Tightly regulated FIC domain proteins modulate bacterial topoisomerases by adenylylation

Inauguraldissertation

zur Erlangung der Würde eines Doktors der Philosophie

vorgelegt der

Philosophisch-Naturwissenschaftlichen Fakultät

der Universität Basel

von

Frédéric V. Stanger

aus Frankreich

Basel, 2016

Genehmigt von der Philosophisch-Naturwissenschaftlichen Fakultät auf Antrag von

Prof. Dr. Tilman Schirmer

Prof. Dr. Christoph Dehio

Basel, den 16. September 2014

Prof. Dr. Jörg Schibler

Dekan

Namensnennung-Keine kommerzielle Nutzung-Keine Bearbeitung 3.0 Schweiz
(CC BY-NC-ND 3.0 CH)

Sie dürfen: **Teilen** — den Inhalt kopieren, verbreiten und zugänglich machen

Unter den folgenden Bedingungen:

Namensnennung — Sie müssen den Namen des Autors/Rechteinhabers in der von ihm festgelegten Weise nennen.

Keine kommerzielle Nutzung — Sie dürfen diesen Inhalt nicht für kommerzielle Zwecke nutzen.

Keine Bearbeitung erlaubt — Sie dürfen diesen Inhalt nicht bearbeiten, abwandeln oder in anderer Weise verändern.

Wobei gilt:

- **Verzichtserklärung —** Jede der vorgenannten Bedingungen kann **aufgehoben** werden, sofern Sie die ausdrückliche Einwilligung des Rechteinhabers dazu erhalten.
- **Public Domain (gemeinfreie oder nicht-schützbare Inhalte) —** Soweit das Werk, der Inhalt oder irgendein Teil davon zur Public Domain der jeweiligen Rechtsordnung gehört, wird dieser Status von der Lizenz in keiner Weise berührt.
- **Sonstige Rechte —** Die Lizenz hat keinerlei Einfluss auf die folgenden Rechte:
    - Die Rechte, die jedermann wegen der Schranken des Urheberrechts oder aufgrund gesetzlicher Erlaubnisse zustehen (in einigen Ländern als grundsätzliche Doktrin des **fair use** bekannt);
    - Die **Persönlichkeitsrechte** des Urhebers;
    - Rechte anderer Personen, entweder am Lizenzgegenstand selber oder bezüglich seiner Verwendung, zum Beispiel für **Werbung** oder Privatsphärenschutz.
- **Hinweis —** Bei jeder Nutzung oder Verbreitung müssen Sie anderen alle Lizenzbedingungen mitteilen, die für diesen Inhalt gelten. Am einfachsten ist es, an entsprechender Stelle einen Link auf diese Seite einzubinden.

Quelle: http://creativecommons.org/licenses/by-nc-nd/3.0/ch/ Datum: 12.11.2013

Table of Contents

Statement of my thesis

This work was performed in the groups of Prof. Tilman Schirmer and Prof. Christoph Dehio in the Focal Area Structural Biology and Biophysics and the Focal Area Infection Biology, respectively, at the Biozentrum of the University of Basel.

My PhD advisory Committee consisted of:

Prof. Tilman Schirmer

Prof. Christoph Dehio

Prof. Timm Maier

My thesis is written in a cumulative format. It consists of an abstract, an introduction covering several aspects related to my work, a result section composed of three accepted scientific research articles, three scientific research articles in preparation and an unpublished results section followed by some concluding remarks.

Abstract

Abstract

Proteins containing FIC (filamentation induced by cAMP) domains are conserved through evolution and found ubiquitously in all domains of life and viruses. Fic proteins catalyze adenylylation, or AMPylation, the transfer of an adenosine-5'-monophosphate moiety (AMP) from an ATP substrate onto a target protein. The adenylylation activity of two bacterial proteins, VopS from *Vibrio parahaemolyticus* and IbpA from *Histophilus somni* was discovered recently. VopS and IbpA are translocated into eukaryotic cells and adenylylate the small GTPases RhoA, Rac1 and Cdc42 in the switch I region, resulting in the inhibition of downstream effector binding and ultimately collapse of the actin cytoskeleton and cell death. Due to their cytotoxic activity in eukaryotic cells but also in bacteria, Fic proteins need to be tightly regulated.

To contribute to the understanding of the regulation mechanism of Fic proteins and inhibition of their targets, I applied biochemical, biophysical and mainly X-ray crystallographic analysis. This work was achieved in close collaboration with microbiologists.

In *research article I*, we show that adenylylation competent Fic proteins containing the HxFx[D/E]GNGRxxR motif are inhibited by a conserved α-helix (α_{inh}) that contains a [S/T]xxxE[G/N] inhibition motif. The α_{inh} helix can be found on a separate protein that forms a tight complex with the Fic protein, or at the N-terminus or C-terminus compared to the Fic active site. These three possibilities lead to the classification of Fic proteins into class I, II and III, respectively. The strictly conserved glutamate of this motif competes with the binding of the γ-phosphate of the ATP substrate of Fic proteins. In *research article II*, we structurally demonstrate that this inhibitory mechanism applies independent of the position of the α_{inh} helix relative to the Fic active site motif.

In the *research article III* we identify GyrB and ParE, the B-subunits of the bacterial topoisomerases DNA gyrase and topoIV, as new bacterial targets for class I Fic proteins. Furthermore, we show that the activity of Fic proteins promotes persister formation and that the ATPase activity of GyrB is blocked by Fic-mediated adenylylation of GyrB. As the structural consequences of ATP hydrolysis in GyrB remained elusive, I revealed in *research article IV* all nucleotide bound states along the ATP hydrolysis pathway by thorough X-ray crystallographic analysis. Upon ATP hydrolysis, an obligatory rigid-body domain motion of the transducer relative to the ATPase domain occurs in the immediate post-hydrolysis state ($ADP{\cdot}P_i$).

In *research article V*, we dissect the regulation mechanism of the class III Fic protein NmFic that contains the α_{inh} helix at the C-terminus. NmFic is in a monomer-tetramer equilibrium and structurally unable to bind a target in the tetramer form. Dissociation of the tetramer relieves the inhibition of this Fic protein and allows adenylylation of GyrB. Interestingly, NmFic is also auto-adenylylated. Auto-adenylylation of NmFic leads to conformational changes in the α_{inh} helix and the neighboring α1 helix, with the Fic core being unchanged. We show that the presence of the strictly conserved tyrosine Y183 which is auto-adenylylated is crucial for both Fic protein activities. Thus, we propose that class III Fic proteins are tightly regulated by oligomerization and auto-adenylylation *via* a double-lock mechanism.

The inhibition of bacterial topoisomerases by Fic proteins of class I and III remains to be investigated at a structural level. I have shown that adenylylation of GyrB expulses the ATP-lid loop from its original position and I developed a new strategy to trap the Michaelis-Menten complex of a Fic protein and its cognate target by using covalent cross-linking of the Fic protein with the target *via* a functionalized ATP substrate.

Taken together, these results provide the first level of understanding of the regulation of FIC domain proteins and Fic-mediated inhibition of bacterial topoisomerases.

Introduction

1. Introduction

1.1. Bacterial pathogenesis

1.1.1. Bacterial effector proteins

To establish a replicative niche in their reservoir host, bacteria have evolved a wide range of virulence factors. These effector proteins are secreted by pathogens into host cells *via* designated secretion systems, to manipulate the recipient cell and make it a more favorable environment for the replication of the pathogenic bacteria[1]. Pathogens contain a variety of effectors, ranging from the single effector protein CagA in *Helicobacter pylori*[2] to hundreds of effectors in the case of *Legionella pneumophilae*[3].

In the pathogen, effector proteins are inactive due to the lack of a cognate target or binding to an inactivating binding partner (antitoxin) that interferes either with target recognition or active site obstruction. Also, type III secretion system chaperones of translocators interact with hydrophobic patches of the effector proteins (e.g. YopB or VopD from *Yersinia*) that mediate the membrane attachment within the host cells[4].

Bacterial effector proteins can be classified in two major categories. The first one directly mimics the host cell activities, where the effector proteins can either be a homologous protein or result from convergent evolution, having a similar structure and function but without obvious primary sequence identity, e.g. YopE from *Yersinia pseudotuberculosis*[5,6]. The second category of effector proteins modifies the host proteins by post-translational modification thereby subverting host cell activities more indirectly[7] (see section 1.1.4.).

Many bacterial effector proteins target members of the Rho family GTPases, the well-studied RhoA, Rac and Cdc42. These proteins are key regulators of many cellular processes, e.g. cell cycle control or actin cytoskeleton regulation, which makes them ideal targets of bacterial effector proteins. Interestingly, some effector proteins act as Rho GTPases mimics but others modulate Rho GTPases by covalent modification.

1.1.2. Secretion systems

To reach the host cell, bacterial effector proteins need to be transported through the pathogen and host-cell membranes. In Gram-negative bacteria, six secretion systems have been described. On one-hand, Type I, III, IV and VI secretion systems secrete effector

molecules in one-step, across the inner membrane, the periplasm and outer membrane. On the other-hand, Type II and V secretion systems secrete effectors in two-steps, first to the periplasm and then across the outer membrane. Type III secretion system (T3SS)[8] and type IV secretion system (T4SS) are the best characterized secretion machineries of effector proteins[9].

T3SS evolved from the bacterial flagellum[10] and consists of a secretion apparatus located at the inner membrane, a needle filament (injectisome) that crosses the periplasm and outer membrane towards the eukaryotic plasma membrane where the translocon is found[11].

Host-interacting T4SS evolved multiple times independently from bacterial conjugation systems[12] and mediate the translocation of DNA and effector proteins into eukaryotic cells[13]. Canonical type IV secretion systems are composed of 12 different proteins named VirB1-VirB11 and VirD4. Recent electron microscopy structure of the Type IV secretion system[14] from the *Escherichia coli* conjugative plasmid R388 reveals a three Megadalton complex constituted of VirB3-VirB10 that spans the inner membrane, periplasm and outer membrane. This complex can be divided into three subunits: the inner membrane complex constituted of VirB3-VirB4, the stalk formed by VirB10 and the outer membrane complex made by VirB7, VirB9-VirB10. The exact localization of VirB3-VirB5-VirB6-VirB8 has not yet been unambiguously determined.

1.1.3. Toxin-antitoxin systems

There are many differences between toxins and effectors: for example, toxins inhibit cellular functions whereas effector proteins can modulate host cell functions[15]. Some toxins are found in so-called toxin-antitoxin (TA) systems, which consist of two genes that are encoded in an operon. The antitoxin is usually encoded upstream of the toxin[16].

The regulation of toxin-antitoxin systems is crucial for the activity of the system. Three major classes of antitoxins regulate the TA loci[17]: a type I antitoxin is an antisense RNA than inhibits the translation of the toxin, a type II antitoxin is a protein that binds to the toxin and prevents toxic activity or target binding and a type III antitoxin is an RNA that blocks the toxin through direct binding. In type II and III TA systems, the degradation of the more labile antitoxin leads to the activation of the toxin that can have several roles such as stabilization of genomic parasites, selfish alleles, gene regulation, bacteriophage defense (abortive infection), growth control, persister cell formation or programmed cell arrest[18]. Thereof, phage infection and persister formation are the most important functions.

A general mechanism of action of effector proteins and toxins is post-translational modifications of host cell targets, resulting in alteration of host cell functions.

1.1.4. Pathogen-mediated post-translational modifications

Post-translational modification (PTM) is a widespread mechanism used by both eukaryotic and bacterial cells to modify target proteins *via* the covalent attachment or removal of functional groups. In particular, post-translational modifications are key strategies used by bacterial and viral pathogens to modulate host factors critical for infection. The first evidence for pathogen-mediated post-translational modification was given in 1969, when Collier and Cole[19] showed that Diphteria toxin from *Corynebacterium diphteriae* ADP-ribosylates the host Elongation Factor 2 (EF-2), resulting in the inhibition of translation and subsequent cell death.

In about 45 years of research, many more pathogen-mediated post-translational modifications have been described. These modifications range from the addition of a few atoms, e.g. a phosphate group, to a polypeptide chain, e.g. ubiquitin. The most occurring pathogen-mediated post-translational modification of host cell proteins are phosphorylation, acetylation, ADP-ribosylation, adenylylation (AMPylation), glycosylation, eliminylation, proteolysis, ubiquitination or SUMOylation/de-SUMOylation, of which all are reversible PTMs except eliminylation and proteolysis that are irreversible modifications[20-22] (Figure 1.1).

1.1.4.1. Phosphorylation

Phosphorylation is the transfer of the gamma-phosphate from ATP substrate onto specific amino acids by enzymes called kinases (Figure 1.1.a). The modification of histidine into phosphohistidine is transient, with a short half-life in the range of several seconds at acidic pH[23], whereas the phosphorylation of serine, threonine and tyrosine is more stable[24]. In similar acidic conditions but with elevated temperature (100°C), free phosphoserine or phosphothreonine have a half-life of 18h, and phosphotyrosine of about 5 hours[25]. The environment also affects the stability of these phosphorylations, i.e. the pH and surrounding amino acids that will affect charge distribution and stabilize the phospho-amino acids, as observed in the case of a phosphohistidine with a half-life of 12 days in histone H4 at pH 7.6 and room temperature[26]. Phosphorylation is the first PTM that was described in 1954 by Burnett and Kennedy[27], in mitochondria. YpkA (also called YopO) from *Yersinia*[28], SteC from *Salmonella*, legK1-legK5 from *Legionella* or OspG from *Shigella* are various bacterial

effector proteins that phosphorylate different eukaryotic target proteins on Ser/Thr residues *via* their kinase domain, subverting host defense processes[29].

Interestingly, the phosphorylation of amino acids is a fully reversible process that can be catalyzed by enzymes called phosphatases (Figure 1.1.a). These enzymes catalyze the dephosphorylation of previously phosphorylated residues. The type III effector protein YopH from *Yersinia*[30] is a protein tyrosine phosphatase (PTP) that is essential for the virulence of the bacterium. SptP from *Salmonella*[31] also contains a PTP domain that increases pathogen replication.

1.1.4.2. Acetylation

Acetylation is the addition of an acetate group on serine, threonine or lysine residues of host cell proteins (Figure 1.1.b). YopJ/YopP from *Yersinia*[32] or VopA from *Vibrio parahaemolyticus*[33] acetylates MAPK kinases, blocking a phosphorylation acceptor site or the ATP binding site of the enzyme, respectively. Listeriolysin O from *Listeria monocytogenes* seems to be involved in the increase of Histone H3 and H4 acetylation but also in the decrease of the acetylation of H3, suggesting a function of deacetylation, the reverse process[34].

1.1.4.3. ADP-ribosylation

ADP-ribosylation was first described for diphteria toxin in the late 1960's. An ADP-ribose moiety is transferred from a nicotinamide adenine dinucleotide (NAD+) substrate onto target protein (Figure 1.1.c). Cholera toxin (*V. cholera*) and pertussis toxin (*B. pertussis*) ADP-ribosylate arginine and cysteine residues from G-alphaS, respectively. The C3 toxin from *Clostridium* modifies asparagine residues from Rho or Rac[35]. Pathogen-mediated ADP-ribosylation also occurs on a diphtamide (modified histidine) residue from elongation factor 2, in the case of diphteria toxin (*C. diphteria*) or Exotoxin A (*P. aeruginosa*).

The modification of these diverse amino acids results in the host cell perturbation, by a permanent activation or inactivation of cellular functions. Again, this reaction is reversible and ADP-ribose can be removed by ADP-ribosyl hydrolases[36], of which the best described is the ribosylarginine hydrolase that specifically cleaves ADP-ribose from arginine residues[37].

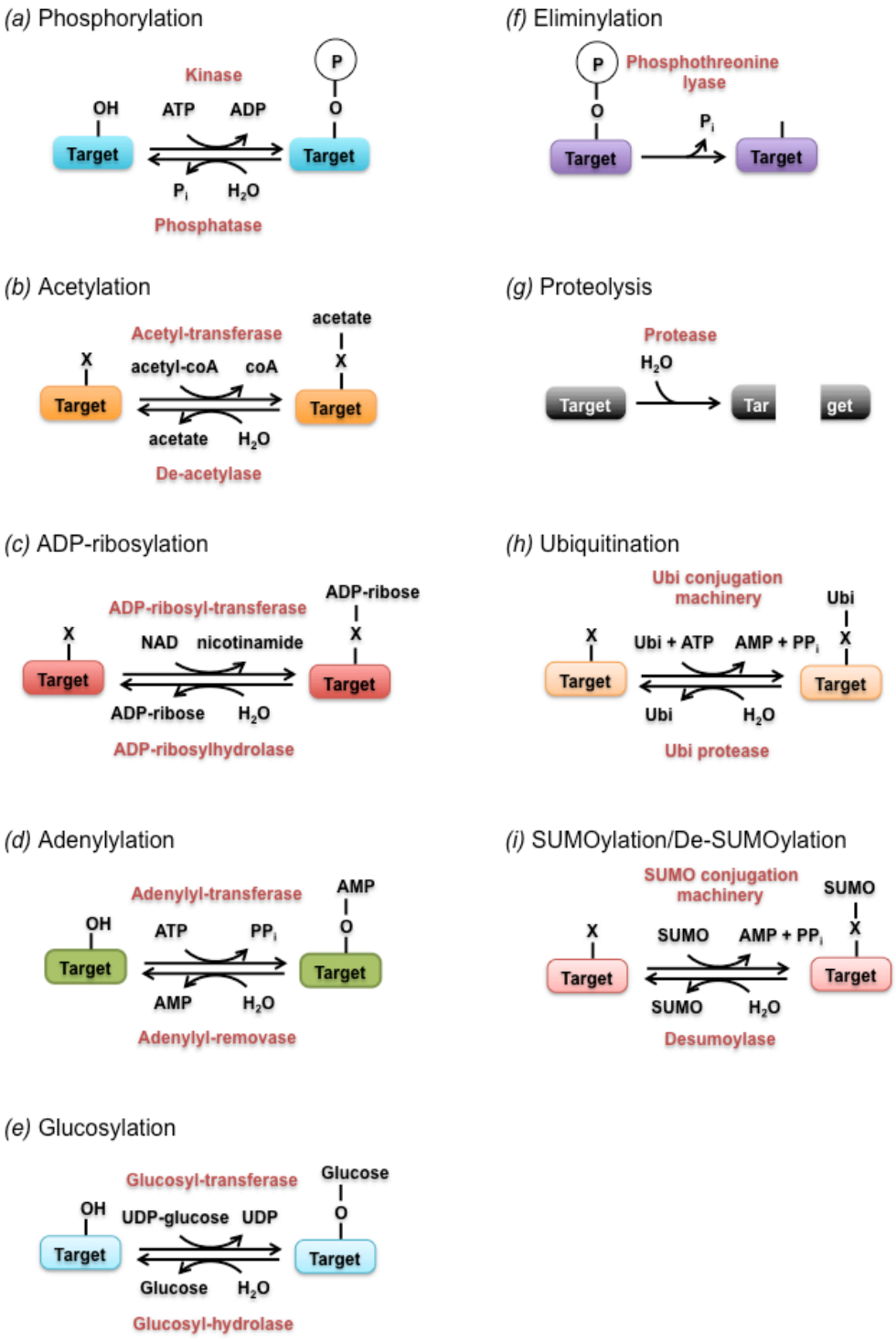

Figure 1.1. Pathogen-mediated post-translational modifications. *(a)* Phosphorylation of hydroxyl groups (Ser, Thr or Tyr) by kinase and the reverse reaction dephosphorylation. *(b)* Acetylation of Lys, Ser or Thr residues (depicted as X) by acetyltransferase and the reverse reaction deacetylation by deacetylase, *(c)* ADP-ribosylation of Arg, Cys or Asn residues (X). *(d)* Adenylylation of Ser, Thr or Tyr side chains by adenylyl-transferase and reverse reaction. *(e)* Glucosylation of hydroxyl groups (Ser, Thr) by glucosyltransferase. *(f)* Irreversible eliminylation of phosphorylated tyrosine side chains, resulting in dehydrobutyrine. *(g)* Irreversible proteolysis by proteases. *(h)* Ubiquitination and de-ubiquitination of lysine side chains. *(i)* Similarly to ubiquitination, the mechanism of SUMOylation and de-SUMOylation. Modified from [21,22].

1.1.4.4. Adenylylation

Adenylylation or AMPylation, i.e. the transfer of an AMP moiety onto a hydroxyl side chain (Figure 1.1.d), is a post-translational modification that has first been described as part of the regulation mechanism of glutamine synthetase (described in section 1.2.2.2). Interestingly, adenylylation is also a pathogen-mediated PTM that has been demonstrated for the *L. pneumophilae* effector protein DrrA[38], which shares the same fold as glutamine synthetase[39], yet without obvious sequence identity. Additionally, Fic proteins are effectors that constitute a new family of adenylyl-transferase with a distinct fold and will be described in section 1.3. This PTM will be detailed in section 1.2. and in the context of Fic-mediated adenylylation in section 1.4.1.

1.1.4.5. Glucosylation (glycosylation)

Pathogen-mediated glucosylation (or glycosylation) consists in the transfer of carbohydrate on serine or threonine residues that has only been described for GTPases targets (Figure 1.1.e). Toxin A and B (TcdA and TcdB, respectively) from *Clostridium difficile* modify the small GTPase Rho by O-glucosylation on Thr37 (Rac and Cdc42 on Thr35) of the switch I region, resulting in the collapse of the actin cytoskeleton[40]. Additionally, Lgt family proteins from *Legionella pneumophilae* induce cytotoxicity through glycosylation of a serine residue in the elongation factor 1A[41].

1.1.4.6. Eliminylation

Eliminylation is the irreversible reaction catalyzed by phosphothreonine lyase (Figure 1.1.f). The effector proteins OpsF from *Shigella* and SpvC from *Salmonella* are phosphothreonine lyases that specifically catalyze an eliminylation reaction on a phosphothreonine of MAP kinase (MAPK) that is essential for MAPK activity[42,43]. The reaction is similar to a dephosphorylation by phosphatase but removes also the acceptor hydroxyl group such that the threonine can no longer be modified. Phosphothreonine lyase converts a phosphothreonine into dehydrobutyrine, an alkene with an unsaturated Cα-Cβ double bond[43].

1.1.4.7. Proteolysis

Proteolysis is the hydrolysis of polypeptide bonds by a protease, resulting in the cleavage of proteins into smaller polypeptides[44] (Figure 1.1.g). Some effector proteins, like YopT from *Yersinia*, catalyze this irreversible post-translational modification[45]. YopT is a cysteine protease that cleaves N-terminally to prenylated cysteines that form the membrane anchor of small GTPases (RhoA, Rac, Cdc42), resulting in the removal of these signaling hubs from the cell membrane and, consequently, breakdown of the actin cytoskeleton[46].

1.1.4.8. Ubiquitination

Ubiquitination (or ubiquitylation) is the addition of ubiquitin, a 9 kDa protein on lysine side-chains of target proteins (Figure 1.1.h). The effector AvrPtoB from *Pseudomonas syringae* functions as an E3 ubiquitin ligase and targets the host protein kinase Fen. Once ubiquitinated, Fen is degraded in a proteasome-dependent manner, resulting in a disruption of plant immunity[47]. The effectors SopA from *Salmonella* and NleL from *E. coli* mimic mammalian E3 ubiquitin ligases and contribute to pathogenicity of their respective bacterium via mechanisms that remain to be elucidated[48].

1.1.4.9. De-SUMOylation

De-SUMOylation is the removal of a SUMO (small ubiquitin-like modifier) by specific desumoylase (proteases) (Figure 1.1.i). The plant pathogen *Xanthomonas campestris* effector protein XopD contains a cysteine protease specific for proteins modified with SUMO, resulting in the suppression of plant defenses which promotes successful infection[20,49].

1.1.4.10. Others: Nucleotidylylation, uridylylation, phosphocholination

Nucleotidylylation, the addition of NMP, i.e. AMP (introduced in section 1.1.4.4. and further described in section 1.2. and 1.4.1.), GMP, CMP or UMP onto hydroxyl side chains of a target protein has been recently described for the human pathogen *Mycobacterium tuberculosis*[50]. This enzymatic post-translational modification is mediated by FIC (filamentation induced by cAMP) domain proteins.

A plant pathogen effector from *X. campestris*, AvrAC, is an urydylyl-transferase with Fic fold that specifically transfers an UMP moiety from an UTP substrate in a reaction called uridylylylation[51].

The versatile Fic proteins also catalyze phosphocholination, the transfer of a phosphocholine moiety from a CDP-choline substrate[52]. Fic-mediated post-translational modifications will be described further in detail in section 1.4.

1.2. Adenylylation

Adenylylation, also called AMPylation, is the covalent transfer of an adenosine-5'-monophosphate (AMP) moiety from an ATP substrate molecule on a protein, RNA or small molecules. A breakthrough in the late 1960's was the discovery of adenylylation as a stable modification crucial for the regulation mechanism of the glutamine synthetase activity (*E. coli*.)[53]. A less stable, termed transient adenylylation, is a common enzymatic reaction that occurs as an activation step in complex enzymatic reaction (tRNA charging, ubiquitination), generating AMP as an efficient leaving group.

There is some controversy on the nomenclature of the AMP transfer reaction in the adenylylation field. Adenylation and adenylylation/AMPylation have been used to characterize the transfer of an AMP moiety. Since adenylation refers to the transfer of an adenyl group, the "radical from adenine", it is not absolutely correct[54]. Adenylylation (or AMPylation) is more accurate as this is the transfer of an adenylyl group (adenine-ribose-phosphate) and I will therefore use adenylylation in this context.

1.2.1. Transient adenylylation

Transient adenylylation has been shown to occur in many enzymatic reactions, with most of them involving the adenylylation of the carboxyl group of amino acids[55].

1.2.1.1. Aminoacyl tRNA synthetases

Aminoacyl tRNA synthetases (aaRS) catalyze the covalent attachment of an amino acid to its cognate transfer RNA (tRNA) molecule, resulting in the formation of an aminoacyl-tRNA (aa-tRNA), which is often referred to as tRNA charging. This is the first stage of protein synthesis and an obvious pre-requisite for mRNA translation into protein. Most organisms have a specific aaRS for each amino acid. tRNA loading is a two-steps reaction that requires ATP. In a first step, called activation step, ATP binds to the aaRS active site together with the cognate amino acid. The α-carboxyl group of the amino acid attacks the α-phosphate of the ATP molecule, resulting in the formation of a 5'-aminoacyl-adenylate (aminoacyl-AMP) that

remains bound to the active site. In a second step, called transfer step, the aminoacyl group is transferred to the 2'- or 3'-OH of the terminal residue of the amino acid arm (5'-CCA-3') of the tRNA, resulting in a covalent and stable charged tRNA (aa-tRNA) and the release of the AMP moiety[56].

1.2.1.2. E1 activating enzymes

E1 activating enzymes are essential in the context of ubiquitination or SUMOylation. In the case of ubiquitination, the C-terminal glycine residue is activated in presence of ATP, resulting in the formation of a covalent unstable ubiquitin-adenylate (ubiquitin-AMP) and release of PPi. Ubiquitin then binds to a cysteine residue and forms a thiolester bond, with the concomitant release of AMP. In a second step, the activated ubiquitin is transferred to E2, the ubiquitin carrier protein. Finally, the third step catalyzed by E3, the ubiquitin protein ligase, results in the linkage of the C-terminus of ubiquitin to the terminal amino group of a lysine side chain[57].

Similarly to aminoacyl-tRNA synthetases, adenylylation of ubiquitin serves as an activation step.

1.2.2. Stable adenylylation

In contrast to the activation mechanism described for transient adenylylation, stable adenylylation is a stand-alone process in which no further reaction is required. A counteracting enzyme performing a de-adenylylation is needed to remove the covalently bound AMP moiety.

1.2.2.1. Aminoglycoside nucleotidyl transferases

Aminoglycosides are a class of highly potent antibiotics that inhibit protein synthesis by binding to the ribosome. Kanamycin, gentamicin, neomycin and the first aminoglycoside discovered in the 1940's, streptomycin, are few examples of this class of antibiotics. Aminoglycosides bind to the 30S subunit of the ribosome and perturb elongation of the nascent chain resulting in premature termination of translation and therefore unachieved polypeptide chains[58].

Interestingly, the most prevalent resistance mechanism against aminoglycosides utilizes enzymatic modification of the antibiotics. The most widely used modifications are

nucleotydylation (including adenylylation), acetylation or phosphorylation, each of them being catalyzed by a specific transferase. These aminoglycoside modifying enzymes are often plasmid encoded[58].

Two nucleotydyl-transferases (ANT(4′) and ANT(2″)-I) from *Staphylococcus aureus* have been extensively studied in the context of aminoglycoside modification[59]. The crystal structure of the kanamycin nucleotydyl-transferase ANT(4′) from *S. aureus* has been solved in complex with kanamycin and a non-hydrolysable ATP analog (AMPCPP)[60]. This enzyme is not specific for ATP and can bind any nucleotides, which is in-line with the few interactions of the adenine portion with the kanamycin nucleotydyl-transferase. More interactions occur in the α, β, and γ phosphate region of the ATP analog moiety. The enzyme has also a broad spectrum of aminoglycoside substrates, mainly from the kanamycin and neomycin families, resulting in a resistance to a broad spectrum of antibiotics. The mechanism deciphered from the crystal structure (PDB: 1KNY) suggests a nucleophilic attack from the 4'-OH group of the aminoglycoside on the α-phosphate of the ATP molecule.

1.2.2.2. The historical case of glutamine synthetase

Glutamine synthetase (GS) has an essential role in the uptake of ammonia in bacteria. The enzyme catalyzes the condensation of ammonia with glutamate to form glutamine. Several inhibitors and activators tightly regulate the activity of glutamine synthetase. One of the central regulation mechanisms is the adenylylation of glutamine synthetase, which is under the control of glutamine synthetase adenylyl transferase (GS-AT) located at the C-terminus of the enzyme[53] (Figure 1.2.a). This domain catalyzes the adenylylation of a specific tyrosine residue (Y397 in *Salmonella typhimurium*). Interestingly, this enzyme contains an N-terminal adenylyl removase (AR) domain that catalyzes the opposite reaction, i.e. the de-adenylylation of this residue and a central regulatory (R) domain. Remarkably, both AR and AT domains share 24% identity and a β-polymerase fold, characteristic of many adenylyl transferase enzymes[39]. The root mean square deviation (rmsd) between the C-alpha positions of the AR and AT domains of this enzyme is 2.4 Å, as revealed by the comparison of both crystal structures (PDB: 1V4A and 3K7D, respectively)[39,61].

The regulation mechanism of glutamine synthetase is of high complexity. The enzyme forms a dodecamer (12 GS) as observed in the first crystal structure obtained of GS[62]. The 12 subunits are organized in a ring form, with a 6-fold axis passing through the hole of the ring.

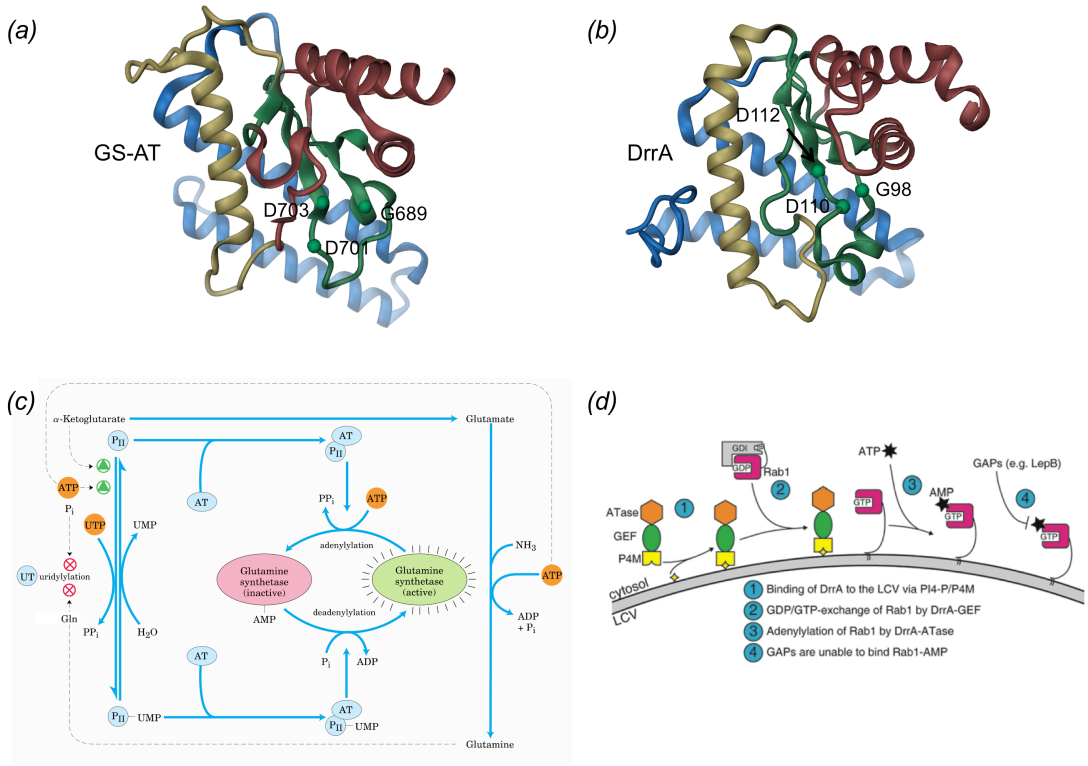

Figure 1.2. Structure and function of the glutamine synthetase adenylyl transferase (GS-AT) and the *Legionella* effector protein DrrA. *(a)* Structure of GS-AT (PDB: 3K7D) compared to *(b)* the structure of DrrA (PDB: 3NKU), The crucial residues of the catalytic active site G-X_{11}-D-X-D are depicted as green balls, adopted from [38]. *(c)* Unexpected complex regulation of glutamine synthetase, taken from [63]. *(d)* Mechanism of GTPase inactivation by DrrA, taken from [64].

This 3D structure also reveals the position of the adenylylated residue, at the interface between subunits and close to the active site. It has been demonstrated that the adenylylation of Y397 decreases the activity of GS. This residue is located close to the active site of the enzyme, but there are, so far, no evidences that adenylylation of GS induces steric clashes with the substrate since a crystal structure of GS-AMP is still lacking. The degree of inhibition is dependent on the number of adenylylated subunit within the dodecamer. GS-AT, the enzyme that adenylylates GS, is activated by glutamine, the product of GS, leading to feedback inhibition of glutamine synthetase. Additionally, GS-AT is inhibited by α-ketoglutarate, the precursor of glutamate, the substrate of GS. The N-terminal adenylyl removase (AR) domain of GS-AT deadenylylates GS by phosphorolysis, i.e. the attack of an inorganic phosphate on the phosphate of Y397-AMP, forming ADP. The AR domain of GS-AT is activated by α-ketoglutarate and inhibited by glutamine. But the regulation of glutamine synthetase is even more complex and involves a regulatory protein called P_{II}. P_{II} is itself

regulated by uridylylation (transfer of an UMP moiety) at a tyrosine residue. GS-AT forms a complex with P_{II} in either the uridylylated (P_{II}-UMP) or deuridylylated (P_{II}) form. The GS-AT/P_{II}-UMP complex stimulates the deadenylylation of glutamine synthetase whereas the complex of GS-AT/P_{II} stimulates the adenylylation of glutamine synthetase. The uridylylation/deuridylylation of P_{II} is catalyzed by an uridylyltransferase, with the uridylylation being activated by α-ketoglutarate and inhibited by glutamine. This unusually complex mechanism of regulation of glutamine synthetase is summarized (Figure 1.2.c). The tight control of this enzyme is crucial regarding its central metabolic role as an entry point for reduced nitrogen.

1.2.2.3. DrrA, an effector from *Legionella pneumophilae*

The bacterial effector protein DrrA (also called SidM) from *Legionella pneumophilae*[38,65] is a multi-domain protein, with an N-terminal adenylyl-transferase domain, a central guanine nucleotide exchange factor (GEF) domain and a C-terminal P4M domain, responsible for membrane attachment. The activity of DrrA had been first described as a GEF for Rab1[65]. Recently, it has been shown that the N-terminal adenylyl-transferase domain is responsible for the cytotoxicity of DrrA (Figure 1.2.d). The crystal structure of the N-terminal domain of DrrA has been determined recently[38] (PDB: 3NKU). Interestingly, DrrA has a similar fold to the C-terminal domain of glutamine synthethase adenylyl transferase (GS-AT) (see previous section 1.2.2.2.) (Figure 1.2.b compared to 1.2.a). Mutation of the catalytic active site aspartates of the G-X_{11}-D-X-D motif of DrrA abolishes the adenylylation activity of the enzyme. Additionally, DrrA specifically adenylylates the conserved tyrosine Y77 of the switch II region of the small GTPase Rab1b. The crystal structure of the adenylylated form of Rab1 (Rab1-Y77AMP) has been determined (PDB: 3NKV) and doesn't display significant structural changes compared to a native form of Rab1, with the covalently attached AMP moiety located close to the surface of the protein. It is undisputed that the N-terminal domain of DrrA is responsible for Rab1 adenylylation and induces cytotoxicity in mammalian cells, but the exact mechanism of action is not yet clear[64].

1.2.2.4. Fic proteins: a new family of adenylyl-transferases

Recently, several effector proteins have been described as adenylyl-transferases, with similar effect as DrrA. VopS, an effector protein from *Vibrio parahaemolyticus*, adenylylates Rho GTPases, resulting in disruption of downstream signaling in host cells[66,67]. This adenylyl-transferase belongs to a family of protein called Fic proteins (filamentation induced

by cAMP) that do neither share sequence identity with glutamine synthetase adenylyl-transferase nor structural similarities. FIC domain proteins are one of the main focuses of my PhD thesis and will be discussed further in detail in the following sections.

1.3. Fic proteins

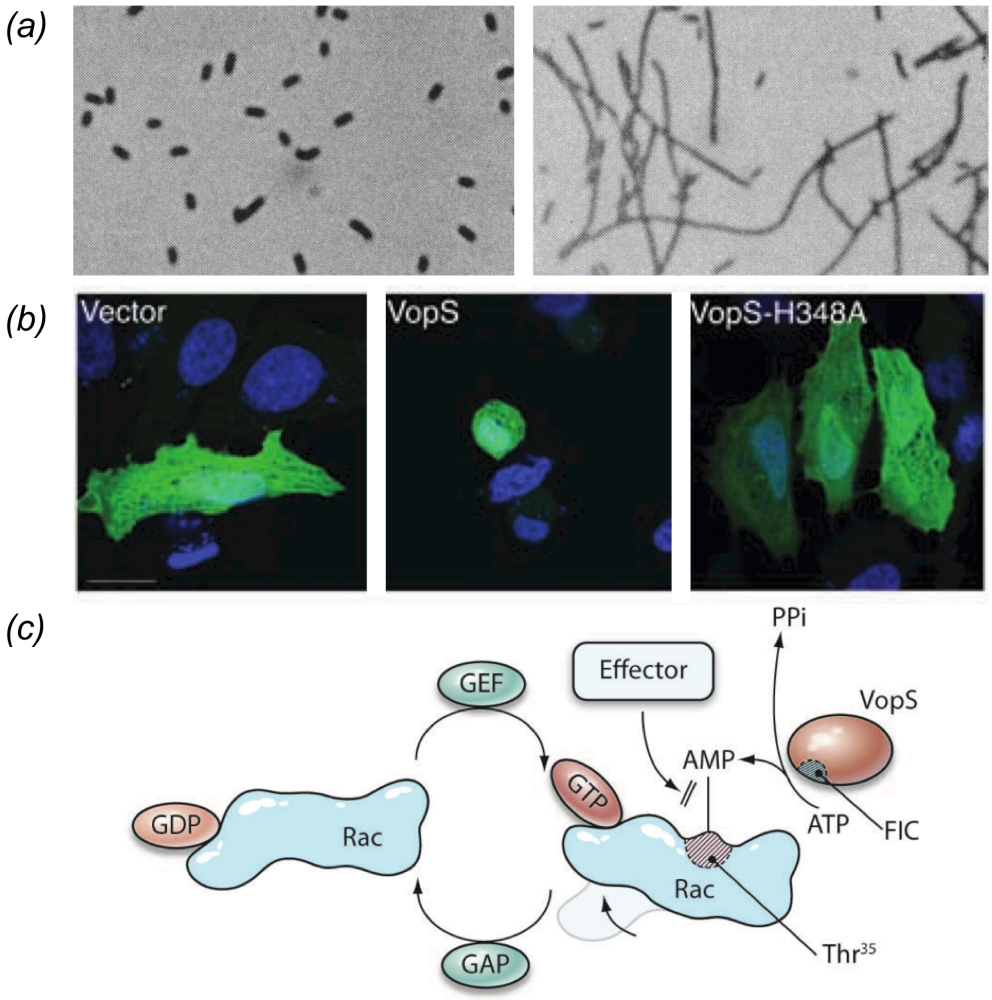

Figure 1.3. Fic-mediated interference with cell vialbility. *(a)* Filamentation of *E.coli* fic-1 mutant when grown at 43°C in presence of 1.5 mM cAMP (right) compared to normal growth and division (left). *(b)* Effect of VopS expression in HeLa cells with from left to right the vector control expressing GFP, expression of GFP-VopS in HeLa inducing cell rounding phenotype and expression of the catalytically inactive mutant VopS-H348A fused to GFP that behaves like the vector control. *(c)* Mechanism of Rho GTPases inactivation by VopS. Adenylylation of Rac on Thr35 of the switch I region inhibits effector binding and downstream signaling. Adopted from [66,68,69].

1.3.1. Discovery of the name-giving *fic* gene

Fic (filamentation induced by cAMP) has been first described by Utsumi *et al.*[68], in the 1980's for an *E. coli* mutant. They have found that an increase in the intracellular cAMP (1.5 mM) level induced cell filamentation in a *fic-1* mutant at elevated temperature (43°C), and could map a glycine to arginine mutation in the Fic protein (G55R) (Figure 1.3.a). In 1991, Komano *et al.*[70], showed that a deletion of the *fic* gene in *E. coli* resulted in an auxotrophic bacteria for p-aminobenzic acid or folate, suggesting that Fic protein is involved in the synthesis of this compound. This would indicate that the Fic protein and cAMP are involved in the regulation mechanism of cell division via a folate mechanism. In this deletion strain, the *fic* gene was replaced by a kanamycin resistance (Km^1) gene. Closer analysis of the *E. coli fic* gene locus showed that the promoter of the *pabA* (p-aminobenzoate synthase) gene lies within the *fic* gene and was therefore also removed by this deletion mutant.

Despite these early results[68,70-74], the function of FIC domain proteins remained elusive until 2009 and the discovery of the adenylyl-transferase activity of the effector protein VopS from *Vibrio parahaemolyticus*[66]. Concurrently, the catalytic activity of the effector protein IbpA from *Histophilus somni* has been deciphered as adenylylation of Rho GTPases[75].

1.3.2. FIC domain effector proteins

As already mentioned, the focus on Fic proteins started when the enzymatic activity of this family of enzyme has been discovered in 2009[66]. The injection of *Vibrio parahaemolyticus* effector proteins via a functional Type III secretion system into eukaryotic host cells induces cell rounding via inhibition of Rho family GTPases[76]. The injection of a single effector, VopS, leads to a similar severe cell rounding phenotype and inhibition of the Rho GTPases Rac1, RhoA and Cdc42. A sequence analysis of the C-terminal domain of VopS, so-called FIC domain, revealed a strictly conserved histidine residue in a stretch of highly conserved amino acids, revealing a putative active site. The mutation of this histidine to alanine, thereafter referred as H/A, abolished the cytotoxicity of VopS (Figure 1.3.b). Mass spectrometry analysis of Rac1 expressed with VopS revealed a mass shift of 329 Da compared to Rac1 co-expressed with the H/A mutant of VopS. This mass corresponds to the covalent attachment of a 5'-adenosine monophosphate moiety (AMP) to the Rho GTPase, that has been assigned to the threonine 35 (Thr35) of the switch I region of Rac1 or Cdc42 and Thr37 of RhoA. Hence, VopS modifies Rho family GTPases by adenylylation in the switch I

region, resulting in the inhibition of downstream effector binding by steric hindrance (Figure 1.3.c).

Concurrently, another effector protein, IbpA from the respiratory pathogen *Histophilus somni* has been shown to adenylylate the Rho GTPases RhoA, Rac and Cdc42, resulting in the disruption of the actin cytoskeleton[75].

Moreover, the FIC domain is conserved from bacteria to human, with the human HypE protein (huntingtin yeast-interacting protein E, also called FICD) also catalyzing adenylylation[75].

Taken together, these two studies on the Fic proteins VopS, IbpA and HypE set the basis of Fic-mediated adenylylation of small GTPases. The consensus active site motif has been defined as HPFxxGNGR, with the first histidine of the motif crucial for the catalytic activity of Fic proteins[66,67,75].

1.3.3. Three dimensional structure of Fic proteins

Crystal structures of Fic proteins were solved by structural genomics groups prior to any knowledge were gained on the function of these proteins. Four Fic proteins were solved: from *Helicobacter pylori*, - HpFic (PDB: 2F6S), from *Neisseria meningitidis* - NmFic (PDB: 2G03), from *Bacteroides thetaiotaomicron* - BtFic (PDB: 3CUC) and from *Shewanella oneidensis* - SoFic (PDB: 3EQX)[77] (Appendix 8.4.). These four structures revealed an alpha-helical topology. FIC domain proteins, due to their size and compact fold, appeared as an ideal substrate for structural studies and crystallographic structure determination.

The core of the FIC domain is made of four α-helices arranged in an up and down bundle, as defined by the Pfam[78] protein families database (http://pfam.xfam.org). These four helices, numbered α2-α5 in the smaller Fic proteins observed, NmFic or HpFic, are decorated with additional helices. Helices α6-α7 lies almost perpendicularly to the Fic core helices (Figure 1.4.b). The active site motif (Figure 1.4.a), further defined by the HPFx[D/E]GN[G/K][79] motif lies in a loop between α-helices α4-α5. A β-hairpin involved in target binding is located between helices α2-α3 and is often referred to as FLAP[79,80].

Intriguingly, an alpha helix (called α') can be encoded N-terminally or C-terminally to the Fic active center and completes the Fic core[79]. The relevance of this α-helix will be discussed in section 3.1., *research article I* and section 3.2., *research article II*.

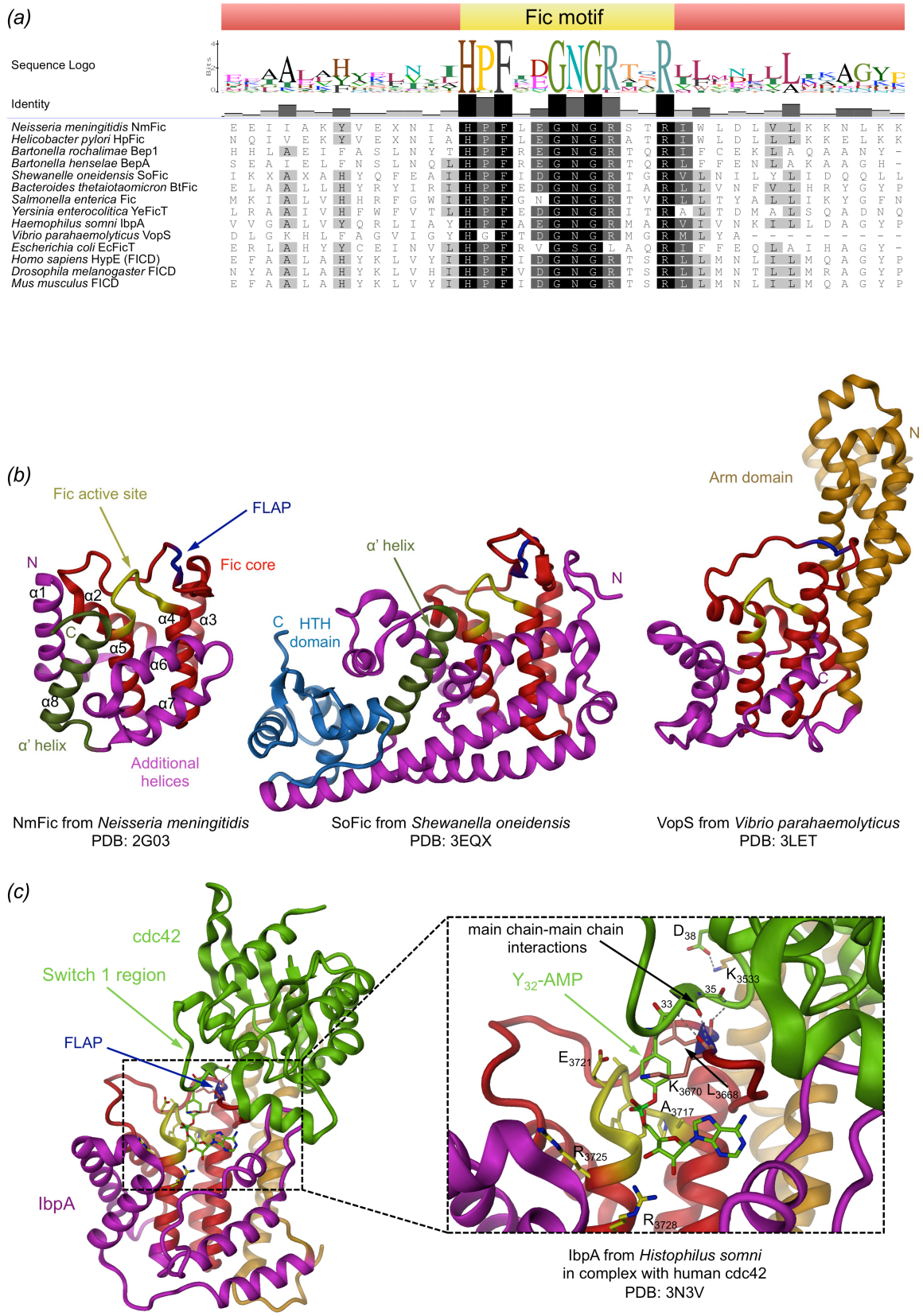

Figure 1.4. Structure of Fic proteins. *(a)* Fic active site motif conservation in bacteria and animals, with consensus sequence logo. *(b)* Topology of Fic proteins with standard colors used for all the figures: Fic core in red, Fic active site in yellow, helix α' in dark green, arm domain in orange, FLAP in dark blue, HTH domain in

light blue, additional helices in magenta. N or C represents the N-terminus or C-terminus of the crystallized fragment, respectively. From left to right, the small NmFic single domain protein, the SoFic protein containing a C-terminal HTH domain and the first Fic protein described as adenylylator, VopS. *(c)* Complex structure of IbpA (standard Fic colors) with Cdc42 (green). The inset shows the IbpA active site details with Cdc42 binding to the FLAP of IbpA. Main chain-main chain interactions are displayed as dashed lines and residues involved in interactions are depicted and the residue number shown. K3670 and L3668 from IbpA form a clamp around the adenylylated residue of Cdc42 (Y32).

A three-dimensional comparison of the structures of Fic proteins revealed a structural homology with Doc, a protein of the plasmid addiction system of the bacteriophage P1[81], and with AvrB from *Pseudomonas syringae*. The Pfam database classifies Fic and Doc proteins together. Indeed, Fic, Doc and AvrB share a same fold as displayed in Figure 1.5.

The crystal structures of VopS[82] (PDB: 3LET) and IbpA[80] (PDB: 3N3U) confirm the three-dimensional structures aforementioned. Fic proteins are often multi-domain proteins. For example, SoFic from *S. oneidensis* contains an N-terminal helix-turn-helix (HTH) domain[77], often involved in transcription regulation (PDB: 3EQX) (Figure 1.4). The structure of the *Bartonella effector protein* BepA[83] (PDB: 2VZA) reveals the same core structure with an additional C-terminal oligonucleotide-binding (OB) domain, which function remains elusive (Appendix 8.4).

1.3.4. Active site motif

The active site has been located in an eight amino acids loop between helices α4-α5 of the Fic core that extends in the first helical turn of the helix α5 by four amino acids. This active center is conserved in Fic and Doc family proteins.

The crystal structures revealed an anion-binding nest located at the N-terminal end of the helix α5 in Fic proteins. The β-hairpin, together with parts of helices α6-α7 participates in forming a pocket for the base of the nucleotide. The conserved first histidine of the HPFx[D/E]GN[G/K] motif, present in Fic proteins is crucial for activity[82,84,85].

The catalytic mechanism has been proposed based on the crystal structure of the IbpA/Cdc42 complex[80]. The catalytic histidine acts as a general base that, upon target binding, deprotonates the incoming hydroxyl side chain. The deprotonated hydroxyl (O^-) poised in line with the Pα-Oαβ bond of the ATP substrate, will perform a nucleophilic attack on the alpha-phosphate, resulting in the covalent transfer of AMP onto the target hydroxyl side chain and release of pyrophosphate (PPi). The phenylalanine of the active site loop is buried into the

active Fic core and crucial for the folding and conformation of the loop[86]. The glutamic acid (or aspartic acid) coordinates the metal ion (Mg^{2+}) binding, metal that is interacting with the α- and β- phosphate of the ATP substrate. The following residues, GNGR, form the anion binding pocket, also referred to as anion binding nest[87], and accommodates the α- and β-phosphates, via main chain interactions of the first turn of helix α5 and side chains or the arginine residue. The last residue of the active site motif located at the C-terminus of the catalytic loop forms hydrogen bonds with the ribose and locks the nucleotide. This is described further in details in section 3.1, *research article I* and section 3.2, *research article II*.

The Fic active site can be described as containing several major parts that appear to be generally conserved: the hydrophobic base-binding pocket, the anion-hole, the metal binding site and the ribose-coordinating subsite[88].

The sequence alignment (Figure 1.4.a) of Fic proteins shows a high conservation of the 12 residues of the Fic active site motif.

1.3.5. Target recognition

Knowledge on the target recognition of Fic proteins was gained with the first complex structure[80] of a Fic protein, IbpA, with its cognate target, Cdc42. In this complex, the arm domain of IbpA participates in the main interactions, with two major interfaces: the first one between IbpA and the switch I region of Cdc42 (~ 440 $Å^2$) and the second between IbpA and the switch II region of Cdc42 (~ 610 $Å^2$). In the switch I region, where the modifiable tyrosine of Cdc42 is located (Y32), Y32 and P34 from Cdc42 make hydrophobic interactions with L3668 and K3670 from IbpA (Figure 1.4.c). The leucine and lysine residues from IbpA form a clamp that locks the position of the modifiable tyrosine. Three additional main chain-main chain hydrogen bonds are formed between the FLAP (β-hairpin) of IbpA and the switch I region of Cdc42 (Figure 1.4.c). These main chain-main chain interactions have also been observed in the AvrB/RIN4 complex (Figure 1.5.b). It is therefore very unlikely that the environment of the active site raises target specificity, but more likely that additional domains serve the target specificity, i.e. the arm domain in the case of IbpA. Comparison of the structure of VopS from *Vibrio parahaemolyticus* with the structure of IbpA revealed a similar arm domain, possibly explaining the shared target between VopS and IbpA, i.e. the small GTPases family RhoA, Rac and Cdc42.

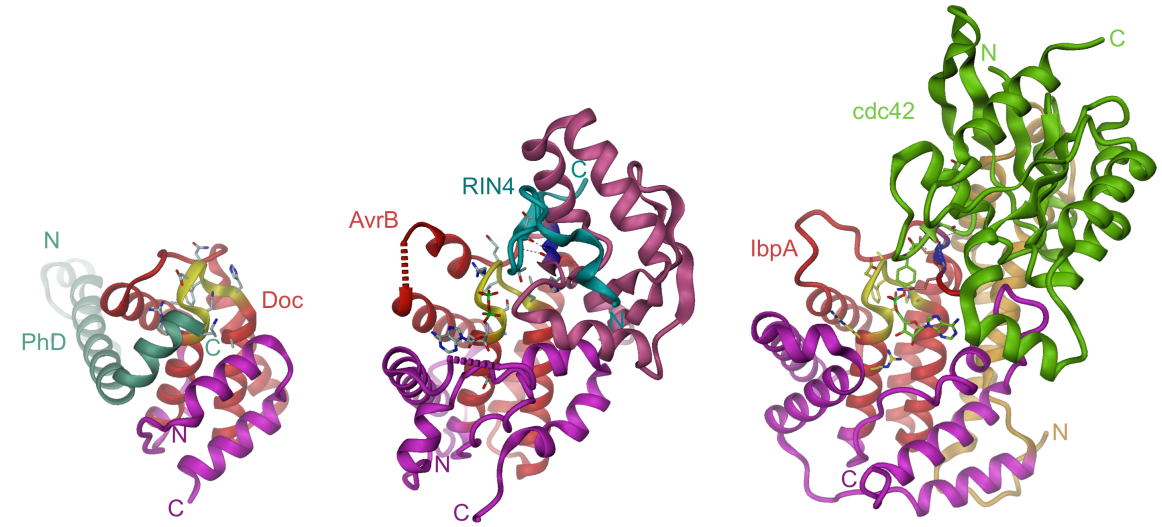

Figure 1.5. Comparison of the Fold of Doc, AvrB and the Fic protein IbpA. These 3 proteins fold in a similar manner, with the core (in red) common to the 3 proteins. *(a)* Doc (death on curing, standard Fic colors) from the Bacteriophage P1 in complex with its cognate antitoxin PhD (prevents host death, green). *(b)* AvrB from the plant pathogen *Pseudomonas syringae* in complex (standard Fic colors) with its target RIN4 (resistance to *Pseudomonas maculicula* protein 1 [RPM1]–interacting protein, blue)[89,90]. A threonine (Y166) that is known to be phosphorylated is positioned in the binding site of AvrB and the side product of the phosphorylation reaction, ADP, is shown (superimposed from PDB: 2NUN). *(c)* The Fic protein IbpA from *Histophilus somni* (standard Fic colors) in complex with its target Cdc42 (green), revealing the adenylylation of Y32 from the switch I region of Cdc42 (for details, see Figure 1.4.).

1.4. Fic-catalyzed post-translational modifications

In the 1990's, Fic proteins were believed to be regulator of the synthesis of p-aminobenzoate (folate) (see section 1.3.1.). Since 2009, we know that Fic proteins harbor a catalytic activity that is called adenylylation, the covalent transfer of an adenosine 5'-monophosphate on a target hydroxyl group. Nevertheless, Fic proteins are more versatile, and can also catalyze different post-translational modifications. Substrates of Fic proteins are diverse nucleoside-diphosphate derivatives such as ATP[67,75], UTP[51], NTP[50] or CDP-choline[52]. The modification performed by Fic proteins depends on slight variations in the active site, i.e. replacement of some crucial residue involved in substrate binding that will therefore switch the substrate specificity.

1.4.1. Adenylylation

Adenylylation is performed by the vast majority of Fic proteins, according to the conserved active site motif. This post-translational modification has already been introduced in section 1.1.4.4. (Figure 1.1.d and Figure 1.4.c). Many bacterial and eukaryotic effector proteins perform adenylylation. VopS from *Vibrio parahaemolyticus*[66], IbpA from *Histophilus somni*[75,91], NmFic from *Neisseria meningitidis*[80], HpFic from *Helicobacter pylori*[80], BepA from *Bartonella henselae*[83], SoFic from *Shewanella oneidensis*[77] are FIC domain proteins of which the adenylylation activity has been demonstrated *in vitro*. The human Fic protein Hype (hungtingtin yeast-interaction protein E, also called FICD) [75,91] and its ortholog in *Drosophila* which has been characterized in more detail [79,92] are also adenylyl-transferases. The HxFx[D/E]GNGRxxR active site motif is required for Fic-mediated adenylylation (see section 3.1., *research article I*).

The covalent transfer of an AMP moiety onto target hydroxyl acceptor groups usually results in inhibition of downstream signaling in host cells. The transfer of the bulky AMP group on Rho GTPase interferes with downstream effector binding[67,69,93].

1.4.2. Nucleotidylylation

Interestingly, BepA from *Bartonella henselae* can use ATP, GTP or CTP without any distinction[83], as shown by *in vitro* radioactive assays using these different nucleotides with the α-phosphate radioactively labeled. VopS also displays equal preferences for ATP and GTP and can therefore also serve as a guanylyl-transferase[91], whereas the MtFic protein from *Mycobacterium tuberculosis* can utilize all types of nucleotides (ATP, GTP, CTP or UTP). All substrates bind to the Fic active site with similar binding free energies ranging from – 6.0 to – 6.9 kcal/mol, with a slight preference for ATP. Because of the relative abundance of ATP (~ 10 mM) in prokaryotic cell (*E. coli*) over UTP, GTP and CTP (~ 8 mM, 5 mM and 3 mM, respectively)[94], the natural substrate of MtFic may be ATP and result in an adenylylation activity of this Fic protein. The relevance of nucleotidylylation (or NMPylation), i.e. the non-specific usage of any nucleotide, remains to be investigated[50].

1.4.3. Uridylylation

In contrast, uridylylation or UMPylation, the covalent transfer of an UMP moiety onto target proteins, uses the specific substrate UTP. AvrAC, a type III effector protein from the plant pathogen *Xanthomonas campestris*, enhances virulence by specifically targeting two host kinases of the plant model *Arabidopis thaliana*[51]. These two kinases, BIK1 and RIPK, are key mediators of the plant immune signaling. Feng *et al.* demonstrated that the FIC domain containing protein AvrAC was not able to use ATP as substrate. Mass spectrometry analysis revealed that AvrAC is auto-modified with several components of 306 Da, corresponding to the addition of uridine-5'-monophosphate, which was further confirmed by *in vitro* assays using radioactively labeled α-^{32}P-UTP. The uridylylation of BIK1 or RIPK on conserved Ser and Thr (Ser236 and Thr237 of BIK1) by the potent AvrAC enzyme occurs on critical phosphorylation sites of these kinases. These residues are part of the activation loop of the kinases and uridylylated residues are resistant to phosphatase activity. uridylylation acts on these kinases as a protection of the phosphorylation sites, preventing the phosphorylation of BIK1 and RIPK that is required for subsequent signal transduction. The uridylylation of the two kinases BIK1 and RIPK by AvrAC from *Xanthomonas* has a similar effect as the acetylation of the activation loop of human MAP kinases by YopJ from *Yersinia*, though with a different and bulkier group (uridylyl *vs* acetyl, respectively) covalently attached to the hydroxyl acceptor group of the host kinase (see section 1.1.4.2).

1.4.4. Phosphocholination

AnkX, a type IV effector protein from the facultative intracellular bacterium *Legionella pneumophila*, prevents microtubule-dependent vesicular transport in the host cell[95]. AnkX catalyzes the phosphocholination, i.e. the transfer of a phosphocholine group from a cytidine-diphosphate-choline (CDP-choline) substrate onto a target protein, the small GTPase Rab1 or Rab35[52]. The activity of the FIC domain of this large multidomain protein has been probed by a mutation of the catalytic histidine of this degenerated HPFxDANGRxxV Fic motif. The adaptability of the Fic motif allowed the switch of substrate between ATP and CDP-choline. AnkX modifies Rab1 and Rab35 during infection, which modulates membrane transport through the endocytic and exocytic pathways of the host cell.

The substrate, CDP-choline, shares a nucleoside diphosphate group with all other substrates known to bind Fic proteins. A thorough structural analysis[96] of Fic-mediated

phosphocholination revealed the structure of AnkX in the different substrate (CDP-choline, PDB: 4BET) and product (CMP/choline, PDB: 4BES or CMP, PDB: 4BER) bound states. In AnkX, the Fic motif has the same conformation as in adenylylating Fic proteins (VopS or IbpA), with the catalytic histidine playing the same crucial role[52,96]. The crystal structure of the catalytically inactive mutant $AnkX_{H/A}$ in complex with CDP-choline reveals that the substrate binds in an inverted manner when compared to the AMP moiety of ATP. Additionally, a unique feature of AnkX is the cytidine binding pocket, located at the other end of the substrate.

Furthermore, comparison of the structure of the phosphocholinating enzyme AnkX with the adenylylating enzyme IbpA in complex with Cdc42 suggests a similar mechanism of phosphoryl transfer that for the adenylylating Fic enzymes. The β-phosphate of CDP-choline superimposes with the α-phosphate of the AMP group bound to Y32 of Cdc42 in the IbpA/Ccd42 complex[80]. Furthermore, the structure reveals that the scissile bond in CDP-choline is the Pβ-Oαβ compared to the Pα-Oαβ in adenylylating enzymes, which is consistent with the transfer of phosphocholine and release of cytidine-monophosphate. Evolutionary, a main advantage of the head-to-tail binding of CDP-choline with respect to ATP is that both phosphocholination and adenylylation reactions can be achieved using the same catalytic residues and therefore reaction mechanisms.

1.4.5. Phosphorylation

Structurally related to Fic proteins, Doc has recently been shown to be a new family of kinases[97,98]. Doc, from the toxin-antitoxin system Doc/PhD (death-on curing / prevent host death), is a potent inhibitor of bacterial translation that was thought to sterically obstructs the A site of ribosome in a non-catalytic manner, but is here refuted. It has been recently shown that Doc phosphorylates the elongation factor EF-Tu on a conserved threonine residue (Thr382), making it unable to bind aa-tRNAs and therefore inhibiting translation. *In vitro* experiments using α-^{32}P-ATP or γ-^{32}P-ATP revealed that Doc is unable to adenylylate EF-Tu and specifically phosphorylates the target protein. Doc preferentially binds EF-Tu, another GTPase substrate of the Fic/Doc superfamily, in its GDP-bound form, with a 30-fold higher affinity than the GTP analog bound form. The affinity for the substrate AMPPNP or GMPPNP has been measured in the millimolar range when no target was present, and increased by 10^5 fold in presence of EF-Tu, suggesting that several residues of the target are involved in substrate binding, or that the target binding helps structuring the FLAP (β-hairpin)

and therefore increases the target binding. In solution structural analysis by SAXS (small angle X-ray scattering) and NMR (nuclear magnetic resonance) reveals the interface between Doc and EF-Tu and allows chemical shift mapping of the residues involved in ATP binding, respectively. Modeling of the ATP substrate based on the chemical shift upon binding predicts that ATP binds more towards the C-terminal part of the active site loop than the N-terminal, i.e. in an inverted mode compared to the adenylylation competent form.

Therefore, it is likely that the γ-phosphate of ATP in Doc adopts the position of the α-phosphate in the adenylylating form, resulting in a transfer of phosphate instead of AMP. The plasticity of the Fic active site is an intriguing evolutionary mechanism to generate new enzymatic activities. The HxFxDANKR motif of Doc's active site differs from the HxF[D/E]GNGR consensus motif for adenylylation. The mutation of the second glycine of the adenylylation competent motif to a lysine is crucial for the inversion of substrate binding mode. When superimposing Doc on the IbpA/adenylylated-Cdc42 complex, the lysine K37 from Doc sterically clashes with the ATP molecule in the adenylylation competent conformation. Moreover, the binding of PhD, the cognate antitoxin of Doc, would interfere with both substrate (ATP) binding and target (EF-Tu) binding.

Intriguingly, Doc can also dephosphorylate EF-Tu. Castro-Roa *et al.* postulated that the level of GDP/GTP and the conformation of EF-Tu in the GDP- or GTP-bound form participates in the regulation of Doc kinase or phosphatase activity. When Doc phosphorylates EF-Tu, the translation is blocked bringing the cells to dormancy. During bacterial stasis, the high level of GDP and baseline level of unphosphorylated EF-Tu may have restart translation and turn Doc into a phosphatase, but this tempting hypothesis needs to be validated.

Kinase activity has also been speculated for AvrB from *Pseudomonas syringae*, a protein structurally related to Fic/Doc family proteins. AvrB induces the phosphorylation of RIN4, a key regulator of the basal host defense responses in the plant model *Arabidopsis*[89,90]. Lee *et al.*[89] were not able to show any direct phosphorylation of neither RIN4 nor other nonspecific substrates by AvrB. Further structural analysis revealed that ADP binds to the active center of AvrB[90]. Interestingly, the substrate binding mode in AvrB is similar to the one described for Doc[97]. AvrB though lacks the catalytic histidine of the active site motif, but a histidine that is part of the FLAP (H217) may have evolved to compensate this mutation and thereafter act as catalytic histidine. A mutant of this histidine lacks catalytic activity and target binding[90]. It has been proposed that AvrB may act as a "protokinase" that lacks intrinsic phosphor-transfer

activity that may be enhanced by association with accessory proteins[90]. Thought RIN4 binds to AvrB and gets phosphorylated in an AvrB-dependent manner, there is no direct evidence of a kinase activity of AvrB.

In summary, the plasticity of the Fic/Doc active center allows the binding of several ligands or a single ligand in different conformation, e.g. ATP, yielding different catalytic activities of these enzymes bearing the same fold. It has been demonstrated that diphosphate-nucleoside can bind to the Fic active site in two different "inverted" conformations, either with the base towards the N-terminal end motif or towards the C-terminal end of the Fic, resulting in adenylylation, uridylylation or phosphocholination and phosphorylation, respectively. With the knowledge acquired to date, it can be deduced that Fic/Doc family proteins are phosphoryl transferases sharing diphosphate-nucleoside substrates. Noteworthy, Fic proteins also tend to preferentially target GTPases[88].

1.5. Regulation of Fic proteins

Fic proteins, because of their high cytotoxicity in eukaryotic cells or bacteriostatic effect in bacteria, need to be tightly regulated.

To date, apart from a few evidences about Fic protein regulation, most is rather speculative. Two mechanisms of regulation seem however possible, via an additional domain fused to the Fic protein or via the auto-modification of the Fic protein that has been constantly observed *in vitro*[51,79,80,83,99,100]. Moreover, the presence of an helix α' that is found permuted at the N-terminus or C-terminus of Fic proteins, already mentioned by Kinch *et al.*[79], plays a key role in the regulation of adenylylation competent Fic proteins and will be further described in section 3.1., *research article I* and section 3.2, *research article II*.

1.5.1. Domain organization of Fic proteins

IbpA, HypE, SoFic or AnkX are multi-domains Fic proteins, in contrast with NmFic or HpFic that are single domain proteins (Figure 1.6).

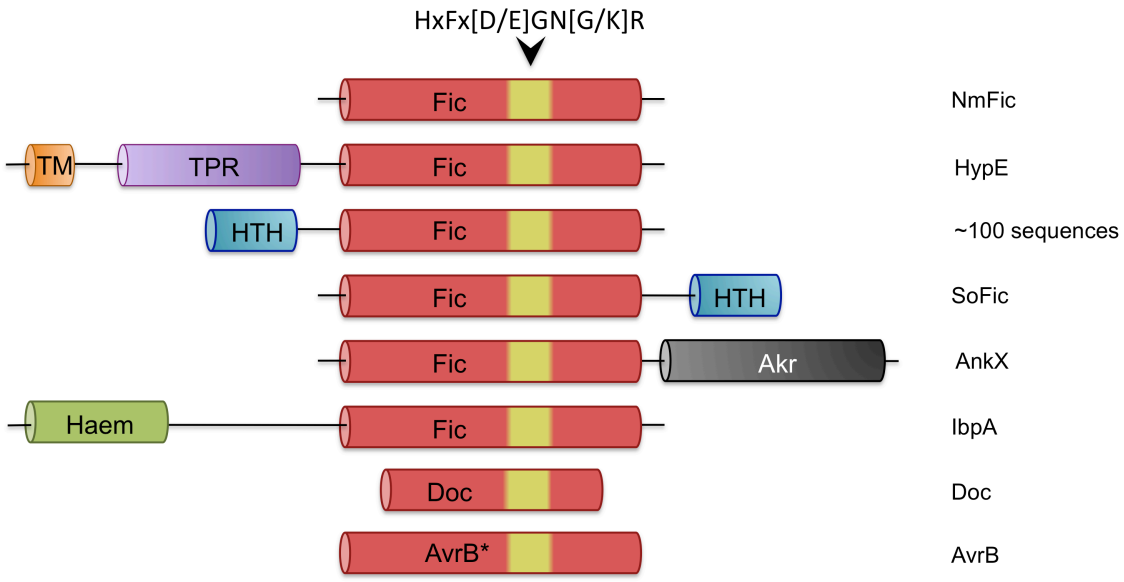

Figure 1.6. Domain organization of Fic, Doc and AvrB proteins. An example of each investigated protein is given next to the scheme of domain organization, except for HTH-Fic, where no protein was studied to date. The nomenclature is as follow: Fic: filamentation induced by cAMP, TM: transmembrane, TPR: tetratricopeptide repeat, HTH: helix-turn-helix DNA binding domain, Akr: ankyrin repeat, Haem: haemagglutination activity domain, Doc: death on curing, AvrB: avirulence protein B. Adopted from [79].

1.5.1.1. Multiple domain Fic proteins

IbpA from *Histophilus somni* is a large multidomain Fic protein. It consists of an N-terminal filtamentous haemagglutinin-like domain (FHA-like) followed by coiled coils and two consecutive Fic domains that have been shown to be functionally redundant, and finally a C-terminal cysteine protease domain homologous to YopT from *Yersinia*[75]. IbpA is not injected into the host cell, but secreted into the environment. The large FHA protein creates a fibrillar network around the bacterium. Following the attachment of *H. somni* to the host cell, it is speculated that portions of IbpA (notably the C-terminus containing the FIC domain) are pinocytosed by the host cell. The cytoplasm is then exposed to Fic proteins and the cytotoxicity of the latter.

The human HypE protein contains an N-terminal signal sequence and transmembrane domain, a central tetratricopeptide repeat (TPR) and a C-terminal Fic domain. The TPR domain may serve as a cellular targeting sequence. HypE also targets Rho family GTPases, probably unspecifically, but the physiological target and role of HypE are still under investigations (personal communication). Histone H3 has recently been identified as a

substrate for HypE[101] but the physiological relevance of the modification of histone H3 has not yet been described.

The structure of the Fic protein from *Shewanella oneidensis*, SoFic, has been solved by the JCSG joint center for structural genomics[77]. A helix-turn-helix (HTH) DNA binding domain is located at the C-terminal end of SoFic. Interestingly, SoFic forms a dimer in the crystal structure that is likely to be physiological and has been predicted as such by the Eppic prediction server[102]. Additionally, the distance between the winged helix-turn-helix domains within the dimer may be suitable for double-stranded DNA binding. This HTH may thus regulate the expression of the Fic protein. Moreover, other fusions of HTH domains and Fic proteins can be found by sequence analysis, with the helix-turn-helix domain either at the N-terminus or at the C-terminus. According to *Kinch et al.*[79], the HTH domain fused to Fic proteins is reminiscent to the N-terminal HTH domain from PhD that regulates the expression of the Doc/PhD toxin-antitoxin system[103].

The only known protein that catalyzes phosphocholination, AnkX, contains an N-terminal Fic domain and up to twelve predicted ankyrin repeats at the C-terminus. Ankyrin repeats consist of 30-34 amino acids residues that have been characterized exclusively in mediating protein-protein interactions. In eukaryotes, ankyrin repeats is the second most abundant class of interaction mediating proteins, after immunoglobulins[104]. In the case of bacterial effectors, ankyrin repeats may play a similar role, in targeting host factors and contributing to the localization of Ank proteins. Interestingly, the loops contained in the helix-turn-helix of AnkX are longer that in eukaryotic repeats. To date, the function of most Ank proteins remains unknown. In the phosphocholine-transferase AnkX, the ankyrin repeats has a role in intramolecular interaction and constrains the Fic domain of AnkX, which is observed for the first time in the context of ankyrin repeats. Yet, the exact role of these repeats is unclear and it is conceivable that the extended loops of the helix-turn-helix of the ankyrin modules of AnkX participate in interactions with the target Rab1.

VopS doesn't contain any additional domain except the N-terminal arm domain that has been reported to be involved in target specificity.

1.5.1.2. Single domain Fic proteins

NmFic from *Neisseria meningitidis* or HpFic from *Helicobacter pylori* are single domain Fic proteins that need to be self-regulated. Yet, no evidences for such mechanism are

available and it remains to be investigated. This will be discussed in the context of section 3.5., *research article V*.

1.5.2. Auto-modification of Fic proteins

Auto-phosphorylation of kinases is a ubiquitous well-understood mechanism of regulation of kinases[105-108]. Are there any parallels with the auto-modification of Fic proteins?

The auto-modification has been observed extensively, for all Fic proteins investigated so far (Figure 1.7). Nevertheless, the physiological role of this auto-modification remains elusive. At first, it has been postulated that the auto-adenylylated Fic proteins observed in radioactive assays represent a transient histidine modified intermediate. This would be in favor of a ping-pong mechanism of AMP transfer catalyzed by Fic proteins, where the Fic catalytic histidine is auto-adenylylated in a first step and the AMP moiety is then transferred to the target protein in a second step. Such a mechanism would explain why the histidine of the Fic motif is crucial for activity, but this hypothesis has been refuted by kinetic analysis of VopS mediated adenylylation of Cdc42[79], showing that adenylylation is a direct transfer mechanism. In such a mechanism, the histidine serves as a general base during catalysis, which is consistent with the pH profile of VopS activity, demonstrating that VopS is less active at low pH[82].

Similarly, auto-phosphocholination of AnkX has also been demonstrated. Phosphocholination was only observed if a larger excess of CDP-choline was used in the reaction sample. *Goody et al.*[100] suggest a phosphocholinated intermediate that is hydrolytically unstable and does not accumulate, in-line with a ping-pong mechanism. This is in contrast with the direct AMP transfer demonstrated for the adenylylator VopS. But this mechanistic difference between these two enzymes is quite surprising, even though the transfer occurs on the β-phosphate of CDP-choline for AnkX and the α-phosphate of ATP for VopS. Again, this intermediate transfer on the catalytic Fic motif histidine has been refuted by the thorough crystallographic work by Campanacci *et al.*[96], demonstrating that the β-phosphate of the CDP-choline substrate is superimposable with the position of the α-phosphate of the AMP group in the IbpA-Cdc42 complex structure. This strongly suggests a similar mechanism for Fic proteins catalyzing phosphocholination and adenylylation.

The auto-adenylylation or auto-phosphocholination of Fic proteins are therefore not resulting from a transient intermediate formation (His-AMP), but a stable modification of serine, threonine or tyrosine residues from the Fic protein itself. Recently, it has been

proposed that auto-modification is a side reaction that uses the same mechanism as target modification, but targeting residues located in poorly folded regions of the Fic protein located outside of the catalytic region[96]. Thus, the relevance of auto-modification of Fic protein is still under debate and will be discussed in the context of section 3.5., *research article V*.

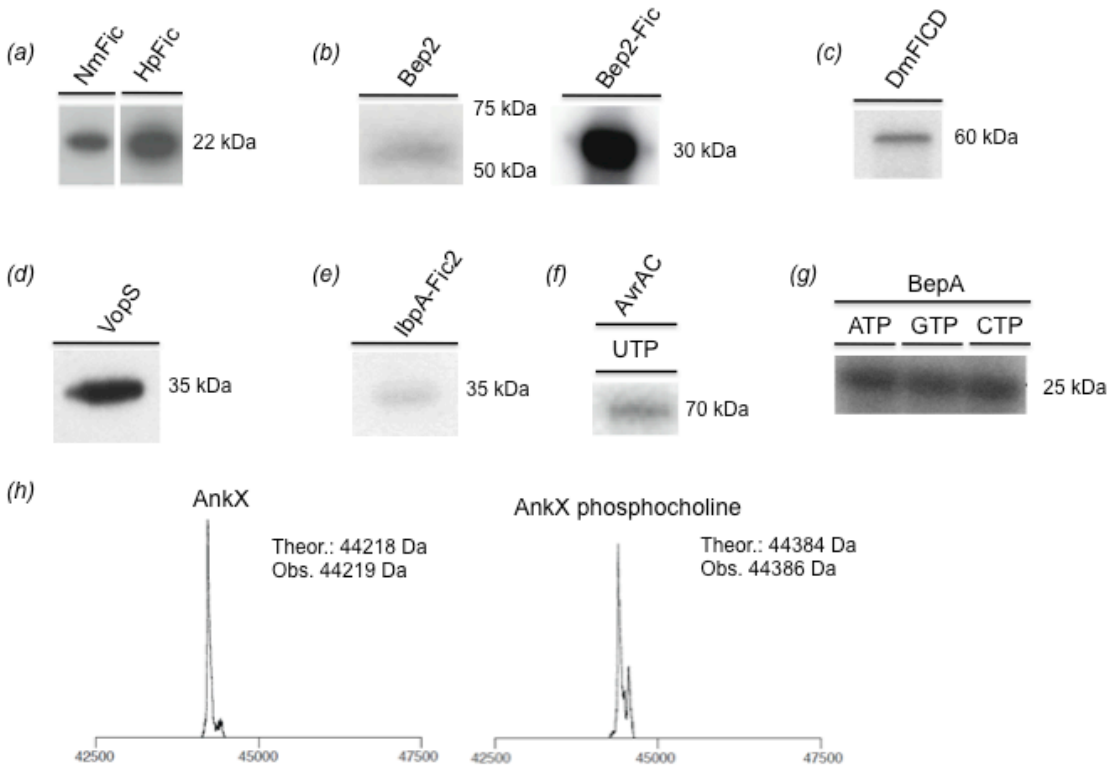

Figure 1.7. Auto-modification of Fic proteins. The auto-modification is monitored by *in vitro* labeling assay using α-^{32}P labeled tri-nucleotide substrate and revealed by autoradiography *(a-g)* or by mass spectrometry analysis *(h)*. Auto-adenylylation of *(a)* NmFic from *Neisseria meningitidis* and HpFic from *Helicobacter pylori*, *(b)* Bep2 from *Bartonella rochalimae* expressed in cell lysate or purified Bep2-Fic, *(c)* DmFICD from *Drosophila melanogaster*, *(d)* VopS from *Vibrio parahaemolyticus*, *(e)* IbpA-Fic2 from *Histophilus somni*. *(f)* Auto-uridylylation of AvrAC from *Xanthomonas campestris*. *(g)* Auto-adenylylation, auto-guanylylation or auto-citydylation of BepA from *Bartonella henselae*. *(h)* Auto-phosphocholination of AnkX from *Legionella pneumophilae* revealed by a mass shift (+ 167 Da) upon incubation with the substrate CDP-choline. Adopted from [51,79,80,83,99,100].

1.6. Targets of Fic proteins

The understanding of the catalytic activity of Fic protein is *per se* of remarkable interest for basic research, but the effect of Fic-mediated activity is *via* host cell target modification. Interestingly, the variety of Fic-mediated post-translational modifications seems to results in the modification of a narrow range of protein folds, with a preference for GTPases.

1.6.1. Eukaryotic targets

1.6.1.1. Adenylylated targets

VopS and IbpA of the pathogens *Vibrio parahaemolyticus* and *Histophilus somni*, respectively, target the Rho family GTPases RhoA, Rac and Cdc42[66,75]. This modification leads to a cell rounding phenotype in the eukaryotic host cell, via collapse of the actin cytoskeleton. IbpA bound Cdc42 appears to mimic the GDP dissociation inhibitor (GDI)-bound state of Rho GTPases. Both switch I and switch II regions of Cdc42 adopt this conformation. IbpA, by exerting a GDI-mimicry activity, can modify Rho GTPases in the cell independent of their nucleotide bound states. The arm domain of IbpA and VopS, only observed so far in these Fic-proteins, has a crucial role in the affinity for all Rho family GTPases.

In contrast to the rather low target specificity of VopS and IbpA, the effector protein Bep1 from *Bartonella rochalimae* specifically adenylylates Rac1 (A. Harms, *master thesis* 2010)[109]. Bep1 doesn't contain any arm domain but a so-called Bep-element (A. Harms, *master thesis* 2010)[109], a β-hairpin located directly N-terminally to the FLAP, only found in several species of *Bartonella* that evolved in parallel and therefore assigned to lineage 3 and lineage 4[110]. This Bep-element may confer target specificity to Rac1 similarly to the arm domain of IbpA and VopS for Rho GTPases RhoA, Rac and Cdc42.

Our group recently developed a new method using isotope-labeled substrate (ATP) combined with mass spectrometry based analysis to identify new adenylylated targets[99]. When target hunting using this method, the adenylylator Bep2 from *Bartonella rochalimae* was incubated with crude cell lysates and ATP isotopes. This resulted in the identification of the filamenting protein vimentin. This new target was confirmed by further *in vitro* assays. Interestingly, Bep2 targets a new class of protein of the host cell cytoskeleton. Vimentin doesn't show any structural homology to GTPase but is directly regulated by small GTPases[111].

Additionally to vimentin, Bep2 also targets β-tubulin from the αβ-tubulin heterodimeric complexes[112]. These complexes can polymerase to form microtubules, crucial components of the cytoskeleton, maintaining the structure of the cell but also involved in intracellular transport[113]. An αβ-tubulin-interacting factor called TOG (tumor overexpressed gene) is involved in fast microtubule growth[114]. The adenylylation site of β-tubulin has been mapped by mass spectrometry analysis to residues Y106 or T107 of β-tubulin. These residues are

involved in interactions with an arginine from TOG[115]. Interestingly, the modeling of an AMP moiety on the tyrosine 106 from β-tubulin doesn't result in any steric clashes, but rather in conceivable interactions between the α-phosphate, the N6 of the adenine ring and the hydroxyl groups from the ribose of the transferred AMP group with arginine 116 and threonine 118 of TOG and glutamate 410 of β-tubulin, respectively. The adenylylation of tubulin by Bep2 may results in a tighter binding of TOG on αβ-tubulin, resulting in a sequestration of TOG on αβ-tubulin dimers and altering of microtubules formation (K. Pieles, *PhD thesis*, 2013)[112]. This hypothesis in currently under investigation by Kathrin Pieles and Simon Marlaire in the group of Christoph Dehio.

The *Bartonella henselae* effector BepA also adenylylates a host target protein that remains to be identified[83].

1.6.1.2. Phosphocholinated targets

The effector AnkX from *Legionella pneumophila* transfers a phosphocholine group on a conserved serine side chain from Rab1 (Ser79 in Rab1A or Ser76 in Rab1B) and Rab35 GTPases[52]. This corresponds to the switch II region of these GTPases. Interestingly, this residue in located directly next to the Tyr80 of Rab1A, a residue adenylylated by the *Legionella* effector DrrA, an adenylylator that doesn't contain any FIC domain. Rab1 and Rab35 phosphocholination results in interferences with binding of these two GTPases with guanine nucleotide exchange factors (GEFs), which is required for the function of the enzyme. This shows that *Legionella* has evolved two structurally different proteins catalyzing two distinct post-translational modifications that modulate the function of host vesicle transport in a similar manner.

1.6.2. Bacterial targets

1.6.2.1. Phosphorylated targets

The Doc toxin from the bacteriophage P1 specifically phosphorylates the elongation factor EF-Tu at the C-terminal end, not at the switch I or switch II region of GTPases as seen for other Fic domain proteins[97,98]. The phosphorylation of EF-Tu results in the blockage of aminoacyl tRNA binding, thus inhibiting translation.

1.6.2.2. Adenylylated targets

Adenylylation of bacterial targets has been recently unraveled by our research groups using mass spectrometry analysis coupled to educated guess, by Alexander Harms *et al.,* and is developed further in section 3.3., *research article III*. The adenylylation of bacterial topoisomerases by VbhT, the Fic protein from *Bartonella schoenbuchensis*, the distantly related YeFicT from *Yersinia enterocolitica* or PaFicT from *Pseudomonas aeruginosa*, results in bacteriostasis of our model organism *E. coli*. These three Fic proteins are Class I Fic proteins (as defined by Engel, Goepfert et al., section 3.1., *research article I*) consisting of a FicT protein (toxin) co-expressed with a small FicA protein (antitoxin), of a classical Type II TA system. Additionally, NmFic from the Class III Fic protein (as defined by Engel, Goepfert et al., section 3.1., *research article I*) from *Neisseria meningitidis* also targets bacterial topoisomerases. The activity of NmFic will be discussed in section 3.5., *research article V*.

1.7. Bacterial type IIA topoisomerases

Bacterial topoisomerases are a new class of Fic protein targets and therefore a central focus of my PhD thesis. DNA topoisomerases control the topology of DNA molecules and were first described by James Wang in 1971[116].

1.7.1. General introduction

Many cellular processes affect the structure of chromosomal DNA. During transcription, the structure of double stranded DNA gets positively supercoiled by polymerases and helicases[117]. During replication or recombination events, chromosomal knots or catenates are generated[118]. These two examples result in so-called topological problems, that needs to be resolved for cell survival. Topoisomerases are the crucial players in this context, and able to alter the DNA topology (Figure 1.8.).

These fascinating molecular machines manipulate DNA molecules by a mechanism of strand passage. In short, a double-stranded DNA molecule is cleaved, generating a DNA break, a gap is opened in the cleaved segment and a DNA strand is passed through the break. Nature has evolved two major types of topoisomerase, type I creates a single-stranded DNA break and type II creates a double-stranded DNA break[119].

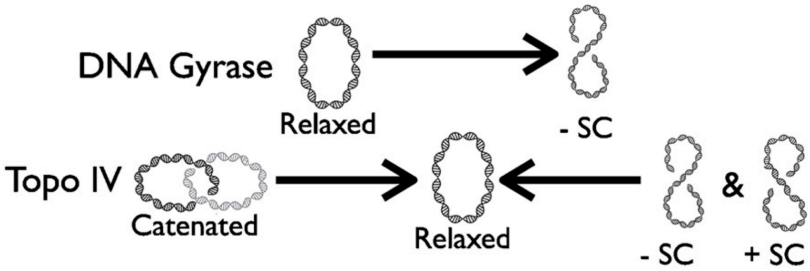

Figure 1.8. Specific activity of DNA gyrase and TopoIV. DNA gyrase introduces negative supercoils into covalently closed dsDNA molecules (top). TopoIV decatenates DNA molecules and also relaxes negatively or positively supercoiled DNA molecules (bottom). Taken from [120].

Topoisomerase II are large enzymes of around 400 kDa formed by heterotetramers in bacteria and dimers in eukaryotes (Figure 1.9.a-c.). The model DNA gyrase from *Escherichia coli*, formed by $GyrA_2GyrB_2$, has been extensively studied. The different structural information's obtained for the DNA gyrase show a three-gates structure that obeys to a two-gates mechanism.

GyrB contains several domains: an N-terminal GHKL ATPase domain, a central transducer domain and a C-terminal TOPRIM domain, of which each has a specific function. The N-terminal domain catalyzes ATP hydrolysis upon ATP-binding mediated dimerization, the central domain transfers the signal of ATP hydrolysis and the C-terminal domain is involved in DNA-binding. GyrA contains an N-terminal winged helix domain that contains the catalytic tyrosine, followed by a so-called tower or shoulder domain, a coiled-coil and a C-terminal DNA binding domain (CTD) (Figures 1.9.a and 1.9.b.).

1.7.2. Distinct roles/functions of DNA gyrase and TopoIV

Two paralogues type IIA topoisomerase are encoded in the bacterial genome, DNA gyrase and topo IV (Figure 1.8.). These two topoisomerases are not functionally redundant and have distinct functions. Supercoiling of DNA is crucial for cell viability and compacting the DNA. Most DNA molecules occur as negatively supercoiled. Negative supercoiling prepares DNA for processing that requires the separation of DNA strands such as replication or transcription, by providing energy for DNA-protein interactions. Positive DNA supercoiling is as efficient for condensation of DNA material but it makes the strand separation more difficult[121]. DNA gyrase introduces negative supercoils into covalently closed dsDNA molecules, which results in a maintained chromosome during transcription.

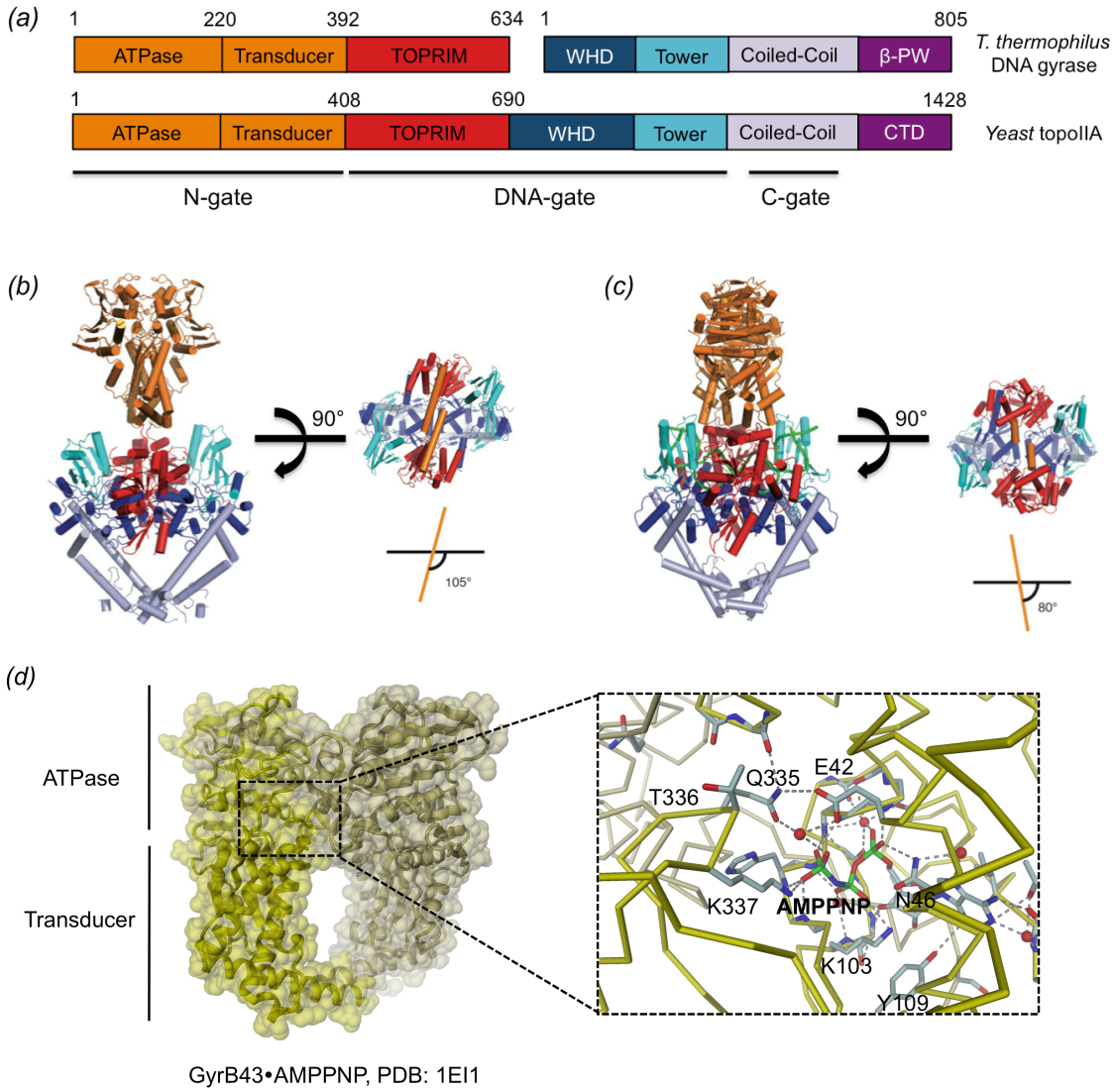

Figure 1.9. Domain architecture and structure of type IIA topoisomerases. *(a)* Comparison of the domain organization of bacterial DNA gyrase and eukaryotic topoisomerases II. *(b)* Structure of DNA gyrase from *Thermus thermophilus* (same color code as in *(a)*) compared with *(c)* the structure of yeast topoIIA bound to a 30 base-pair dsDNA molecule. *(d)* Crystal structure of the 43-kDa N-terminal fragment of GyrB (GyrB43) in complex with AMPPNP shown as ribbon and semi-transparent surface. Inset of the ATP binding site with crucial residues depicted. Adopted from [122,123,124].

Distinctly, topo IV removes catenants and knots[125,126], separating daughter chromosomes after replication[127].

These two enzymes are structurally related and both form heterotetramer: $GyrA_2GyrB_2$ for DNA gyrase and $ParC_2ParE_2$ for topo IV.

1.7.3. Structure of type II DNA topoisomerases

Bacterial topoisomerases form A_2B_2 heterotetramer ($GyrA_2GyrB_2$). Structural information for each domain is available from high-resolution crystallographic structures.

Wigley *et al.*[123] obtained the first structural information of DNA gyrase, by crystallizing the 43-kDa N-terminal fragment of GyrB (GyrB43). This revealed a tight dimer containing two domains, an N-terminal GHKL-type ATPase domain, and an additional domain, termed transducer domain, that delimits a hole (N-gate chamber) of about 20 Å diameter[123] (Figure 1.9.d).

Several residues from different domains form the ATP binding site of GyrB. The GHKL-ATPase domain of GyrB constitutes the scaffold of the binding site, together with the N-terminal arm domain of GyrB and two residues from the transducer domain. The phosphates groups of the ATP analog ligand are bound to the amine groups of a glycine-rich loop, found at the N-terminus of an α-helix. The N-terminal arm interacts with the adenine ring, thus the two protomers of the dimer participate in ATP binding. The two residues, glutamine 335 and lysine 337 from the transducer domain protrude into the ATPase domain binding site and interact directly or *via* a water-molecule with the γ-phosphate of the ligand. This may provide a mechanism of signaling of the ATP hydrolysis event[123].

GyrA, on the other end, is specialized in DNA binding with its C-terminal β-pinwheel DNA binding domain. GyrA dimerization forms the C-gate.

Recently, knowledge on the entire structural organization of topoisomerases has emerged, for the yeast (*Saccharomyces cerevisiae*) topoIIA (yTopoII) obtained by X-ray crystallography[128] at low resolution (4.4 Å) and for the bacterial DNA gyrase of *Thermus thermophilus* by cryo-electron microscopy[122], revealing the architecture of this macromolecule (Figure 1.9.b-c.). Interestingly, the comparison of the domain organization in these both structures, from yeast or the bacteria *T. thermophilus* reveals the same domain architecture. This revealed the orientation of the ATPase and transducer domains respectively to the DNA-gate. The structure of GyrB43 obtained in complex with AMPPNP by Wigley *et al.* already revealed a crossover of the C-terminal helices. The electron density shows that the ATPase and transducer domains are located at the top of the DNA gate and that the following TOPRIM domain in the sequence of either yTopoII or GyrB is swapped. The ATPase region of one protomer within the dimer contacts the TOPRIM domain of its partner, confirming the role of the C-terminal crossover helix of the transducer domain in closing the N-gate chamber.

The cryo-electron microscopy map obtained for *T. thermophilus* DNA gyrase reveals the position of the C-terminal β-pinwheels DNA binding domain. This demonstrates how DNA is asymmetrically wrapped around these domains. The data show how the ATPase domain and the β-pinwheel domains cooperate through their spatial proximity to introduce negative supercoils (Figure 1.9.b-c.).

1.7.4. DNA gyrase mechanism

Type II topoisomerases operate via a so-called two-gates mechanism, even though the structures of DNA gyrase revealed three gates. The N-gate is found at the interface formed by $GyrB_2$, the DNA-gate at the center of the enzyme, formed by $GyrA_2GyrB_2$, and the C-gate is formed by a $GyrA_2$ dimer. At the beginning of the catalytic cycle of the topoisomerase, a double-stranded segment of DNA, called the G-segment (gate segment) binds to the DNA gate, in the cleavage-ligation region[129], also termed A'-region of the enzyme[130]. This is the segment that will be cleaved by conserved tyrosine of the winged helix domain of GyrA, resulting in a covalent bond between the G-segment and GyrA. A second segment of DNA, called the T-segment (transport segment) then binds to the enzyme[131,132]. This segment gets trapped in the N-gate, after closing of this gate by dimerization of the N-terminal ATPase[123,124] domains of GyrB upon ATP binding[129,133]. Hydrolysis of a first ATP molecule triggers conformational changes coupled to the opening of the DNA-gate. This opening is dependent on the flexion of the coiled coil arms or GyrA[134], resulting in a separation of the winged helix domains of GyrA, located at the DNA-gate interface[135]. The G-segment is passed from the N-gate *via* the cleaved G-segment in the DNA-gate to the C-gate[136,137]. The G-segment is then resealed and the DNA-gate closed. The opening of the C-gate leads to the release of the T-segment. Hydrolysis of the second ATP bound to the GyrB dimer and products release reset the enzyme, now ready for another cycle of strand passage (Figure 1.10).

This complex mechanism confers unidirectionallity of strand passage from the N-gate to the C-gate, via the cleaved double stranded DNA segment bound to the DNA-gate. The control of this reaction is believed to be via the ATP hydrolysis mechanism and the timed and coordinated opening and closing of the three gates.

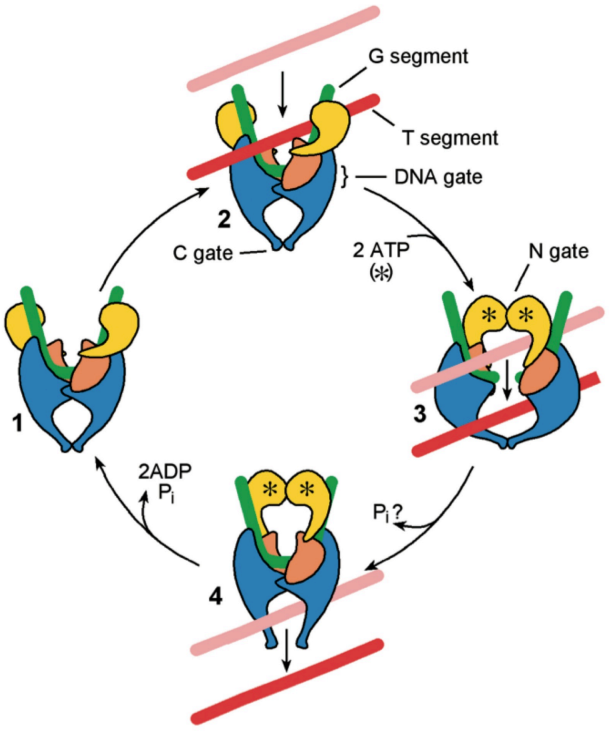

Figure 1.10. Mechanism of type IIA topoisomerases. GyrB is depicted in yellow (ATPase and transducer domains) and orange (Toprim domain), GyrA is depicted in blue. First, the G-segment binds to the DNA-gate (step 1). Upon ATP binding, the T-segment gets trapped in the N-gate (step 2). Upon cleavage of the G-segment and concomitant ATP hydrolysis, the T-segment gets pushed through the G-segment into the C-gate (step 3). Upon Pi and ADP release, the N-gate reopens which reset the enzyme (step 4). Taken from [138].

Yet, the exact role and consequences of ATP hydrolysis are still under debate[128,139] and will be further discussed in section 3.4., *research article IV*, providing new high resolution structural evidences of domain motions upon ATP hydrolysis in *E. coli* GyrB.

1.7.5. The proposed role of ATP binding and hydrolysis in DNA gyrase

ATP hydrolysis is required for the introduction of negative supercoils into relaxed DNA molecules of from positively supercoiled DNA to negatively supercoiled[138,140-145]. Structural information has been gathered on different nucleotide states bound to the ATPase domain of topoisomerases. Conformational changes were observed in some cases. The structure of the human topoII (type IIA topoisomerase) has been determined in complex with AMPPNP (a non hydrolysable ATP analog) or with ADP[146], and the archaeal TopoVI (type IIB topoisomerase) with many nucleotide states from AMPPNP, ADP·Pi to ADP[147,148].

ATP binding, first, is required for dimerization of the N-gate, which can be structurally explained by the presence of an N-terminal “arm” or “strap” domain. This arm, a 15 amino

acids stretch, extends from the N-terminus of one protomer and embraces its partner. Interestingly, mutation of crucial residues of this arm, i.e. Tyr5 that directly interacts with the ATP bound to the active site, abolishes the dimerization. Also, a deletion of this 15 amino acids strap abolishes the propensity to dimerize[124].

Secondly, it is undisputed that ATP hydrolysis leads to conformational changes. Baird *et al.*[144], showed that the hydrolysis of one ATP molecule is sufficient for DNA gyrase activity. For that purpose, they observed in a mutant (E66Q) of yeast topoII the binding of ATP but slow hydrolysis event, resulting in a twenty-fold decrease of decatenation. It shows that ATP hydrolysis is required to accelerate strand passage. Generating a heterodimer of wild-type/E66Q-mutant yeast topoII only reduces the decatenation by a two-fold factor, suggesting that one hydrolysis event is sufficient to stimulate strand passage.

Conclusions concerning the direct effect of ATP hydrolysis, i.e. production of ADP·Pi, and/or Pi release were drawn from the crystal structures of human topoII in complex with AMPPNP or ADP and from the archael topoVI structures along the ATPase cycle.

The structure of N-terminal domain of the human topoII[146] (hTopoII) reveals a similar dimer as observed for the bacterial GyrB fragment[123]. The comparison of the hTopoII in complex with AMPPNP (PDB: 1ZXM) and in complex with ADP (PDB: 1ZXN) reveals rotation of the transducer domain relative to the ATPase domain, resulting in a larger N-gate hole upon hydrolysis. The authors attributed this domain reorganization to the hydrolysis and subsequent phosphate release event. Noteworthy, a close inspection of the nucleotide binding site reveals a sulfate ion next to the ADP product and may therefore mimic an ADP·Pi state. The quaternary structure rearrangement involves a conformational change of the QTK loop, part of the transducer domains that protrudes into the ATP binding site and mediates contacts with the nucleotide. This loop and particularly its conserved lysine residue has been described as a sensor and relay residue for the nucleotide bound status of the enzyme.

For the archaeal topoVI structures, the situation is quite different. A conformational change is observed between the monomeric nucleotide-free (apo) or ADP-bound structure and the other nucleotide bound states (AMPPNP, ADP·AlF_4, ADP·Pi or also ADP in the dimer state)[147,148]. Here, the ADP structure can adopt both conformation, i.e. the monomer or dimer form. Interestingly, the conformation of the equivalent residues of the QTK loop of human topoII, called switch loop, is changed dramatically depending on the nucleotide state. This results in a domain reorientation, with the transducer domain rotating respectively to the

ATPase domain by around 11°. It is here postulated that this domain rearrangement serves to communicate the status of the ATPase site to the cleavage-ligation region of the enzyme, the DNA-gate, resulting in G-segment cleavage and opening. Yet, the molecular mechanisms of Pi release are not fully understood[139]. Nowadays, it seems to be believed in the topoisomerase field that ATP hydrolysis serves to guide DNA towards negative supercoiling[122], therefore providing unidirectionallity in the strand passage mechanism.

In the context of bacterial DNA gyrase, the structures of the 43-kDa N-terminal fragment (GyrB43) of *E. coli* in complex with nucleotides along the ATP hydrolysis pathway will be discussed in section 3.4., *research article IV*.

1.7.6. DNA gyrase is a toxin target

The well-characterized CcdB toxin from the CcdB/CcdA toxin-antitoxin (TA) system targets DNA topoisomerase[149]. CcdB (control of cell death protein B) is encoded on the F plasmid from *E. coli* that is remarkably maintained in bacterial cell lines, even with its very low copy number. The role of the TA systems on the F plasmid is the maintenance of this plasmid in daughter cells during cell division by a post-segregation killing mechanism. CcdA (antitoxin) and CcdB (toxin) are two small proteins encoded in an operon and forms a very tight complex. Post-segregationnal killing mechanisms are based on the different stability of the expressed toxin and antitoxin proteins. It has been shown that the Lon protease is involved in the degradation of the CcdA antitoxin, which results in an active CcdB toxin. This toxin causes activation of the SOS system and ultimately leads to bacterial cell death, via targeting of the subunit A of DNA gyrase (GyrA). A CcdB dimer binds to a GyrA dimer with a dissociation constant (Kd) of around 0.4 nM[150], therefore inhibiting the DNA gyrase. The mechanism of GyrA poisoning by CcdB has been elucidated using structural informations of a $GyrA_2$/$CcdB_2$ complex (PDB: 1X75)[151,152] (Figure 1.11.a-b.). This structure shows that a CcdB dimer binds to GyrA in its open conformation, i.e. an open conformation of the DNA gyrase DNA-gate. This demonstrates that CcdB can bind to GyrA just after DNA cleavage and before T-segment passage. Ultimately, it results in an inhibition of DNA gyrase by CcdB induced covalent DNA gyrase/G-segment complex that locks the DNA molecule on the gyrase. Thus, this blocks the cellular polymerases[153,154], leading to double-stranded DNA breaks that induce the SOS response and ultimately cell death[155].

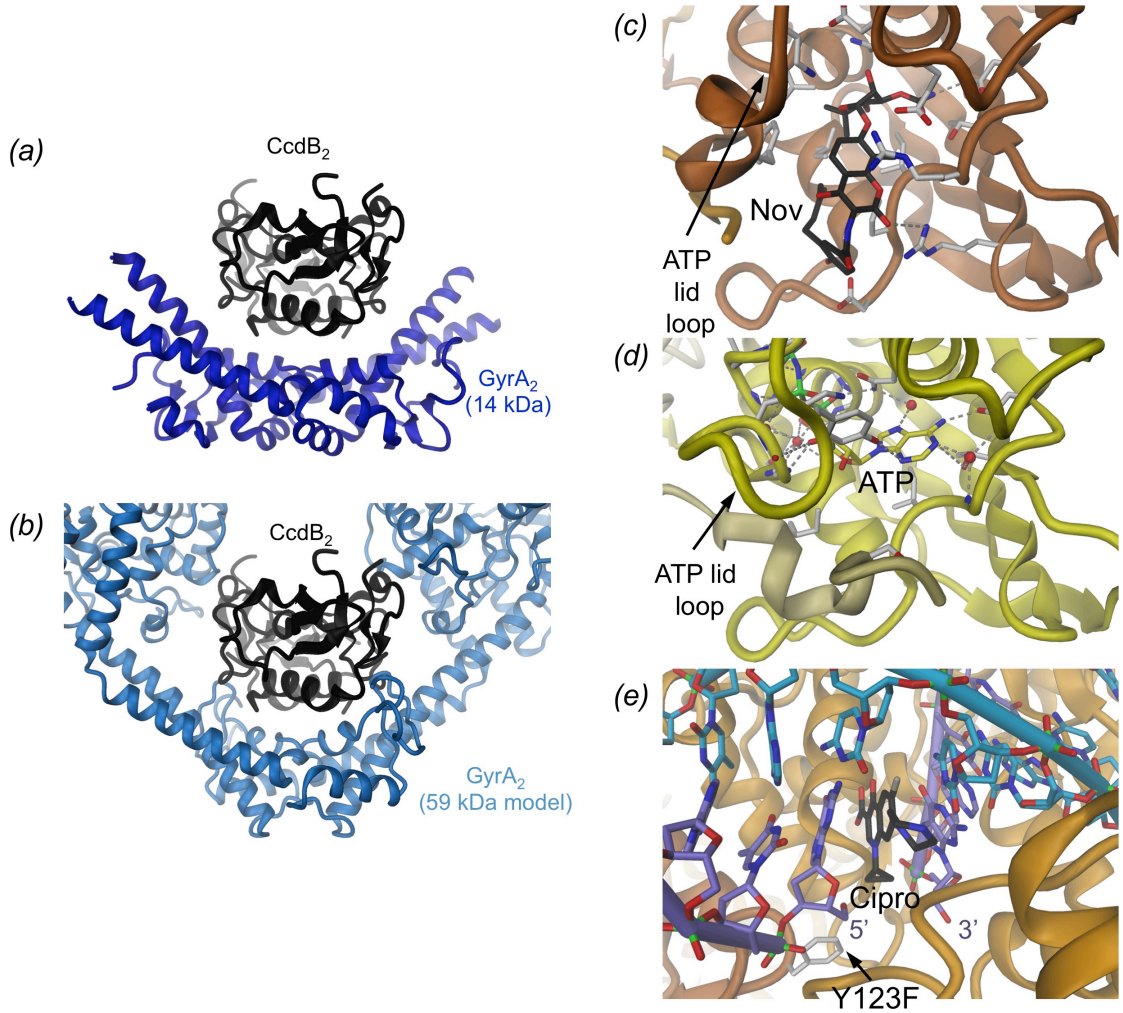

Figure 1.11. Structural insight into the inhibition of DNA gyrase by toxins or antibiotics. *(a)* CcdB (black) binds to GyrA dimer (14 kDa fragment, blue) in an opened conformation and prevents the closure of the GyrA dimer (PDB code: 1X75). *(b)* Model of GyrA (59 kDa fragment, light blue) based on the open conformation of yeast topoII in the opened conformation shows an embedded CcdB (PDB code: 1BGW). *(c)* Novobiocin (Nov, black C atoms) bound to the 43-kDa fragment of GyrB (PDB code: 1KIJ) compared to *(d)* ATP (yellow C atoms) bound to the same fragment of GyrB (PDB code: 1EI1). Note the different conformation of the ATP lid loop disrupted by novobiocin binding and the type of interactions, mostly hydrophobic for novobiocin and polar for the ATP substrate. *(e)* Inhibition of DNA gyrase by criprofloxacin (Cipro, black C atoms) bound to GyrA and double-nicked double-stranded DNA (one strand with violet C atoms and the other with blue C atoms) (PDB code: 2XCT). Ciprofloxacin stacks between two base pairs. Note the position of the Y123F mutant of the catalytic tyrosine that has been demonstrated to form a covalent bond with the 5' -end of the cleaved dsDNA molecule. Ciprofloxacin prevents the attack of the 3'-hydroxyl group of the DNA molecule, resulting in dsDNA breaks.

Other plasmid-encoded proteins like microcin B17 or the ParE toxin also poison DNA gyrase[156]. It is likely that more, yet unrevealed toxins, also target DNA gyrase. Section 3.3., *research article III* focused on Class I Fic toxins (as defined in section 3.1., *research article I*) that inhibit (but do not poison) bacterial topoisomerases by adenylylation to subvert DNA topology and promote persistence.

1.7.7. DNA gyrase is a valuable drug target

DNA gyrase is the only enzyme able to introduce negative supercoils dependent on ATP hydrolysis, which makes it unique in the pool of DNA topoisomerases. As such, bacterial DNA gyrase is a valuable antibiotic target[157,158]. A distinction can be made between catalytic inhibitors of DNA gyrase (i.e. aminocoumarins) or DNA gyrase poisons (i.e. quinolones)[159].

Aminocoumarin drugs like novobiocin are potent competitive inhibitors of DNA gyrase, blocking the ATP binding in the ATPase domain of GyrB[160,161]. Novobiocin tightly binds to the ATPase domain of GyrB and ParE (*E. coli*) with an affinity (K_i) of 14 nM and 110 nM, respectively. They are natural compounds isolated from *Streptomyces* species. High-resolution crystal structures of GyrB in complex with aminocoumarin provided important information on the binding mode of the inhibitor (Figure 1.11.c compared to the ATP binding mode in Figure 1.11.d).

Quinolones target GyrA resulting in inhibition of supercoiling, double stranded DNA breaks and ultimate bacterial killing, a similar effect than the toxin CcdB, but the interaction of quinolones and CcdB with GyrA are distinct. Quinolones are the most successful antibacterial compounds targeting the DNA gyrase, of which ciprofloxacin is a very potent inhibitor that is bactericidal. Many quinolones have been commercialized with success. Quinolones inhibit DNA supercoiling and relaxation mediated by DNA gyrase via a covalent bond between the catalytic tyrosines of GyrA and the 5' end of the cleaved dsDNA molecules. Again, high-resolution X-ray structures provided valuable structural information about the binding sites of quinolones on DNA gyrase (Figure 1.11.e). To summarize, quinolones like ciprofloxacin and the CcdB toxin are poisoning DNA gyrase and are therefore intrinsically bactericidal.

Aim of my Thesis

2. Aim of my Thesis

Fic proteins catalyze adenylylation, the transfer of an AMP moiety onto a target protein. Expression in *E. coli* of the Fic protein from *Neisseria meningitidis* or *Bartonella schoenbuchensis*, NmFic or VbhT respectively, results in severe growth defect of the model organism *E. coli*. This phenotype correlates with the adenylylation of bacterial topoisomerases.

The aim of my PhD thesis, started in October 2010, was to decipher the regulatory mechanism of Fic proteins and contribute to the understanding of Fic-mediated target inhibition.

For that purpose, I first focused on class III Fic protein (NmFic from *N. meningitidis*) that contains a C-terminal inhibition motif, undergoes oligomerization and auto-adenylylation. I also focused on the target of NmFic: the B subunit of bacterial DNA gyrase (GyrB), a type IIA topoisomerase.

I used, amongst others, mainly X-ray crystallography, biochemical and biophysical analysis to unravel the details of the regulation mechanism of Fic proteins and Fic-mediated target inhibition.

Results

3. Results

3.1. *Research article I* (Engel, Goepfert *et al.*, *Nature*, 2012)

Adenylylation control by intra- or intermolecular active-site obstruction in Fic proteins

Philipp Engel*, Arnaud Goepfert*, Frédéric V. Stanger, Alexander Harms, Alexander Schmidt, Tilman Schirmer & Christoph Dehio

* These authors contributed equally to this work

Nature, Volume 482, Issue 7383, 2012 Jan 22nd, Pages 107-110

3.1.1. Statement of my own contributions

I contributed to the *research article I* by cloning most of the recombinant plasmids used in this work. I expressed, purified crystallized and determined the structure of $NmFic_{wt}$ in complex with AMPPNP, the inhibited form of NmFic. I took part to the experimental design, in particular the design of structure-based mutations of the different Fic proteins tested for relief of inhibition. I participated in the data analysis of the structures determined in the frame of this study. I also participated in the production of the Supplementary Movie that summarizes the findings of this publication from a structural point of view.

The manuscript was written by Philipp Engel, Arnaud Goepfert, Tilman Schirmer and Christoph Dehio.

3.1.2. "Adenylylation control by intra- or intermolecular active-site obstruction in Fic proteins"

LETTER

doi:10.1038/nature10729

Adenylylation control by intra- or intermolecular active-site obstruction in Fic proteins

Philipp Engel[1]†*, Arnaud Goepfert[1,2]*, Frédéric V. Stanger[1,2], Alexander Harms[1], Alexander Schmidt[3], Tilman Schirmer[2] & Christoph Dehio[1]

Fic proteins that are defined by the ubiquitous FIC (filamentation induced by cyclic AMP) domain are known to catalyse adenylylation (also called AMPylation); that is, the transfer of AMP onto a target protein. In mammalian cells, adenylylation of small GTPases through Fic proteins injected by pathogenic bacteria can cause collapse of the actin cytoskeleton and cell death[1,2]. It is unknown how this potentially deleterious adenylylation activity is regulated in the widespread Fic proteins that are found in all domains of life and that are thought to have critical roles in intrinsic signalling processes. Here we show that FIC-domain-mediated adenylylation is controlled by a conserved mechanism of ATP-binding-site obstruction that involves an inhibitory α-helix (α_{inh}) with a conserved (S/T)XXXE(G/N) motif, and that in this mechanism the invariable glutamate competes with ATP γ-phosphate binding. Consistent with this, FIC-domain-mediated growth arrest of bacteria by the VbhT toxin of *Bartonella schoenbuchensis* is intermolecularly repressed by the VbhA antitoxin through tight binding of its α_{inh} to the FIC domain of VbhT, as shown by structure and function analysis. Furthermore, structural comparisons with other bacterial Fic proteins, such as Fic of *Neisseria meningitidis* and of *Shewanella oneidensis*, show that α_{inh} frequently constitutes an amino-terminal or carboxy-terminal extension to the FIC domain, respectively, partially obstructing the ATP binding site in an intramolecular manner. After mutation of the inhibitory motif in various Fic proteins, including the human homologue FICD (also known as HYPE), adenylylation activity is considerably boosted, consistent with the anticipated relief of inhibition. Structural homology modelling of all annotated Fic proteins indicates that inhibition by α_{inh} is universal and conserved through evolution, as the inhibitory motif is present in ~90% of all putatively adenylylation-active FIC domains, including examples from all domains of life and from viruses. Future studies should reveal how intrinsic or extrinsic factors modulate adenylylation activity by weakening the interaction of α_{inh} with the FIC active site.

In two Fic proteins, IbpA and VopS, that are translocated by pathogenic bacteria into host cells, the ubiquitous FIC domain has been shown to catalyse adenylylation[1–4]. The crystal structure of the effector domain IbpA(FIC2) in complex with its adenylylated host target Cdc42 has been reported[5] and a catalytic mechanism has been proposed[5,6]. IbpA- or VopS-mediated adenylylation of Rho-family GTPases abolishes downstream signalling in human cells and, thus, causes actin cytoskeleton collapse and cell death[1,2]. By contrast, overexpression of a human Fic protein with similar target specificity, HYPE, had only a marginal effect[1]. This suggests that the potentially deleterious adenylylation activity is tightly regulated in HYPE and probably in most of the almost 3,000 Fic proteins that are proposed to have important roles in intrinsic signalling processes in bacteria, archaea and eukaryotes.

VbhT is a bacterial Fic protein of the mammalian pathogen *B. schoenbuchensis*[7,8]. It is composed of an N-terminal FIC domain and a C-terminal BID domain (Fig. 1a). The BID domain facilitates protein translocation into mammalian or bacterial target cells through a type IV secretion system or conjugation machinery[9], respectively, but the target cell and functional role of VbhT are unknown. VbhT arrests growth when expressed in *Escherichia coli* (Fig. 1c and Supplementary Fig. 1a). Growth arrest is repressed by mutation of histidine to alanine (VbhT(H136A)) in the conserved FIC motif HXFX(D/E)GNGRXXR. In other Fic proteins, this signature motif has been shown to be essential for target protein adenylylation activity[1,2,10], therefore suggesting that toxicity is related to adenylylation of endogenous proteins. Indeed, wild-type VbhT, but not VbhT(H136A), catalysed *in vitro* adenylylation of a putative *E. coli* target protein of approximately 80 kilodaltons (kDa) (Fig. 1d). Furthermore, *E. coli* cells showed filamentation after expression of wild-type VbhT, but not of VbhT(H136A) (Supplementary Fig. 2). A similar phenotype has been described for what is thought to be a hyperactive mutant of the *E. coli* Fic protein[11]. Co-expression of VbhT with VbhA, encoded by the small open reading frame *vbhA*

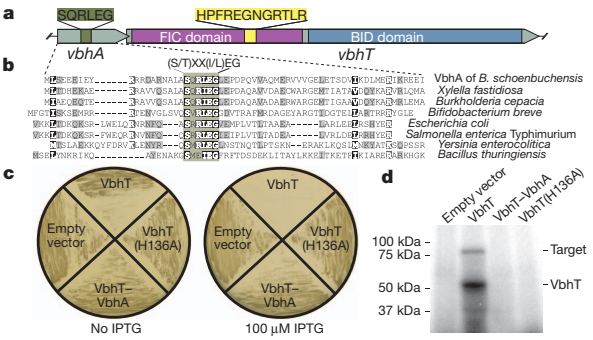

Figure 1 | The small protein VbhA represses the toxic effect (growth arrest) that is mediated by the adenylylation activity of VbhT in *E. coli*. **a**, Genetic organization of the type-IV-secretion-system-associated locus of *B. schoenbuchensis*, which is composed of the overlapping *vbhA* and *vbhT* genes. The FIC and BID domains that are encoded by *vbhT* are shown in different colours. Protein translations of the regions encoding the conserved motif of VbhA and the FIC motif of VbhT are depicted. **b**, Protein alignment of VbhA and a subset of the 158 homologues that are encoded upstream of *fic* loci in different bacteria (see also Supplementary Fig. 4). The most conserved region shows a (S/T)XX(I/L)EG consensus. Sequence accessions and strain designations are given in Supplementary Fig. 4. **c**, Growth of *E. coli* on lysogeny broth (LB) plates after IPTG-induced expression of different VbhT and VbhA constructs. Expression of VbhT shows a toxic effect, whereas bacterial growth is not affected when VbhT(H136A) is expressed or when VbhT and VbhA are co-expressed (VbhT–VbhA). All *E. coli* strains revealed normal growth without induction. Growth curve experiments in LB gave analogous results (Supplementary Fig. 1). **d**, Adenylylation assay with crude cell lysates of *E. coli* ectopically expressing the same constructs as in panel **c**.

[1]Focal Area Infection Biology, Biozentrum, University of Basel, CH-4056 Basel, Switzerland. [2]Core Program Structural Biology and Biophysics, Biozentrum, University of Basel, CH-4056 Basel, Switzerland. [3]Proteomics Core Facility, Biozentrum, University of Basel, CH-4056 Basel, Switzerland. †Present address: Department of Ecology and Evolutionary Biology, Yale University, New Haven, CT 06520-8106, USA. *These authors contributed equally to this work.

RESEARCH LETTER

immediately upstream of *vbhT* (Fig. 1a), completely repressed VbhT toxicity, as shown by wild-type-like bacterial growth, normal cell morphology, and inhibition of VbhT-dependent adenylylation (Fig. 1 and Supplementary Figs 1a and 2). We also observed VbhT-mediated toxicity and its repression by VbhA in *B. schoenbuchensis*, the natural carrier of this toxin and antitoxin, and in the related species *Bartonella henselae* (Supplementary Fig. 3).

The inhibitory action of VbhA on the VbhT toxin, and the genetic organization of the respective genes in an operon are reminiscent of toxin–antitoxin modules that are found in many bacterial genomes, often associated with mobile genetic elements[12]. A comprehensive analysis of the upstream region of FIC-domain-encoding genes (PFAM pf02661) identified 158 bacterial *vbhA* homologues that probably function as antitoxins. Although the sequences are rather diverse, a central (S/T)XX(I/L)EG motif is conspicuous (Fig. 1b and Supplementary Fig. 4). The high-resolution (1.5 Å) crystal structure of VbhA in complex with the FIC domain of VbhT (VbhT(FIC)) (Supplementary Table 1) shows that VbhA is folded into three anti-parallel helices that tightly embrace VbhT(FIC) (Fig. 2a) with the N-terminal helix (α_{inh}), adopting a location that is analogous but distinct to that of the antitoxin Phd in its complex with Doc[13] (Supplementary Fig. 5). Doc is a Fic protein with a degenerate, probably adenylylation-incompetent FIC motif[14] that may have adopted another toxic activity (Supplementary Information, section 1). The VbhA antitoxin motif locates to the C-terminal part of α_{inh} and is positioned close to the putative ATP-binding site[10] at the N-cap of the helix that follows the active loop of VbhT(FIC). This suggests that the antitoxin competes with ATP binding. VbhA residues Ser 20 and Glu 24 of the inhibitory motif form a hydrogen bond and a salt bridge, respectively, with the conserved Arg147 of VbhT following the active loop.

Intriguingly, structural comparison with other bacterial Fic proteins of known fold (Fic proteins from *S. oneidensis* (SoFic)[14,15] and from *N. meningitidis* (NmFic)[14] (Fig. 2b, c), and from *Bacteroides theataiotaomicron* (BtFic)[14] and from *Helicobacter pylori* (HpFic)[14] (Supplementary Fig. 6)) reveals that a structural equivalent of α_{inh} can be part of the FIC domain fold itself. Moreover, these proteins also show the SXXXE(G/N) inhibitory motifs that are, with respect to the FIC active site, arranged exactly as in the VbhA-VbhT(FIC) complex. Along the polypeptide chain, however, these α_{inh} occur at two distinct locations either in the N-terminal part (SoFic and BtFic) or at the C terminus (NmFic and HpFic). Thus, Fic proteins containing α_{inh} can be grouped into three classes (Fig. 2d) depending on whether α_{inh} is provided by an interacting antitoxin (class I) or whether it is part of the FIC fold as an N-terminal helix (class II) or a C-terminal helix (class III).

To investigate the distribution of class II and class III Fic proteins, we predicted the structures of all PFAM FIC domain entries by homology modelling (Supplementary Information, section 1). Including the class I proteins that are identified above, two-thirds of all Fic proteins were classified (Fig. 2e and Supplementary Table 2), with a strong dominance of class II, the class to which human HYPE belongs (Supplementary Tables 3 and 4). The proportion of classified Fic proteins increases to 90% when considering only adenylylation-competent Fic proteins that are defined by compliance with the HXFX(D/E)GNGRXXR motif (Supplementary Text). This suggests co-evolution of catalytic and inhibitory function. The inhibition motifs that are derived from Psi-Blast (class I) and structural predictions (classes II and III) are shown in Fig. 2f with the overall consensus being (S/T)XXXE(G/N). The strict conservation of the glutamate is striking and indicates that the observed ionic interaction with the second arginine of the conserved FIC motif (Figs 2a–c) is crucial for inhibition. Phylogenetic distribution of class I

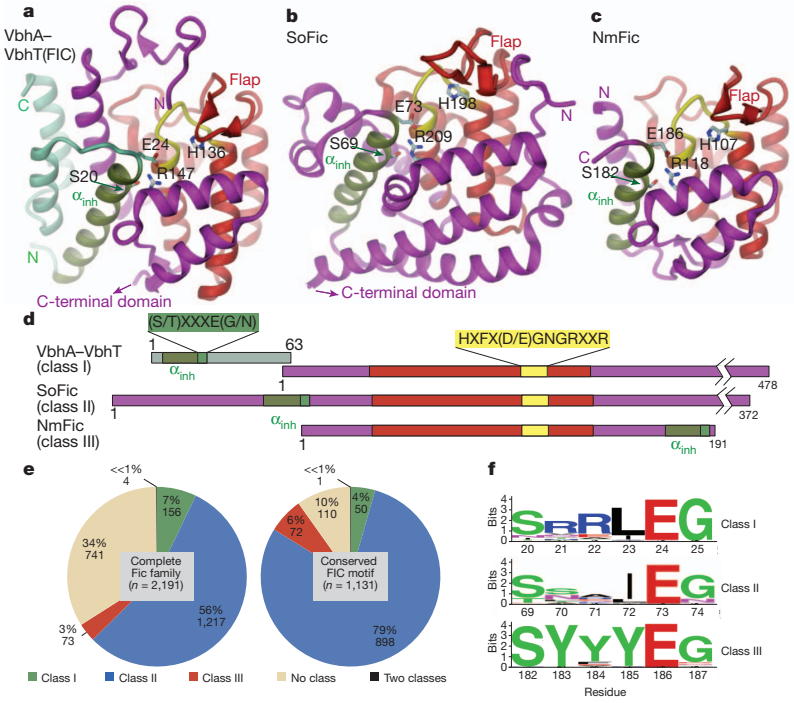

Figure 2 | Structures and classification of Fic proteins according to the position of the inhibitory motif along the polypeptide chain. Structures are shown in cartoon (FIC core as defined by PFAM, red; active site loop with histidine, yellow; inhibitory helix (α_{inh}) with SXXXE(G/N) motif, green) with important residues in full. **a**, Complex of VbhT(FIC) with antitoxin VbhA (green). **b**, SoFic (from *S. oneidensis*, PDB code 3EQX) with C-terminal domain omitted. **c**, NmFic (from *N. meningitidis*, PDB code 2G03). **d**, Linear organization of motifs in the proteins presented in panels **a**–**c**. **e**, Distribution of the three Fic protein classes for the entire family in the PFAM database (left) and the subset of Fic proteins with the conserved FIC motif HXFX[(D/E)GNGRXXR that is likely to convey adenylylation activity (right; see also Supplementary Information, section 1). **f**, Sequence profiles for the inhibition site of the three Fic protein classes.

and class III Fic proteins indicates that each is of monophyletic origin (Supplementary Fig. 7). Fic proteins with a degenerate FIC motif are dispersed over the tree, with the exception of the large cluster of Doc-like toxins. This suggests that there is recurrent degeneration of the conserved FIC motif with concomitant loss of adenylylation activity. Consistent with this, deterioration of the FIC motif seems to correlate with the absence of a recognizable inhibitory motif (Supplementary Fig. 7). Fic proteins with a degenerate FIC motif may display catalytic activities different from adenylylation, such as phosphocholination, as reported for the *Legionella pneumophila* effector AnkX[16].

Owing to our discovery of the prevalence of the inhibitory motif in Fic proteins, we carried out a detailed analysis of its functional and structural role. For this, NmFic (class III, Fig. 2c) was chosen, as it is the smallest active Fic family protein with known crystallization condition (Supplementary Table 1). As reported before[6], NmFic exhibits *in vitro* auto-adenylylation activity (Fig. 3d). The acceptor site was traced to Y183 of α_{inh} by mass spectrometry (Supplementary Information, section 1, and Supplementary Fig. 8). On the basis of the location of Y183 relative to the active site, auto-adenylylation is probably catalysed intermolecularly after partial unfolding or detachment of α_{inh}. Addition of *E. coli* lysate to NmFic did not reveal additional bands on the autoradiograph, and this indicated that there are no NmFic targets in *E. coli* or that the activity of NmFic is inhibited. The latter was shown to be correct as mutation of the inhibitory motif (S182A/E186A, NmFic(SE/AA)) resulted in transfer of radioactivity onto an ~80-kDa *E. coli* protein and enhanced auto-adenylylation with an additional acceptor site (Y188; Fig. 3d and Supplementary Fig. 9). Deletion of the entire α_{inh} helix (NmFic(Δ8)) led to similar target protein adenylylation, proving that the activity resides in the FIC domain core. However, only weak auto-adenylylation was apparent owing to the lack of the acceptor tyrosines in this deletion mutant (Fig. 3d and Supplementary Fig. 8c).

To investigate the inhibitory mechanism, crystals of NmFic proteins were soaked with the non-hydrolysable ATP analogue adenylyl imidodiphosphate (AMPPNP) (Supplementary Table 1). The NmFic–AMPPNP structure revealed nucleotide binding but with the γ-phosphate disordered (Fig. 3a). Notably, the orientation of the α-phosphate seems to be non-productive, as the position that is in line with the scissile Pα-O3α bond is occluded by H107 and N113 (Supplementary Fig. 10a and Supplementary Movie). To reveal the situation in an inhibition-relieved mutant, the structure of NmFic(SE/AA) was determined to 3.0 Å (Supplementary Fig. 11). Electron density was lacking for α_{inh}, indicating disorder, whereas the nucleotide conformation was well defined. In the NmFic(Δ8)–AMPPNP structure, the same nucleotide conformation was observed (Fig. 3b) and, owing to its high resolution (1.7 Å), the structural basis for the observed relief of inhibition in these mutants became evident. Whereas the adenosine moiety adopts the same position as in the wild-type, the γ-phosphate of the nucleotide is bound to R118, occupying the same position as the carboxylate of the inhibitory E186 in the wild type. As a consequence, the α-phosphate is found to be re-oriented, and the new orientation permits in line attack of a target side chain onto the α-phosphorus to accomplish AMP transfer (Fig. 3c, Supplementary Fig. 10 and Supplementary Movie).

The exact role of the inhibitory glutamate was investigated further by mutagenesis of Fic proteins from the three regulatory classes. In wild-type NmFic, Cα and Cβ of the glutamate are close to the position that is attained by the γ-phosphate position in NmFic(Δ8) (Fig. 3c). Still, an E to G single point mutant may provide sufficient space and main-chain flexibility to allow γ-phosphate binding. Indeed, similar to NmFic(Δ8)and NmFic(SE/AA), the mutant NmFic(E186G) resulted in growth inhibition of *E. coli* (Supplementary Fig. 1b). Likewise, co-expression of VbhT(FIC) and VbhA(E24G), as representatives for class I, caused *E. coli* growth defects (Supplementary Fig. 1a). We also included SoFic, a bacterial class II protein, in this analysis. Consistent with the effects of E to G single point mutants in NmFic and VbhA, mutant SoFic(E73G) revealed a negative effect on *E. coli* growth

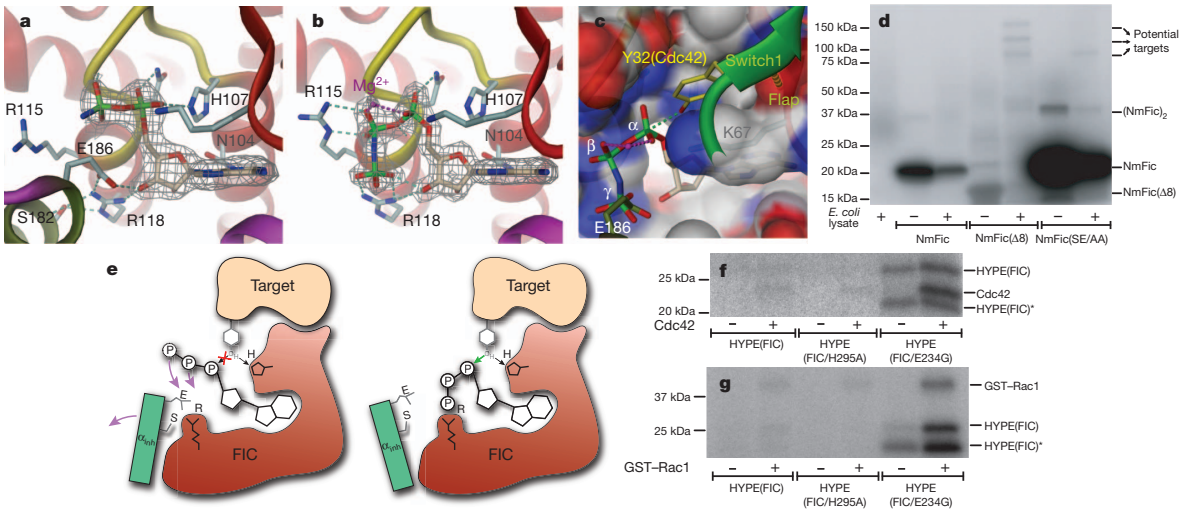

Figure 3 | Structure and function of wild-type and mutant NmFic reveals a general inhibition mechanism corroborated by HYPE protein analysis. **a**, Active site of NmFic with bound ATP analogue AMPPNP. The γ-phosphate seems to be disordered and has not been modelled. **b**, Active site of NmFic(Δ8) with bound AMPPNP and Mg^{2+}. The γ-phosphate occupies the position taken by E186 of the SXXXEG motif in the wild-type (as shown in **a**). Also shown are $2Fo - Fc$ maps that are contoured at 1.2σ and cover the ligands. **c**, Surface representation of the active site of NmFic(Δ8) with modifiable Y32 (yellow) of the Cdc42 switch1 loop (green) in a position that is obtained from a superposition of the active site loops of NmFic over the IbpA(FIC2)–Cdc42 complex[5]. **d**, Autoradiography of an SDS gel after incubation of wild-type and mutant NmFic with [α-^{32}P]ATP in the presence or absence of *E. coli* lysate. The mutants, but not the wild-type, catalyse AMP transfer onto *E. coli* target proteins. **e**, Scheme of a general inhibition mechanism for Fic proteins. The α_{inh} helix (green) with the (S/T)XXXE(G/N) motif prevents productive ATP binding. It is only after dissociation of the helix that the ATP γ-phosphate attains the position close to a conserved arginine (indicated by "R") of the FIC motif. This is accompanied by reorientation of the α-phosphate to allow in-line attack of the target hydroxyl side chain after proton transfer to the active histidine as proposed before[5]. **f**, **g**, Autoradiography after incubation of HYPE(FIC) with α-^{32}P-ATP in the presence or absence of Cdc42 (**f**) or GST-tagged Rac1 (GST–Rac1) (**g**). HYPE(FIC/E234G) shows enhanced auto-adenylylation and target adenylylation. HYPE(FIC)* denotes a degradation product of HYPE(FIC).

RESEARCH LETTER

(Supplementary Fig. 1c) and strongly enhanced auto-adenylylation (Supplementary Fig. 12). A similar marked effect on auto-adenylylation was observed after mutation of the corresponding residue in human HYPE (HYPE(FIC/E234G)), another class II protein (Fig. 3f, g). It is known that HYPE catalyses Cdc42 and Rac1 adenylylation[1,4]. The rather low adenylylation activity of wild-type HYPE on these substrates is markedly enhanced in the HYPE(FIC/E234G) mutant (Fig. 3f, g), demonstrating that the relief of inhibition by α_{inh} enhances not only auto-adenylylation but also AMP transfer onto bona fide protein targets.

From this study a general mechanism for the inhibition of the FIC-domain-mediated adenylylation has emerged that invokes a glutamate finger from α_{inh} to inter- or intramolecularly block part of the ATP binding site (Fig. 3e). Dissociation of the toxin–antitoxin complex (class I) or intramolecular loosening of the contact between α_{inh} and the FIC domain active site (classes II and III) allows ordered binding of the entire ATP moiety with the α-phosphate in an orientation that is productive for accepting an incoming target hydroxyl side chain.

Class I proteins might exert functions similar to the classical bacterial toxin–antitoxin modules[12], whereas class II and III Fic proteins seem to regulate intrinsic cellular functions that are related to physiological adaptation and cell homeostasis. Conservation of class II Fic proteins in all three kingdoms of life (Supplementary Table 2) emphasizes the important role of the regulatory mechanisms described here. How the adenylylation activity is activated by weakening the interaction of α_{inh} with the FIC active site in class II and class III Fic proteins is one of many important questions for future research. We also anticipate our study to be a starting point for rational approaches to modulate the adenylylation activities of Fic proteins—approaches that should aid in elucidating the diverse biological functions of these widespread signalling proteins.

METHODS SUMMARY

Toxicity experiments were performed with *E. coli* strain MG1655, which encodes an IPTG (isopropyl-β-D-thiogalactoside)-inducible T7 polymerase (strain AB472). Protein expression was controlled by the addition of either 100 μM IPTG (induction) or 1% glucose (repression). A PSI-BLAST search for homologues with VbhA of *B. schoenbuchensis* was conducted to identify Fic proteins belonging to class I. Class II and class III proteins were classified by structure predictions using the program HHpred[17]. We analysed all 2,189 proteins of the FIC PFAM family (pf02661, release 24). Adenylylation assays were carried out using bacterial crude cell lysates for VbhT constructs or purified proteins for NmFic, SoFic and HYPE constructs. For structure determination, VbhA and VbhT(FIC) were co-expressed in the BL21(DE3) strain of *E. coli*, and NmFic, SoFic(Δ8) and NmFic(SE/AA) in the BL21-AI strain of *E. coli*. VbhA-VbhT(FIC) and NmFic were purified by affinity chromatography followed by size exclusion chromatography. An additional anion exchange chromatography step was performed for NmFic(Δ8)and NmFic(SE/AA). Diffraction data were collected at beamline X06SA of the Swiss Light Source. For NmFic(Δ8)and NmFic(SE/AA), we obtained phases by molecular replacement using the NmFic structure (PDB code 2G03) as a search model. The VbhA–VbhT(FIC) complex was solved by molecular replacement using a fragment of BepA (PDB code 2JK8).

Full Methods and any associated references are available in the online version of the paper at www.nature.com/nature.

Received 4 July; accepted 24 November 2011.
Published online 22 January 2012.

1. Worby, C. A. *et al.* The fic domain: regulation of cell signaling by adenylylation. *Mol. Cell* **34,** 93–103 (2009).
2. Yarbrough, M. L. *et al.* AMPylation of Rho GTPases by *Vibrio* VopS disrupts effector binding and downstream signaling. *Science* **323,** 269–272 (2009).
3. Roy, C. R. & Mukherjee, S. Bacterial FIC proteins AMP up infection. *Sci. Signal.* **2,** pe14 (2009).
4. Mattoo, S. *et al.* Comparative analysis of *Histophilus somni* immunoglobulin-binding protein A (IbpA) with other Fic domain-containing enzymes reveals differences in substrate and nucleotide specificities. *J. Biol. Chem.* **286,** 32834–32842 (2011).
5. Luong, P. *et al.* Kinetic and structural insights into the mechanism of AMPylation by VopS Fic domain. *J. Biol. Chem.* **285,** 20155–20163 (2010).
6. Xiao, J., Worby, C. A., Mattoo, S., Sankaran, B. & Dixon, J. E. Structural basis of Fic-mediated adenylylation. *Nature Struct. Mol. Biol.* **17,** 1004–1010 (2010).
7. Dehio, C. *et al. Bartonella schoenbuchii* sp. nov., isolated from the blood of wild roe deer. *Int. J. Syst. Evol. Microbiol.* **51,** 1557–1565 (2001).
8. Engel, P. *et al.* Parallel evolution of a type IV secretion system in radiating lineages of the host-restricted bacterial pathogen *Bartonella*. *PLoS Genet.* **7,** e1001296 (2011).
9. Schulein, R. *et al.* A bipartite signal mediates the transfer of type IV secretion substrates of *Bartonella henselae* into human cells. *Proc. Natl Acad. Sci. USA* **102,** 856–861 (2005).
10. Palanivelu, D. V. *et al.* Fic domain-catalyzed adenylylation: insight provided by the structural analysis of the type IV secretion system effector BepA. *Protein Sci.* **20,** 492–499 (2011).
11. Utsumi, R., Nakamoto, Y., Kawamukai, M., Himeno, M. & Komano, T. Involvement of cyclic AMP and its receptor protein in filamentation of an *Escherichia coli* fic mutant. *J. Bacteriol.* **151,** 807–812 (1982).
12. Engelberg-Kulka, H., Amitai, S., Kolodkin-Gal, I. & Hazan, R. Bacterial programmed cell death and multicellular behavior in bacteria. *PLoS Genet.* **2,** e135 (2006).
13. Garcia-Pino, A. *et al.* Doc of prophage P1 is inhibited by its antitoxin partner Phd through fold complementation. *J. Biol. Chem.* **283,** 30821–30827 (2008).
14. Kinch, L. N., Yarbrough, M. L., Orth, K. & Grishin, N. V. Fido, a novel AMPylation domain common to Fic, Doc, and AvrB. *PLoS ONE* **4,** e5818 (2009).
15. Das, D. *et al.* Crystal structure of the Fic (Filamentation induced by cAMP) family protein SO4266 (gi|24375750) from *Shewanella oneidensis* MR-1 at 1.6 Å resolution. *Proteins* **75,** 264–271 (2009).
16. Mukherjee, S. *et al.* Modulation of Rab GTPase function by a protein phosphocholine transferase. *Nature* **477,** 103–106 (2011).
17. Söding, J., Biegert, A. & Lupas, A. N. The HHpred interactive server for protein homology detection and structure prediction. *Nucleic Acids Res.* **33,** W244–W248 (2005).

Supplementary Information is linked to the online version of the paper at www.nature.com/nature.

Acknowledgements We thank T. Glatter for mass spectrometry analysis of samples at the Core Proteomics facility. We thank the staff of beamline X06SA of the Swiss Light Source for assistance with data acquisition. We are grateful to G. Pluschke for providing the genomic DNA of *Neisseria meningitidis*, the ASU Biodesign Institute for providing the plasmid enclosing the *Shewanella oneidensis* Fic protein and S. Mattoo and J. Dixon for providing the pET-GSTX plasmids enclosing HYPE and HYPE(H295A). We also thank D. Bumann and A. Boehm for providing plasmid pC10E and *E. coli* strain AB472, respectively. This work was supported by grants 3100-061777 and 3100-138414 from the Swiss National Science Foundation (to C.D. and T.S., respectively), and grant 51RT 0_126008 (InfectX) in the frame of the SystemsX.ch Swiss Initiative for Systems Biology (to C.D.).

Author Contributions P.E., F.V.S. and A.H. cloned recombinant plasmids. P.E. discovered and physiologically characterized VbhT–VbhA as a toxin–antitoxin module and carried out the bioinformatic analysis. A.G. expressed, purified and crystallized VbhA–VbhT(FIC), NmFic(SE/AA) and NmFic(Δ8), and determined their structures. F.V.S. expressed, purified and crystallized NmFic with AMPPNP and determined the structure. A.G. and A.H. performed the adenylylation assays. A.H carried out the growth curve experiments. A.S. conducted the mass spectrometry analysis. All authors contributed to experimental design and data analysis. The manuscript was written by P.E., A.G., T.S. and C.D.

Author Information The atomic coordinates of VbhA–VbhT(FIC) and the complexes of NmFic, NmFic(SE/AA) and NmFic(Δ8) with AMPPNP have been deposited in the Protein Data Bank under accession codes 3SHG, 3S6A, 3SN9 and 3SE5, respectively. Reprints and permissions information is available at www.nature.com/reprints. The authors declare no competing financial interests. Readers are welcome to comment on the online version of this article at www.nature.com/nature. Correspondence and requests for materials should be addressed to C.D. (Christoph.Dehio@unibas.ch) or T.S. (Tilman.Schirmer@unibas.ch).

METHODS

Identification of VbhA homologues. VbhA of *B. schoenbuchensis* was queried against a database composed of translated open reading frames (>10 amino acids) identified in the 500-bp upstream region of all *fic* loci (PFAM release 24, 2,189 proteins). Nine rounds of Psi-Blast were performed and hits with an *E*-value <1 manually validated.

***E. coli* toxicity tests and cell filamentation.** *E. coli* AB472, a derivative of MG1655, was transformed with VbhT-expressing plasmids and always handled in LB containing 1% glucose. A single colony was picked, resuspended in 20 µl of LB and plated on LB plates containing 100 µM IPTG (induction) or 1% glucose (repression). Plates were incubated overnight at 37 °C. Growth curves were acquired by measuring optical density of liquid cultures in LB containing 100 µM IPTG that had been inoculated from overnight cultures of single colonies and were grown at 30 °C with continuous shaking. Cell filamentation was visualized by co-transformation of plasmid pC10E that constitutively expresses GFP and examined using fluorescence microscopy.

Conjugation experiments for VbhT toxicity tests in *Bartonella*. Plasmids were introduced into *Bartonella* strains by conjugation from *E. coli* using three-parental mating. *Bartonella* strains were grown for 36–48 h at 35 °C with 5% CO_2 on Columbia base agar plates supplemented with 5% defibrinated sheep blood and 100 µg ml^{-1} streptomycin. *E. coli* β2150 that harbours helper plasmid pRK2013, and *E. coli* β2150 that contains the VbhT-expressing plasmid were grown overnight at 37 °C in LB supplemented with 50 µg ml^{-1} kanamycin or 30 µg ml^{-1} chloramphenicol, respectively, and both media were also supplemented with diaminopimelic acid (DAP) and 1% glucose. After 16 h of incubation, *E. coli* strains were diluted 1:50 in fresh LB medium and grown to a optical density (OD) at 595 nm (OD_{595nm}) of 0.4–0.8. Subsequently, each *E. coli* strain was diluted to OD_{595nm} of 0.25, washed once and resuspended in supplemented M199 medium (containing 10% FCS and 1% glucose). *Bartonella* strains were collected in 1 ml and resuspended in 60 µl of M199 (OD_{595nm} = 1). Each *Bartonella* suspension was mixed with 20 µl of *E. coli* β2150 that harbours pRK2013 and 20 µl of *E. coli* β2150 that harbours the VbhT-expressing plasmid. The conjugation mix was distributed on a conjugation filter on a columbia blood agar (CBA) plate supplemented with 150 µl DAP and 150 µl 1% glucose. After 6 h of incubation under *Bartonella* growth conditions as described before, the bacteria were washed off the filter with 1 ml supplemented M199. Dilutions of bacterial suspensions were plated on lysogeny broth agar (LA) supplemented with DAP, 1% glucose and 30 µg ml^{-1} chloramphenicol for selecting donors, on CBA supplemented with 1.2 µg ml^{-1} chloramphenicol for selecting transconjugants, and on CBA supplemented with 100 µg ml^{-1} streptomycin for selecting recipients. Agar plates were incubated under *Bartonella* growth conditions and colony-forming units were counted after 1 day for donors and after 7 days for recipients and transconjugants.

***In vitro* adenylylation assay.** Adenylylation activity of VbhT was assessed in an assay using lysates of ectopically expressing *E. coli*. Bacterial pellets were resuspended in reaction buffer (50 mM Tris-HCl pH 8.0, 150 mM NaCl, 0.1 mM EGTA, 15 mM $MgCl_2$, 140 µg ml^{-1} RNase A and protease inhibitor cocktail (Roche)) and lysed by sonication. After clearing lysates by centrifugation, supernatants were used for experimentation or stored at −20 °C.

Adenylylation reactions were prepared by supplementing 15 µl supernatant from expression cultures with 10 µCi [α-^{32}P]ATP (Hartmann Analytic) and 25 µl blank *E. coli* supernatant. Adenylylation activity of NmFic and SoFic constructs was assessed by incubating 60 µg purified protein with 10 µCi [α-^{32}P]ATP (Hartmann Analytic) and 25 µl blank *E. coli* supernatant. Reactions were incubated for 1 h at 30 °C, resolved by SDS–PAGE, and adenylylation was probed by autoradiography. For HYPE(FIC) assays, 15 ng of pure protein was incubated with 1.6 µg of purified GTPases.

Protein expression and purification. pFVS0011 vector (encoding VbhA and VbhT(FIC)) was transformed into *E.coli* BL21 (DE3). *E. coli* cultures were grown at 37 °C in LB medium supplemented with 50 µg ml^{-1} of kanamycin to an OD_{595nm} of 0.6 before induction with 0.3 mM IPTG for 16 h at 23 °C. Vectors pFVS0015 (carrying the *NmFic* gene), pFVS0016 (encoding NmFic(Δ8)), pFVS0037 (encoding NmFic(SE/AA)) were transformed into BL21-AI cells. Cells were incubated overnight in 750 ml LB medium that was supplemented with 50 µg ml^{-1} kanamycin and 1% glucose at 23 °C at 200 r.p.m. until OD_{595nm} of 2 was reached. Bacterial pellets were resuspended in terrific broth medium containing 50 µg ml^{-1} kanamycin to obtain an OD_{595nm} of approximately 1. Protein expression was induced at 23 °C with 0.1% arabinose and 0.5 mM IPTG for 23 h at 200 r.p.m. Plasmids harbouring *HYPE*(*FIC*) and *SoFic* constructs were transformed in *E. coli* Rosetta (DE3) cells and BL21-AI cells, respectively. The proteins were expressed as described for NmFic.

Cells containing overexpressed VbhA–VbhT(FIC) and NmFic were resuspended in lysis buffer containing 20 mM Tris (pH 7.5), 250 mM NaCl and 25 mM imidazole and disrupted using French press. Cell debris was pelleted by ultracentrifugation and the supernatant was applied to a His-Trap column (GE Healthcare). The stable complex was eluted with a gradient of elution buffer containing 20 mM Tris (pH 7.5), 250 mM NaCl and 500 mM imidazole. The protein was then concentrated and injected on a Superdex 75 16/60 gel filtration column (GE Healthcare) equilibrated with 10 mM Tris (pH 7.5) and 100 mM NaCl. The pure proteins were concentrated to 6 mg ml^{-1} for VbhA–VbhT(FIC) and 53 mg ml^{-1} for NmFic.

The same purification protocol was used for NmFic(Δ8) and NmFic (SE/AA), but with an additional intermediate purification step. After affinity purification, the proteins were adjusted to 20 mM Tris (pH 8.5), 25 mM NaCl, applied to a Resource-Q anion exchange column (Amersham Biosciences) and eluted with a linear gradient of NaCl. Peak fractions were concentrated and further purified by gel filtration chromatography. Purified proteins in 10 mM Tris (pH 7.8), 100 mM NaCl were concentrated to 30 mg ml^{-1} for NmFic(Δ8) and 51 mg ml^{-1} for NmFic(SE/AA). SoFic and SoFic(E73G) were purified as described previously[15]. HYPE(FIC), HYPE(FIC/H295A) and HYPE(FIC/E234G) were purified in the same way as NmFic. GST-tagged Cdc42 and Rac1 were expressed and purified as described previously[18,19].

Crystallization. All crystals were obtained at 20 °C (except for NmFic crystals, which were obtained at 4 °C) using the hanging-drop vapour diffusion method after mixing 1 µl protein solution with 1 µl reservoir solution. VbhA–VbhT(FIC) and NmFic(SE/AA) crystallized in 23% (w/v) PEG 3350 and 0.2 M di-ammonium tartrate, and were cryoprotected with 25% (w/v) PEG 3350, 0.2 M di-ammonium tartrate and 10% glycerol. NmFic crystallized in 5% 2-propanol, 0.1 M MES pH 6.0 and 0.1 M Ca-acetate, and was transferred into 8% 2-propanol, 0.1 M MES pH 6.0, 0.1 M Mg-acetate and 15% glycerol, then into 30% glycerol for cryoprotection. NmFic(Δ8) crystallized with 44% (v/v) PEG 600, 0.1 M Na-citrate pH 5.6. No cryoprotection was needed for data collection. In each case, the substrate analogue complex was produced by crystal soaking for 2 h with 10 mM AMPPNP, 10 mM $MgCl_2$.

Structure determination. Statistics of data collection and refinement are given in Supplementary Table 1. Diffraction data were collected at beamline X06SA (PXIII) of the Swiss Light Source (λ = 1.0 Å) at 100 K on a MAR CCD detector, processed using MOSFLM[20], and scaled with SCALA[21]. The structures were determined by molecular replacement (PHASER[22]) using a BepA fragment (PDB code 2JK8[10], residues 30–194) or the uncomplexed NmFic structure (PDB code 2G03, unpublished, Midwest Center for Structural Genomics) as models for structure solution of VbhA–VbhT(FIC) and the different NmFic proteins, respectively. A structure solution of wild-type and mutant NmFic in complex with AMPPNP was straightforward, whereas a weak solution (RFZ = 5.1, TFZ = 3.6) with poor phasing power was obtained for VbhA–VbhT(FIC). The partial model lacking VbhA was refined by rigid-body refinement using REFMAC5 (ref. 23) with three bodies to an R_{free} of 52%. Model extension using the module AutoBuild of the PHENIX package[24] yielded an almost complete model (R/R_{free} = 30.8%/35.2%). The remainder of the molecule was traced manually with COOT[25] and then by full refinement using PHENIX[24]. The Ramachandran plot showed that more than 99% of the residues are in favoured regions of the four structures. The figures were generated with Dino (http://www.dino3d.org).

Prediction of inhibition motif in Fic proteins. All Fic proteins (PFAM release 24, 2,189 proteins) were subjected to a profile-to-profile comparison with sequences from the PDB using HHpred[17]. HHpred builds an alignment of homologues for each query sequence by using iterations of PSI-BLAST searches against the non-redundant database. Secondary structures are then predicted on the PSI-BLAST alignment using PSIPRED[26]. On the basis of this data, a profile Hidden Markov Model (HMM) is generated. Each query profile is compared with the pre-computed HMMs of the proteins in the PDB to identify structural homologues. In terms of query profiles, the PDB profiles include secondary structure information derived from their three-dimensional structure. We analysed the pairwise profile alignments of each Fic protein with the eight different Fic family members deposited in the PDB. A Fic protein was predicted to belong to class II or class III if the templates' inhibitory motifs were aligned to a corresponding query sequence in the profile alignments (see Supplementary Information, section 1).

Phylogenetic analysis of Fic proteins. Phylogenetic trees of the Fic family were inferred with FastTree 2 (ref. 27) and RAxML 7.0.4 (ref. 28). Trees were built on the amino acid alignment provided by the PFAM database. Unaligned overhanging ends were trimmed off and identical sequences were reduced to one representative. We used local support values based on the Shimodaira–Hasegawa test to estimate the reliability of the tree inferred with FastTree2. The RaxML tree was inferred using the PROTMIXWAGF model and 25 rate categories.

Liquid chromatography–mass spectrometry analysis. 2.5 µM of purified NmFic, NmFic(Δ8) or NmFic(SE/AA) were incubated in reaction buffer (10 mM Tris, pH 8, 100 mM NaCl) in the presence or absence of 50 µM ATP and 50 µM $MgCl_2$ for 1 h. Proteins were reduced in 5 mM TCEP, alkylated in

RESEARCH LETTER

10 mM iodacetamid and digested with sequencing grade trypsin (Promega). The generated peptides were purified with C18 Microspin columns (Harvard Apparatus) and analysed using liquid chromatography–mass spectrometry (LC–MS) or MS on an easy nano-LC system coupled to an LTQ-Orbitrap-Velos mass spectrometer (both from Thermo-Fisher Scientific), as recently described[29] using a linear gradient from 95% solvent A (0.15% formic acid, 2% acetonitrile) and 5% solvent B (98% acetonitrile, 0.15% formic acid) to 35% solvent B over 40 min. The data acquisition mode was set to obtain one high-resolution MS scan in the Fourier Transform (FT) part of the mass spectrometer at a resolution of 60,000 (full width at half maximum) and MS–MS scans in the linear ion trap of the 20 most intense ions. The resulting MS2 scans were searched against a *N. meningitidis* protein database containing the target protein sequence, including NmFic and NmFic(SE/AA) sequences, that was obtained from EBI (http://www.ebi.ac.uk) using the SEQUEST search algorithm provided in the Proteome Discoverer software package (Thermo-Fisher Scientific). *In silico* trypsin digestion was performed after lysine and arginine (unless followed by proline), with a tolerance of two missed cleavages in fully tryptic peptides. Database search parameters were set to allow phosphoadenosine modification (+329.05252 Da) of threonine and tyrosine residues as variable modification and carboxyamidomethylation (+57.021464 Da) of cysteine residues as fixed modification. The fragment mass tolerance was set to 0.8 Da and the precursor mass tolerance to 15 p.p.m.

Strain construction. For toxicity experiments, the *vbhT* wild-type gene (FN645515) from *B. schoenbuchensis* R1 was cloned into pRSF-Duet1 (pPE0017, His_6-tagged *vbhT*). VbhT(H136A) (pPE0034) was constructed by introducing a two-base-pair point mutation in the FIC motif of *vbhT* of pPE0017, as described elsewhere[30]. Plasmid co-expressing VbhT and VbhA (VbhT/VbhA) was constructed by cloning *vbhA* (FN645515) amplified from *B. schoenbuchensis* R1 into pRSF-Duet1 (pPE0020, HA-tagged *vbhA*). *vbhT* was then cloned into pPE0020, resulting in pPE0021. To construct VbhT-expressing plasmids for *Bartonella*, *vbhT* from *B. schoenbuchensis* R1 was cloned into vector pMMB206 (ref. 31) (pVbhT, HA-tagged *vbhT*). pVbhT(H136A) was constructed from pVbhT as described before.

The in-frame deletion of the complete *vbhA/vbhT* operon in *B. schoenbuchensis* (*Bsch ΔvbhA/vbhT*) was generated as described previously by a two-step gene replacement procedure[9]. The mutagenesis vector pPE3005 was constructed by ligating a cassette with the flanking regions of the in-frame deletion into pTR1000[9].

For protein purification, the full-length *vbhA* gene and part of the *vbhT* gene encoding the FIC domain (*vbhT*(*FIC*)), amino acid residues 1–198, His_6-tagged) were amplified from plasmid pPE0021 and cloned into the pRSF-Duet1 vector (pFVS0011). VbhA(E24G)/VbhT(FIC) expression plasmid (pFVS0065) was generated by introducing a two-base-pair mutation in pFVS0011. The *NmFic* gene was amplified with an N-terminal His_6-tag from *N. meningitidis* from coding region of amino acid residues 11–191 and from coding region of amino acid residues 11–167 to generate plasmids expressing NmFic (pFVS0015) and NmFic(Δ8) (pFVS0016), respectively. The S182A/E186A double mutant construct (NmFic(SE/AA)) was generated by introducing two subsequent point mutations in pFVS0015. The E186G mutant construct (NmFic(E186G)) was generated by the same approach. The *SoFic* gene was amplified from plasmid (ASU biodesign institute, Clone ID SoCD00104192) and cloned with an N-terminal His_6-tag into pRSF-Duet1 (pFVS0040). The SoFic(E73G) plasmid (pFVS0058) was generated by introducing a two-base-pair point mutation in pFVS0040. GST–HYPE(E234G) (pFVS0064) was generated by introducing point mutations in the plasmid containing GST–HYPE. From these plasmids, shorter constructs (HYPE(FIC), HYPE(FIC/E234G) and HYPE(FIC/H295A)) only carrying the FIC domain of HYPE (from amino acids 187 to 437) were generated. For the expression of human Cdc42 and Rac1, the *Cdc42–Q61L* and *Rac1–Q61L* coding sequences were amplified from plasmid pRK5myc L61 Cdc42[32] and pRK5FLAG L61 Rac1 (ref. 32) and cloned into pGex6p1 with an N-terminal GST-tag, resulting in pAH088 and pAH060, respectively. The wild-type variants of Cdc42 and Rac1 were generated from the mutant constructs through polymerase chain reaction (PCR)-based site-directed mutagenesis[30] (resulting in pAH059 and pAH071). All primers and the resulting vectors are summarized in Supplementary Tables 5 and 6.

18. Self, A. J. & Hall, A. Purification of recombinant Rho/Rac/G25K from *Escherichia coli*. *Methods Enzymol.* **256,** 3–10 (1995).
19. Smith, S. J. & Rittinger, K. Preparation of GTPases for structural and biophysical analysis. *Methods Mol. Biol.* **189,** 13–24 (2002).
20. Leslie, A. G. The integration of macromolecular diffraction data. *Acta Crystallogr. D* **62,** 48–57 (2006).
21. Collaborative Computational Project, Number 4. The CCP4 suite: programs for protein crystallography. *Acta Crystallogr. D* **50,** 760–763 (1994).
22. McCoy, A. J. *et al.* Phaser crystallographic software. *J. Appl. Crystallogr.* **40,** 658–674 (2007).
23. Murshudov, G. N., Vagin, A. A. & Dodson, E. J. Refinement of macromolecular structures by the maximum-likelihood method. *Acta Crystallogr. D* **53,** 240–255 (1997).
24. Adams, P. D. *et al.* PHENIX: a comprehensive Python-based system for macromolecular structure solution. *Acta Crystallogr. D* **66,** 213–221 (2010).
25. Emsley, P. & Cowtan, K. Coot: model-building tools for molecular graphics. *Acta Crystallogr. D* **60,** 2126–2132 (2004).
26. Jones, D. T. Protein secondary structure prediction based on position-specific scoring matrices. *J. Mol. Biol.* **292,** 195–202 (1999).
27. Price, M. N., Dehal, P. S. & Arkin, A. P. FastTree 2—approximately maximum-likelihood trees for large alignments. *PLoS ONE* **5,** e9490 (2010).
28. Stamatakis, A. RAxML-VI-HPC: maximum likelihood-based phylogenetic analyses with thousands of taxa and mixed models. *Bioinformatics* **22,** 2688–2690 (2006).
29. Schmidt, A. *et al.* Absolute quantification of microbial proteomes at different states by directed mass spectrometry. *Mol. Syst. Biol.* **7,** 510 (2011).
30. Zheng, L., Baumann, U. & Reymond, J. L. An efficient one-step site-directed and site-saturation mutagenesis protocol. *Nucleic Acids Res.* **32,** e115 (2004).
31. Dehio, C. & Meyer, M. Maintenance of broad-host-range incompatibility group P and group Q plasmids and transposition of Tn5 in *Bartonella henselae* following conjugal plasmid transfer from *Escherichia coli*. *J. Bacteriol.* **179,** 538–540 (1997).
32. Rhomberg, T. A., Truttmann, M. C., Guye, P., Ellner, Y. & Dehio, C. A translocated protein of *Bartonella henselae* interferes with endocytic uptake of individual bacteria and triggers uptake of large bacterial aggregates via the invasome. *Cell. Microbiol.* **11,** 927–945 (2009).

SUPPLEMENTARY INFORMATION

doi:10.1038/nature10729

Content:

1. Supplementary Text

1.1 Defining an adenylylation competent FIC signature motif

Based on sequence conservation, previous mutagenesis results, and the structure of the competent NmFic(Δ8)/AMPPNP complex (Supplementary Fig. 10b), we have defined the HxFx[D/E]GNGRxxR profile as the crucial core motif for catalytically active Fic proteins with respect to adenylylation. The histidine residue (H) has been shown in several studies[1,2] to be essential for activity and probably acts as a general base for deprotonation of the target side-chain hydroxyl group[2,3]. The phenylalanine (F) is part of the hydrophobic core and important for correct positioning of the active loop. It remains unclear whether other hydrophobic residues could replace the phenylalanine. Strikingly, all Fic proteins so far shown to exhibit adenylylation activity harbour a phenylalanine at this position. The carboxylic side-chain of the aspartic/glutamic acid (D/E) probably coordinates the divalent cation (Mg^{2+} or Mn^{2+}) that is required for activity (data not shown). However, in the competent substrate complex structure (Supplementary Fig. 10b) it is partly disordered. As predicted before[2] and confirmed by the competent AMPPNP complex structure (Supplementary Fig. 10b), the three backbone amide nitrogens of GNG are involved in α- and β- phosphate binding. No other residue than a glycine is allowed for the two G positions, since side-chains would clash with the core of the protein or the ATP substrate, respectively. The asparagine side-chain is involved in positioning of the α-phosphate and establishes two H-bonds with the backbone amide and carbonyl group of the active site phenylalanine residue. Finally, the two arginines are forming a salt-bridge with the β- and γ-phosphate, respectively (Supplementary Fig. 10b). For all residues of the motif, single point mutants have been constructed except for the first glycine and first arginine that showed reduced or negligible auto-adenylylation and/or target adenylylation[1-5], thereby highlighting the

importance of these conserved residues. Thus, based on current structural and biochemical knowledge, we can assume that Fic proteins with a motif conforming to the consensus HxFx[D/E]GNGRxxR are likely to represent AMP transferases. In contrast, proteins divergent from this motif have most probably lost adenylylation activity.

1.2 Prediction and analysis of the three regulatory classes of Fic proteins

While class I proteins were identified by Psi-Blast for the detection of VbhA-homologous peptides encoded in the upstream region of *fic* loci, we used a structure based approach to detect class II and class III Fic proteins. The program HHpred predicts structures of distant homologs from proteins deposited in structure databases[6]. The analysis is based on a profile-to-profile comparison of Hidden Markov Models (HMMs) generated from Psi-Blast and secondary structure predictions (see Online Methods). We conducted an HHpred analysis for each protein in the FIC family (PFAM release 24, 2,189 proteins) using the protein structure database PDB. The PDB contains structures of FIC domains from eight different proteins: (i) 3dd7, DocH66Y of prophage P1 in complex with the C-terminal domain of Phd; (ii) 2jk8, BepA of *Bartonella henselae,* a type IV secretion system effector protein; (iii) 3n3u, IbpA of *Histophilus somni*, a protein secreted into host cells; (iv) 3let, VopS of *Vibrio parahaemolyticus*, a Type III secretion system effector protein; (v) 2f6s, Fic protein of *Helicobacter pylori* (HpFic); (vi) 2g03, Fic protein of *Neisseria meningitidis* (NmFic); (vii) 3eqx, Fic protein of *Shewanella oneidensis* (SoFic); (viii) 3cuc, Fic protein of *Bacteroides thetaiotaomicron* (BtFic). For all Fic proteins analyzed with HHpred, we detected significant structural homology with these eight FIC domain structures in the PDB. Based on the corresponding HHpred alignments, we validated each Fic protein for the presence of an N-terminal (class II) or C-terminal (class III) inhibition motif. Fic proteins were predicted to fall into one of these two classes, if the structural alignments with the two structural prototypes of

a class (for class II, SoFic and BtFic; for class III, NmFic and HpFic) included the region comprising their inhibition motif. The segment of the query sequence aligning with the inhibition motifs of a given class was then identified as the putative inhibition motif of the query protein. Only proteins for which both alignments predicted the same inhibition motif were categorized into the corresponding class.

Supplementary Tables 4a-e show that for most proteins, predicted to fall into one of the two classes, the corresponding template structures resulted in the highest homology scores among the eight Fic proteins in our HHpred analysis. Further, the inhibition motifs independently predicted from the two template structures, turned out to be the same for most Fic proteins. Finally, only four proteins were identified to belong to more than one of the three classes. Altogether, this demonstrates the high specificity of our analysis for the prediction of these regulatory features.

Strikingly, the consensus sequence of all motifs from class I, II, and III converges towards the general inhibition motif [S/T]xxxE[G/N]. The glutamate (E24 of VbhA), thereby, displays the most conserved amino acid, which is consistent with the presented mechanism of inhibition (Fig. 3).

As mentioned in the main text, in comparison to the entire family, the total number of proteins predicted to fall into one of the three regulatory classes is significantly increased in the subset of Fic proteins harbouring the adenylylation-competent FIC motif HxFx[D/E]GNGRxxR (see Supplementary Text 1.1). Thus, the inhibition motif seems to be a specific feature of proteins with adenylylation activity and indicates co-evolution of these two functional features. In contrast to this general trend, the relative number of class I proteins (regulated by an antitoxin-like protein) decreases in the subset of Fic proteins with a conserved FIC motif. This can be explained by the fact that a significant fraction of class I comprises proteins from *E. coli* and related species which harbour a serine instead of an

asparagine and a leucine instead of arginine (1st position) in the active loop. It remains to be elucidated whether HxFx[D/E]GSGLxxR either can still mediate adenylylation or has evolved another activity which is regulated by a similar mechanism as adenylylation.

Interestingly, class I and III are restricted to bacteria (which present 90% of all Fic proteins), while in archaea and eukaryotes only class II inhibition motifs were predicted (Supplementary Table 2). Most of the metazoan Fic proteins including the human homolog HYPE as well as some of the fungal Fic proteins are predicted to contain a class II regulatory motif suggesting that this regulatory mechanism of adenylylation activity is conserved in all domains of life.

1.3 Prediction of regulatory classes for selected Fic proteins

The classification based on the presence/absence of an inhibition motif is listed in Supplementary Table 3 for a subset of Fic proteins which were previously studied. For VopS, the effector protein of *Vibrio parahaemolyticus*, our analysis did not predict an inhibition motif. This is in agreement with the 3D structure of VopS[3], which does not reveal any regulatory helix positioned next to the FIC active site.

In case of the second bacterial virulence factor for which adenylylation activity in eukaryotic host cells was described, IbpA[4], our analysis predicted an N-terminal inhibition motif (class II). However, the 3D structure of IbpA does not show this predicted inhibition motif to be located in the active center of the FIC domain[1]. Thus, our prediction for IbpA may be a false positive. Both VopS and IbpA are translocated into eukaryotic host cells, where they adenylylate proteins of the Rho family GTPases. This leads to the collapse of the actin cytoskeleton and subsequently to cell death[4,5]. In general, effector proteins of bacterial pathogens that aim at killing or dramatically subverting the cells of their eukaryotic hosts (e.g.

immune cells) by adenylylation of cellular targets might not need to be regulated. Further, due to their specificity for eukaryotic targets, they may not be toxic for the bacterium before translocation and would thus not require an inhibited state.

However, for effector proteins of *Bartonella,* our Psi-Blast analysis identified homologs of VbhA located upstream of the effector gene loci. In contrast to VopS and IbpA, the effector proteins of *Bartonella* seem to have a much more subtle effect on host cells[7]. It remains to be elucidated whether for *Bartonella* effector proteins co-translocation of a VbhA-homolog into host cells allows regulation of adenylylation activity.

Like the bacterial virulence factors IbpA or VopS, the human Fic protein HYPE, was shown to adenylylate the GTPases RhoA, Rac1, and Cdc42[4]. The conserved N-terminal inhibition motif identified for HYPE and other mammalian Fic proteins might explain why HYPE, in contrast to IbpA or VopS, did not show any cytotoxic effect on mammalian cells[4]. Thus, the here-identified regulatory mechanism might be essential for the tight regulation of mammalian Fic proteins and their integration into key signaling pathways of mammals.

Doc proteins share the same structural fold as Fic proteins and are thus grouped into the FIC PFAM family (which is also referred to as Fic/Doc family). They constitute the toxins of toxin-antitoxin modules homologous to the post-segregational killing system Doc/Phd of Bacteriophage P1[8]. In our phylogenetic analysis (Supplementary Fig. 7), Doc proteins form a separate cluster clearly distinct from the remaining Fic proteins. Furthermore, their core motif (Supplementary Table 3) is highly divergent from the adenylylation competent motif as defined above (see Supplementary Text 1.1). Consistently, our HHpred and Psi-Blast analyses did not identify any adenylylation-inhibiting motif for Doc-related proteins. Nevertheless, Doc activity is inhibited by the antitoxin Phd which binds in a similar way as VbhA to VbhT (Supplementary Fig. 5). Doc-mediated toxicity on bacteria results from binding to the 30S ribosomal subunit, but the exact underlying mechanism of Doc-mediated toxicity remains

elusive and adenylylation activity has not been reported[9]. Still, inhibition of Doc toxicity by mutation of the histidine in the central motif of the FIC domain indicates its involvement in mediating the toxic effect[10]. For Doc as well as for other Fic proteins carrying a motif divergent from the adenylylation-competent consensus profile, the FIC domain could mediate other enzymatic activities[11]. Catalytic versatility of the FIC domain fold would further explain why this protein family is so abundant in a wide range of organisms.

1.4 Mass spectrometry (MS) results for the identification of the auto-adenylylation site of NmFic

In order to specifically pinpoint the location of the adenylylation in the FIC domain and to verify the results obtained for the adenylylation assay (Fig. 3d), a mass spectrometric analysis of the trypsinized NmFic protein samples was performed. As apparent from Supplementary Fig. 8a, the majority of the adenylylation could be identified at position Y6 in the displayed peptide sequence. Additional conformation was obtained by the identification of the same adenylylation site on the same peptide containing the C-terminal glycine as consequence of incomplete proteolysis (Supplementary Fig. 8b). However, due to the close proximity of the tyrosine residues, it cannot be excluded that Y7 or Y8 are also modified. Comparative analysis of the NmFic and NmFic(Δ8) mutant clearly indicates a strong increase in adenylylation for this domain (Supplementary Fig. 8c). Notably, we covered the whole protein sequence by MS analysis and could only identify adenylylation at the C-terminal tyrosine residues of this protein, indicating exclusive adenylylation of this protein at these sites and confirming the results obtained in Fig. 3d.

MS analysis of the NmFic(SE/AA) mutant revealed a higher degree of adenylylation, which is indicated by the identification of more and multiple adenylylated peptide species (Supplementary Fig. 9), again, confirming the observations made in Fig. 3d.

2. Supplementary Figures

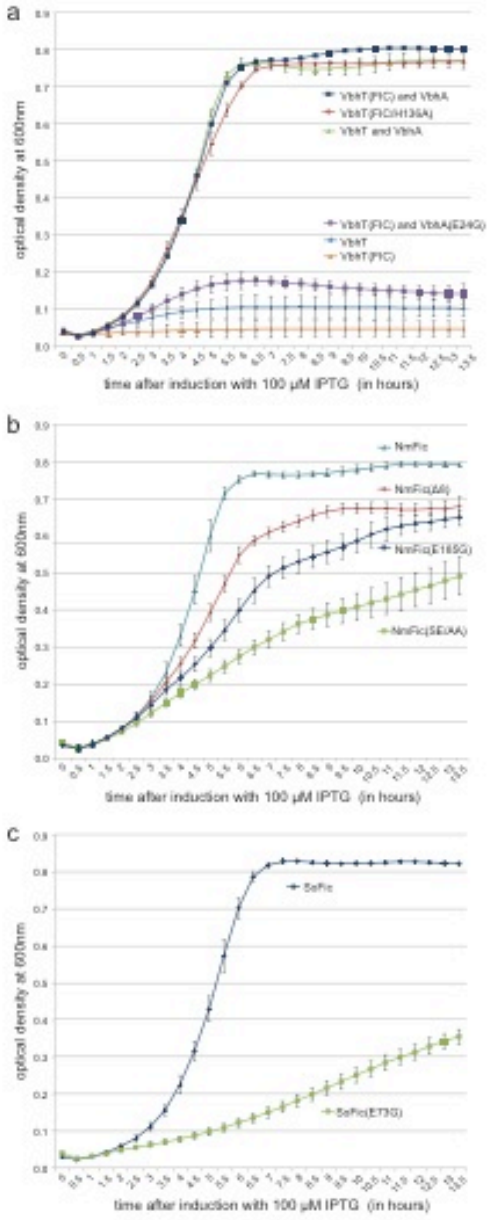

Supplementary Figure 1. Growth curves of *E. coli* MG1655 expressing different constructs of (a) VbhA-VbhT, (b) NmFic, or (c) SoFic. Cultures were inoculated with 5 µl

of an overnight culture and induced with 100 μM IPTG. Bacterial growth was measured by monitoring the optical density at 600 nm every 30 minutes. All experiments were carried out in quadruplicates.

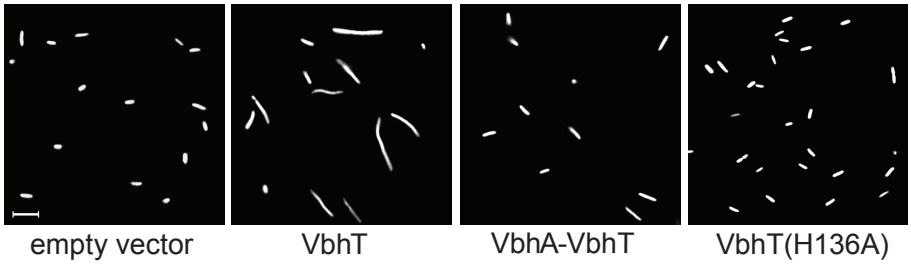

Supplementary Figure 2. Cell filamentation of *E. coli* upon expression of VbhT is repressed by co-expression of VbhA. Fluorescence microscopy of *E. coli* harbouring a GFP-reporter plasmid (pC10E) in addition to the same VbhA-VbhT-expression plasmids as presented in Fig. 1c (scale bar, 5 μm). Cell filamentation of *E. coli* observed upon VbhT expression is not evident for VbhT(H136A) or VbhA-VbhT.

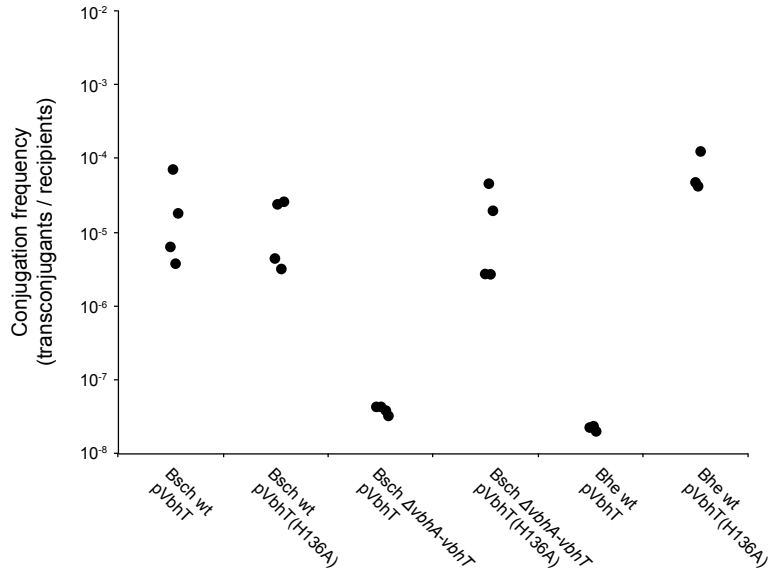

Supplementary Figure 3. Conjugation of VbhT expression plasmids into *Bartonella schoenbuchensis* and *Bartonella henselae* reveals toxicity of VbhT in the absence of *vbhA*. Conjugation frequencies are given by the number of transconjugants per recipient as determined by dilution plating and counting of colony forming units on media selective for either transconjugants or recipients. Conjugation of a plasmid expressing VbhT wild-type (pVbhT) into *B. schoenbuchensis* wild-type (Bsch wt) resulted in a conjugation frequency of about 10^{-5}. In contrast, conjugation of the same plasmid into *B. schoenbuchensis* harbouring a deletion of the complete *vbhA-vbhT* operon (Bsch Δ*vbhA-vbhT*) or into *B. henselae* wild-type (Bhe wt), which does not encode *vbhA,* gave no transconjugants in four and three independent experiments, respectively. This resulted in conjugation frequencies < 10^{-7} (when taking the detection threshold in our experiments into account). The inability to conjugate the plasmid into these strains was dependent on a functional FIC motif: a plasmid expressing VbhT with an adenylylation-deficient FIC motif (pVbhT(H136A)) could be conjugated into Bsch Δ*vbhA-vbhT* and Bhe wt with a similar frequency as into Bsch wt.

RESEARCH SUPPLEMENTARY INFORMATION

Supplementary Figure 4. Protein alignment of translated ORFs with homology to VbhA encoded in the upstream region *of fic* gene loci. We used Psi-Blast to query the VbhA protein sequence against all translated ORFs (>10 aa) found in the 500 bp upstream of loci

encoding Fic proteins. In total, this analysis identified 158 ORFs with homology to VbhA. 127 ORFs are overlapping with the corresponding *fic* gene, together constituting putative operons. From the remaining 31 ORFs, 20 are less than 100 bp away from the annotated start codon of the *fic* gene. In the depicted alignment, sequences identical to each other were reduced to one representative resulting in 87 aligned sequences including VbhA. Overhanging ends were trimmed. Start and end positions of the aligned sequences are indicated. The consensus sequence logo is depicted on top of the alignment indicating the conserved central motif. The alignment was generated with MUSCLE[12] (implemented in Geneious v5.3.6) and manually curated. Shading of amino acids indicates degree of conservation. Sequences used in the alignment of Fig. 1b are highlighted in red color.

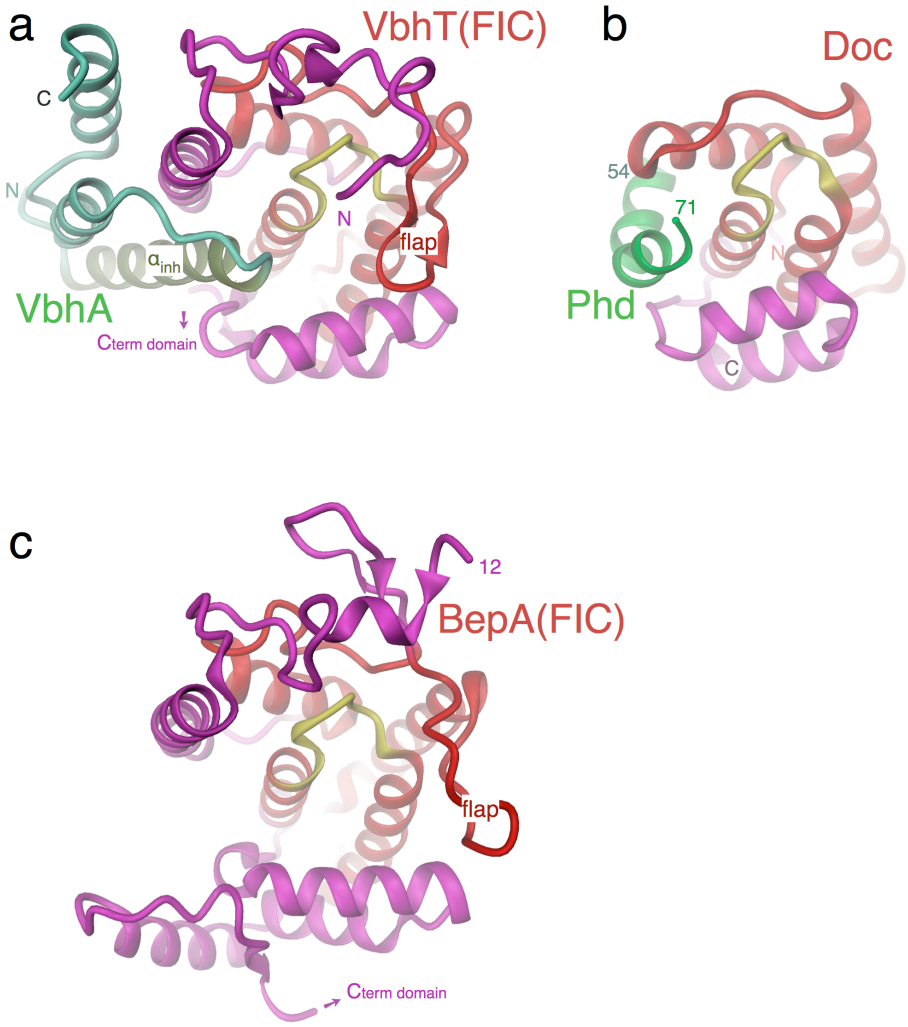

Supplementary Figure 5. Comparison of FIC domain folds and FIC/antitoxin interactions. a, VbhA-VbhT(FIC) from *B. schoenbuchensis*. The VbhT(FIC) structure is highly similar to that of BepA(FIC)[2] (rmsd of 1.6 Å for 169 C_α-positions, panel c). **b**, Doc/Phd from Bacteriophage P1[13], PDB code 3dd7). **c**, BepA(FIC) from *B. henselae*[2]. Representations of the structures as in Fig. 2.

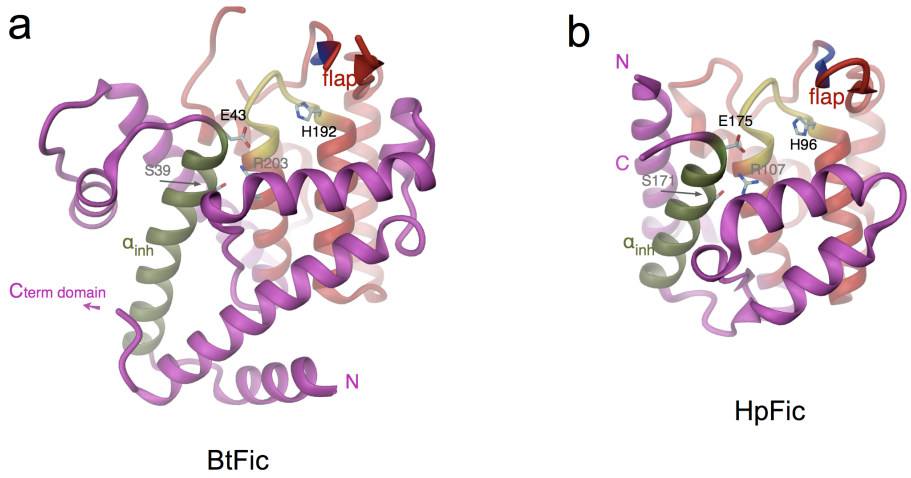

Supplementary Figure 6. Fic protein structures BtFic (BT2513 from *Bacteroides thetaiotaomicron*, PDB code 3CUC) (a) and HpFic (HP1159 from *Helicobacter pylori*, PDB code 2F6S) (b). Structures are shown in cartoon representation as in Fig. 2 (Fic core as defined by PFAM, red; active site loop with histidine, yellow; inhibitory helix (α_{inh}) with C-terminal SxxxEG motif, green; termini labeled with N and C) with important residues in full. Note that BtFic and HpFic are class II and III Fic proteins, respectively, and are close structural homologs of SoFic(Fig. 2b) and NmFic (Fig. 2c).

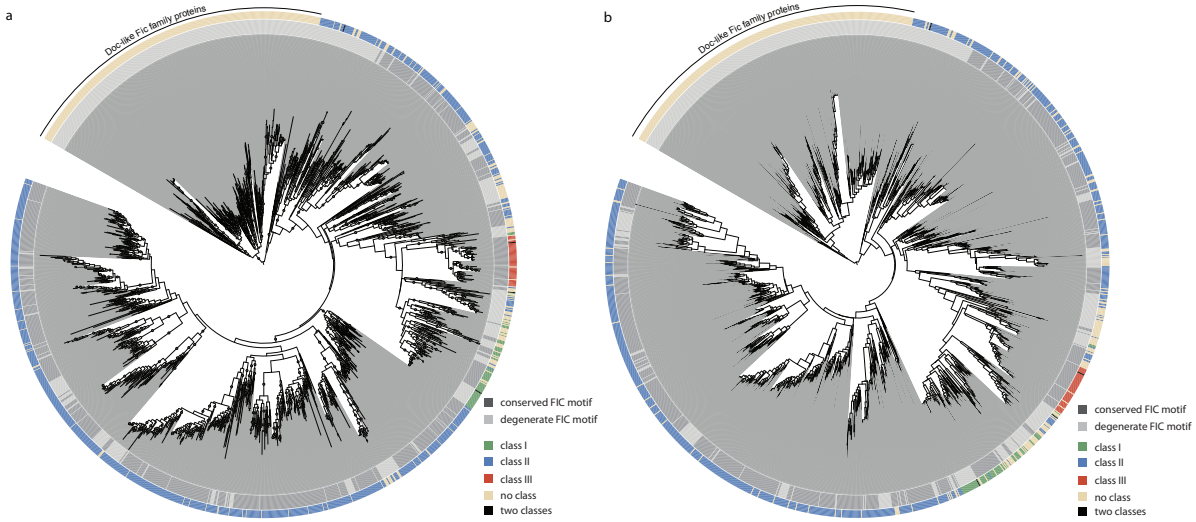

Supplementary Figure 7. **Phylogenetic trees of Fic proteins.** a, Approximately-maximum-likelihood tree inferred with FastTree2. Local support values were calculated as implemented in FastTree2[14] using the Shimodaira-Hasegawa test. Circles indicate branches with local support values > 0.9. b, Maximum-likelihood tree inferred with RAxML[15] using the PROTMIXWAG model. Dark and light grey coloring on the inner circle indicates the presence (conserved) or absence (degenerate) of the adenylylation competent motif, respectively. The outer circle depicts the class assigned to each Fic protein conforming the coloring of Fig. 2e. The large cluster of Doc-like proteins lacking the conserved FIC motif is indicated. An interactive version of the tree with species and accession number labels for each leaf can be accessed via the following link http://itol.embl.de/shared/Engel2011.

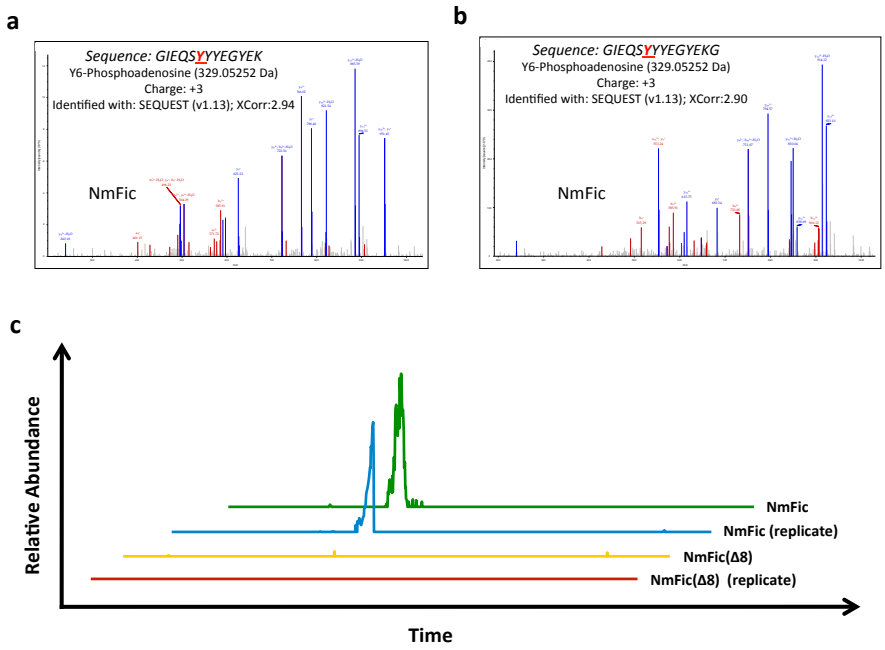

Supplementary Figure 8. LC-MS/MS analysis of adenylylated NmFic protein. a, MS/MS-spectrum of the fully cleaved peptide GIEQSYYYEGYEK at a charge state of 3 using CID. The identified adenylylation sites are underlined in the peptide sequence and indicated in red. All correctly assigned y- and b- fragment ions are indicated in blue and red, respectively, unassigned fragment ions are shown in gray. **b,** MS/MS-spectrum of the incompletely cleaved peptide GIEQSYYYEGYEKG showing the same modification. **c,** Extracted ion chromatograms of the fully cleaved peptide displayed in panel a for the different samples analyzed.

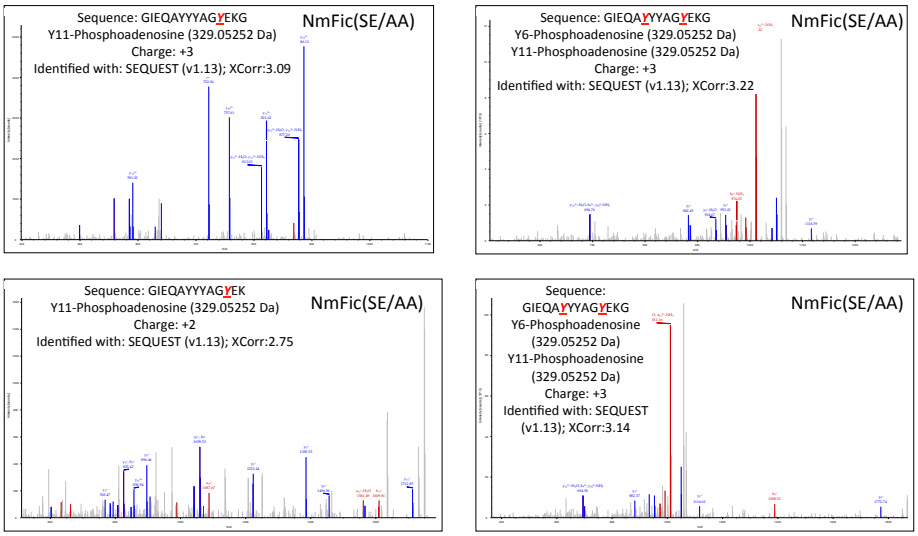

Supplementary Figure 9. LC-MS/MS analysis of adenylylated NmFic(SE/AA) protein. Four MS/MS-spectra are displayed showing the most significant adenylylated peptide sequences identified in the NmFic(SE/AA) mutant. The identified adenylylation sites are underlined in the peptide sequence and indicated in red. All correctly assigned y- and b-fragment ions are indicated in blue and red, respectively, unassigned fragment ions are shown in gray.

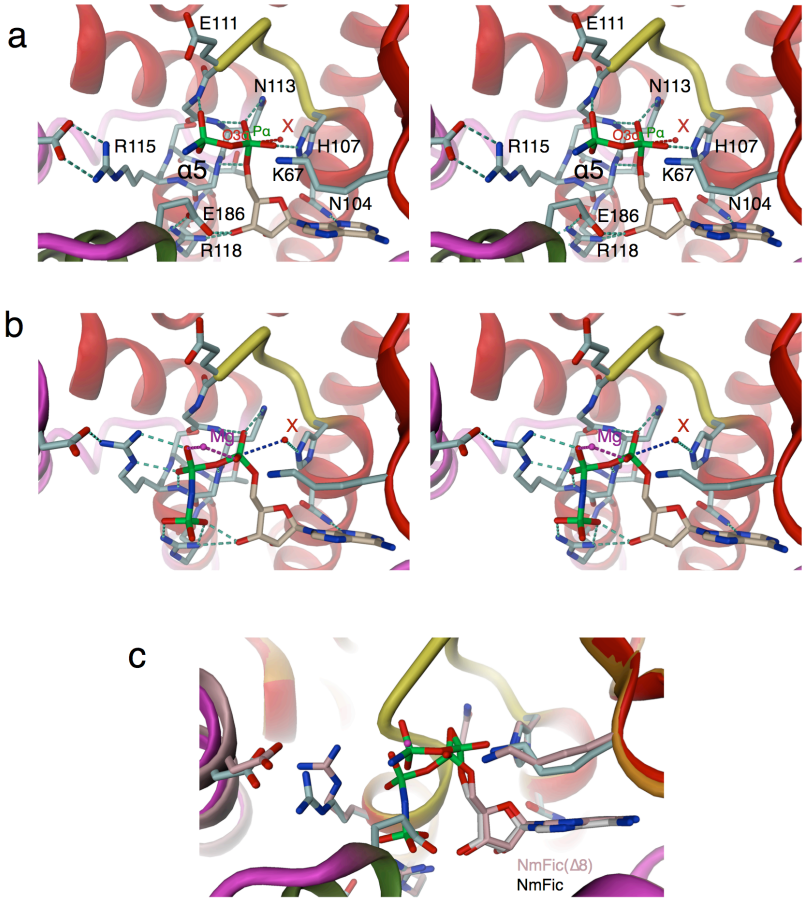

Supplementary Figure 10. AMPPNP binding to NmFic and NmFic(Δ8). The stereoviews of NmFic (a) and NmFic(Δ8) (b) show the detailed interactions of the nucleotide with the Fic active site with H-bonds marked by stippled lines in aquamarine. The structure represenations show similar views as in Figs 3a and b, but with the N-terminal end of helix α5 shown in full to visualize the capping interactions of the α- and β-phosphate with the helix. Additionally, the position that would have to be adopted by a target hydroxyl group for productive nucleophilic attack inline with the scissile Pα-O3α bond is indicated by a small red sphere (marked X) with the X - Pα distance set to 3.0 Å. (c) Superposition of NmFic (gray carbons) and NmFic(Δ8) (orange carbons).

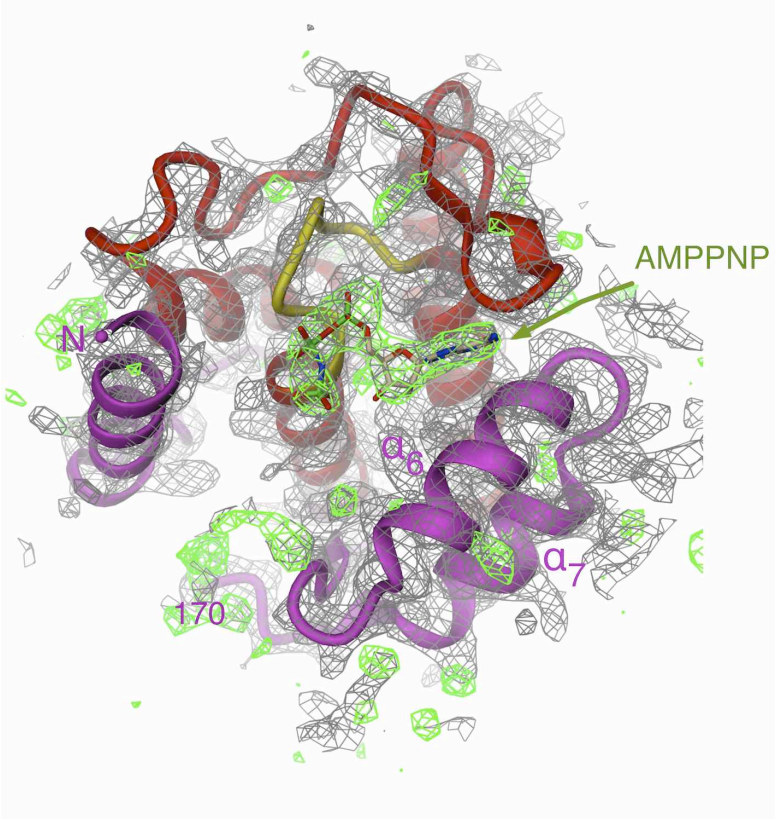

Supplementary Figure 11. Crystal structure of NmFic(SE/AA). The schematic cartoon of chain A is shown in the same representation as in Fig. 2a. Note that (as in all other 15 molecules of the asymmetric unit) helix α_{inh} which follows α7 is disordered as evidenced by missing electron density. The AMPPNP substrate analog, however, is fully resolved and found in the same conformation and orientation as in the corresponding NmFic(Δ8)/AMPPNP structure (Fig. 3b). The ligand has been omitted from phasing. The 2Fo-Fc density map is shown in grey (1.2 σ), the Fo-Fc map in green (3.0 σ).

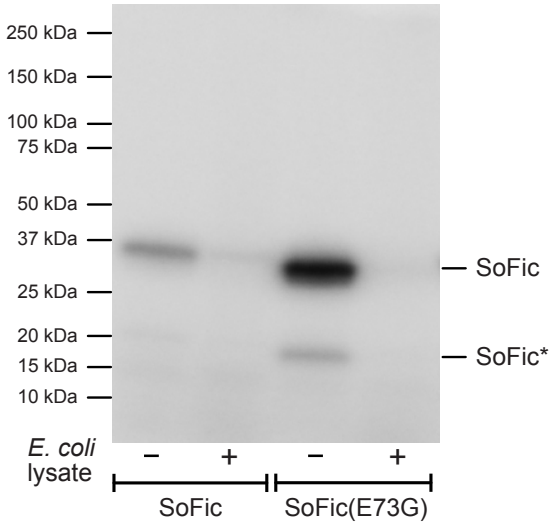

Supplementary Figure 12. Autoradiography of an SDS-gel after incubation of SoFic and SoFic(E73G) with α-^{32}P-ATP in the presence or absence of *E. coli* lysate. Auto-adenylylation is drastically increased in the SoFic(E73G) mutant. SoFic* indicates a truncated version of SoFic as evidenced by mass spectrometry. No target bands are revealed upon incubation with *E. coli* lysate. It is conceivable that the target is a small, unresolved peptide or DNA.

RESEARCH SUPPLEMENTARY INFORMATION

3. Supplementary Tables

Supplementary Table 1. Data collection and refinement statistics.

	VbhA-VbhT(FIC)	NmFic	NmFic(Δ8)	NmFic(SE/AA)
Data collection				
Space group	C2	$P6_422$	$P2_1$	$P2_1$
Cell dimensions				
a, *b*, *c* (Å)	106.34, 40.37, 73.79	148.96, 148.96, 75.80	73.94, 65.03, 75.99	110.31, 136.92, 114.66
α, β, γ (°)	90.00, 121.40, 90.00	90.00, 90.00, 120.00	90.00, 107.08, 90.00	90.00, 100.26, 90.00
Resolution (Å)	45.21-1.50(1.58-1.50) *	65.35-2.15(2.27-2.15) *	37.03-1.7(1.79-1.70) *	87.07-3.02(3.19-3.02) *
R_{sym} or R_{merge}	6.3(23.8)	9.3(46.9)	6.9(37.3)	11.2(35.2)
$I/\sigma I$	9.1(2.0)	18.5(4.0)	9.8(2.6)	6.9(2.2)
Completeness (%)	96.2(74.8)	99.1(93.9)	97.7(95.4)	89.0(43.1)
Redundancy	3.8(2.0)	13.6(8.8)	4.0(3.5)	3.8(2.1)
Refinement				
Resolution (Å)	15.0-1.50	15.0-2.15	15.0-1.7	15.0-3.02
No. reflections	41,211(4,622)	27,218(3,678)	73,865(10,470)	58,488(4,120)
R_{work}/ R_{free}	18.0/21.5	18.8/21.3	15.9/19.7	22.2/24.8
No. atoms				
Protein	2173	1681	5076	21120
Ligand/ion	2 TAR	1 ANP	4 ANP, 4 MG, 4 P6G	16 ANP
Water	255	189	424	-
B-factors				
Protein	22.1	37.2	18.4	66.4
Ligand/ion	22.2	44.8	34.6	36.5
Water	31.1	47.8	24.4	-
R.m.s deviations				
Bond lengths (Å)	0.012	0.012	0.010	0.009
Bond angles (°)	1.3	1.2	1.3	1.1

*Highest resolution shell is shown in parenthesis.

Supplementary Table 2. Distribution of Fic proteins from different domains of life in the three regulatory classes I to III.

	Data analyzed			Distribution of Fic proteins into the different regulatory classes I to III													
				class I[d]		class II[e]		class III[f]		no class		class I and II		class I and III		class II and III	
Domain	**Dataset[a]**	**Proteins[b]**	**Domains[c]**	#	%	#	%	#	%	#	%	#	%	#	%	#	%
All	FIC family	2189	2191	156	7.12	1217	55.55	73	3.33	741	33.82	1	0.05	1	0.05	2	0.09
	conserved FIC motif	1129	1131	50	4.42	898	79.40	72	6.37	110	9.73	0	0.00	0	0.00	1	0.09
Bacteria	FIC family	2072	2074	154	7.03	1146	52.30	73	3.33	697	31.81	1	0.05	1	0.05	2	0.09
	conserved FIC motif	1058	1059	50	4.42	834	73.74	72	6.37	102	9.02	0	0.00	0	0.00	1	0.09
Archaea	FIC family	49	49	0	0.00	30	1.37	0	0.00	19	0.87	0	0.00	0	0.00	0	0.00
	conserved FIC motif	26	26	0	0.00	26	2.30	0	0.00	0	0.00	0	0.00	0	0.00	0	0.00
Eukaryota	FIC family	59	59	0	0.00	38	1.73	0	0.00	21	0.96	0	0.00	0	0.00	0	0.00
	conserved FIC motif	40	40	0	0.00	35	3.09	0	0.00	5	0.44	0	0.00	0	0.00	0	0.00
Viruses	FIC family	5	5	0	0.00	2	0.09	0	0.00	3	0.14	0	0.00	0	0.00	0	0.00
	conserved FIC motif	4	4	0	0.00	2	0.18	0	0.00	2	0.18	0	0.00	0	0.00	0	0.00
Unclass[g]	FIC family	1	1	0	0.00	1	0.05	0	0.00	0	0.00	0	0.00	0	0.00	0	0.00
	conserved FIC motif	1	1	0	0.00	1	0.09	0	0.00	0	0.00	0	0.00	0	0.00	0	0.00
Other[g]	FIC family	3	3	2	0.09	0	0.00	0	0.00	1	0.05	0	0.00	0	0.00	0	0.00
	conserved FIC motif	1	1	0	0.00	0	0.00	0	0.00	1	0.09	0	0.00	0	0.00	0	0.00

[a] we analyzed the entire FIC PFAM family (PFAM release 24) as well as a subset of Fic proteins harbouring an adenylylation-competent core motif (conserved FIC motif, HxFx[D/E]GNGRxxR),
[b] number of proteins analyzed,
[c] number of domains analyzed; two proteins harbour two FIC domains,
[d] class I, antitoxin-like ORF harbouring inhibition motif,
[e] class II, N-terminal inhibition motif,
[f] class III, C-terminal inhibition motif,
[g] Unclass" stands for unclassified Fic proteins, "Other" comprises three Fic proteins from plasmid sequences sampled from the environment

Supplementary Table 3. Prediction of class I, class II, and class III inhibition motifs for selected Fic proteins.

						HHpred results[d]																	
						class II structures						class III structures						Structures without class II or III regulatory features					
		predicted regulatory features (class I-III)[c]				SoFic (3eqx)			BtFic (3cuc)			NmFic (2g03)			HpFic (2f6s)			Doc (3dd7)		BepA (2jk8)		VopS (3let)		IbpA (3n3u)	
Fic protein[a]	FIC motif[b]	class I	class II	class III	none	rank#	score	motif	rank#	score	motif	rank#	score	motif	rank#	score	motif	rank#	score	rank#	score	rank#	score	rank#	score
BepA (CAD89506)	HPFREGNGRTQR	yes[e]	no	no	no	7	84	no	4	130	no	3	226	no	2	240	no	8	41	1	686	6	92	5	105
IbpA_FIC1 (BAC78649)	HPFAEGNGRMAR	no	yes	no	no	3	237	GSAVDD	2	250	GSAVDD	5	162	no	6	155	no	8	59	7	137	4	207	1	427
IbpA_FIC2 (BAC78649)	HPFAEGNGRMAR	no	yes[f]	no	no	4	210	TKVIED	3	228	TKVIED	6	163	no	7	149	no	9	57	8	129	5	194	1	488
VopS (BAC59949)	HGFTDGNGRMGR	no	no	no	no	4	48	no	3	50	no	2	52	no	6	43	no	8	24	7	41	1	426	5	47
Doc (CAA66833)	HIFNDANKRTAL	no	no	no	no	6	72	no	3	79	no	4	75	no	5	73	no	1	279	2	86	8	71	7	72
E.coli_Fic (AAA23773)	HPFRVGSGLAQR	yes[g]	no	no	no	6	170	no	4	197	no	3	233	no	2	240	no	8	60	1	326	7	141	5	178
Hype/FicD (AAO89351)	HPFIDGNGRTSR	no	yes	no	no	4	267	TVAIEG	1	379	TVAIEG	5	226	no	6	209	no	8	81	7	193	2	366	3	292
SoFic (AAN57237)	HPFIDGNGRTGR	no	yes	no	no	1	616	SSEIEN	2	286	SSEIEN	4	171	no	6	156	no	8	58	7	150	5	169	3	270
BtFic (AAO77620)	HPFEDGNGRIAR	no	yes	no	no	2	283	SNHLEG	1	492	SNHLEG	5	216	no	6	193	no	8	77	7	180	4	242	3	269
NmFic (NP_273311)	HPFLEGNGRSTR	no	no	yes	no	6	150	no	4	193	no	1	363	SYYYEG	2	338	SYYYEG	8	61	3	218	7	143	5	171
HpFic (ACI27853)	HPFLEGNGRATR	no	no	yes	no	7	145	no	4	187	no	2	316	SYYYEG	1	348	SYYYEG	8	63	3	208	6	148	5	171

[a]protein name and genbank accession
[b]grey shading indicates conserved FIC motif (HxFx[D/E]GNGRxxR)
[c]based on Psi-Blast and HHpred analysis, class I: antitoxin-like ORF harbouring inhibition motif; class II: N-terminal inhibition motif; class III: C-terminal inhibition motif
[d]results of the HHpred alignments with each of the eight template structures from the FIC family, the rank of each alignment, the alignment score, and the presence of an inhibition motif for class II and class III are indicated.
[e]accession of the antitoxin-like ORF: YP_034061
[f]in the IbpA xtal structure (3n3u) the identified motif locates to a loop preceding a helix α6 that is roughly in the position of a canonical α_{inh} (see Supplementary Text)
[g]accession of the antitoxin-like ORF: NP_417821

Supplementary Table 4. Classification of all PFAM FIC domain-containing proteins according to the presence of an antitoxin or an intrinsic inhibition motif. Due to its bulkiness, the table is provided as an extra file in Excel format on http://www.nature.com/nature.

Supplementary Table 5. List of primers used in this study.

Primer name	Sequence (5'-3')
prPE484	CCGCTCGAGGTGAGGAAATATGAGGGTAGC
prPE485	CCGCTCGAGTTACCTTGTAATTCCCTTTGAAG
prPE500	CCGGAATTCAAGAAGGAGATATACATGAGACCATGGCCTACCCATAC
prPE501	CCGGAATTCTTACCTTGTAATTCCCTTTGAAG
prPE519	GGAAGATCTTCATATTTCCTCACGTTTTATCCG
prPE520	GGGAATTCCATATGGCCTACCCATACGATGTTCCAGATTACGCGGCCGCGATGTTGAGCGAGGAAGAAATC
prPE526	CGGGATCCAGCTGCACTTTATAATGTTCCTC
prPE527	ATTACATCTCCTTCAATTACCTA
prPE530	TAGGTAATTGAAGGAGATGTAATTAATTGCAATTATATTATTTCTTGAC
prPE517	CGGGATCCCATCAATGCTTGAAGGAATATGG
prAH095	CGGGATCCATGCAGACAATTAAGTGTGTTG
prAH097	CCGCTCGAGTTAGAATATACAGCACTTCCT
prAH106	CGGGATCCATGCAGGCCATCAAGTGTGT
prAH107	CCGCTCGAGTTACAACAGCAGGCATTTTC
prAH116	GAATGCGTTGGCCCCGTTTCGAGAAGGTAATGGACGTAC
prAH127	CCTTCTCGAAACGGGGCCAACGCATTCAATTCGCCCATG
prAH138	GGGATACAGCTGGACAGGAAGATTATGACAGATTACGCCCCC
prAH139	CTGTCATAATCTTCCTGTCCAGCTGTATCCCATAAGCCCAG
prAH181	CTTTTTGATACTGCAGGGCAAGAGGATTATGACAGATTACG
prAH182	CATAATCCTCTTGCCCTGCAGTATCAAAAAGTCCAAGAGTATATGG
prAG041	GCGCCCATGGTGTTGAGCGAGGAAGAAATCG
prAG042	CGCGGATCCTCATATTTCCTCACGTTTTATCC
prFVS037	GGGAATTCCATATGGTGAGGAAATATGAGGGTAGC
prFVS001	CGACCTCGAGTTAGTGATGGTGATGGTGATGTGTAAATTCAGTGAGGTTTCTAC
prFVS007	GGGAATTCCATATGCATCACCATCACCATCACATGAAATCCATAGACGAACAAAG
prFVS008	CGACCTCGAGTCAGCCTTTTTCATACCCTTCG
prFVS009	CGACCTCGAGTTAGTCAGTCAGGTTGTCCTTTAAC
prFVS010	CAGGCCTATTATTACGCAGGGTATGAAAAAG
prFVS011	CCTGCGTAATAATAGGCCTGCTCGATAC
prFVS026	GTATCGAGCAGGCGTATTATTACGCAGGGTATG
prFVS027	GTAATAATACGCCTGCTCGATACCTTTAAAGATG
prFVS032	GGGAATTCCATATGCATCACCATCACCATCACGAATGGCAAGCTGAACAAGC
prFVS033	CGACCTCGAGTTAAAGCGCATAACGGCTGAAC
prFVS063	CGTTTAGGCGGTTTGGAACCAGATCCACAAG
prFVS064	CTGGTTCCAAACCGCCTAAACGTTGACTAGC
prFVS067	CCAAGGCAGTAGCGAGATTGGCAATATCGTTACCACCAC
prFVS068	GATATTGCCAATCTCGCTACTGCCTTGGGCTTCGAGCAG
prFVS076	GTGGCCATCGGCGGCAACACCCTCACCCTCTC
prFVS077	GTGTTGCCGCCGATGGCCACTGTGTGGTAG
prFVS082	GTATTATTACGGCGGGTATGAAAAAGGCTGAC
prFVS083	CATACCCGCCGTAATAATACGACTGCTCG
prFVS088	GGGAATTCCATATGCATCACCATCACCATCACGTGGAAGAGATCGACCAGAG
prFVS089	CCGCTCGAGTCACGAGTACTCAGTTGTGGCAAAAAG

Supplementary Table 6. List of plasmids constructed in this study.

Plasmid name	Description	Primers used	
		fwd	rev
pPE0017	VbhT (MCS1) in pRSFDuet1	prPE484	prPE485
pPE0020	VbhA (MCS2) in pRSFDuet1	prPE520	prPE519
pPE0021	VbhT (MCS1) + VbhA (MCS2) in pRSFDuet1	-	-
pPE0034	VbhT His136Ala (MCS1) in pRSFDuet1	prAH116	prAH127
pPE1018	HA-VbhT in pMMB206 (pVbhT)	prPE500	prPE501
pPE1031	HA-VbhT(H136A) in pMMB206 (pVbhT(H136A))	prAH116	prAH127
pPE3005	VbhA-VbhT deletion fragment in pTR1000	prPE526	prPE517
pFVS0011	VbhA (MCS1) + VbhT 1-198 (MCS2) in pRSFDuet1	prAG037	prFVS001
pFVS0012	VbhT 1-198 (MCS2) in pRSFDuet1	prAG037	prFVS001
pFVS0015	NmFic 11-191 (MCS2) in pRSFDuet1	prFVS007	prFVS008
pFVS0016	NmFic 11-167 Δ8 (MCS2) in pRSFDuet1	prFVS007	prFVS009
pFVS0023	NmFic 11-191 Glu186Ala (MCS2) in pRSFDuet1	prFVS010	prFVS011
pFVS0037	NmFic 11-191 Ser182Ala Glu186Ala (MCS2) in pRSFDuet1	prFVS026	prFVS027
pFVS0040	SoFic 1-372 (MCS2) in pRSFDuet1	prFVS032	prFVS033
pFVS0058	SoFic 1-372 Glu73Gly (MCS2) in pRSFDuet1	prFVS067	prFVS068
pFVS0059	NmFic 11-191 Glu186Gly (MCS2) in pRSFDuet1	prFVS082	prFVS083
pFVS0065	VbhA Glu24Gly (MCS1) + VbhT 1-198 (MCS2) in pRSFDuet1	prFVS063	prFVS064
pFVS0080	VbhA Glu24Gly (MCS1) + VbhT 1-198 His136Ala (MCS2) in pRSFDuet1	prAH116	prAH127
GST-HypE	GST-HypE in pET-GSTx (kindly provided by Jack Dixon)	-	-
GST-HypE$_{H/A}$	GST-HypE His295Ala in pET-GSTx (kindly provided by Jack Dixon)	-	-
pFVS0064	GST-HypE Glu234Gly in pET-GSTx	prFVS076	prFVS077
pFVS0085	HypE(FIC) 187-437 (MCS2) in pRSFDuet1	prFVS088	prFVS089
pFVS0087	HypE(FIC) 187-437 His295Ala (MCS2) in pRSFDuet1	prFVS088	prFVS089
pFVS0091	HypE(FIC) 187-437 Glu234Gly (MCS2) in pRSFDuet1	prFVS088	prFVS089
pFVS0058	SoFic 1-372 Glu73Gly (MCS2) in pRSFDuet1	prFVS067	prFVS068
pAH059	GST-Cdc42 Gln61Leu		
pAH088	GST-Cdc42		
pAH060	GST-Rac1 Gln61Leu		
pAH071	GST-Rac1		

4. References

1 Xiao, J., Worby, C. A., Mattoo, S., Sankaran, B. & Dixon, J. E. Structural basis of Fic-mediated adenylylation. *Nat Struct Mol Biol* **17**, 1004-1010 (2010).

2 Palanivelu, D. V. *et al.* Fic domain-catalyzed adenylylation: insight provided by the structural analysis of the type IV secretion system effector BepA. *Protein Sci* **20**, 492-499 (2011).

3 Luong, P. *et al.* Kinetic and structural insights into the mechanism of AMPylation by VopS Fic domain. *J Biol Chem* **285**, 20155-20163 (2010).

4 Worby, C. A. *et al.* The fic domain: regulation of cell signaling by adenylylation. *Mol Cell* **34**, 93-103 (2009).

5 Yarbrough, M. L. *et al.* AMPylation of Rho GTPases by *Vibrio* VopS disrupts effector binding and downstream signaling. *Science* **323**, 269-272 (2009).

6 Soding, J., Biegert, A. & Lupas, A. N. The HHpred interactive server for protein homology detection and structure prediction. *Nucleic Acids Res* **33**, W244-248 (2005).

7 Schmid, M. C. *et al.* A translocated bacterial protein protects vascular endothelial cells from apoptosis. *PLoS Pathog* **2**, e115 (2006).

8 Lehnherr, H., Maguin, E., Jafri, S. & Yarmolinsky, M. B. Plasmid addiction genes of bacteriophage P1: doc, which causes cell death on curing of prophage, and phd, which prevents host death when prophage is retained. *J Mol Biol* **233**, 414-428 (1993).

9 Liu, M., Zhang, Y., Inouye, M. & Woychik, N. A. Bacterial addiction module toxin Doc inhibits translation elongation through its association with the 30S ribosomal subunit. *Proc Natl Acad Sci U S A* **105**, 5885-5890 (2008).

10 Magnuson, R. & Yarmolinsky, M. B. Corepression of the P1 addiction operon by Phd and Doc. *Journal of bacteriology* **180**, 6342-6351 (1998).

11 Mukherjee, S. *et al.* Modulation of Rab GTPase function by a protein phosphocholine transferase. *Nature* **477**, 103-106 (2011).

12 Edgar, R. C. MUSCLE: a multiple sequence alignment method with reduced time and space complexity. *BMC Bioinformatics* **5**, 113 (2004).

13 Garcia-Pino, A. *et al.* Doc of prophage P1 is inhibited by its antitoxin partner Phd through fold complementation. *J Biol Chem* **283**, 30821-30827 (2008).

14 Price, M. N., Dehal, P. S. & Arkin, A. P. FastTree 2--approximately maximum-likelihood trees for large alignments. *PLoS One* **5**, e9490 (2010).

15 Stamatakis, A. RAxML-VI-HPC: maximum likelihood-based phylogenetic analyses with thousands of taxa and mixed models. *Bioinformatics* **22**, 2688-2690 (2006).

3.2. *Research article II* (Goepfert *et al.*, *PLoS ONE*, 2013)

Conserved Inhibitory Mechanism and Competent ATP Binding Mode for Adenylyltransferases with Fic Fold

Arnaud Goepfert, Frédéric V. Stanger, Christoph Dehio & Tilman Schirmer

PLoS ONE, Volume 8, Issue 5, May 2013

3.2.1. Statement of my own contributions

My contribution to the *research article II* consisted initially in the cloning of the recombinant plasmids used for protein over-expression. I also expressed, purified and crystallized $NmFic_{E186G}$.

The crystal structures were determined by Arnaud Goepfert and the manuscript was written by Arnaud Goepfert, Christoph Dehio and Tilman Schirmer.

3.2.2. "Conserved Inhibitory Mechanism and Competent ATP Binding Mode for Adenylyltransferases with Fic Fold"

OPEN ACCESS Freely available online

PLOS ONE

Conserved Inhibitory Mechanism and Competent ATP Binding Mode for Adenylyltransferases with Fic Fold

Arnaud Goepfert[1,2], Frédéric V. Stanger[1,2], Christoph Dehio[1]*, Tilman Schirmer[2]*

1 Focal Area Infection Biology, Biozentrum, University of Basel, Basel, Switzerland, **2** Focal Area Structural Biology and Biophysics, Biozentrum, University of Basel, Basel, Switzerland

Abstract

The ubiquitous FIC domain is evolutionarily conserved from bacteria to human and has been shown to catalyze AMP transfer onto protein side-chain hydroxyl groups. Recently, it was predicted that most catalytically competent Fic proteins are inhibited by the presence of an inhibitory helix α_{inh} that is provided by a cognate anti-toxin (class I), or is part of the N- or C-terminal part of the Fic protein itself (classes II and III). *In vitro*, inhibition is relieved by mutation of a conserved glutamate of α_{inh} to glycine. For the class III bacterial Fic protein NmFic from *Neisseria meningitidis*, the inhibitory mechanism has been elucidated. Here, we extend above study by including bacterial class I and II Fic proteins VbhT from *Bartonella schoenbuchensis* and SoFic from *Shewanella oneidensis*, respectively, and the respective E->G mutants. Comparative enzymatic and crystallographic analyses show that, in all three classes, the ATP substrate binds to the wild-type FIC domains, but with the α-phosphate in disparate and non-competent orientations. In the E->G mutants, however, the tri-phosphate moiety is found reorganized to the same tightly bound structure through a unique set of hydrogen bonds with Fic signature motif residues. The γ-phosphate adopts the location that is taken by the inhibitory glutamate in wild-type resulting in an α-phosphate orientation that can be attacked in-line by a target side-chain hydroxyl group. The latter is properly registered to the Fic active center by main-chain β-interactions with the β-hairpin flap. These data indicate that the active site motif and the exposed edge of the flap are both required to form an adenylylation-competent Fic protein.

Citation: Goepfert A, Stanger FV, Dehio C, Schirmer T (2013) Conserved Inhibitory Mechanism and Competent ATP Binding Mode for Adenylyltransferases with Fic Fold. PLoS ONE 8(5): e64901. doi:10.1371/journal.pone.0064901

Editor: Eric Cascales, Centre National de la Recherche Scientifique, Aix-Marseille Université, France

Received March 13, 2013; **Accepted** April 19, 2013; **Published** May 30, 2013

Funding: This work was supported by grants 31003A 312979 and 3100 138414 from the Swiss National Science Foundation (to CD and TS, respectively) and grant 51RT 0_126008 (InfectX) in the frame of the SystemsX.ch Swiss Initiative for Systems Biology (to CD). The funders had no role in study design, data collection and analysis, decision to publish, or preparation of the manuscript.

Competing Interests: The authors have declared that no competing interests exist.

* E-mail: tilman.schirmer@unibas.ch (TS); christoph.dehio@unibas.ch (CD)

Introduction

Adenylyl transferases (ATases) utilize adenosine triphosphate (ATP) to covalently modify proteins, nucleic acids, or small molecules with adenosine monophosphate (AMP), a reaction known as adenylylation or AMPylation. The ubiquitous FIC domain (pfam 02661) found in proteins of all domains of life and viruses has only recently been shown to confer ATase activity. Thus, the bacterial T3SS effector protein VopS from *Vibrio parahaemolyticus* and the surface antigen IbpA from *Histophilus somni* covalently attach the bulky AMP moiety onto a specific threonine or tyrosine, respectively, of the switch I region of Rho family GTPases [1,2]. This abrogates binding of downstream effectors and results in actin cytoskeleton collapse and concomitant cell detachment and death. Mutational and bioinformatics analysis indicated that Fic proteins containing a strictly conserved HxFx(D/E)GNGRxxR signature motif in the active center typically display adenylylation activity [1,2,3,4,5], while Fic proteins with an active center deviating from this consensus are considered to have adopted different activities. Indeed, the host-targeted effector protein AnkX of *Legionella pneumophila* exhibiting an HxFxDANGRxxV signature motif displays phosphocholination activity towards the GTPase Rab1 [6].

The FIC domain is structurally characterized by a conserved central core of four helices (α2 to α5) that is flanked by three helices (α1, α6 and α7) found in diverse dispositions in different Fic proteins [3,7]. Helices α4 and α5 are joined by a loop that together with the N-terminal cap of helix α5 forms the active center represented by a signature motif with the consensus sequence HxFx(D/E)GNGRxxR. The catalytic mechanism of adenylylation was deduced from the crystal structure of the second FIC domain of IbpA in complex with the adenylylated Cdc42 target [4] and from biochemical studies [5] and shown to involve nucleophilic attack of the target side-chain hydroxyl onto the ATP α-phosphate. The triphosphate binding site at the anionic nest at the N-terminus of helix α5 was characterized by the crystal structure of BepA from *Bartonella henselae* in complex with pyrophosphate, the side product of the reaction [3]. An ATP substrate complex structure was obtained recently for the Fic protein of *Neisseria meningitidis* [8] corroborating the catalytic mechanism. The histidine of the signature motif is critical for deprotonation of the incoming target hydroxyl group [5], whereas the phenylylanine is part of the hydrophobic core of the domain. The remaining residues of the motif are involved in ATP/Mg^{2+} binding and loop stabilization [3,8].

We recently demonstrated that the Fic protein VbhT from *Bartonella schoenbuchensis* causes bacterial growth arrest when overexpressed in *Bartonella* or *E. coli* and that this effect can be repressed by co-expression with the anti-toxin VbhA, a small protein encoded upstream of VbhT [8]. As shown by structure

analysis, VbhA forms a tight complex with the FIC domain of VbhT with the conserved glutamate (E_{inh}) from the inhibitory helix α_{inh} partly obstructing the ATP binding site, which gave a first clue regarding the inhibitory mechanism mediated by VbhA binding.

Exhaustive bioinformatic analysis coupled with homology modeling revealed that the (S/T)xxxE(G/N) signature motif of α_{inh} is not only found in several other putative anti-toxin sequences coded immediately upstream of Fic proteins, but is often part of the FIC domain itself either preceding helix α1 or immediately following helix α7 [8]. Thus, a classification system was introduced grouping the Fic proteins for which an anti-toxin with an inhibitory helix α_{inh} had been found into class I and those with an equivalent of α_{inh} in the N- or C-terminal part of the Fic protein into classes II and III, respectively. Indeed, 90% of the Fic proteins with the canonical FIC signature motif could be classified accordingly, suggesting that all these enzymes are inhibited in their enzymatic activity.

The physiological stimulus or condition for relief of α_{inh}-mediated inhibition is not yet known. For T4SS Fic proteins of class I (such as VbhT or BepA [9]), however, it appears likely that, for injection into host cells, the Fic protein has to unfold and will be translocated without the antitoxin. For class II and III proteins, detachment, unfolding, or proteolytic cleavage of the α_{inh} helix may cause relief of inhibition. In fact, a truncation mutant of the class III Fic protein from *N. meningitidis* (NmFic) lacking the entire C-terminal α_{inh} helix showed strong ATase activity and allowed to study the catalytic and inhibitory mechanism in detail [8]. A more subtle means to relieve inhibition, which is applicable to Fic proteins of all three classes, is the replacement of the inhibitory glutamate by glycine. *In vivo*, such E->G mutations showed a detrimental effect on bacterial growth [8]. For the human HYPE protein (class II), the corresponding mutant protein catalyzed *in vitro* AMP transfer to the small GTPases Rac1 and Cdc42, whereas only marginal effect was seen with the wild-type proteins [8].

Here, we assayed in a systematic approach Fic representatives of the three Fic classes and their E->G mutants for *in vitro* adenylylation showing that the mutation causes inhibition relief across the Fic classes. Binding of ATP substrate or AMPPNP substrate analog to the wild-type and the E->G mutant proteins was studied by protein crystallography to reveal the inhibitory mechanism and to get further insight into catalysis. This yielded a consistent molecular mechanism that most likely applies to most adenylylation competent Fic proteins irrespective of class.

Materials and Methods

Cloning

The full-length *vbhA* gene and part of the *vbhT* gene (amino acid residues 1–248, His_6-tagged) were amplified from plasmid pPE0021 and cloned into the pRSF-Duet1 vector leading to plasmid pAG0077 (VbhA/VbhT(FIC)). The full-length *vbhA* gene and part of the *vbhT* gene encoding the FIC domain (amino acid residues 1–198, His_6-tagged) were PCR-amplified from plasmid pPE0021 and cloned into the pRSF-Duet1 vector (pFVS0011). A two-base pair mutation is then introduced in pFVS0011 to obtain plasmid pFVS0065 ($VbhA_{E24G}$/VbhT(FIC)). The *fic* gene of *Neisseria meningitidis* was PCR-amplified with an N-terminal His_6-tag from *Neisseria meningitidis* from coding region of amino acid residues 11–191 to generate plasmid expressing NmFic (pFVS0015). The E186G mutant construct ($NmFic_{E186G}$, pFVS0059) was generated by introducing a two-base pair mutation in pFVS0015. The *fic* gene of *Shewanella oneidensis* was PCR-amplified from plasmid (ASU biodesign institute, Clone ID SoCD00104192) and cloned with an N-terminal His_6-tag into pRSF-Duet1 (pFVS0040). The $SoFic_{E73G}$ plasmid (pFVS0058) was generated by introducing a two-base pair point mutation in pFVS0040.

Protein Expression and Purification

Vectors pAG0077 (VbhA/VbhT(FIC)), pFVS0040 (SoFic) and pFVS0015 (NmFic) were transformed into *E.coli* BL21 (DE3). *E. coli* cultures were grown at 37°C in LB medium supplemented with 50 µg/ml of kanamycin to an OD_{595} of 0.6 before induction with 0.3 mM IPTG for 16 h at 23°C. Vectors pFVS0065 ($VbhA_{E24G}$/VbhT(FIC)), pFVS0059 ($NmFic_{E186G}$), pFVS0058 ($SoFic_{E73G}$) were transformed into BL21-AI cells**.** Cells were incubated in 750 ml LB medium supplemented with 50 µg/ml kanamycin and 1% glucose at 37°C at 200 rpm until an OD_{595} value of 1.5 was reached. Bacterial pellets were resuspended in 1 L of Terrific Broth media containing 50 $\mu g/ml^{-1}$ kanamycin. Protein expression was induced at 23°C with 0.1% arabinose and 0.1 mM IPTG for 23 h at 200 rpm.

Cells containing overexpressed VbhA/VbhT(FIC) and NmFic were resuspended in lysis buffer containing 20 mM Tris (pH 7.5), 250 mM NaCl, and 25 mM imidazole and disrupted using French press. Cell debris were pelleted by ultracentrifugation and the supernatant was applied to a His-Trap column (GE Healthcare). The proteins were eluted with a gradient of elution buffer containing 20 mM Tris (pH 7.5), 250 mM NaCl, and 500 mM imidazole. The proteins were then concentrated and injected on a Superdex 75 16/60 gel filtration column (GE Healthcare) equilibrated with 10 mM Tris (pH 7.6) and 100 mM NaCl. The pure proteins were concentrated to 3.7 mg/ml for VbhA/VbhT(FIC) and 30 mg/ml for NmFic.

The same purification protocol as described above was used for $VbhA_{E24G}$/VbhT(FIC) and $NmFic_{E186G}$ with an additional intermediate purification step. After affinity purification, the proteins were adjusted to 20 mM Tris (pH 8.5), 25 mM NaCl, applied to a Resource-Q anion exchange column (Amersham Biosciences), and eluted with a linear gradient of 1 M NaCl. Peak fractions were concentrated and further purified by gel filtration chromatography. Purified proteins in 10 mM Tris (pH 7.6), 100 mM NaCl were concentrated to 4.1 mg/ml for $VbhA_{E24G}$/VbhT(FIC) and 33 mg/ml for $NmFic_{E186G}$. Cells containing overexpressed SoFic and $SoFic_{E73G}$ were resuspended in lysis buffer containing 50 mM HEPES (pH 8.0), 50 mM NaCl, 1 mM TCEP, 10% glycerol and 10 mM Imidazole and disrupted using French press. Cell debris were pelleted by ultracentrifugation and the supernatant was applied to a His-Trap column (GE Healthcare). The proteins were eluted with a gradient of elution buffer containing 50 mM HEPES (pH 8.0), 50 mM NaCl, 1 mM TCEP, 10% glycerol and 300 mM imidazole. The proteins were then concentrated and injected on a Superdex 75 16/60 gel filtration column (GE Healthcare) equilibrated with 20 mM HEPES (pH 8.0), 200 mM NaCl and 1 mM TCEP. The pure proteins were concentrated to 21.8 mg/ml for SoFic and 12 mg/ml for $SoFic_{E73G}$.

Protein Crystallization

For crystallization, the hanging-drop vapor diffusion method was used with 1 µl protein solution mixed with 1 µl reservoir solution. The VbhA/VbhT(FIC) and $VbhA_{E24G}$/VbhT(FIC) complexes were concentrated to 3.7 mg/ml and 4.1 mg/ml, respectively, and crystallized at 20°C using a reservoir solution composed of 15% (w/v) PEG 4000, 0.1 M MES pH 6.5. Whereas, the wild-type crystal was soaked with 5 mM ATP, and 5 mM

$MgCl_2$, the mutant was co-crystallized with 10 mM ATP, and 10 mM $MgCl_2$. For data collection, crystals were transferred to reservoir solutions supplemented with 20% glycerol and flash frozen in liquid nitrogen. SoFic and $SoFic_{E73G}$ were concentrated to 21.8 mg/ml and 12 mg/ml, respectively, and co-crystallized with either 5 mM ATP or 5 mM AMPPNP and supplemented with 5 mM $MgCl_2$ in a solution composed of 21% (w/v) PEG 3350 and 0.2 M NaF pH 7.1 at 4°C. For data collection, crystals of the protein-ligand complex were cryoprotected by transfer to a reservoir solution supplemented with 15% (v/v) PEG 200 and flash cooled in liquid nitrogen. For crystallization of $NmFic_{E186G}$ (33 mg/ml), a reservoir solution composed of 4 M potassium formate, 0.1 M Bis-Tris propane pH 9.0, 2% (w/v) PEG MME 2000 was used. Crystals were soaked with 5 mM AMPPNP and 5 mM $MgCl_2$ and then cryoprotected with 20% glycerol prior flash-cooling in liquid nitrogen.

Data Collection, Structure Determination, and Refinement

Diffraction data were collected at the Swiss Light Source at 100 K and processed using XDS [10]. The structures were solved by molecular replacement using the apo structures of VbhA/VbhT(FIC) (PDB code 3SHG), SoFic (PDB code 3EQX) or NmFic (PDB code 2G03) as search models using Phaser [11]. Several rounds of iterative model building and refinement were performed using Coot [12] and PHENIX [13] or REFMAC5 [14], respectively. 5% of the data were excluded from refinement and used for cross-validation. The geometry of the final model was assessed using MolProbity [15] showing >99% of the residues in the core and allowed regions of the Ramachandran plot. Data collections and refinement statistics are summarized in Table 1. The atomic coordinates and structure factors of VbhA/VbhT(FIC)/ATP, $VbhA_{E24G}$/VbhT(FIC)/ATP, SoFic/ATP, $SoFic_{E73G}$/AMPPNP, and $NmFic_{E186G}$/AMPPNP have been deposited in the Protein Data Bank under accession codes 3ZC7, 3ZCB, 3ZCN, 3ZEC and 3ZLM, respectively. The figures were generated with Dino (A. Philippsen unpublished, http://www.dino3d.org).

In vitro Adenylylation Assay

Adenylylation activity of VbhA/VbhT(FIC), SoFic and NmFic constructs was assessed by incubating 125 ng, 1.25 µg and 2.5 µg of purified protein, respectively, with 10 µCi α-^{32}P-ATP (Hartmann Analytic) in a buffer containing 50 mM Tris pH 8.0, 150 mM NaCl, 0.1 mM EGTA, 15 mM $MgCl_2$, and protease inhibitor cocktail (Roche). Reactions were incubated for 1 h at 30°C, resolved by SDS–PAGE, and subjected to autoradiography.

Results

Constitutive Inhibition is Relieved by Truncation of the Inhibitory Glutamate in All Three Fic Classes

For the comparative structure/function study on the inhibitory mechanism of Fic proteins from the various classes we chose as representatives the FIC domain of VbhT (residues 1 to 198) from *Bartonella schoenbuchensis* in complex with its cognate antitoxin VbhA (VbhA/VbhT(FIC); class I), Fic protein SO_4266 *from Shewanella oneidensis* (SoFic; class II) and Fic protein NMB0255 from *Neisseria meningitidis* (NmFic; class III).

Auto-adenylylation is a convenient read-out to assess adenylylation activity of Fic proteins. It does not require the presence of a physiological protein target that may, in fact, not yet been known as in the case of SoFic. Autoradiographies of SDS-PAGE gels after incubation with α-^{32}P-ATP (Fig. 1) show that auto-adenylylation is virtually absent in the wild-type Fic proteins of all three classes, i.e. for VbhA/VbhT(FIC), SoFic, and NmFic (see also ref. 8), but is drastically boosted in the respective E->G mutants suggesting a common inhibitory mechanism.

ATP Binds to Wild-type Fic Proteins in Disparate and Catalytically Incompetent Conformations

Fig. 2 shows the high-resolution structures of VbhA/VbhT(FIC) (class I) and SoFic (class II), both in complex with ATP. Whereas VbhA/VbhT(FIC) crystallized isomorphously to the unliganded wild-type crystals ([8], PDB code 3SHG), SoFic yielded crystals of monoclinic space group, i.e. distinct to the orthorhombic form of the apo structure ([16], PDB code 3EQX). In the two structures the nucleotide is clearly visible, albeit with elevated B-factors (40 $Å^2$) in VbhA/VbhT(FIC). Only marginal structural changes are induced upon substrate binding (rms deviations between the Cα-positions of apo and complex form of 0.4 Å and 0.8 Å for VbhA/VbhT(FIC) and SoFic, respectively).

In both structures the ATP substrate is found at analogous sites (Fig. 2) with the base filling a pocket formed by α4, α6, and the β-hairpin flap, the ribose 3′-hydroxyl H-bonded to the conserved glutamate of α_{inh}, and the triphosphate moiety interacting with the anionic nest formed by the N-terminus of α5. The same binding mode has been observed for class III NmFic [8]. In all three structures, also the ribose 2′-hydroxyl is forming an H-bond, but to non-homologous protein side-chains. Similarly, the binding subsite for the base is not conserved on the residue level. However, in each case, hydrophobic residues are contributed by helix α6 and by the flap. A weak H-bond is formed between the adenine N3 and N133 in VbhT(FIC). A homologous interaction (with N104) is found in NmFic [8].

Most relevant for catalysis is the orientation of the α-phosphate that has to be accessible for nucleophilic attack by the target side-chain hydroxyl group. In VbhA/VbhT(FIC) and SoFic, as in NmFic [8], the position that is in-line with the scissile Pα-O3α bond is not accessible for an attacking group (Fig. 2). Such a group positioned there would severely clash with atoms of the enzyme. Thus, in Fic proteins of all three classes, catalytically non-competent orientation of the α-phosphate appears to be the reason for the lack of adenylylation activity.

Interestingly, while the α-phosphate is locked in a secured position in each of the structures, it shows distinct orientations among the three proteins that can be traced back to differences in the binding mode of the β- and γ-phosphates (Fig. 2C). Though interacting with the same protein groups (anionic nest; histidine, asparagine, and first arginine of the signature motif), the detailed H-bonding patterns are different (e.g. the main chain amide of the second glycine of the motif interacts with the bridging O3β in VbhA/VbhT(FIC), and with the non-bridging O1β in SoFic).

It seems that during convergent evolution of α_{inh}-mediated adenylylation inhibition in the different Fic protein classes no strict constraints for the ATP binding mode were operational apart from the requirement for a non-competent orientation for the reacting phosphate.

Truncation of the Inhibitory Glutamate Allows the ATP Substrate to Bind in a Catalysis Competent Conformation

Relief of Fic protein inhibition was achieved previously by expression of VbhT without its cognate antitoxin VbhA or by replacing in NmFic the SxxxE inhibition motif by AxxxA or – most drastically - by deleting the entire α_{inh} [8]. The conserved glutamate of α_{inh}, E_{inh}, was identified to be crucial for the inhibitory effect, since mere truncation of its side-chain (E->G

Table 1. Data collection and refinement statistics.

Protein	VbhA/VbhT(FIC)	$VbhA_{E24G}$/VbhT(FIC)	SoFic	$SoFic_{E73G}$	$NmFic_{E186G}$
Ligand	ATP	ATP	ATP	AMPPNP	AMPPNP
PDB code	3ZC7	3ZCB	3ZCN	3ZEC	3ZLM
Data collection					
Wavelength (Å)	1.000	0.979	0.979	0.979	1.000
Detector	MAR225 CCD	PILATUS 2M	MAR225 CCD	MAR225 CCD	PILATUS 2M
Space group	C2	C2	$P2_1$	$P2_12_12_1$	$P6_422$
Cell dimensions					
a, *b*, *c* (Å)	106.5, 40.6, 73.7	106.5, 40.3, 73.9	37.8, 164.9, 70.2	71.3, 80.6, 141.8	149.1, 149.1, 76.4
$\alpha\ \beta\ \gamma$ (°)	90.0, 121.6, 90.0	90.0, 121.4, 90.0	90.0, 94.4, 90.0	90.0, 90.0, 90.0	90.0, 90.0, 120.0
Resolution (Å)	45.4−2.1 (2.2−2.1)	45.4−1.9 (2.1−1.9)	35.5−1.7 (1.8−1.7)	42.7−2.2 (2.3−2.2)	49.3−2.0 (2.1−2.0)
R_{sym} or R_{merge} (%)	8.5 (33.8)	5.7 (33.4)	4.4 (41.3)	10.5 (52.8)	6.3 (72.7)
CC(1/2) (%)	99.8 (93.6)	99.9 (93.1)	99.9 (87.1)	99.8 (90.3)	100.0 (97.9)
I/σ	18.9 (5.7)	14.5 (3.4)	22.9 (3.4)	17.6 (4.5)	31.1 (5.7)
Completeness (%)	99.2 (92.3)	99.2 (97.0)	99.5 (96.7)	100.0 (100.0)	99.9 (100.0)
Multiplicity	5.4 (4.9)	3.6 (3.6)	3.9 (3.4)	7.4 (7.5)	21.4 (22.6)
Refinement					
Resolution (Å)	15.0−2.10	30.0−1.94	15.0−1.70	15.0−2.20	30.0−2.00
No. reflections	15,769 (2,342)	18,923 (1,355)	93,100 (2,837)	42,085 (3,956)	32,490 (2,338)
R_{work}/R_{free} [%]	16.6/23.0	19.4/23.4	16.7/20.2	16.5/21.1	18.2/19.9
Mol./a.u	1	1	2	2	1
No. atoms					
Protein	2172	2011	5961	5984	1458
Ligand/ion	1 ATP	1 ATP, 1 MG	2 ATP	2 ANP, 1 MG	1 ANP, 1 MG
Water	226	134	981	695	135
Average B ($Å^2$)					
Protein	22.0	25.0	21.9	20.7	45.9
Ligand/ion	39.7	27.5/11.4	21.9	12.9/28.9	40.1/64.8
Water	28.4	32.1	33.7	28.0	49.3
R.m.s deviations					
Bond lengths (Å)	0.007	0.011	0.008	0.009	0.010
Bond angles (°)	1.0	1.3	1.2	1.2	1.2

Values for the highest resolution shell are shown in brackets.
doi:10.1371/journal.pone.0064901.t001

mutation) rendered recombinantly overexpressed Fic proteins of all three classes toxic to *E. coli* [8].

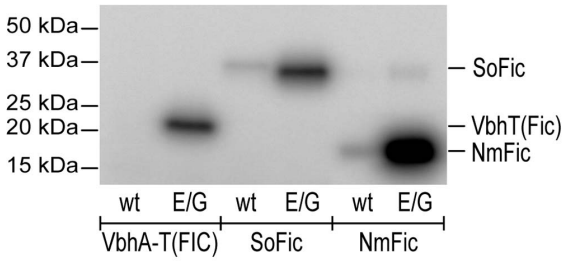

Figure 1. AMP transfer catalyzed by Fic proteins and their inhibition-relieved variants. Autoradiography of VbhA/VbhT(FIC), SoFic and NmFic (wt, wild type; E/G, E->G mutant) after incubation with radioactively labeled α-^{32}P-ATP.
doi:10.1371/journal.pone.0064901.g001

In vitro, the mutation has a drastic effect in that auto-adenylylation is boosted in all three representative Fic proteins (Fig. 1). This opens the door for studying the action of any active Fic protein *in vivo*, even without knowing the physiological stimulus for inhibition relief.

To reveal the underlying inhibition relief mechanism, crystal structures of the three mutant proteins in complex with ATP or AMPPNP were determined to high resolution. Although, in solution the mutants show auto-adenylylation, no such modification is observed in the crystal structures. For $NmFic_{E186G}$ this is not surprising, since the complex structure has been obtained by soaking and auto-adenylylation would require partial unfolding of α_{inh} carrying the modifiable tyrosine (Y183) [8]. The $VbhA_{E24G}$/VbhT(FIC) and $SoFic_{E73G}$ complexes were co-crystallized. Since we do not see adenylylated residues, the extend of modifications may be either minor, locate to flexible loops or only the unmodified fraction may have crystallized. Figs. 3A–C show that in all three cases, the nucleotide is well resolved and, in contrast to

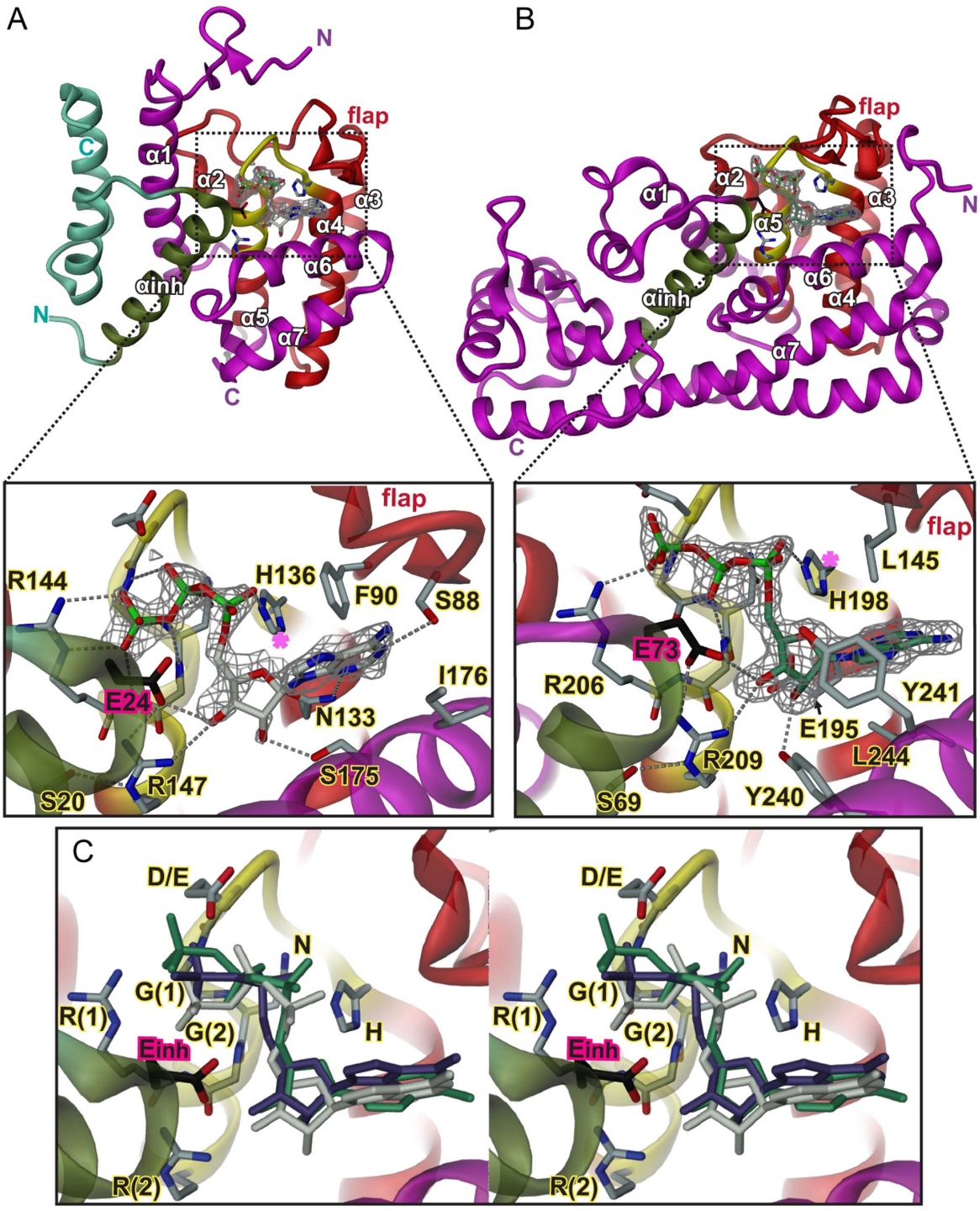

Figure 2. Crystal structures of wild-type Fic proteins representing classes I to II in complex with ATP substrate. (A) VbhA/VbhT(FIC), (B) SoFic. Structures are shown in cartoon representation (red, FIC core as defined by PFAM; yellow, active site loop and N-terminal end of helix α5; dark-green, inhibitory helix α_{inh}). In (A), the fold of the antitoxin is shown in dark-green and steel-blue. Selected residues are shown in full with the inhibitory glutamate (E24 or E73, respectively) colored in dark. The 2Fo-Fc simulated annealing omit maps covering the ligand are contoured at 1.1 σ. In both structures, the orientation of the α-phosphate prevents nucleophilic attack of a putative target side-chain hydroxyl onto the ATP substrate, since the position inline with the scissile Pα-O3α bond (magenta star) is unattainable. C) Stereo view of the superposition of the ATP nucleotides

shown in panel A and B with AMPPNP from the complex structure of the class III NmFic protein (PDB 3S6A [8]) within the active site of the VbhA/VbhT(FIC) complex (same as in panel A). The nucleotides of the various complexes are distinguished by their colors (white for the ATP bound to VbhA/VbhT(FIC), green for the ATP bound to SoFic, and blue for the AMPPNP of the NmFic complex. Note that the AMPPNP γ-phosphate in NmFic is found disordered [8] and therefore not shown. The residues of the HxFx(D/E)GNGRxxR Fic signature motif are labeled, the two glycine and the two arginine residues are distinguished by a "1" or "2" in brackets. The phenylalanine (not shown) is part of the hydrophobic core. The inhibitory glutamate from α_{inh} is labeled as E_{inh}.
doi:10.1371/journal.pone.0064901.g002

the wild-type complexes, shows a unique conformation and relative position within the binding site (Fig. 3D).

While the base and ribose moieties interact with the mutant in the same way as with the wild-type proteins (compare with Fig. 2, see also Fig. 3a in [8] for NmFic), the triphosphate has adopted a strongly curved conformation with the terminal γ-phosphate approaching closely the ribose moiety and forming a tight salt-bridge with the second arginine of the FIC motif (R(2): R147, R209, or R118, respectively).

The position and orientation of the triphosphate is defined by a multitude of specific interactions (Fig. 3A–C). In all structures, the α- and β-phosphate moieties form four H-bonds with the four exposed backbone amide groups of the compound anion binding nest [17] at the N-terminal end of helix α5. In addition, the first arginine of the signature motif (R(1): R144, R206, or R115, respectively) forms a salt-bridge with the β-phosphate involving two H-bonds and the asparagine of the motif (N142, N204, or N113, respectively) interacts with a non-bridging oxygen of the α-phosphate.

In all the structures, a magnesium ion is present albeit with high B-factor for $NmFic_{E186G}$ (63 $Å^2$). The metal bridges the α- and β-phosphate and is coordinated in addition by the conserved D/E residue of the Fic signature motif in $VbhA_{E24G}$/VbhT(FIC) and $SoFic_{E73G}$ (E140, D202, respectively). It is particularly well resolved in the former structure where three well-defined water molecules complete its octahedral coordination shell (Fig. 3A). Interestingly, the divalent cation is observed only in the adenylylation competent complexes, but not in the wild-type complexes. Indeed, magnesium is indispensable for Fic mediated ATase activity (data not shown) and is probably important for fine-tuning of the α- and β-phosphate orientation within the compound anion binding nest and for stabilization of the transition state.

Overall, the three structures display a unique mode of ATP binding that can be attained only in the mutants, since the γ-phosphate effectively adopts the position that is taken by the inhibitory glutamate in the wild-type proteins (Fig. 4). Most relevantly, the reorganization of the triphosphate in the binding site results in a α-phosphate orientation that is now prone for in-line attack by an incoming target side-chain (Fig. 3D). Clearly, the conservation of this binding mode across the FIC classes shows that it is essential for FIC function.

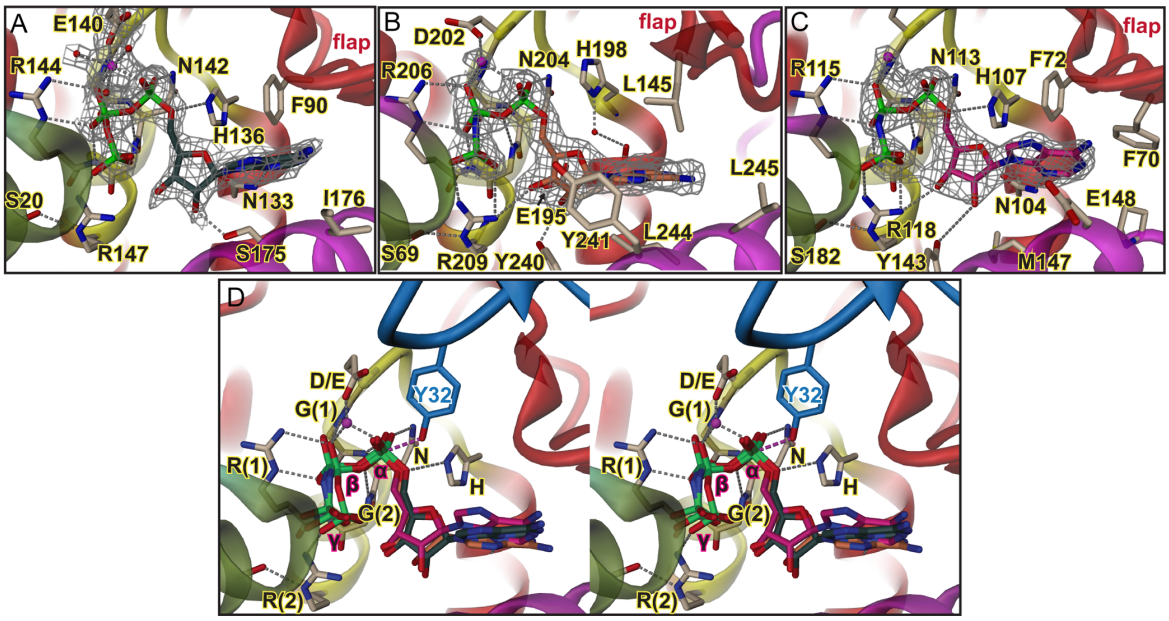

Figure 3. Crystal structures of E->G mutated Fic proteins representing classes I to III in complex with substrate or substrate analog. A, $VbhA_{E24G}$/VbhT(FIC) in complex with ATP/Mg^{2+}; B, $SoFic_{E73G}$, C, $NmFic_{E186G}$, both in complex with AMPPNP/Mg^{2+}. Representation as in Fig. 2 with magnesium ions shown as magenta spheres. The 2Fo-Fc simulated annealing omit maps covering the nucleotide/Mg^{2+} ligands are contoured at 1.1 σ. D, Stereo view of the superposition of the ligand structures shown in panels B and C onto the $VbhA_{E24G}$/VbhT(FIC) complex (same as in panel A). Note that the nucleotides of the various complexes are distinguished by their carbon color ($VbhA_{E24G}$/VbhT(FIC) ATP in green, $SoFic_{E73G}$ AMPPNP in orange and $NmFic_{E186G}$ AMPPNP in pink). The residues of the HxFx(D/E)GNGRxxR signature motif are labeled as in Fig. 2C with the phenylalanine not shown. Also shown is the modifiable hydroxyl side-chain Y32 of Cdc42 (blue) after superposition of the IbpA(FIC2)/Cdc42 complex [4] onto $VbhA_{E24G}$/VbhT(FIC). For the superposition, only the Fic active site loops were used. The α-phosphate moieties appear well-suited for in-line attack of the target hydroxyl group (broken line in magenta).
doi:10.1371/journal.pone.0064901.g003

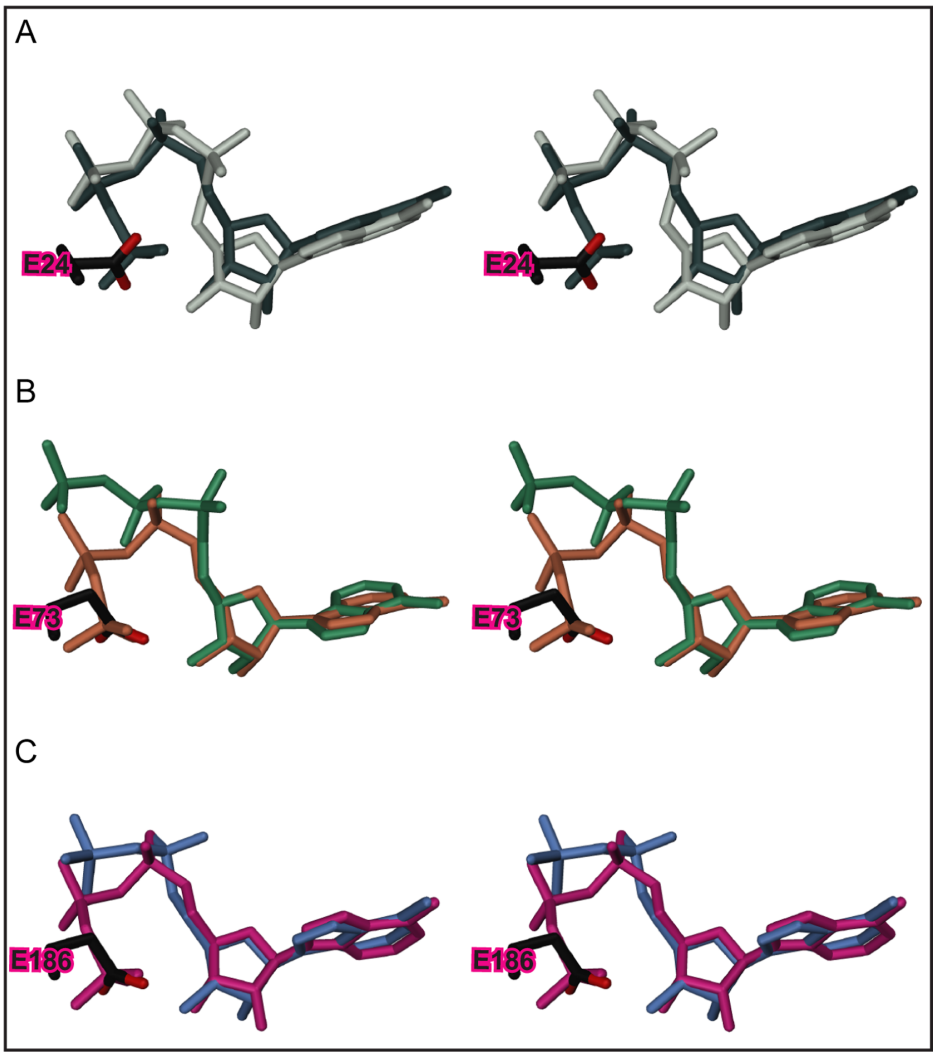

Figure 4. Comparison of triphosphate nucleotide structures as bound to wild-type and E->G mutated Fic proteins from class I to III. Stereo views of the ligand structures after superposition of the FIC domains (not shown). Also shown is the inhibitory glutamate of the wild-type structures. A, ATP as bound to VbhA/VbhT wild-type (white) and the E24G mutant (dark green). B, ATP and AMPPNP as bound to SoFic wild-type (green) and the E73G mutant (orange), respectively. C, AMPPNP as bound to NmFic (blue) and the E186G mutant (pink). Note that the AMPPNP γ-phosphate in NmFic is found disordered [8] and therefore not shown.
doi:10.1371/journal.pone.0064901.g004

Target Registration to the FIC Active Site

The conservation of the FIC active site and the ATP substrate binding mode prompts for a precise alignment of the incoming side-chain hydroxyl with the scissile Pα-O3α bond. The beta-hairpin flap partly covering the active site appears to represent a "target dock" that ensures this precise positioning of the target backbone stretch immediately following the modifiable hydroxyl side-chain and thus registers the side-chain to the active site as has been proposed before (2). This was deduced mainly from the only known Fic protein/target complex structure IbpA(FIC)/Cdc42 [4] where the AMPylated Y32 of Cdc42 is part of a segment (switch 1 loop) in extended conformation and complements inter-molecularly the β-hairpin of the flap (Fig. 5A).

This notion is further corroborated by the structure of the wild-type VbhA/VbhT(FIC) complex presented here that revealed additional density close to the flap above the active site (Fig. 5B). This was interpreted as a four residue peptide in extended conformation that is associated antiparallely to the edge of the two-stranded β-hairpin of the flap via three main chain-main chain H-bonds. Location and side-chain densities are consistent with the peptide representing residues 203 to 206 of a symmetry mate (note that the ordered part of the VbhT(FIC) construct ends with residue F197). Very similarly, peptide density is present at an equivalent location in the A-chain of $SoFic_{E73G}$ and could be attributed to the N-terminus (residues 0 to 3) of a symmetry related B-chain as also reported for the isomorphous crystal structure of wild-type SoFic (Fig. 5C) [16].

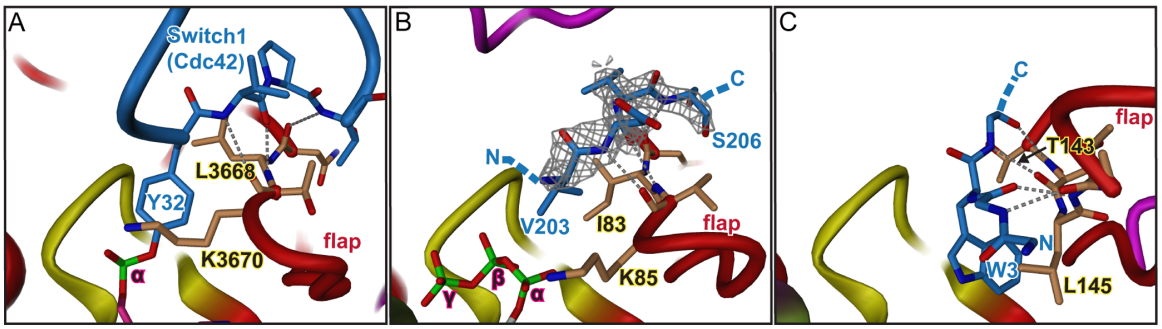

Figure 5. Sequence independent registration of peptide or target protein to the FIC flap. The bound peptide/protein segment (blue) and the target dock (brown) are shown in full. Main chain-main chain H-bonds are depicted as stippled lines. A, Product complex of IbpA(Fic2) with Cdc42 target [4]. Tyrosine 32 from the switch1 region of Cdc42 is adenylylated. B, VbhA/VbhT(FIC) complexed with residues 203 to 206 of a symmetry related molecule. The 2Fo-Fc simulated annealing omit map covering the residues 203 to 206 is contoured at 1.1 σ. Note that the preceding 7 residues are disordered and not shown. C, SoFic complexed with residues 0 to 4 of a symmetry related molecule (PDB 3EQX) [16]. The side-chains of residues 0, 1 and 4 are disordered and not displayed for clarity reason. Note that Y32 in panel A, V203 in panel B and W3 in panel C are in equivalent positions.
doi:10.1371/journal.pone.0064901.g005

Comparison of Figures 5A–C suggests that a tyrosine instead of the valine in position 203 of the symmetry related VbhT(FIC) chain or of the tryptophan in position 3 of the symmetry related SoFic chain would indeed be well poised to attack the ATP α-phosphate. Furthermore, it has been shown for IbpA that the side-chains of the target dock residues Leu3668 and Lys3670 form a hydrophobic clamp that fix the target tyrosine side-chain (Fig. 5C) [4]. Side-chains of residues I83 and K85 in VbhT(FIC) and residues T143 and L145 in SoFic, that hold the valine and tryptophan, respectively, may in a similar way clamp down the modifiable side-chain (Fig. 5A–B). Taken together, these observations show that the flap has propensity for peptide binding as it is well known for exposed beta-sheet edges in other proteins [18,19,20] and ensures productive alignment of the target hydroxyl side-chain with the bound ATP substrate.

Probably, sequence independent positioning of the backbone flanking the modifiable target residue confers an evolutionary advantage. While exposed loops in extended conformation of many proteins may easily dock to the flap, other parts of the enzyme would confer target affinity and specificity (as seen in the IbpA(FIC)/Cdc42 complex [4]) that were free to adopt during evolution without compromising on the catalytic mechanism. Notably, peptide registration to the active site via main-chain interactions is known also for serine proteases [21] and protein kinases [22,23].

Discussion

The vast majority of Fic proteins are characterized by a conserved HxF[D/E]GNGRxxR active site motif and catalyses adenylylation, an enzymatic activity that involves nucleophilic attack of a target hydroxyl group onto the α-phosphate of ATP. Productive AMP transfer therefore relies on the proper juxtaposition of the reaction partners. The inhibition-relieved (E->G) mutant structures of Fic proteins from the three distinct classes shed light on the importance of the active site [D/E]GNGRxxR residues to enable catalytically competent ATP substrate binding. Indeed, in the three classes, these residues, by way of a large hydrogen-bonding network, enable a unique mode of ATP binding to orientate favorably the α-phosphate relative to the target side-chain hydroxyl group (Fig. 3). The latter is registered to the FIC active site in-line with the scissile Pα-O3α bond *via* sequence-independent main chain-main chain interactions with the target dock at the edge of the FIC flap (Fig. 5). Thus, the FIC active site and the target dock are two indivisible structural elements that have been exposed to high functional constraints to ensure productive catalysis. Fic proteins with degenerated active site signature motifs and/or devoid of a flap-like structure are likely to have adopted new functions.

In Fic proteins of the three inhibition classes, the inhibitory glutamate plays the same role. It out-competes the γ-phosphate for binding to arginine R(2) of the FIC signature motif (Fig. 4). This results in an α-phosphate orientation that does not permit an attack of the incoming target side-chain hydroxyl group. Interestingly, though the active sites are structurally well conserved, the nucleotide triphosphates show variation in their binding to the Fic proteins of the three classes (Fig. 2). This is in contrast to the uniform binding mode found in the inhibition relieved mutants (Fig. 3) and shows that the mode of ATP binding to the inhibited enzyme *per se* was not under evolutionary constraints.

Knowledge of the universal catalytic and inhibitory mechanism of Fic mediated AMP transfer will now pave the way for further studies towards the physiological roles of Fic proteins and particularly the identification of their protein targets. It may also prompt rational structure based design of small molecule inhibitors targeting the ATP binding pocket or novel peptides that mimic the inhibitory helix to neutralize bacterial virulence factors which kill their host *via* uncontrolled Fic-mediated adenylylation activity.

Acknowledgments

We thank the staff of beam-line X06DA of the Swiss Light Source (Villigen, Switzerland) for assistance with data acquisition. We gratefully acknowledge Gerd Pluschke for kindly providing the genomic DNA of *Neisseria meningitidis* and the ASU Biodesign Institute for providing the plasmid enclosing the *Shewanella oneidensis* Fic protein.

Author Contributions

Conceived and designed the experiments: AG CD TS. Performed the experiments: AG FVS. Analyzed the data: AG TS. Wrote the paper: AG CD TS.

References

1. Worby CA, Mattoo S, Kruger RP, Corbeil LB, Koller A, et al. (2009) The fic domain: regulation of cell signaling by adenylylation. Molecular cell 34: 93–103.
2. Yarbrough ML, Li Y, Kinch LN, Grishin NV, Ball HL, et al. (2009) AMPylation of Rho GTPases by Vibrio VopS disrupts effector binding and downstream signaling. Science 323: 269–272.
3. Palanivelu DV, Goepfert A, Meury M, Guye P, Dehio C, et al. (2011) Fic domain-catalyzed adenylylation: insight provided by the structural analysis of the type IV secretion system effector BepA. Protein science : a publication of the Protein Society 20: 492–499.
4. Xiao J, Worby CA, Mattoo S, Sankaran B, Dixon JE (2010) Structural basis of Fic-mediated adenylylation. Nature structural & molecular biology 17: 1004–1010.
5. Luong P, Kinch LN, Brautigam CA, Grishin NV, Tomchick DR, et al. (2010) Kinetic and structural insights into the mechanism of AMPylation by VopS Fic domain. The Journal of biological chemistry 285: 20155–20163.
6. Mukherjee S, Liu X, Arasaki K, McDonough J, Galan JE, et al. (2011) Modulation of Rab GTPase function by a protein phosphocholine transferase. Nature 477: 103–106.
7. Kinch LN, Yarbrough ML, Orth K, Grishin NV (2009) Fido, a novel AMPylation domain common to fic, doc, and AvrB. PloS one 4: e5818.
8. Engel P, Goepfert A, Stanger FV, Harms A, Schmidt A, et al. (2012) Adenylylation control by intra- or intermolecular active-site obstruction in Fic proteins. Nature 482: 107–110.
9. Schulein R, Guye P, Rhomberg TA, Schmid MC, Schroder G, et al. (2005) A bipartite signal mediates the transfer of type IV secretion substrates of Bartonella henselae into human cells. Proceedings of the National Academy of Sciences of the United States of America 102: 856–861.
10. Kabsch W (2010) Xds. Acta crystallographica Section D, Biological crystallography 66: 125–132.
11. McCoy AJ, Grosse-Kunstleve RW, Adams PD, Winn MD, Storoni LC, et al. (2007) Phaser crystallographic software. Journal of applied crystallography 40: 658–674.
12. Emsley P, Lohkamp B, Scott WG, Cowtan K (2010) Features and development of Coot. Acta crystallographica Section D, Biological crystallography 66: 486–501.
13. Adams PD, Afonine PV, Bunkoczi G, Chen VB, Davis IW, et al. (2010) PHENIX: a comprehensive Python-based system for macromolecular structure solution. Acta crystallographica Section D, Biological crystallography 66: 213–221.
14. Murshudov GN, Vagin AA, Dodson EJ (1997) Refinement of macromolecular structures by the maximum-likelihood method. Acta crystallographica Section D, Biological crystallography 53: 240–255.
15. Chen VB, Arendall WB 3rd, Headd JJ, Keedy DA, Immormino RM, et al. (2010) MolProbity: all-atom structure validation for macromolecular crystallography. Acta crystallographica Section D, Biological crystallography 66: 12–21.
16. Das D, Krishna SS, McMullan D, Miller MD, Xu Q, et al. (2009) Crystal structure of the Fic (Filamentation induced by cAMP) family protein SO4266 (gi|24375750) from Shewanella oneidensis MR-1 at 1.6 A resolution. Proteins 75: 264–271.
17. Watson JD, Milner-White EJ (2002) A novel main-chain anion-binding site in proteins: the nest. A particular combination of phi,psi values in successive residues gives rise to anion-binding sites that occur commonly and are found often at functionally important regions. Journal of molecular biology 315: 171–182.
18. Hill CP, Yee J, Selsted ME, Eisenberg D (1991) Crystal structure of defensin HNP-3, an amphiphilic dimer: mechanisms of membrane permeabilization. Science 251: 1481–1485.
19. Nassar N, Horn G, Herrmann C, Scherer A, McCormick F, et al. (1995) The 2.2 A crystal structure of the Ras-binding domain of the serine/threonine kinase c-Raf1 in complex with Rap1A and a GTP analogue. Nature 375: 554–560.
20. Doyle DA, Lee A, Lewis J, Kim E, Sheng M, et al. (1996) Crystal structures of a complexed and peptide-free membrane protein-binding domain: molecular basis of peptide recognition by PDZ. Cell 85: 1067–1076.
21. Wilmouth RC, Clifton IJ, Robinson CV, Roach PL, Aplin RT, et al. (1997) Structure of a specific acyl-enzyme complex formed between beta-casomorphin-7 and porcine pancreatic elastase. Nature structural biology 4: 456–462.
22. Hubbard SR (1997) Crystal structure of the activated insulin receptor tyrosine kinase in complex with peptide substrate and ATP analog. The EMBO journal 16: 5572–5581.
23. Yang J, Cron P, Good VM, Thompson V, Hemmings BA, et al. (2002) Crystal structure of an activated Akt/protein kinase B ternary complex with GSK3-peptide and AMP-PNP. Nature structural biology 9: 940–944.

3.3. *Research article III* (Harms *et al.*, in preparation for *Cell*)

Fic toxins subvert DNA topology by adenylylation of topoisomerases to promote bacterial persistence

Alexander Harms, Frédéric V. Stanger, Patrick D. Scheu, Imke G. de Jong, Timo Glatter, Kenn Gerdes, Tilman Schirmer & Christoph Dehio

In preparation for *Cell*.

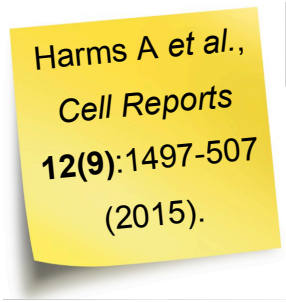

3.3.1. Statement of my own contributions

I participated to the *research article III* by cloning recombinant plasmids used for protein over-expression. I expressed and purified VbhTA, $VbhTA_{E24G}$ and the 43-kDa N-terminal fragment of *E. coli* GyrB. I assessed the inhibition of GyrB by VbhT using an FPLC-based nucleotide quantification assay that I have adapted for that purpose, revealing that the ATPase activity of GyrB is inhibited by $VbhTA_{E24G}$.

I took part in the experimental design and contributed to data analysis and writing of the manuscript.

3.3.2. "Fic toxins adenylylate topoisomerases to subvert DNA topology and promote persistence"

Research Article

Fic toxins subvert DNA topology by adenylylation of topoisomerases to promote bacterial persistence

Alexander Harms[1], Frédéric V. Stanger[1,2], Patrick D. Scheu[3], Imke G. de Jong[1], Timo Glatter[4], Kenn Gerdes[3,5], Tilman Schirmer[2] & Christoph Dehio[1]

[1]*Focal Area Infection Biology, Biozentrum, University of Basel, CH-4056 Basel, Switzerland;*
[2]*Focal Area Structural Biology and Biophysics, Biozentrum, University of Basel, CH-4056 Basel, Switzerland;*
[3]*Centre for Cell & Molecular Biosciences, Newcastle University, NE2 4AX Newcastle upon Tyne, United Kingdom;*
[4]*Proteomics Core Facility, Biozentrum, University of Basel, CH-4056 Basel, Switzerland;*
[5]*Department of Biology, University of Copenhagen, DK-2200 Copenhagen, Denmark*

Corresponding author:
Prof. Christoph Dehio
Biozentrum, University of Basel
Klingelbergstrasse 70
CH-4056 Basel, Switzerland
Tel.: +41-61-267 2140
Fax.: +41-61-267 2118
e-mail: christoph.dehio@unibas.ch

Summary

Research on the large family of Fic proteins containing a FIC (filamentation induced by cAMP) domain has primarily studied scattered representatives that had secondarily evolved into host-targeted virulence factors of bacterial pathogens. However, most Fic proteins are genuine bacterial proteins whose functions have remained unknown. Here we uncover one major group of bacterial Fic proteins as toxins of a conserved toxin-antitoxin gene family that act via the adenylylation of DNA gyrase and topoisomerase IV (topo IV), the two bacterial type IIA topoisomerases. Adenylylation inactivates both targets *in vitro*. *In vivo*, Fic toxins robustly disable topo IV, resulting in DNA catenation and knotting, while the level of gyrase inhibition causing DNA relaxation differs among diverse representatives. Subversion of DNA topology by Fic toxins causes a reversible growth arrest and promotes the formation of multidrug-tolerant persister cells. The activation of a Fic toxin-antitoxin system *in vivo* was found to depend on protease Lon.

Highlights

- One group of ubiquitous FIC domain proteins form a conserved toxin-antitoxin family
- Fic toxins inhibit DNA gyrase and topoisomerase IV activities via adenylylation
- Target inhibition distorts cellular DNA topology causing reversible growth arrest
- Fic toxins induce a phenotypic switch to the multidrug-tolerant persister state

Introduction

Fic proteins containing a FIC (filamentation induced by cAMP) domain are found in all kingdoms of life and typically catalyze adenylylation (also known as AMPylation), the covalent transfer of an adenosine-5' monophosphate (AMP) moiety onto target proteins (Engel et al., 2012; Kinch et al., 2009). They are particularly abundant in prokaryotes with around 20'000 representatives (InterPro domain IPR003812), indicating that Fic proteins are pervasive, yet understudied players in the physiology of diverse microbes. Previous research on Fic proteins focused on a few scattered representatives that had secondarily evolved into host-targeted virulence factors and that in part displayed peculiar biochemical activities such as phosphocholination or uridylylation (Feng et al., 2012; Mukherjee et al., 2011; Yarbrough et al., 2009).

We recently showed that the prevalent adenylylation activity of Fic proteins is controlled by a conserved inhibitory α-helix that binds into the FIC domain active site and forces the ATP substrate to bind in an adenylylation-incompetent state (Engel et al., 2012). Fic proteins could be grouped into three major classes (I-III) based on the positioning of this α-helix relative to the FIC domain core, and the release of that inhibition always resulted in bacterial growth arrest (Goepfert et al., 2013b). These results were reminiscent of the enigmatic "filamentation induced by cAMP" phenotype caused by a mutant of the prototypic *Escherichia coli* Fic protein that gave the name to the domain family (Utsumi et al., 1982). Fic of *E. coli* belongs to class I of Fic proteins which is defined as having their inhibitory α-helix in a separate small protein that is typically encoded upstream of the *fic* gene with slight overlap (Engel et al., 2012). This genetic arrangement and the inhibition of toxic class I Fic proteins via binding to a separate "anti-toxin" are hallmarks of type II toxin-antitoxin modules (TA modules) (Gerdes and Maisonneuve, 2012; Goepfert et al., 2013a). Type II TA modules comprise a toxin that blocks cell growth and an antitoxin protein that controls toxin activity by tight binding until it is degraded in response to nutritional and environmental stresses (Brzozowska and Zielenkiewicz, 2013). Bacterial chromosomes encode multitudes of type II TA modules (Pandey and Gerdes, 2005) that have been proposed to exert many different functions including post-segregational killing, bacteriophage defense, and programmed cell death (Magnuson, 2007; Van Melderen, 2010). The only known common function of TA systems is that of bacterial persistence (multidrug tolerance) (Gerdes and Maisonneuve, 2012; Schuster and Bertram, 2013). We recently described the TA-like

appearance of class I Fic proteins and introduced a new nomenclature terming the FIC domain toxins FicT (previously Fic; e.g., EcFicT for Fic of *E. coli*) and the antitoxins FicA (previously YhfG) (Goepfert et al., 2013a). Interestingly, the Doc toxin of the Doc-Phd toxin-antitoxin system of bacteriophage P1 was recently shown to be a kinase that inhibits bacterial growth via the phosphorylation of EF-Tu (Castro-Roa et al., 2013). Doc represents a remote, deeply branching clade of Fic proteins that is believed to derive from canonical, adenylylating Fic proteins via inversion of the nucleotide substrate binding site and appearance of a novel antitoxin, Phd, that inhibits Doc by blocking substrate binding (Castro-Roa et al., 2013; Engel et al., 2012; Garcia-Pino et al., 2008). Their evolutionary connection to Doc and their toxin/antitoxin-like features suggested that also the original, primordial class I Fic proteins form a type II TA system that acts via the adenylylation of targets within bacteria (Goepfert et al., 2013a). However, the molecular function and biological role of the ubiquitous, yet enigmatic FicTA modules remained elusive.

Here we characterize FicTA modules as a toxin-antitoxin system that targets DNA gyrase and topoisomerase IV via adenylylation of an invariant tyrosine at their ATP binding site. Adenylylation fully inhibits both targets *in vitro* and reversibly arrests bacterial growth. Using a wide range of different techniques we show that Fic toxin expression results in strong DNA knotting and catenation combined with a varying degree of DNA relaxation in *E. coli*, indicating that Fic toxins can inactivate both targets *in vivo*. Remarkably, we find that the impairment of cellular physiology due to Fic toxin activity converts bacteria into multidrug-tolerant persister cells. Moreover, we show that activation of a FicTA system *in vivo* depends on protease Lon.

Results

Ectopic expression of Fic toxins results in a reversible inhibition of bacterial growth that depends on adenylylation

We previously established the VbhTA system of *Bartonella schoenbuchensis* as a model for class I Fic proteins and demonstrated that the antitoxin VbhA inhibits the adenylylation activity of the VbhT toxin as well as the associated growth inhibition in *Escherichia coli* (Engel et al., 2012). Since VbhT is unique among class I Fic proteins in that it harbors a C-terminal type IV secretion signal (called BID domain), we decided to investigate the

molecular and biological functions of VbhT along with a more typical representative of class I, i.e., the YeFicTA system of *Yersinia enterocolitica* str. 8081 (see *Extended Results* in the Supplemental Information). For comparison, we also included the PaFicTA system of *Pseudomonas aeruginosa* PAO1, a very distant homolog.

We observed strong inhibition of *E. coli* growth upon expression of VbhT or YeFicT from a single-copy vector in the absence of their VbhA or YeFicA antitoxins, respectively (Figures 1A and 1B). This effect was dose-dependent (Figure 1C) and required the Fic toxins' adenylylation activity because mutation of the catalytic histidine within the FIC domain signature motif HXFX(D/E)GNGRXXR into alanine ("H/A" mutants) abolished Fic toxicity (Figure 1A). Subsequent expression of the cognate antitoxins reversed the growth inhibition (Figure 1D), demonstrating that Fic toxin activity leads to a classical bacteriostatic condition that is a common feature of many TA systems (Pedersen et al., 2002). We note that the ectopic expression of VbhT appears to be less potent in growth inhibition than that of YeFicT or the FIC domain of VbhT alone (VbhT(fic); Figures 1B and 1C), possibly due to differential expression of the constructs or because the BID domain of VbhT sterically reduces toxin activity.

Fic toxins adenylylate GyrB and ParE of different bacteria

To unravel the molecular mechanism of the reversible growth inhibition caused by the Fic toxins' adenylylation activity we next aimed at uncovering the identity of the adenylylated target(s). For this purpose we performed *in vitro* adenylylation assays with lysates of *E. coli* that had expressed VbhT and used a pull-down approach similar to the one published by Grammel et al. (2011) for target identification. Though we failed to achieve significant enrichment of potential targets, we serendipitously discovered an adenylylated peptide that belonged to GyrB of *E. coli* (data not shown). The theoretical molecular weight of GyrB (89.95 kDa) fits well with the apparent molecular weight of the *bona fide* endogenous target adenylylation detected by autoradiography in adenylylation assays with VbhT (Figure 2A and our previous work (Engel et al., 2012)) which we calculated to be approximately 90 kDa using the ImageQuant software (Molecular Dynamics). Ectopic expression of GyrB both of *E. coli* or *B. schoenbuchensis* unambiguously showed that this protein is adenylylated by VbhT in bacterial lysates *in vitro* (Figure 2A). Given the very high similarity in sequence, structure, and function to GyrB (Bellon et al., 2004) we further suspected that its paralog ParE may also be targeted by VbhT. Indeed, like for GyrB, ectopic expression of ParE of *E. coli* and

B. schoenbuchensis clearly demonstrated adenylylation by VbhT (Figure 2A). However, unlike for GyrB, no adenylylation of endogenous ParE is detectable by visual inspection of autoradiographs of our adenylylation experiments with cleared lysates of *E. coli* expressing VbhT (Figure 2A). We believe that this discrepancy is caused by differential target abundance with each cell of *E. coli* containing approximately 10 times more molecules of GyrB than of ParE (Alexander Schmidt, personal communication).

GyrB and ParE are the B subunits of the two bacterial type IIA topoisomerases DNA gyrase and topoisomerase IV (topo IV) which control cellular DNA topology by maintaining negative supercoiling respectively removing DNA catenation and knotting. Therefore, they are essential for all cellular activities involving the processing of closed circular DNA like bacterial chromosomes (Sissi and Palumbo, 2010). Due to their vital role for bacterial physiology the type IIA topoisomerases are the target of several groups of antimicrobials, bacteriocins, as well as the CcdBA and ParDE type II TA systems (Sissi and Palumbo, 2010). These toxins, the bacteriocins, as well as quinolone-based antimicrobials are poisons that prevent resealing of the DNA cleavage inherent to type II topoisomerase activity and ultimately result in cell death (Chen et al., 1996; Deghorain et al., 2013; Heddle et al., 2001). In contrast, aminocoumarin drugs like novobiocin merely inactivate the enzymes by blocking their ATP binding which abrogates the cellular control of DNA topology but does not directly trigger cell death (Hardy and Cozzarelli, 2003).

Adenylylation at the ATP binding site inhibits DNA gyrase and topo IV *in vitro*

Using mass spectrometry, we identified the adenylylation sites on GyrB and ParE of *E. coli* to be homologous tyrosines 109 and 105, respectively (Figure S2). This residue is involved in ATP binding as part of the "ATP lid" and highly conserved among type IIA topoisomerase B subunits (Brino et al., 2000; Wigley et al., 1991). Since their functionality generally depends on concurrent ATP hydrolysis (Bates et al., 2011), we hypothesized that adenylylation may inactivate DNA gyrase and topo IV by interfering with the ATPase cycle, which could explain the marked growth arrest upon Fic toxin expression. We therefore assayed the hydrolysis of ATP by a GyrB ATPase model construct (Ali et al., 1993) and found that adenylylation indeed completely blocked the target's ATPase activity (Figure 2B). Subsequently, we used recombinant DNA gyrase and topo IV to assess the effect of adenylylation on the signature activities of both targets on suitable DNA substrates *in vitro*. As expected, adenylylation prevented supercoiling of a relaxed reporter plasmid by DNA

gyrase and decatenation of kDNA, a meshwork of catenated DNA rings, by topo IV (Figure 2C). Interestingly, the slow kinetics of ATP hydrolysis inhibition upon addition of VbhT to GyrB (apparent in Figure 2B) and the requirement to pre-incubate VbhT and gyrase or topo IV prior to addition of their respective DNA substrates in order to achieve full inhibition (Figure 2C) suggest that Fic toxins may be slow enzymes at least *in vitro*.

Fic toxins achieve only partial inhibition of DNA gyrase *in vivo*

We then investigated whether Fic toxins also inactivate DNA gyrase and topo IV *in vivo*. Any inhibition of DNA gyrase would decrease the negative supercoiling of cellular DNA. We therefore used plasmid pAH160, a high-copy number vector originally designed for rhamnose-inducible protein expression, isolated from *E. coli* expressing Fic toxins to directly visualize changes in DNA topology via high-resolution agarose gel electrophoresis with chloroquine to resolve negative supercoiling (see *Experimental Procedures*). As expected, the treatment of *E. coli* with a high concentration of novobiocin that completely inactivates DNA gyrase resulted in collapse of the negative supercoiling (Figure 3A). However, a dose of Fic toxin expression that impaired bacterial growth (two hours of full induction; see Figure 1B) caused only a slight stretch of the topoisomer distribution towards DNA relaxation. This result was not consistent with a strong inhibition of DNA gyrase by Fic toxins *in vivo* and therefore seemed to contradict our *in vitro* results. However, we suspected that the transient nature of local DNA relaxation for the single topological domain of our simple reporter plasmid may have masked more prominent effects of a potential partial inhibition of DNA gyrase by VbhT and YeFicT. We therefore used another reporter plasmid encoding a relaxation-induced P*gyrB::gfpmut2* GFP promoter fusion to record any DNA gyrase inhibition inside single cells by flow cytometry. For validation, we confirmed that *E. coli* harboring this plasmid showed dose-dependent induction of GFP fluorescence upon inhibition of DNA gyrase with different concentrations of novobiocin (Figure 3B). In this system the expression of VbhT or YeFicT resulted in a rather weak, but detectable induction of GFP fluorescence, while VbhT(fic) elicited a stronger response (Figure 3B). However, Rovinskiy, Agbleke *et al.* (2012) convincingly argued that plasmid-based assays may generally underestimate the physiological effects of an incomplete DNA gyrase inhibition. We therefore constructed a chromosomal P*gyrB::gfpmut2* reporter and measured the effect of Fic toxin expression on the supercoiling of the nucleoid. Like with the plasmid-based assay (Figure 3B), the treatment with different concentrations of novobiocin caused a dose-dependent induction of GFP fluorescence, while Fic toxin expression only resulted in weak (VbhT and YeFicT) or

moderate (VbhT(fic)) DNA relaxation (Figure 3C). These findings mirror our results from high resolution agarose gel electrophoresis and thus indicate that VbhT and YeFicT are unlikely to achieve levels of DNA gyrase inhibition *in vivo* that would greatly contribute to growth inhibition. The more prominent effect with the VbhT(fic) construct may be due to differences in expression or reflect an evolution of the VbhT FIC domain to stronger activity in order to partially compensate for the hindrance by its BID domain. Despite that, VbhT(fic) is not a more potent toxin than YeFicT (Figure 1B and 1C), suggesting that DNA gyrase inhibition is no necessary driving force of Fic toxicity.

Robust inhibition of topo IV by Fic toxins *in vivo*

The inactivation of topo IV is known to result in DNA knotting and catenation which induce a classical phenotype called *par* hallmarked by cell filamentation and the sequestration of unsegregated DNA at the cell center (Kato et al., 1990). We therefore used fluorescence microscopy to study cell shape and DNA partitioning in *E. coli* expressing Fic toxins (Figure 4A). As expected from our biochemical data, the expression of YeFicT, VbhT, or VbhT(fic) greatly inhibited DNA segregation and bacterial cell division, resulting in a strong *par* phenotype (Figure 4A and 4B). Interestingly, the nucleoids in cells expressing VbhT(fic) and YeFicT – but not VbhT – are highly condensed which may indicate super-condensation as a stress response (Meyer and Grainger, 2013). As an independent readout for topo IV inhibition *in vivo* we re-analyzed the pAH160 samples that had been used for the detection of DNA relaxation by high resolution agarose gel electrophoresis (see Figure 3A). After nicking to remove all supercoiling the samples were run on plain agarose gels to resolve DNA knotting and catenation. Plasmid isolated from *E. coli* that had expressed any of the Fic toxin constructs showed detectable DNA knots and a clear ladder of catenanes with various node numbers evidencing robust topo IV inhibition (Figure 4C and 4D). The seemingly weak extent of all DNA knotting with pAH160 is likely an artifact of the small size of this reporter plasmid (4359 bp) and still evidences considerable knotting of the nucleoid, since the topological entanglement and size of chromosomal DNA greatly favor knotting and complicate unknotting compared to small plasmids (Witz et al., 2011). We therefore conclude that the growth inhibition upon VbhT and YeFicT expression is primarily caused by the inhibition of topo IV via consequent distortions of DNA topology.

Bacterial genetics confirm that Fic toxin expression impairs DNA segregation and replication fork movement

It is intuitive that the catenanes formed upon Fic toxicity would impair DNA segregation and cell division. Consistently, we find that the inactivation of topoisomerase III or XerCD recombination which can both partially complement a topo IV deficiency in DNA segregation makes *E. coli* hypersensitive to Fic toxicity (Figure 5A). Moreover, others have shown that the inactivation of topo IV results in an inhibition of DNA replication and transcription via DNA knotting as well as an impaired topological control of replication forks that is aggravated in different ways by DNA gyrase inhibition (Deibler et al., 2007; Khodursky et al., 2000; Lopez et al., 2012; Witz et al., 2011; Witz and Stasiak, 2010). DNA knots continuously arise in the tangled nucleoid from random strand passages that occur whenever cellular DNA handling cuts open the chromosome, e.g., during processes of replication, recombination, or repair, and they cannot be removed in the absence of functional topo IV (Deibler et al., 2001). We therefore expected that the viability of bacteria expressing Fic toxins should depend on replication fork repair and restart via fork reversal and various recombination pathways. Indeed, we found that *E. coli* deficient in the *recABCD* or *ruvABC* machineries were hypersensitive to Fic toxicity (Figure 5A). Importantly, the same genes are also involved in a number of different DNA repair pathways on top of recombinational fork repair, e.g., the processing of double-strand breaks. We therefore verified that the single inactivation of *recA* (which is essential for double-strand break repair (Wigley, 2013)) does not abolish the reversibility of Fic toxicity in our experimental system (Figure 5B). However, the dual inactivation of exonuclease V and homologous recombination which represent the two branches of replication fork restart after fork reversal results in detectable lethality upon Fic toxin expression (*recB* as well as *recDA* mutant in Figure 5B). We therefore conclude that frequent replication fork arrest impairs chromosome replication during Fic toxicity (De Septenville et al., 2012). Fork arrest is a main trigger of the SOS response, a cascade of genes whose expression is induced upon DNA damage (Erill et al., 2007). We indeed detected an activation of the SOS response upon Fic toxin expression, but these effects were clearly distinct from the strong activation observed with gyrase poisons like ciprofloxacin or the CcdB toxin (Figure 5C). Though most factors encoded by SOS genes are more or less directly involved in DNA repair, the SulA protein expressed in response to severe DNA damage directly blocks cell division via the inhibition of septation (Huisman et al., 1984), thus buying

overtime for DNA repair functions. Irreversible blocks of cell division via SOS activation and SulA were proposed to be involved in a number of toxicity phenomena like thymineless death (Fonville et al., 2010). Similarly, we find that – under the relatively low level of Fic toxicity that we used – the inability to launch the SOS response (in a *lexA3* mutant) or the inactivation of *sulA* made the bacteria considerably more tolerant to Fic toxin expression than the control strain (Figure 5A). However, the contribution of the SOS response to growth inhibition is only minor at the higher levels of Fic toxicity that we generally used for phenotypic characterization (Figure S3A and S3B), suggesting that SulA-mediated growth inhibition is no necessary component of Fic toxicity.

A distant homolog shows the same activities and phenotypes as YeFicT and VbhT

To confirm DNA gyrase and topo IV inhibition as the general mechanism of class I Fic toxins we finally compared the results obtained with VbhT and YeFicT to those with PaFicT of *Pseudomonas aeruginosa* PAO1, a very distant homolog (see *Extended Results*). As expected, PaFicT expression in *E. coli* results in bacterial growth inhibition which requires the native FIC domain active site and is inhibited by the cognate PaFicA antitoxin (Figure 6A and Figure 6B). The expression of PaFicT induces a *par* phenotype (Figure 6C) and results in considerable DNA gyrase inhibition that is even stronger than the one achieved with VbhT(fic) (Figure 6D and Figure 6E). Like novobiocin, PaFicT induces strong DNA knotting but no catenation, suggesting that the expression of this toxin causes a strong inhibition of both type IIA topoisomerases and thereby immediately stops DNA replication (Figure 6F) (Khodursky et al., 2000). In conclusion, our results show that diverse Fic toxins target DNA gyrase and topo IV to inhibit bacterial growth. While VbhT, YeFicT, and PaFicT all appear to achieve a strong inhibition of topo IV upon expression in *E. coli*, the extent of DNA gyrase inhibition varied for the different toxins.

Fic toxins induce persister formation in *Escherichia coli*

Given that TA system activation is the main path for the generation of persisters, i.e., bacterial cells exhibiting multidrug tolerance, we wondered whether Fic toxins could have a biological role in this context (Gerdes and Maisonneuve, 2012). We therefore expressed VbhT and YeFicT in *E. coli* and subsequently challenged the bacteria with either of three antibiotics (ciprofloxacin, kanamycin, or ampicillin) that kill via entirely different mechanisms. Remarkably, while the antibiotic treatment eliminated all but 1 in 10’000 of the

cells in the vector control, 10% of the bacteria expressing Fic toxins survived for any drug (Figure 7A). Under physiological conditions toxin activity is generally unleashed via protease-mediated antitoxin degradation in response to certain triggers or stochastically in a subpopulation of cells (Brzozowska and Zielenkiewicz, 2013; Maisonneuve et al., 2013). We therefore asked whether any of the proteolytic systems in *E. coli* could activate Fic toxins *in vivo* to inhibit bacterial growth. Interestingly, *lac*-driven ectopic expression of the *yeficAT* module resulted in detectable growth inhibition, suggesting that one or more of the resident proteases in *E. coli* degrade part of the YeFicA pool inside the cells (Figure 7B). After the biochemical investigation of YeFicA degradation by *E. coli* proteases was not conclusive (data not shown), we tested *E. coli* mutants that are deficient in ClpP, HslV, or Lon protease activities and found that the growth inhibition upon *yeficAT* overexpression was fully dependent on Lon. Consistently, a targeted activation of Lon via the stringent response with DL-serine hydroxamate aggravated the growth defect in *clpP* and *hslV* mutants as well as the control strain, while the *lon* mutant was unaffected (Figure 7B). It is well established that Lon controls the majority of bacterial TA systems and recent work demonstrated that it is itself stochastically activated in part of the population to drive persister formation via TA system activation (Brzozowska and Zielenkiewicz, 2013; Maisonneuve et al., 2013). We therefore conclude that YeFicTA and its homologs are a classical type II TA system that acts via a novel mechanism, the inactivation of type IIA topoisomerases via adenylylation of their B subunits.

Discussion

In this study we characterized diverse representatives of class I Fic proteins and showed that they act as toxins of FicTA toxin-antitoxin modules. We determined the conserved molecular mechanism by which class I Fic toxins disable bacterial physiology as the adenylylation and concomitant inactivation of DNA gyrase and topo IV which are individually essential for bacterial growth. VbhT, YeFicT, and PaFicT all caused a robust inhibition of topo IV upon expression in *E. coli*, but the extent of DNA gyrase inhibition differed, possibly reflecting divergent histories of host adaptation. Though a robust inhibition of topo IV alone is sufficient to inhibit bacterial growth, any additional inhibition of DNA gyrase aggravates this effect because both decatenation and unknotting activities of topo IV

are guided by the negative supercoiling of the nucleoid (Witz et al., 2011; Witz and Stasiak, 2010).

Mechanistically, Fic toxins therefore resemble the distantly related Doc toxin that blocks translation via the phosphorylation of EF-Tu (Castro-Roa et al., 2013). The other known topoisomerase-targeting TA systems CcdBA and ParDE are bactericidal plasmid addiction modules that trigger lethal double-strand breaks by poisoning gyrase activity via non-covalent interaction with the A subunit (Deghorain et al., 2013). Importantly, the only weak activation of the SOS response (Figure 5C) and the reversibility of bacterial growth inhibition (Figure 1D) even upon *recA* deficiency (Figure 5B) exclude such a poisoning mechanism for Fic proteins. Instead, these toxins are enzymes that merely inhibit topoisomerase activity by post-translational modification of the B subunits. Consequently, Fic toxins do not kill bacterial cells, but induce a reversible bacteriostatic condition that is known as bacterial persistence and features multidrug tolerance. Various toxin-antitoxin modules are known to promote persister formation by mechanisms mostly involving interference with translation or membrane integrity (Maisonneuve and Gerdes, 2014; Wang et al., 2012). Here we show for the first time that also the collapse of bacterial DNA topology provides a path to the persister state that is independent of the SOS response triggered by DNA damage. Future studies will further elucidate the molecular mechanism of persister formation via topoisomerase inhibition.

Experimental Procedures

Bacterial strains and plasmids

E. coli strains and plasmids used and constructed in the course of this study are described in the Supplemental Information. All primers are listed in Table S1. All vectors and all details of their construction are listed in Table S2.

Toxicity tests

Unless stated differently, experiments were performed with *E. coli* K-12 MG1655 Δ*ecficAT* (AHE573) and derivatives using a two-plasmid system with toxin genes under P*lac*

control and antitoxin genes under P*ara* control. Detailed procedures are described in the Supplemental Information.

Persister assays

Bacterial persistence was quantified similarly as described by Dörr *et al*. (2010) using a procedure that is described in detail in the Supplemental Information.

Protein expression and purification

Different VbhT constructs were expressed and purified as described previously (Engel et al., 2012). Details as well as the procedures for other constructs are described in the Supplemental Information.

ATP hydrolysis assay

The ATPase activity of GyrB was monitored using an FPLC coupled assay analyzing the nucleotide composition of the sample (Zähringer et al., 2011) based on the conditions described by Brino *et al.* (2000). For details, see the Supplemental Information.

Identification of AMPylation sites by LC-MS analysis

Recombinant *E. coli* DNA gyrase and topo IV (TopoGEN Inc.) were adenylylated *in vitro* with purified VbhT(fic)-VbhA(E/G), tryptically digested, C18-purified, and analysed by LC-MS/MS as described previously (Engel et al., 2012). Mass tolerance was set to 15 ppm for precursor ions and 0.6 Da for fragment ions. Converted MS data were searched using Mascot against a SwissProt *E. coli* decoy database containing target sequences of VbhTA. Search results were evaluated using Scaffold 3 (Proteome Software).

In vitro adenylylation assays

The adenylylation activity of Fic proteins was assessed using cleared lysates of ectopically expressing *E. coli* and [α-32P]-ATP (Hartmann Analytic) as described previously (Engel et al., 2012).

In vitro topoisomerase assays

In vitro supercoiling or decatenation assays of recombinant DNA gyrase or topoisomerase IV of *E. coli* (TopoGEN Inc.) were performed according to the supplier's recommendations. Details of the experimental procedure are described in the Supplemental Information.

Flow cytometry with GFP promoter fusions

The response of P*gyrB* (for DNA relaxation (Menzel and Gellert, 1983)) and P*sulA* (for SOS induction) promoters to Fic toxin expression was probed using plasmid-encoded *gfpmut2* promoter fusions of the collection created by Zaslaver *et al.* (2006) and pUA139, the parental plasmid without promoter, or chromosomal derivatives thereof (AHE1156 and AHE1158; see *Strain Construction*). For details, see the Supplemental Information.

High-resolution agarose gel electrophoresis

Changes in cellular DNA topology upon Fic toxin expression were assessed using the pAH160 reporter plasmid isolated from snap-frozen samples of *E. coli* AHE938 cultures with the Wizard Plus SV Minipreps DNA Purification kit (Qiagen). Details of the experimental procedure for high-resolution agarose gel electrophoresis to resolve DNA supercoiling, knotting, and catenation are described in the Supplemental Information.

Fluorescence microscopy

E. coli AHE573 that had expressed Fic toxins for 2 hours were stained with membrane dye FM4-64 (Molecular Probes) ad 2.5 µg/ml and DNA dye DAPI (4',6'-diamidino-2-phenylindole, Roche) ad 5 µg/ml for 30 minutes in LB medium in the dark and then

transferred onto microscopy slides coated with 1% agarose. Images were acquired using an Olympus IX71 microscope equipped with a CoolSnap HQ2 camera, LED illumination, and a 100x phase contrast objective (all from Applied Precision). Filter sets were Ex: 390/18, Em: 435/48 (DAPI) and Ex: 542/27, Em: 594/45 (TRITC). Snapshots were taken using SoftWorx 5.5 software and the pictures were adjusted for publication using ImageJ (http://rsbweb.nih.gov/ij/download.html) and Photoshop CS5 extended 12.0.4x64 (Adobe). For quantification at least 100 cells per strain and experiment were evaluated regarding cell shape and DNA segregation.

Authors Contributions

A.H. and F.V.S. cloned recombinant plasmids. F.V.S. expressed and purified protein constructs. A.H., F.V.S., P.D.S., and I.G.d.J. performed the experiments. T.G. conducted the mass spectrometry analysis. All authors participated in experimental design and data analysis. The manuscript was written by A.H., F.V.S., P.D.S., I.G.d.J, K.G., T.S., and C.D.

Acknowledgments

We are grateful to Guy Cornelis for genomic DNA of *Yersinia enterocolitica* strain 8081, Urs Jenal for genomic DNA of *Pseudomonas aeruginosa* PAO1, and Philipp Engel for helpful discussions. We thank Olin Silander for access to different *Escherichia coli* libraries and the Coli Genetic Stock Center (CGSC) for strains BW25113 and K996. Maxime Quebatte and Dirk Bumann are acknowledged for advice on flow cytometry. This work was supported by grants 3100-132979 and 3100-138414 from the Swiss National Science Foundation (to C.D. and T.S., respectively), ERC Advanced Investigator Grant FICModFun (340330) to C.D., and ERC Advanced Investigator Grant PERSIST (294517) to K.G. A.H. is a fellow of the Fellowships for Excellence PhD program of the Biozentrum, University of Basel.

References

Ali, J.A., Jackson, A.P., Howells, A.J., and Maxwell, A. (1993). The 43-kilodalton N-terminal fragment of the DNA gyrase B protein hydrolyzes ATP and binds coumarin drugs. Biochemistry *32*, 2717-2724.

Bates, A.D., Berger, J.M., and Maxwell, A. (2011). The ancestral role of ATP hydrolysis in type II topoisomerases: prevention of DNA double-strand breaks. Nucleic Acids Res *39*, 6327-6339.

Bellon, S., Parsons, J.D., Wei, Y., Hayakawa, K., Swenson, L.L., Charifson, P.S., Lippke, J.A., Aldape, R., and Gross, C.H. (2004). Crystal structures of *Escherichia coli* topoisomerase IV ParE subunit (24 and 43 kilodaltons): a single residue dictates differences in novobiocin potency against topoisomerase IV and DNA gyrase. Antimicrob Agents Chemother *48*, 1856-1864.

Brino, L., Urzhumtsev, A., Mousli, M., Bronner, C., Mitschler, A., Oudet, P., and Moras, D. (2000). Dimerization of *Escherichia coli* DNA-gyrase B provides a structural mechanism for activating the ATPase catalytic center. J Biol Chem *275*, 9468-9475.

Brzozowska, I., and Zielenkiewicz, U. (2013). Regulation of toxin-antitoxin systems by proteolysis. Plasmid *70*, 33-41.

Castro-Roa, D., Garcia-Pino, A., De Gieter, S., van Nuland, N.A., Loris, R., and Zenkin, N. (2013). The Fic protein Doc uses an inverted substrate to phosphorylate and inactivate EF-Tu. Nat Chem Biol *9*, 811-817.

Chen, C.R., Malik, M., Snyder, M., and Drlica, K. (1996). DNA gyrase and topoisomerase IV on the bacterial chromosome: quinolone-induced DNA cleavage. J Mol Biol *258*, 627-637.

Cox, M.M., Goodman, M.F., Kreuzer, K.N., Sherratt, D.J., Sandler, S.J., and Marians, K.J. (2000). The importance of repairing stalled replication forks. Nature *404*, 37-41.

De Septenville, A.L., Duigou, S., Boubakri, H., and Michel, B. (2012). Replication fork reversal after replication-transcription collision. PLoS Genet *8*, e1002622.

Deghorain, M., Goeders, N., Jové, T., and Melderen, L. (2013). Type II Toxin-Antitoxin Loci: The *ccdAB* and *parDE* Families. In Prokaryotic Toxin-Antitoxins, K. Gerdes, ed. (Springer Berlin Heidelberg), pp. 45-67.

Deibler, R.W., Mann, J.K., Sumners de, W.L., and Zechiedrich, L. (2007). Hin-mediated DNA knotting and recombining promote replicon dysfunction and mutation. BMC Mol Biol *8*, 44.

Deibler, R.W., Rahmati, S., and Zechiedrich, E.L. (2001). Topoisomerase IV, alone, unknots DNA in *E. coli*. Genes Dev *15*, 748-761.

Dörr, T., Vulic, M., and Lewis, K. (2010). Ciprofloxacin causes persister formation by inducing the TisB toxin in *Escherichia coli*. PLoS Biol *8*, e1000317.

Engel, P., Goepfert, A., Stanger, F.V., Harms, A., Schmidt, A., Schirmer, T., and Dehio, C. (2012). Adenylylation control by intra- or intermolecular active-site obstruction in Fic proteins. Nature *482*, 107-110.

Erill, I., Campoy, S., and Barbe, J. (2007). Aeons of distress: an evolutionary perspective on the bacterial SOS response. FEMS Microbiol Rev *31*, 637-656.

Feng, F., Yang, F., Rong, W., Wu, X., Zhang, J., Chen, S., He, C., and Zhou, J.M. (2012). A *Xanthomonas* uridine 5'-monophosphate transferase inhibits plant immune kinases. Nature *485*, 114-118.

Fonville, N.C., Bates, D., Hastings, P.J., Hanawalt, P.C., and Rosenberg, S.M. (2010). Role of RecA and the SOS response in thymineless death in *Escherichia coli*. PLoS Genet *6*, e1000865.

Garcia-Pino, A., Christensen-Dalsgaard, M., Wyns, L., Yarmolinsky, M., Magnuson, R.D., Gerdes, K., and Loris, R. (2008). Doc of prophage P1 is inhibited by its antitoxin partner Phd through fold complementation. J Biol Chem *283*, 30821-30827.

Gerdes, K., and Maisonneuve, E. (2012). Bacterial persistence and toxin-antitoxin loci. Annu Rev Microbiol *66*, 103-123.

Goepfert, A., Harms, A., Schirmer, T., and Dehio, C. (2013a). Type II Toxin-Antitoxin Loci: The fic Family. In Prokaryotic Toxin-Antitoxins, K. Gerdes, ed. (Springer Berlin Heidelberg), pp. 177-187.

Goepfert, A., Stanger, F.V., Dehio, C., and Schirmer, T. (2013b). Conserved inhibitory mechanism and competent ATP binding mode for adenylyltransferases with Fic fold. PLoS One *8*, e64901.

Grainge, I., Bregu, M., Vazquez, M., Sivanathan, V., Ip, S.C., and Sherratt, D.J. (2007). Unlinking chromosome catenanes *in vivo* by site-specific recombination. EMBO J *26*, 4228-4238.

Grammel, M., Luong, P., Orth, K., and Hang, H.C. (2011). A chemical reporter for protein AMPylation. J Am Chem Soc *133*, 17103-17105.

Hardy, C.D., and Cozzarelli, N.R. (2003). Alteration of *Escherichia coli* topoisomerase IV to novobiocin resistance. Antimicrob Agents Chemother *47*, 941-947.

Heddle, J.G., Blance, S.J., Zamble, D.B., Hollfelder, F., Miller, D.A., Wentzell, L.M., Walsh, C.T., and Maxwell, A. (2001). The antibiotic microcin B17 is a DNA gyrase poison: characterisation of the mode of inhibition. J Mol Biol *307*, 1223-1234.

Huisman, O., D'Ari, R., and Gottesman, S. (1984). Cell-division control in Escherichia coli: specific induction of the SOS function SfiA protein is sufficient to block septation. Proc Natl Acad Sci USA *81*, 4490-4494.

Kato, J., Nishimura, Y., Imamura, R., Niki, H., Hiraga, S., and Suzuki, H. (1990). New topoisomerase essential for chromosome segregation in *E. coli*. Cell *63*, 393-404.

Khodursky, A.B., Peter, B.J., Schmid, M.B., DeRisi, J., Botstein, D., Brown, P.O., and Cozzarelli, N.R. (2000). Analysis of topoisomerase function in bacterial replication fork movement: use of DNA microarrays. Proc Natl Acad Sci USA *97*, 9419-9424.

Kinch, L.N., Yarbrough, M.L., Orth, K., and Grishin, N.V. (2009). Fido, a novel AMPylation domain common to fic, doc, and AvrB. PLoS One *4*, e5818.

Lopez, V., Martinez-Robles, M.L., Hernandez, P., Krimer, D.B., and Schvartzman, J.B. (2012). Topo IV is the topoisomerase that knots and unknots sister duplexes during DNA replication. Nucleic Acids Res *40*, 3563-3573.

Magnuson, R.D. (2007). Hypothetical functions of toxin-antitoxin systems. J Bacteriol *189*, 6089-6092.

Maisonneuve, E., Castro-Camargo, M., and Gerdes, K. (2013). (p)ppGpp controls bacterial persistence by stochastic induction of toxin-antitoxin activity. Cell *154*, 1140-1150.

Maisonneuve, E., and Gerdes, K. (2014). Molecular mechanisms underlying bacterial persisters. Cell *157*, 539-548.

Menzel, R., and Gellert, M. (1983). Regulation of the genes for *E. coli* DNA gyrase: homeostatic control of DNA supercoiling. Cell *34*, 105-113.

Meyer, A.S., and Grainger, D.C. (2013). The *Escherichia coli* Nucleoid in Stationary Phase. Adv Appl Microbiol *83*, 69-86.

Mukherjee, S., Liu, X., Arasaki, K., McDonough, J., Galan, J.E., and Roy, C.R. (2011). Modulation of Rab GTPase function by a protein phosphocholine transferase. Nature *477*, 103-106.

Pandey, D.P., and Gerdes, K. (2005). Toxin-antitoxin loci are highly abundant in free-living but lost from host-associated prokaryotes. Nucleic Acids Res *33*, 966-976.

Pedersen, K., Christensen, S.K., and Gerdes, K. (2002). Rapid induction and reversal of a bacteriostatic condition by controlled expression of toxins and antitoxins. Mol Microbiol *45*, 501-510.

Perez-Cheeks, B.A., Lee, C., Hayama, R., and Marians, K.J. (2012). A role for topoisomerase III in *Escherichia coli* chromosome segregation. Mol Microbiol *86*, 1007-1022.

Rovinskiy, N., Agbleke, A.A., Chesnokova, O., Pang, Z., and Higgins, N.P. (2012). Rates of gyrase supercoiling and transcription elongation control supercoil density in a bacterial chromosome. PLoS Genet *8*, e1002845.

Schuster, C.F., and Bertram, R. (2013). Toxin-antitoxin systems are ubiquitous and versatile modulators of prokaryotic cell fate. FEMS Microbiol Lett *340*, 73-85.

Sissi, C., and Palumbo, M. (2010). In front of and behind the replication fork: bacterial type IIA topoisomerases. Cell Mol Life Sci *67*, 2001-2024.

Utsumi, R., Nakamoto, Y., Kawamukai, M., Himeno, M., and Komano, T. (1982). Involvement of cyclic AMP and its receptor protein in filamentation of an *Escherichia coli fic* mutant. J Bacteriol *151*, 807-812.

Van Melderen, L. (2010). Toxin-antitoxin systems: why so many, what for? Curr Opin Microbiol *13*, 781-785.

Wang, X., Lord, D.M., Cheng, H.Y., Osbourne, D.O., Hong, S.H., Sanchez-Torres, V., Quiroga, C., Zheng, K., Herrmann, T., Peti, W., *et al.* (2012). A new type V toxin-antitoxin system where mRNA for toxin GhoT is cleaved by antitoxin GhoS. Nat Chem Biol *8*, 855-861.

Wigley, D.B. (2013). Bacterial DNA repair: recent insights into the mechanism of RecBCD, AddAB and AdnAB. Nat Rev Microbiol *11*, 9-13.

Wigley, D.B., Davies, G.J., Dodson, E.J., Maxwell, A., and Dodson, G. (1991). Crystal structure of an N-terminal fragment of the DNA gyrase B protein. Nature *351*, 624-629.

Witz, G., Dietler, G., and Stasiak, A. (2011). DNA knots and DNA supercoiling. Cell cycle *10*, 1339-1340.

Witz, G., and Stasiak, A. (2010). DNA supercoiling and its role in DNA decatenation and unknotting. Nucleic Acids Res *38*, 2119-2133.

Yarbrough, M.L., Li, Y., Kinch, L.N., Grishin, N.V., Ball, H.L., and Orth, K. (2009). AMPylation of Rho GTPases by *Vibrio* VopS disrupts effector binding and downstream signaling. Science *323*, 269-272.

Zähringer, F., Massa, C., and Schirmer, T. (2011). Efficient enzymatic production of the bacterial second messenger c-di-GMP by the diguanylate cyclase YdeH from *E. coli*. Appl Biochem Biotechnol *163*, 71-79.

Zaslaver, A., Bren, A., Ronen, M., Itzkovitz, S., Kikoin, I., Shavit, S., Liebermeister, W., Surette, M.G., and Alon, U. (2006). A comprehensive library of fluorescent transcriptional reporters for *Escherichia coli*. Nat Methods *3*, 623-628.

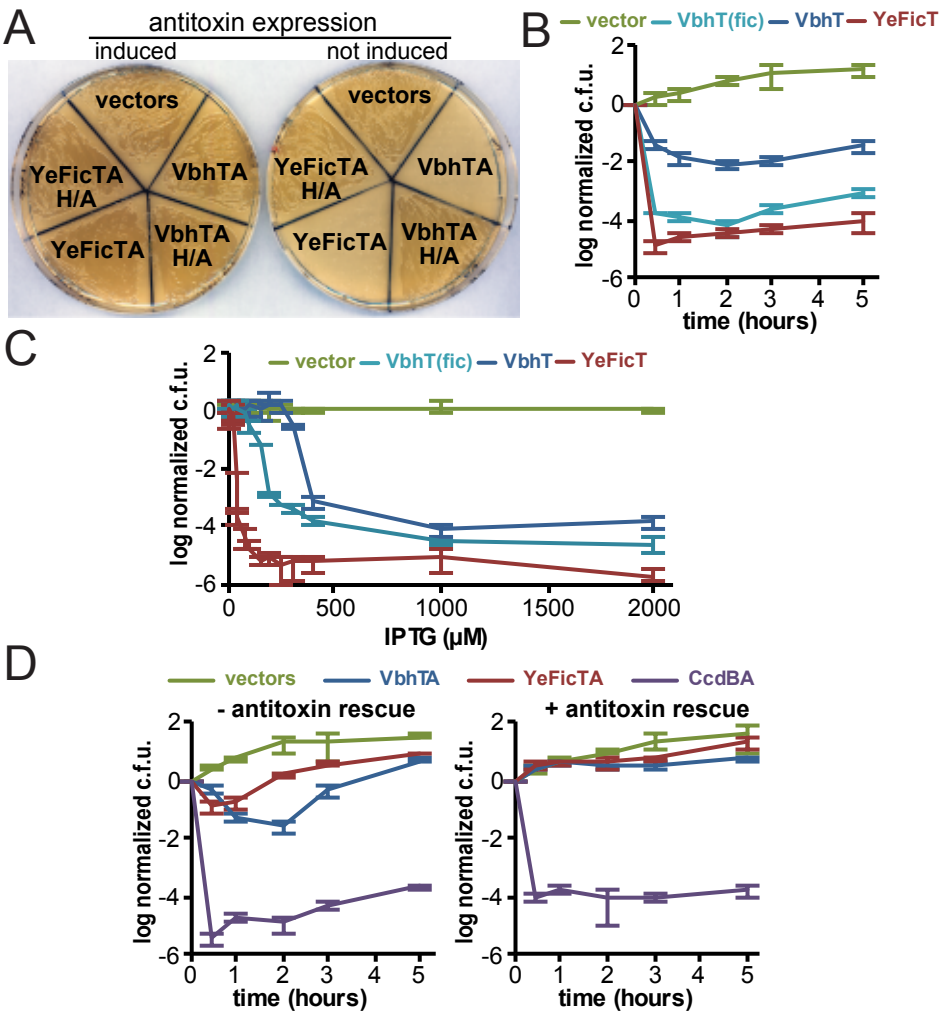

Figure 1. Fic toxins reversibly inhibit bacterial growth. (A) VbhT and YeFicT, but not catalytically inactive mutants (H/A), inhibit *E. coli* growth on LB agar plates in the absence of cognate VbhA or YeFicA antitoxins. The signature motifs of all FicTA modules investigated in this study are compared in Figure S1. **(B)** We followed the colony forming units (c.f.u. / ml) of exponentially growing *E. coli* cultures in which Fic toxin expression had been induced with 2000 µM of isopropyl β-D-thiogalactopyranoside (IPTG). The curves show a marked growth inhibition by YeFicT or only the FIC domain of VbhT (VbhT(fic)) and a lower potency of VbhT.**(C)** *E. coli* harboring plasmids for the expression of Fic toxins under P*lac* control were spotted onto agar plates containing different concentrations of IPTG. The decrease in c.f.u. depended on the dose of Fic toxin expression and mirrored the differential potency of the Fic toxin constructs as shown in (B). **(D)** The c.f.u. / ml of exponentially growing *E. coli* cultures harboring plasmids for the expression of toxins under P*lac* and cognate antitoxins under P*ara* control were monitored over time after the induction of Fic toxin expression by spotting on LB agar plates containing glucose (to inhibit toxin expression) or arabinose (to induce antitoxin expression). We find that the growth inhibition by Fic toxins, but not gyrase-poisoning toxin CcdB, is reversed by subsequent antitoxin expression. Weaker Fic toxicity in (D) compared to (B) is likely the consequence of leaky antitoxin expression. All data points and error bars are mean and s.d. of biological triplicates.

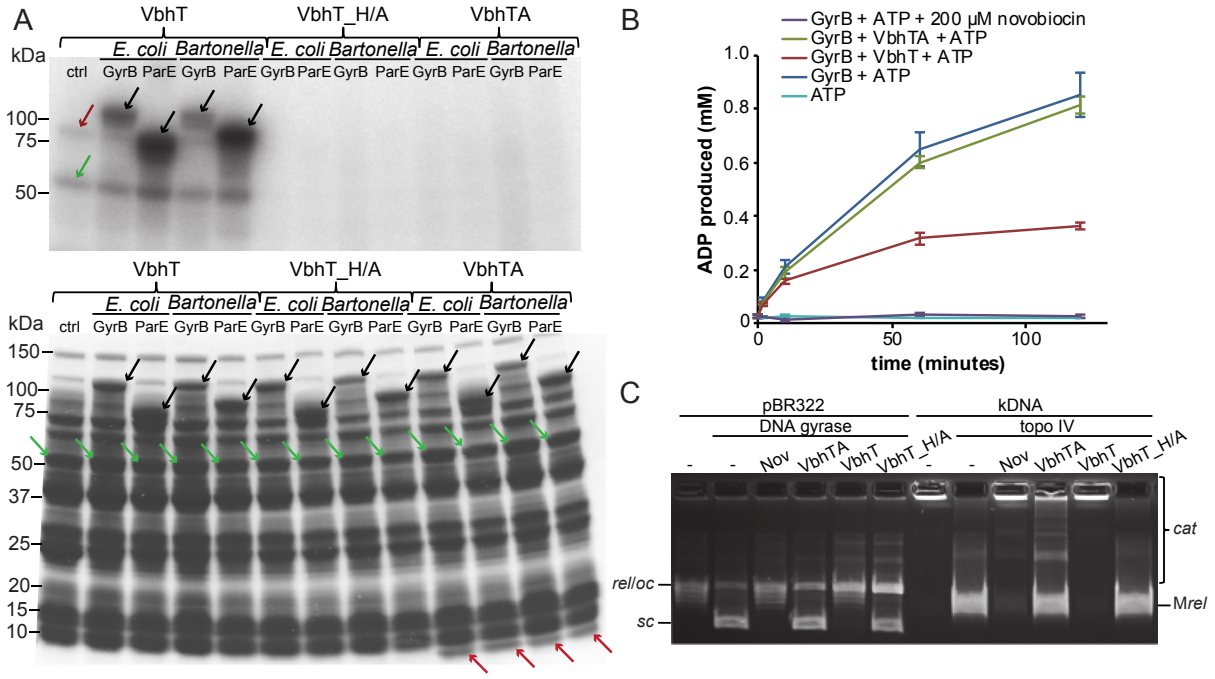

Figure 2. Fic toxins adenylylate DNA gyrase and topo IV which results in target inhibition *in vitro*. (A) Cleared lysates of *E. coli* that had expressed different VbhT constructs or target candidates were mixed, incubated with [α-32P]-ATP to trace adenylylation, and then analyzed using SDS-PAGE and autoradiography. The autoradiograph (top) shows VbhT auto-adenylylation (58 kDa; green arrow) and adenylylation of endogenous GyrB (90 kDa; red arrow) as well as ectopically expressed GyrB and ParE of *E. coli* and *B. schoenbuchensis* (as GST-fusions; black arrows). The Coomassie stain (bottom) of the same gel shows the presence of all ectopically expressed proteins (green: VbhT, magenta: VbhA, black: GST-GyrB and GST-ParE). Using mass spectrometry we mapped the adenylylation sites to be tyrosine 109 in *E. coli* GyrB and tyrosine 105 in *E. coli* ParE (Figure S2). **(B)** The ATPase activity of an N-terminal GyrB construct was assayed as the production of ADP by FPLC. The data show that adenylylation inhibits the ATPase activity of GyrB, albeit with slow kinetics (note the slow cessation of ADP production with VbhT). **(C)** The supercoiling and decatenation activities of recombinant DNA gyrase and topo IV were probed by monitoring the supercoiling (*sc*) of relaxed pBR322 (*rel*) and the decatenation of highly catenated kDNA (*cat*) into monomers (M*rel*) *in vitro*. The targets were pre-incubated with different Fic toxin constructs for one hour prior to the addition of DNA substrates. The agarose gel resolving the reaction products shows that both enzymes are fully inhibited by adenylylation as well as by novobiocin, though no considerable effect of adenylylation was apparent without pre-incubation, suggesting that Fic toxins are slow enzymes at least *in vitro* (data not shown). All data points and error bars are mean and s.d. of biological triplicates. *oc* = open circular (nicked) plasmid. In (B) and (C) VbhT, VbhT_H/A, and VbhTA denote corresponding constructs of VbhT(fic)A for technical reasons (see *Extended Experimental Procedures*).

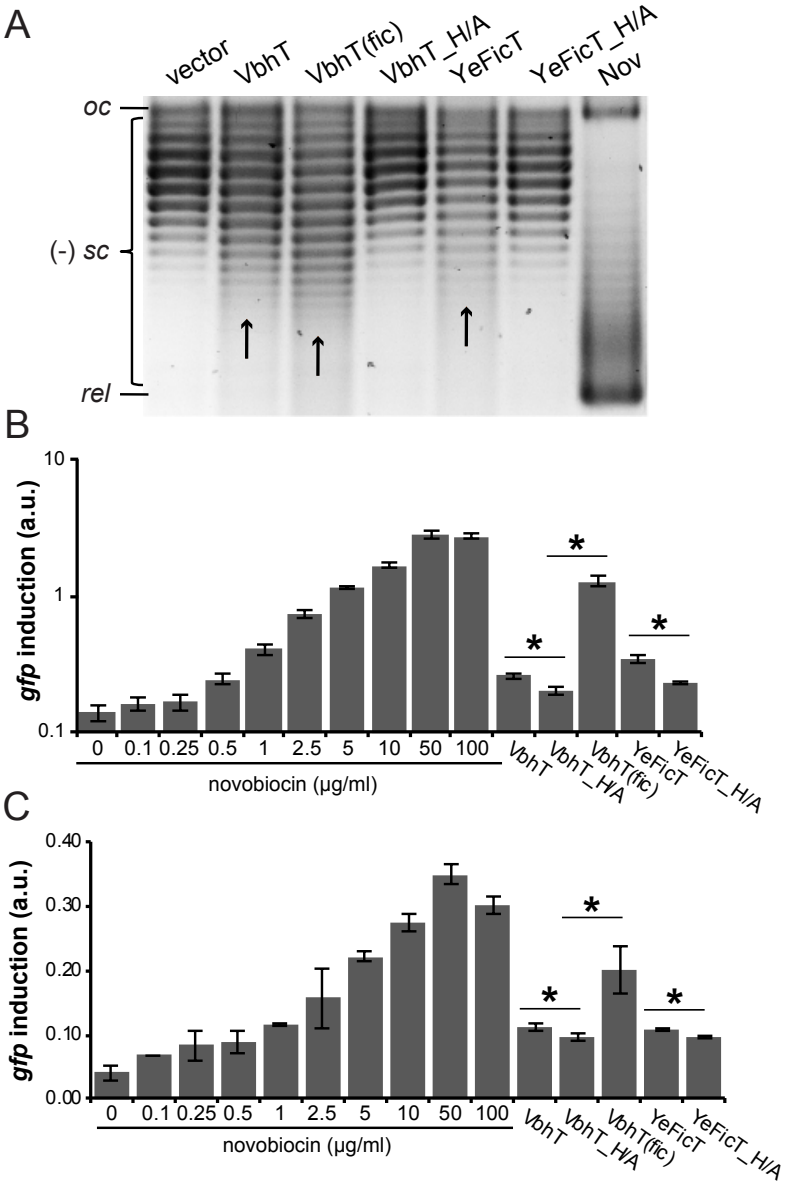

Figure 3. Fic toxins achieve only partial inhibition of DNA gyrase *in vivo*. (A) Reporter plasmid pAH160 was analyzed by high resolution agarose gel electrophoresis (in presence of 12.5 µg/ml chloroquine to resolve negative supercoiling) following isolation from *E. coli* that had expressed different Fic toxin constructs for two hours. The gel shows only a slight stretching of the pAH160 topoisomer distribution towards DNA relaxation (arrows), indicative of weak inhibition of DNA gyrase, while high concentrations of novobiocin (Nov; 100 µg/ml) fully abrogate the negative supercoiling. **(B)** The induction of a relaxation-sensitive P*gyrB::gfpmut2* module on a reporter plasmid was analyzed by flow cytometry in *E. coli* that had expressed different Fic toxin constructs for two hours. While novobiocin elicits a dose-dependent response (10 µg/ml fully inhibit DNA gyrase in *acrA*-deficient *E. coli* (Khodursky et al., 2000)), only a weak or intermediate induction of GFP expression is apparent with Fic toxins ($p<0.01$, unequal variance t-test). **(C)** A chromosomal P*gyrB::gfpmut2* module was used to assay nucleoid relaxation as described for the plasmid sensor in (B). Similarly, a significant but weak relaxation can be detected for VbhT or YeFicT, while the VbhT(fic) construct elicits a stronger induction of GFP fluorescence (all ($p<0.05$, unequal variance t-test). All data points and error bars are mean and s.d. of biological triplicates.

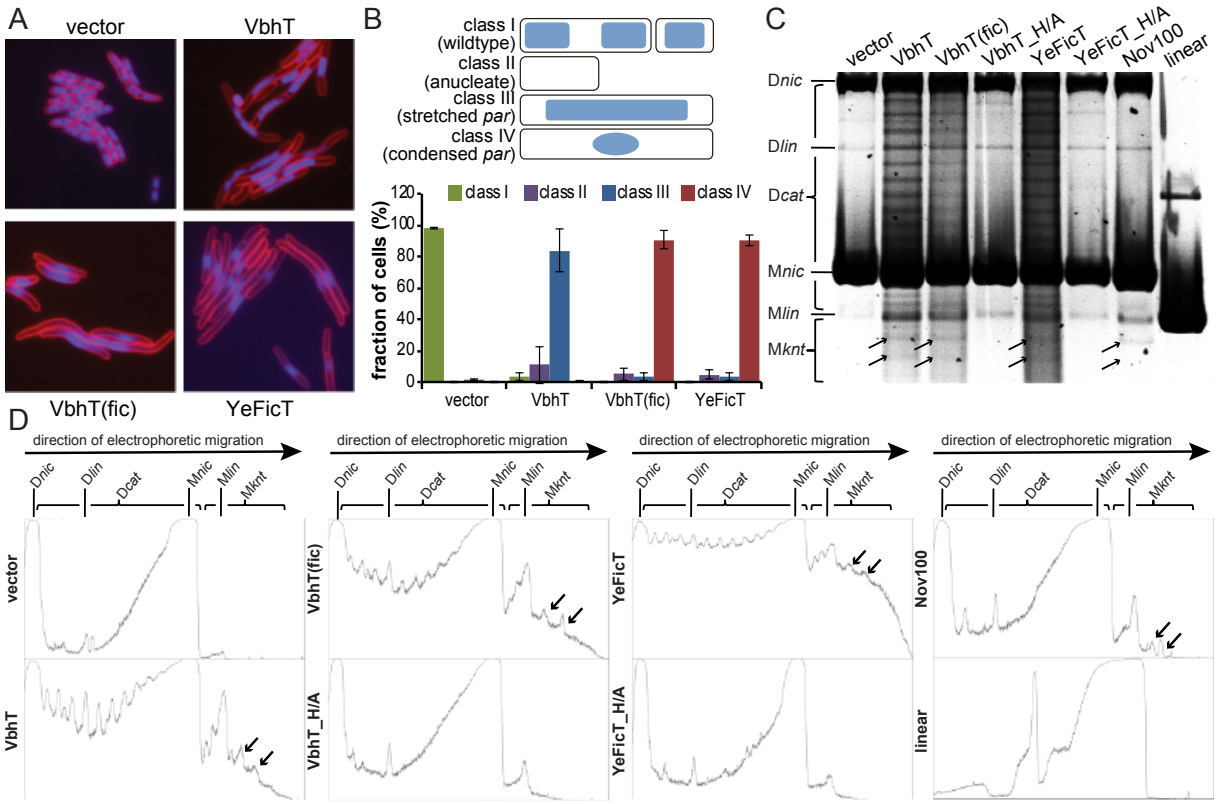

Figure 4. Fic toxin expression results in robust inhibition of topo IV *in vivo*. (A) *E. coli* that had expressed different Fic toxin constructs for two hours were stained with FM4-64 (membranes; red) and DAPI (DNA, blue) and analyzed by fluorescence microscopy. Fic toxin expression induces a "*par*" phenotype with cell filamentation and unsegregated nucleoids, indicative of strong topo IV inhibition. **(B)** Classification and quantification of the *par* phenotype show stretched nucleoids with VbhT and condensed nucleoids with VbhT(fic) and YeFicT. All data points are mean values of three independent experiments with error bars denoting s.d. **(C)** Nicking of the DNA samples used for Figure 3A separates nicked (*nic*) / linear (*lin*) dimers (*D*) and monomers (*M*) and reveals catenation (D*cat*) and knotting (M*knt*, arrows) upon Fic toxin expression. High concentrations of novobiocin (100 µg/ml, *Nov100*) immediately inactivate DNA gyrase (note collapsed supercoiling in Figure 3A) and topo IV, leading primarily to DNA knotting in the absence of DNA replication. **(D)** A lane plot was created for the gel shown in (C) using ImageJ (http://rsbweb.nih.gov/ij/download.html). Two bands of monomeric, knotted pAH160 reporter plasmid (arrows) are clearly visible for VbhT, VbhT(fic), and YeFicT expression as well as upon for treatment with 100 µg/ml novobiocin (inhibiting topo IV) but are absent in controls.

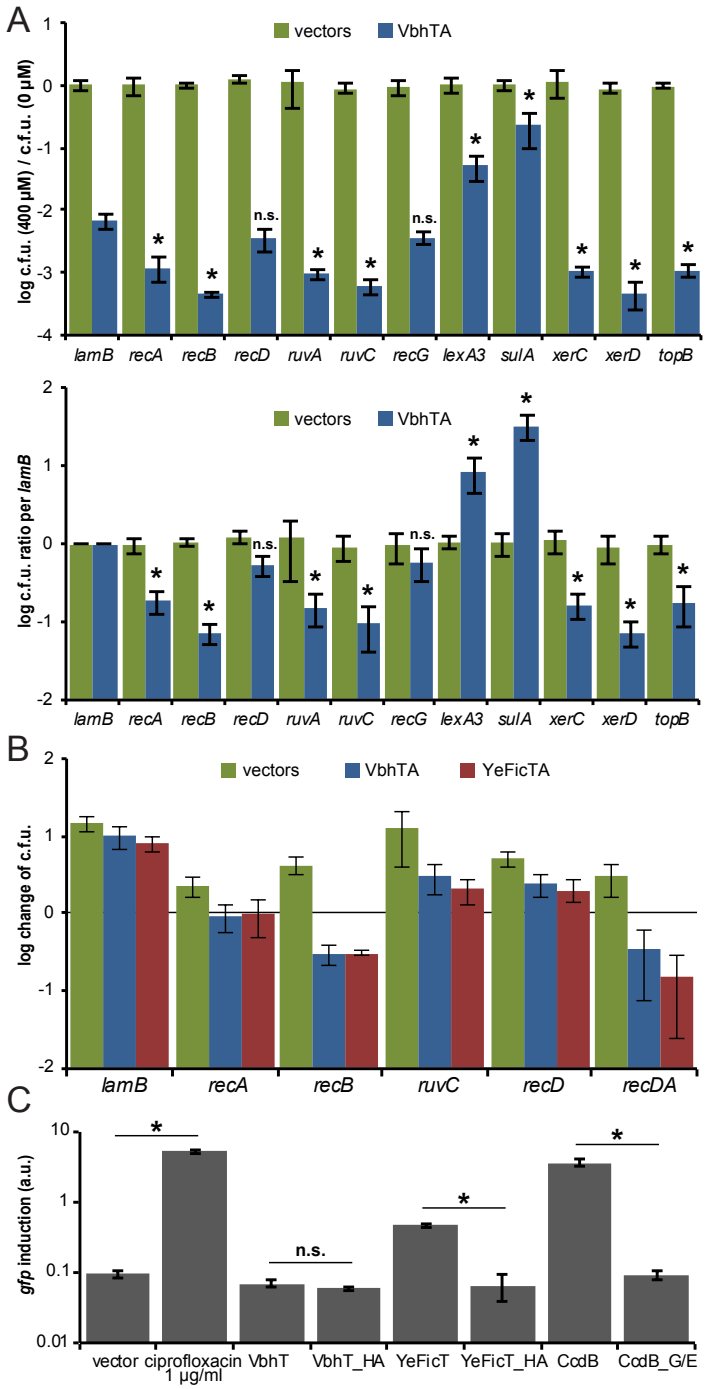

Figure 5. Fic toxin expression impairs DNA segregation and blocks replication fork movement (A) The differential susceptibility of various *E. coli* K-12 single gene mutants and an isogenic *lexA3* strain harboring Fic toxin as well as antitoxin vectors (to improve plasmid stability in hypersensitive strains via leaky expression) was quantified by forming the ratio of c.f.u. obtained on LB agar supplemented with 400 µM IPTG (to induce Fic toxin expression) over those on LB agar without IPTG (top) and subsequent normalization to the ratio obtained with *lamB* that served as an internal control (bottom). We detect an increased sensitivity to VbhT expression in mutants defective for XerCD recombination (*xerC* / *xerD*) or topoisomerase III (*topB*) which can partially complement topo IV regarding decatenation (Cox et al., 2000; Grainge et al., 2007; Perez-Cheeks et al., 2012).

Moreover, bacteria with defects in replication fork reversal, homologous recombination, and Holliday junction processing (*recA*, *recB*, *ruvA*, *ruvC*) are hypersensitive to Fic toxicity, while the sole inactivation of *recD,* part of Exonuclease V, or *recG*, one of the factors that can drive replication fork reversal, did not have a clear effect. Conversely, the inability to induce the SOS response (*lexA3*) or suppress cell division following SOS induction (*sulA*) makes *E. coli* more tolerant under the conditions tested ($p<0.05$, unequal variance t-test). n.s. = not significant **(B)** The reversibility of Fic toxicity (see Figure 1D) was assayed in different *E. coli* mutants by induction of antitoxin expression on LB agar plates subsequent to Fic toxin expression in liquid culture. Fic toxicity is reversible in the *lamB* control and *recA* / *recD* / *ruvC* single mutants (log change of c.f.u. ≥ 0), while dual inactivation of exonuclease V as well as homologous recombination activities in *recB* or *recDA* mutants results in detectable lethality (values ≤ 0), indicative of replication fork reversal driving fork repair after blockade (De Septenville et al., 2012). **(C)** The induction of the SOS response was probed using flow cytometry recording fluorescence from a plasmid-encoded P*sulA::gfpmut2* module with a procedure identical to the detection of DNA relaxation via a P*gyrB::gfpmut2* reporter (Figure 3B). The results show that YeFicT expression leads to some activation of the SOS response, but much weaker than gyrase-poisoning toxin CcdB or DNA-damaging drugs like ciprofloxacin (all $p<0.05$, unequal variance t-test), while the effects of VbhT expression were not significant (n.s.). The expression of inactive toxin mutants (FicT_H/A or CcdB_G100E) had no effect. All data points are mean values of three independent experiments with error bars denoting s.d.

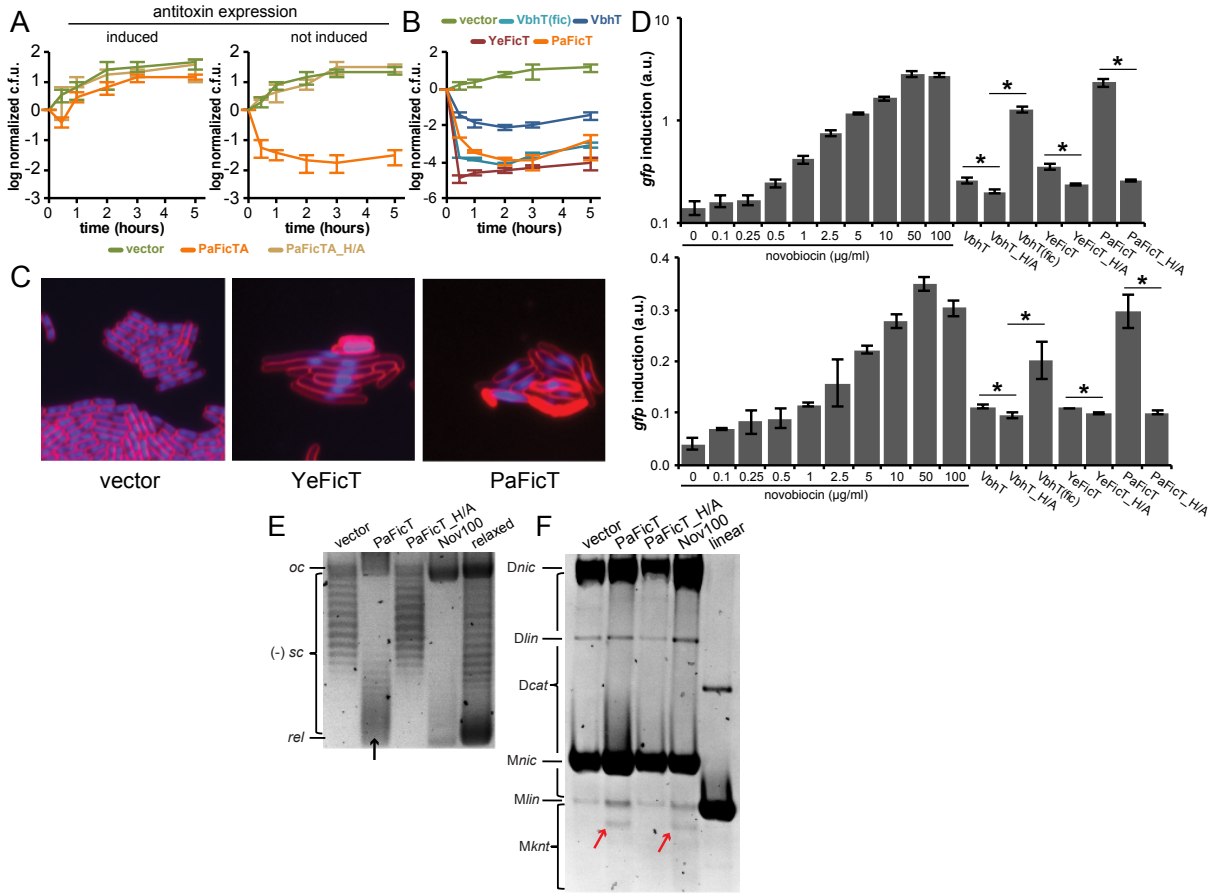

Figure 6. The PaFicTA system shows phenotypes similar to those observed with VbhTA and YeFicTA. (A) The c.f.u. / ml of exponentially growing *E. coli* cultures harboring plasmids for the expression of toxins under P*lac* and cognate antitoxins under P*ara* control were monitored over time. Toxin expression was induced with 2000 µM of IPTG in all cultures at t=0 and the results were compared for the presence and absence of a simultaneous induction of antitoxin expression with 0.2% L-arabinose. While the vector control and PaFicT_H/A expression showed no difference, the expression of PaFicT in the absence of PaFicA induction resulted in growth inhibition. **(B)** The growth inhibition of exponentially growing *E. coli* cultures in which PaFicT expression had been induced with 2000 µM of (IPTG) at t=0 was compared to the effects of other Fic toxins (see Figure 1B). Expression of the PaFicT construct resulted in a decrease of c.f.u. / ml by four logs that is most similar to the results obtained with the VbhT(fic) construct. Weaker growth inhibition with PaFicT in (A) compared to (B) is likely the consequence of leaky PaFicA expression. **(C)** Cell shape and DNA segregation of *E. coli* that had expressed PaFicT were analyzed as shown for the other toxins in Figure 4A (membranes: red, DNA: blue). The condensed nucleoid morphology and only weak filamentation upon PaFicT expression mostly resemble the phenotype obtained upon VbhT(fic) expression (see Figure 4A). **(D)** The induction of a plasmid-encoded (top) or chromosomal (bottom) P*gyrB::gfpmut2* module upon PaFicT expression was monitored as described for the other toxins in Figure 3B and Figure 3C. Expression of PaFicT results in strong DNA relaxation that is even more pronounced than the effects of VbhT(fic) expression, evidencing an ample inhibition of DNA gyrase ($p<0.01$, unequal variance t-test). **(E and F)** The DNA topology of a pAH160 reporter plasmid was analyzed using high resolution agarose gel electrophoresis as shown for the other toxins in Figure 3A and Figure 4C. The near-complete relaxation of plasmid DNA upon expression of PaFicT as revealed by chloroquine agarose

gel electrophoresis (E) is even stronger than the relaxation obtained with VbhT(fic), confirming the results shown in (D). An electrophoretic analysis of nicked reporter plasmid in (F) shows that PaFicT expression results in DNA knotting, but no detectable catenation. These results indicate a strong inhibition of both DNA gyrase and topo IV by PaFicT which rapidly inhibits DNA replication and thus the formation of catenanes (like novobiocin; (Khodursky et al., 2000)). All data points are mean values of three independent experiments with error bars denoting s.d.

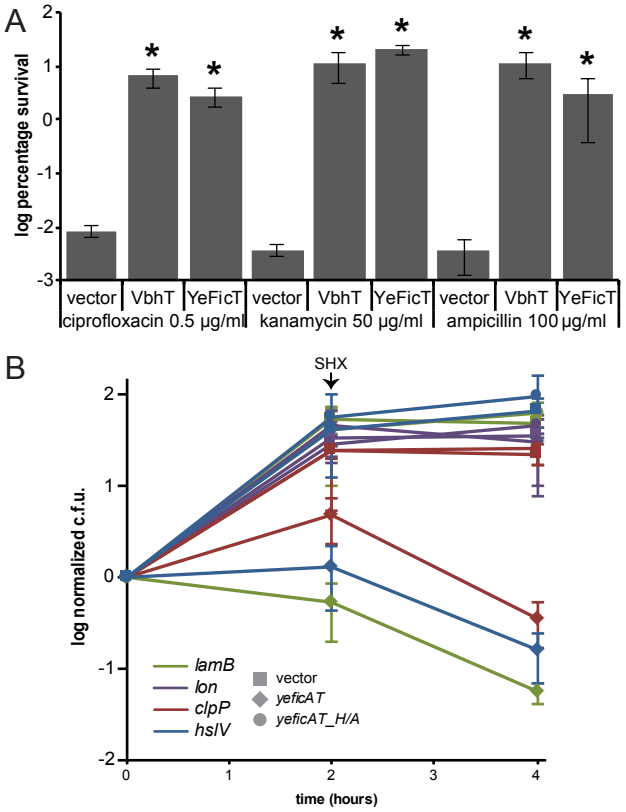

Figure 7. Fic toxin expression induces persister formation and can be activated *in vivo* by Lon. **(A)** Exponentially growing *E. coli* were induced to express Fic toxins for two hours and then challenged with a lethal concentration of one of three different antibiotics for three more hours so that only persisters would survive. C.f.u. / ml were determined before and after drug challenge; the data show a 1,000fold increased proportion of persisters in *E. coli* expressing Fic toxins ($p<0.001$, unequal variance t-test). This effect is largely independent of the weak SOS activation by Fic toxins (Figure S3C; see Figure 5C). **(B)** *E. coli* harboring a plasmid-encoded *yeficAT* module under P*lac* control were induced with 2000 µM IPTG and c.f.u. were recorded over time. It is apparent that the ectopic coexpression of *yeficAT* results in growth inhibition unless *lon* is inactivated. The growth defect is aggravated by Lon activation via the stringent response (+SHX = DL-serine hydroxamate). We confirmed that YeFicT toxicity is not generally reduced in the *lon* mutant and did not detect a similar effect with *vbhAT(fic)* (Figure S4A and S4B). All data points are mean values of three independent experiments with error bars denoting s.d.

Supplemental Information

Extended Results

Using a panel of diverse model proteins to study Fic toxins

In our previous work we established VbhT of *Bartonella schoenbuchensis* as a model system for class I FIC domain proteins and showed that its cognate antitoxin VbhA inhibits both the adenylylation activity of VbhT as well as the associated growth inhibition in *E. coli* (Engel et al., 2012). However, while most class I Fic proteins singly comprise a FIC domain, VbhT uniquely harbors a discernable type IV secretion signal at its C-terminus, a BID (Bep Intracellular Delivery) domain. BID domains are present in relaxases of a number of conjugation systems as well as the closely related host-targeted effectors of the genus *Bartonella* (Schulein et al., 2005), suggesting that VbhT may be secreted into a target cell (prokaryotic or eukaryotic) by the Vbh type IV secretion system (T4SS) encoded close-by. It was therefore possible that VbhT could have secondarily acquired a new function which may or may not rely on a different / altered biochemical activity than that of the other class I Fic proteins. We therefore decided to study VbhT along with other, more typical representatives to elucidate the molecular function and biological role of these proteins.

The prototypic EcFicT protein of *Escherichia coli* was the first Fic protein to be described and the "filamentation induced by cAMP" phenotype of its *fic-1* allele gave the name to the domain family (Utsumi et al., 1982). Being a genuine *E. coli* protein, EcFicT would have been an ideal candidate for a biological characterization in this classical model organism along with VbhT. However, we found that EcFicT is unlikely to be representative of the bulk of class I Fic proteins because it belongs to an atypical subgroup that is only found in *Enterobacteria* and harbors a secondarily deteriorated FIC domain active site motif (Figure S1). Consequently, EcFicT did not show adenylylation activity or inhibit bacterial growth (our unpublished results). However, we still used a Δ*ecficAT* derivative of *E. coli* str. K-12 substr. MG1655 for most experiments to exclude functional crosstalk of any kind between endogenous EcFicTA and the other model systems.

Instead of EcFicT we decided to characterize YeFicT of *Yersinia enterocolitica* str. 8081, an organism closely related to *E. coli* (Thomson et al., 2006). YeFicT has 37% protein sequence identity to EcFicT and 32% protein sequence identity to the FIC domain of VbhT of *B. schoenbuchensis*. Most importantly, YeFicT appears to be an average single-domain class I

Fic protein with a conserved FIC domain active site motif. Though not originally annotated in genome of *Y. enterocolitica* str. 8081, we identified the small ORF *yeficA* encoded upstream of *yeficT* with slight overlap as a candidate antitoxin with inhibitory α-helix and identical length to *vbhA*.

Finally, we studied a rather distant relative of our other model proteins to assess whether our findings may generally apply to all class I Fic proteins. For this purpose we chose PaFicT of *Pseudomonas aeruginosa* PAO1 with 22.1%, 16.6%, and 22.0% protein sequence identity in the conserved regions to YeFicT, EcFicT, and VbhT, respectively. Like for YeFicT, we identified the small ORF *paficA* encoded upstream of *paficT* with slight overlap that may serve as an antitoxin. Interestingly, the signature motifs of both the FIC domain in PaFicT (HXFX(D/E)GNGRXX**L** with a leucine instead of the final arginine) and PaFicA (SXXX**D**(G/N)) with an aspartate instead of the glutamate) slightly diverge from the canonical motifs as defined by Engel, Goepfert *et al.* (2012) (see Figure S1).

Extended Experimental Procedures

Bacterial handling and growth conditions.

Escherichia coli were transformed with one or more plasmids using TSS transformation (Chung et al., 1989) and always handled in LB liquid or solid medium containing appropriate antibiotics as well as 1% w/v D-glucose to suppress basal expression of any construct prior to the inoculation of experimental cultures. Unless stated differently, experiments were performed with exponentially growing derivatives of *E. coli* K-12 harboring pNDM220 derivatives (encoding Fic toxin constructs) and, whenever indicated, pBAD33 derivatives (encoding Fic antitoxins) as well as occasional other plasmids. For the enumeration of colony forming units (c.f.u.) bacterial cultures were serially diluted and spotted on LB agar plates which were thereafter incubated at 37°C for up to several days before counting. Selection for different genotypes or plasmid maintenance was performed with ampicillin ad 30 μg/ml (pNDM220 and derivatives) or 100 μg/ml (pGex-6p1 and derivatives), chloramphenicol ad 34 μg/ml, gentamicin ad 20 μg/ml, kanamycin ad 50 μg/ml, and tetracycline ad 12 μg/ml.

Plasmid Construction

Plasmids were constructed using standard procedures of restriction-based cloning or sequence- and ligation-independent cloning (SLIC) with enzymes obtained from New England Biolabs. For phenotypic analyses, toxin genes or *ficAT* modules were cloned into pNDM220 (Gotfredsen and Gerdes, 1998) under control of a particularly tight P*lac* (for pAH154 or pAH157 series, respectively) and antitoxin genes were cloned into pBAD33 under control of P*araB* (for pAH153 series), resulting in a two-plasmid expression system as it was used previously for the analysis of toxin-antitoxin interactions (Jorgensen et al., 2009). The *yeficA* and *paficA* antitoxin genes were identified as ORFs encoded by nucleotides 1’867’230-1’867’042 and 1’480’066-1’479’788 in the genomes of *Yersinia enterocolitica* str. 8081 (NC_008800) and *Pseudomonas aeruginosa* PAO1 (NC_002516.2), respectively. YeFicT and PaFicT are proteins YP_001005954.1 and NP_250057.1. For biochemical analyses and protein purification, toxins and / or antitoxins were cloned into pRSFDuet-1 (Novagen) and target candidates as glutathione S-transferase (GST) fusions into pGex-6p-1 (GE Healthcare). Point mutations and deletions were introduced via PCR into suitable template plasmids as described by Liu and Naismith (2008). Occasional sub-cloning of PCR products was

performed using the StrataClone blunt PCR cloning kit (Agilent). Plasmid construction was always confirmed by DNA sequencing.

Strain Construction

E. coli strains used for phenotypic analyses were generated from *E. coli* str. K-12 substr. MG1655 and protein expression was performed in *E. coli* BL21 or derivatives. Strains were constructed using the method of Datsenko and Wanner (2000). For the deletion of *ecficAT* in *E. coli* K-12 MG1655 the original locus was amplified with prAH361/362, sub-cloned, and the deletion allele was produced via amplification with prAH359/360. Subsequent allelic replacement via a *kanR* / *sacB* cassette (amplified from pJM05 (MacKichan et al., 2008) with prAH363/364) in the *ecficAT* locus resulted in strain AHE573 (*E. coli* str. K-12 substr. MG1655 Δ*ecficAT*. The deletion allele was constructed in a way to not affect expression of downstream gene *pabA* by leaving the last 55bp of the *ecficT* gene. The *lexA3* allele was moved via P1vir transduction from *E. coli* K996 (CGSC#: 7786) into AHE573 or, to yield a strain isogenic with the KEIO collection (Baba et al., 2006), into *E. coli* BW25113 (CGSC#: 7636) with selection for the *malE::tn10* marker close-by, resulting in AHE961 (*E. coli* K-12 Δec*ficAT lexA3 malE::tn10*) and AHE963 (*E. coli* BW25113 *lexA3 malE::tn10*). The *endA* gene in AHE573 was replaced by the inactive *endA** allele of BL21 (DE3) Gold (Agilent) to inactivate endonuclease I and improve the quality of isolated plasmids for high resolution agarose gel electrophoresis, resulting in AHE745 (*E. coli* K-12 Δec*ficAT endA**). Primers were prAH351/352 to amplify *endA* or *endA** and prAH366/367 for the locus-specific double-selectable cassette. The *acrA* gene in AHE745 was replaced with a gentamicin resistance cassette (amplified with prAH559/560 from pRS96 (Schulein et al., 2005)) to obtain a highly novobiocin-sensitive strain as it was used by Hardy and Cozzarelli (2003) (AHE938, *E. coli* K-12 Δ*ecficAT endA* acrA::genR*). For the construction of a chromosomal DNA relaxation sensor we first trimmed the promoter fragment of the pP*gyrB::gfpmut2* vector of Zaslaver *et al.* (2006) down to the P*gyrB* promoter as listed by RegulonDB (Schein et al., 2006) by site-directed mutagenesis with primers prAH909/910, creating plasmid pP*gyrB::gfpmut2*_v1. A cassette containing a kanamycin cassette as well as the P*gyrB::gfpmut2* module was amplified from pP*gyrB::gfpmut2*_v1 using primers prAH925/926 and integrated into the *gapC* locus of AHE938 using lambda Red recombineering, creating strain AHE1158 (*E. coli* K-12 Δ*ecficAT endA* acrA::genR*

gapC::PgyrB::gfpmut2_v1). A promoterless control was created analogously using plasmid pUA139 as the template for amplification, creating strain AHE1156 (*E. coli* K-12 Δ*ecficAT endA* acrA::genR gapC::pUA139*). The construction of all strains was confirmed by DNA sequencing.

Toxicity tests

Experiments were generally performed with *E. coli* K-12 MG1655 Δ*ecficAT* (AHE573) and derivatives or, when indicated, single gene mutants of the KEIO collection (Baba et al., 2006). The growth of *E. coli* expressing Fic toxins was qualitatively assessed on LB agar plates inducing Fic toxin expression with 2000 µM of Isopropyl β-D-thiogalactopyranoside (IPTG) in presence or absence of 0.2% w/v L-arabinose to induce antitoxin expression. For growth curves, Fic toxin expression was induced at t = 0 with 2000 µM of IPTG and the change in c.f.u. (on LB agar plates containing 1% D-glucose) was quantified by normalization to the c.f.u. at t = 0. When appropriate, the c.f.u. counts on plates containing 0.2% L-arabinose were enumerated in parallel. When indicated, the stringent response was induced with DL-serine hydroxamate (Sigma) ad 0.5 mg/ml. Differences in the susceptibility of various *E. coli* single gene mutants of the KEIO collection to Fic toxicity were assessed using the continuous expression of VbhT with 400 µM IPTG induction and the *lamB* mutant as an isogenic control. We chose this relatively low level of *lac* promoter induction and VbhT instead of YeFicT to avoid problems with saturating toxicity, leaky expression (especially in hypersensitive mutants), and an insufficient dynamic range to detect both increased and decreased susceptibility. The reversibility of Fic toxin expression by antitoxin induction upon plating on 0.2% L-arabinose with different *E. coli* mutants (Figure 5B) was tested after 90 minutes of Fic toxin induction to reliably detect both VbhT and YeFicT toxicity (see Figure 1D).

Persister assays

E. coli that had expressed Fic toxins for two hours were challenged with lethal concentrations of one of three different antibiotics (0.5 µg/ml ciprofloxacin, 50 µg/ml kanamycin, or 100 µg/ml ampicillin) so that only persisters would survive. Ampicillin was

added in combination with 10 µg/ml clavulanate to inactivate the β-lactamase encoded on pNDM220 and derivatives (Vakulenko et al., 1998). Three hours after drug challenge the bacteria were washed extensively in LB medium containing 20 mM $MgSO_4$ and plated in serial dilutions on LB agar plates containing 1% D-glucose. Persister frequencies were calculated by forming the ratio of c.f.u. counts after and before drug challenge.

Protein Expression and Purificaiton

VbhT constructs were generally expressed and purified as described previously (Engel et al., 2012). For purification, VbhT was expressed in form of truncated constructs devoid of the BID domain and together with its VbhA antitoxin for technical reasons (Engel et al., 2012). Note that purified "active" VbhT therefore indicates the presence of mutant VbhA(E24G) that is unable to inhibit the adenylylation activity of VbhT. The N-terminal 43 kDa fragment (1-392) of *E. coli* GyrB (Ali et al., 1993) was expressed from pFVS0109 in *E. coli* BL21 (DE3). Cultures were grown at 37°C in LB medium supplemented with 50 µg/ml of kanamycin and 0.1% D-glucose to an OD600 of 0.6 and then protein expression was induced with 0.35 mM IPTG for 16h at 23°C. Subsequently, bacteria were pelleted and resuspended in lysis buffer containing 50mM Tris pH 7.5, 1 mM EDTA, 5 mM DTT and disrupted using French press. Cell debris was removed by ultracentrifugation and the supernatant applied to a His-trap column (GE Healthcare). Proteins were eluted with a gradient of elution buffer containing 50mM Tris pH 7.5, 1 mM EDTA, 5 mM DTT and 500 mM imidazole. The protein was then concentrated and injected on a Superdex 75 16/60 gel filtration column (GE Healthcare) equilibrated with 50 mM Na-phosphate buffer pH 7.2, 1 mM EDTA and 5 mM DTT.

ATP hydrolysis assay

50 µM of a well-characterized N-terminal 43 kDa fragment of GyrB (Ali et al., 1993) was incubated with 10 µM of purified VbhT constructs (i.e., 5-fold excess of target), 1 mM ATP, and 1 mM $MgCl_2$ for up to 120 minutes. At 0, 2, 10, 60 and 120 minutes, an aliquot of each reaction was boiled for 5 minutes at 99°C and spun down at 16 000 *g* for 5 minutes to pellet the precipitated proteins. The supernatant composed of nucleotides was loaded on a Resource Q column (GE Healthcare) equilibrated with 5 mM ammonium bicarbonate pH 9.0.

Nucleotides were eluted with a gradient of elution buffer containing 1 M ammonium bicarbonate pH 9.0. Samples were analyzed by FPLC and nucleotide peak areas were integrated using the Unicorn software (GE Healthcare). The ATPase activity of GyrB was visualized as the production of ADP over time.

In vitro topoisomerase assays

Supercoiling and decatenation activities of recombinant type IIA topoisomerases of *E. coli* (TopoGEN Inc.) were performed according to the supplier's recommendations with one unit of enzyme per reaction and supplemented with novobiocin ad 5 μg/ml (to fully inhibit both topoisomerases) or 50 pmol of different purified constructs of VbhAT(fic) as indicated. Reactions were incubated for 30 minutes at 30°C and then 0.54 μg of relaxed pBR322 (DNA gyrase / supercoiling assays) or kDNA (topo IV / decatenation assays) was added. After incubation at 37°C for one hour the reactions were stopped with Universal Stop Buffer and treated with proteinase K to resolve any potential DNA – protein linkages. The DNA was purified by chloroform – isoamyl alcohol extraction, resolved by electrophoresis in 1.1% agarose gels, stained with the GR Green Nucleic Acid Stain (Biolabo SA), and imaged at a Safe Imager (Invitrogen) equipped with an EOS 40D camera (Canon). Recombinant DNA gyrase and topo IV, DNA substrates, and 5x Universal Stop Buffer were obtained from TopoGEN Inc. (Columbus, Ohio).

Flow cytometry with GFP promoter fusions

GFP fluorescence (excited at 488 nm) and forward scatter of exponentially growing *E. coli* AHE938 (with plasmid reporters) or AHE1156 / AHE1158 (chromosomal reporters) were recorded with a FACSCalibur flow cytometer (Becton Dickinson) two hours after drug treatment or the induction of Fic toxin expression. Data of ca. 25'000 cells per sample were analyzed using the FlowJo software (Tree Star) to obtain mean GFP fluorescence and mean forward scatter values. Fluorescence values were corrected for background fluorescence at the given experimental condition (determined with *E coli* AHE938 harboring pUA139 or AHE1156). Subsequently, we removed distortions of apparent fluorescence caused by differences in cell size via normalization to the forward scatter because Renggli *et al*. (2013) recently demonstrated that the distortions of both values show a strong linear correlation.

High-resolution agarose gel electrophoresis

For the analysis of DNA supercoiling, topoisomers of our pAH160 plasmid reporter were separated in gels containing 1% of agarose (Eurogentec) and 12.5 µg/ml of chloroquine (AppliChem) at 1.5 V/cm in the dark. Gels were washed extensively in water to remove chloroquine, stained with the GR Green Nucleic Acid Stain (Biolabo SA), and imaged at a Safe Imager (Invitrogen) equipped with an EOS 40D camera (Canon). As a control for DNA relaxation we treated reporter pAH160 with topoisomerase I (New England Biolabs) as suggested by the supplier. For the analysis of DNA catenation and knotting, plasmid supercoiling was removed by nicking with Nt.BbvCI (New England Biolabs) and topoisomers were resolved and visualized as described above without chloroquine. The presence of pNDM220 derivatives (size > 10'000 bp) in all samples did not impede analysis due to their low abundance and the huge size difference to pAH160 (4359 bp).

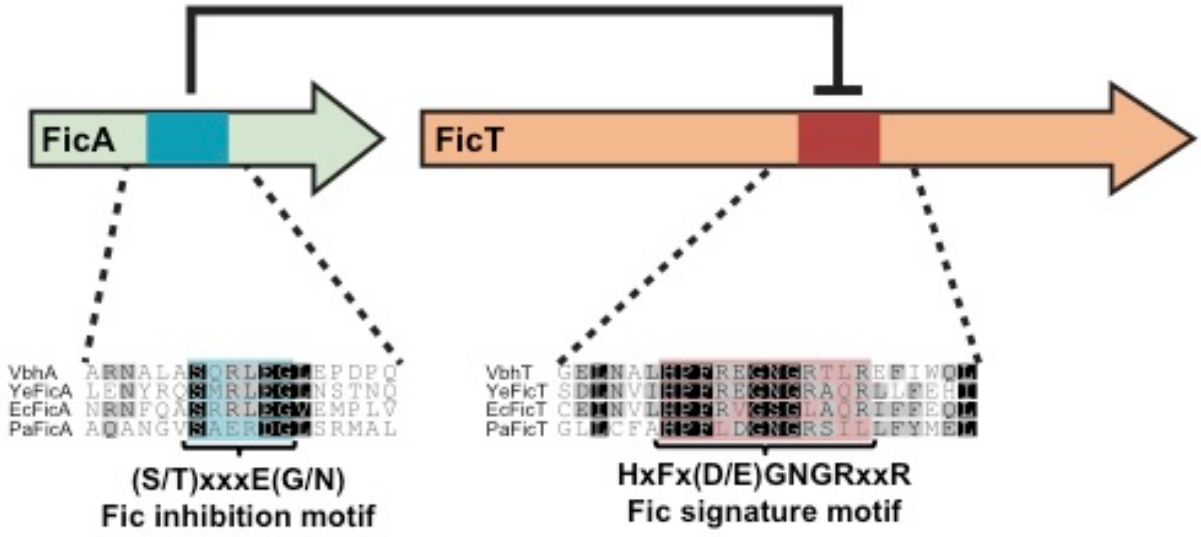

Figure S1. Comparison of FicA and FicT signature motifs of FicTA modules investigated in this study, Related to Figure 1. Protein sequences of FicA and FicT homologs were aligned using ClustalW (implemented in Geneious v.7.0.5), manually curated, and the signature motifs were extracted for illustration. Shading of amino acids indicates the degree of conservation according to the Blosum62 score matrix. The sequence alignments show that only EcFicT largely diverges from the canonical HXFX(D/E)GNGRXXR motif of Fic proteins as defined by Engel, Goepfert *et al.* (2012) (see also *Extended Results* in the Supplemental Information). All four FicA homologs contain an (SXXXE(G/N)) motif with the inhibitory glutamate being a chemically similar aspartate in PaFicA.

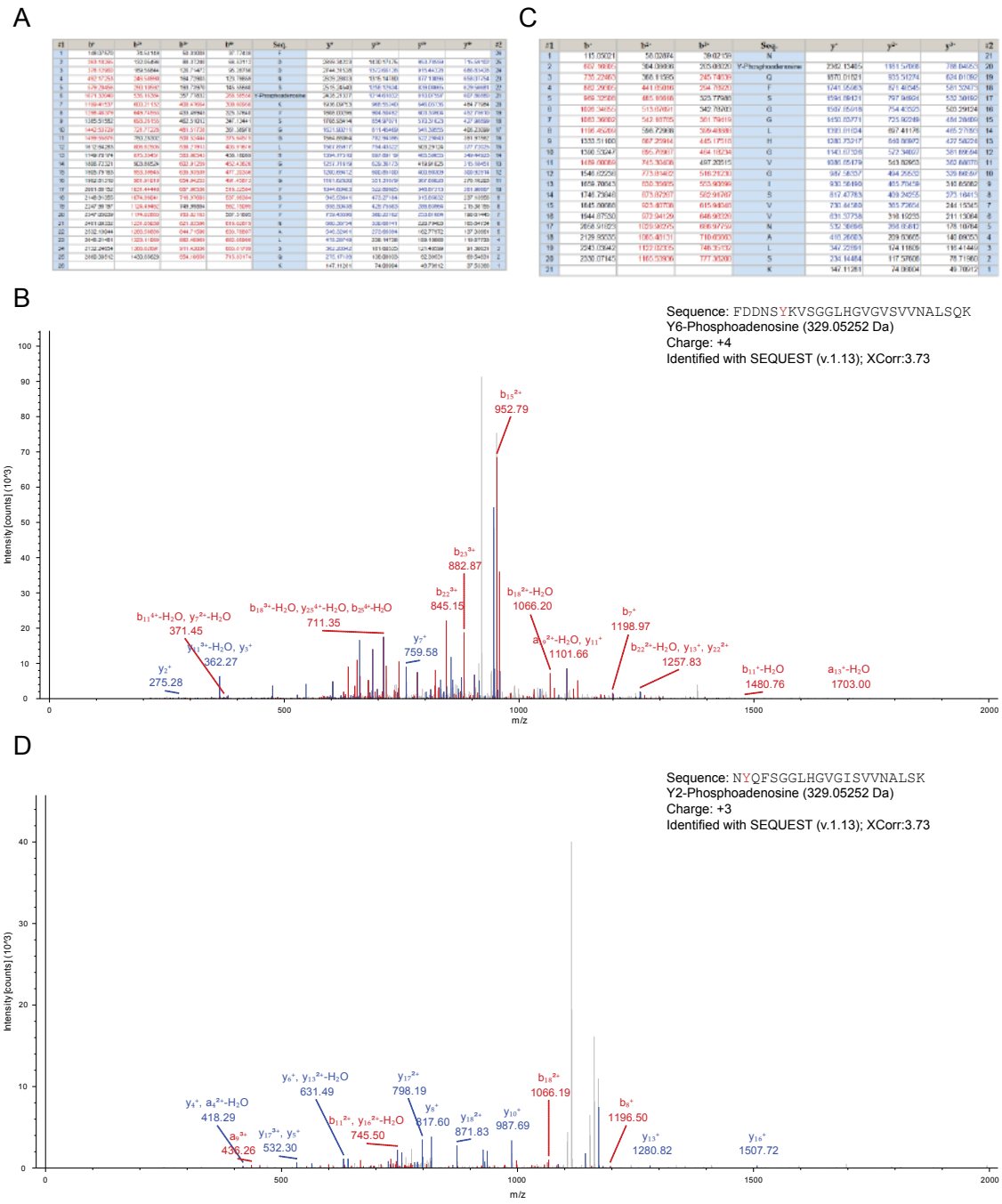

Figure S2. VbhT adenylylates Tyr109 and Tyr105 of *E. coli* GyrB and ParE, respectively, Related to Figure 2. Ion series and MS/MS spectra for detected adenylylated residues on GyrB **(A, B)** and ParE **(C, D)** are shown (see *Experimental Procedures*). The identified modified residue is marked in red. SEQUEST Xcorr search scores, peptide charge states and peptide sequence are shown in (B) and (D).

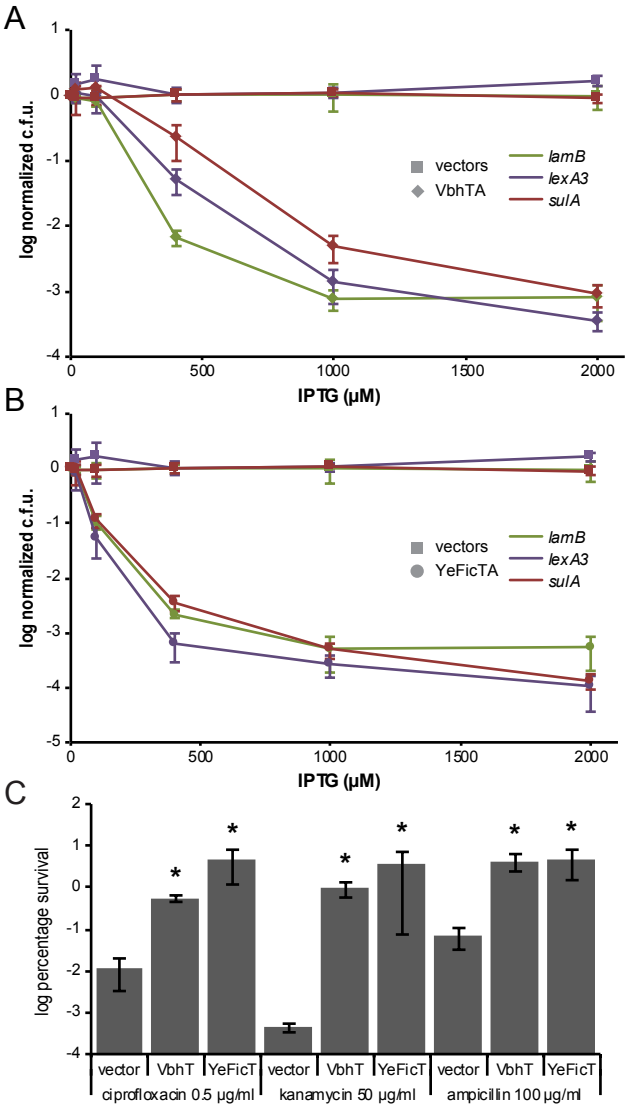

Figure S3. The minor SOS induction by Fic toxins does not greatly contribute to growth inhibition or persister formation, Related to Figure 5 and Figure 7. (A and B) We quantified the differential susceptibility of *E. coli lexA3* and *sulA* mutants as well as the *lamB* control to Fic toxicity by forming the ratio of c.f.u. obtained on LB agar supplemented with different concentrations of IPTG (to induce Fic toxin expression) over those on LB agar without IPTG. Both for VbhT (A) and YeFicT (B) the data show that the SOS response contributes to growth inhibition only at low levels of *ficT* expression and plays no role at 2000 µM of IPTG that we generally used for phenotypic characterization. **(C)** The persister formation of a *lexA3* derivative of AHE573 was quantified as for the parental strain (Figure 7A) and still revealed greatly increased fractions of persister cells upon Fic toxin expression ($p<0.05$, unequal variance t-test), showing that an inability to launch the SOS response does not greatly affect the phenotype. We note an unexpectedly increased tolerance of the vector control to ampicillin compared to AHE573 (Figure 7A), but an identical effect can also be seen in the data of Dörr *et al.* (2009) (figure 1, panel D) with the same concentration of ampicillin (100 µg/ml) and the same duration of drug challenge (3h). Data points are mean values of three independent experiments with error bars denoting s.d.

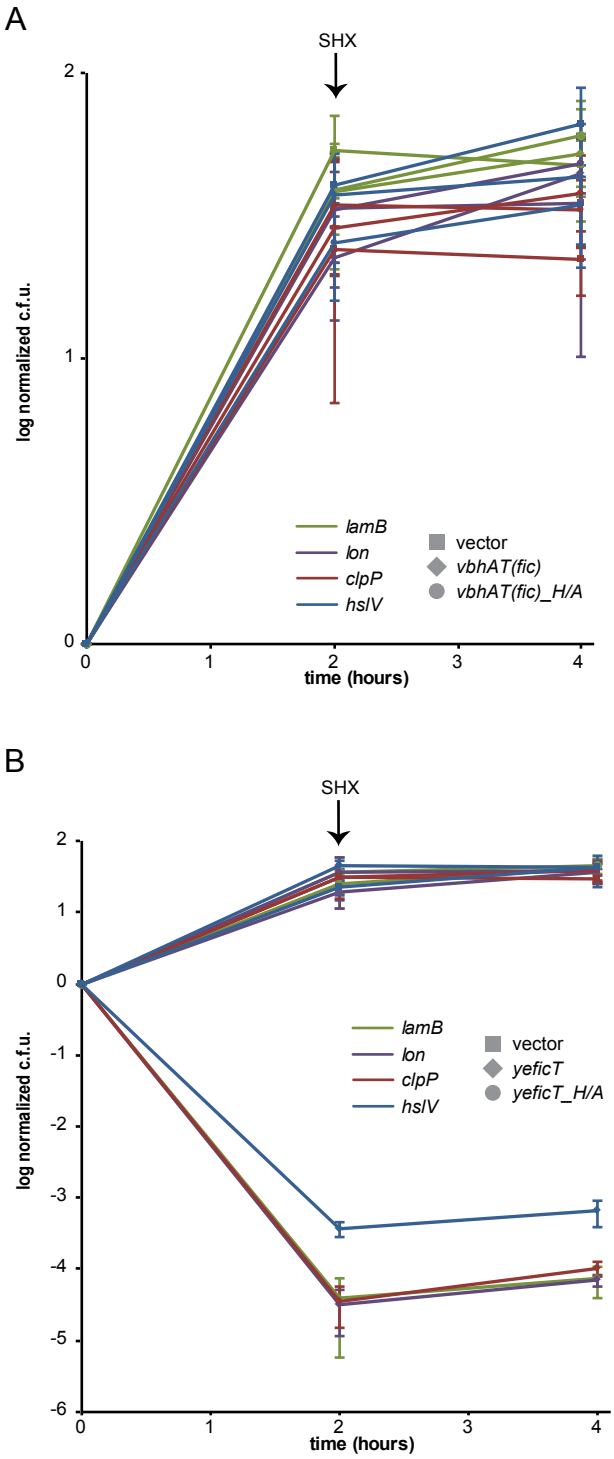

Figure S4. Additional results on Fic toxin activation by antitoxin degradation *in vivo*, Related to Figure 6. (A) The experiment of Figure 6B was repeated with *vbhAT(fic)* instead of *yeficAT*. No growth inhibition that would evidence toxin activation *in vivo* can be detected. **(B)** The experiment of Figure 6B was repeated with *yeficT* instead of *yeficAT* expression. The data show that the *lon* mutant is not less susceptible to Fic toxicity than the other mutants.

Table S1. List of oligonucleotides used in this study. Related to Experimental Procedures.

Primer name	*Sequence (5'-3')*
prAH116	GAATGCGTTGGCCCCGTTTCGAGAAGGTAATGGACGTAC
prAH127	CCTTCTCGAAACGGGGCCAACGCATTCAATTCGCCCATG
prAH260	GAGCGGGATCCATGTCGAATTCTTATGACTCC
prAH262	CTCCCGCTCGAGTTAAATATCGATATTCGCCGC
prAH286	GAGCGAGATCTATGACGCAAACTTATAACGCT
prAH288	CTCCCGCTCGAGTTAAACCTCAATCTCCGCCA
prAH289	GAGCGGGATCCATGAGTGATGAAACAACCTCA
prAH291	CTCCCGCTCGAGTTAGATATCAAGATTGGCAACA
prAH351	CATAATCGCGTAGTTCGTGG
prAH352	ATATGGTTGGCGGCATCTTC
prAH359	GCGCGGGCGCACTGCAGATGATATTTA
prAH360	GCAGTGCGCCCGCGCGAGAAATCATTA
prAH361	GATTTCGGTTACGCGGTATTT
prAH362	GAATAACGTCAAGGGAGATC
prAH363	GGTAGTTATCCTTTCCGCTAAAGTCCTGCCGTAATGATTTCTCGCGCGGGCGACATCATAACGGTTCTGG
prAH364	CAGATTCCCCGGCTTCGCTTACCACTTTGCTAAATATCATCTGCAGTGCGGGAATCGAAATCTCGTGATG
prAH366	CCAAAACAGCTTTCGCTACGTTGCTGGCTCGTTTTAACACGGAGTAAGTGCGACATCATAACGGTTCTGG
prAH367	GGTTGTACGCGTGGGGTAGGGGTTAACAAAAAGAATCCCGCTAGTGTAGGGGAATCGAAATCTCGTGATG
prAH412	ATCCTCCAAAATCGGATCTGGAAGTTCTGTTCCAGGGGCCCCTGGGATCCATGAGCGATAATAATAAAGATCTT
prAH413	CCGAAACGCGCGAGGCAGATCGTCAGTCAGTCACGATGCGGCCGCTCGAGTTAGATATCGAGATTATGAGCAA
prAH447	TTAATGTTATCGCCCCTTTCCGTGAAGGTAATGG
prAH448	CACGGAAAGGGGCGATAACATTAAGATCAGAATAGTA
prAH485a	GAGCGGGGATCCATAGGAGGAACAATTTTGTGAACAGCGATAAATACGG
prAH487	CTCCCGCGAATTCTTAACGAATACAGCGGGCG
prAH488	GAGCGGGGTACCATAGGAGGAACAATATGACGAGTCTGGCTGAGAA
prAH489	CTCCCGCAAGCTTTCACCGCGAACTCGGCTG
prAH490	GAGCGGGGTACCATAGGAGGAACAATATGTTGAGCGAGGAAGAAATC
prAH491	CTCCCGCAAGCTTTCATATTTCCTCACGTTTTATC
prAH496	GAGCGGGGTACCATAGGAGGAACAATATGAAGCAGCGTATTACAGTG
prAH497	CTCCCGCAAGCTTTCACCAGTCCCTGTTCTCG
prAH515	GAGCGGAGATCTATAGGAGGAACAATTTTGTGAGGAAATATGAGGGTAG
prAH516	CTCCCGCGAATTCTTACCTTGTAATTCCCTTTGAAG
prAH521	GAGCGGGGATCCATAGGAGGAACAATTTTATGCAGTTTAAGGTTTACACC
prAH522	CTCCCGCGAATTCTTATATTCCCCAGAACATCAG
prAH551	GTTCTGGGAAATATAAGAATTCACTGGCCG
prAH552	TTATATTTCCCAGAACATCAGGTTAATG
prAH559	CATTGACCAATTTGAAATCGGACACTCGAGGTTTACATATGAACAAAAACGCCAAGGATCTGATGGCGC
prAH560	TAAAGAAATTAGGCATGTCTTAACGGCTCCTGTTTAAGTTAAGACTTGGATTAGGTGGCGGTACTTGGG
prAH755	TGAATTTACATAAGAATTCACTGGCCGTCG
prAH756	GTGAATTCTTATGTAAATTCAGTGAGGTTTCTA
prAH909	GATTAACCCAAGTATAAAGAAGGAGATATACATATGAGTAAAGGAG
prAH910	GTATATCTCCTTCTTTATACTTGGGTTAATCCGTTATTTTACCCTT
prAH925	CCTCCGCCGAGAAATCGCAGGCGCATCTTGATGCTGGTGCGAAGAAGGTGGTATCATCAACAGGCTTACCC
prAH926	GCGGAGGTTTTTTCCTCCGCCTGTGCGCGTCAGAGTTTAGCGAATTTTTCCATAGACAGCCTGAAACAGG
prAH933	TCATCCACTCCCGCAAGCTTCCAGGTATCTCTTT

prAH935	GAGCGGGGTACCATAGGAGGAACAATTTTATGAGTTTCGATCCCTTTGG
prAH936	CTCCCGCGAATTCTTAGGGTTCGGAGTCGG
prAH937	CTTTGCGGCGCCCTTTCTAGACGGCAAC
prAH938	GAAAGGGCGCCGCAAAGCAAAGAAGTCC
prAH945	GAGCGGGGTACCATAGGAGGAACAATATGGAAAGGGGTTTACCG
prAH950	GTTCGAGGAATGGTACCGAGCTCGAATT
prAH952	ACCATTCCTCGAACAATATGGAAAGGGGTTTA
prFVS107	GGGAATTCCATATGCATCACCATCACCATCACTCGAATTCTTATGACTCCTCCAG
prFVS114	CGACCTCGAGTTAGGTCATTTCACGCGCGCGACG

This table lists all oligonucleotides used for the construction of strains and plasmids in this study.

Table S2. List of vectors used in this study. Related to Experimental Procedures.

Plasmid name	Description	Source / Reference	Primers used for insert PCR		Primers used for site-directed mutagenesis		Template for primer operation	Details on molecular cloning		
			fwd	rev	fwd	rev		restriction enzymes (insert)	vector backbone	restriction enzymes (vector)
pBAD33	Empty vector (p15A *ori*, *ParaB*)	Guzman *et al.* (1995)	-	-	-	-	-	-	-	-
pAH153_*ccdA*	*ccdA* in pBAD33	this study	prAH496	prAH497	-	-	*E. coli* Novablue	KpnI, HindIII	pBAD33	KpnI, HindIII
pAH153_*vbhA*	*vbhA* in pBAD33	this study	prAH490	prAH491	-	-	*B. schoenbuchensis*	KpnI, HindIII	pBAD33	KpnI, HindIII
pAH153_*paficA*	*paficA* in pBAD33	this study (site-directed mutagenesis to weaken ribosomal binding site)	prAH945	prAH933	prAH962	prAH950	*P. aeruginosa* PAO1	KpnI, HindIII	pBAD33	KpnI, HindIII
pAH153_*yeficA*	*yeficA* in pBAD33	this study	prAH488	prAH489	-	-	*Y. enterocolitica* 8081	KpnI, HindIII	pBAD33	KpnI, HindIII
pNDM220	Empty vector (mini-R1 *ori*, P*lac*)	Gottfredsen and Gerdes (1998)	-	-	-	-	-	-	-	-
pAH154_*ccdB*	*ccdB* in pNDM220	this study	prAH521	prAH522	-	-	*E. coli* Novablue	BamHI, EcoRI	pNDM220	BamHI, EcoRI
pAH154_*ccdB_*G/E	*ccdB*-Gly100Glu in pNDM220	this study	-	-	prAH551	prAH552	pAH154_*ccdB*	-	-	-
pAH154_*paficT*	*paficT* in pNDM220	this study	prAH935	prAH936	-	-	*P. aeruginosa* PAO1	KpnI, EcoRI	pNDM220	KpnI, EcoRI
pAH154_*paficT_*H/A	*paficT*-His 136Ala in pNDM220	this study	-	-	prAH937	prAH938	pAH154_*paficT*	-	-	-
pAH154_*vbhT*	*vbhT* in pNDM220	this study	prAH515	prAH516	-	-	*B. schoenbuchensis*	BglII, EcoRI	pNDM220	BamHI, EcoRI
pAH154_*vbhT(fic)*	*vbhT(fic)* in pNDM220	this study	-	-	prAH755	prAH756	pAH154_*vbhT*	-	-	-
pAH154_*vbhT_*H/A	*vbhT*-His136Ala in pNDM220	this study	-	-	prAH116	prAH127	pAH154_*vbhT*	-	-	-
pAH154_*yeficT*	*yeficT* in pNDM220	this study	prAH485a	prAH487	-	-	*Y. enterocolitica* 8081	BamHI, EcoRI	pNDM220	BamHI, EcoRI
pAH154_*yeficT_*H/A	*yeficT*-His 136Ala in pNDM220	this study	-	-	prAH447	prAH448	pAH154_*yeficT*	-	-	-
pAH157_*vbhAT*	*vbhAT* module in pNDM220	this study	prAH490	prAH516	-	-	*B. schoenbuchensis*	KpnI, EcoRI	pNDM220	KpnI, EcoRI
pAH157_*vbhAT(fic)*	*vbhAT* module with *vbhT(fic)* in pNDM220	this study	-	-	prAH755	prAH756	pAH157_*vbhAT*	-	-	-
pAH157_*vbhAT(fic)_*H/A	*vbhAT* module with *vbhT(fic)*-His136Ala in pNDM220	this study	-	-	prAH116	prAH127	pAH157_*vbhAT(fic)*	-	-	-
pAH157_*yeficAT*	*yeficAT* module in pNDM220	this study	prAH488	prAH487	-	-	*Y. enterocolitica* 8081	KpnI, EcoRI	pNDM220	KpnI, EcoRI
pAH157_*yeficAT_*H/A	*yeficAT* module with *yeficT(fic)*-His136Ala in pNDM220	this study	-	-	prAH447	prAH448	pAH157_*yeficAT*	-	-	-
pGex-6p-1	Empty vector (ColE1 *ori*, P*tac*)	GE Healthcare	-	-	-	-	-	-	-	-
pAH111	*E. coli gyrB* in pGex-6p-1 (GST-fusion)	this study	prAH260	prAH262	-	-	*E. coli* K-12 MG1655	BamHI, XhoI	pGex-6p-1	BamHI, XhoI
pAH119	*E. coli parE* in pGex-6p-1 (GST-fusion)	this study	prAH286	prAH288	-	-	*E. coli* K-12 MG1655	BglII, XhoI	pGex-6p-1	BamHI, XhoI
pAH120	*B. schoenbuchensis gyrB* in pGex-6p-1 (GST-fusion)	this study	prAH289	prAH291	-	-	*B. schoenbuchensis*	BamHI, XhoI	pGex-6p-1	BamHI, XhoI
pAH139	*B. schoenbuchensis parE* in pGex-6p-1 (GST-fusion)	this study	prAH412	prAH413	-	-	*B. schoenbuchensis*	BamHI, XhoI	pGex-6p-1	BamHI, XhoI
pRSFDuet-1	Empty vector (RSF1030 *ori*, P*T7* MCS1, P*T7* MCS2)	Novagen	-	-	-	-	-	-	-	-
pFVS0011	VbhA (MCS1, HA-tagged) + VbhT 1-198 (MCS2, His6-tagged) in pRSFDuet1	Engel, Goepfert *et al.* (2012)	-	-	-	-	-	-	-	-
pFVS0012	VbhT 1-198 (MCS2, His6-tagged) in pRSFDuet1	Engel, Goepfert *et al.* (2012)	-	-	-	-	-	-	-	-
pFVS0065	VbhA Glu25Gly (MCS1, HA-tagged) + VbhT 1-198 (MCS2, His6-tagged) in pRSFDuet1	Engel, Goepfert *et al.* (2012)	-	-	-	-	-	-	-	-
pFVS0080	VbhA Glu25Gly (MCS1, HA-tagged) + VbhT 1-198 His136Ala (MCS2, His6-tagged) in pRSFDuet1	Engel, Goepfert *et al.* (2012)	-	-	-	-	-	-	-	-
pPE0017	VbhT (MCS1) in pRSFDuet-1 (His6-tagged)	Engel, Goepfert *et al.* (2012)	-	-	-	-	-	-	-	-
pPE0021	VbhT (MCS1, His6-tagged) and VbhA (MCS2, HA-tagged) in pRSFDuet-1	Engel, Goepfert *et al.* (2012)	-	-	-	-	-	-	-	-
pPE0034	VbhT-H138A (MCS1) in pRSFDuet-1 (His6-tagged	Engel, Goepfert *et al.* (2012)	-	-	-	-	-	-	-	-
pFVS0109	*E. coli gyrB* 2-392 (MCS2, N-ter His6-tagged) in pRSFDuet-1	this study	prFVS107	prFVS114	-	-	*E. coli* K-12 MG1655	NdeI, XhoI	pRSFDuet-1	NdeI, XhoI
pAH160	Empty vector (RSF1030 *ori* of pRSFDuet-1, *rhaRS+PmaB* of *E. coli* K-12)	this study	prAH684, prAH1586	prAH685, prAH1587	-	-	*E. coli* K-12 MG1655 (prAH584/5), pRSFDuet-1 (prAH586/7)	- (fragments fused via SLIC)		
pPgyrB::*gfpmut2*	P*gyrB* reporter in pSC101 *ori* plasmid	Zaslaver *et al.* (2006)	-	-	-	-	-	-	-	-
pPgyrB::*gfpmut2*_v1	optimized P*gyrB* reporter in pSC101 *ori* plasmid	This study	-	-	prAH909	prAH810	pPgyrB::*gfpmut2*	-	-	-
pPsulA::*gfpmut2*	P*sulA* reporter in pSC101 *ori* plasmid	Zaslaver *et al.* (2006)	-	-	-	-	-	-	-	-
pUA139	promoterless parental vector of GFP fusions by Zaslaver et al.(Zaslaver et al., 2006)	Zaslaver *et al.* (2006)	-	-	-	-	-	-	-	-

This table lists all plasmids used throughout this study and contains all relevant details of their construction.

Supplemental References

Ali, J.A., Jackson, A.P., Howells, A.J., and Maxwell, A. (1993). The 43-kilodalton N-terminal fragment of the DNA gyrase B protein hydrolyzes ATP and binds coumarin drugs. Biochemistry *32*, 2717-2724.

Baba, T., Ara, T., Hasegawa, M., Takai, Y., Okumura, Y., Baba, M., Datsenko, K.A., Tomita, M., Wanner, B.L., and Mori, H. (2006). Construction of *Escherichia coli* K-12 in-frame, single-gene knockout mutants: the Keio collection. Mol Syst Biol *2*, 2006 0008.

Chung, C.T., Niemela, S.L., and Miller, R.H. (1989). One-step preparation of competent *Escherichia coli*: transformation and storage of bacterial cells in the same solution. Proc Natl Acad Sci USA *86*, 2172-2175.

Datsenko, K.A., and Wanner, B.L. (2000). One-step inactivation of chromosomal genes in Escherichia coli K-12 using PCR products. Proc Natl Acad Sci USA *97*, 6640-6645.

Dörr, T., Lewis, K., and Vulić, M. (2009). SOS Response Induces Persistence to Fluoroquinolones in *Escherichia coli*. PLoS Genet *5*, e1000760.

Engel, P., Goepfert, A., Stanger, F.V., Harms, A., Schmidt, A., Schirmer, T., and Dehio, C. (2012). Adenylylation control by intra- or intermolecular active-site obstruction in Fic proteins. Nature *482*, 107-110.

Gotfredsen, M., and Gerdes, K. (1998). The *Escherichia coli relBE* genes belong to a new toxin-antitoxin gene family. Mol Microbiol *29*, 1065-1076.

Hardy, C.D., and Cozzarelli, N.R. (2003). Alteration of *Escherichia coli* topoisomerase IV to novobiocin resistance. Antimicrob Agents Chemother *47*, 941-947.

Jorgensen, M.G., Pandey, D.P., Jaskolska, M., and Gerdes, K. (2009). HicA of *Escherichia coli* defines a novel family of translation-independent mRNA interferases in bacteria and archaea. J Bacteriol *191*, 1191-1199.

Liu, H., and Naismith, J.H. (2008). An efficient one-step site-directed deletion, insertion, single and multiple-site plasmid mutagenesis protocol. BMC Biotechnol *8*, 91.

MacKichan, J.K., Gerns, H.L., Chen, Y.T., Zhang, P., and Koehler, J.E. (2008). A SacB mutagenesis strategy reveals that the *Bartonella quintana* variably expressed outer membrane proteins are required for bloodstream infection of the host. Infect Immun *76*, 788-795.

Renggli, S., Keck, W., Jenal, U., and Ritz, D. (2013). Role of autofluorescence in flow cytometric analysis of *Escherichia coli* treated with bactericidal antibiotics. J Bacteriol *195*, 4067-4073.

Schein, C.H., Volk, D.E., Oezguen, N., and Paul, A. (2006). Novel, structure-based mechanism for uridylylation of the genome-linked peptide (VPg) of picornaviruses. Proteins *63*, 719-726.

Schulein, R., Guye, P., Rhomberg, T.A., Schmid, M.C., Schroder, G., Vergunst, A.C., Carena, I., and Dehio, C. (2005). A bipartite signal mediates the transfer of type IV secretion substrates of *Bartonella henselae* into human cells. Proc Natl Acad Sci USA *102*, 856-861.

Thomson, N.R., Howard, S., Wren, B.W., Holden, M.T., Crossman, L., Challis, G.L., Churcher, C., Mungall, K., Brooks, K., Chillingworth, T.*, et al.* (2006). The complete genome sequence and comparative genome analysis of the high pathogenicity *Yersinia enterocolitica* strain 8081. PLoS Genet *2*, e206.

Utsumi, R., Nakamoto, Y., Kawamukai, M., Himeno, M., and Komano, T. (1982). Involvement of cyclic AMP and its receptor protein in filamentation of an *Escherichia coli fic* mutant. J Bacteriol *151*, 807-812.

Vakulenko, S.B., Geryk, B., Kotra, L.P., Mobashery, S., and Lerner, S.A. (1998). Selection and characterization of β-lactam-β-lactamase inactivator-resistant mutants following PCR mutagenesis of the TEM-1 β-lactamase gene. Antimicrob Agents Chemother *42*, 1542-1548.

Zaslaver, A., Bren, A., Ronen, M., Itzkovitz, S., Kikoin, I., Shavit, S., Liebermeister, W., Surette, M.G., and Alon, U. (2006). A comprehensive library of fluorescent transcriptional reporters for *Escherichia coli*. Nat Methods *3*, 623-628.

3.4. *Research article IV* (Stanger *et al.*, *PLoS ONE*, in press)

Structure of the N-terminal gyrase B fragment in complex with ADP·Pi reveals rigid-body motion induced by ATP hydrolysis

Frédéric V. Stanger, Christoph Dehio & Tilman Schirmer

***PLoS ONE*, in press.**

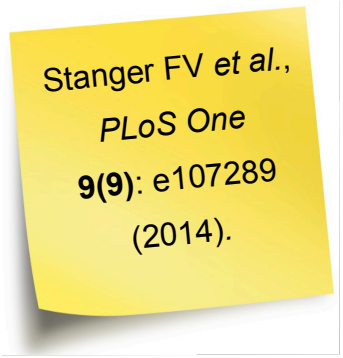

3.4.1. Statement of my own contributions

I designed and performed all experiments described in the *research article IV*. I cloned, expressed, purified and crystallized the N-terminal 43-kDa fragment of GyrB comprising the ATPase and transducer domains in complex with different nucleotides or analogs. I then determined the crystallographic structures.

Tilman Schirmer and myself analyzed the data. The manuscript was written by myself, Christoph Dehio and Tilman Schirmer. I prepared and assembled all the figures and tables presented in the manuscript.

3.4.2. "Structure of GyrB in complex with ADP·Pi reveals rigid-body motions induced by ATP hydrolysis"

OPEN ACCESS Freely available online

PLOS ONE

Structure of the N-Terminal Gyrase B Fragment in Complex with ADP·P_i Reveals Rigid-Body Motion Induced by ATP Hydrolysis

Frédéric V. Stanger[1,2], Christoph Dehio[2], Tilman Schirmer[1]*

1 Focal Area Structural Biology and Biophysics, Biozentrum, University of Basel, Basel, Switzerland, **2** Focal Area Infection Biology, Biozentrum, University of Basel, Basel, Switzerland

Abstract

Type II DNA topoisomerases are essential enzymes that catalyze topological rearrangement of double-stranded DNA using the free energy generated by ATP hydrolysis. Bacterial DNA gyrase is a prototype of this family and is composed of two subunits (GyrA, GyrB) that form a $GyrA_2GyrB_2$ heterotetramer. The N-terminal 43-kDa fragment of GyrB (GyrB43) from *E. coli* comprising the ATPase and the transducer domains has been studied extensively. The dimeric fragment is competent for ATP hydrolysis and its structure in complex with the substrate analog AMPPNP is known. Here, we have determined the remaining conformational states of the enzyme along the ATP hydrolysis reaction path by solving crystal structures of GyrB43 in complex with ADP·BeF_3, ADP·P_i, and ADP. Upon hydrolysis, the enzyme undergoes an obligatory 12° domain rearrangement to accommodate the 1.5 Å increase in distance between the γ- and β-phosphate of the nucleotide within the sealed binding site at the domain interface. Conserved residues from the QTK loop of the transducer domain (also part of the domain interface) couple the small structural change within the binding site with the rigid body motion. The domain reorientation is reflected in a significant 7 Å increase in the separation of the two transducer domains of the dimer that would embrace one of the DNA segments in full-length gyrase. The observed conformational change is likely to be relevant for the allosteric coordination of ATP hydrolysis with DNA binding, cleavage/re-ligation and/or strand passage.

Citation: Stanger FV, Dehio C, Schirmer T (2014) Structure of the N-Terminal Gyrase B Fragment in Complex with ADP·P_i Reveals Rigid-Body Motion Induced by ATP Hydrolysis. PLoS ONE 9(9): e107289. doi:10.1371/journal.pone.0107289

Editor: Kornelius Zeth, University of the Basque Country, Spain

Received July 8, 2014; **Accepted** August 12, 2014; **Published** September 9, 2014

Data Availability: The authors confirm that all data underlying the findings are fully available without restriction. Coordinates and structure factors have been deposited in the Protein Data Bank with accession numbers 4PRV, 4PRX, 4PU9, 4R1F.

Funding: This work was supported by the European Research Council (ERC) Advanced Investigator Grant (ERC-2013-AdG) "FIC-Mediated Post-Translational Modifications at the Pathogen-Host Interface: Elucidating Structure, Function and Role in Infection" (FICModFun) 340330 (to CD) and Swiss National Science Foundation grants 3100-132979 (to CD) and 31003A-138414 (to TS). The funders had no role in study design, data collection and analysis, decision to publish, or preparation of the manuscript.

Competing Interests: The authors have declared that no competing interests exist.

* Email: tilman.schirmer@unibas.ch

Introduction

Type II DNA topoisomerases are essential enzymes that catalyze topological rearrangement of double-stranded DNA (dsDNA) to maintain chromosomes in an appropriate state. In particular, DNA gyrase introduces negative supercoils into covalently closed dsDNA molecules using the free energy generated by ATP hydrolysis. Bacterial DNA gyrase is a prototype of this family composed of two subunits (GyrA, GyrB) and forms a $(GyrAGyrB)_2$ dimer of around 400 kDa.

The dimerization interface is composed of three contact areas or gates (N-, DNA-, C-gate) that open-up successively and in a coordinated fashion to allow DNA passage (Fig. 1). The current view on the enzymatic mechanism is the following two-gate mechanism (reviewed in [1–5]). The enzymatic cycle starts by the binding of a segment of double-stranded DNA (gate-segment, G) to the DNA-gate, followed by the trapping of another segment (transfer-segment, T) through the ATP-actuated closure, i.e. dimerization, of the N-gate. Subsequent cleavage of the G-segment and opening of the DNA-gate allows transfer of the T-segment through the gate. Finally, the G-segment gets resealed and the T-segment is released by opening of the C-gate.

The GyrB subunit is comprised of three domains: the N-terminal ATPase domain (GHKL family), the transducer domain, and the C-terminal TOPRIM domain. First insight into the detailed structure of bacterial topoisomerases was obtained with the crystal structure of a 43 kDa N-terminal fragment of *E. coli* GyrB (GyrB43) that comprises the ATPase domain and the central transducer domain [6]. The structure showed a tight dimer with contacts mainly mediated by the ATPase domains (N-gate). The dimer delimits a central hole with a diameter of 20 Å, large enough to accommodate double-stranded DNA (Fig. 1).

The structure was determined in the presence of the substrate analog AMPPNP that is bound to the canonical site of the GHKL-type ATPase domain, but also interacts with the QTK loop of the transducer domain and an N-terminal "brace" of the other subunit of the dimer. Latter interaction explains why only the dimeric form of the GyrB43 fragment is competent for ATP hydrolysis as evidenced by the greater than first-order dependence of the reaction-rate on enzyme concentration [7] and how the presence

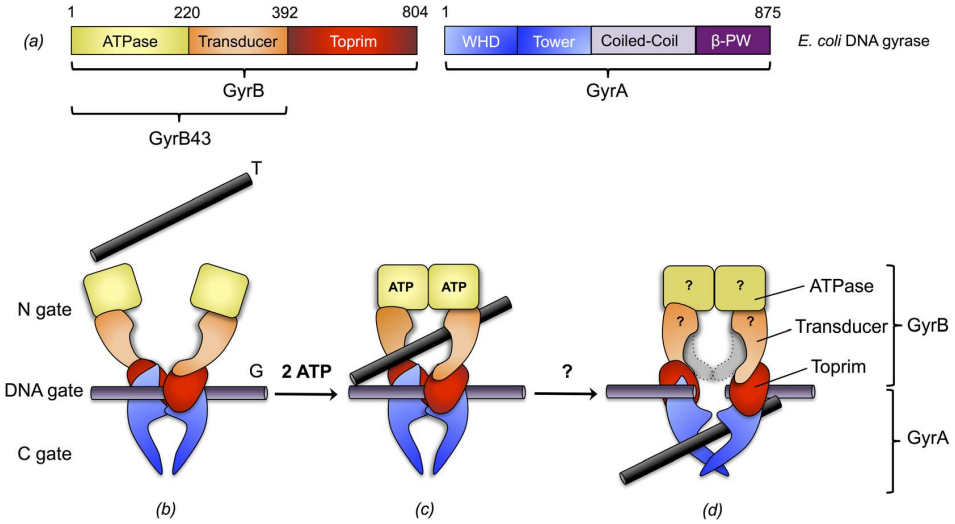

Figure 1. Domain architecture of *E. coli* DNA gyrase and model of DNA gyrase mechanism. (a) Domain architecture of *E. coli* DNA gyrase. GyrB is composed of an ATPase (yellow), a transducer (orange) and a toprim (red) domain. GyrA is composed of a winged-helix (WHD, blue), a tower (blue), a coiled-coil (light purple) and a β-pinwheel (β-PW, purple) domain. (*b*) A double-stranded DNA segment (G-segment) is captured at the DNA-gate, the N-gate is open to allow access of the T-segment. (*c*) Upon ATP binding, the ATPase domains dimerize and the T-segment gets trapped. (*d*) This is followed by ATP hydrolysis, G-segment cleavage, DNA-gate opening and T-segment translocation. The domain colored in light-grey represents the transducer domain in the preceding orientation. The mechanistic details of this step are not clear, in particular whether prior to P_i release the enzyme conformation is changed and how ATP hydrolysis and DNA passage are coordinated. For clarity, the coiled-coil and β-pinwheel domains of GyrA are omitted in (b-d). Adopted from references [3,5].
doi:10.1371/journal.pone.0107289.g001

of ATP stabilizes the closed conformation of the N-gate in GyrB [8].

The different steps of DNA gyrase action have to be tightly coordinated. In particular, G-segment cleavage and translocation of the T-segment should occur only after N-gate closure to prevent non-productive DNA cleavage and to ensure unidirectional segment translocation. Thus, not surprisingly, it could be shown that e.g. ATP hydrolysis is stimulated by the presence of DNA [9]. The question arises whether the ATP hydrolysis event *per se*, i.e. the post-hydrolysis state prior to product release, can be sensed by the enzyme to facilitate or even energize the next catalytic step. In this context it is noteworthy that the substrate is found deeply buried in the GyrB active site without an obvious exit route for the products [6].

Structures of type II topoisomerases have been determined previously for archael topoVI-B' in complex with various nucleotides [10,11] and for human topoII (htopoII) in complex with AMPPNP and ADP [12], highlighting some of the structural changes occurring along the ATP hydrolysis pathway. Both studies discuss the central role of the conserved lysine (K337 in *E. coli* GyrB) that is proposed to sense the nucleotide state and to relay this information to the center of the enzyme.

Here we report the structures of bacterial GyrB43 in complex with (i) the pre-hydrolysis analog ADP·BeF_3, (ii) the post-hydrolysis ADP·P_i and (iii) the product ADP. Compared to the AMPPNP complex structure [6,13], the post-hydrolysis state, i.e. the ternary complex of GyrB43 with ADP and P_i, shows a substantial domain reorientation, the significance of which is discussed in the context of full-length DNA gyrase.

Materials and Methods

Cloning

The gene of *E. coli gyrB* (residues 1-392) was amplified by PCR from *E. coli* genomic DNA using the primer set prFVS107/prFVS114 (5′-GGGAATTCCATATG*CATCACCATCACCATCAC*TCGAATTCTTATGACTCCTCCAG-3′ and 5′-CGACCTCGAGTTAGGTCATTTCACGCGCGCGACG-3′). The DNA sequence corresponding to the N-terminal His_6-tag is in italics. The amplified DNA fragment was then simultaneously digested with NdeI and XhoI and ligated in the MCS2 of the pRSFDuet-1 vector (Novagen) digested with the same restriction enzymes, resulting in plasmid pFVS0109.

Protein expression, extraction and purification

The pFVS0109 plasmid was transformed into Ca^{2+}-competent *E. coli BL21 (DE3)*. Cells were grown at 37°C in LB medium supplemented with 50 µg/mL of kanamycin and 0.1% glucose to an OD_{600} of 0.6 before induction with 500 µM isopropyl 1-thio-D-galactopyranoside (IPTG) for 5 hours at 37°C. Cells were then harvested by centrifugation. Cells containing overexpressed GyrB43 were resuspended in lysis buffer containing 50 mM Tris pH 7.5, 1 mM EDTA, 5 mM DTT and 5 mM imidazole and disrupted using French press. Cell debris were pelleted by ultracentrifugation at 200 000 *g* and the supernatant was applied to two 1 mL HisTrap column (GE Healthcare) plugged in series. The protein of interest was eluted with a gradient of elution buffer containing 50 mM Tris pH 7.5, 1 mM EDTA, 5 mM DTT and 500 mM imidazole. The eluted fractions containing GyrB protein were then loaded on a 5 mL HiTrap Q column (GE Healthcare) pre-equilibrated with loading buffer (50 mM Tris pH 7.5, 1 mM

EDTA, 5 mM DTT). Proteins were eluted with a gradient of elution buffer containing 50 mM Tris pH 7.5, 1 mM EDTA, 5 mM DTT and 1 M NaCl. The protein was then concentrated and injected on a Superdex 75 16/60 gel filtration column (GE Healthcare) equilibrated with 50 mM Na-phosphate pH 7.2, 1 mM EDTA and 5 mM DTT. The different batches of pure protein leading to the crystallization of GyrB in complex with ADP·P_i, ADP·BeF_3 or ADP were concentrated to 36 mg/mL.

GyrB43/nucleotide complexes crystallization

Crystals were obtained at 20°C using the sitting-drop vapour diffusion method after mixing 0.2 µL protein solution with 0.2 µL reservoir solution equilibrating against a reservoir of 80 µL. For crystallization of GyrB43 in complex with ADP·P_i, the protein solution was prepared by incubating GyrB with a 15 fold molar excess of ATP and $MgCl_2$. This allowed the ATPase reaction to start and produce the reaction products: ADP·P_i. GyrB43 in complex with ADP·P_i crystallized after one week in 0.1 M tri-ammonium citrate pH 6.5 and 25% (w/v) PEG 2000. Crystals were soaked in the reservoir solution supplemented with 20% glycerol for cryoprotection. The protein sample leading to the crystallization of GyrB43 in complex with ADP was prepared similarly to the ADP·P_i sample. GyrB43 in complex with ADP crystallized after a week in 10% (w/v) PEG 20000, 20% (v/v) PEG MME 550, 0.02 M each carboxylic acid, 0.1 M bicine/Trizma base pH 8.5 (Morpheus screen [14]). For crystallization of GyrB43 in complex with ADP·BeF_3, a prerequisite is the formation of a stable ADP·BeF_3 complex. This was achieved by incubating 20 mM ADP with 500 mM NaF and 100 mM $BeCl_2$ for 16 hours at 4°C [8]. The protein solution was prepared by incubating GyrB43 with a 15 fold molar excess of ADP·BeF_3 and $MgCl_2$. Crystals grew after a week in 0.2 M NaF, 0.1 M Bis-Tris propane pH 6.5 and 20% (w/v) PEG 3350. Crystals were soaked in the reservoir solution supplemented with 20% glycerol for cryoprotection. All crystals were then flash frozen in liquid nitrogen and stored until data collection.

Data collection, processing, structure determination and refinement

Diffraction data were collected at the Swiss Light Source (Villigen, Switzerland) at 100 K and processed using XDS [15] and scaled either with XSCALE [15] or aimless [16]. GyrB43 structures were solved by molecular replacement using the previously published structure of the 43-kDa N-terminal fragment of GyrB (PDB entry 1EI1 [13]) as search model using Phaser [17]. Several rounds of iterative model building and refinement were performed using Coot [18] and Refmac5 [19] or PHENIX [20]. 5% of the data were excluded from refinement and used for cross-validation. For the remodeling of the sulfate and asparagine side chain of human topoIIA in complex with ADP·SO_4 (PDB code: 1ZXN), the re-refined model was obtained from the PDB_REDO databank [21]. Iterative model building and refinement was performed as described above. The geometry of the final model was assessed using MolProbity [22] showing >99% of the residues in the core and allowed regions of the Ramachandran plot. Data collections and refinement statistics are summarized in Table 1 and Table 2, respectively.

Structure analysis

Superimpositions were made using Modtrafo (T. Schirmer unpublished, http://www.biozentrum.unibas.ch/schirmer/modtrafo). Root mean square deviation (RMSD) were calculated using lsqman [23]. To obtain the change in domain orientation, the different structures were superimposed on their respective ATPase domains. Then, the respective transducer domains were superimposed and the resulting rotation matrix analyzed by Modtrafo in terms of polar angles (Ω, φ, κ) with Ω, φ defining the orientation of the rotation axis and κ the rotation angle.

Figures were prepared with Dino (A. Philippsen unpublished, http://www.dino3d.org).

Accession numbers

Coordinates and structure factors have been deposited in the Protein Data Bank (PDB) with accession numbers 4PRX, 4PU9 and 4PRV for GyrB43·ADP·P_i, GyrB43·ADP·BeF_3 and GyrB43·ADP, respectively. The re-refined and corrected coordinates of htopoII·ADP·SO_4 have been deposited in the PDB with accession number 4R1F.

Results

Overall structures

To understand better the effect of ATP hydrolysis on the mechanism of GyrB at the atomic level, we aimed to obtain further structures along the reaction pathway, in particular the ADP·P_i complex structure representing the post-hydrolysis state. A 43 kDa N-terminal fragment of GyrB from *E. coli* (GyrB43) comprising the ATPase and the transducer domain [6,13] was overexpressed and purified. The fragment was found to be competent for ATP hydrolysis as assessed by an FPLC based nucleotide quantification method [24] yielding k_{cat} and K_m values of $2.7 \cdot 10^{-3}$ s^{-1} and 0.45 mM, respectively. These values are similar to those determined previously for this fragment [7,13]. GyrB43 was crystallized in presence of ATP substrate (12.5 mM) that was expected to get hydrolyzed to ADP and P_i. In addition, a high background phosphate concentration (50 mM sodium phosphate buffer) was employed to saturate the γ-phosphate binding site.

Crystals of orthorhombic space group $C222_1$ with one monomer per asymmetric unit were obtained that diffracted to 1.8 Å. Data collection statistics are given in Table 1. The structure was solved by molecular replacement using the structure of GyrB43 (*E. coli*) in complex with AMPPNP that had been determined in a different space-group previously (PDB entry 1EI1 [13], Fig. 2a), as search model. The electron density map (2Fo-Fc) calculated with the molecular replacement phases showed well-defined density for the ATPase domain, but rather poor density for the transducer domain. The difference density (Fo-Fc) showed disagreement in the QTK loop region (334–337), which is the part of the transducer domain that extends into the ATP-binding pocket. These observations provided the first indication of a global conformational change.

Rigid- and jelly-body refinement improved the electron density in the transducer domain and caused a drop in the R_{free} from 46.7% to 35.1%. Subsequently, residues 330–340 comprising the QTK loop were rebuilt based on a respective omit-map. An ADP and an adjacent phosphate molecule could be placed unambiguously in the map. Final refinement yielded a GyrB43·ADP·P_i model (Fig. 2b) with R_{work} and R_{free} values of 16.3% and 20.3%, respectively (Table 2). The model comprises all residues from 4 to 378 except segment 304–314 at the tip of the transducer domain.

In addition, the structures of GyrB43 in complex with ADP·BeF_3 (2.4 Å) and in complex with ADP (2.0 Å) were solved. In both cases, plate-like crystals of the same $C222_1$ space-group, but with cell constants distinct to those of the GyrB43·ADP·P_i form were obtained. Both structures (Figs. 2c, d) were solved by molecular replacement using the same search model (PDB entry

Table 1. Data collection statistics.

	GyrB43 in complex with ADP·P_i	GyrB43 in complex with ADP·BeF_3	GyrB43 in complex with ADP
X-ray source	SLS X06SA (PXI)	SLS X06DA (PXIII)	SLS X06DA (PXIII)
X-ray detector	Pilatus 6M	Pilatus 2M	Pilatus 2M
Wavelength (Å)	1.0000	0.9793	1.0000
Space group	C 2 2 2_1	C 2 2 2_1	C 2 2 2_1
Cell dimensions a, b, c (Å)	77.6, 131.6, 92.4	88.1 143.2 79.9	88.2, 142.5, 79.1
Matthews coefficient ($Å^3Da^{-1}$)	2.9	3.1	3.1
Solvent content (%)	57.9	59.3	59.3
Molecules in asymmetric unit	1	1	1
Resolution limits (Å)	46.19–1.80 (1.86–1.80)	44.08–2.40 (2.49–2.40)	75.03–2.00 (2.07–2.00)
R_{merge}†(%)	9.9 (112.5)	7.0 (32.8)	7.1 (59.4)
R_{meas}‡(%)	10.4 (115.5)	7.6 (35.1)	7.7 (67.0)
CC 1/2	99.9 (80.5)	99.9 (97.4)	99.9 (93.7)
$<I/\sigma(I)>$	16.4 (2.0)	21.1 (6.1)	21.4 (3.3)
Total reflections	473′415 (42′913)	137′915 (13′976)	192′676 (17′839)
Unique reflections	44′052 (4′261)	20′072 (1′966)	30′053 (3′203)
Wilson B-factor	25.0	36.3	23.5
Multiplicity	10.7 (10.1)	6.9 (7.1)	6.4 (5.6)
Completeness (%)	99.7 (97.4)	99.6 (99.5)	88.2 (95.8)
Mosaicity	0.16	0.46	0.19

Numbers in parentheses belong to the outer shell.
†$R_{merge} = \sum_{hkl}\sum_i |I_i(hkl) - <I(hkl)>| / \sum_{hkl}\sum_i I_i(hkl)$, where $I_i(hkl)$ is the observed intensity for a reflection and $<I(hkl)>$ is the average intensity obtained from multiple observations of symmetry-related reflections.
‡$R_{meas} = \sum_{hkl} [N/(N-1)]^{1/2} \sum_i |I_i(hkl) - <I(hkl)>| / \sum_{hkl}\sum_i I_i(hkl)$, where $I_i(hkl)$ is the observed intensity for a reflection, $<I(hkl)>$ is the average intensity obtained from multiple observations of symmetry-related reflections and N is the number of observations of intensity I(hkl).
doi:10.1371/journal.pone.0107289.t001

1EI1) as for the aforementioned structure of the GyrB43·ADP·P_i complex. Again, the ligands could be unambiguously modeled into the Fo-Fc maps. Data collection statistics are given in Table 1. The quality of the electron density maps allowed the tracing of 95% and 94% of the polypeptide chain except segments 305–315, 389–392 for GyrB43·ADP·BeF_3 and 303–315, 387–392 for the structure of GyrB43·ADP, respectively. Final refinement statistics are given in Table 2.

Rigid domain reorientations

Structural comparisons of the individual domains of the three newly determined GyrB43 structures in complex with ADP·P_i, ADP·BeF_3 and ADP with the previously published structure of GyrB43·AMPPNP reveals that both the transducer and the ATPase domain structures are virtually identical in all complexes with root mean square deviation (rmsd) values between 0.32 and 0.57 Å (Table 3). Still, there are considerable conformational changes between the structures as evident from Fig. 2. In particular, the hole delimited by the two transducer domains of the dimer is larger in GyrB43·ADP·BeF_3 and GyrB43·ADP·P_i than in the GyrB43·AMPPNP [6,13] and GyrB43·ADP structures.

Changes in the arrangement of the two domains are revealed when superimposing the subunits on their ATPase domains (Fig. 3), showing large differences in the respective Cα atoms positions of the transducer domains. The largest rmsd (2.9 Å) occurs between the ternary GyrB43·ADP·P_i complex and the restrained GyrB43·AMPPNP substrate complex (Figs. 3a, c and Table 3). The domain re-arrangement is a relative 12° rotation (without translation component) with the rotation axis oriented roughly along the long axis of the monomer and passing through the domain interface (Fig. 3a). Thereby, the transducer β-sheet rolls over the C-terminal helix of the ATPase domain (residues 222 to 232). This part of the interface is mostly hydrophobic. Interacting residues close to the rotation axis are e.g. L197, I222, V226 of the N-terminal and A255, V322 of the C-terminal domain. Interestingly, a rotation about approximately the same axis but by only 6° is needed to superimpose the transducer domain of GyrB43·ADP·BeF_3 onto that of GyrB43·AMPPNP (Fig. 3b, c). No domain reorientation is observed for the binary GyrB43·ADP complex. Table 3 shows that upon superposition of the ATPase domain the transducer domain is still well aligned (rmsd of Cα positions: 0.8 Å).

To further characterize the long-range structural changes, intra-subunit distances were measured within the dimer structures. The changes in the distances are given in Fig. 4. Upon ATP hydrolysis, the QTK loops (Q335 and T336) of the two subunits get closer together at the dimerization interface, whereas residues at the surface of the N-gate chamber (N294, L282) or the C-terminal end (D377) of the transducer domain considerably increase their inter-subunit distance (by up to 7 Å) (see morphing in Movie S1). Accordingly, we define the conformations of the GyrB43·ADP·BeF_3 and the GyrB43·ADP·P_i complex "semi-open" and "open", respectively (Fig. 2). Latter structural change may well have relevance for the communication of the ATP hydrolysis event to the core of the gyrase enzyme (see Discussion).

Crystal packing analysis

In general, variation in protein domain arrangements observed in non-isomorphous crystals can be due to distinct crystal packing

Table 2. Refinement statistics.

	GyrB43 in complex with ADP·P_i	GyrB43 in complex with ADP·BeF_3	GyrB43 in complex with ADP	htopoII in complex with ADP·SO_4
PDB code	4PRX	4PU9	4PRV	4R1F
Resolution limits (Å)	46.19–1.80 (1.86–1.80)	44.08–2.40 (2.49–2.40)	75.03–2.00 (2.07–2.00)	30.00–2.51 (2.60–2.51)
R_{work} * (%)	16.3 (23.7)	21.9 (28.0)	20.7 (38.5)	20.2 (27.6)
R_{free} **(%)	20.3 (34.2)	27.3 (35.3)	25.9 (43.3)	24.1 (34.5)
Number of non-hydrogen atoms	3′063	2′979	3′015	12′360
macromolecules	2′787	2′899	2′861	12′093
ligands	39	32	28	133
solvent	237	48	126	134
Protein residues	363	374	369	1647
R.m.s.d from ideal				
Bond lengths (Å)	0.022	0.016	0.018	0.012
Bond angles (°)	2.11	1.97	1.89	1.46
Ramachandran favored *** (%)	98	93	97	95
Ramachandran outliers *** (%)	0.28	0.81	0.27	0.54
Clashscore ***	1.09	4.32	2.13	5.35
Average B values (Å^2)	30.3	42.2	29.5	64.3
macromolecules	30.0	42.4	29.6	64.5
ligands	21.3	30.0	22.3	56.0
solvent	36.1	40.3	29.8	55.1

Numbers in parentheses refer to the outer shell.
* $R_{work} = \sum_{hkl}|| F_{obs}| - |F_{calc}||/\sum_{hkl}|F_{obs}|$
** R_{free} is the R value calculated for 5% of the data set that was not included in the refinement.
*** Molprobity.
doi:10.1371/journal.pone.0107289.t002

forces. Therefore, the various crystal packings were analyzed in detail.

The GyrB43·ADP·P_i crystal form is distinct to that of the published GyrB43·AMPPNP structure [13], still the molecular packings are related (Fig. 5). Despite the distinct intra-dimer distance between the transducer domains (marked by a black dot in Fig. 5a), GyrB43 dimers are arranged to similar layers (Fig. 5a) due to a conserved ATPase-transducer domain crystal contact with an interface of ~490 Å^2 (Fig. 5b). Layers are packed onto each other according to the crystallographic 2_1 axes along b *via* weak ATPase-ATPase contacts mediated by the "base" of this domain. These interactions are dissimilar between the two crystal forms with a smaller area in the GyrB43·AMPPNP form (218 Å^2) compared to the GyrB43·ADP·P_i form (387 Å^2). Transducer domains are very weakly or not at all involved in inter-layer contacts in the AMPPNP or ADP·P_i complex, respectively.

The similarity in packing is reflected in relations between cell parameters/symmetry elements of the two forms (Fig. 5c). In the

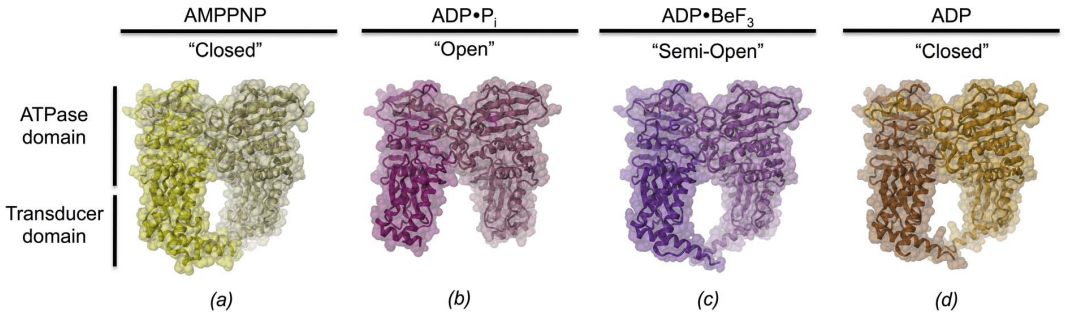

Figure 2. Conformational states of GyrB43 along the ATP hydrolysis reaction path. The various states have been trapped by co-crystallization with the appropriate nucleotides. The dimeric structures are shown in cartoon representation with semi-transparent molecular surface overlaid. Subunits are distinguished by a slight variation in colour hue. View perpendicular to the molecular dyad. (a) AMPPNP complex (PDB entry 1EI1 [13]), (b) ADP·P_i complex, (c) ADP·BeF_3 complex and (d) ADP complex. Note the distinct opening angles defined by the two transducer domains with the AMPPNP and ADP complexes in a "closed" conformation, the ADP·BeF_3 complex in a "semi-open" and the ADP·P_i complex in "open" conformation.
doi:10.1371/journal.pone.0107289.g002

Table 3. Pair-wise fit of GyrB43 domains after superposition of the ATPase domains (regular) or transducer domains (italics).

	rmsd (Å) of ATPase domain (20-220)			
rmsd (Å) of transducer domain (221–392)	AMPPNP	ADP·BeF_3	ADP·P_i	ADP
AMPPNP		0.422	0.389	0.393
ADP·BeF_3	*0.565*		0.328	0.317
	1.592			
ADP·P_i	*0.391*	*0.423*		0.354
	2.875	1.579		
ADP	*0.501*	*0.369*	*0.354*	
	0.644	1.519	2.891	

The values give the rmsd (Å) of the corresponding Cα positions. When superimposing the ATPase domains dimer, the pairwise rmsd range from 0.46 Å to 0.93 Å.
doi:10.1371/journal.pone.0107289.t003

$P2_12_12$ form (GyrB43·AMPPNP), the molecular dyad symmetry of GyrB43 is non-crystallographic, whereas, in the $C222_1$ form, it coincides with the crystallographic 2-fold symmetry along the long axis (b axis). The positions of local two-fold symmetry axis of GyrB43·AMPPNP are depicted in green on Fig. 5c. In space group $P2_12_12$, the symmetry is broken by a slight shift of the local symmetry axis along the horizontal direction (Fig. 5c) by 5% to x = 0.29 compared to its theoretical position at a quarter in space group $C222_1$.

Concerning the GyrB43·ADP complex, the structure was obtained in a crystal form unrelated to that of GyrB43·AMPPNP. Still the two structures are virtually identical (see preceding section) ruling out any crystal packing artifacts. Finally, the GyrB43·ADP·BeF_3 crystal structure was obtained in a form isomorphous to that of GyrB43·ADP. Thus, the observed domain rotation can be attributed to the presence of the BeF_3 moiety. Altogether, one can conclude that the observed distinct relative orientations of the transducer domains are most likely not due to any crystal packing artifacts, but should be a direct consequence of the distinct complexation states of the ATP pocket.

Ligand binding

In the following, we describe in detail the structural changes in GyrB43 that accompany ATP hydrolysis and are coupled to the observed domain orientations. As described first for GyrB43 in complex with AMPPNP [6,13], the nucleotide is deeply buried in the core of the ATPase domain, with the triphosphate moiety located at the N-terminal end of helix α6 (residues 118–126). The active sites of both *E. coli* GyrB43·AMPPNP complex structures [6,13] are virtually identical (Fig. S1) although the structure determined by Brino *et al*. (PDB code: 1EI1) [13] contains a mutation (Y5S) in the N-terminal arm. Furthermore, inter-species comparison between GyrB from *E. coli* (PDB code: 1EI1) [13] and *Mycobacterium tuberculosis* (PDB code: 3ZKB) [25] reveals a very well conserved ligand-protein interaction network (Fig. S1). Figures 6a and 7a show that the terminal γ-phosphate moiety is held firmly in place with its terminal oxygens forming a multitude of H-bonds with main-chain amide nitrogens of the N-terminus of helix α6 and of the preceding glycine-rich loop. Furthermore, the phosphate forms a salt-bridge with K337 from the transducer domain and interacts indirectly via a water molecule with Q335 (also from the transducer domain) and with E42. Q335, in turn, forms an H-bond with the main-chain carbonyl of residue 26 from the ATPase domain (Fig. 6a and Fig. S3a). In the unreleased GyrB43·AMPPNP structure [6], Q335 forms a direct H-bond with the gamma-phosphate of the ligand and lacks the interaction with carbonyl 26.

The structure of GyrB43 in complex with ADP and P_i shows the immediate post-hydrolysis state at high resolution (1.8 Å) (Fig. 6b, Fig. S3b and Fig. 7b). Although the distance between the β- and the now liberated distal phosphorus is found significantly increased by 1.5 Å to 4.5 Å, all protein - ligand interactions are virtually unchanged compared to the AMPPNP complex. In particular, despite inverted configuration, two of the oxygens of the phosphate ion (O2, O3) are bonded to the same main-chain amide nitrogens 115–116 and 118–119 as the γ-phosphate in the AMPPNP complex (compare panels (a) and (b) of Figure 6). The phosphate oxygen O3 forms a short H-bond (2.50 Å) with the terminal phosphate of ADP. In the small GTPase Rab11, an analogous interaction (between GDP and P_i) has been identified by crystallography [26] and by FTIR [27]. The phosphate oxygen O4, the oxygen that evidently has been added upon hydrolysis, projects out of the binding site and interacts with the δ-nitrogen group of H116. Furthermore, it forms a water mediated H-bond with Q335 from the transducer domain. The side-chain amino-group of K337 has moved by 1.0 Å, but is still within H-bonding distance to the now liberated phosphate group. Strikingly, the position of the QTK loop (residues 335–337) with respect to the ligand(s) is considerably distinct in the pre- and post-hydrolysis structure (by about 2.5 to 3 Å) (Fig. 6). This is due to the relative rigid-body motion of the transducer domain described previously. The movement appears to avoid a clash (1.7 Å) that would occur between the Q335 side-chain in AMPPNP complex position and the liberated phosphate group (Fig. 6c). Noteworthy, the side-chain cannot escape sidewise, since its movement is severely restricted by hydrophobic residues of the ATP lid loop (residues 99–120, shown in surface representation in Fig. 7). Rather, the glutamine side-chain amide group finds a new favorable position 3.5 Å apart, where it interacts with its counterpart of the other subunit (Q335*) and main-chain carbonyl 25 of the ATPase domain.

The atom positions of the ADP·BeF_3 ligand in the respective complex are almost indistinguishable to that of the AMPPNP ligand (Fig. S2a compared with Fig. 6a and stereoviews in Fig. S3a compared with Fig. S3c). The substituents of the beryllium atom are arranged tetrahedrally and the beryllium - β-phosphorus distance (2.9 Å) is only marginally shorter than the γ – β-phosphorus distance (3.1 Å). The only major difference is the loss

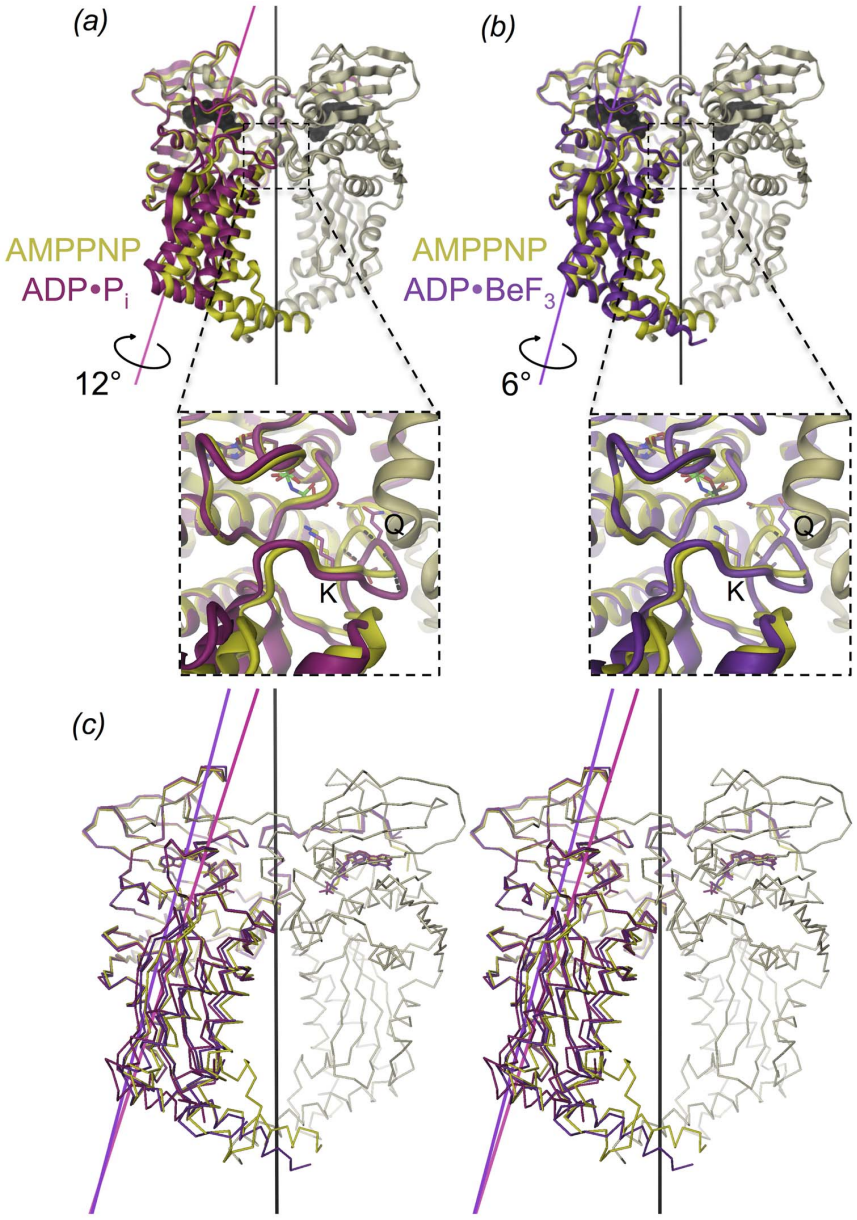

Figure 3. Structure comparison of (a) GyrB43·ADP·P_i (magenta) and (b) GyrB43·ADP·BeF_3 (violet) with GyrB43·AMPPNP (shown as a dimer with yellow/grey colour with molecular dyad in black). The structures are superimposed on their ATPase domain (residues 20–220). The rotation axes for the domain reorientation of the transducer domain with respect to the ATPase domain are indicated. These form an angle of 21.5° and 14.5° with the molecular dyad for GyrB·ADP·P_i and GyrB·ADP·BeF_3, respectively. The insets show the QTK loop of the transducer domain that is rotated relative to the ATPase domain in response to the nucleotide state (dashed lines); Q: Q335, K: K337. (c) Stereoview of the overlay of the three aforementioned structures.
doi:10.1371/journal.pone.0107289.g003

of the (indirect) interaction with Q335 due to the aforementioned transducer domain rotation. Finally, the structure of the GyrB43·ADP complex is globally (Table 3) and locally (Fig. S2b and Fig. S3d) almost identical to that of GyrB43·AMPPNP (Fig. 6a and Fig. S3a). The only difference is the presence of a water molecule in the approximate position of the absent γ-phosphate. As expected from the unchanged domain organization, the Q335 side-chain interacts with residue 26 in the same way as in the AMPPNP complex structure.

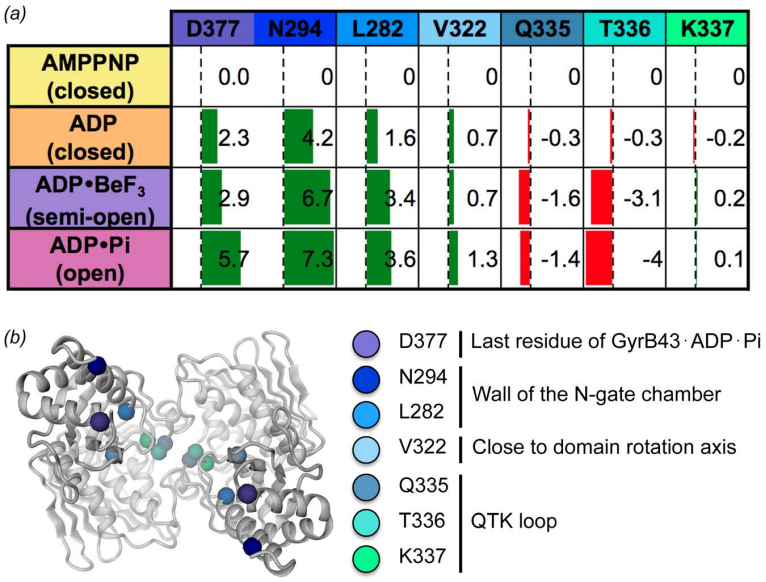

Figure 4. Quantification of nucleotide induced structural changes within dimeric GyrB43. (a) Inter-subunit distance changes between symmetry related residues of selected transducer domain Cα-atoms. The changes have been calculated relative to the AMPPNP complex structure, green bars indicate an increase in distance, red bar indicate a decrease. (b) Cartoon representation of dimeric GyrB43 (ADP·P_i state) with the residues used for the calculations in (a) indicated. View along the symmetry axis from the C-terminal side.
doi:10.1371/journal.pone.0107289.g004

In the three newly solved structures, a magnesium ion is found coordinated by the α- and β-phosphate moieties, one water molecule and the side-chain of N46. In the ADP·P_i complex, the coordination of the cation seems somewhat distorted to an additional weak interaction with the orthophosphate (O4 - Mg^{2+} distance: 3.1 Å).

Summarizing, the detailed analysis of the ATP binding site revealed pronounced changes in the vicinity of the γ-phosphate subsite upon ATP hydrolysis. How these relate to the observed rigid body motions, which in turn seem crucial for the coordination of gyrase activity will be discussed below.

Discussion

The endergonic process of negative DNA supercoiling is driven by ATP hydrolysis [28]. ATP binding to the ATPase domain of the GyrB subunit causes N-gate closing and ensures directional transfer of the trapped DNA T-segment through the DNA-gate. Closure of the N-gate may also exert a pinching force that is mediated by the transducer domains on the trapped DNA segment to facilitate transfer through the DNA-gate [3]. It has been demonstrated that ATP hydrolysis occurs sequentially for yeast topoisomerase II [29]. Hydrolysis of the first ATP molecule is sufficient for the catalysis of DNA cross-passage, while only upon hydrolysis of the second ATP molecule the ATPase domains dissociate to reset the enzyme. In contrast, *B. subtilis* GyrB appears to hydrolyze ATP synchronously [30]. Considering the close homology, a similar mechanism would be expected also for bacterial DNA gyrase.

Here, we have studied the nucleotide-state dependent conformations of GyrB43 prior to nucleotide release, i.e. prior to ATPase domain dissociation, with the aim to provide further and detailed structural information about the coordination of ATP hydrolysis and strand passage.

Nucleotide-dependent topoisomerase II conformations

The triphosphate-nucleotide complexed conformations of the ATPase/topoisomerase fragments match closely for the bacterial [6,13], eukaryotic [12], and archaeal [10,11] structures. It has been dubbed "restrained" conformation [11] due to the tight packing of the transducer domain against the ATPase domain and the multiple interactions of the ligand with the ATP binding site. These include interactions with the ATP lid loop, the N-terminal segment of adjacent subunit and the glycine rich loop that tightly embraces the γ-phosphate. Moreover, residues of the QTK loop (being part the transducer domain) are also engaged in ATP binding. For the slightly truncated subunit B of archaeal topoisomerase VI (topoVI-B'), comparison of the restrained (dimeric) AMPPNP complex with the "relaxed" (monomeric) nucleotide-free state revealed a relative reorientation of the two domains [11] giving a first hint for the potential of allosteric communication via these domains. In the dimeric structures of topoVI- B', the ADP, ADP·P_i and the ADP·AlF_4 complexes all showed the restrained conformation [11]. This suggested that ATP hydrolysis would elicit no large-scale structural response in topoVI.

In contrast, human topoisomerase II shows a semi-open ADP complex characterized by an 8° outward rotation of the transducer domain when compared with its restrained/closed AMPPNP conformation [12] (Fig. S4a). Closer inspection and re-refinement of the original structure (PDB code: 1ZXN), however, revealed that the γ-phosphate binding subsite is not empty, but occupied by a sulfate ion in 3 of the 4 molecules of the asymmetric unit (the active site of the fourth molecule contains a glycerol molecule). The corrected structure (Fig. S4b) with improved statistics (R_{work}/

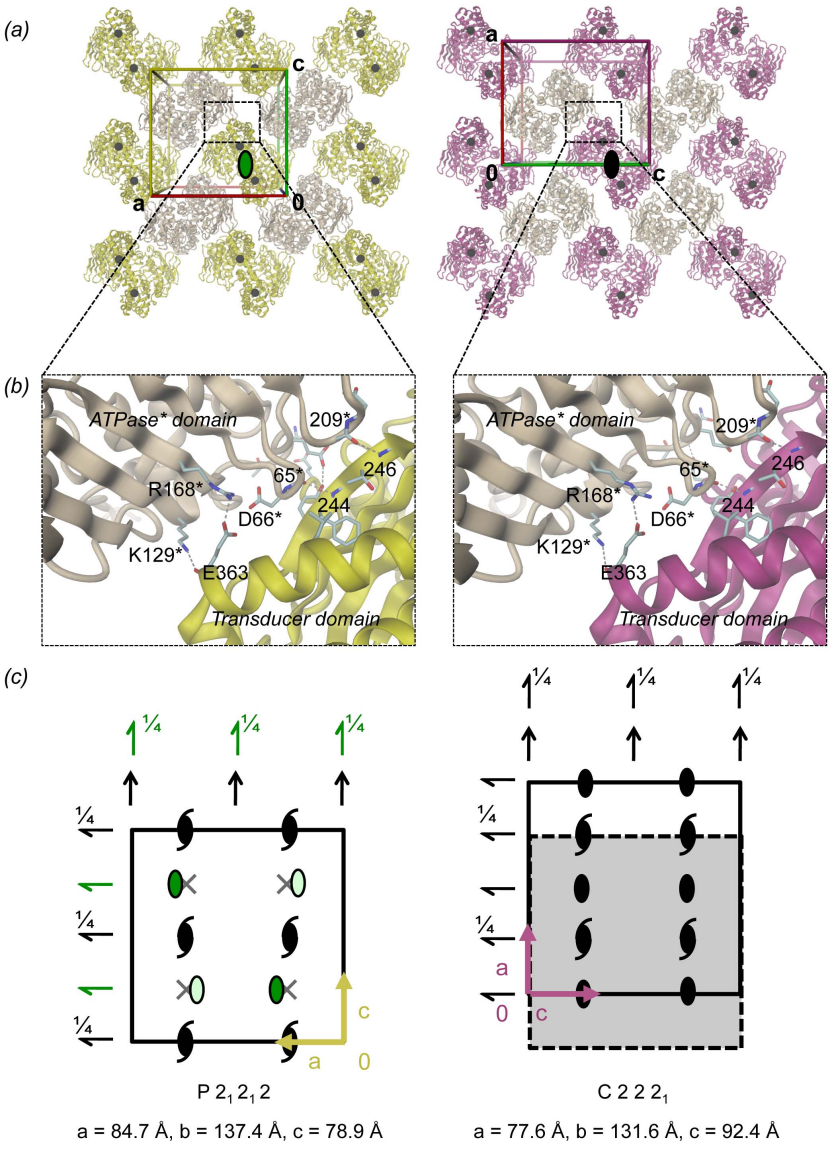

Figure 5. GyrB43 crystal packing of the $P2_12_12$ (left, GyrB43·AMPPNP complex) and the $C222_1$ (right, GyrB43·ADP·P_i complex) form. (a) The molecular packing is shown within a slab perpendicular to b and centered at y = 1/4. In both forms, dimers are oriented with their molecular dyads parallel to b (viewing direction). In the $P2_12_12$ form (left) the molecular dyad is local (green elliptical symbol), in the $C222_1$ form (right) the molecular dyad is crystallographic (black symbol). In each case, neighbouring dimers are related by horizontal 2-fold screw-axes. Black spheres represent the position of residue D377 at the end of the transducer domain (also depicted in Fig. 4b). (b) Details of the major crystal contact formed in both packings between the transducer domain and the ATPase domain of a symmetry related dimer. (c) Representation of the symmetry elements, same view as in panel (a). Unit cells are indicated by solid line. With respect to the arrangement of symmetry elements, the dashed rectangle of the scheme at the right is equivalent to the unit cell of the left scheme. Local symmetry elements are indicated in green.
doi:10.1371/journal.pone.0107289.g005

R_{free} (%) of 20.2/24.1) has been deposited in the Protein Data Bank (PDB code: 4R1F). Thus, the structure apparently represents an ADP·SO_4 mimic of the post-hydrolysis state and the domain rotation may well be of functional relevance (Fig. S4, see also below).

For bacterial gyrase, all of the conformational states along the ATP hydrolysis pathway are now known. The canonical, restrained structure is attained both in presence of AMPPNP [6,13] and ADP, as for topoVI-B'. This indicates that the γ-phosphate is not required to restrain the conformation of the enzyme. The effect of ATP hydrolysis would then be the

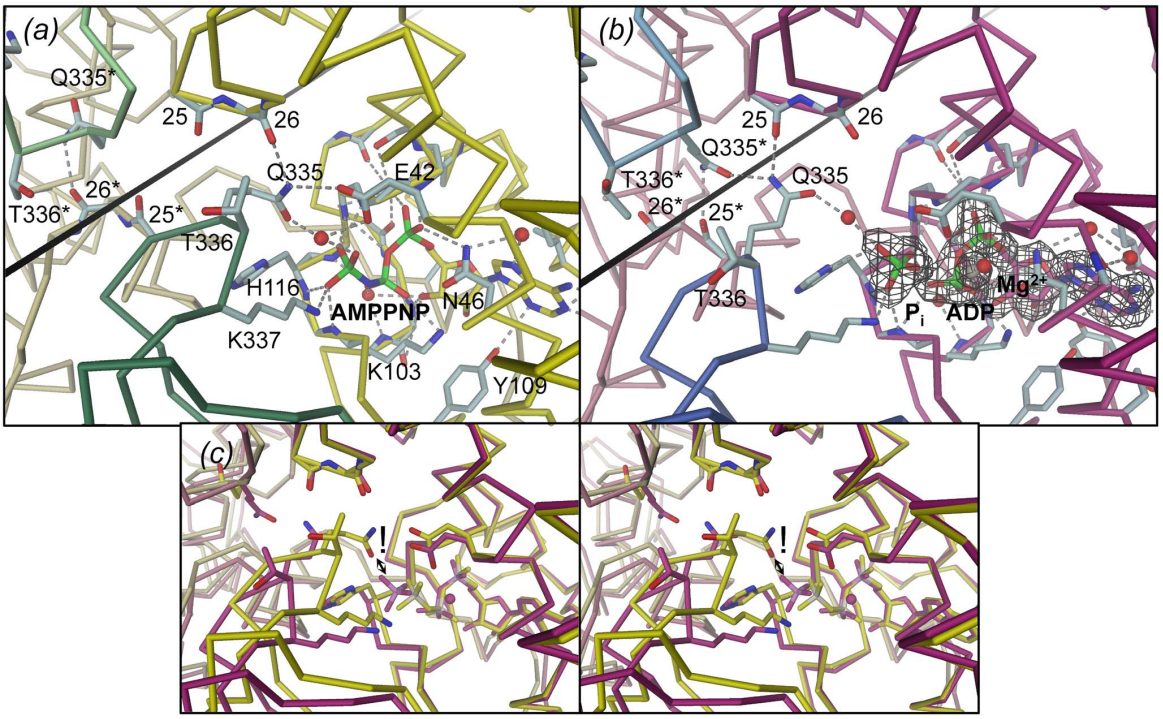

Figure 6. Structures of the GyrB43 nucleotide binding site as determined for (a) the substrate analog complex GyrB43·AMPPNP (PDB entry 1EI1 [13]**) and (b) the post-hydrolysis complex GyrB43·ADP·P_i with Fo-Fc omit map shown at a contour level of 3.0 σ.** Note the distinct interaction of the QTK loop (transducer domain) with the 25–26 loop (ATPase domain) in the two states. The rotation axis for the relative domain reorientation is shown as straight line (same in Fig. 3a) (c) Stereoview of the superimposition of the structures shown in (a) and (b) after superposition on their ATPase domain. The exclamation mark indicates the steric clash that would occur between Q335 in the AMPPNP complex conformation (yellow) with the P_i moiety of the post-hydrolysis state (magenta).
doi:10.1371/journal.pone.0107289.g006

enhancement of nucleotide dissociation to reset the enzyme to the monomeric ATPase state [5]. This is in contrast to, e.g., small GTPases that act like a "loaded spring" and switch to a relaxed state upon GTP hydrolysis and phosphate release [31].

Here, we have shown for the bacterial GyrB43 fragment that there is an additional effect of ATP hydrolysis that occurs prior to phosphate release and may be of functional significance. The ADP·P_i post-hydrolysis state is characterized by a virtually unchanged ATPase dimer structure, but with the transducer domains reoriented as rigid bodies by 12° relative to their position in the substrate analog complex (see morphing in Movie S1).

Interestingly, also human topoII may undergo a similar structural transition as inferred by the comparison of the respective AMPPNP and ADP·SO_4 complexes (Fig. S4). As for bacterial gyrase, the pivot of the motion is at the center of the interface between the C-terminal ATPase domain helix and the transducer β-sheet, but the direction of the rotation axis is different (Fig. S4a). In contrast, the archaeal topoisomerase IIB enzyme topoVI exhibits no structural change upon ATP hydrolysis [11]. This can be attributed to a distinct QTK loop with only the lysine conserved in this distantly related topoisomerase family (Fig. S5), see below.

The conformational change observed in GyrB43 can be traced back to the significant, but small (1.5 Å) increase in the distance between the β-phosphate and the terminal γ-phosphate or phosphate moiety, respectively. The direct structural consequences of the shifted γ-phosphate position on the local organization of the binding site and particularly on the position of the QTK loop will be discussed in the following section.

The central role of the QTK loop in bacterial and eukaryotic topoisomerases (topoisomerases IIA)

All topoisomerases IIA studied so far adopt the restrained/closed conformation in complex with tri-phosphate substrate analogs. In contrast, the post-hydrolysis complex has adopted the open state, since the phosphate would severely clash with Q335 from the QTK loop of the transducer domain in the restrained state (Fig. 6c). Close inspection of the restrained structure reveals that such strain cannot be relieved by a simple side-chain rotation of the tightly buried glutamine. Also, there is no apparent route for the phosphate to leave the binding site, since the previously described tunnel [13] seems too narrow (Fig. 7). Instead, the observed movement of the entire transducer domain appears mandatory to accommodate the post-hydrolysis state in which the side-chain of Q335 forms a new set of H-bonds, i.e. with its symmetry mate Q335* and a main-chain carbonyl of the ATPase domain.

Thus, Q335 appears to fulfill a central role by acting as a two-state switch in response to the nucleotide state of the ATPase domain. Indeed, an early biochemical *in vivo* study on *E. coli*

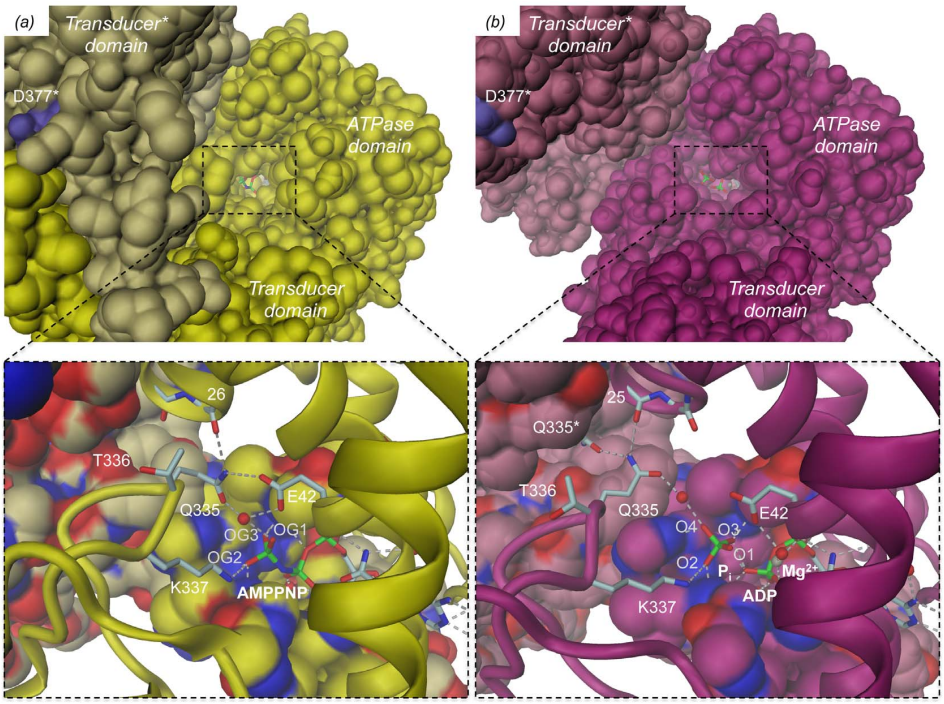

Figure 7. Surface representation of GyrB43 demonstrating the deeply buried nucleotide (stick model). View along the narrow tunnel leading to nucleotide. (a) GyrB43·AMPPNP complex, (b) GyrB43·ADP·P_i complex. The insets show close-ups of the nucleotide sites with the ATP lid loop (residues 99–120) and the adjacent subunit of the dimer in surface representation (same colour codes as Fig. 2). Note, that upon ATP hydrolysis glutamine 335 cannot escape "downwards" to relieve a clash with the P_i moiety due to the presence of the ATP lid. Instead the entire transducer domain moves to the side.
doi:10.1371/journal.pone.0107289.g007

gyrase [9] had already identified this glutamine as indispensable for the regulation of ATP hydrolysis by DNA binding. A later study on a QTK deletion mutant of human topoII again showed deregulation of the enzyme with DNA cleavage no longer controlled by the nucleotide state of the enzyme [32].

The equivalent of the QTK loop in archaea carries no glutamine (Fig. S5) and exhibits a distinct main-chain geometry [10]. Therefore, the nucleotide-binding pocket is considerably more spacious. This explains why the post-hydrolysis state can be accommodated in the restrained conformation and why no ATP hydrolysis induced structural changes have been observed [11]. Whether also in archaeal topoisomerases the event of ATP hydrolysis can be signaled to the core of the enzyme remains to be investigated.

Coordination of ATP hydrolysis and supercoiling activity

Modification of DNA topology needs the coordinated catalysis of various steps. Therefore, it is not surprising that DNA binding positively affects ATPase activity as shown for *E. coli* gyrase [33]. The simplest explanation for this allosteric regulation is that T-segment binding to the N-gate chamber of gyrase induces a change in the relative disposition of the two transducer domains which in turn is coupled to local changes in the ATPase active site [29]. Since the transducer domain carries the active lysine (K337), a reorientation of the transducer domain with respect to the ATPase dimer with the bound ATP substrates should indeed affect ATP hydrolysis.

Such DNA induced domain reorientation has, to our knowledge, not yet been observed directly. It is likely, however, that for such communication the in-built domain mobility described in detail here is exploited again. In the restrained state, the side-chain amino-group of K337 is in H-bonding distance to the γ-phosphate of the substrate analog and, thus, probably capable to stabilize the negative charge of the transition state [9]. In the other, open conformation of the enzyme, the K337 amino-group is pulled out of the nucleotide pocket by 1.0 Å, probably sufficient to significantly de-tune the enzyme [9].

Is there signaling also in the opposite direction, from the active sites of the ATPase dimer to the core of the enzyme? This could then synchronize ATP hydrolysis with the other catalytic steps. Here, we have shown by detailed structural studies that prior to phosphate release a well-defined, obligatory state is attained and that this post-hydrolysis state is characterized by a significantly increased distance between the distal transducer ends of the GyrB43 fragment. We propose that this ATP hydrolysis induced movement initiates a series of events starting with G-segment cleavage that would be followed by DNA-gate opening and T-segment passage. The refined mechanistic scheme for the enzymatic cycle of full-length gyrase based on the current two-gate model [2] is shown in Fig. 8. It has been suggested that part of the free energy generated by ATP hydrolysis may be used to actively push the T-segment through the DNA gate [3]. This would indeed be consistent with the observed rigid-body rearrangement.

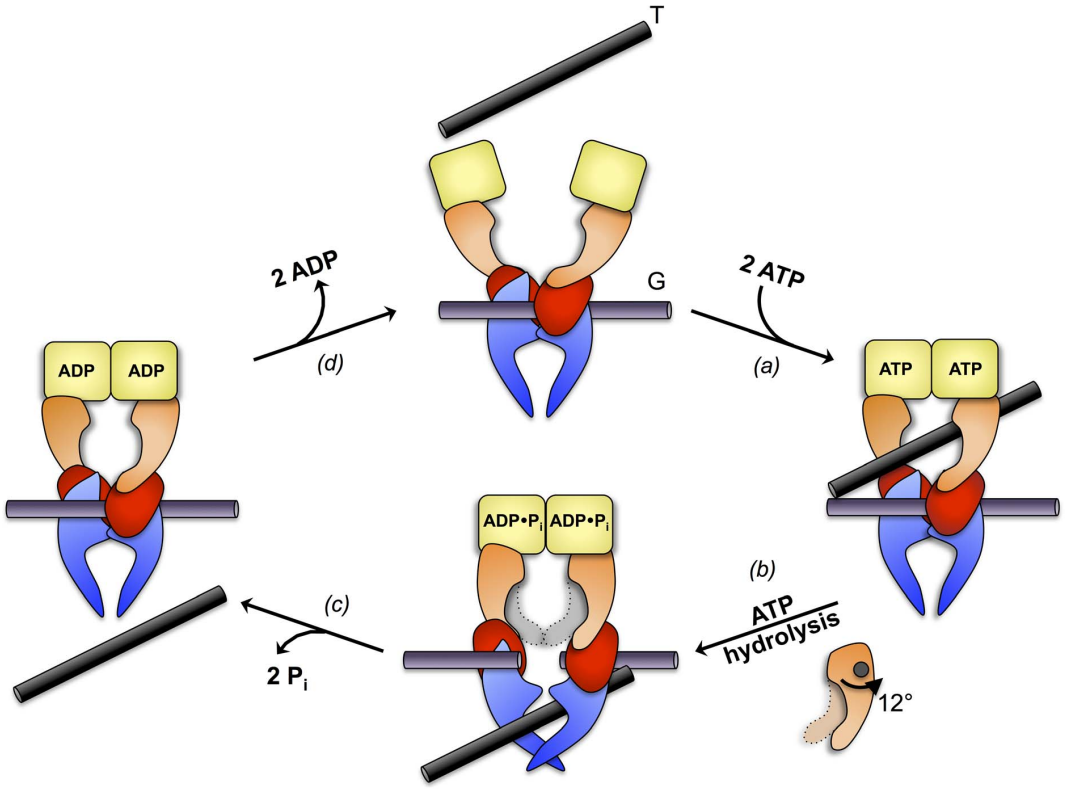

Figure 8. Refined mechanistic scheme of DNA gyrase activity, based on reference [2]**, representation as in Fig. 1.** The N-gate of the $GyrA_2GyrB_2$ heterotetramer with bound G-segment at the central DNA-gate (top) closes upon ATP binding thereby trapping a T-segment in the upper chamber (step a). Hydrolysis of the two ATP molecules causes a 12° rotation of the respective transducer domains relative to the ATPase domain (step b). We propose that this conformational change is coupled to DNA gate opening and T-segment translocation. Subsequent P_i release would be coordinated with G-segment re-ligation and DNA-gate closure (step c). Finally, ADP release results in dissociation of the ATPase domains and a reset of the enzyme (step d).
doi:10.1371/journal.pone.0107289.g008

Supporting Information

Figure S1 Comparison of various GyrB structures in complex with AMPPNP. (a) Superimposition of the *E. coli* GyrB43·AMPPNP structure determined by Wigley *et al.* (unreleased, personal communication, note that AMPPNP had been modeled as ATP) [6] in brown onto our reference structure *E. coli* GyrB43·AMPPNP determined by Brino *et al.* (PDB code: 1EI1) [13] in yellow. (b) Superimposition of *M. tuberculosis* GyrB·AMPPNP in blue-green onto our reference structure *E. coli* GyrB43·AMPPNP (PDB code: 1EI1) [13] in yellow. Structure of the ligand binding site of (c) *E. coli* GyrB·AMPPNP determined by Wigley *et al.* and (d) *M. tuberculosis* GyrB·AMPPNP (PDB code: 3ZKB). Hydrogen bonds are depicted as grey dashed lines. (e) Close-up stereoview of the active sites of the two structures shown in (a). (f) Close-up stereoview of the active sites of the two structures shown in (b).
(TIF)

Figure S2 Details of the binding sites of GyrB43 in complex (a) with ADP·BeF_3 and (b) ADP. H-bonds are depicted by dashed grey lines. The Fo-Fc omit electron density maps are shown at a contouring level of 3.0 sigma.
(TIF)

Figure S3 Stereoviews of the details of the binding sites of GyrB43 in complex with (a) AMPPNP, (b) ADP·P_i, (c) ADP·BeF_3 and (d) ADP. H-bonds are depicted by dashed grey lines. The Fo-Fc omit electron density maps are shown at a contouring level of 3.0 sigma.
(TIF)

Figure S4 (a) Superimposition of the human topoII in complex with AMPPNP (PDB entry 1ZXM, dark blue) and in complex with ADP (light blue) [12]. (b) Active site details of htopoII in complex with AMPPNP (left) or ADP·SO_4 (right), with the Fo-Fc omit electron density map for ADP, SO_4 and Mg^{2+} shown at a contouring level of 3.0 sigma. (c) Stereoview of the structures shown in (b) after superposition on their ATPase domain. The exclamation mark indicates the steric clash that would occur between Q376 in the AMPPNP complex conformation (dark blue) with the SO_4 moiety of the post-hydrolysis mimic state (light blue).
(TIF)

Figure S5 Sequence alignment of the region encompassing the QTK loop from representative species of bacteria, eukaryotes and archaea. The QTK loop is strictly conserved in topoIIA but absent from topoIIB.
(TIF)

Movie S1 Morphing between the GyrB43·AMPPNP complex (PDB entry 1EI1 [13]**) and the post-hydrolysis complex GyrB43·ADP·P_i, shown in cartoon representation with semi-transparent molecular surface overlaid with the same colors as in Fig. 2 (AMPPNP state in yellow and ADP·P_i state in magenta).** The molecular two-fold axis is shown as a black line. Views perpendicular (left) and along (right) the molecular dyad.
(MOV)

Acknowledgments

We thank Alexander Harms, Amit Sundriyal and Timm Maier for critical reading of the manuscript. We thank the staff of beam-lines X06DA and X06SA of the Swiss Light Source (Villigen, Switzerland) for their excellent support. We are grateful to Dale B. Wigley for sharing the coordinates of wild-type *E. coli* GyrB43.

Author Contributions

Conceived and designed the experiments: FVS CD TS. Performed the experiments: FVS. Analyzed the data: FVS TS. Contributed to the writing of the manuscript: FVS CD TS.

References

1. Corbett KD, Berger JM (2004) Structure, molecular mechanisms, and evolutionary relationships in DNA topoisomerases. Annu Rev Biophys Biomol Struct 33: 95–118.
2. Schoeffler AJ, Berger JM (2008) DNA topoisomerases: harnessing and constraining energy to govern chromosome topology. Q Rev Biophys 41: 41–101.
3. Sissi C, Palumbo M (2010) In front of and behind the replication fork: bacterial type IIA topoisomerases. Cell Mol Life Sci 67: 2001–2024.
4. Bates AD, Berger JM, Maxwell A (2011) The ancestral role of ATP hydrolysis in type II topoisomerases: prevention of DNA double-strand breaks. Nucleic Acids Res 39: 6327–6339.
5. Gubaev A, Klostermeier D (2014) The mechanism of negative DNA supercoiling: A cascade of DNA-induced conformational changes prepares gyrase for strand passage. DNA Repair (Amst) 16C: 23–34.
6. Wigley DB, Davies GJ, Dodson EJ, Maxwell A, Dodson G (1991) Crystal structure of an N-terminal fragment of the DNA gyrase B protein. Nature 351: 624–629.
7. Ali JA, Jackson AP, Howells AJ, Maxwell A (1993) The 43-kilodalton N-terminal fragment of the DNA gyrase B protein hydrolyzes ATP and binds coumarin drugs. Biochemistry 32: 2717–2724.
8. Gubaev A, Klostermeier D (2011) DNA-induced narrowing of the gyrase N-gate coordinates T-segment capture and strand passage. Proc Natl Acad Sci USA 108: 14085–14090.
9. Smith CV, Maxwell A (1998) Identification of a residue involved in transition-state stabilization in the ATPase reaction of DNA gyrase. Biochemistry 37: 9658–9667.
10. Corbett KD, Berger JM (2003) Structure of the topoisomerase VI-B subunit: implications for type II topoisomerase mechanism and evolution. EMBO J 22: 151–163.
11. Corbett KD, Berger JM (2005) Structural dissection of ATP turnover in the prototypical GHL ATPase TopoVI. Structure 13: 873–882.
12. Wei H, Ruthenburg AJ, Bechis SK, Verdine GL (2005) Nucleotide-dependent domain movement in the ATPase domain of a human type IIA DNA topoisomerase. J Biol Chem 280: 37041–37047.
13. Brino L, Urzhumtsev A, Mousli M, Bronner C, Mitschler A, et al. (2000) Dimerization of Escherichia coli DNA-gyrase B provides a structural mechanism for activating the ATPase catalytic center. J Biol Chem 275: 9468–9475.
14. Gorrec F (2009) The MORPHEUS protein crystallization screen. J Appl Crystallogr 42: 1035–1042.
15. Kabsch W (2010) XDS. Acta Crystallogr D Biol Crystallogr 66: 125–132.
16. Evans PR, Murshudov GN (2013) How good are my data and what is the resolution? Acta Crystallogr D Biol Crystallogr 69: 1204–1214.
17. McCoy AJ, Grosse-Kunstleve RW, Adams PD, Winn MD, Storoni LC, et al. (2007) Phaser crystallographic software. J Appl Crystallogr 40: 658–674.
18. Emsley P, Lohkamp B, Scott WG, Cowtan K (2010) Features and development of Coot. Acta Crystallogr D Biol Crystallogr 66: 486–501.
19. Murshudov GN, Skubák P, Lebedev AA, Pannu NS, Steiner RA, et al. (2011) REFMAC5 for the refinement of macromolecular crystal structures. Acta Crystallogr D Biol Crystallogr 67: 355–367.
20. Adams PD, Afonine PV, Bunkóczi G, Chen VB, Davis IW, et al. (2010) PHENIX: a comprehensive Python-based system for macromolecular structure solution. Acta Crystallogr D Biol Crystallogr 66: 213–221.
21. Joosten RP, Joosten K, Murshudov GN, Perrakis A (2012) PDB_REDO: constructive validation, more than just looking for errors. Acta Crystallogr D Biol Crystallogr 68: 484–496.
22. Chen VB, Arendall WB, Headd JJ, Keedy DA, Immormino RM, et al. (2010) MolProbity: all-atom structure validation for macromolecular crystallography. Acta Crystallogr D Biol Crystallogr 66: 12–21.
23. Kleywegt GJ (1996) Use of non-crystallographic symmetry in protein structure refinement. Acta Crystallogr D Biol Crystallogr 52: 842–857.
24. Zähringer F, Massa C, Schirmer T (2011) Efficient enzymatic production of the bacterial second messenger c-di-GMP by the diguanylate cyclase YdeH from E. coli. Appl Biochem Biotechnol 163: 71–79.
25. Agrawal A, Roué M, Spitzfaden C, Petrella S, Aubry A, et al. (2013) Mycobacterium tuberculosis DNA gyrase ATPase domain structures suggest a dissociative mechanism that explains how ATP hydrolysis is coupled to domain motion. Biochem J 456: 263–273.
26. Pasqualato S, Cherfils J (2005) Crystallographic evidence for substrate-assisted GTP hydrolysis by a small GTP binding protein. Structure 13: 533–540.
27. Kötting C, Blessenohl M, Suveyzdis Y, Goody RS, Wittinghofer A, et al. (2006) A phosphoryl transfer intermediate in the GTPase reaction of Ras in complex with its GTPase-activating protein. Proc Natl Acad Sci USA 103: 13911–13916.
28. Bates AD, Maxwell A (2007) Energy coupling in type II topoisomerases: why do they hydrolyze ATP? Biochemistry 46: 7929–7941.
29. Baird CL, Harkins TT, Morris SK, Lindsley JE (1999) Topoisomerase II drives DNA transport by hydrolyzing one ATP. Proceedings of the National Academy of Sciences 96: 13685–13690.
30. Goettler T, Klostermeier D (2007) Dissection of the nucleotide cycle of B-subtilis DNA gyrase and its modulation by DNA. J Mol Biol 367: 1392–1404.
31. Vetter IR (2001) The Guanine Nucleotide-Binding Switch in Three Dimensions. Science 294: 1299–1304.
32. Bendsen S, Oestergaard VH, Skouboe C, Brinch M, Knudsen BR, et al. (2009) The QTK loop is essential for the communication between the N-terminal atpase domain and the central cleavage—ligation region in human topoisomerase IIalpha. Biochemistry 48: 6508–6515.
33. Maxwell A, Gellert M (1984) The DNA dependence of the ATPase activity of DNA gyrase. Journal of Biological Chemistry 259: 14472–14480.

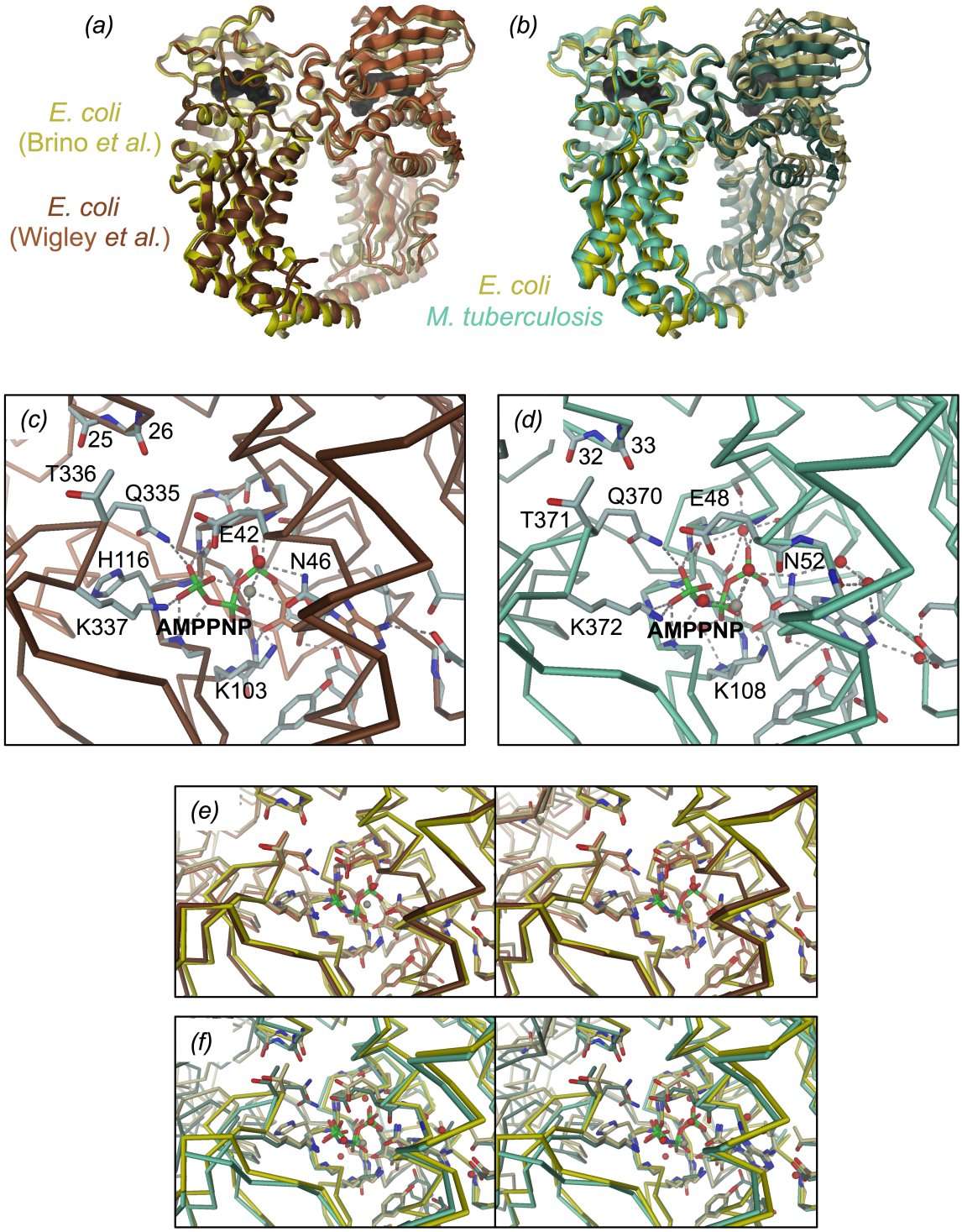
(a)
E. coli
(Brino et al.)
E. coli
(Wigley et al.)
(b)
E. coli
M. tuberculosis
(c)
25
26
T336
Q335
E42
H116
N46
K337
AMPPNP
K103
(d)
32
33
Q370
E48
T371
N52
K372
AMPPNP
K108
(e)
(f)

Figure S1.

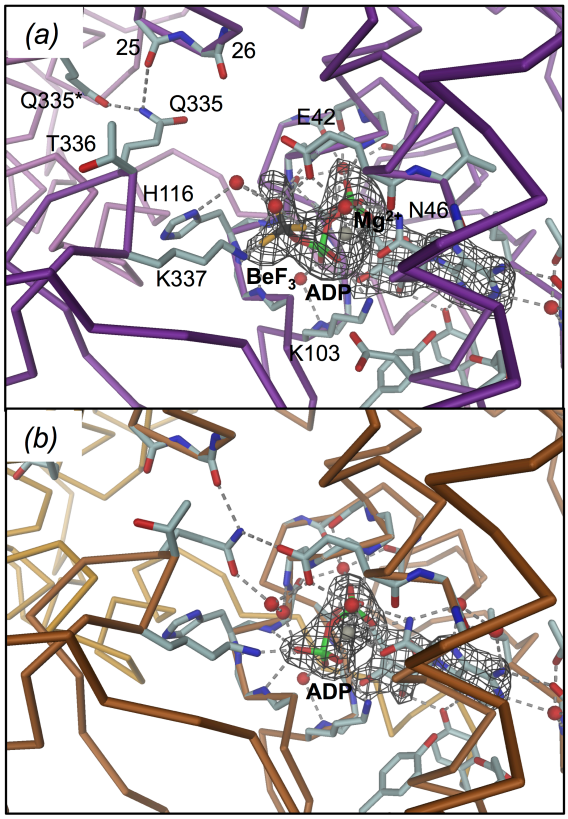

Figure S2.

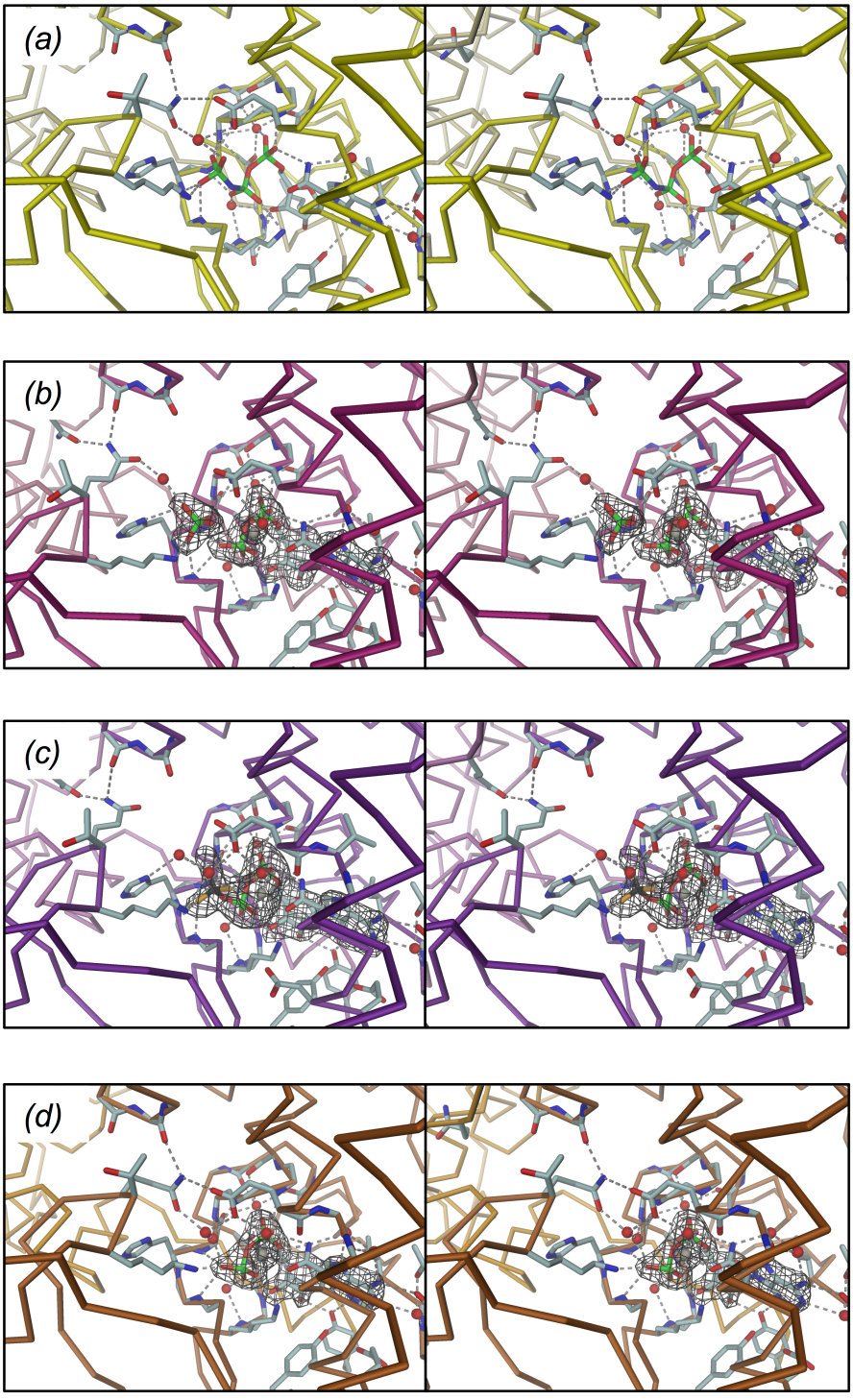

Figure S3.

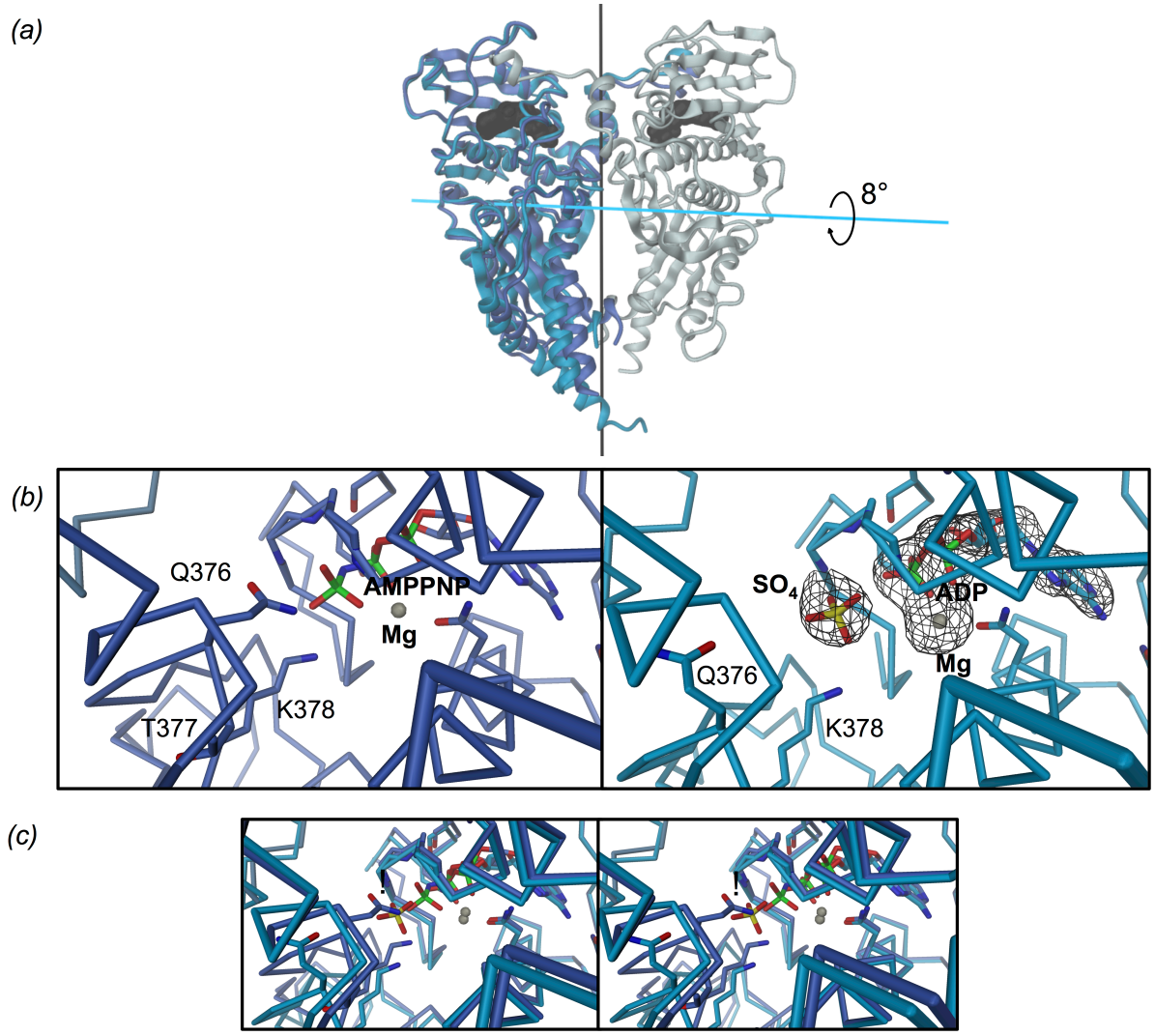

Figure S4.

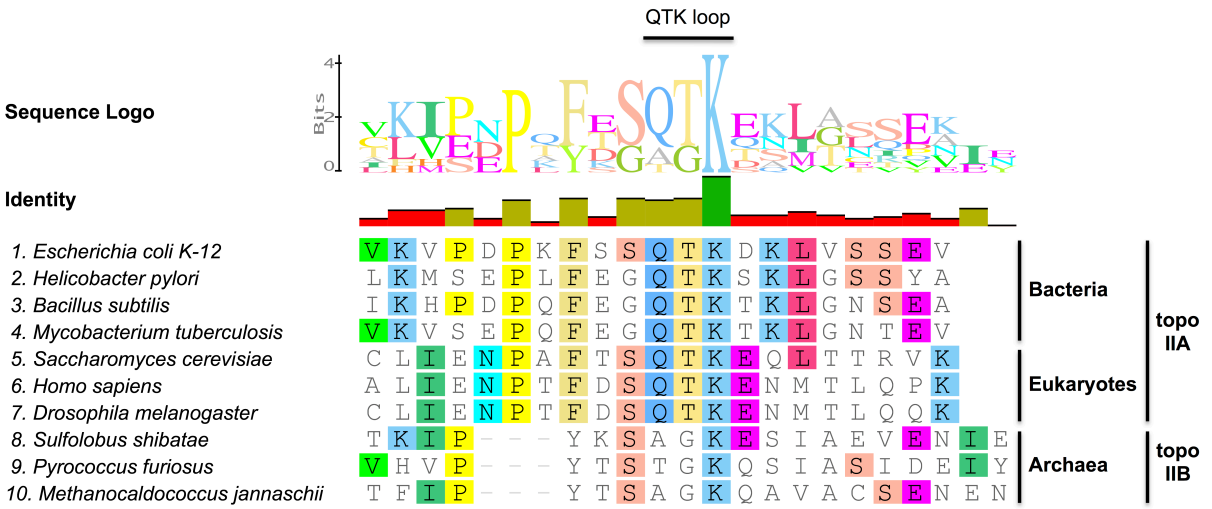
QTK loop
Sequence Logo
Bits
Identity
1. Escherichia coli K-12
2. Helicobacter pylori
3. Bacillus subtilis
4. Mycobacterium tuberculosis
5. Saccharomyces cerevisiae
6. Homo sapiens
7. Drosophila melanogaster
8. Sulfolobus shibatae
9. Pyrococcus furiosus
10. Methanocaldococcus jannaschii
Bacteria
Eukaryotes
Archaea
topo IIA
topo IIB

Figure S5.

3.5. *Research article V* (Stanger *et al.*, in preparation for *JBC*)

Target Adenylylation by class III Fic proteins is regulated by a double-lock mechanism: oligomerization and auto-adenylylation

Frédéric V. Stanger, Björn M. Burmann, Alexander Harms, Adam Mazur, Timothy Sharpe, Christoph Dehio, Sebastian Hiller and Tilman Schirmer

Manuscript in preparation

Format: Research article for the *Journal of Biological Chemistry*

3.5.1. Statement of my own contributions

I contributed to the *research article V* by designing and performing the experiments and analyzing the data. I cloned, expressed, purified, crystallized and determined the crystal structures of NmFic mutants. I analyzed the oligomeric state of NmFic by size exclusion chromatography coupled to multi angle laser light scattering (SEC-MALLS) and analyzed the growth defect of the respective mutants by spotting experiment.

The target (GyrB) of NmFic was discovered by Alexander Harms. Björn M. Burmann conducted the NMR analysis of NmFic. The SEC-MALLS analysis was performed and analyzed by myself, Timothy Sharpe and Adam Mazur. I wrote the manuscript together with all authors that provided input on their specific experiments. I prepared and assembled all the figures and tables presented in the manuscript.

3.5.2. "Target adenylylation by class III Fic proteins is regulated by a double-lock mechanism: oligomerization and auto-adenylylation"

Target adenylylation by class III Fic proteins is regulated by a double-lock mechanism: oligomerization and auto-adenylylation

Frédéric V. Stanger[1,2], Björn M. Burmann[1], Alexander Harms[2], Adam Mazur[3], Timothy Sharpe[4], Christoph Dehio[2], Sebastian Hiller[1] and Tilman Schirmer[1]

[1]Focal Area Structural Biology and Biophysics, Biozentrum, University of Basel, Basel, Switzerland

[2]Focal Area Infection Biology, Biozentrum, University of Basel, Basel, Switzerland

[3]Research IT, Biozentrum, University of Basel, Basel, Switzerland

[4]Biophysics Facility, Biozentrum, University of Basel, Basel, Switzerland

Corresponding authors:

Prof. Tilman Schirmer	Prof. Sebastian Hiller	Prof. Christoph Dehio
Biozentrum, University of Basel		
Klingelbergstrasse 70		
CH-4056 Basel, Switzerland		
Tel.: +41-61-267-20-89	Tel.: +41-61-267-20-82	Tel.: +41-61-267-21-40
Fax.: +41-61-267-21-09	Fax.: +41-61-267-21-09	Fax.: +41-61-267-21-18
tilman.schirmer@unibas.ch	sebastian.hiller@unibas.ch	christoph.dehio@unibas.ch

Abstract

Fic proteins containing the HxFx[D/E]GNGRxxR motif catalyze adenylylation, the transfer of an AMP moiety from ATP onto target proteins. This activity has severe consequences on the cellular stability and appears to be tightly controlled. Recently, it has been shown that adenylylation-competent Fic proteins are specifically inhibited by an α-helix (α_{inh}), which can be found at different locations relative to the Fic active site. Mutation of the conserved glutamate of the inhibitory motif relieves the inhibition of Fic proteins. Yet, it has remained unclear how intrinsic and extrinsic factors contribute to the control of Fic protein activation.

Here, we investigate the heterologous expression of the class III Fic protein NmFic of *Neisseria meningitidis* in *Escherichia coli* that causes a severe growth defect. We report the structural and functional characterization of NmFic and its activation mechanism. We find that NmFic is in a monomer–tetramer equilibrium. Both, the target docking site and the active site, are located towards the center of this tetramer and are accessible only in the monomeric form. Mutation of crucial residues at the interfaces that disrupts the tetramer activates the protein. Furthermore, we show that trans-auto-adenylylation of NmFic leads to significant conformational changes and that the presence of the auto-adenylylated tyrosine Y183, part of the α_{inh} helix, is required for the activity of the Class III Fic protein. We also show that adenylylation of the bacterial target GyrB from the DNA gyrase complex by NmFic blocks negative supercoiling of DNA and bacterial cell division.

Overall, these data provide the first insight into an intrinsic regulatory mechanism of a Fic protein via oligomerization and auto-adenylylation.

Introduction

Fic proteins containing FIC domains (pfam 02661) are found in all kingdoms of life as well as in viruses. They have originally been described to be involved in filamentation induced by cAMP (1), but until recently, their molecular role had remained elusive. Yarbrough *et al*. (2) deciphered the catalytic activity of the Type III effector protein VopS from *Vibrio parahaemolyticus* as adenylylation of the host cell Rho GTPases, resulting in collapse of the actin cytoskeleton and subsequent cell death. Enzymatically, Fic proteins containing the canonical HxFx[D/E]GNGRxxR motif catalyze adenylylation (or AMPylation), the covalent transfer of an AMP moiety from an ATP substrate onto a target protein (3, 4).

Fic proteins with an active site deriving from this consensus sequence likely catalyze other post-translational modifications. AnkX from *Legionella pneumophila* harbouring an HxFxDANGRxxV motif has been shown to catalyze the phosphocholination of the small GTPase Rab1 (5, 6). Doc of bacteriophage P1, a protein related to the Fic family proteins, contains the HxFxDANKRxxL active site motif, conferring a kinase activity and the phosphorylation of the translation elongation factor EF-Tu (7, 8).

The crystal structures of several FIC domain proteins have been determined (3, 9-12). Fic/Doc proteins contain a conserved central core of four helices that is flanked by additional Fic elements found in different positions (13). A loop joining the third and fourth helix of the Fic core forms the Fic active site motif. The complex structure of the Fic protein from *Histophilus somni* (IbpA) with its cognate target (Cdc42) reveals the stabilization of the modified residue by the β-hairpin region of the Fic protein, thus making the FLAP (or β-hairpin) a critical region of the Fic protein for target binding. The catalytic mechanism of Fic-mediated adenylylation has been inferred from this structure, where the catalytic histidine of the active site motif acts as a general base and deprotonates the attacking hydroxyl group, which in turn performs a nucleophilic attack on the α-phosphate of the ATP substrate. This results in the formation of a covalent phosphodiester bond between the AMP moiety and the modified amino acid.

The activity of Fic proteins is tightly regulated. A conserved inhibition motif, part of an inhibitory alpha-helix (α_{inh}), is located in the close vicinity of the active site (3). It has been demonstrated that the strictly conserved glutamate of this motif plays a key role in obstructing the γ-phosphate position of the ATP substrate, therefore inhibiting competent substrate binding in adenylylating Fic proteins. Interestingly, this inhibition motif is either found on a

separate small protein that forms a tight complex with the Fic protein, or at the N-terminus or C-terminus compared to the Fic active site within the same polypeptide chain (3, 12). These three possibilities lead to a classification of Fic proteins into class I, II and III, respectively (3, 12). The mutation of this glutamate residue to glycine relieves the inhibition of Fic proteins, thus increasing the adenylylation activity (3, 12).

Yet, the intrinsic or extrinsic factors that affect the conformation of this inhibitory α-helix and therefore the catalytic activity have not been investigated. This regulation may depend on additional domains found in multi-domain Fic proteins or localization of Fic proteins fused to a signal sequence. For the single domain class III Fic proteins, scattered through all classes of proteobacteria likely due to horizontal gene transfer, the regulation mechanism is most probably inherent. Interestingly, the class III Fic protein NmFic from *Neisseria meningitidis* (*N. meningitidis*) is auto-adenylylated on two tyrosine residues, Y183 and Y188, located in the vicinity of the inhibition motif (3). The strictly conserved tyrosine Y183 is buried, pointing towards the Fic core. Modeling of auto-adenylylation of this residue results in steric clashes, suggesting a conformational change upon auto-adenylylation.

Recently, it has been shown that Fic proteins also target bacterial proteins (3) which results in bacterial growth arrest. ParE of the topoIV complex and GyrB of the DNA gyrase complex are adenylylated by the Class I Fic protein VbhT from *Bartonella schoenbuchensis* (Harms *et al., in preparation*).

We here show that the class III Fic protein NmFic, containing the α_{inh} helix at the C-terminus, specifically adenylylates GyrB, resulting in growth arrest. We report the structure-function characterization of the regulation mechanism of the class III Fic protein NmFic via a new double-lock mechanism. Interestingly, NmFic forms a tetramer with the active site and target binding-site buried in the center of the tetramer, inaccessible for target binding. NmFic undergoes a monomer-tetramer equilibrium where the active and target binding sites are accessible in the monomeric form. Disruption of the tetramer by repellant mutations results in bacterial growth arrest by activation of the Fic protein. Ultimately, we show that auto-adenylylation of the conserved tyrosine Y183 leads to drastic conformational changes, e.g. of the α_{inh} helix, that are crucial for the class III Fic protein activity. We anticipate that this double-lock mechanism by oligomerization and auto-adenylylation is conserved through all class III Fic proteins.

Material and Methods

Plasmid construction

pRSF-Duet1 derivatives were cloned as described previously (3) and used for over-expression of proteins for purification. For phenotypic analyses, *nmfic* genes were cloned into pNMD220 (14) under the control of a particularly tight P*lac*. Site-directed mutagenesis was performed following the protocol described by Zheng *et al*. (15). A list of used plasmids and respective oligonucleotides can be found in Table S1 and Table S2.

Expression – Isotope labeling – Purification

Plasmids pFVS0015, pFVS0051, pFVS0083, pFVS0109, pFVS0135, pFVS0137, pFVS0138, pFVS0143 were transformed into *E. coli* BL21 (λDE3) cells. Plasmids pFVS0059, pFVS0125, pFVS0126 and pFVS0134 were transformed into *E. coli* BL21 AI cells. NmFic and GyrB43 (residues 1-392) proteins were expressed and purified as described previously in (3) or (16), respectively. For NMR analysis, [*U*-^{13}C,^{15}N]-labeled NmFic was obtained by growing the expression cells in M9 minimal media (17) supplemented with ($^{15}NH_4$)Cl (Cambridge Isotope Labs) and D-[^{13}C]-glucose (Sigma Aldrich) using standard NmFic expression and purification conditions.

SEC-MALLS analysis

Size exclusion chromatography coupled to multi-angle laser light scattering (SEC-MALLS) was employed for the determination of the oligomeric state and elution concentration of NmFic wild-type and various mutants at different concentrations. SEC-MALLS analysis was performed as described previously (18). The column was equilibrated in 10 mM Tris pH 7.6 and 100 mM NaCl at 4°C.

SEC-MALLS derived apparent mass values (MW^{app}) for $NmFic_{wt}$, $NmFic_{E102R}$ (mutant 1) and $NmFic_{E156R}$ (mutant 2) measured in a range of various elution concentrations were fitted simultaneously to obtain the dimerization affinities (K_{D1} and K_{D2}), assuming that both interaction interfaces are independent. Therefore, $NmFic_{E102R}$ and $NmFic_{E156R}$ are assumed to form only dimers, as one of the interfaces was mutated, and $NmFic_{wt}$ is in monomer-tetramer equilibrium, which involves both interfaces. The equilibria were modeled as fast-exchange processes with respect to the timescale of chromatographic separation, since all the samples yielded a single MALLS peak. The theoretical MW^{app} values were calculated from mass

concentrations ($c_{m,i}$) and molecular weights (MW_i) of populated species (monomer and dimer for the interface mutants; monomer, dimers, trimer and tetramer for the other NmFic variants):

$$MW^{app} = \frac{\sum_i c_{m,i} MW_i}{\sum_i c_{m,i}} \quad (1)$$

The global non-linear least-squares fitting was performed using Levenberg-Marquardt algorithm (19, 20). All routines were implemented in the Python language using NumPy and SciPy numerical libraries (21).

Monomer-tetramer equilibrium analysis

The equilibrium concentrations of individual species for $NmFic_{wt}$ were calculated using numerical solution of the set of mass action law equations (22) describing the monomer-tetramer oligomerization scheme (Fig. S3). The reaction extents were used as state variables and inequality constraints were imposed to ensure the correctness of the results. Optimization of reaction extents values was accomplished using Sequential Least SQuares Programming (SLSQP) method (23) as implemented in the SciPy library (21).

Spotting experiment

Escherichia coli K-12 MG1655 were transformed with pNDM220 derivative plasmids using TSS transformation (24) and handled in LB liquid medium containing appropriate antibiotics as well as 1% (w/v) D-glucose to suppress basal expression before the inoculation of experimental cultures. For the counting of colony forming units (CFU/mL), bacterial cultures were serially diluted and spotted on LB agar plates containing 0, 50 μM, 100 μM, 250 μM, 500 μM, 1000 μM or 2000 μM of isopropyl β-D-thiogalactopyranoside (IPTG) and 30 μg/mL ampicillin which were then incubated at 37°C.

***In vitro* adenylylation assay**

Adenylylation assays were performed using crude cell lysate of ectopically expressing *E. coli* as described previously (3) or using purified proteins as described in (12). Adenylylation activity of NmFic was assessed by incubating 5 μM NmFic protein with 10 μCi [α-^{32}P]-ATP (Hartmann analytic) and 25 μM GyrB43. In addition to radioactively labeled ATP, 62.5 μM of cold ATP was added and 200 μM of novobiocin, a potent inhibitor of GyrB43 to prevent immediate hydrolysis of ATP by GyrB43.

In vivo Supercoiling assay

In vivo supercoiling assays were performed as described previously (Harms *et al*., *in preparation*).

NMR spectroscopy

NMR experiments were performed on a Bruker AscendII 700 MHz spectrometer running Topspin 3.0 and equipped with a cryogenically cooled triple-resonance probe. All experiments were performed in NMR-buffer (25 mM MES, 150 mM NaCl, pH 6.5) at 25°C. For the sequence-specific backbone resonance assignments of NmFic and adenylylated-NmFic, the following experiments were recorded: 2D ^{15}N-^{1}H TROSY-HSQC (25), 3D HNCA (26, 27), 3D HNCACB (26-28), 3D HNCO (29), and 3D HN(CA)CO (30). For the analysis of the dynamic properties of NmFic and adenylylated-NmFic the following experiments were measured: ^{15}N{^{1}H}-NOE (31), T_1(^{15}N) (32), TRACT (33). NMR data were processed with PROSA (34) and analyzed with CARA, XEASY (35), and Topspin3.0 (Bruker Biospin). Nonlinear least-square fits of relaxation data were done with Matlab (MathWorks). R_2(^{15}N) values were derived from R_a(^{15}N) and R_b(^{15}N). Error bars for R_1(^{15}N), R_a(^{15}N), and R_b(^{15}N) were calculated by a statistical bootstrapping scheme and error bars for the ^{15}N{^{1}H}-NOE from the spectral noise. Secondary chemical shifts were calculated relative to the random-coil values of Kjaergaard and Poulsen (36).

The chemical shift changes of the amide moiety upon ATP were fitted by non-linear regression analysis to Equation 2 by using standard software. Δ_{obs} corresponds to the chemical shift difference at a given titration point and Δ_{max} is the maximal chemical shift difference at the last titration point.

$$\Delta_{obs} = \Delta_{max} \frac{(K_D + [ATP]_0 + [NmFic]_0) - \sqrt{(K_D + [ATP]_0 + [NmFic]_0)^2 - (4[NmFic]_0[ATP]_0)}}{2[NmFic]_0} \quad (2)$$

Crystallization

NmFic$_{E156R}$ and NmFic$_{E156R,Y183F}$ (10 and 8 mg/mL, respectively) crystallized in 500 μL of precipitant solution containing 10 mM Tris pH 7.8 and 100 mM NaCl using the batch crystallization method at 4°C.

All other crystals were obtained using the sitting-drop vapor-diffusion method by mixing 0.2 μL protein solution with 0.2 μL reservoir solution equilibrating against a reservoir of 80 μL at 20°C except $NmFic_{wt}$ (tetramer form) that crystallized in 7% (v/v) 2-propanol, 0.1 M MES pH 6.0, 0.05 M calcium acetate at 4°C. $NmFic_{E102R}$ crystallized after one month in 8% (v/v) Tacsimate pH 6.0, 20% (w/v) PEG 3350 and $NmFic_{E102R,E156R}$ crystallized after ten days in 8% (v/v) Tacsimate pH 5.0, 30% (w/v) PEG 1500. $NmFic_{Y183F,E186G}$ crystallized in 0.1 M Tris pH 8.0, 30% (w/v) Jeffamine M-600 pH 7.0. For data collection, crystals were cryoprotected by soaking into a reservoir solution supplemented with 15-30% glycerol and subsequently flash-frozen in liquid nitrogen.

Structure determination

X-ray data were collected at the Swiss Light Source (Villigen, Switzerland) on beamline X06SA (PXI) or X06DA (PXIII) at 100 K and a wavelength of 1.000 Å or 0.800 Å (Table 1). Diffraction data were indexed and integrated using iMosflm (37) or XDS (38) and subsequently merged and scaled using XSCALE (38) or aimless (39). $NmFic_{wt}$ diffracted to 3.10 Å. $NmFic_{E156R}$, $NmFic_{E102R}$ and $NmFic_{E102R,E156R}$ diffracted to 0.99 Å, 2.35 Å and 1.90 Å, respectively. $NmFic_{Y183F,E186G}$ and $NmFic_{E156R,Y183F}$ respectively diffracted to 2.20 Å and 1.00 Å. Data collection and processing statistics are summarized in Table 1. Structures were determined by molecular replacement using Phaser (40) with $NmFic_{wt}$ (PDB: 3S6A (3)), devoid from ligand or ordered solvent, as search model. Several rounds of model building and refinement were performed using Coot (41) and Refmac5 (42) or phenix.refine (43). 5% of the data were excluded from refinement and used for cross-validation. The geometry of the final model was assessed using MolProbity (44) showing > 99% of the residues in the core and allowed regions of the Ramachandran plot. Final refinement yielded NmFic models with reasonable R_{work}/R_{free} values for their respective resolution ranges (45). Refinement statistics are summarized in Table 2.

Figures were prepared with Dino (A. Philippsen unpublished, http://www.dino3d.org).

Results

NmFic undergoes a monomer–tetramer equilibrium

Crystals of $NmFic_{wt}$ grown at high protein concentration belong to the space group $P6_5$ and contain four molecules per asymmetric unit. These four molecules form a non-crystallographic 222 tetramer that contains two equivalent dimers (Fig. 1 *(a,b)* and Fig. S1 *(b)*). The same tetramer form is observed for $NmFic_{\Delta 8}$, a deletion mutant of the α_{inh} helix ($\alpha 8$) that had been previously determined from non-isomorphous crystals (3). Isologous contacts are observed at the interfaces of $NmFic_{wt}$ between subunits A-B, C-D and A-D, B-C, respectively (Fig. 1). The first interface (buried surface area of 420.3 +/- 1.1 $Å^2$) forms hydrophobic interactions and two symmetrical salt-bridges between residues R149 and E156 of two neighboring monomers (Fig. 1 *(d)*). The second interface (826.1 +/- 11.3 $Å^2$) forms the same type of interactions, with salt-bridges between residues R71 and E102 (Fig. 1 *(c)*). The residues involved in these interfaces are conserved in class III Fic proteins as shown by the multiple sequence alignment (Fig. S2). Consequently, analysis of the oligomeric state of $NmFic_{wt}$ in solution revealed the presence of multimeric forms in a concentration dependent manner (Fig. S1 *(a)*). Size exclusion chromatography coupled to multi-angle laser light scattering (SEC-MALLS) was performed, revealing a single peak that varies in elution volume and apparent molar mass (from 22 kDa to 88 kDa) with varying total protein concentration. This shows that the protein is in a monomer–tetramer equilibrium in fast exchange with respect to the timescale of chromatographic separation (Fig. 2 *(a)*).

The Fic active site is located in the center of the tetramer and the β-hairpin forming the target-binding site (FLAP) is deeply buried (Fig. 1 *(a,b,e)*, yellow and light blue, respectively). Modeling of the binding of a small target fragment based on the superimposition of the IbpA/Cdc42 complex structure (PDB: 4ITR (10)) on the FLAP region of NmFic reveals several steric clashes (depicted by stars on Fig. 1 *(e)*). It is therefore well conceivable that NmFic in this tetrameric form is incompetent for target binding and that a lower oligomeric state, i.e. monomer or dimer, is the active species.

To test this hypothesis, we engineered variants of NmFic carrying single amino acid mutations (glutamic acid to arginine) of the salt-bridges formed at both dimerization interfaces, $NmFic_{E102R}$ and $NmFic_{E156R}$. The crystallographic structures of $NmFic_{E102R}$ and $NmFic_{E156R}$ were determined (Tables 1-2). These structures reveal that the dimerization interfaces are maintained as in the tetrameric wild-type protein (Fig. 3). The interface areas

for $NmFic_{E102R}$ and $NmFic_{E156R}$ are 418.6 Å^2 and 779.4 Å^2, respectively, and thus virtually identical to the tetramer (420.3 ± 1.1 Å^2 and 826.1 ± 11.3 Å^2, respectively). Residue E102 is involved in a salt-bridge with E71 of the FLAP in the wild-type protein and the mutation $NmFic_{E102R}$ leads to an increase in flexibility of the FLAP region as evidenced by the lack of electron density for residues 62–77. The high-resolution structure (0.99 Å) of $NmFic_{E156R}$ reveals the exact same dimer as observed within the tetrameric crystal form (RMSD of 0.989 Å for Cα atoms).

The multimerization equilibrium of these two proteins, as well as the double mutant, was assessed by SEC-MALLS. As expected, these mutants do not form a tetrameric species, but undergo a monomer–dimer equilibrium (22 kDa – 44 kDa) via the remaining interface (Fig. 2 *(a)*). The combination of both mutations in $NmFic_{E102R,E156R}$ reveals a constant mass of 22 kDa (monomer) at various protein concentration (Fig. 2 *(a)*). From these data, the dimerization constants (K_d) for $NmFic_{E102R}$ (mutant 1) and $NmFic_{E156R}$ (mutant 2) were determined to K_{d1} = 7.4 ± 1.4 μM and K_{d2} = 59.9 ± 11.8 μM, respectively. Note that the smaller dimerization interface features the higher affinity. The independent global fitting of the monomer–dimer–tetramer equilibrium of the wild-type protein yielded 7.6 ± 1.1 μM and 61.3 ± 8.8 μM for K_{D1} and K_{D2}, respectively (Fig. S3, Fig. 2 *(a)* and Table 3). These values are virtually identical in the precision of the experiment, indicating directly that the two interfaces are not connected by cooperativity. Based on the dissociation constants, the concentration-dependences of monomeric, dimeric, trimeric and tetrameric species of $NmFic_{wt}$ were calculated (Fig. 2 *(b)*). At total NmFic concentrations below 2 μM, NmFic is mostly present as monomers, whereas above this threshold, tetrameric species populate. Importantly, since most protein is sequestered as tetramers, the monomer concentration reaches a value of just 5 μM at a total NmFic concentration of 1 mM (Fig. 2 *(b)*). In contrast, the monomer concentrations in the Fic mutants are much larger, with 60 μM and 150 μM for mutant 1 ($NmFic_{E102R}$) and mutant 2 ($NmFic_{E156R}$) respectively at 1 mM total concentration (Fig. 2 *(c) and* S4). As monomer and tetramer are the predominant species, the monomer-tetramer equilibrium of $NmFic_{wt}$ can also be fitted with a single effective dissociation constant K_{Def} of 21.8 ± 1.0 μM (Table 3).

NmFic targets GyrB of the DNA gyrase complex

As the next step, we aimed to identify the target of NmFic within *E. coli*. VbhT, a Fic protein from the α-proteobacteria *Bartonella schoenbuchensis* adenylylates its own ParE and GyrB, as well as the homologous proteins from *E. coli* (Harms *et al., in preparation*). In turn,

though VbhT adenylylates both proteins, the *in vivo* supercoiling activity of GyrB is only faintly affected by VbhT when the decatanation activity of ParE is drastically inhibited by the expression of the Fic protein VbhT. Because of the similar growth defect phenotype of *E. coli* induced by expression of VbhT and the inhibition-relieved mutant of NmFic ($NmFic_{E186G}$) (3, 12), we tested the adenylylation of *E. coli* GyrB and ParE by $NmFic_{E186G}$. Interestingly, this inhibition-relieved mutant of the class III Fic protein from *N. meningitidis* (3, 12) specifically adenylylates *E. coli* GyrB but not ParE, suggesting a different mechanism of the bacterial growth inhibition (Fig. 4 *(a)*). Furthermore, $NmFic_{E186G}$ adenylylates GyrB of *N. meningitidis* stronger than the homologous in *E. coli* (Fig. 4 *(a)*). Mutation of the adenylylated tyrosine 109 from *E. coli* GyrB (to alanine or phenylalanine) completely abolishes the adenylylation of GyrB, showing that GyrB is specifically adenylylated on this residue. The tyrosine 109 from GyrB is located in the N-terminal ATPase domain of GyrB and conserved in bacterial topoisomerases. This residue is part of the ATP lid-loop (46) and involved in a weak contact with the N3 of the adenine ring of the ATP substrate of GyrB (47). The adenylylation of GyrB results in the inhibition of ATP hydrolysis (Harms *et al.*, *in preparation*), which is required for the DNA supercoiling activity of DNA gyrase that is essential for bacterial growth (48, 49).

Like novobiocin at the high concentration of 100 μg/mL, the expression of $NmFic_{E186G}$ in *E. coli* results in collapse of the negative supercoiling of a reporter plasmid (Fig. 4 *(b)*). No effect can be observed with the catalytically inactive $NmFic_{H107A,E186G}$ mutant, showing that the observed loss of supercoiling activity directly results from the adenylylation of GyrB by the inhibition-relieved mutant $NmFic_{E186G}$ (Fig. 4 *(b)*). This is in contrast with the effect of VbhT on GyrB, which does not inhibit the *in vivo* supercoiling activity of GyrB (Harms *et al.*, *in preparation*).

Tetramerization deficient mutants induce growth defects and adenylylate GyrB

Knowledge of the target enabled us to evaluate the activity of NmFic mutants of the dimerization interfaces *in vitro* by adenylylation assay. For *in vivo* characterization (*E. coli* model), bacteria (*E. coli* K12 MG1655) were transformed with plasmids containing *nmfic* genes, grown in liquid culture, and serial dilutions of exponentially growing bacteria were spotted on LB-agar plates supplemented with increasing amounts of IPTG (form none to 2 mM) (Fig. 5 *(a)*). Colony forming units were counted allowing the quantification of bacterial growth defect upon expression of the different NmFic mutants. Compared to the

wild-type or the catalytically inactive mutant in which the first histidine of the Fic active site motif has been mutated (2), $NmFic_{E102R}$ (mutant 1), $NmFic_{E156R}$ (mutant 2) and $NmFic_{E102R,E156R}$ (monomer) mutants show a severe growth defect in dependence of the induction level (Fig. 5 *(a,b)*). This growth defect was quantified for each mutant, resulting in the loss of 1.5, 3.0, and 1.5 log10 CFU/mL of viability for $NmFic_{E102R}$, $NmFic_{E156R}$ and $NmFic_{E102R,E156R}$, respectively. In addition to the loss in colony number, the colonies exhibited a drastically smaller size (Fig. 5 *(a)*). Furthermore, expression of the combination of the dimerization interface mutants with the H107A mutation (catalytically inactive) abolishes the growth defect of *E. coli*, similarly to the expression of wild-type tetrameric NmFic (Fig. 5 *(a,b)*). These observations evidence that the catalytic activity of NmFic is responsible for the growth defect of bacteria expressing the dimerization interface mutants. *In vitro*, an adenylylation assay revealed that purified NmFic mutants of the dimerization interface adenylylate the target GyrB (N-terminal fragment containing the ATPase and transducer domains). These results are in agreement with the *in vivo* results, clearly showing that the catalytically inactive mutants are unable to transfer radioactively labeled α-^{32}P-AMP on GyrB (Fig. 5 *(c)* and Fig. S5). These observations rely so far on the total concentration of NmFic proteins expressed for *in vivo* quantification or the total concentration of pure protein in the *in vitro* assays.

It is interesting to compare the growth defect to the NmFic monomer concentration rather than the total concentration. For that purpose, a conversion factor (ratio) between IPTG and total NmFic concentration was applied, with a concentration of 100 μM of inducer (IPTG) leading to 1 μM of total NmFic protein (Fig. 6 *(a)*), based on different IPTG/$NmFic_{total}$ ratios that were tested graphically (Fig. 6 (b) and Fig. S6 *(a-c)*). At this ratio, the concentration of monomer in the $NmFic_{wt}$ (forming tetramer) stays rather low (< 1 μM) at a total NmFic concentration of 10-20 μM. This is in contrast with the mutant 1, mutant 2 and monomer mutant, in which the monomer concentration is very close to the total NmFic concentration. Fig. 6 *(b)* shows that for $NmFic_{wt}$, a sufficient concentration of monomeric Fic protein cannot be achieved with the maximal level of induction that can be used experimentally. This points towards a threshold level of NmFic that can be tolerated by the cell and here not obtained in wild-type NmFic, where the tetramer acts as a sponge that stores the active NmFic species. Taken together, these results reveal a first level of regulation of NmFic by oligomerization.

Structural investigation of auto-adenylylated NmFic by NMR

To understand the effect of auto-adenylylation of NmFic, we investigated the changes induced by auto-modification of a catalytically inactive monomer mutant ($NmFic_{E102R,H107A,E156R}$) in solution using high-resolution nuclear magnetic resonance (NMR). NmFic is auto-adenylylated on two tyrosines positioned in the close vicinity of the conserved inhibitory glutamate, that is part of the α_{inh} helix (helix 8) (3). Modeling of auto-adenylylation on tyrosine 183 and 188 results in steric clashes with the Fic core, suggesting a putative conformational change upon auto-adenylylation of NmFic. Intriguingly, tyrosine Y183 is strictly conserved in class III Fic proteins. We obtained well-dispersed NMR spectra for a native and an auto-adenylylated sample (inactive monomer mutant that was adenylylated by the addition of trace amounts of hyperactive $NmFic_{\Delta 8}$, Fig. S7). Sequence-specific resonance assignments were obtained for 95% and 93% for native and adenylylated $NmFic_{E102R,H107A,E156R}$, respectively. Analysis of the chemical shift changes upon auto-adenylylation revealed that the helix 1, the inhibitory helix 8 (α_{inh}) and the FLAP region (Fig. 7) are the most affected regions upon adenylylation. The changes in the helix 1 are highly likely a direct result of the auto-adenylylation of helix 8 possibly leading repulsion of both helices from the Fic core. This movement will then lead to the activation of NmFic by active-site opening, with auto-adenylylation being the intrinsic factor that expulses the inhibition motif from the ATP binding site, relieving the inhibition of class III Fic proteins. We used the chemical shifts of the backbone $^{13}C\alpha$ and $^{13}C\beta$ nuclei to identify the secondary-structure elements of both NmFic forms in solution. NmFic features eight α-helices in solution, that corresponds in their number and positioning to the crystalline structure (Fig. S8). In addition, residues 62–66 of the FLAP region exhibit a small β-sheet. These secondary elements remain upon adenylylation, showing only a slight decrease of about 15% percent of helical content in helix 1.

The opening of the γ-phosphate binding site upon adenylylation, leads to a two-fold increase of the affinity of ATP binding compared to the native unadenylylated form, with respective dissociation constants of 4.0 ± 1.2 mM and 7.8 ± 1.1 mM (Table 4 and Fig. S9). These constants are rather high, but are in excellent agreement with similar observations for Doc, the toxin of bacteriophage P1 that phosphorylates EF-Tu, with a K_D of 7.2 mM for an ATP analog in the absence of target. Strikingly, upon pre-formation of a Doc–EF-Tu complex, the affinity for the substrate increases by ~ 10^5-fold to 0.26 μM (7). This effect can be deduced to the fact that the FLAP region is responsible for target binding but also needs to provide important residues for ATP binding and the base-binding pocket. We observed a high

degree of flexibility in the FLAP-region on the picosecond–nanosecond timescale by measurement of $^{15}N\{^{1}H\}$-NOE measurements. This dynamic behavior was further evidenced by a reduction in the T_1-relaxation time as well as by the absence of electron density in this region in crystal structures. Therefore a significant increase of the substrate affinity upon GyrB binding and subsequent stabilization of the FLAP to enhance ATP binding in-line with the Doc–EF-Tu interaction can be expected.

Presence of the auto-adenylylated tyrosine 183 of NmFic is required for activity

To investigate further the role of auto-adenylylation, we mutated the tyrosine 183 and tested the effect *in vivo*. Since $NmFic_{wt}$ is known to be inhibited by a tight tetramer formation, we investigated the effect of Y183 on the inhibition-relieved mutant $NmFic_{E186G}$ (3, 12). Comparison of $NmFic_{E186G}$ to $NmFic_{Y183F,E186G}$ shows that the growth defect phenotype of $NmFic_{E186G}$ is completely abolished by the Y183F mutation (Fig. 8 *(a)*). To rule out any significant structural changes upon Y183F mutation, we compared the crystal structures of both aforementioned proteins. Both structures are very similar, with root mean square deviation (RMSD) of 0.306 Å for the Cα atoms (0.684 Å for all atoms) after superimposition (50) (Fig. 8 *(b)*). These *in vivo* and structural results clearly indicate that the auto-adenylylation of residue Y183 is crucial for the activity of the protein. Additionally, the combination of mutants of the dimerization interface (mutant 1, mutant 2 and monomer mutant) with the mutation of Y183 also re-established normal growth of *E. coli* cells (Fig. 8 *(a)*), while leading to no structural changes as evidenced by the RMSD of 0.228 Å for the Cα atoms (0.428 Å for all atoms) for the mutant 2 ($NmFic_{E156R}$) and the mutant 2 Y183F ($NmFic_{E156R,Y183F}$) obtained at 1.0 Å resolution (Fig. 8 *(c)*).

The SEC-MALLS analysis of the inhibition-relieved $NmFic_{E186G}$ mutant reveals a less stable tetramer that $NmFic_{wt}$ (Fig. 9 *(a)* and Table 3) with a tetramerization K_{Def} of 190.0 ± 9.5 μM ($NmFic_{E186G}$) compared to 21.8 ± 1.0 μM ($NmFic_{wt}$), albeit the mutation is far away from oligomerization interfaces. A double mutation Y183F, E186G has an opposite effect, making the tetramer much tighter (Table 3). There may be an effect of auto-adenylylation on the lower affinity of $NmFic_{E186G}$ since the purified protein is expected to be partially auto-modified, as revealed by an increased A_{260}/A_{280} ratio (data not shown). The monomer concentration of the E186G mutant compared to the total concentration reveals that this mutant, even though still forming a tetramer, has monomer levels very close to the dimer mutants (Fig. 9 *(b)*).

Altogether, combination of solution NMR analysis, crystallographic analysis and *in vivo* growth analysis reveals that the auto-adenylylation of NmFic is a required mechanism of relief of inhibition in class III Fic proteins. This layer of control is accompanied by the regulation through tetramerization to tightly control the adenylylation of the target GyrB.

Discussion

Fic proteins need to be tightly regulated due to their highly toxic activity both in the prokaryotic and eukaryotic cells (2, 3) (Harms *et al*., *in preparation*). The crystal structure shows that tetrameric Fic can not be competent for target binding, due to burying of the target binding site in the core of the tetramer. On a first level of regulation, disassembly of the tetrameric state is thus essential for activation of the Fic protein. Our activation model assumes that the cell can compensate for the deleterious effects of a small intracellular concentration of monomeric NmFic, up to a level at which the inhibition of DNA gyrase by NmFic is not bacteriostatic. *In vitro* oligomerization analysis yields a maximal level of 2 μM for monomeric Fic. This value could be modulated *in vivo*, due to molecular crowding effects in the cytosol or additional binding partners that would facilitate the tetramer formation. A level of 1-2 μM of monomer, corresponding to 600-1200 molecules per bacteria, would be sufficient to inhibit the 1300 GyrB molecules (A. Schmidt, personal communication), thus the DNA gyrase machinery and negative supercoiling in the cell, resulting in cell growth arrest.

Dimers and monomers of NmFic are toxic for *E. coli*, but the toxicity does not accumulate from dimers to monomer (Fig. 5). At rather low concentration, the concentration of monomer is very close to the total protein concentration (Fig. 2 *(c)*), and therefore no significant difference is expected. The mutant 1 and monomer are less toxic than the mutant 2, which can not be rationalized from the interfaces. Nonetheless, both mutant 1 and monomer mutant harbor the E102R mutation, residue that is located below the target binding site (FLAP) and may contribute to target binding, since it is unlikely that three main chain–main chain hydrogen bonds of the FLAP are sufficient for target binding and specificity. Alternatively, this mutation may also slightly alter GyrB binding. We can not exclude that a dimer (mutant 1, mutant 2 or both) is/are also active in a natural environment. Nonetheless, the low abundance of these species within the monomer-tetramer equilibrium of wild-type NmFic (Fig. 2 *(b)*) makes it highly unlikely that the dimers have a major role in the activity of NmFic in the cell.

The neutralization of toxic proteins is a common scheme in biology. Binding of antitoxins to toxins is a quite common way to neutralize toxins of all kind prior to their intended activation in time or location. The *E. coli* relB/RelE protein complex is a characteristic example of such a toxin-antitoxin system (14). The relBE toxin-antitoxin system acts as transcriptional autoregulation system. In the case of nutritional starvation, transcription from the relBE operon gets dramaticaly increased and the level of RelB antitoxin is reduced by Lon-dependent proteolysis, a common mechanism of antitoxin degradation (51). The liberation of the RelE toxin results in cellular growth arrest (52). Keeping a protein in an inactivated oligomeric state, like tetramerization for NmFic, is an elegant way to control protein function that can be activated directly by an external trigger. In this case, the protein acts as its own antitoxin. Similar activation mechanism can also be found for the bacterial chaperone trigger factor, directly interacting in the monomeric form with a large variety of nascent chains on the ribosome (53), which is in the cytosol in a monomer-dimer equilibrium that can be modulated depending on the growth conditions (54, 55). Trigger factor dimerizes with an apparent K_D of 18 μM, in the same range as the effective K_{Def} of $NmFic_{wt}$ (21.8 ± 1.0 μM). Furthermore, the plant Ultraviolet-B radiation photoreceptor UVR8, responsible for adaptation to UV, is inactive as a dimer but active as a monomer. In the ground state, inactive, UVR8 is present as a homodimer that monomerizes within seconds of UV-B irradiation (56). The active monomer then interacts with COP1, resulting in changes in gene expression, acclimation and UV-B tolerance (57).

A second level of control is provided by auto-adenylylation of NmFic. We propose that this auto-adenylylation is the intrinsic factor that expulses the strictly conserved glutamate of the inhibition motif, thus relieving the inhibition of class III Fic proteins. This is evidenced by *in vivo* effects of the mutation of the strictly conserved Y183 within class III Fic proteins. Additionally, the investigation of the auto-adenylylation in solution by NMR reveals chemical shift changes of residues belonging to the α_{inh} helix, the helix that is responsible for the inhibition of competent ATP binding (3, 12). Changes in the chemical shifts of the helix α1 are likely an effect of the movement of helix α8, since this is the adjacent helix that will be affected by the introduction of the adenylylation on Y183. The observed changes within the FLAP is likely due to the binding of the target in the auto-adenylylated form, whereas the target here is the intermolecular helix α8.

Is there a link between the oligomerization and auto-adenylylation? First, it is worth noting that a target cannot bind to the tetrameric form of NmFic, i.e. here the helix 8 acting as an intermolecular target. Auto-adenylylation occurs via binding of the helix α8 (α_{inh}) on the FLAP of another monomer and covalent transfer of AMP on the tyrosine 183. Once auto-adenylylated, the helix α8 cannot fold back to its original inhibitory position, relieving the auto-inhibition. Interestingly, the $NmFic_{E186G}$ mutant of the inhibitory glutamate has a much lower affinity for both forms of dimers within the tetramer as observed by the shifted monomer-tetramer equilibrium towards higher concentration (Table 3). The helix α8 lies on the surface of the tetramer and is not involved in dimerization interfaces. Additionally, $NmFic_{E186G}$ is found endogenously auto-adenylylated. This observation indicates a putative link between oligomerization and auto-adenylylation, where adenylylation has an enhancing effect on monomerization. The auto-adenylylation of the mutant 1, mutant 2 and monomer mutant are required for the activity of these proteins, as evidenced by the experimental *in vivo* growth data. The monomer and dimer mutants are also active, showing that the auto-adenylylation is not only involved in disrupting the oligomer but rather in an own activity. Altogether, the informations obtained on auto-adenylylation show that the auto-adenylylation *per se* is required for the activity of the protein, expulsing the inhibitory helix from the ATP binding site, but most likely needs the monomerization of NmFic beforehand. Commonly, auto-adenylylation has been observed for most Fic proteins investigated so far (10, 11, 13, 58-60) but its putative role within the functional cycle of these proteins was not yet addressed. Therefore, the regulatory function of auto-adenylylation for class III Fic proteins may indicate that auto-modification is also involved in the control of catalytic activities of class I and class II FIC domains and could thus be a general feature of Fic proteins.

In summary, our experiments suggest a model for Fic activation (Fig. 10). Upon an initiation signal that remains still elusive, the NmFic tetramer is disrupted which liberates the FLAP, enabling target binding. The disruption of the tetramer is followed by a second layer of regulation, auto-adenylylation. This modification of monomers leads to full activation of the protein by expulsion of the inhibitory alpha helix. Once a certain level of auto-adenylylated monomer is present in the cell, adenylylation of GyrB from the DNA gyrase subunit blocks efficiently the bacterial growth, resulting in a bacteriostatic effect. Our study revealed the tight two-step regulation of class III Fic proteins and identified its biological role as a negative regulator of the DNA-gyrase machinery.

Author contribution

F.V.S. and A.H. cloned recombinant plasmids. F.V.S. expressed, purified, crystallized and determined the X-ray structure of protein constructs and analyzed the *E. coli* growth upon expression of NmFic. A.H. discovered the target of NmFic, performed adenylylation and supercoiling assay. B.M.B. conducted the NMR analysis of NmFic. F.V.S., A.M. and T.Sh. performed and analyzed the SEC-MALLS experiments. All authors participated in experimental design, data analysis and wrote the manuscript.

Acknowledgments

We thank the staff of beam-lines X06DA and X06SA of the Swiss Light Source (Villigen, Switzerland) for excellent support. We gratefully acknowledge Gerd Pluschke for kindly providing the genomic DNA of *Neisseria meningitidis*. This work was supported by the ERC Advanced Investigator Grant (ERC-2013-AdG) FICModFun 340330 (to C.D.), and SNF grants 3100-132979 (to C.D.) and 31003A-138414 (to T.S.).

Table 1. Data collection statistics.

	wt	E102R	E156R	E102R-E156R	Y183F-E186G	E156R-Y183F
X-ray source	SLS X06DA (PXIII)	SLS X06SA (PXI)	SLS X06DA (PXIII)	SLS X06DA (PXIII)	SLS X06DA (PXIII)	SLS X06DA (PXIII)
X-ray detector	MAR225 CCD	Pilatus 6M	Pilatus 2M	Pilatus 2M	Pilatus 2M	Pilatus 2M
Wavelength (Å)	1.00853547/6	1.000	0.800	1.000	1.000	0.800
Space group	P 6_5	P 2 2_1 2_1	P 2 2_1 2_1	P 2 2_1 2_1	P 6_4 2 2	P 2 2_1 2_1
Cell dimensions (Å) a, b, c	131.92, 131.92, 167.74	48.56, 81.91, 97.53,	35.33, 50.54, 130.14	35.40, 39.75, 132.75	148.64 148.64 75.98	35.38 50.70 129.78
Matthews coeff. (Å^3/Da)	5.06	2.53	2.73	2.45	5.84	2.74
Solvent content (%)	75.50	50.98	54.67	49.39	78.79	54.79
Mol. per asym. unit	4	2	1	1	1	1
Resolution limits (Å)	14.95 - 3.10 (3.21 - 3.10)	62.72 - 2.35 (2.43 - 2.35)	47.15 - 0.99 (1.02 - 0.99)	66.37 - 1.50 (1.55 - 1.50)	53.13 - 2.20 (2.28 - 2.20)	32.91 - 1.00 (1.04 - 1.00)
Total reflections	58397 (5680)	120000 (12268)	839576 (79738)	53547 (2947)	560845 (53518)	784149 (73569)
Unique reflections	29964 (2991)	16808 (1666)	129866 (12557)	8894 (474)	25596 (2494)	122935 (11501)
Multiplicity	1.9 (1.9)	7.1 (7.4)	6.5 (6.4)	6.0 (6.2)	21.9 (21.5)	6.4 (6.4)
Completeness (%)	99.74 (99.70)	99.89 (100.00)	99.47 (97.58)	74.68 (99.57)	99.93 (99.76)	96.84 (91.52)
Mosaicity	1.22	0.19	0.10	0.27	0.47	0.21
⟨ I/σ(I) ⟩	11.08 (3.35)	21.93 (4.57)	29.81 (3.47)	26.97 (19.17)	20.95 (1.91)	25.42 (3.43)
R_{merge} † (%)	6.35 (24.31)	7.52 (47.95)	3.16 (54.76)	4.59 (5.64)	16.73 (212.70)	3.90 (49.68)
R_{meas} ‡ (%)	8.98	8.12	3.43	5.03	17.13	4.26
$CC_{1/2}$ (%)	99.0 (84.4)	99.9 (93.0)	100.0 (86.9)	99.9 (99.9)	99.9 (84.1)	100.0 (85.0)
CC* (%)	99.7 (95.7)	100.0 (98.2)	100.0 (96.4)	100.0 (100.0)	100.0 (95.6)	100.0 (95.9)

Number in parentheses belong to the outer shell.

† $R_{merge} = \sum_{hkl}\sum_i |I_i(hkl) - \langle I(hkl)\rangle| / \sum_{hkl}\sum_i I_i(hkl)$, where $I_i(hkl)$ is the observed intensity for a reflection and $\langle I(hkl)\rangle$ is the average intensity obtained from multiple observations of symmetry-related reflections.

‡ $R_{meas} = \sum_{hkl}[N/(N-1)]^{1/2}\sum_i |I_i(hkl) - \langle I(hkl)\rangle| / \sum_{hkl}\sum_i I_i(hkl)$, where $I_i(hkl)$ is the observed intensity for a reflection, $\langle I(hkl)\rangle$ is the average intensity obtained from multiple observations of symmetry-related reflections and N is the number of observations of intensity I(hkl).

Table 2. Refinement statistics.

	wt	E102R	E156R	E102R-E156R	Y183F-E186G	E156R-Y183F
PDB code	N/A	N/A	N/A	N/A	N/A	N/A
Resolution limits (Å)	14.95 - 3.10 (3.21 - 3.10)	62.72 - 2.35 (2.43 - 2.35)	47.15 - 0.99 (1.02 - 0.99)	66.37 - 1.50 (1.55 - 1.50)	53.13 - 2.20 (2.28 - 2.20)	32.91 - 1.00 (1.04 - 1.00)
R_{work} * (%)	18.20 (23.94)	21.43 (23.08)	12.24 (16.21)	20.83 (25.58)	17.31 (31.92)	14.65 (18.21)
R_{free} ** (%)	22.82 (30.82)	25.84 (26.76)	13.13 (16.98)	25.59 (36.61)	20.97 (34.82)	15.50 (19.19)
Number of non-H atoms	5967	2705	1848	1449	1608	1847
- macromolecules	5860	2685	1619	1342	1459	1618
- ligands	107	-	8	-	31	8
- water	-	20	221	107	118	221
Protein residues	712	326	181	162	178	181
RMSD bond lengths (Å)	0.014	0.014	0.026	0.019	0.012	0.028
RMSD bong angles (°)	1.79	1.46	2.22	1.80	1.28	2.45
Ramachandran favored/allowed * (%)**	96.7 / 99.7	99.7 / 100.0	100.0 / 100.0	99.4 / 100.0	100.0 / 100.0	100.0 / 100.0
Ramachandran outliers * (%)**	0.3	0.0	0.0	0.0	0.0	0.0
Clashscore ***	1.79	1.87	6.61	3.73	5.10	6.26
Wilson B-factor	34.97	33.80	8.36	16.72	34.72	7.95
Average B values ($Å^2$)	29.90	37.50	12.00	22.10	46.10	11.40
- macromolecules	29.20	37.60	10.80	21.50	45.50	10.10
- ligands	71.00	-	18.30	-	45.40	18.60
- solvent	-	28.00	20.90	28.70	54.00	20.50

Numbers in parentheses refer to the outer shell.

* $R_{work} = \sum_{hkl} || F_{obs}| - |F_{calc} || / \sum_{hkl} |F_{obs}|$

** R_{free} is the R value calculated for 5% of the data set that was not included in the refinement.

*** Molprobity

Table 3. Dissociation constants for the dimerization of NmFic *via* the interface 1 (K_{D1}) or interface 2 (K_{D2}).

		K_{D1} [µM]	K_{D2} [µM]	Effective K_D [µM] **
$NmFic_{E102R}$	Local fitting	7.4 ± 1.1	-	-
	Global fitting	7.6 ± 1.1	-	-
$NmFic_{E156R}$	Local fitting	-	59.9 ± 11.8	-
	Global fitting	-	61.3 ± 8.8	-
$NmFic_{wt}$		7.6 ± 1.1	61.3 ± 8.8	21.8 ± 1.0
$NmFic_{Y183F}$ *		7.2 ± N/A	56.2 ± 2.7	20.4 ± 1.0
$NmFic_{E186G}$ *		66.1 ± N/A	511.9 ± 25.9	190.0 ± 9.5
$NmFic_{Y183F,E186G}$ *		3.6 ± N/A	28.1 ± 1.9	10.3 ± 0.7

* Both dissociation constants were not fitted individually, but with a ratio of $K_{D2} = 7.74 * K_{D1}$, assuming both interfaces are affected similarly by the mutations that are not part of the interface.

** The effective K_D (K_{Def}) represents a value of the dissociation constant where $K_{D1} = K_{D2}$.

Table 4. Dissociation constants for the interaction of NmFic or auto-adenylylated NmFic with ATP for selected residues.

Residue	Native NmFic K_D [mM]	Auto-adenylylated NmFic K_D [mM]
K140	7.0 ± 0.7	5.7 ± 0.8
T141	9.0 ± 1.4	4.8 ± 1.3
I105	6.7 ± 0.3	3.0 ± 0.9
G69	9.0 ± 0.4	3.2 ± 0.4
G68	7.3 ± 0.7	3.2 ± 0.5
Median	**7.8 ± 1.1**	**4.0 ± 1.2**

α

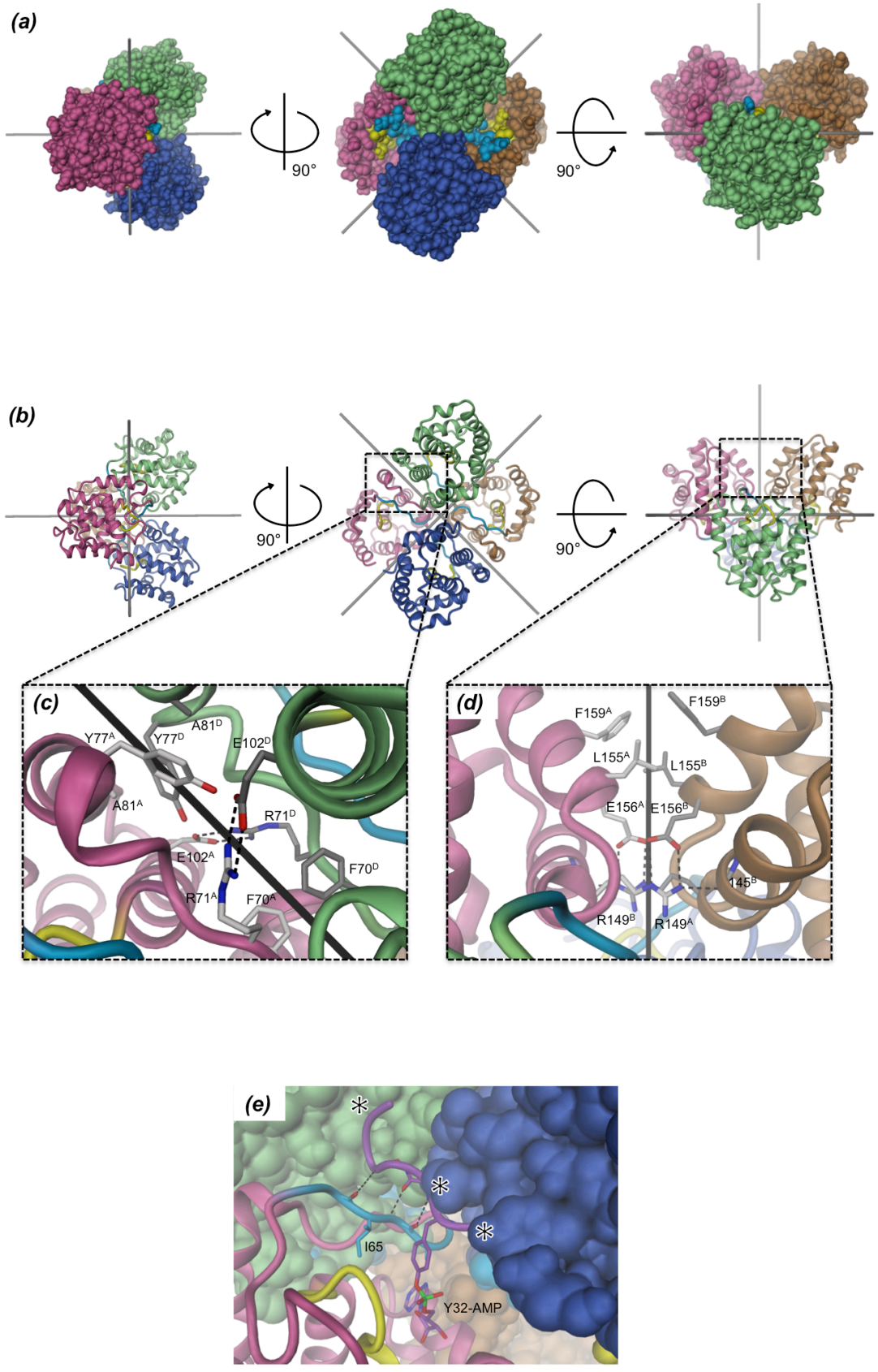
(a)
90°
90°
(b)
90°
90°
(c)
Y77A
Y77D
A81D
E102D
A81A
R71D
E102A
F70D
R71A
F70A
(d)
F159A
F159B
L155A
L155B
E156A
E156B
145B
R149B
R149A
(e)
I65
Y32-AMP

Figure 1. Tetrameric structure of the class III Fic protein NmFic. *(a)* Crystal structure of the NmFic 222 tetramer in $P6_5$ crystal form shown in surface representation. Local symmetry axes are indicated by black lines: monomer A in pink, B in brown, C in blue and D in green. The Fic active site motif is highlighted in yellow and the FLAP in light blue. Equivalent dimers within the tetramer are formed by AB, CD and AD, BC *(b)* Cartoon representation as in *(a)*. *(c)* Close-up view of the AD dimerization interface, with contact area of ~ 826 $Å^2$. *(d)* Close-up view of the AB dimerization interface, with contact area of ~ 421 $Å^2$. Hydrogen-bonds are depicted as dashed black lines. Indices of the labeled residues refer to the respective monomers. *(e)* Superimposition of the switch I region of Cdc42 (violet) on NmFic based on the IbpA/Cdc42 complex structure (PDB: 4ITR (10)). The main-chain of the target sterically clashes with the other subunits (shown as blue and green surfaces) of the NmFic tetramer (clashes indicated by black stars).

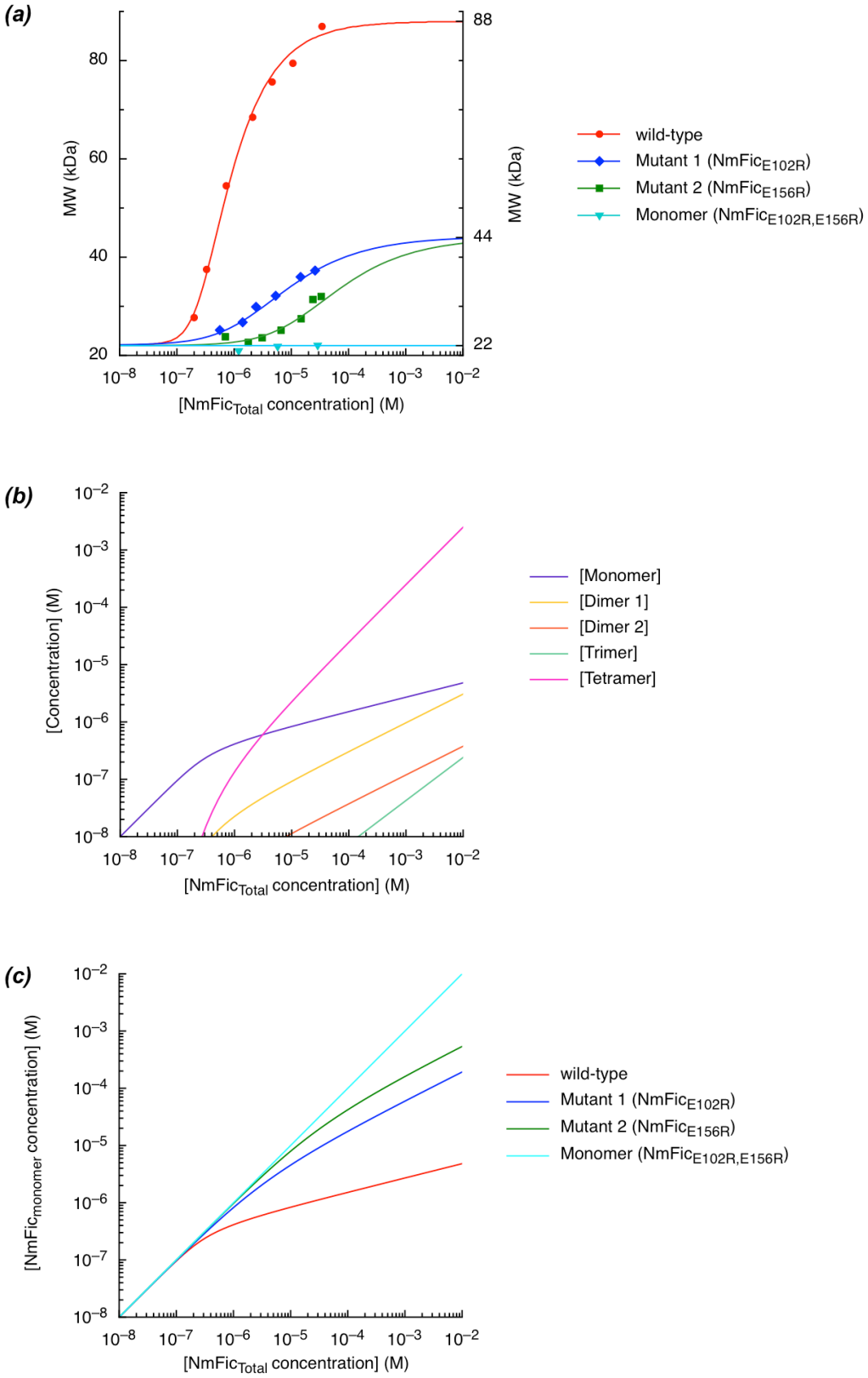
(a)
MW (kDa)
88
80
60
44
40
22
20
10−8 10−7 10−6 10−5 10−4 10−3 10−2
[NmFicTotal concentration] (M)
wild-type
Mutant 1 (NmFicE102R)
Mutant 2 (NmFicE156R)
Monomer (NmFicE102R,E156R)
(b)
[Concentration] (M)
10−2 10−3 10−4 10−5 10−6 10−7 10−8
10−8 10−7 10−6 10−5 10−4 10−3 10−2
[NmFicTotal concentration] (M)
[Monomer]
[Dimer 1]
[Dimer 2]
[Trimer]
[Tetramer]
(c)
[NmFicmonomer concentration] (M)
10−2 10−3 10−4 10−5 10−6 10−7 10−8
10−8 10−7 10−6 10−5 10−4 10−3 10−2
[NmFicTotal concentration] (M)
wild-type
Mutant 1 (NmFicE102R)
Mutant 2 (NmFicE156R)
Monomer (NmFicE102R,E156R)

Figure 2. Dynamic monomer–oligomer equilibrium of NmFic. *(a)* Concentration dependence of the effective molecular weight as determined by MALLS for different variants of NmFic. The points are experimental data points, the lines are the result of a non-linear fit of the monomer–oligomer model of Figure S3. The resulting dissociation constants are shown in Table 3. *(b)* Molecular concentrations of oligomeric species of $NmFic_{wt}$ as a function of the total protein concentration, as calculated from the dissociation constants K_{D1} and K_{D2}. *(c)* Concentration of monomeric protein as a function of total protein concentration for different variants of NmFic, as indicated.

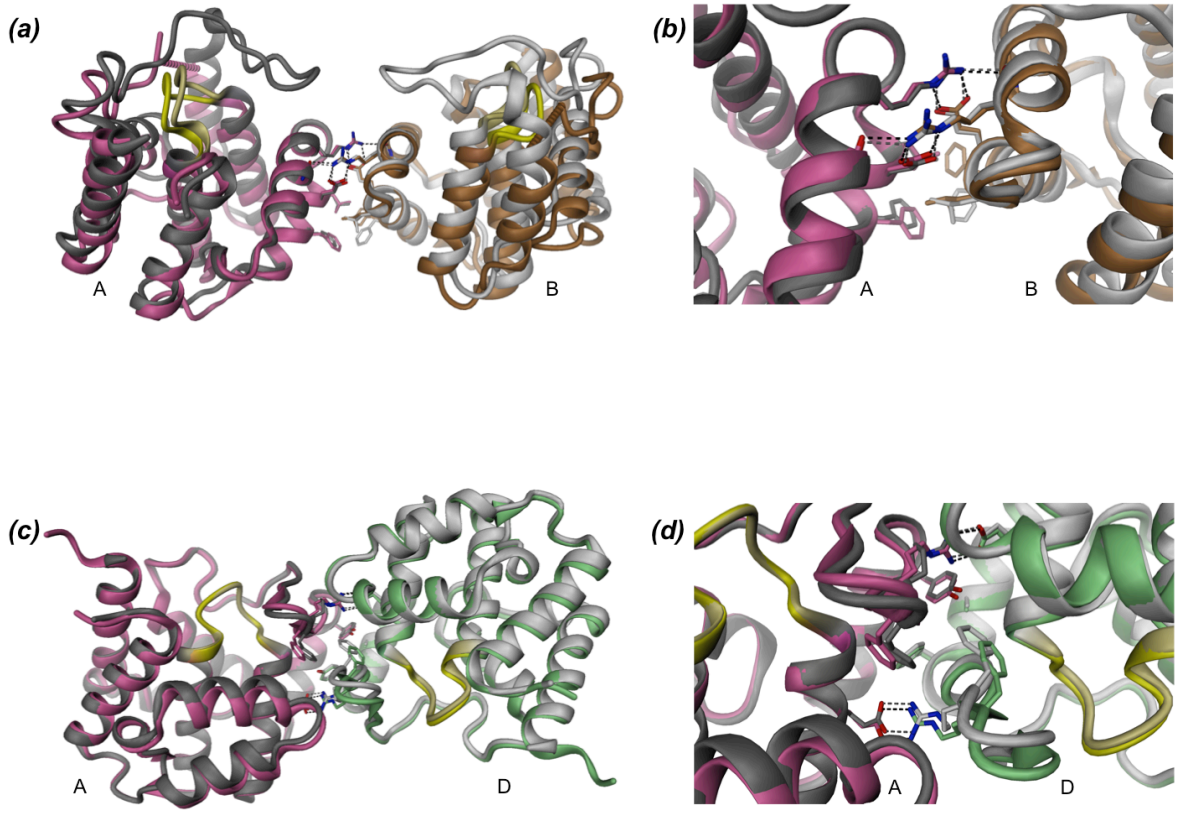

Figure 3. Crystal structures of NmFic$_{E102R}$ and NmFic$_{E156R}$. *(a)* Structure of NmFic$_{E102R}$ (pink/orange) superimposed with the AB dimer as part of the NmFic$_{wt}$ tetramer (dark/light gray). The active site is colored in yellow in both structures. The FLAP region is not observed in the crystal structure due its flexibility and absence of crystal contacts (top). Only the corresponding molecules are shown for clarity. *(b)* Close-up view of the conserved hydrophobic and hydrophilic interactions between the tetramer form and the NmFic$_{E102R}$ form. *(c)* Structure of NmFic$_{E156R}$ (pink/green) superimposed with the AD dimer as part of the NmFic$_{wt}$ tetramer (dark/light gray). *(d)* Details of the conserved interaction site.

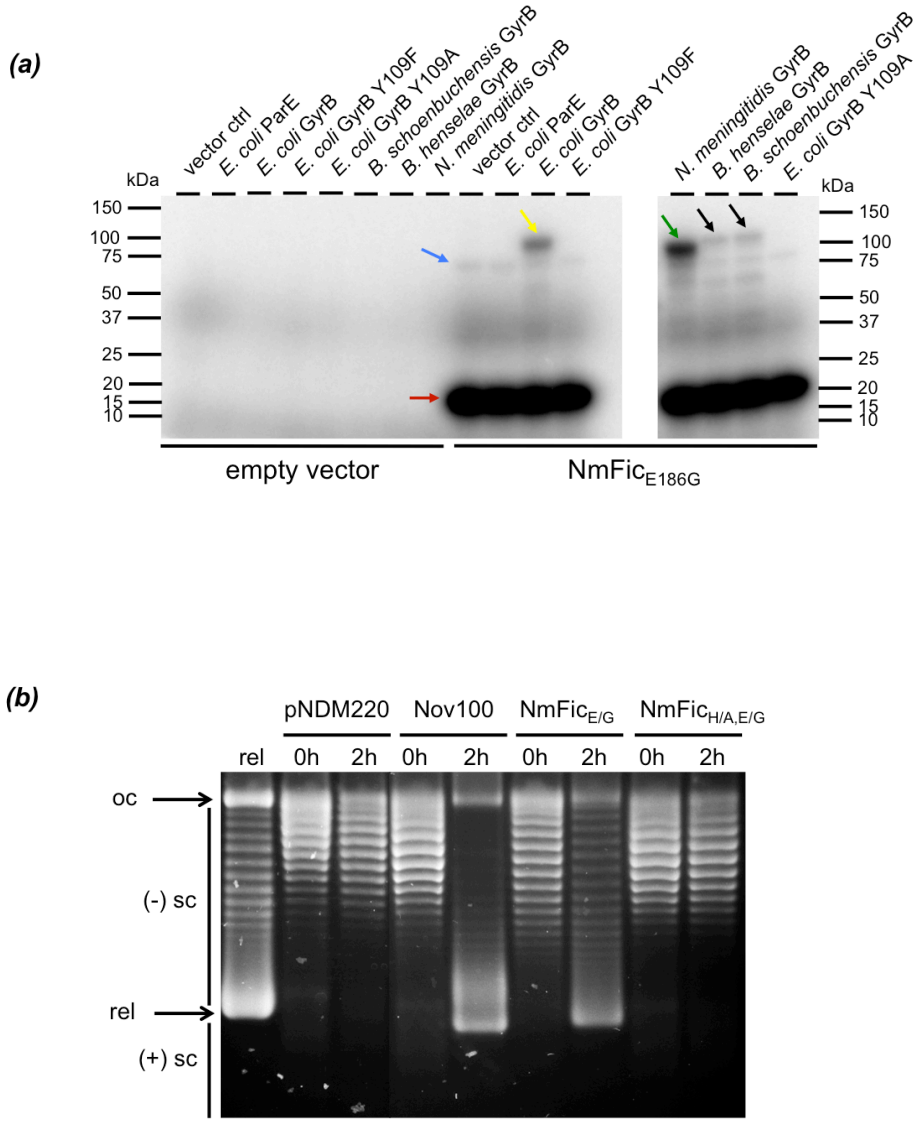

Figure 4. *In vitro* adenylylation of DNA gyrase by NmFic and *in vivo* inhibition of negative supercoiling. *(a)* Autoradiogram of *in vitro* adenylylation assay using α-^{32}P-ATP with crude cell lysates of *E. coli* ectopically expressing full-length and GST-tagged GyrB or ParE constructs from various organisms, incubated with pure inhibition-relieved NmFic$_{E186G}$. The red arrow indicates the auto-adenylylation of NmFic, the blue arrow the adenylylation of endogenously expressed GyrB, the yellow arrow the adenylylation of GST-tagged GyrB from *E. coli*, the green arrow the adenylylation of GST-GyrB from *N. meningitidis* and black arrows the adenylylation of GST-GyrB from *Bartonella* species. *(b)* Complete *in vivo* inhibition of the negative supercoiling ((-)sc) activity of DNA gyrase by the inhibition-relieved NmFic$_{E186G}$ protein at a similar level as the potent inhibitor novobiocin revealed by chloroquine agarose gel electrophoresis.

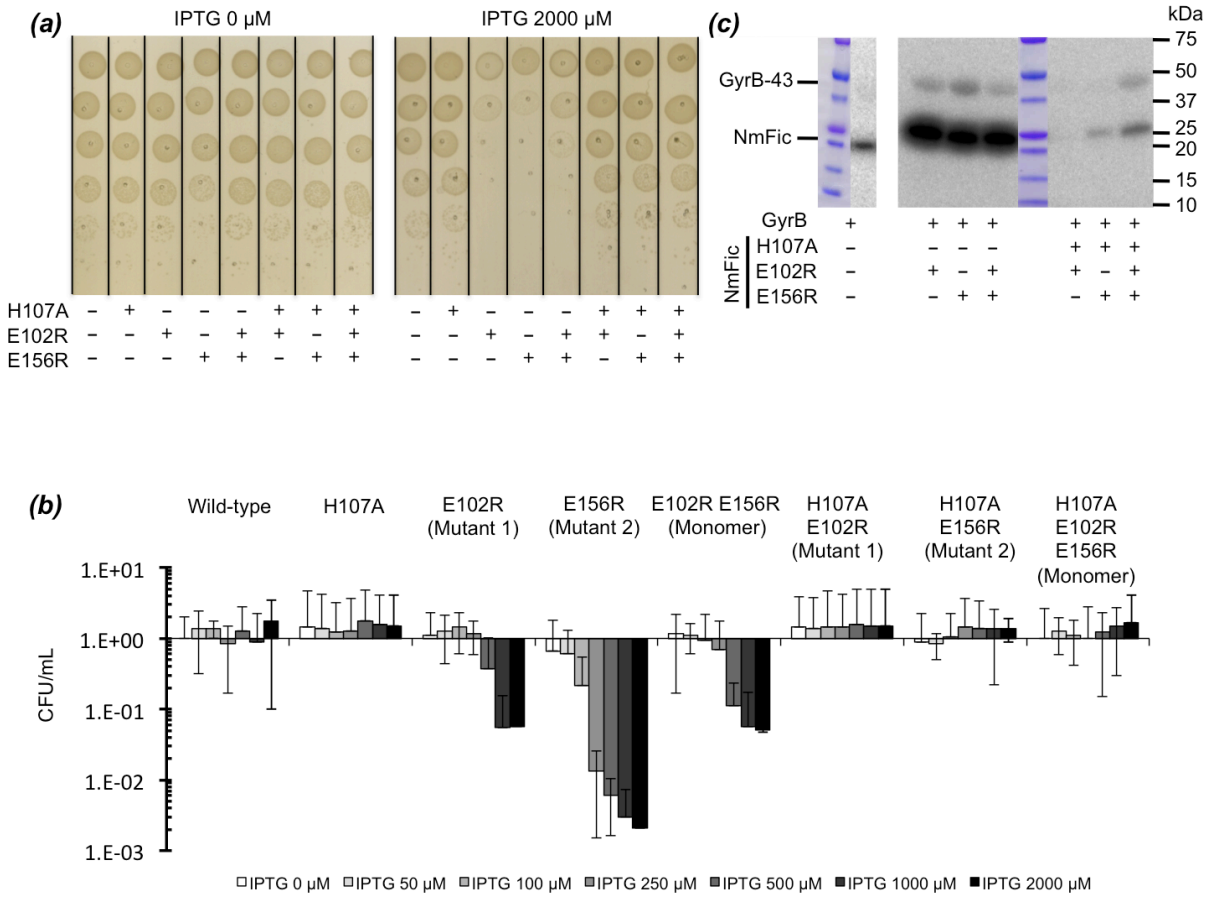

Figure 5. Growth defect of *E. coli* expressing NmFic variants. *(a)* Spotting experiment of *E. coli* MG1655 (λDE3) expressing NmFic derivatives on plates containing 0 or 2000 μM of the expression inducer IPTG. Note the remarkable growth defect, both in colony number and colony size, of the $NmFic_{E102R}$, $NmFic_{E156R}$ and $NmFic_{E102R,E156R}$ mutants. *(b)* Quantification of *E. coli* growth defect. The bars represent the average of three independent experiments and the error bars represent the standard deviation. *(c) In vitro* adenylylation assay with purified NmFic proteins and purified GyrB43 (N-terminal 43-kDa fragment comprising the ATPase and transducer domains).

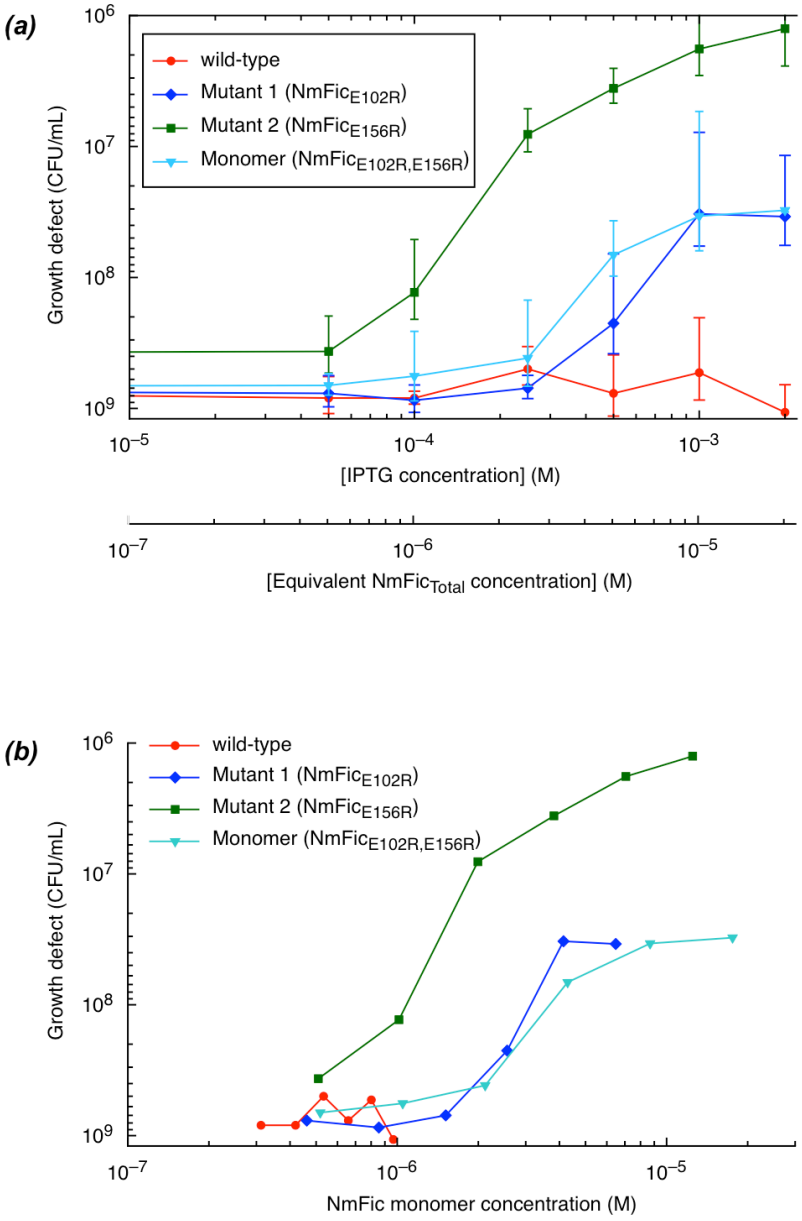

Figure 6. Bacterial growth defect correlates with the concentration of monomeric NmFic. *(a) E. coli* growth defect depending on IPTG concentration or equivalent of NmFic total concentration, assuming 100 μM IPTG correspond to 1 μM NmFic total protein (2nd horizontal axis). *(b) E. coli* growth defect depending on the monomer concentration of NmFic, assuming the same ratio as in *(a)*.

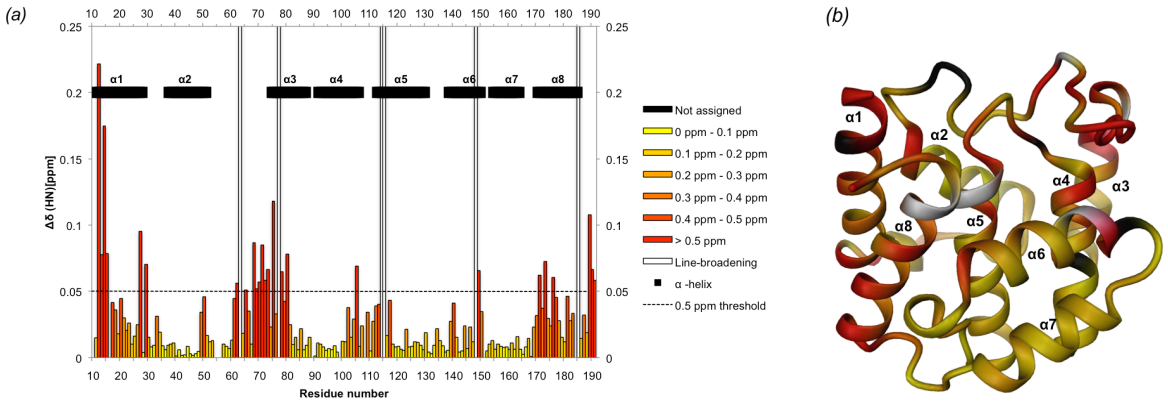

Figure 7. Structural perturbations of NmFic by auto-adenylylation. *(a)* Combined chemical shifts difference of the backbone amide moiety, Δδ(HN) between unmodified and auto-adenylylated $NmFic_{E102R,H107A,E156R}$ as function of the residue number. Unassigned residues are colored in black and residues exhibiting significant line-broadening in the adenylylated form are depicted in white. *(b)* Plot of the same chemical shift differences on the structure of monomeric NmFic using the same color code as in panel *(a)*. The largest chemical shift differences cluster in helices α1 and α8 (α_{inh}), and in the FLAP region.

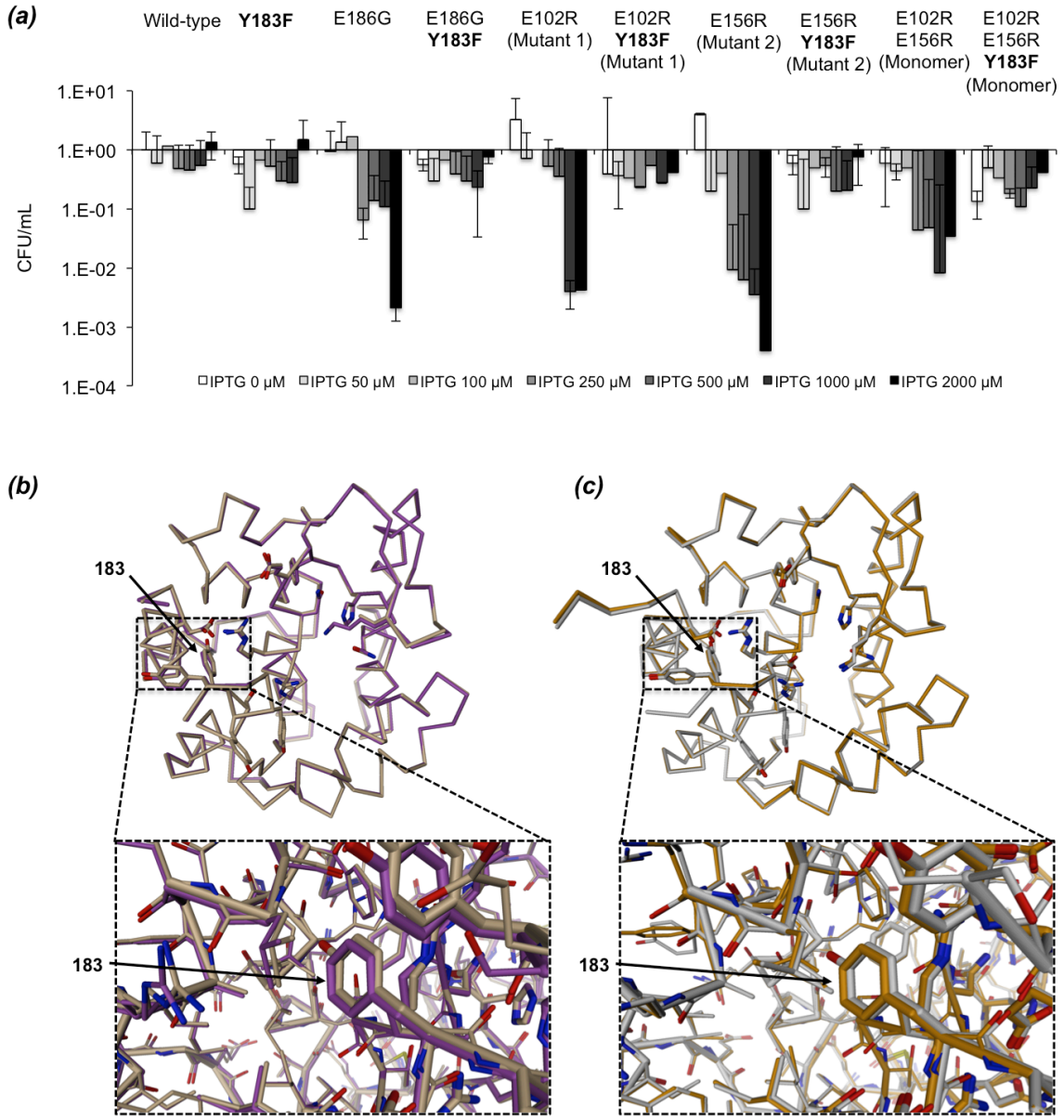

Figure 8. Mutation of Y183 abolishes the growth defect of NmFic without affecting the local protein structure. *(a)* Quantification of the *E. coli* growth defect. The bars represent the average of two independent experiments and the error bars the standard deviation. *(b)* Superimposition of $NmFic_{E186G}$ (beige) and $NmFic_{Y183F,E186G}$ (violet) with an RMSD of 0.306 Å for the Cα positions. *(c)* Superimposition of $NmFic_{E156R}$ (light gray) and $NmFic_{E156R,Y183F}$ (orange), with an RMSD of 0.228 Å for the Cα positions.

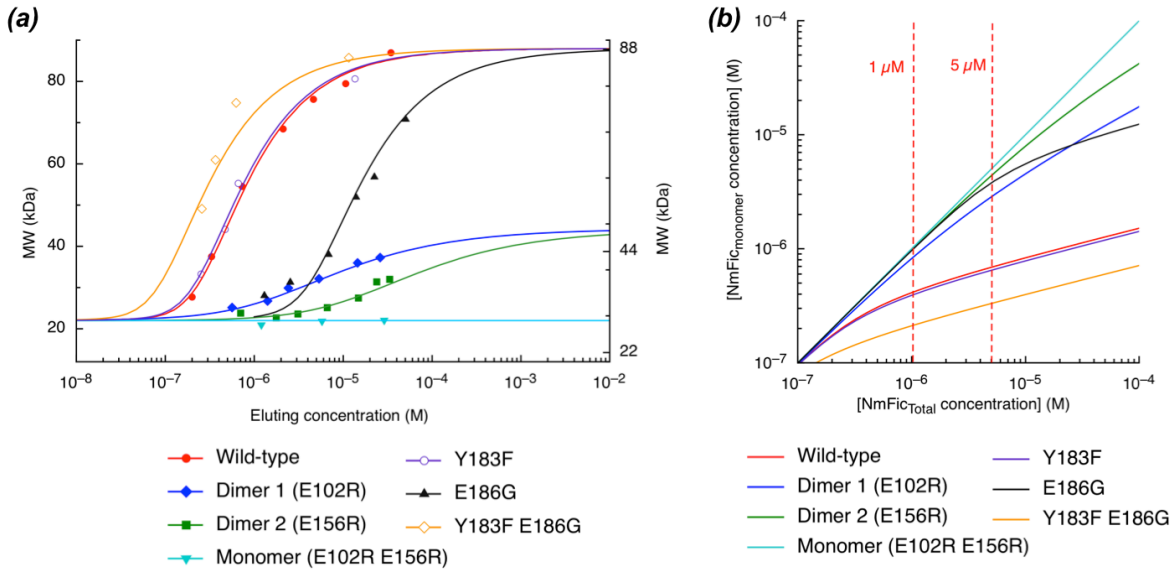

Figure 9. Dynamic monomer–oligomer equilibrium of NmFic mutants. *(a)* SEC-MALLS analysis of the oligomeric state of NmFic mutants of the auto-adenylylated tyrosine (Y183F, purple), of the inhibitory glutamate (E186G, black) or combination of both mutations (Y183F E186G, yellow). Respective dissociation constants are reported in Table 3. For comparison, wild-type, mutant 1, mutant 2, and monomer mutant are shown in the same colors as in Fig. 2. *(b)* Comparison of the monomer concentration ($NmFic_{monomer}$) versus total protein concentration ($NmFic_{Total}$) for the wild-type protein and mutants of the dimerization interface or of the auto-adenylylated tyrosine 183, using the same color code as in panel *(a)*.

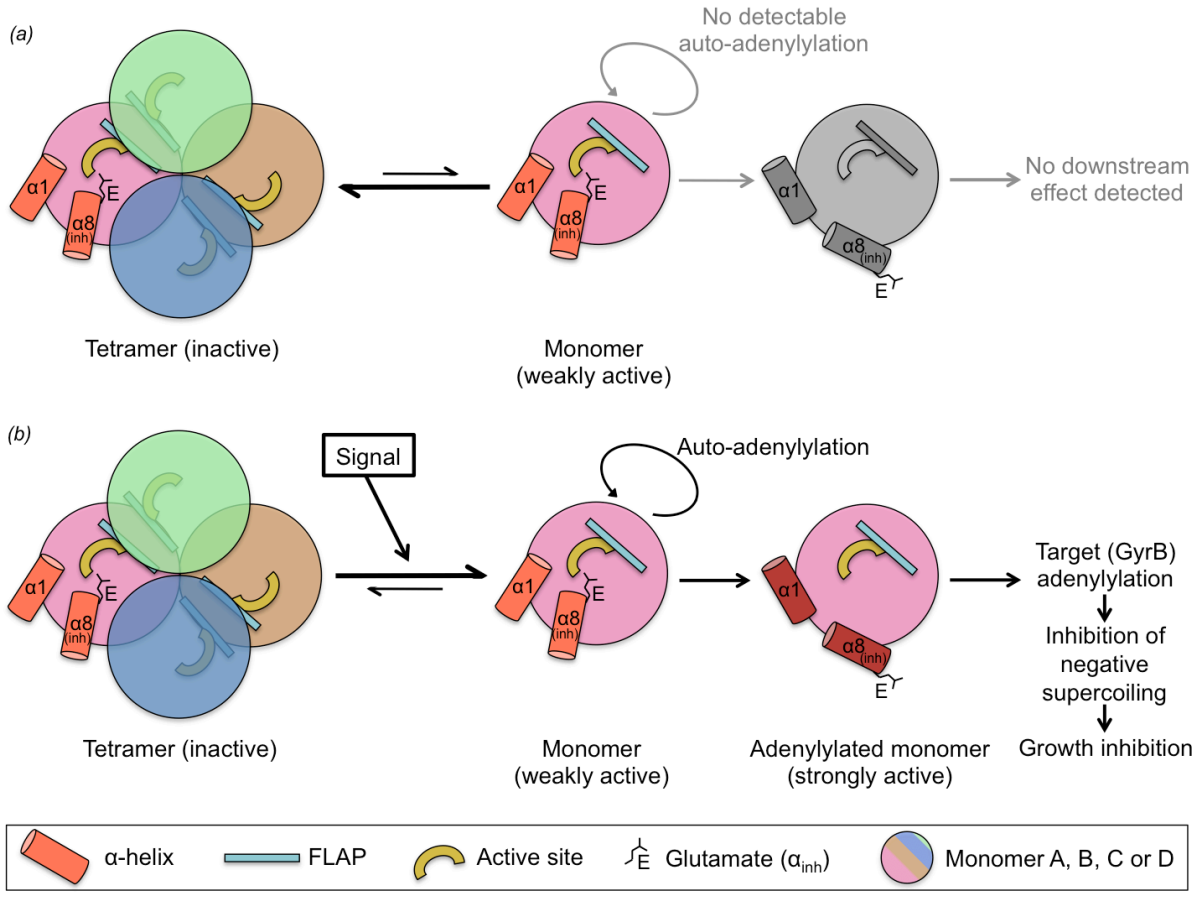

Figure 10. Regulation mechanism of class III Fic proteins. *(a)* In normal conditions, the monomer-tetramer equilibrium is in favor of the tetramer formation. *(b)* Upon a certain signal, the monomer-tetramer equilibrium is pushed towards the monomer. The monomer is then auto-adenylylated, which results in a conformational change of the helix α8 (α_{inh}) and the neighboring helix α1. The Fic protein is now active and able to adenylylate its target GyrB, leading to the inhibition of negative supercoiling and inhibition of bacterial growth.

Table S1. List of Plasmids.

Plasmid	Backbone	Description	Primer (fw)	Primer (rv)	Restriction sites	Source
pRSF-Duet1	pRSF-Duet1	Empty vector (RSF1030 *ori*, P*T7*)				Novagen
pFVS0015	pRSF-Duet1	$NmFic_{wt}$				Engel *et al.*
pFVS0051	pRSF-Duet1	$NmFic_{H107A}$	prFVS149	prFVS150		this study
pFVS0059	pRSF-Duet1	$NmFic_{E186G}$				Goepfert *et al.*
pFVS0083	pRSF-Duet1	$NmFic_{Y183F,E186G}$	prFVS096	prFVS092		this study
pFVS0109	pRSF-Duet1	*E. coli* GyrB 1-392 N_{ter} His_6-tag	prFVS107	prFVS114	NdeI/XhoI	this study
pFVS0117	pRSF-Duet1	$NmFic_{H107A,E186G}$	prFVS082	prFVS083		this study
pFVS0125	pRSF-Duet1	$NmFic_{E102R}$	prFVS119	prFVS120		this study
pFVS0126	pRSF-Duet1	$NmFic_{E156R}$	prFVS121	prFVS122		this study
pFVS0134	pRSF-Duet1	$NmFic_{E102R,E156R}$	prFVS119	prFVS120		this study
pFVS0135	pRSF-Duet1	$NmFic_{E156R,Y183F}$	prFVS091	prFVS092		this study
pFVS0137	pRSF-Duet1	$NmFic_{E102R,H107A}$	prFVS149	prFVS150		this study
pFVS0138	pRSF-Duet1	$NmFic_{H107A,E156R}$	prFVS149	prFVS150		this study
pFVS0143	pRSF-Duet1	$NmFic_{E102R,H107A,E156R}$	prFVS149	prFVS150		this study
pNMD220	pNDM220	Empty vector (mini-R1 ori, PLac)				Gotfredsen *et al.*
pAH154_NmFic_wt	pNDM220	$NmFic_{wt}$	prAH525	prAH526	BamHI/EcoRI	this study
pAH154_NmFic_E186G	pNDM220	$NmFic_{E186G}$	prAH537	prAH538		this study
pFVS0146	pNDM220	$NmFic_{Y183F}$	prFVS091	prFVS092		this study
pFVS0147	pNDM220	$NmFic_{Y183F,E186G}$	prFVS096	prFVS092		this study
pFVS0149	pNDM220	$NmFic_{E102R}$	prFVS119	prFVS120		this study
pFVS0150	pNDM220	$NmFic_{E156R}$	prFVS121	prFVS122		this study
pFVS0151	pNDM220	$NmFic_{H107A}$	prFVS149	prFVS150		this study
pFVS0173	pNDM220	$NmFic_{E102R,E156R}$	prFVS119	prFVS120		this study
pFVS0174	pNDM220	$NmFic_{E102R,Y183F}$	prFVS091	prFVS092		this study

Plasmid	Backbone	Description	Primer (fw)	Primer (rv)	Restriction sites	Source
pFVS0175	pNDM220	$NmFic_{E156R,Y183F}$	prFVS091	prFVS092		this study
pFVS0177	pNDM220	$NmFic_{E102R,H107A}$	prFVS149	prFVS150		this study
pFVS0178	pNDM220	$NmFic_{E102R,E156R,Y183F}$	prFVS091	prFVS092		this study
pFVS0179	pNDM220	$NmFic_{H107A,E156R}$	prFVS149	prFVS150		this study
pFVS0197	pNDM220	$NmFic_{E102R,H107A,E156R}$	prFVS149	prFVS150		this study

Table S2. List of DNA oligonucleotides and their respective sequences.

Primer	Sequence (5'-3')
prFVS082	GTATTATTACGGCGGGTATGAAAAAGGCTGAC
prFVS083	CATACCCGCCGTAATAATACGACTGCTCG
prFVS091	GAGCAGTCGTTTTATTACGAAGGGTATGAAAAAG
prFVS092	GTAATAAAACGACTGCTCGATACCTTTAAAG
prFVS096	GAGCAGTCGTTTTATTACGGCGGGTATGAAAAAG
prFVS107	GGGAATTCCATATGCATCACCATCACCATCACTCGAATTCTTATGACTCCTCCAG
prFVS114	CGACCTCGAGTTAGGTCATTTCACGCGCGCGACG
prFVS119	CAAATATGTTCGTATGAACATTGCCCATCC
prFVS120	CAATGTTCATACGAACATATTTGGCGATGATTTC
prFVS121	CAACGATTTACGUCTGCGCTTTTTGTTAAAG
prFVS122	CAAAAAGCGCAGACGTAAATCGTTGACGGGGCTG
prFVS149	GAACATTGCCGCCCCGTTTTTGGAGGGTAATGGCAG
prFVS150	CAAAAACGGGGCGGCAATGTTCATTTCAACATATTTG
prAH525	GAGCGGGGATCCATAGGAGGAACAATTTTATGAAATCCATAGACGAACAAAG
prAH526	CTCCCGCGAATTCTCAGCCTTTTTCATACCCTTC
prAH537	TTATTACGGCGGGTATGAAAAAGGCTGAGAA
prAH538	TTCATACCCGCCGTAATAATACGACTGCTCG

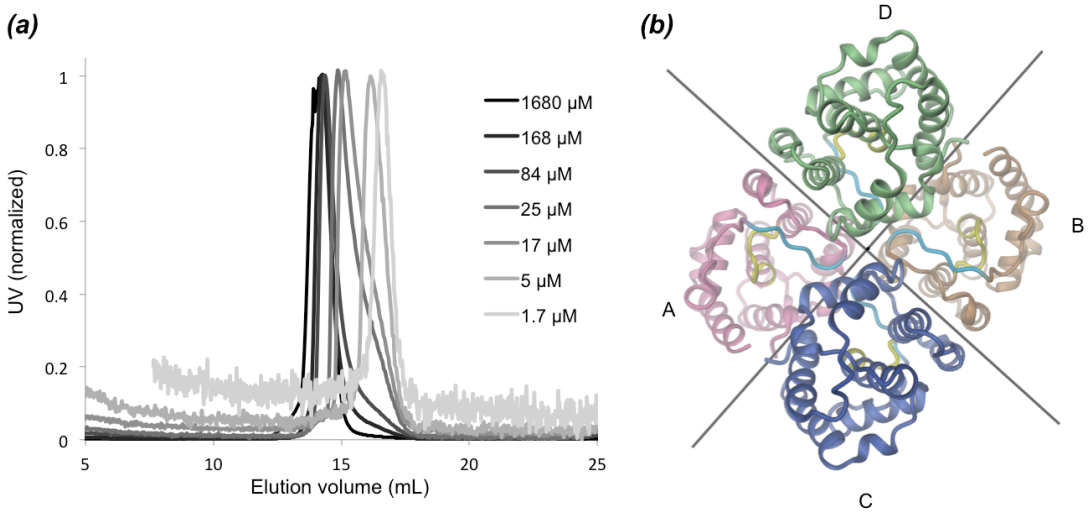

Figure S1. Dynamic equilibrium of NmFic$_{wt}$ from monomer to tetramer. *(a)* Dynamic equilibrium of NmFic$_{wt}$ on the time-scale of the Size Exclusion Chromatography (SEC) experiment. SEC analysis using an analytical S75 16/60 column (GE Healthcare) with a flowrate of 0.5 mL/min loaded with 50 μL of wild-type NmFic at various loading concentrations (gray-scale from dark-gray [1680 μM] to light-gray [1.7 μM]). *(b)* The NmFic 222 tetramer observed in the P6$_5$ crystal form shown as ribbon representation (same as Fig. 1).

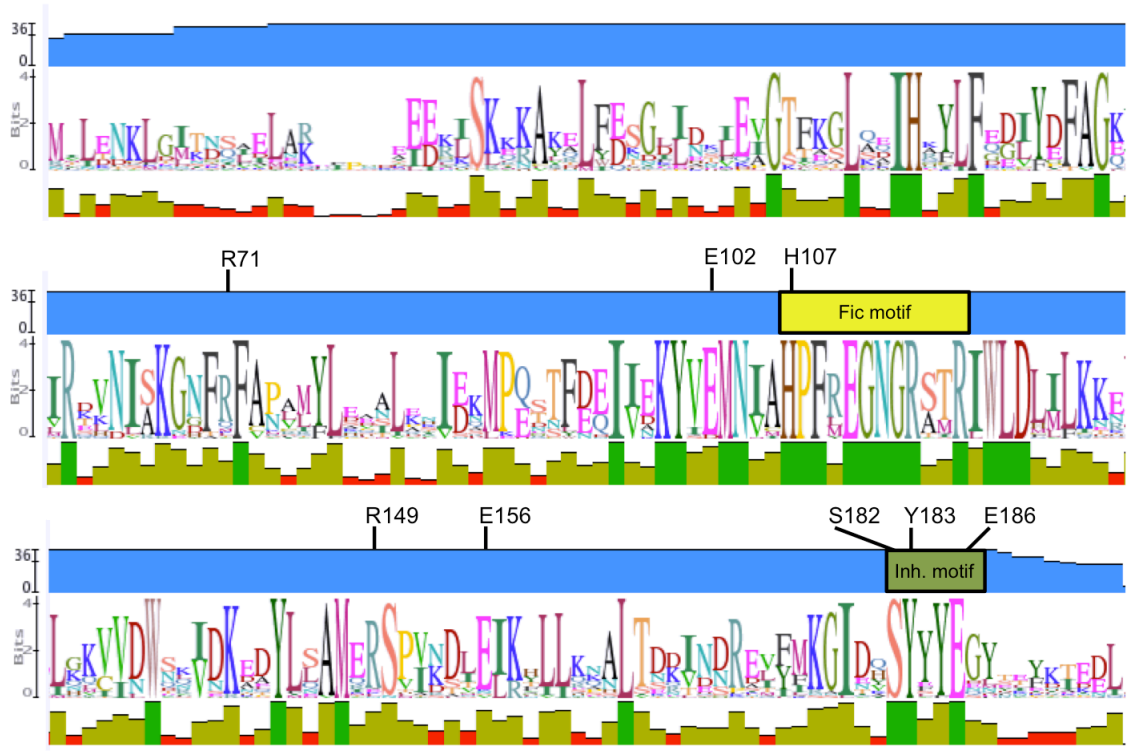

Figure S2. Amino acid conservation in class III Fic proteins. The alignment contains one representative sequence for each of 41 organisms. The alignment was calculated using MUSCLE (Multiple Sequence Comparison by Log-Expectation) (61) (http://www.geneious.com).

(a)

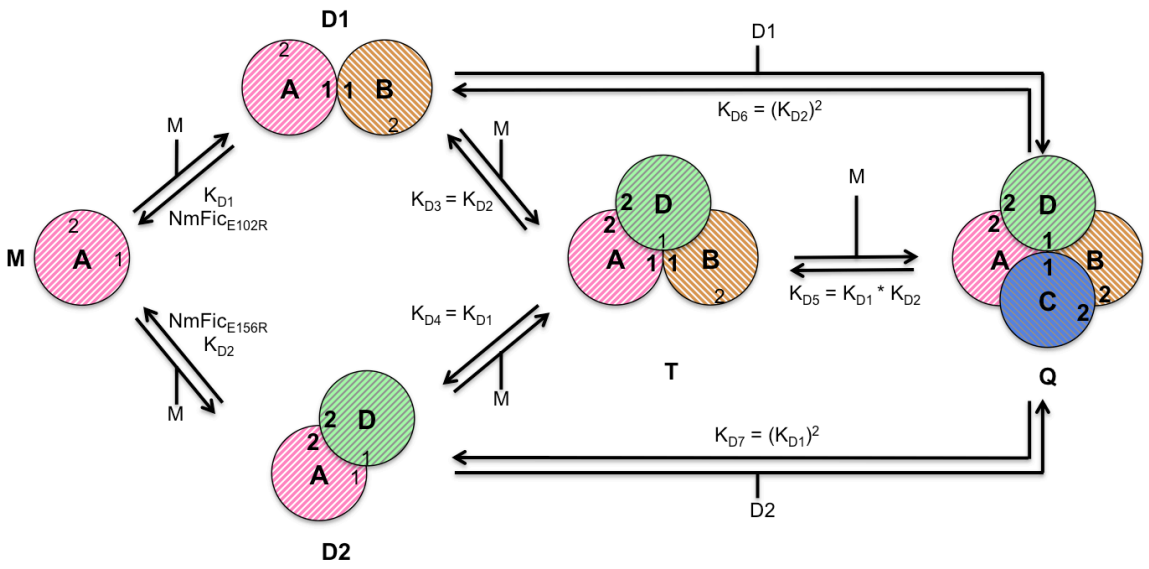

(b)

$$2 * M \leftrightarrows D1 \qquad K_{D1} = \frac{[D1]}{[M]^2} \qquad (3)$$

$$2 * M \leftrightarrows D2 \qquad K_{D2} = \frac{[D2]}{[M]^2} \qquad (4)$$

$$M + D1 \leftrightarrows T \qquad K_{D3} = K_{D2} \qquad (5)$$

$$M + D2 \leftrightarrows T \qquad K_{D4} = K_{D1} \qquad (6)$$

$$M + T \leftrightarrows Q \qquad K_{D5} = K_{D1} * K_{D2} \qquad (7)$$

$$2 * D1 \leftrightarrows Q \qquad K_{D6} = (K_{D2})^2 \qquad (8)$$

$$2 * D2 \leftrightarrows Q \qquad K_{D7} = (K_{D1})^2 \qquad (9)$$

Figure S3. Thermodynamic model of NmFic multimerization. *(a)* Schematic view of the equilibrium and *(b)* set of mass action law equations. (M = monomer, D1 = dimer 1, D2 = dimer 2, T = trimer, Q = tetramer).

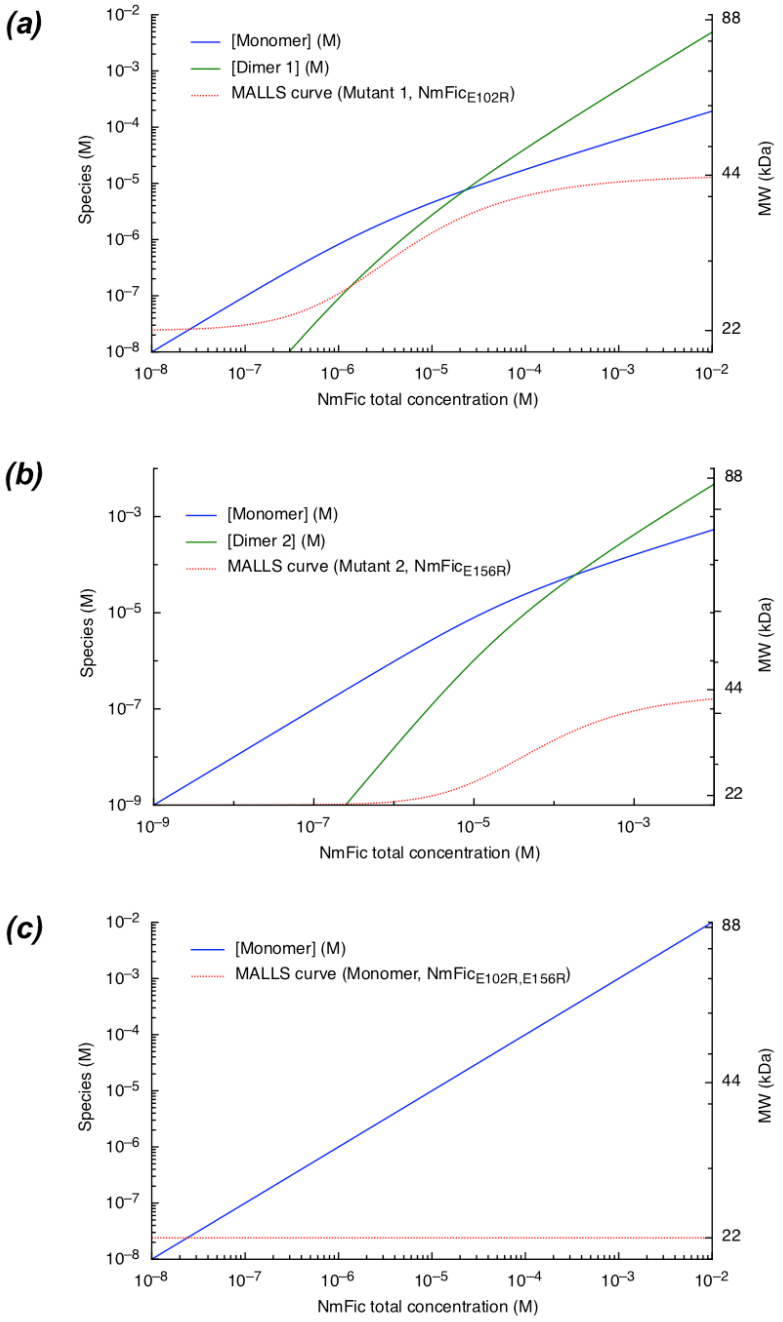

Figure S4. Dynamic equilibrium of NmFic tetramerization-deficient mutants. Species profile calculated with the equilibrium constants *(a)* K_{D1} for NmFic$_{E102R}$, *(b)* K_{D2} for NmFic$_{E156R}$ and *(c)* NmFic$_{E102R,E156R}$. The red curves represent the fitted experimental MALLS data.

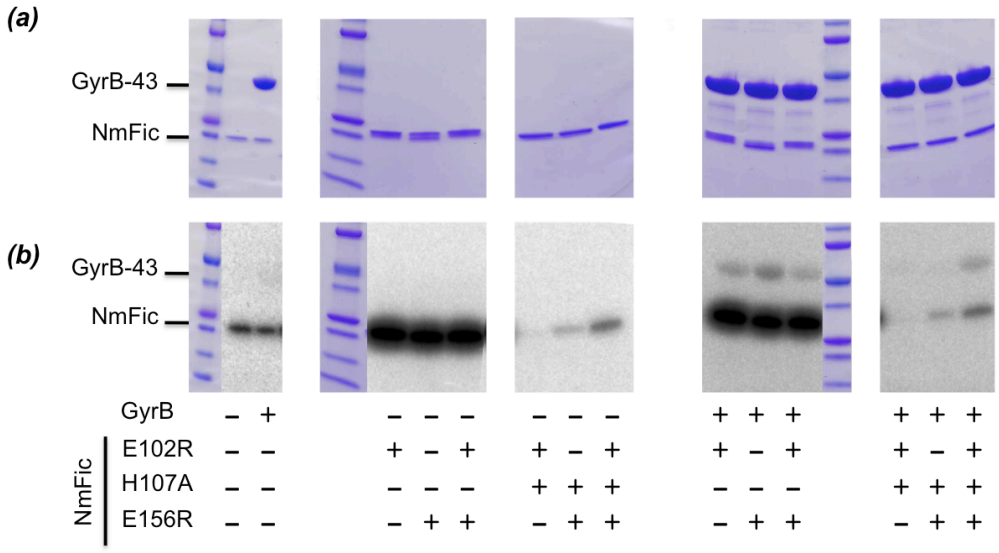

Figure S5. Adenylylation assay with pure NmFic proteins and pure GyrB43. *(a)* SDS-PAGE and *(b)* autoradiography of the SDS-PAGE gel after incubation of NmFic variants with [α-^{32}P]-ATP and pure GyrB proteins. The dimerization interface mutants catalyze the adenylylation of the target protein GyrB.

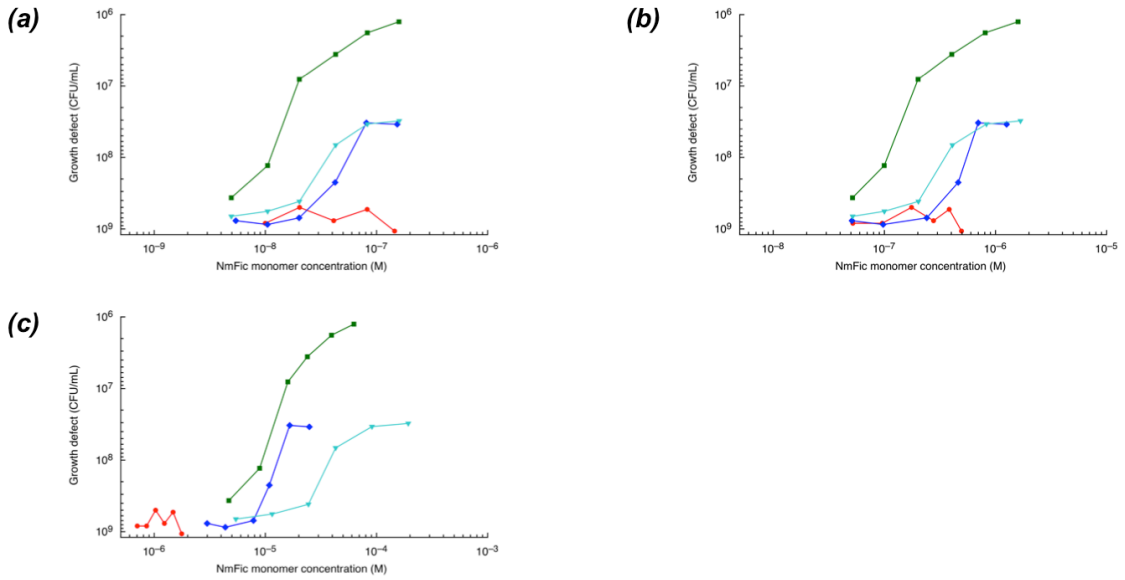

Figure S6. Calculated IPTG/[NmFic$_{monomer}$] ratios. Different equivalence and the resulting plots as in Figure 6 *(b)*, with *(a)* 100 μM IPTG = 0.01 μM NmFic, *(b)* 100 μM IPTG = 0.1 μM NmFic and *(c)* 100 μM IPTG = 10 μM NmFic.

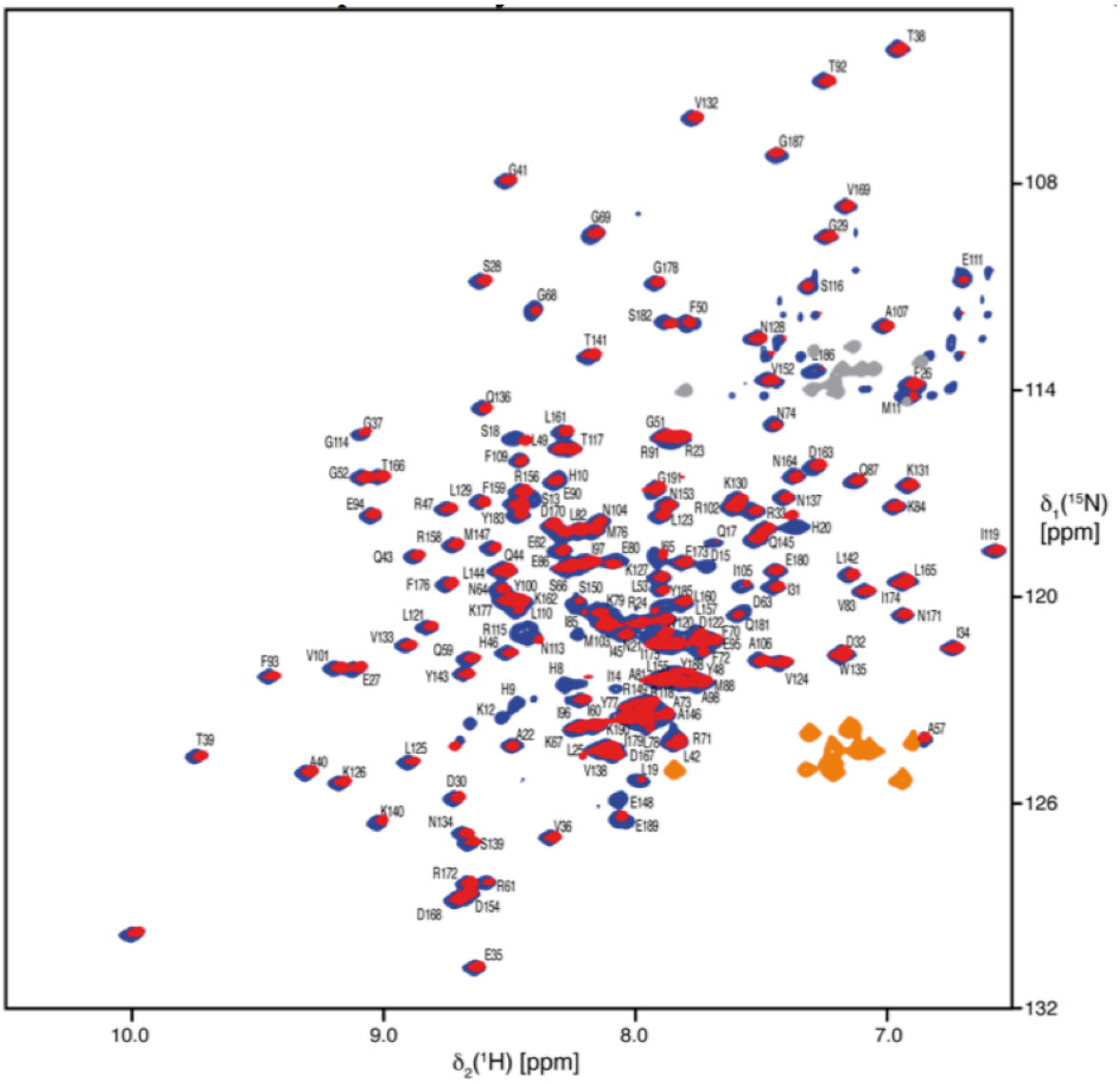

Figure S7. NMR fingerprint spectra of unmodified and auto-adenylylated NmFic. Overlay of 2D [^{15}N,^{1}H]-HSQC spectra of 0.5 mM [*U*-^{13}C,^{15}N]-labelled monomeric, inactive NmFic ($NmFic_{E102R,H107A,E156R}$) (blue) and of 0.25 mM [*U*-^{13}C,^{15}N]-labelled adenylylated monomeric inactive NmFic ($NmFic_{E102R,H107A,E156R}$) (red). Measurements were performed at 700 MHz in25 mM MES pH 6.5, 150 mM NaCl, at 25°C. The sequence specific resonance assignment is indicated.

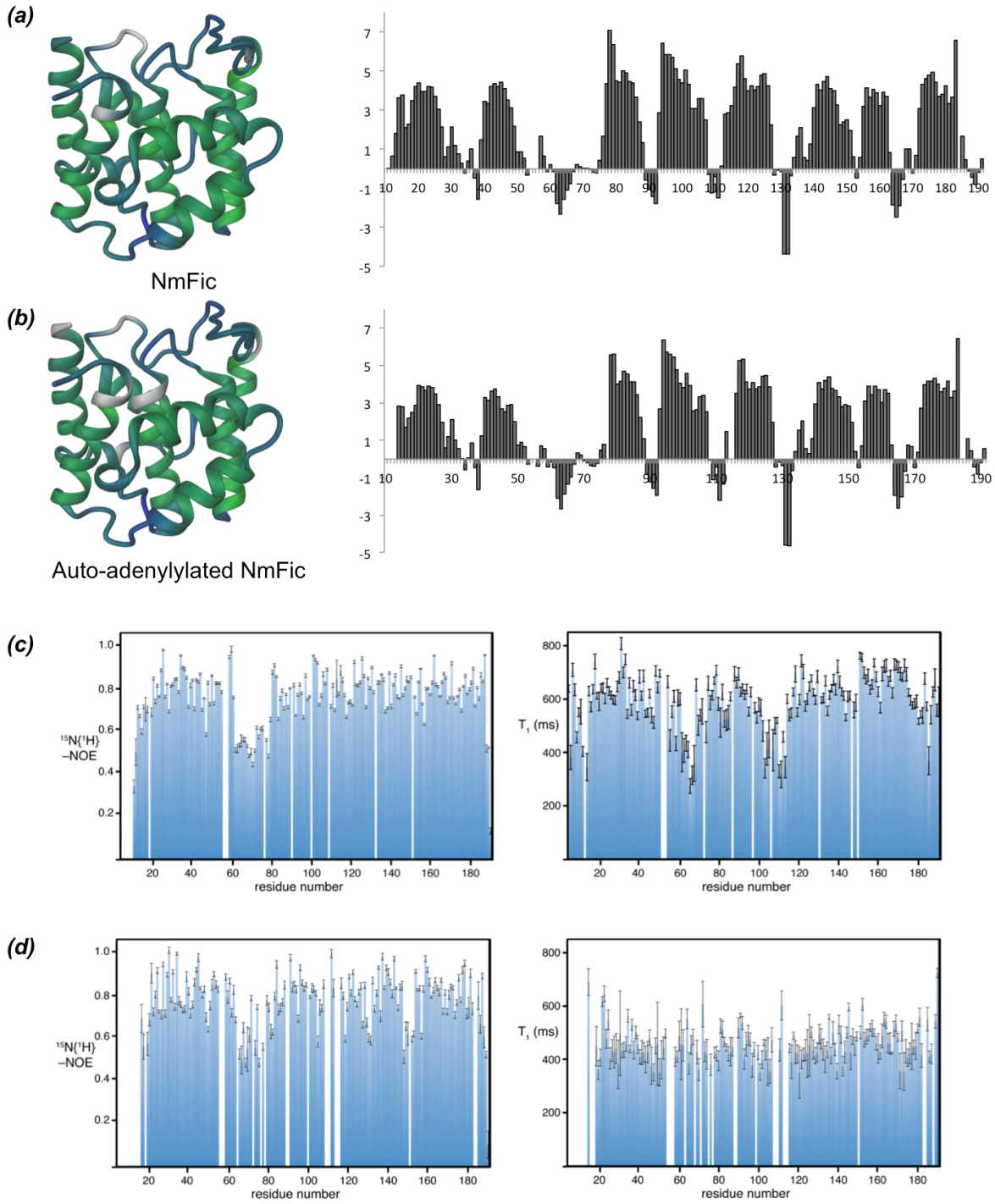

Figure S8. Secondary structure analysis of unmodified and adenylylated NmFic. Combined secondary chemical shifts for ^{13}Cα and 13Cβ of (a) unmodified and (b) adenylylated NmFic$_{E102R,H107A,E156R}$, plotted against the amino acid residue number. A 1–2–1 weighting function for residues (*i*-1) – *i* – (*i*+1) has been applied to the raw data. Consecutive stretches of positive and negative values indicate α-helix and β-sheet secondary structure elements, respectively. Heteronuclear NOE (left) and T_1 relaxation (right) experiment of (c) unmodified NmFic and *(d)* auto-adenylylated NmFic.

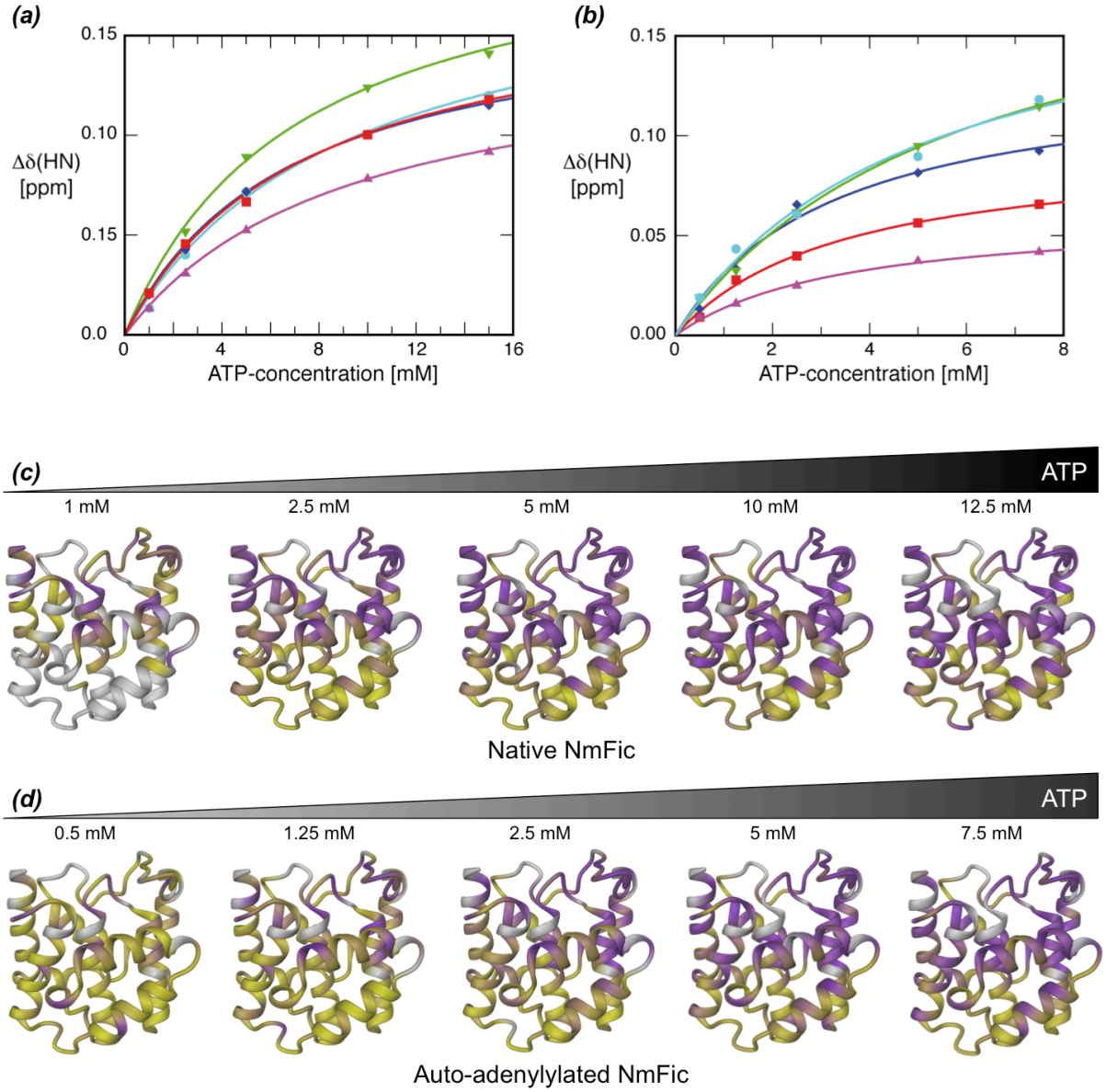

Figure S9. Effect of ATP binding on the NmFic monomer. Backbone amide chemical shift perturbations for selected residues upon titrating of *(a)* ATP to [*U*-^{13}C,^{15}N]–NmFic$_{E102R,H107A,E156R}$ (starting concentration 500 µM) and *(b)* ATP to adenylylated [*U*-^{13}C,^{15}N]–NmFic$_{E102R,H107A,E156R}$ (starting concentration 250 µM). The lines represent nonlinear least–squares best–fits of the normalized changes in the ^{1}H and ^{15}N chemical shifts using a bimolecular equilibrium binding model. The optimized value of the equilibrium dissociation constant is 7.8 ± 1.2 mM for *(a)* and 4.0 ± 1.1 mM for *(b)*. Chemical shift differences of the amide moiety of *(c)* native monomeric NmFic and *(d)* auto-adenylylated monomeric NmFic with Δδ(HN) as a function of the ATP concentration, relative to apo NmFic with a gradient from yellow (unchanged chemical shift) to purple (chemical shift change of 0.05 ppm and above). *(c)* Native monomeric NmFic and *(d)* auto-adenylylated monomeric NmFic.

References

1. Utsumi, R., Nakamoto, Y., Kawamukai, M., Himeno, M., and Komano, T. (1982) Involvement of cyclic AMP and its receptor protein in filamentation of an Escherichia coli fic mutant. J Bacteriol 151, 807–812
2. Yarbrough, M. L., Li, Y., Kinch, L. N., Grishin, N. V., Ball, H. L., and Orth, K. (2009) AMPylation of Rho GTPases by Vibrio VopS disrupts effector binding and downstream signaling. Science 323, 269–272
3. Engel, P., Goepfert, A., Stanger, F. V., Harms, A., Schmidt, A., Schirmer, T., and Dehio, C. (2012) Adenylylation control by intra- or intermolecular active-site obstruction in Fic proteins. Nature 482, 107–110
4. Garcia-Pino, A., Zenkin, N., and Loris, R. (2014) The many faces of Fic: structural and functional aspects of Fic enzymes. Trends in Biochemical Sciences 39, 121–129
5. Mukherjee, S., Liu, X., Arasaki, K., McDonough, J., Galán, J. E., and Roy, C. R. (2011) Modulation of Rab GTPase function by a protein phosphocholine transferase. Nature 477, 103–106
6. Campanacci, V., Mukherjee, S., Roy, C. R., and Cherfils, J. (2013) Structure of the Legionella effector AnkX reveals the mechanism of phosphocholine transfer by the FIC domain. EMBO J 32, 1469–1477
7. Castro-Roa, D., Gieter, S. D., Nuland, N. A. J. V., Loris, R., Garcia-Pino, A., and Zenkin, N. (2013) The Fic protein Doc uses an inverted substrate to phosphorylate and inactivate EF-Tu. Nat Chem Biol, 1–9
8. Cruz, J. W., Rothenbacher, F. P., Maehigashi, T., Lane, W. S., Dunham, C. M., and Woychik, N. A. (2014) Doc toxin is a kinase that inactivates elongation factor tu. J Biol Chem 289, 7788–7798
9. Luong, P., Kinch, L. N., Brautigam, C. A., Grishin, N. V., Tomchick, D. R., and Orth, K. (2010) Kinetic and structural insights into the mechanism of AMPylation by VopS FIC domain. Journal of Biological Chemistry 285, 20155
10. Xiao, J., Worby, C. A., Mattoo, S., Sankaran, B., and Dixon, J. E. (2010) Structural basis of Fic-mediated adenylylation. Nat Struct Mol Biol 17, 1004–1010
11. Palanivelu, D. V., Goepfert, A., Meury, M., Guye, P., Dehio, C., and Schirmer, T. (2011) Fic domain-catalyzed adenylylation: insight provided by the structural analysis of the type IV secretion system effector BepA. Protein science : a publication of the Protein Society 20, 492–499
12. Goepfert, A., Stanger, F. V., Dehio, C., and Schirmer, T. (2013) Conserved inhibitory mechanism and competent ATP binding mode for adenylyltransferases with fic fold. PLoS ONE 8, e64901
13. Kinch, L. N., Yarbrough, M. L., Orth, K., and Grishin, N. V. (2009) Fido, a novel AMPylation domain common to fic, doc, and AvrB. PLoS ONE 4, e5818

14. Gotfredsen, M., and Gerdes, K. (1998) The Escherichia coli relBE genes belong to a new toxin-antitoxin gene family. Mol Microbiol 29, 1065–1076

15. Zheng, L., Baumann, U., and Reymond, J.-L. (2004) An efficient one-step site-directed and site-saturation mutagenesis protocol. Nucleic Acids Res 32, e115

16. Brino, L., Urzhumtsev, A., Mousli, M., Bronner, C., Mitschler, A., Oudet, P., and Moras, D. (2000) Dimerization of Escherichia coli DNA-gyrase B provides a structural mechanism for activating the ATPase catalytic center. J Biol Chem 275, 9468–9475

17. Sambrook, J., Fritsch, E. F., and Maniatis, T. (1989) Molecular Cloning: A Laboratory Manual, 2nd Ed, Cold Spring Harbor Laboratory

18. Sundriyal, A., Massa, C., Samoray, D., Zehender, F., Sharpe, T., Jenal, U., and Schirmer, T. (2014) Inherent regulation of EAL domain-catalyzed hydrolysis of second messenger cyclic di-GMP. J Biol Chem 289, 6978–6990

19. Levenberg, K. (1944) A method for the solution of certain non-linear problems in least squares. Quarterly Journal of Applied Mathmatics II, 164–168

20. Marquardt, D. W. (1963) An Algorithm for Least-Squares Estimation of Nonlinear Parameters. Journal of the Society for Industrial and Applied Mathematics 11, 431–441

21. van der Walt, S., Colbert, S. C., and Varoquaux, G. (2011) The NumPy Array: A Structure for Efficient Numerical Computation. Computing in Science & Engineering 13, 22–30

22. Paz-García, J. M., Johannesson, B., Ottosen, L. M., Ribeiro, A. B., and Rodríguez-Maroto, J. M. (2013) Computing multi-species chemical equilibrium with an algorithm based on the reaction extents. Computers & Chemical Engineering 58, 135–143

23. Kraft, D. (1994) Algorithm 733: TOMP–Fortran modules for optimal control calculations. ACM Transactions on Mathematical Software (TOMS) 20, 262–281

24. Chung, C. T., Niemela, S. L., and Miller, R. H. (1989) One-step preparation of competent Escherichia coli: transformation and storage of bacterial cells in the same solution. Proc Natl Acad Sci USA 86, 2172–2175

25. Pervushin, K., Riek, R., Wider, G., and Wüthrich, K. (1997) Attenuated T2 relaxation by mutual cancellation of dipole-dipole coupling and chemical shift anisotropy indicates an avenue to NMR structures of very large biological macromolecules in solution. Proc Natl Acad Sci USA 94, 12366–12371

26. Grzesiek, S., and Bax, A. (1992) Improved 3D Triple-Resonance NMR Techniques Applied to a 31-kDa Protein. Journal of Magnetic Resonance 96, 432–440

27. Kay, L. E., Ikura, M., Tschudin, R., and Bax, A. (2011) Three-dimensional triple-resonance NMR Spectroscopy of isotopically enriched proteins. 1990. J. Magn. Reson. 213, 423–441

28. Bax, A., and Ikura, M. (1991) An efficient 3D NMR technique for correlating the proton and 15N backbone amide resonances with the alpha-carbon of the preceding

residue in uniformly 15N/13C enriched proteins. J. Biomol. NMR 1, 99–104

29. Grzesiek, S., Anglister, J., Ren, H., and Bax, A. (1993) 13C line narrowing by 2H decoupling in 2H/13C/15N enriched proteins. Application to triple resonance 4D J connectivity of sequential amides. J Am Chem Soc 115, 4369–4370

30. Clubb, R. T., Thanabal, V., and Wagner, G. (1992) A constant-time three-dimensional triple-resonance pulse scheme to correlate intraresidue 1HN, 15N, and 13C' chemical shifts in 15N-13C-labelled proteins. Journal of Magnetic Resonance 97, 213–217

31. Zhu, G., Xia, Y., Nicholson, L. K., and Sze, K. H. (2000) Protein Dynamics Measurements by TROSY-Based NMR Experiments. Journal of Magnetic Resonance 143, 423–426

32. Zhu, L., Sharp, J. D., Kobayashi, H., Woychik, N. A., and Inouye, M. (2010) Noncognate Mycobacterium tuberculosis toxin-antitoxins can physically and functionally interact. J Biol Chem 285, 39732–39738

33. Lee, D., Hilty, C., Wider, G., and Wüthrich, K. (2006) Effective rotational correlation times of proteins from NMR relaxation interference. Journal of Magnetic Resonance 178, 72–76

34. Güntert, P., Dötsch, V., Wider, G., and Wüthrich, K. (1992) Processing of multi-dimensional NMR data with the new software PROSA. J. Biomol. NMR 2, 619–629

35. Bartels, C., Xia, T.-H., Billeter, M., Güntert, P., and Wüthrich, K. (1995) The program XEASY for computer-supported NMR spectral analysis of biological macromolecules. J. Biomol. NMR 6, 1–10

36. Kjaergaard, M., and Poulsen, F. M. (2011) Sequence correction of random coil chemical shifts: correlation between neighbor correction factors and changes in the Ramachandran distribution. J. Biomol. NMR 50, 157–165

37. Battye, T. G. G., Kontogiannis, L., Johnson, O., Powell, H. R., and Leslie, A. G. W. (2011) iMOSFLM: a new graphical interface for diffraction-image processing with MOSFLM. Acta Crystallogr D Biol Crystallogr 67, 271–281

38. Kabsch, W. (2010) XDS. Acta Crystallogr D Biol Crystallogr 66, 125–132

39. Evans, P. R., and Murshudov, G. N. (2013) How good are my data and what is the resolution? Acta Crystallogr D Biol Crystallogr 69, 1204–1214

40. McCoy, A. J., Grosse-Kunstleve, R. W., Adams, P. D., Winn, M. D., Storoni, L. C., and Read, R. J. (2007) Phaser crystallographic software. J Appl Crystallogr 40, 658–674

41. Emsley, P., Lohkamp, B., Scott, W. G., and Cowtan, K. (2010) Features and development of Coot. Acta Crystallogr D Biol Crystallogr 66, 486–501

42. Murshudov, G. N., Skubák, P., Lebedev, A. A., Pannu, N. S., Steiner, R. A., Nicholls, R. A., Winn, M. D., Long, F., and Vagin, A. A. (2011) REFMAC5 for the refinement of macromolecular crystal structures. Acta Crystallogr D Biol Crystallogr 67, 355–367

43. Adams, P. D., Afonine, P. V., Bunkóczi, G., Chen, V. B., Davis, I. W., Echols, N., Headd, J. J., Hung, L.-W., Kapral, G. J., Grosse-Kunstleve, R. W., McCoy, A. J., Moriarty, N. W., Oeffner, R., Read, R. J., Richardson, D. C., Richardson, J. S., Terwilliger, T. C., and Zwart, P. H. (2010) PHENIX: a comprehensive Python-based system for macromolecular structure solution. Acta Crystallogr D Biol Crystallogr 66, 213–221

44. Chen, V. B., Arendall, W. B., Headd, J. J., Keedy, D. A., Immormino, R. M., Kapral, G. J., Murray, L. W., Richardson, J. S., and Richardson, D. C. (2010) MolProbity: all-atom structure validation for macromolecular crystallography. Acta Crystallogr D Biol Crystallogr 66, 12–21

45. Urzhumtseva, L., Afonine, P. V., Adams, P. D., and Urzhumtsev, A. (2009) Crystallographic model quality at a glance. Acta Crystallogr D Biol Crystallogr 65, 297–300

46. Dutta, R., and Inouye, M. (2000) GHKL, an emergent ATPase/kinase superfamily. Trends in Biochemical Sciences 25, 24–28

47. Wigley, D. B., Davies, G. J., Dodson, E. J., Maxwell, A., and Dodson, G. (1991) Crystal structure of an N-terminal fragment of the DNA gyrase B protein. Nature 351, 624–629

48. Gross, C. H., Parsons, J. D., Grossman, T. H., Charifson, P. S., Bellon, S., Jernee, J., Dwyer, M., Chambers, S. P., Markland, W., Botfield, M., and Raybuck, S. A. (2003) Active-site residues of Escherichia coli DNA gyrase required in coupling ATP hydrolysis to DNA supercoiling and amino acid substitutions leading to novobiocin resistance. Antimicrob Agents Chemother 47, 1037–1046

49. Bates, A. D., Berger, J. M., and Maxwell, A. (2011) The ancestral role of ATP hydrolysis in type II topoisomerases: prevention of DNA double-strand breaks. Nucleic Acids Res 39, 6327–6339

50. Kleywegt, G. J. (1996) Use of non-crystallographic symmetry in protein structure refinement. Acta Crystallogr D Biol Crystallogr 52, 842–857

51. Li, G.-Y., Zhang, Y., Inouye, M., and Ikura, M. (2008) Structural mechanism of transcriptional autorepression of the Escherichia coli RelB/RelE antitoxin/toxin module. J Mol Biol 380, 107–119

52. Christensen, S. K., and Gerdes, K. (2003) RelE toxins from bacteria and Archaea cleave mRNAs on translating ribosomes, which are rescued by tmRNA. Mol Microbiol 48, 1389–1400

53. Oh, E., Becker, A. H., Sandikci, A., Huber, D., Chaba, R., Gloge, F., Nichols, R. J., Typas, A., Gross, C. A., Kramer, G., Weissman, J. S., and Bukau, B. (2011) Selective ribosome profiling reveals the cotranslational chaperone action of trigger factor in vivo. Cell 147, 1295–1308

54. Kaiser, C. M., Chang, H.-C., Agashe, V. R., Lakshmipathy, S. K., Etchells, S. A.,

Hayer-Hartl, M., Hartl, F. U., and Barral, J. M. (2006) Real-time observation of trigger factor function on translating ribosomes. Nature 444, 455–460

55. Patzelt, H., Kramer, G., Rauch, T., Schönfeld, H.-J., Bukau, B., and Deuerling, E. (2002) Three-state equilibrium of Escherichia coli trigger factor. Biol. Chem. 383, 1611–1619

56. Rizzini, L., Favory, J.-J., Cloix, C., Faggionato, D., O'Hara, A., Kaiserli, E., Baumeister, R., Schäfer, E., Nagy, F., Jenkins, G. I., and Ulm, R. (2011) Perception of UV-B by the Arabidopsis UVR8 protein. Science 332, 103–106

57. Heijde, M., and Ulm, R. (2012) UV-B photoreceptor-mediated signalling in plants. Trends in Plant Science 17, 230–237

58. Pieles, K., Glatter, T., Harms, A., Schmidt, A., and Dehio, C. (2014) An experimental strategy for the identification of AMPylation targets from complex protein samples. Proteomics 14, 1048–1052

59. Feng, F., Yang, F., Rong, W., Wu, X., Zhang, J., Chen, S., He, C., and Zhou, J.-M. (2012) A Xanthomonas uridine 5′-monophosphate transferase inhibits plant immune kinases. Nature 485, 114–118

60. Goody, P. R., Heller, K., Oesterlin, L. K., Müller, M. P., Itzen, A., and Goody, R. S. (2012) Reversible phosphocholination of Rab proteins by Legionella pneumophila effector proteins. EMBO J 31, 1774–1784

61. Edgar, R. C. (2004) MUSCLE: multiple sequence alignment with high accuracy and high throughput. Nucleic Acids Res 32, 1792–1797

3.6. Towards an understanding of the structure-function of Fic-mediated inhibition of bacterial topoisomerases

In *research article III*, we identified the bacterial topoisomerases GyrB and ParE as targets of VbhT from *Bartonella schoenbuchensis*. GyrB is part of the DNA gyrase complex ($GyrA_2GyrB_2$) that catalyzes the introduction of negative supercoils into covalently closed double-stranded DNA molecules. ParE, together with ParC, forms the molecular nanomachine topoIV specialized in the decatenation of DNA molecules, separating daughter chromosomes during replication. In *research article V*, we could show that NmFic specifically targets GyrB but not ParE.

On the molecular level, GyrB and ParE are adenylylated on a conserved tyrosine, Y109 of *E. coli* GyrB or Y105 of *E. coli* ParE, that is part of the ATP lid-loop. In this chapter, I aim to reveal the molecular details of GyrB or ParE adenylylation.

3.6.1. Enzymatic reactions

$$\text{GyrB} + \text{ATP} \leftrightarrow \text{GyrB}\bullet\text{ATP} \rightarrow \text{GyrB} + \text{ADP} + \text{Pi} \quad (1)$$

$$\text{Fic} + \text{ATP} + \text{GyrB} \leftrightarrow \text{Fic}\bullet\text{ATP}\bullet\text{GyrB} \rightarrow \text{Fic} + \text{GyrB-AMP} + \text{PPi} \quad (2)$$

$$\text{GyrB-AMP} + \text{ATP} \leftrightarrow \text{GyrB-AMP}\bullet\text{ATP} \quad (3)$$

3.6.2. Crystal structure of the adenylylated form of GyrB

To understand the effect of the adenylylation of GyrB, I crystallized the adenylylated form of GyrB43 in complex with ATP. GyrB43 consists of the N-terminal 43-kDa fragment of GyrB comprising the ATPase and transducer domains (residues 1-392). The crystal diffracted to 2.6 Å and the structure was solved by molecular replacement. The structure reveals a conserved dimer between the native form (PDB: 1EI1) and the newly determined adenylylated form of GyrB (RMSD of 1.05 Å for the Cα positions). Strikingly, adenylylated GyrB adopts a different conformation of the ATP-lid loop (Figure 3.6.1 and Table 3.6.1), with an RMSD of 4.65 Å for the Cα positions of this region. The loop is expulsed from the cavity

that forms the ATP binding site. Intriguingly, the natural substrate ATP (not an ATP analog) is bound to the active site of the ATPase domain and not hydrolyzed. A weak H-bond has been described between the N3 of the adenine and the hydroxyl group of $Y109^{123}$. Interactions between the ligand (ATP) in adenylylated GyrB or ligand analog (AMPPNP) in native GyrB are very similar (compare Figure 3.6.1.b and 3.6.1.c), except the loss of the weak interaction between the hydroxyl group of Y109 and the N3 of the adenine. The latter observation, i.e. non-hydrolyzed ATP, raises the question whether the adenylylation of GyrB has an effect on the catalytic activity of the ATPase domain.

Table 3.6.1. Pair-wise fit of adenylylated GyrB43 and native GyrB43 after superposition of the ATPase domains of the subunit A. The values give the RMSD (Å) of the corresponding Cα positions.

	RMSD (Å)		
	Dimer	**Monomer A**	**Monomer B**
Residues 4-386	1.05	0.99	1.11
Residues 4-103 and 113-386 (all except the ATP lid loop)	0.78	0.64	0.89
Residues 104-112 (ATP lid loop)	4.65	4.95	4.32

As shown in *research article III* (Figure 2B from *research article III*), adenylylation of GyrB by $VbhTA_{E24G}$ completely abolishes the ATPase activity of GyrB. Further, I tested different ratios of $VbhTA_{E24G}$ to GyrB, keeping GyrB constant (25 µM) and increasing $VbhTA_{E24G}$ from 0 to 50 µM (Figure 3.6.2). The rate of inhibition of GyrB by $VbhTA_{E24G}$ is concentration-dependent and a low concentration of $VbhTA_{E24G}$ completely blocks the ATPase activity of GyrB after an extended time, i.e. after full target adenylylation has been achieved. Adenylylation of GyrB acts as a non-competitive inhibition of the ATPase activity of GyrB.

This shows that $VbhTA_{E24G}$ efficiently adenylylates GyrB and thus blocks its ATPase activity. Nonetheless, I was not able to observe a stable complex *in vitro*, even at high protein concentration (> 250 µM).

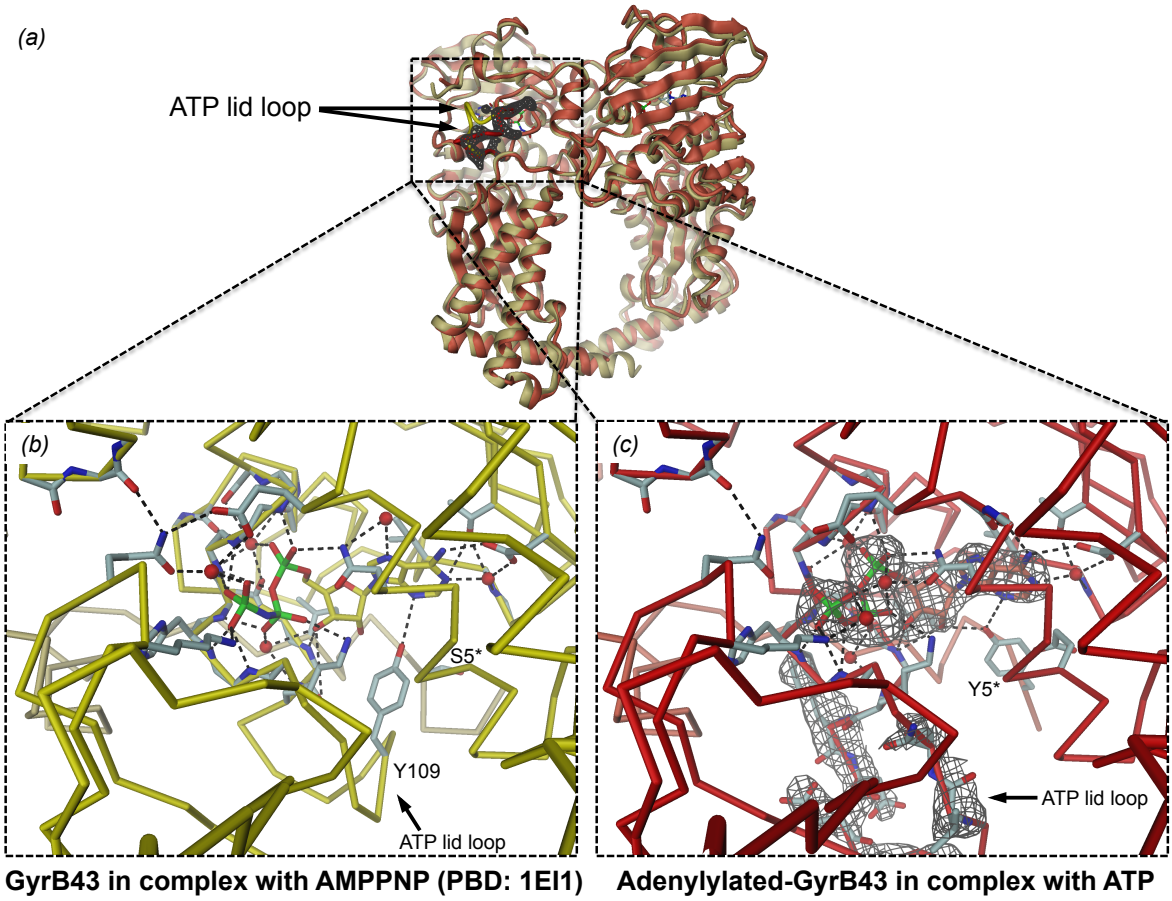

Figure 3.6.1. Crystal structure of adenylylated GyrB compared to native GyrB. *(a)* Superimposition of adenylylated GyrB and native GyrB reveals a conserved fold and conformation (light yellow for native GyrB and light red for adenylylated GyrB). The ATP lid-loop adopts a different conformation upon adenylylation (native GyrB colored in yellow and adenylylated GyrB colored in red). The Fo-Fc omit map (dark gray) is shown for adenylylated GyrB, where only the main chain has been observed due to lack of crystal contacts and high flexibility of the loop. *(b)* Details of the active site of native GyrB and *(c)* details of the active site of adenylylated GyrB, revealing a non-hydrolyzed ATP molecule in the Fo-Fc omit map (dark gray). The Fo-Fc omit map is also shown for the ATP lid-loop (residues 103-112). Hydrogen bonds are depicted as black dashed lines in *(b)* and *(c)*.

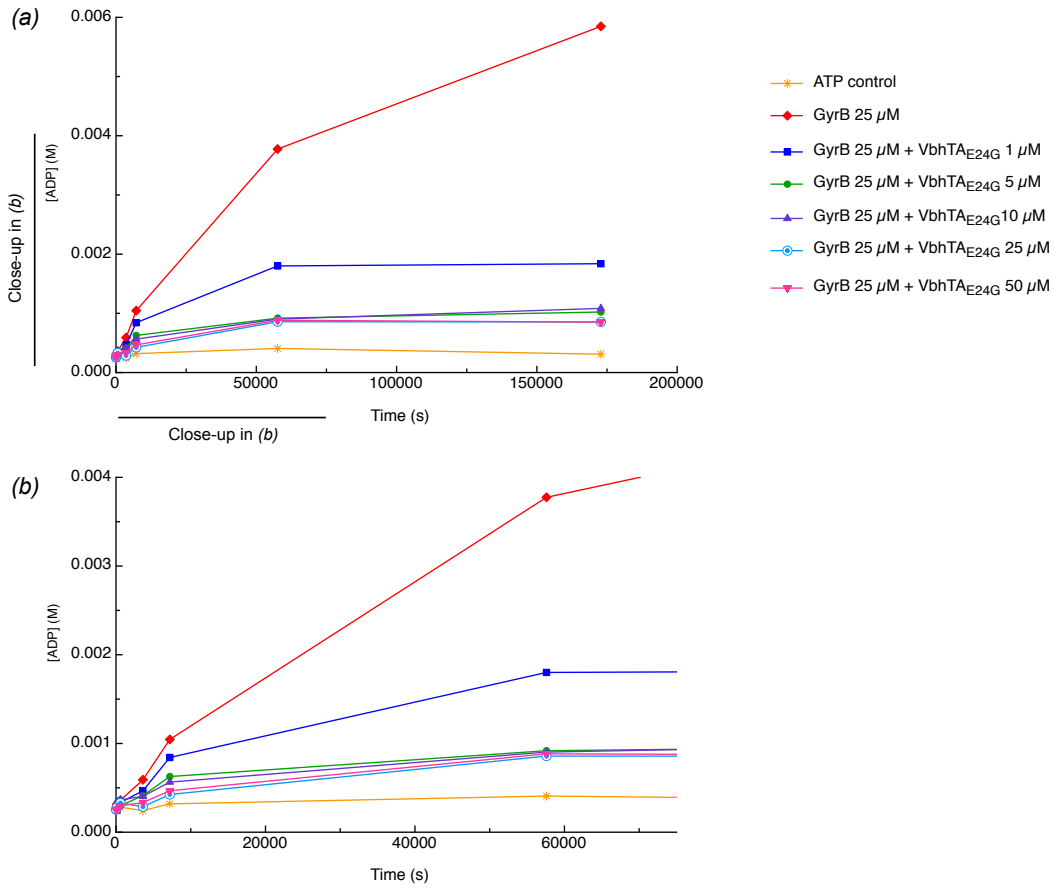

Figure 3.6.2. Inhibition of the ATPase activity of GyrB by VbhTA$_{E24G}$ in a concentration-dependent manner. *(a)* Full time course of the inhibition of GyrB by VbhTA$_{E24G}$ and *(b)* zoom-in on the early time points of *(a)*.

3.6.3. Crystallization strategies

As a first crystallization strategy, I tried to form a GyrB:Fic (the Fic protein being here NmFic or VbhTA) complex using GyrB and Fic proteins purified in separate batches. Purified GyrB and Fic were mixed in a 1:1 ratio (250 µM each) with a 10-fold molar excess of ATP (or AMPPNP) and $MgCl_2$[80]. The protein mixture was incubated for 2 hours on ice and subjected to crystallization screening. No crystals containing GyrB:Fic complexes were obtained, only crystals containing either the Fic protein or GyrB. The structures of Fic proteins couldn't be used further as these were identical to the already known structures, but GyrB structures revealed new conformations dependent on the nucleotide state that have been described in section 3.4., *research article IV*.

In order to enhance the chances of crystallization of a complex, I implemented or developed different strategies: (i) the fluorescent trace-labeling of GyrB or the Fic protein to monitor the crystallization of each partner in the crystal, (ii) the fusion of Fic-GyrB based on a model of putative interactions using a flexible $(G4S)_X$ linker, and (iii) the cross-linking of the Fic protein with GyrB via a functionalized ATP substrate that will be covalently attached to both proteins.

3.6.2.1. Fluorescent trace-labeling of each protein

Fluorescent trace-labeling has been developed by Forsythe *et al.*[162] in the group of Marc Pusey[163] to monitor the appearance of very small crystals and discriminate between salt crystals and protein crystals. However, the applicability of fluorescent trace-labeling of proteins for crystallization goes beyond these original applications. It can be adapted to monitor the appearance of crystals containing a complex of proteins for example. At the time of adapting the technique in the lab for this purpose, a ready-to-use kit was not available (now available from Molecular Dimensions, MD1-72). Therefore, I adapted the protocol from Forsythe *et al.* and also obtained advices from Marc Pusey. The labeling procedure allowed the labeling of 0.1-0.5% of the proteins on random lysine side chains, in good agreement with published values. I used carboxyrhodamine (CR) and tetramethylrhodamine carboxylic acid (TAMRA).

To visualize the fluorescence, I used a Leica DM6000 microscope with the N2.1 filter (Figure 3.6.3.a). As a pilot experiment, I couldn't find a better compromise in terms of fluorophore and filters with a fluorophore containing a succinimidyl ester group allowing the random labeling of lysine side chains. Importantly, flat bottom plates should be used for lower background fluorescence and better crystal detection. Despite the suboptimal setup, fluorescent crystals were obtained (Figure 3.6.3.b), both with CR or TAMRA. Each crystallization drop contained only one fluorophore, i.e. one drop contained labeled GyrB and unlabeled Fic protein, the next drop contained fluorescent Fic protein and non-fluorescent GyrB and as control, the last drop only contained unlabeled Fic protein and GyrB. Interestingly, the presence of fluorescent trace-labeled protein did not impede the crystallizability of the proteins. No crystals containing fluorescent GyrB and fluorescent Fic proteins could be obtained.

Nonetheless, this technique is very powerful for the detection of crystals and can theoretically be applied to various different protein complexes.

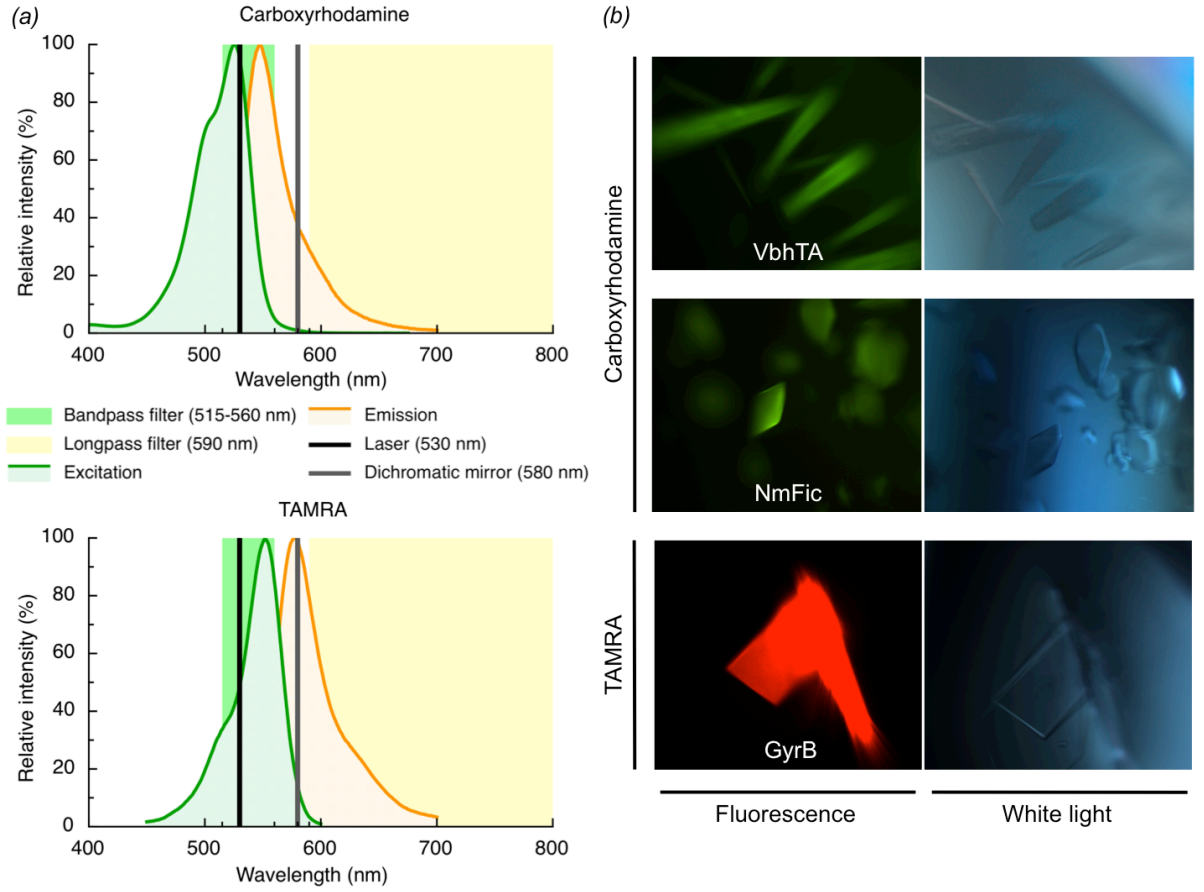

Figure 3.6.3. Crystallization of fluorescent trace-labeled proteins. *(a)* Absorption and emission spectrum of carboxyrhodamine (top) and TAMRA (bottom) compared to the setup of the Leica DM6000 microscope with filter N2.1. *(b)* Fluoresecent crystals obtained using the setup shown in *(a)*.

3.6.2.2. Fusion of GyrB-Fic proteins using a flexible linker

Natural flexible linkers are found between domains of proteins, allowing conformational changes. Non-natural linkers can be used to produce chimeras, i.e. multi-domain proteins from two different proteins that are not naturally found together or are even from different organisms. Engineered fusion proteins can also be used for the crystallization of low-affinity complexes or for non-crystallizing components[164]. As an example, the full-length *E. coli* gyrase complex structure recently obtained by electron microscopy was a fusion protein of the GyrA and GyrB polypeptide chains of *Thermus thermophilus*[122].

The superimposition of the adenylylated-GyrB on Cdc42 and NmFic or VbhTA on IbpA from the IbpA/Cdc42 complex (PDB: 4ITR) revealed that the C-terminus of the helix α8 of NmFic or the C-terminus of VbhA from the VbhTA complex are at about 21-25 Å of the N-terminus of GyrB. Therefore, a chimera was engineered between NmFic-GyrB and VbhA-GyrB using a flexible $(GGGGS)_{2\text{-}4}$ linker[165]. Soluble fusion proteins were obtained and subjected to crystallization screening. Again, no crystals containing a full fusion protein could be obtained, only degradation products, e.g. GyrB.

3.6.2.3. Cross-linking the Fic protein with its cognate target via a functionalized ATP substrate analog

3.6.2.3.1. A serine interacts with the 2'-OH of the ribose

In $VbhTA_{E24G}$ in complex with ATP, a serine interacts with the 2'-OH of the ribose via hydrogen-bond. In NmFic, the position of the serine is occupied by a methionine. Interesingly, the modeling of a cysteine in both proteins instead of the serine or methionine results in an appropriate distance for S-S cross-linking if a sulfur would be on the 2' position of the ribose. Ligand cross-linking will here allow the trapping of a covalent complex between the Fic protein and the adenylylated GyrB via the transferred AMP moiety.

3.6.2.3.2. 2'-SH-ATP custom synthesis

2'-SH-ATP was custom synthesized by Trilink Biotechnologies, Inc. and obtained as a 100 mM solution containing 10 mM of DTT to prevent the formation of 2'-SH-ATP dimers.

3.6.2.3.3. Can 2'-SH-ATP be used by a Fic protein to adenylylate GyrB?

A pre requisite for the feasability of this project is the binding of the modified ATP to the Fic protein, in particular to the mutated Fic protein containing a serine to cysteine mutation at position 175. The ATPase activity of GyrB was monitored using the same assay as described previously, with 2'-SH-ATP as substrate (see section 3.3., *research article III* and section 3.6.1.). Additionally, the inhibition of GyrB by $VbhTA_{E24G}$ and $VbhT_{S175C}A_{E24G}$ was tested using 2'-SH-ATP. First, GyrB is able to hydrolize 2'-SH-ATP, though slower than the natural substrate ATP (Figure 3.6.4). Noteworthy, 2'-SH-ATP is also a substrate for the Fic protein VbhT ($VbhT_{S175C}A_{E24G}$) as shown by the inhibition of substrate hydrolysis by GyrB (Figure

3.6.4). This result confirms the feasability of the protein-substrate-protein cross-link via the functionalyzed ATP molecule covalently transferred to GyrB as a functionalyzed AMP.

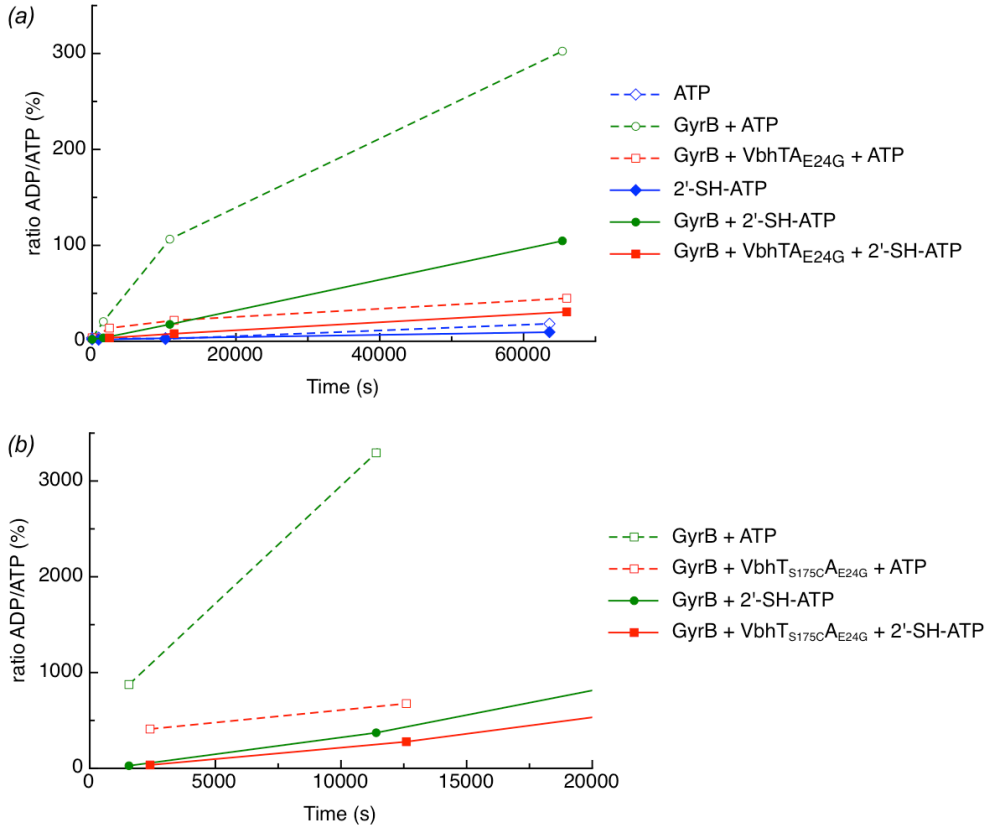

Figure 3.6.4. Inhibition of GyrB by VbhTA$_{E24G}$ or VbhT$_{S175C}$A$_{E24G}$ using functionalized ATP. *(a)* Inhibition of GyrB by VbhTA$_{E24G}$ using ATP or 2'-SH-ATP and *(b)* inhibition of GyrB by VbhT$_{S175C}$A$_{E24G}$ using ATP or 2'-SH-ATP.

3.6.2.3.4. Structure of VbhT$_{S175C}$A$_{E24G}$ with covalently bound 2'-SH-ATP

VbhT$_{S175C}$A$_{E24G}$ was co-crystallized with the ligand analog 2'-SH-ATP and $MgCl_2$. Crystals diffracted to 1.8 Å and well-defined electron density was obtained for the protein region and the ligand (Figure 3.6.5). The 2'-SH-ATP ligand was covalently bound to VbhT$_{S175C}$ via a disulfide bond (S-S) between the 2'SH group of the ligand and the SH group of cysteine 175. The ribose pucker is different in the natural ligand and the functionalized ligand 2'-SH-ATP, 2'-endo and 3'-endo respectively. Strikingly, the base (adenine) and the tri-phosphate superimposes very well despite the distortion of the ribose conformation. This flexibility of the ribose was anticipated by the few interactions observed between the ribose

and the protein in the structure of $VbhTA_{E24G}$ in complex with ATP (Figure 3.6.5). These interactions include a weak hydrogen bond between the 3'-OH of the ribose and the side chain of arginine R147 (3.2 Å distance) and a strong hydrogen bond between the 2'-OH of the ribose and the side chain of serine S175 (2.4 Å). The hydrogen bond between serine 175 and the 2'-OH of the ribose is replaced by a covalent disulfide bond between the cysteine 175 and the 2'-SH in $VbhT_{S175C}A_{E24G}$:2'-SH-ATP, as anticipated by the design of the functionalized ligand and mutant protein. The distance between the two sulfur atoms of the disulfide bond has been refined to 2.1 Å, slightly larger that the ideal value of 2.05 Å[166] and is in good agreement with the electron density (Figure 3.6.5). The CS-SC dihedral angle is of 98°, close to the ideal value at which the S-S bond strength is the highest that had been determined to 90°[167]. The comparison of the structure of $VbhT_{S175C}A_{E24G}$ in a covalent complex with 2'-SH-ATP with the structure of $VbhTA_{E24G}$ in complex with ATP (PDB: 3ZC7) reveals a competent binding of the substrate, now covalently cross-linked to the protein via a disulfide bond (Figure 3.6.5). This will be used for the crystallization of a covalent complex with the adenylylated target GyrB, on which the AMP moiety will act as a linker between the Fic protein and the DNA gyrase subunit.

3.6.2.3.5. Formation of a covalent ternary complex between $VbhT_{S175C}A_{E24G}$, 2'-SH-ATP and GyrB

As mentioned in the previous paragraph, $VbhT_{S175C}A_{E24G}$ forms a covalent complex with the functionalized ligand 2'-SH-ATP that binds in a competent conformation. This complex is then preformed *in vitro* (for a detailed protocol, see section 3.6.4. and Figure 3.6.7) and then mixed with the target GyrB in presence or absence of AMPPNP.

As preliminary medium-throughput method, non-reducing SDS-PAGE analysis was used as readout to discriminate between covalently cross-linked complexes and non-complexed proteins (Figure 3.6.6). Using different concentrations of oxidizing agent (diamide or H_2O_2), I could show that a fraction of complex is obtained with a rather high concentration (10 mM) of diamide or H_2O_2 (oxidizing agent). There is a clear concentration correlation between complex formation and diamide concentration. To further prove that the band observed around 70 kDa is a covalent complex via a disulfide bond, the samples were compared using non-reducing (NR) or reducing (R) loading dye. As anticipated, the cross-linked complex is only observed in presence of non-reducing (NR) loading dye (Figure 3.6.6).

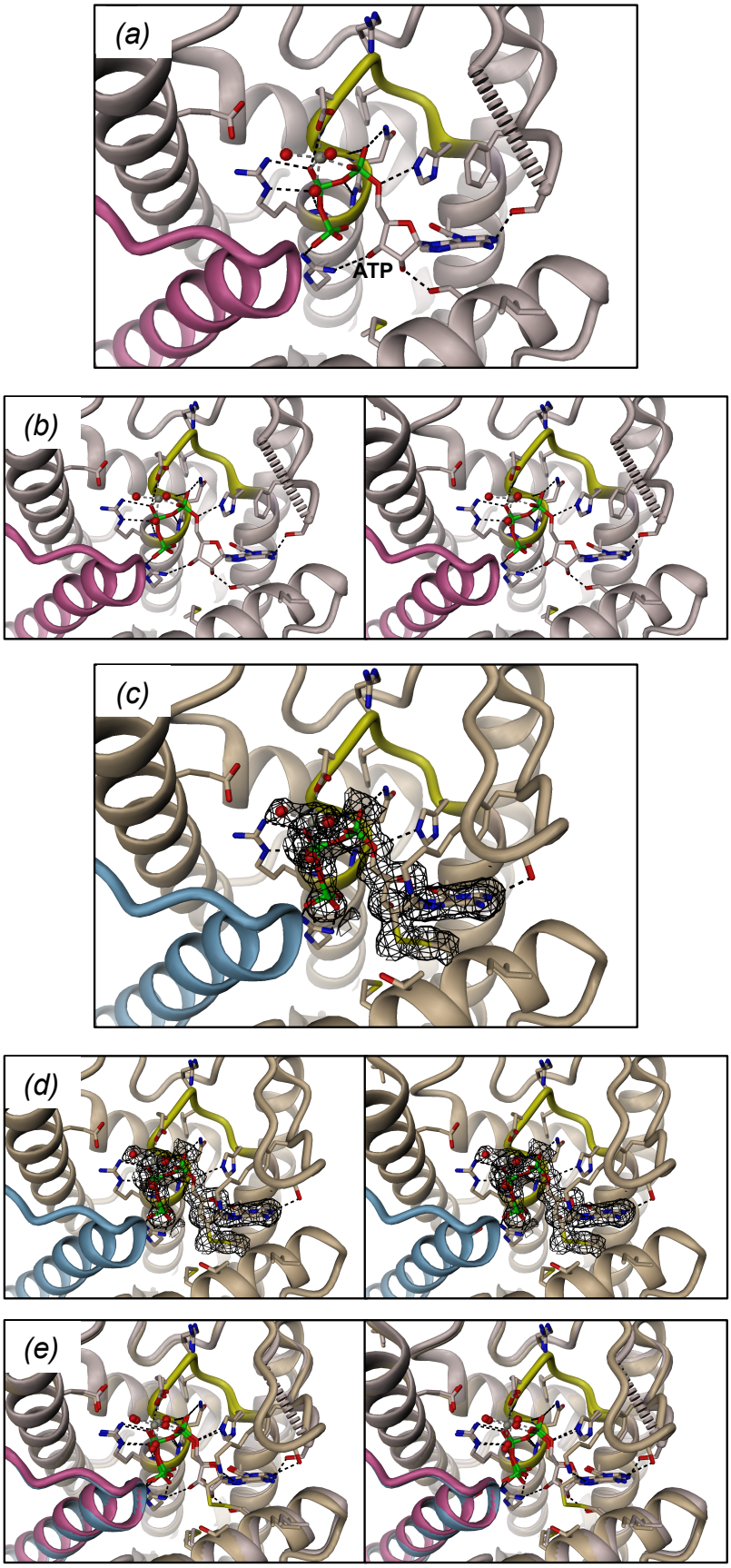
(a)
ATP
(b)
(c)
(d)
(e)

Figure 3.6.5. Crystal structure of $VbhT_{S175C}A_{E24G}$ with covalently bound 2'-S-ATP. *(a)* Details of the active site of $VbhTA_{E24G}$ in complex with ATP (PDB code: 3ZCB). VbhT is colored in light gray with the active site loop colored in yellow. VbhA is colored in pink. *(b)* Stereoview of *(a)*. *(c)* Active site details of $VbhT_{S175C}A_{E24G}$ with covalently bound 2'-S-ATP *via* a disulfide bond between the γ-sulfur of cysteine 175 and the 2'-sulfur of the functionalized ATP. A Fo-Fc omit map contoured at 3 σ is shown in dark gray, VbhT is colored in beige with the active site loop in yellow and VbhA is colored in blue. *(d)* Stereoview of *(c)*. *(e)* Stereoview of the superimposition of $VbhTA_{E24G}$ in complex with ATP and $VbhT_{S175C}A_{E24G}$ with covalently bound 2'-S-ATP.

Unexpectedly, the covalent complex between $VbhT_{S175C}A_{E24G}$, 2'-SH-ATP and GyrB is only obtained in presence of AMPPNP, which is required for the formation of a GyrB homodimer. This suggests that VbhT will preferentially target GyrB in the dimer form, even though we could show *in vitro* by adenylylation assays that VbhT or NmFic targets a fragment of GyrB (15-392) that lacks the N-terminal arm and is therefore dimerization deficient (data not shown).

These preliminary results are a proof of principle that the custom synthesized 2'-SH-ATP is a substrate for the Fic protein that can be covalently bound to the mutated Fic active site *via* a disulfide bond between an engineered cysteine and the thiol group on the 2' position of the ribose. Further, the covalently bound 2'-SH-ATP is in a competent conformation for AMP transfer. 2'-S-AMP covalently bound to the Fic active site is transferred on GyrB, resulting in a covalent quaternary complex $VbhA_{E24G}$/$VbhT_{S175C}$-2'-S-AMP-GyrB.

Varying reducing and oxidizing agents and their respective concentrations or optimizing the time and temperature of each step can improve the conditions in which the complex is obtained. Furthermore, the SDS-PAGE may be too harsh for the complex and the low amount of cross-linked complex may result as an artifact of the readout. Therefore, size exclusion chromatography will be used in the future to discriminate and separate the complex from the non-complexed proteins to obtain a homogeneous sample for further crystallization experiments.

Because crystallization may not be straightforward for such a complex, a combination of cross-linking via the disulfide bond with fluorescent trace labeling may be an elegant way to discover small crystals.

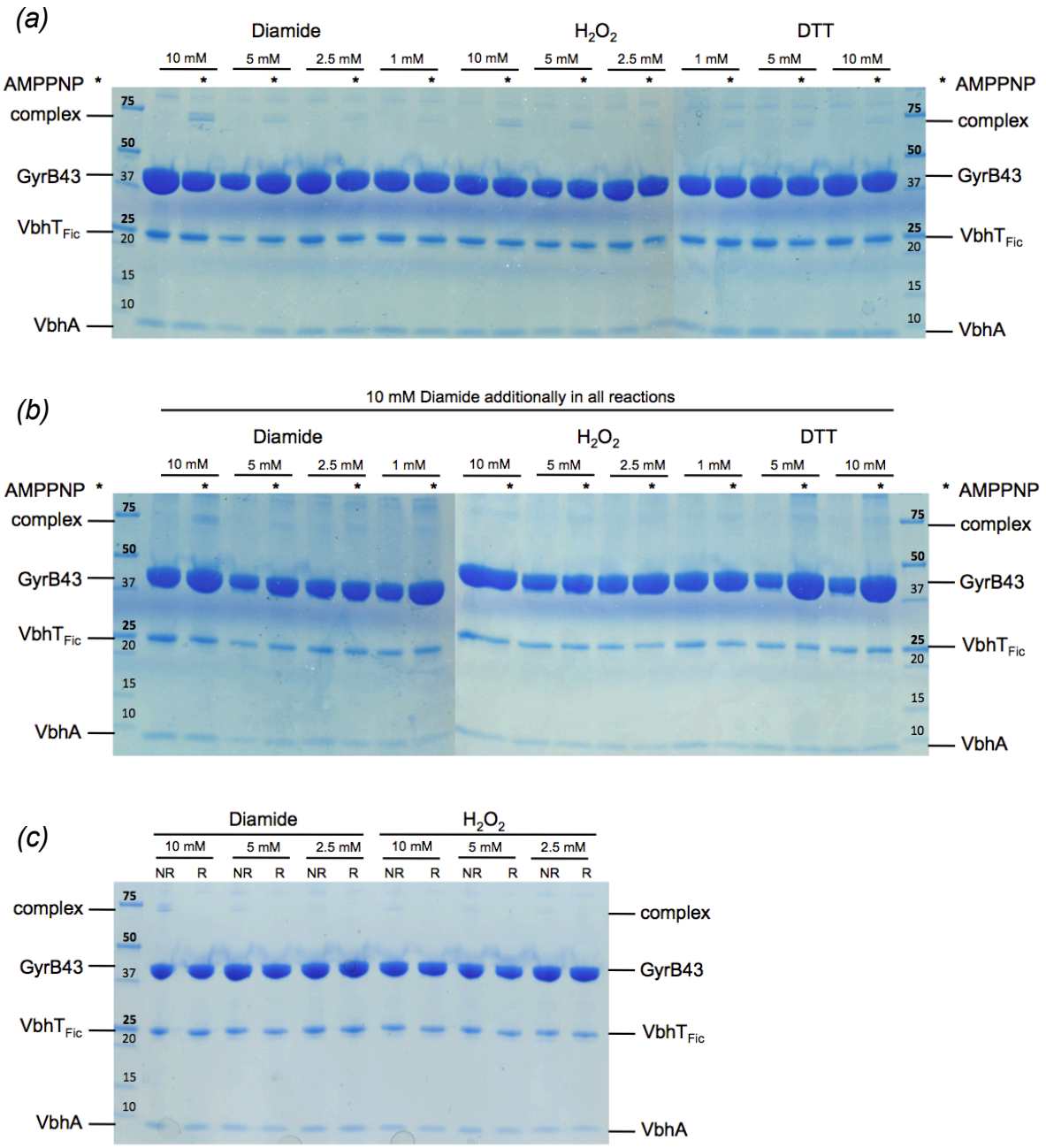

Figure 3.6.6. Evaluation of the formation of a covalent $VbhT_{S175C}A_{E24G}$:2'-S-AMP-GyrB complex by SDS-PAGE analysis. *(a)* SDS-PAGE analysis of samples containing different concentrations of diamide, H_2O_2 or DTT. *(b)* Same samples as in *(a)* with the addition of 10 mM diamide in all reaction during the adenylylation reaction. *(c)* SDS-PAGE gel using non reducing (NR) or reducing (R) loading dye to confirm the covalent $VbhT_{S175C}A_{E24G}$:2'-S-AMP-GyrB complex.

3.6.4. Material and Methods related to section 3.6

Cloning – Recombinant plasmids pFVS0065 (genes encoding VbhT and $VbhA_{E24G}$) and pFVS0109 (gene encoding GyrB43 comprising residues 1-392) were described in section 3.2., *research article II* and section 3.3., *research article III*, respectively. A two-base pair mutation was introduced in plasmid pFVS0065 to obtain plasmid pFVS0229 (genes encoding $VbhT_{S175C}$ and $VbhA_{E24G}$).

Protein expression and purification – Proteins were expressed and purified as described in section 3.2., *research article II* for VbhT/VbhA complexes and as described in section 3.3., *research article III* for GyrB43.

Crystallization – For crystallization, GyrB43, $VbhTA_{E24G}$ and $VbhT_{S175C}A_{E24G}$ were concentrated to 10.75 mg/mL, 8 mg/mL and 4 mg/mL, respectively. Prior to the co-crystallization of adenylylated-GyrB with ATP, GyrB43 was incubated for two hours at 4°C with an equimolar ratio of the adenylylator $VbhTA_{E24G}$ and a 10-fold molar excess of ATP and $MgCl_2$. GyrB43 crystallized (without removal of $VbhTA_{E24G}$ or ligand/ion) in 0.2 M Tri-ammonium citrate pH 7.5 and 22% (w/v) PEG 2000 MME. $VbhT_{S175C}A_{E24G}$ co-crystallized with 5 mM 2'-SH-ATP, 5 mM MgCl2 and 5 mM DTT in a solution containing 0.2 M lithium acetate dihydrate pH 7.9 and 20% (w/v) PEG 3350. Crystals were cryo-protected by transfer in a reservoir solution supplemented with 30% glycerol and subsequently flash frozen and stored in liquid nitrogen until data collection.

Structure determination – X-ray diffraction data were collected at the Swiss Light Source (Villigen, Switzerland) on beamline X06DA (PXIII) at 100 K and a wavelength of 1.0000 Å. Diffraction data were indexed and integrated using XDS[168] and subsequently merged and scaled using XSCALE[168] or Aimless[169] for the structure of adenylylated-GyrB in complex with ATP or the structure of $VbhT_{S175C}A_{E24G}$ in complex with 2'-SH-ATP. Data collection and processing statistics are summarized in Table 3.6.2. Structures were determined by molecular replacement using Phaser with GyrB43 (PDB: 1EI1[124]) and VbhTA (PDB: 3SHG[170]) respectively, devoid from ligand or ordered solvent, as search model. Several rounds of model building and refinement were performed using Coot[171] and Refmac5[172] or phenix.refine[173]. 5% of the data were excluded from refinement and used for cross-validation. The geometry of the final model was assessed using MolProbity[174]. Final refinement yielded models of adenylylated-GyrB in complex with ATP and $VbhT_{S175C}A_{E24G}$

in complex with 2'-SH-ATP with respective R_{work}/R_{free} (%) values of 19.6/26.9 and 16.1/21.1. Refinement statistics are summarized in Table 3.6.3.

Quantification of Fic-mediated inhibition of the ATPase activity of GyrB by FPLC assay – The quantification of the inhibition of GyrB by $VbhTA_{E24G}$ was performed as described in section 3.3., *research article III*. Additionally, the ratio of GyrB:$VbhTA_{E24G}$ protein was increased from 1:50 to 1:1.

Formation of a covalent $VbhT_{S175C}A_{E24G}$:2'-SH-AMP:GyrB complex via crosslink of the thiol group of the engineered ligand – 2'-SH-ATP was designed for the purpose of our experiment and ordered as a custom synthesized ATP analog from Trilink Biotechnologies, Inc. To ensure the monomerization of 2'-SH-ATP, the nucleotide was incubated in a 1:1 ratio with DTT for 2 hours at room temperature (adapted from Sigma Aldrich online protocol for thiol-modified oligonucleotide reduction). $VbhT_{S175C}A_{E24G}$ is then incubated with a 40-fold molar excess of reduced 2'-SH-ATP for 5 hours at room temperature to allow complex formation. To form a covalent complex between the 2'-SH-ATP and $VbhT_{S175C}A_{E24G}$ via the 2'-SH group and the cysteine 175, increasing concentration of oxidizing agent (H_2O_2 or diamide) from 1 to 10 mM were incubated overnight at 4°C with $VbhT_{S175C}A_{E24G}$:2'-SH-ATP. The excess of nucleotide is then removed by size exclusion chromatography and the A_{260}/A_{280} absorption ratio is measured to evaluate the formation of covalent complex (varying between 0.63 and 0.81). GyrB is then added to the sample with or without an 80-fold molar excess of AMPPNP. An aliquot of each sample supplemented with non-reducing loading dye (60 mM Tris-HCl pH 6.8, 2% (w/v) SDS, 10% (v/v) glycerol, 0.01% (w/v) bromophenol blue) is loaded on a 4-20% SDS-PAGE gel and stained. For a pictorial view of the protocol, see Figure 3.6.7.

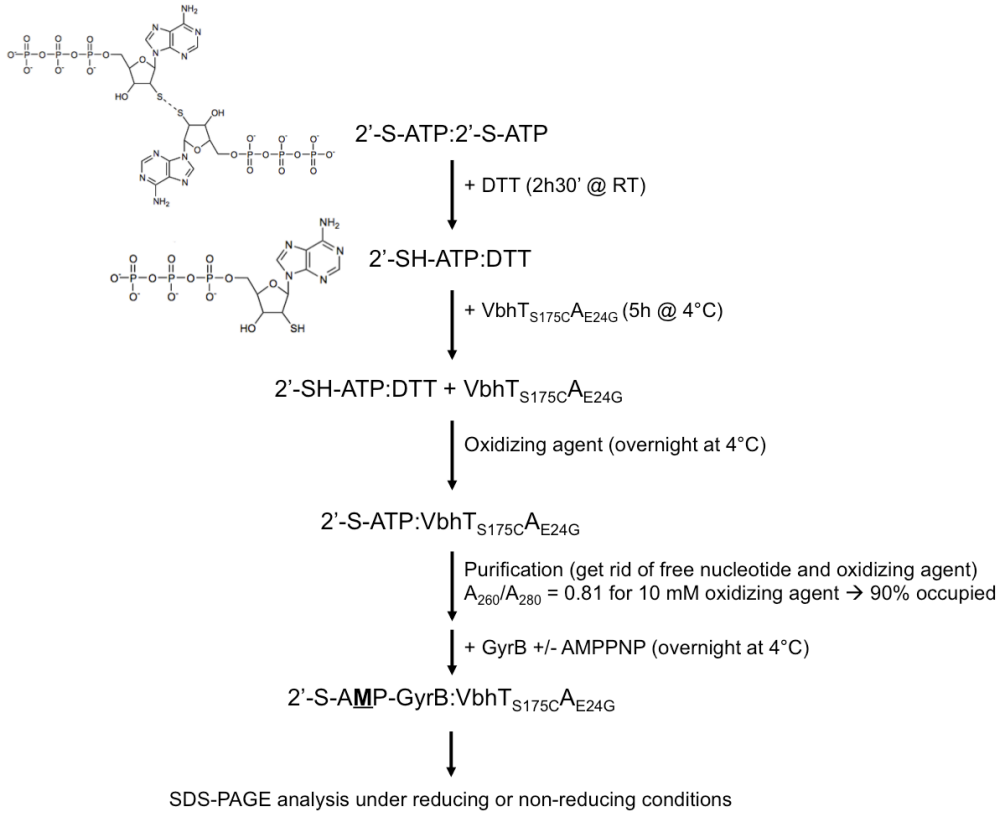

Figure 3.6.7. Pictorial view of the complex formation protocol.

Table 3.6.2. Data collection statistics.

	Adenylylated GyrB43 in complex with ATP	$VbhT_{S175C}A_{E24G}$ in complex with 2'-SH-ATP
X-ray source	SLS X06DA (PXIII)	SLS X06DA (PXIII)
X-ray detector	Pilatus 2M	Pilatus 2M
Wavelength (Å)	1.0000	1.0000
Space group	P 2 2_1 2_1	P 1 2_1 1
Cell dimensions		
a, b, c (Å)	79.33 137.82 85.45	43.805 64.309 45.633
β (°)		94.13
Matthews coeff. ($Å^3$/Da)	2.77	2.21
Solvent content (%)	55.24	43.98
Mol. per asym. unit	2	2 (1 VbhT, 1 VbhA)
Resolution limits (Å)	72.62 - 2.6 (2.69 - 2.60)	45.51 - 1.80 (1.87 - 1.80)
Total reflections	75'686 (6'157)	79'516 (7'554)
Unique reflections	26'998 (2'501)	23'325 (2'273)
Multiplicity	2.8 (2.5)	3.4 (3.3)
Completeness (%)	91.45 (86.24)	99.52 (98.52)
Mosaicity	0.58	0.24
$\langle I / \sigma(I) \rangle$	7.94 (1.53)	7.5 (2.6)
R_{merge} † (%)	12.7 (64.7)	9.7 (42.5)
R_{meas} ‡ (%)	15.46	13.6 (59.5)
$CC_{1/2}$	98.9 (60.8)	99.0 (82.9)

Numbers in parentheses belong to the outer shell.

† $R_{merge} = \sum_{hkl}\sum_i |I_i(hkl) - \langle I(hkl)\rangle| / \sum_{hkl}\sum_i I_i(hkl)$, where $I_i(hkl)$ is the observed intensity for a reflection and $\langle I(hkl)\rangle$ is the average intensity obtained from multiple observations of symmetry-related reflections.

‡ $R_{meas} = \sum_{hkl} [N/(N-1)]^{1/2} \sum_i |I_i(hkl) - \langle I(hkl)\rangle| / \sum_{hkl}\sum_i I_i(hkl)$, where $I_i(hkl)$ is the observed intensity for a reflection, $\langle I(hkl)\rangle$ is the average intensity obtained from multiple observations of symmetry-related reflections and N is the number of observations of intensity I(hkl).

Table 3.6.3. Refinement statistics.

	Adenylylated GyrB43 in complex with ATP	$VbhT_{S175C}A_{E24G}$ in complex with 2'-SH-ATP
PDB code	N/A	N/A
Resolution limits (Å)	72.62 - 2.6 (2.69 - 2.60)	45.51 - 1.80 (1.87 - 1.80)
R_{work} * (%)	19.62 (24.40)	16.15 (18.80)
R_{free} ** (%)	26.92 (33.55)	21.06 (27.45)
Number of non-H atoms	6'033	2'292
- macromolecules	5'862	2'040
- ligands	62	32
- solvent	109	220
Protein residues	766	248
RMSD bond lengths (Å)	0.013	0.021
RMSD bond angles (°)	1.61	1.99
Ramachandran favored/allowed * (%)**	93.7 (98.8)	99.2 (100.0)
Ramachandran outliers * (%)**	1.2	0.0
Clashscore ***	7.11	5.21
Average B values (Å^2)	33.50	17.20
- macromolecules	33.90	16.10
- ligands	19.70	16.50
- solvent	20.90	26.80

Numbers in parentheses refer to the outer shell.

* $R_{work} = \sum_{hkl} || F_{obs}| - |F_{calc}|| / \sum_{hkl} |F_{obs}|$

** R_{free} is the R value calculated for 5% of the data set that was not included in the refinement.

*** Molprobity

3.7. *Research article VI* (Stanger *et al.*, in preparation for *Acta Cryst. F*)

Crystal structure of the *E. coli* class I Fic protein EcFicT in complex with EcFicA

Frédéric V. Stanger, Christoph Dehio & Tilman Schirmer

Manuscript in preparation

Format: Article for *Acta Crystallographica Section F*

3.7.1. Statement of my own contributions

I designed and performed all the experiments presented in the *research article VI*. I cloned, expressed, purified EcFicT/EcFicA and crystallized the toxin/antitoxin complexes. I determined the crystallographic structures, analyzed the data and wrote the manuscript.

3.7.2. "Crystal structure of the *E. coli* class I Fic protein EcFicT in complex with EcFicA"

publBio structural communications

Crystal structure of the *E. coli* class I Fic protein EcFicT in complex with EcFicA

Frédéric V. Stanger[ab], Christoph Dehio[b] and Tilman Schirmer[a]*

[a]Focal Area Structural Biology and Biophysics, Biozentrum, University of Basel, 50/70 Klingelbergstrasse, Basel, CH-4056, Switzerland
[b]Focal Area Infection Biology, Biozentrum, University of Basel, 50/70 Klingelbergstrasse, Basel, CH-4056, Switzerland

Correspondence email: tilman.schirmer@unibas.ch

Keywords: *E. coli* Fic, Class I Fic protein, YhfG, EcFicA, filamentation induced by cAMP

PDB reference:

Synopsis

Two crystal structures of EcFicT/EcFicA of *E. coli* have been determined at high resolution. They reveal a conserved Fic fold with an unusual hydrophobic binding pocket close to the Fic active site that may confer substrate specificity to this Fic protein with a degenerated active site motif.

Abstract

FIC domain proteins are well-conserved through evolution and found in all kingdoms of life and viruses. The vast majority of Fic proteins containing a canonical HxFx[D/E]GNGRxxR Fic motif catalyse a post-translational modification called adenylylation, the transfer of an AMP moiety. Several Fic proteins, including the originally described Fic protein EcFicT from *E. coli*, contain a degenerated Fic active site motif of unknown function. A small gene encoding *ecficA* (or *yhfG*) is located upstream of the ec*ficT* gene. Here, we show that the class I Fic protein EcFicT forms a tight complex with the small protein EcFicA that contains an [S/T]xxxE[G/N] inhibition motif and we determined two high-resolution structures of the complex. We anticipate that the detailed structural information will provide a solid basis for the understanding of the enzymatic activity of this Fic protein.

1. Introduction

Filamentation induced by cAMP (Fic) has been introduced in the early 1980's by Utsumi *et al.* (Utsumi et al., 1982) to describe the phenotype of an *E. coli* temperature sensitive mutant in the *fic* gene. This mutation caused cell filamentation at non-permissive temperature (43°C) in the presence of high concentration of cAMP (1.5 mM). A bacteria expressing the *fic* gene or a knock-out strain of the *fic* gene are viable, but only the *fic-1* gene (G55R mutant) or a complementation of the knock-out with the *fic-1* gene show a filamentation phenotype, suggesting a gain of function mutation of the *fic-1* allele (Kawamukai et al., 1988; 1989).

Yet, the exact biochemical function of the *E. coli* Fic protein (EcFicT) is not clear. Recently, the biochemical activity of the majority of Fic proteins has been revealed by *in vitro* and *in vivo* analysis combined with mass spectrometry (Worby et al., 2009; Yarbrough & Orth, 2009; Woolery et al., 2010). FIC domain proteins containing a canonical HxFx[D/E]GNGRxxR motif catalyze a post-translational modification called adenylylation, the transfer of an AMP moiety from an ATP substrate (Engel et al., 2012). Nevertheless, depending on the composition of the active site, Fic/Doc family proteins also catalyse other post-translational modifications. AnkX from *Legionella pneumophilae* catalyses phosphocholination (Mukherjee et al., 2011) and Doc from the Doc/PhD toxin-antitoxin system from Bacteriophage P1 catalyses phosphorylation (Castro-Roa et al., 2013; Cruz et al., 2014). The Fic active site motif of

EcFicT, consisting of HPFRVGSGLAQR, differs from the adenylylation competent motif or known motifs of Fic proteins catalyzing other post-translation modifications. Neither the modification catalyzed by this protein nor the target is known, if any. Interestingly, a small protein is encoded by the *yhfG* gene upstream of the *fic* gene on the *E. coli* genome, similarly to the type II toxin-antitoxin system VbhT/VbhA (Engel et al., 2012; Goepfert et al., 2012; Goepfert et al., 2013). The small protein YhfG, now renamed EcFicA, contains a conserved [S/T]xxxE[G/N] motif as defined by Engel, Goepfert *et al.*, which defines EcFicTA as a class I Fic protein. We anticipated that EcFicT forms a tight complex with EcFicA and therefore cloned, expressed, purified, crystallized and determined the three-dimensional structure of EcFicT in complex with the small protein EcFicA. We focused on two different mutants: the putative inhibition-relieved mutant $EcFicTA_{E28G}$ of the inhibitory motif and the mutant $EcFicT_{G55R}A$ encoded by the *fic-1* gene described in the 1980's. Here, we propose that the crystal structure of the EcFicTA may serve as a template for bioinformatical analysis and modeling of a putative ligand that can be further challenged by *in vitro* and *in vivo* assays.

2. Materials and methods

2.1. Macromolecule production

Plasmid pPE0038 contains the *ecficT* gene in the MCS1 and the *ecficA* gene in the MCS2 of the pRSFDuet-1 (Novagen), N-terminally fused to a the nucleic acid sequence coding for a His_6-tag and a HA-Tag, respectively, as previously described (Harms et al., submitted).

A single base-pair and double base-pairs mutation were introduced in plasmid pPE0038, resulting in plasmid pFVS0129 containing $EcFicT_{G55R}$/EcFicA and plasmid pFVS0129 containing EcFicT/$EcFicA_{E28G}$, respectively. Details are given in Table 1.

Plasmids pFVS0129 and pFVS0130 were transformed into *E. coli* BL21 (λDE3). EcFicT/EcFicA (Uniprot: P20605/P0ADX5) protein complexes were expressed and purified similarly to the previously described VbhT/VbhA proteins (Engel et al., 2012; Goepfert et al., 2013). $EcFicT_{G55R}$/EcFicA and EcFicT/$EcFicA_{E28G}$ were concentrated to 25 and 28 mg/mL, respectively (Figs. 1a-b).

2.2. Crystallization

Crystals were obtained at 20°C using the sitting-drop vapour diffusion method after mixing 0.2 μL protein solution with 0.2 μL reservoir solution equilibrating against a reservoir of 80 μL. $EcFicT_{G55R}$/EcFicA crystallized after 5 days in 0.2 M $MgCl_2$, 0.1 M Tris pH 8.0 and 20% (w/v) PEG 6000 and EcFicT/$EcFicA_{E28G}$ crystallized after 8 days in 19% (w/v) PEG 1500, 0.1 M MMT (malic acid, MES, Tris) buffer pH 6.0 (Fig. 1c).

2.3. Data collection and processing

For data collection, crystals were cryoprotected by transfer into a reservoir solution supplemented with 20% glycerol and subsequently vitrified in liquid nitrogen. X-ray data were collected at the Swiss Light Source (Villigen, Switzerland) on beamline X06SA (PXI) and X06DA (PXIII) at 100 K with a wavelength of 1.0000 Å (Fig. 1d).

Diffraction data were indexed and integrated using XDS (Kabsch, 2010) and subsequently merged and scaled using XSCALE (Kabsch, 2010) or aimless (Evans & Murshudov, 2013). $EcFicT_{G55R}$/EcFicA and EcFicT/$EcFicA_{E28G}$ diffracted to 2.0 Å and 2.4 Å, respectively. Data collection and processing statistics are summarised in Table 3.

2.4. Structure solution and refinement

First, the structure of $EcFicT_{G55R}$/EcFicA was solved by molecular replacement using the structure of VbhT from the VbhT/VbhA complex as search model (PDB: 3ZC7, Fig. 2a). Analysis of the unit-cell contents using MATTHEWS_COEFF (Matthews, 1968) as implemented in the CCP4 (Winn et al., 2011) suite suggested two

EcFicT/EcFicA complexes per asymmetric unit (2.60 $Å^3.Da^{-1}$, 52.6% solvent). No pathologies were detected by *phenix.xtriage* (Adams et al., 2010). Crystals belonged to the Laue group 6/m as determined by pointless (Evans, 2006), to the point group P6 with unit cell parameters a = 104.69 Å, b = 104.69 Å and c = 110.52 Å. Because of the uncertainties on the space group, all alternative $P6_x$ space groups were tested for molecular replacement using Phaser (McCoy et al., 2007). The best solution (TFZ=11.6 and LLG=206) was obtained in $P6_5$ with two molecules in the asymmetric unit. Initial refinement (R_{work} = 43.6, R_{free} = 47.0) showed some alpha-helical structure (positive Fo-Fc map) in the groove of the Fic protein next to the active site, where an α_{inh} helix is usually found (Engel et al., 2012; Goepfert et al., 2012; 2013). EcFicA was built using Autobuild (Zwart et al., 2008). Several rounds of model building and refinement were performed using Coot (Emsley et al., 2010) and Refmac5 (Murshudov et al., 2011) or phenix.refine (Adams et al., 2010). Final refinement yielded an $EcFicT_{G55R}$/EcFicA model (Fig. 2b) with R_{work}/R_{free} (%) values of 17.7/20.4, respectively. Final refinement statistics are given in Table 4.

Further, crystals of the monoclinic space group I121 were obtained that diffracted to 2.4 Å, with three $EcFicT/EcFicA_{E28G}$ complexes per asymmetric unit according to the Matthews coefficient of 1.93 $Å^3.Da^{-1}$, corresponding to a solvent content of 38.0%. Data collection statistics are given in Table 3. The structure of $EcFicT/EcFicA_{E28G}$ was solved by molecular replacement using the previously solved structure of $EcFicT_{G55R}$/EcFicA as search model, followed by iterative model building and refinement. The final model comprises residues 5-53 of EcFicA and residues 10-195 except the loop 82-88 of the FLAP region of EcFicT. Final refinement statistics are given in Table 4.

3. Results and discussion

Both structures revealed a 33.7 kDa complex formed by EcFicT (25.7 kDa) and EcFicA (8 kDa). EcFicT forms a seven α-helices bundle. A structure close to a β-harpin is located between helices α2-α3, that is known to be involved in target binding (Lee et al., 2004; Xiao et al., 2010) and the Fic active site containing the Fic motif is located between helices α4-α5. EcFicA tightly embraces EcFicT via mainly hydrophobic interactions, analogously to VbhA embraces VbhT. Yet, EcFicA adopts a unique conformation, forming two parallel α-helices linked by ten amino acids, compared to VbhA that contains three anti-parallel α-helices.

The canonical inhibition motif (SRRLEG) located at the C-terminal end of the first helix of EcFicA (α_{inh}) protrudes into the EcFicT active site. Similarly to the previously described structure of the class I Fic protein VbhT/VbhA, the Ser24 and Glu28 of EcFicA interacts via H-bonds with the last arginine residue of the Fic active site motif (HPFRVGSGLAQR) (Fig. 2b).

A few amino acids have been replaced through evolution from the canonical adenylylation competent Fic motif, which makes unlikely that EcFicT catalyzes the transfer of an AMP moiety. There are no steric hindrances on the phosphates or ribose sides of the substrate in the active site when modeling ATP binding but the adenine ring clashes with a glutamine from the FLAP and an asparagine from the helix α6, Q84 and N171 respectively (Fig. 3a). Additionally, crucial residues for substrate binding and catalysis are absent, i.e. the carboxylic acid involved in metal (Mg^{2+}) binding is replaced by a valine, the asparagine part of the anion binding nest is changed in a serine and the first arginine of the canonical Fic motif, crucial for β- and γ-phosphate coordination is replaced by a hydrophobic leucine residue. Altogether, it makes it unlikely that EcFicT catalyzes adenylylation.

Interestingly, there is room on the opposite site from the canonical base-binding pocket of Fic proteins, where a hydrophobic pocket is observed (Fig. 3a). This has already been observed for the phosphorylating protein Doc from the Bacteriophage P1 (Castro-Roa et al., 2013; Cruz et al., 2014) and the phosphocholinating protein AnkX from *Legionella pneumophilae* (Mukherjee et al., 2011; Campanacci et al., 2013).

structural communications

The mutation encoded by the *fic-1* gene that results in a growth defect phenotype doesn't affect the fold of the Fic protein ($EcFicT_{G55R}$), as revealed by a root mean square deviation (rmsd) of 0.513 Å^2 between the Cα position of equivalent atoms in the two newly determined EcFicTA structures (Fig. 3b). This mutation has also no effect on the oligomeric state of the protein (Fig. 1a). Close analysis of the mutated residue, arginine R55 of EcFicT, reveals two H-bonds forming an intra-molecular salt-bridge between the arginine side chain and the neighbouring carboxylic acid side chain of the glutamate E107 (helix α3) (Fig. 3c). From a structural point of view, the G55R mutation may provide more stability to the Fic fold, explaining why only this mutant lead to the filamentation phenotype when expressed in *E. coli* at elevated temperature (43°C) in presence of high level of cAMP (1.5 mM) (Utsumi et al., 1982; Kawamukai et al., 1988; 1989; Komano et al., 1991).

The structure of EcFicTA reveals a conserved Fic fold with a deteriorated Fic motif and an additional hydrophobic binding pocket in the vicinity of the active site loop. Structural information combined with bio-informatical ligand docking analysis may be the basis of a new method to find the substrate of Fic proteins with deteriorated Fic active site motif. Still, *in vivo* and *in vitro* analyses are required to understand the activity of the name-giving Fic protein.

Table 1

Macromolecule production information

	$EcFicT_{G55R}$/EcFicA (pFVS0129)	**EcFicT/$EcFicA_{E28G}$ (pFVS0130)**
Source organism	*Escherichia coli* str. K-12 substr. MG1655	*Escherichia coli* str. K-12 substr. MG1655
DNA source	EcFicT/EcFicA in pRSFDuet-1 (pPE0038)	EcFicT/EcFicA in pRSFDuet-1 (pPE0038)
Forward primer	5′-CTGGTGCGCCGTTTACCGCATTTGCGCACTATC-3′	5′-GTCGCCGTCTTGGCGGCGTCGAGATGCCTTTAGTC-3′
Reverse primer	5′-GTAAACGGCGCACCAGCGGACCAAGCTC-3′	5′-CTCGACGCCGCCAAGACGGCGACTGGCCTGAAAATTAC-3′
Cloning vector	pRSFDuet-1	pRSFDuet-1
Expression vector	pRSFDuet-1	pRSFDuet-1
Expression host	*E. coli* BL21 (λDE3)	*E. coli* BL21 (λDE3)
Complete amino acid sequence of EcFicT[§]	MGSSHHHHHHSQDPNSSSARLQVEMGDKFGEGRDPYLYPGLDIMRNRLNIHQQQRLEQAAYEMTALRAATIELGPLVR**R**LPHLRTIHRQLYQDIFDWAGQLREVDIYQGDTPFCHFAYIEKEGNALMQDLEEEGYLVGLEKAKFVERLAHYYCEINVLHPFRVGSGLAQRIFFEQLAIHAGYQLSWQGIEKEAWNQANQSGAMGDLTALQMIFSKVVSEAGESE	MGSSHHHHHHSQDPNSSSARLQVEMGDKFGEGRDPYLYPGLDIMRNRLNIHQQQRLEQAAYEMTALRAATIELGPLVRGLPHLRTIHRQLYQDIFDWAGQLREVDIYQGDTPFCHFAYIEKEGNALMQDLEEEGYLVGLEKAKFVERLAHYYCEINVLHPFRVGSGLAQRIFFEQLAIHAGYQLSWQGIEKEAWNQANQSGAMGDLTALQMIFSKVVSEAGESE
Complete amino acid sequence of EcFicA[§]	MAYPYDVPDYAAAVKKLTDKQKSRLWELQRNRNFQASRRLEGVEMPLVTLTAAEALARLEELRSHYER	MAYPYDVPDYAAAVKKLTDKQKSRLWELQRNRNFQASRRL**G**GVEMPLVTLTAAEALARLEELRSHYER

[§] Mutations are bold and underlined.

Table 2

Crystallization

	$EcFicT_{G55R}$/EcFicA	**EcFicT/$EcFicA_{E28G}$**
Method	Sitting-drop vapour diffusion	Sitting-drop vapour diffusion
Plate type	Art Robbins Intelli-Plate® 96 well	Art Robbins Intelli-Plate® 96 well
Temperature (K)	293.15	293.15

Protein concentration	25 mg/mL	28 mg/mL
Buffer composition of protein solution	10 mM Tris pH 7.8, 100 mM NaCl	10 mM Tris pH 7.8, 100 mM NaCl
Composition of reservoir solution	0.2 M $MgCl_2$, 0.1 M Tris pH 8.0, 20% (w/v) PEG 6000	19% PEG 1500 (w/v), 0.1 M MMT (malic acid, MES, Tris) buffer pH 6.0
Volume and ratio of drop	1:1	1:1
Volume of reservoir	80 μL	80 μL

Table 3

Data collection and processing

	$EcFicT_{G55R}$/EcFicA	**EcFicT/$EcFicA_{E28G}$**
Diffraction source	SLS X06DA (PXIII)	SLS X06SA (PXI)
Wavelength (Å)	0.9999	1.0000
Temperature (K)	100	100
Detector	Pilatus 2M	Pilatus 6M
Crystal-detector distance (mm)	250	380
Rotation range per image (°)	0.25	0.25
Total rotation range (°)	180	360
Exposure time per image (s)	0.25	0.1
Space group	P 6_5	I 1 2 1
a, *b*, *c* (Å)	104.7, 104.7, 110.5	87.9, 64.4, 143.9
α, β, γ (°)	90.0, 90.0, 120.0	90.0, 100.2, 90.0
Mosaicity (°)	0.14	0.25
Matthews coefficient ($Å^3.Da^{-1}$)	3.1	2.5
Solvent content (%)	60.5	50.9
Resolution range (Å)	90.66 - 2.00 (2.07 - 2.00)	80.41 - 2.40 (2.49 - 2.40)
Total No. of reflections	472’112 (43’939)	208’089 (17’030)
No. of unique reflections	46’196 (4’553)	30’840 (2’735)
Completeness (%)	99.7 (98.7)	98.9 (88.6)
Redundancy	10.2 (9.7)	6.7 (6.2)
$\langle I/\sigma(I)\rangle$	22.7 (2.9)	9.40 (2.07)
R_{meas}‡	10.3	18.7
R_{merge}†	9.7 (86.5)	16.3 (66.0)
CC 1/2	99.9 (83.2)	97.5 (75.9)
Overall *B* factor from Wilson plot ($Å^2$)	24.01	36.42

Values for the outer shell are given in parentheses. ‡ $R_{meas} = \sum_{hkl}[N/(N-1)]^{1/2}\sum_i|I_i(hkl) - \langle I(hkl)\rangle| / \sum_{hkl}\sum_i I_i(hkl)$, where $I_i(hkl)$ is the observed intensity for a reflection, $\langle I(hkl)\rangle$ is the average intensity obtained from multiple observations of symmetry-related reflections and N is the number of observations of intensity I(hkl). † $R_{merge} = \sum_{hkl}\sum_i|I_i(hkl) - \langle I(hkl)\rangle| / \sum_{hkl}\sum_i I_i(hkl)$, where $I_i(hkl)$ is the observed intensity for a reflection and $\langle I(hkl)\rangle$ is the average intensity obtained from multiple observations of symmetry-related reflections.

Table 4

Structure refinement

	$EcFicT_{G55R}$/EcFicA	**EcFicT/$EcFicA_{E28G}$**
Resolution range (Å)	90.66 - 2.0 (2.073 - 2.001)	80.41 - 2.4 (2.486 - 2.4)
Completeness (%)	99.74 (98.70)	98.87 (88.65)
No. of reflections, working set	44197	30840
No. of reflections, test set	2001	1561
Final R_{cryst}* (%)	17.75 (23.40)	21.48 (23.19)
Final R_{free}** (%)	20.40 (28.73)	27.51 (30.03)
No. of non-H atoms	4294	5556

Protein	3887	5393
Ion	6	0
Ligand	0	0
Water	401	163
Total	478	686
R.m.s. deviations		
Bonds (Å)	0.019	0.013
Angles (°)	1.73	1.50
Average *B* factors (Å^2)	30.20	37.80
Protein	29.60	37.90
Ion	40.50	
Ligand		
Water	35.70	34.20
Ramachandran plot		
Favoured regions*** (%)	99.37	98.65
Additionally allowed*** (%)	0.63	1.20
Outliers*** (%)	0.00	0.15
Clashscore***	3.12	3.11

Values for the outer shell are given in parentheses. * $R_{cryst} = \sum_{hkl}|| F_{obs}| - |F_{calc}|| / \sum_{hkl}|F_{obs}|$. ** R_{free} is the R value calculated for 5% of the data set that was not included in the refinement. *** Molprobity (Chen et al., 2010).

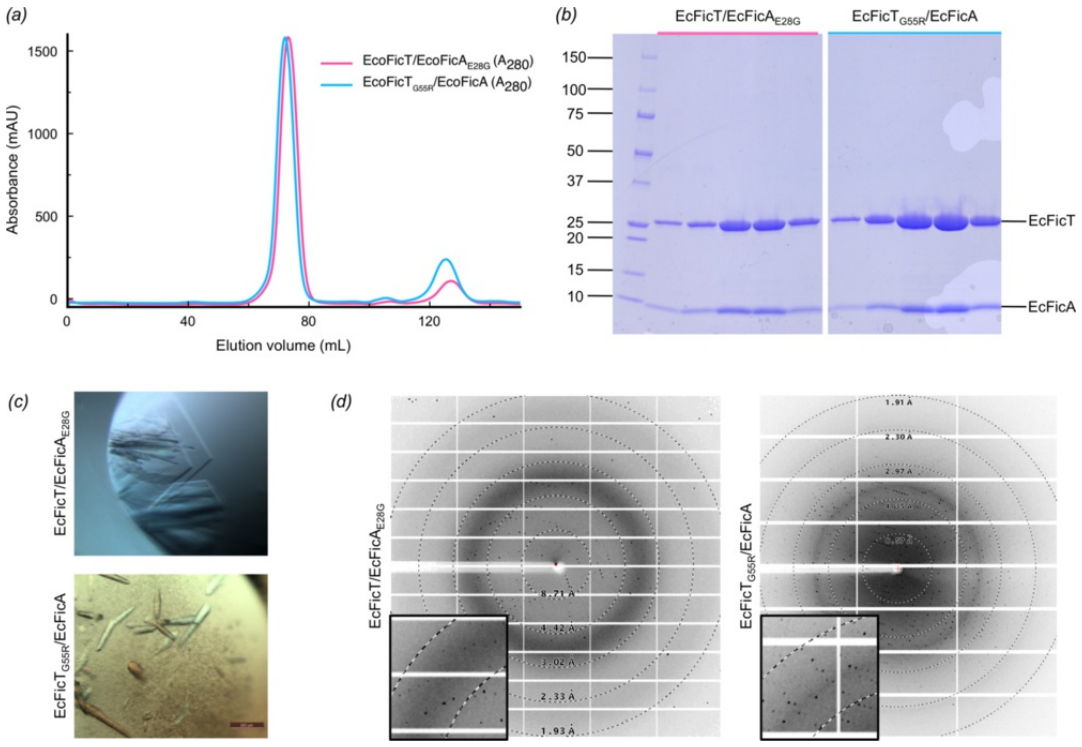

Figure 1

Purification, crystallization of EcFicT/EcFicA complexes and data collection. (a) Size exclusion chromatography (SEC) analysis of EcFicT/EcFicA complexes reveals a 1:1 EcFicT:EcFicA complex in solution (EcFicT/EcFicA$_{E28G}$ in pink and EcFicT$_{G55R}$/EcFicA in blue). (b) SDS-PAGE analysis of the SEC samples. (c) Crystals obtained for both complexes. Despite the poor apparent quality of the crystals, the latter diffracted to 2.4 Å and 2.0 Å. (d) Diffraction pattern of both crystal forms reveal low mosaicity and isomorphic diffraction.

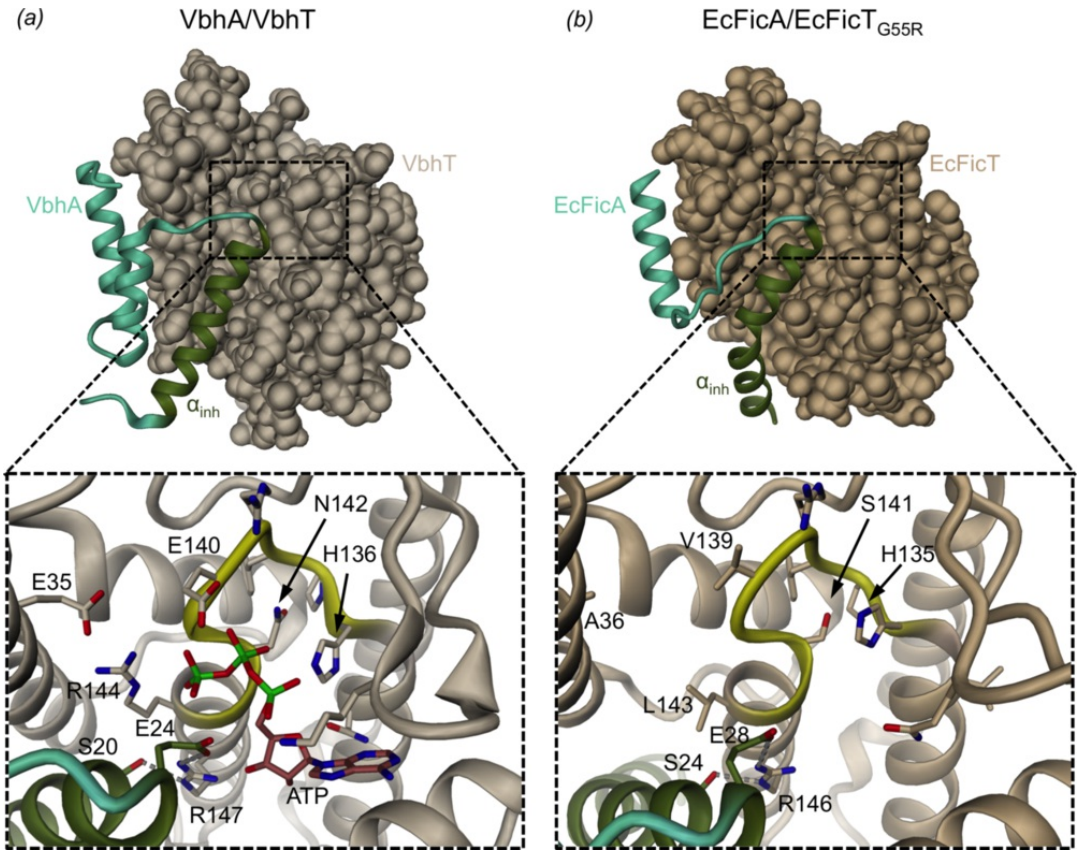

Figure 2

Structural comparison of (a) VbhT/VbhA (PDB: 3ZC7) and (b) EcFicT$_{G55R}$/EcFicA protein complexes. VbhT and EcFicT are displayed as solvent accessible surface representation whereas VbhA and EcFicA are shown as aquamarine ribbon, except the α_{inh} helix in dark green. In the close-up view of the active site, the active site loop is shown in yellow and crucial residues are depicted as sticks. Additionally, H-bonds are shown as dashed gray lines between the last arginine of the Fic active site motif and the serine and glutamate of the inhibition motif.

1.png

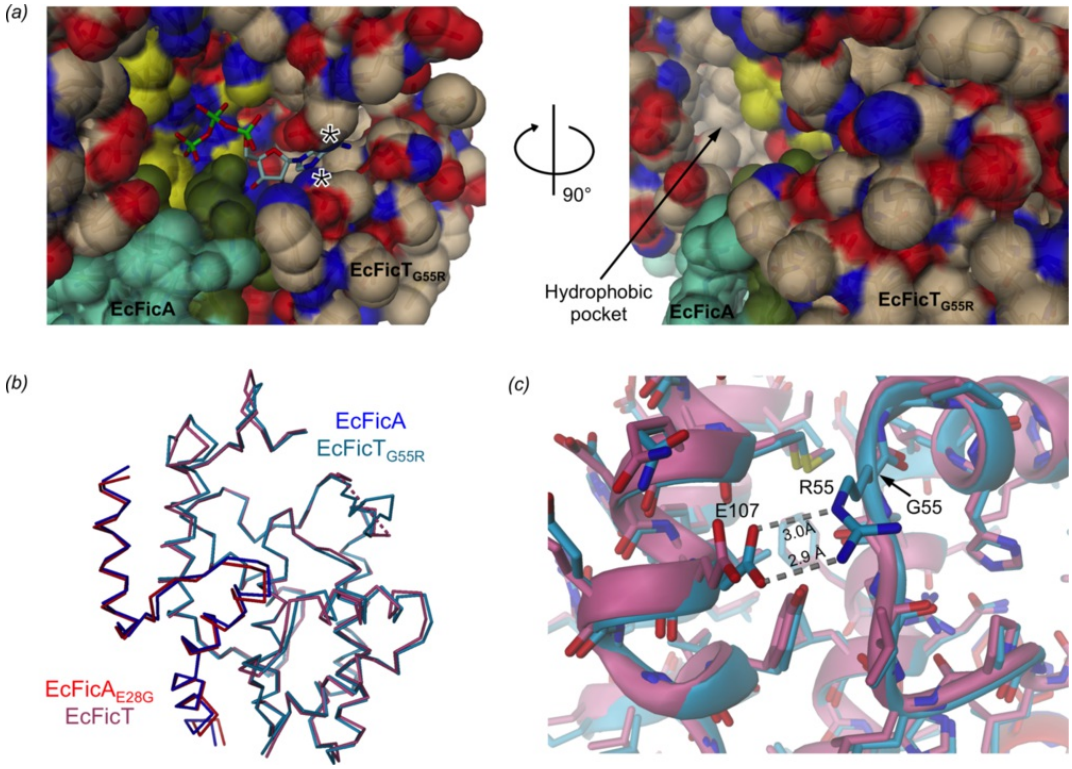

Figure 3

Structural analysis of EcFicT/EcFicA complexes. (a) Modelling of ATP binding (from the VbhT/VbhA complex, PDB: 3ZC7) (Goepfert et al., 2013) in the binding site of EcFicT$_{G55R}$/EcFicA. Steric hindrance are observed between ATP and the adenine-binding pocket, where clashes between the adenine ring and Q84 or N171 are indicated by black stars (left). A rotation of 90° reveals a hydrophobic pocket located on the C-terminal side of the active site loop (right). (a-b) Solvent accessible surface representation of EcFicT/EcFicA, with EcFicA in the same colour as in Fig. 2. EcFicT is shown in beige, except positively and negatively charged atoms that are depicted in blue and red, respectively. (c) Superimposition of EcFicT/EcFicA$_{E28G}$ and EcFicT$_{G55R}$/EcFicA reveals a well-conserved Cα trace (rmsd: 0.513 Å). (d) Details of the salt-bridge formed between residues R55 and E107 in the EcFicT$_{G55R}$/EcFicA complex.

Acknowledgements

We thank Arnaud Goepfert for critical reading of the manuscript. We thank the staff of beam-lines X06DA and X06SA of the Swiss Light Source (Villigen, Switzerland) for their excellent support. This work was supported by ERC Advanced Grant FICModFun 340330 (to CD) and SNF grants 3100-132979 (to CD) and 31003A_138414 (to TS).

References

Adams, P. D., Afonine, P. V., Bunkóczi, G., Chen, V. B., Davis, I. W., Echols, N., Headd, J. J., Hung, L.-W., Kapral, G. J., Grosse-Kunstleve, R. W., et al. (2010). *Acta Crystallogr D Biol Crystallogr*. **66**, 213–221.

242 Campanacci, V., Mukherjee, S., Roy, C. R., & Cherfils, J. (2013). *Embo J*.

243 Castro-Roa, D., Gieter, S. D., Nuland, N. A. J. V., Loris, R., Garcia-Pino, A., & Zenkin, N. (2013). *Nat Chem Biol*. 1–9.

244 Chen, V. B., Arendall, W. B., Headd, J. J., Keedy, D. A., Immormino, R. M., Kapral, G. J., Murray, L. W., Richardson, J.
245 S., & Richardson, D. C. (2010). *Acta Crystallogr D Biol Crystallogr*. **66**, 12–21.

246 Cruz, J. W., Rothenbacher, F. P., Maehigashi, T., Lane, W. S., Dunham, C. M., & Woychik, N. A. (2014). *J Biol Chem*.
247 **289**, 7788–7798.

248 Emsley, P., Lohkamp, B., Scott, W. G., & Cowtan, K. (2010). *Acta Crystallogr D Biol Crystallogr*. **66**, 486–501.

249 Engel, P., Goepfert, A., Stanger, F. V., Harms, A., Schmidt, A., Schirmer, T., & Dehio, C. (2012). *Nature*. **482**, 107–110.

250 Evans, P. (2006). *Acta Crystallogr D Biol Crystallogr*. **62**, 72–82.

251 Evans, P. R. & Murshudov, G. N. (2013). *Acta Crystallogr D Biol Crystallogr*. **69**, 1204–1214.

252 Goepfert, A., Harms, A., Schirmer, T., & Dehio, C. (2012). *Prokaryotic Toxin-Antitoxins*, pp. 177–187. Berlin,
253 Heidelberg: Springer Berlin Heidelberg.

254 Goepfert, A., Stanger, F. V., Dehio, C., & Schirmer, T. (2013). *PLoS ONE*. **8**, e64901.

255 Kabsch, W. (2010). *Acta Crystallogr D Biol Crystallogr*. **66**, 125–132.

256 Kawamukai, M., Matsuda, H., Fujii, W., Nishida, T., Izumoto, Y., Himeno, M., Utsumi, R., & Komano, T. (1988). *J*
257 *Bacteriol*. **170**, 3864–3869.

258 Kawamukai, M., Matsuda, H., Fujii, W., Utsumi, R., & Komano, T. (1989). *J Bacteriol*. **171**, 4525–4529.

259 Komano, T., Utsumi, R., & Kawamukai, M. (1991). *Res Microbiol*. **142**, 269–277.

260 Lee, C. C., Wood, M. D., Ng, K., Andersen, C. B., Liu, Y., Luginbühl, P., Spraggon, G., & Katagiri, F. (2004). *Structure*.
261 **12**, 487–494.

262 Matthews, B. W. (1968). *J Mol Biol*. **33**, 491–497.

263 McCoy, A. J., Grosse-Kunstleve, R. W., Adams, P. D., Winn, M. D., Storoni, L. C., & Read, R. J. (2007). *J Appl*
264 *Crystallogr*. **40**, 658–674.

265 Mukherjee, S., Liu, X., Arasaki, K., McDonough, J., Galán, J. E., & Roy, C. R. (2011). *Nature*. **477**, 103–106.

266 Murshudov, G. N., Skubák, P., Lebedev, A. A., Pannu, N. S., Steiner, R. A., Nicholls, R. A., Winn, M. D., Long, F., &
267 Vagin, A. A. (2011). *Acta Crystallogr D Biol Crystallogr*. **67**, 355–367.

268 Utsumi, R., Nakamoto, Y., Kawamukai, M., Himeno, M., & Komano, T. (1982). *J Bacteriol*. **151**, 807–812.

269 Winn, M. D., Ballard, C. C., Cowtan, K. D., Dodson, E. J., Emsley, P., Evans, P. R., Keegan, R. M., Krissinel, E. B.,
270 Leslie, A. G. W., McCoy, A., et al. (2011). *Acta Crystallogr D Biol Crystallogr*. **67**, 235–242.

271 Woolery, A., Luong, P., & Broberg, C. (2010). *Frontiers in Microbiology*. **1**, 3131–3137.

272 Worby, C. A., Mattoo, S., Kruger, R. P., Corbeil, L. B., Koller, A., Mendez, J. C., Zekarias, B., Lazar, C., & Dixon, J. E.
273 (2009). *Molecular Cell*. **34**, 93–103.

274 Xiao, J., Worby, C. A., Mattoo, S., Sankaran, B., & Dixon, J. E. (2010). *Nat Struct Mol Biol*. **17**, 1004–1010.

275 Yarbrough, M. L. & Orth, K. (2009). *Nat Chem Biol*. **5**, 378–379.

276 Zwart, P. H., Afonine, P. V., Grosse-Kunstleve, R. W., Hung, L.-W., Ioerger, T. R., McCoy, A. J., McKee, E., Moriarty, N.
277 W., Read, R. J., Sacchettini, J. C., et al. (2008). *Methods Mol Biol*. **426**, 419–435.

Concluding remarks

4. Concluding remarks

4.1. Regulation of Fic proteins

Adenylylation is tightly regulated in Fic proteins. The presence of an α'-helix that is located either at the N-terminus or C-terminus compared to the Fic active site had been first mentioned by Kinch *et al*[79] in a structure comparison. In section 3.1., *research article I*, we showed that this α-helix, named α_{inh}, can also be found as part of a separate protein, exemplified by the VbhT/VbhA complex.

4.1.1. The crucial role of the alpha inhibitory helix (α_{inh})

The α_{inh} helix (described in detail in section 3.1., *research article I* and section 3.2., *research article II*) can be found on a separate small protein that forms a tight complex with the Fic protein, or at the N-terminus or C-terminus to the Fic active site within the same polypeptide chain, resulting in the classification of Fic proteins into class I, II and III. The α_{inh} helix acts in all three classes of Fic proteins via a conserved mechanism of active site obstruction. The helix contains an inhibition motif [S/T]xxxE[G/N], with the strictly conserved glutamate playing a key role by competing with the γ-phosphate binding sub-site. In the three classes of Fic proteins, the truncation of the conserved glutamate allows the substrate to bind in the active site in a conformation competent for the transfer of AMP onto a target protein. In turn, when the active site is obstructed by the inhibition motif, the substrate can still bind but is forced into a conformation in which the nucleophilic attack by the deprotonated hydroxyl group from the target side chain is impossible.

Interestingly, Fic proteins target eukaryotic as well as prokaryotic proteins. It has first been revealed that VopS from *Vibrio parahaemolyticus* or IbpA from *Histophilus somni* targets Rho GTPases. We have later shown that the Fic proteins VbhT from *Bartonella schoenbuchensis* and NmFic from *Neisseria meningitidis* target bacterial proteins, which lead to a growth defect phenotype upon expression of the inhibition-relief mutant of these respective proteins (section 3.1., *research article I*). ParE of the topoIV complex and GyrB of the DNA gyrase complex have been identified as bacterial targets of the class I Fic protein VbhT (section 3.3., *research article III*). Interestingly, the class III Fic protein NmFic exclusively targets GyrB (section 3.5., *research article V*).

For class I Fic proteins (VbhT/VbhA), dissociation of the toxin-antitoxin complex allows the relief of inhibition (*research article I*). In section 3.3., *research article III*, we show that the Fic toxin-antitoxin system VbhTA, amongst others, promotes bacterial persister formation *via* a novel physiological pathway involving inhibition of both type IIA topoisomerases with concomitant collapse of DNA topology. For the class III Fic protein NmFic, an intramolecular conformational change resulting in loosening of the interactions between the α_{inh} helix and the Fic core is needed to relieve the inhibition. In section 3.5., *research article V*, we show that the class III Fic protein NmFic is regulated by a double-lock mechanism, *via* oligomerization and auto-adenylylation.

4.1.2. The unexpected role of the oligomeric state

The oligomerization of Fic proteins had so far only been described for the Class II Fic protein SoFic from *Shewanella oneidensis* that contains a C-terminal winged-helix DNA binding domain[77]. SoFic forms a dimer that brings the two helix-turn-helix (HTH) domains in suitable distance for DNA binding[77]. This dimerization and DNA binding may be part of the regulation mechanism of this class II Fic protein, part of the largest sequence cluster of Fic proteins, but further investigations are required to confirm the putative role of the HTH domain or dimerization.

The class III Fic protein NmFic belongs to the smallest class of Fic protein in terms of sequences, but these sequences are scattered through α- to ε-proteobacteria, resulting from horizontal gene transfer. NmFic undergoes a fast monomer-tetramer equilibrium on the time-scale of size exclusion chromatography experiments. The crystal structure of NmFic reveals a tetramer in which the active site and target-binding site (FLAP, β-hairpin) are located towards the center of the tetramer with 222 symmetry. In this form, target binding is impossible due to steric hindrance. The 222 tetramer can be described as a dimer of dimers. Strikingly, mutation of residues located at the dimerization interface that disrupts the interface results in a growth defect of *E. coli* that expresses these mutants. In the monomeric state, the active site and target binding site are accessible.

Oligomerization of NmFic acts as a sponge (buffer) that stores the active species, i.e. the monomers, within the tetramer where the active and target binding sites are not available for the adenylylation of a target protein. This elegant way of neutralizing the toxic protein was unexpected and deciphered by structure-function analysis of NmFic. The de-oligomerization,

i.e. monomerization of NmFic is necessary but not sufficient for the activity of NmFic. A second level of control of NmFic requires the auto-adenylylation of a conserved residue located on the α_{inh} helix, tyrosine 183.

4.1.3. Auto-adenylylation as a new player

Auto-modification of Fic proteins has been observed since the first study revealing the catalytic role of these enzymes[66] and subsequently for all Fic proteins that have been described to date (see section 1.5.2. and section 3.4., *research article IV*). It has been used as a convenient target-independent read-out for Fic protein activity that allowed investigating the role of the Fic active site residues[80] and to reveal the inhibition mechanism of Fic proteins[170,175]. Auto-adenylylation, i.e. the transfer of an AMP moiety onto the Fic protein itself, is similar to the auto-phosphorylation process of kinases[176]. The well-described auto-phosphorylation mechanism can occur intramolecularly (*in cis*) or intermolecularly (*in trans*). The occurrence of auto-modification in Fic proteins stimulated speculative discussion about its role as a putative transient intermediate[82,100], about a nonspecific reaction or whether auto-adenylylation has functional consequences[80]. The transient intermediate that would be supported by a ping-pong mechanism has been first disproven by Luong *et al.*,[82], showing that VopS forms a ternary complex with ATP and the target and that direct AMP transfer occurs on the target.

We investigated the role of auto-adenylylation using our class III model protein NmFic from *Neisseria meningitidis*. NmFic has been shown to be auto-adenylylated on tyrosine Y183 and tyrosine Y188, located within the inhibition motif (section 3.1., *research article I*). As described in section 3.4., *research article IV*, tyrosine Y183 is buried in the core of the Fic protein and strictly conserved in class III Fic proteins. Tyrosine Y188 is exposed to the solvent. Mutation of the conserved tyrosine Y183 abolishes the growth defect induced by the active Fic proteins without perturbation of the fold and without conformational change. Investigation of the structural effect of auto-adenylylation of NmFic by NMR revealed that upon auto-adenylylation, the helices 1 and 8 (α_{inh}) are perturbed.

Auto-adenylylation is likely the intrinsic factor that plays a key role in the relief of inhibition of auto-inhibited Fic proteins. Auto-adenylylation of the alpha-inhibitory helix (α_{inh}) of NmFic (class III) likely expulses this α_{inh}, resulting in a free gamma-phosphate

binding site that allows competent ATP binding in the Fic active site and efficient AMP transfer.

4.2. Fic proteins preferentially recognize NTPases

4.2.1. Adenylylation of GTPases disrupts effector binding

Fic-mediated adenylylation has originally been described as a modification of the small GTPases Rho, Rac and Cdc42[66,75]. This modification occurs in the switch I region of the target. Fic-mediated phosphocholination of Rab proteins occurs in the switch II region of these GTPases[52]. Recently, it has been shown that Doc is a kinase that phosphorylates the translation elongation factor EF-Tu at the C-terminus of this GTPase[97,98]. Adenylylation of GTPases by IbpA or VopS results in collapse of the actin cytoskeleton and cell death. The addition of a bulky group on the Y32 or Rac and Cdc42 or Y34 or RhoA of the switch I region inhibits the interactions with downstream effectors, leading to the phenotype described above.

4.2.2. Adenylylation of bacterial DNA gyrase blocks the ATPase activity of GyrB

We have recently identified a new class of enzymes as Fic targets. The bacterial topoisomerases GyrB and ParE from the DNA gyrase complex and topo IV complex respectively are adenylylated by Fic proteins (section 3.3., *research article III* and section 3.5., *research article V*). The adenylylation occurs in the N-terminal part of GyrB and ParE, within the ATPase domain. The adenylylated residue (Y109 of GyrB and Y105 of ParE) is part of a flexible loop, called the ATP-lid loop that appears to be expulsed from the ligand-binding site upon binding of competitive inhibitors such as novobiocin (section 1.7.7.). Interestingly, also upon adenylylation, the ATP-lid loop of GyrB is distorted from its original position, being expulsed from the active site (section 3.6.1.) but adopting a different conformation than upon novobiocin binding. We have also shown that adenylylation of GyrB abolishes the catalytic activity of the ATPase domain of GyrB, i.e. ATP hydrolysis (section 3.3., *research article III*) but not the binding of ATP to the GyrB active site. ATP hydrolysis is required for DNA gyrase activity, since this molecular nanomachine introduces negative supercoils into covalently closed double-stranded DNA molecules using the free energy generated by ATP hydrolysis.

In the context of the DNA gyrase mechanism, the structural consequences of ATP hydrolysis were not yet understood by the community. As a brief aside, in a context unrelated to Fic-mediated adenylylation, I contributed to the understanding of the ATP hydrolysis mechanism in GyrB by crystallizing all nucleotide bound complexes along the ATP hydrolysis pathway (section 3.4., *research article IV*). GyrB undergoes an obligatory rigid body motion upon ATP hydrolysis, i.e. when going from the substrate complex to the immediate post-hydrolysis products ADP and P_i. This conformational change corresponds to an opening of the N-gate hole and it is well conceivable that the free energy generated by ATP hydrolysis may be used to actively push the T-segment through the DNA gate.

GyrB adenylylation may then lock the gyrase in a closed conformation by inhibiting ATP hydrolysis. The unidirectionality of the T-segment would then be inhibited. Further experimental evidences are required to prove this tempting hypothesis. To further characterize the adenylylation of topoisomerases by Fic proteins, crystallization of a Fic/topoisomerase complex is of central interest. Extensive crystallization trials using different strategies have been tested (section 3.6.3.) without success so far. Nevertheless, the latest strategy using a cross-link of the modified target and the Fic protein *via* the ribose of the transferred AMP and a Fic active site residue seems very promising. For the first time, we were able to observe a complex *in vitro*. We suspect the adenylylation reaction to be a "kiss and run" reaction, in which the modified target gets released from the Fic protein quickly after the modification occurs.

4.2.3. Do Fic proteins target other families of proteins?

ATPase and GTPase, apart from their common catalytic activity of nucleotide hydrolysis, differ in fold or sequence identity. It cannot be excluded that Fic proteins also target unrelated proteins. For example, it has been shown recently that Bep2 from *B. rochalimae* targets tubulin which is a P-loop GTPase (K. Pieles, *PhD thesis*, 2013)[112] but also targets vimentin[99]. Vimentin contains neither a GTPase fold nor an ATPase fold and the adenylylation of tubulin occurs distantly from the P-loop.

Further investigations are required to find new targets of Fic proteins by combining our knowledge on Fic proteins and substrate binding, i.e. that it is highly likely that Fic proteins transfer a phosphate-containing group probably attached to a sugar and most likely requires a substrate that contains an energy-rich phosphodiester bond (see Appendix 8.3. for a

comprehensive list of diphosphate-containing molecules from *E. coli*). This strategy can be tested on the *E. coli* EcFicT protein, where we know that a hydrophobic pocket is in the vicinity of the Fic active motif. Neither the target nor the modification catalyzed by this Fic protein, if any, is known (section 3.7., *research article VI*).

4.3. Is there a common scheme in Fic-mediated target inhibition?

Adenylylation of small GTPases by VopS[66] or IbpA[75] blocks the binding to downstream effectors that lead to cell death[177]. Phosphocholination of Rab1 by the *Legionella* effector AnkX blocks the GTPase in the GTP bound state, which traps Rab1 at the membrane, where the bacterium resides during infection[178]. Phosphorylation of EF-Tu by Doc from the Bacteriophage P1 leads to an inefficient translation elongation that brings the cell to a dormant state[97]. The adenylylation of topoisomerases by Fic proteins that had been recently deciphered (section 3.3., *research article III*) results in bacteriostasis, promoting persister formation. We could show that the ATPase activity of GyrB is impaired by the adenylylation of Y109 in the ATP-lid loop (section 3.6.). A recent hypothesis (K. Pieles, *PhD thesis*, 2013)[112] proposed that adenylylation of tubulin by Bep2 from *B. rochalimae* may strengthen the interaction between tubulin and TOG, a protein required for fast microtubule growth[115]. This may also impede cell viability or promote bacterial infection and needs to be investigated further.

Further investigations are required to understand the mechanism of target inhibition. By combining *in vivo* investigation with biochemical analysis and X-ray crystallography, we can aim to understand and dissect the specificity of recognition of Fic proteins with their cognate targets. The method developed in section 3.6.2.3., which uses covalent complex formation *via* a functionalized ATP molecule is very promising and may be used not only for the co-crystallization of VbhT from *B. schoenbuchensis* or NmFic from *N. meningitidis* with bacterial topoisomerases but also for any other Fic proteins with known targets, like Bep1 from *B. rochalimae* that specifically adenylylates Rac1[109].

As a general feature, FIC domain proteins investigated to date block the biological activity of their target, either by inhibiting downstream effector binding, by blocking the enzymatic activity of the target protein or maybe even by blocking the release of the target protein from partner binding.

References

5. References

1. Mattoo, S., Lee, Y. M. & Dixon, J. E. Interactions of bacterial effector proteins with host proteins. Current Opinion in Immunology 19, 392–401 (2007).
2. Backert, S., Tegtmeyer, N. & Selbach, M. The versatility of Helicobacter pylori CagA effector protein functions: The master key hypothesis. Helicobacter 15, 163–176 (2010).
3. Hubber, A. & Roy, C. R. Modulation of host cell function by Legionella pneumophila type IV effectors. Annu. Rev. Cell Dev. Biol. 26, 261–283 (2010).
4. Page, A.-L. & Parsot, C. Chaperones of the type III secretion pathway: jacks of all trades. Mol Microbiol 46, 1–11 (2002).
5. Pawel-Rammingen, Von, U. et al. GAP activity of the Yersinia YopE cytotoxin specifically targets the Rho pathway: a mechanism for disruption of actin microfilament structure. Mol Microbiol 36, 737–748 (2000).
6. Stebbins, C. E. & Galán, J. E. Structural mimicry in bacterial virulence. Nature 412, 701–705 (2001).
7. Galán, J. E. Common themes in the design and function of bacterial effectors. Cell Host Microbe 5, 571–579 (2009).
8. Galán, J. E. & Collmer, A. Type III secretion machines: bacterial devices for protein delivery into host cells. Science 284, 1322–1328 (1999).
9. Freche, B., Reig, N. & van der Goot, F. G. The role of the inflammasome in cellular responses to toxins and bacterial effectors. Semin Immunopathol 29, 249–260 (2007).
10. Abby, S. S.Eduardo P. C. Rocha. The Non-Flagellar Type III Secretion System Evolved from the Bacterial Flagellum and Diversified into Host-Cell Adapted Systems. PLoS Genet 8, e1002983 (2012).
11. Cornelis, G. R. The type III secretion injectisome, a complex nanomachine for intracellular 'toxin' delivery. Biol. Chem. 391, 745–751 (2010).
12. Frank, A. C., Alsmark, C. M., Thollesson, M. & Andersson, S. Functional divergence and horizontal transfer of type IV secretion systems. Mol. Biol. Evol. 22, 1325–1336 (2005).
13. Cascales, E. & Christie, P. J. The versatile bacterial type IV secretion systems. Nat Rev Microbiol 1, 137–149 (2003).
14. Low, H. H. et al. Structure of a type IV secretion system. Nature 508, 550–553 (2014).
15. Toft, C. & Andersson, S. G. E. Evolutionary microbial genomics: insights into bacterial host adaptation. Nat. Rev. Genet. 11, 465–475 (2010).
16. Wang, X. & Wood, T. K. Toxin/Antitoxin Systems Influence Biofilm and Persister Cell Formation and the General Stress Response. Applied and environmental microbiology (2011).
17. Yamaguchi, Y., Park, J.-H. & Inouye, M. Toxin-antitoxin systems in bacteria and archaea. Annu Rev Genet 45, 61–79 (2011).
18. Magnuson, R. D. Hypothetical functions of toxin-antitoxin systems. J Bacteriol 189, 6089–6092 (2007).

19. Collier, R. J. & Cole, H. A. Diphtheria toxin subunit active in vitro. Science 164, 1179–1181 (1969).

20. Salomon, D. & Orth, K. Lost after translation: post-translational modifications by bacterial type III effectors. Curr Opin Microbiol 16, 213–220 (2013).

21. Ribet, D. & Cossart, P. Pathogen-mediated posttranslational modifications: A re-emerging field. Cell 143, 694–702 (2010).

22. Ribet, D. & Cossart, P. Post-translational modifications in host cells during bacterial infection. FEBS Lett 584, 2748–2758 (2010).

23. Hultquist, D. E. The preparation and characterization of phosphorylated derivatives of histidine. Biochim Biophys Acta 153, 329–340 (1968).

24. Attwood, P. V., Piggott, M. J., Zu, X. L. & Besant, P. G. Focus on phosphohistidine. Amino Acids 32, 145–156 (2007).

25. Duclos, B., Marcandier, S. & Cozzone, A. J. Chemical properties and separation of phosphoamino acids by thin-layer chromatography and/or electrophoresis. Methods in enzymology 201, 10–21 (1991).

26. Matthews, H. R. Protein kinases and phosphatases that act on histidine, lysine, or arginine residues in eukaryotic proteins: a possible regulator of the mitogen-activated protein kinase cascade. Pharmacol. Ther. 67, 323–350 (1995).

27. BURNETT, G. & KENNEDY, E. P. The enzymatic phosphorylation of proteins. J Biol Chem 211, 969–980 (1954).

28. Wiley, D. J. et al. The Ser/Thr kinase activity of the Yersinia protein kinase A (YpkA) is necessary for full virulence in the mouse, mollifying phagocytes, and disrupting the eukaryotic cytoskeleton. Microb Pathog 40, 234–243 (2006).

29. Canova, M. J. & Molle, V. Bacterial serine/threonine protein kinases in host-pathogen interactions. J Biol Chem 289, 9473–9479 (2014).

30. Viboud, G. I. & Bliska, J. B. Yersinia outer proteins: role in modulation of host cell signaling responses and pathogenesis. Annu. Rev. Microbiol. 59, 69–89 (2005).

31. Humphreys, D., Hume, P. J. & Koronakis, V. The Salmonella effector SptP dephosphorylates host AAA+ ATPase VCP to promote development of its intracellular replicative niche. Cell Host Microbe 5, 225–233 (2009).

32. Mukherjee, S. et al. Yersinia YopJ acetylates and inhibits kinase activation by blocking phosphorylation. Science 312, 1211–1214 (2006).

33. Trosky, J. E. et al. VopA inhibits ATP binding by acetylating the catalytic loop of MAPK kinases. J Biol Chem 282, 34299–34305 (2007).

34. Hamon, M. A. et al. Histone modifications induced by a family of bacterial toxins. Proc Natl Acad Sci USA 104, 13467–13472 (2007).

35. Corda, D. & Di Girolamo, M. Functional aspects of protein mono-ADP-ribosylation. EMBO J 22, 1953–1958 (2003).

36. Mashimo, M., Kato, J. & Moss, J. Structure and function of the ARH family of ADP-ribosyl-acceptor hydrolases. DNA Repair (Amst) (2014).

37. Takada, T., Okazaki, I. J. & Moss, J. ADP-ribosylarginine hydrolases. Mol. Cell. Biochem. 138, 119–122 (1994).

38. Müller, M. P. et al. The Legionella effector protein DrrA AMPylates the membrane

traffic regulator Rab1b. Science 329, 946–949 (2010).

39. Xu, Y., Carr, P. D., Vasudevan, S. G. & Ollis, D. L. Structure of the adenylylation domain of E. coli glutamine synthetase adenylyl transferase: evidence for gene duplication and evolution of a new active site. J Mol Biol 396, 773–784 (2010).

40. Just, I. et al. Glucosylation of Rho proteins by Clostridium difficile toxin B. Nature 375, 500–503 (1995).

41. Belyi, Y., Tabakova, I., Stahl, M. & Aktories, K. Lgt: a family of cytotoxic glucosyltransferases produced by Legionella pneumophila. J Bacteriol 190, 3026–3035 (2008).

42. Li, H. et al. The phosphothreonine lyase activity of a bacterial type III effector family. Science 315, 1000–1003 (2007).

43. Brennan, D. F. & Barford, D. Eliminylation: a post-translational modification catalyzed by phosphothreonine lyases. Trends in Biochemical Sciences 34, 108–114 (2009).

44. Rogers, L. D. & Overall, C. M. Proteolytic post-translational modification of proteins: proteomic tools and methodology. Mol. Cell Proteomics 12, 3532–3542 (2013).

45. Shao, F. et al. Biochemical characterization of the Yersinia YopT protease: cleavage site and recognition elements in Rho GTPases. Proc Natl Acad Sci USA 100, 904–909 (2003).

46. Shao, F., Merritt, P. M., Bao, Z. Q., Innes, R. W. & Dixon, J. E. A Yersinia effector and a pseudomonas avirulence protein define a family of cysteine proteases functioning in bacterial pathogenesis. Cell 109, 575–588 (2002).

47. Rosebrock, T. R. et al. A bacterial E3 ubiquitin ligase targets a host protein kinase to disrupt plant immunity. Nature 448, 370–374 (2007).

48. Piscatelli, H. et al. The EHEC type III effector NleL is an E3 ubiquitin ligase that modulates pedestal formation. PLoS ONE 6, e19331 (2011).

49. Canonne, J. et al. The Xanthomonas Type III Effector XopD Targets the Arabidopsis Transcription Factor MYB30 to Suppress Plant Defense. Plant Cell 23, 3498–3511 (2011).

50. Mishra, S. et al. Cloning, Expression, Purification, and Biochemical Characterisation of the FIC Motif Containing Protein of Mycobacterium tuberculosis. Protein Expr Purif (2012).

51. Feng, F. et al. A Xanthomonas uridine 5′-monophosphate transferase inhibits plant immune kinases. Nature 485, 114–118 (2012).

52. Mukherjee, S. et al. Modulation of Rab GTPase function by a protein phosphocholine transferase. Nature 477, 103–106 (2011).

53. Stadtman, E. R. The story of glutamine synthetase regulation. J. Biol. Chem. 276, 44357–44364 (2001).

54. Itzen, A., Blankenfeldt, W. & Goody, R. S. Adenylylation: renaissance of a forgotten post-translational modification. Trends in Biochemical Sciences 1–8 (2011).

55. Schmelz, S. & Naismith, J. H. Adenylate-forming enzymes. Curr Opin Struct Biol 19, 666–671 (2009).

56. Giegé, R. The early history of tRNA recognition by aminoacyl-tRNA synthetases. J. Biosci. 31, 477–488 (2006).

57. Hershko, A. & Ciechanover, A. The ubiquitin system. Annu. Rev. Biochem. 67, 425–479 (1998).

58. Mingeot-Leclercq, M. P., Glupczynski, Y. & Tulkens, P. M. Aminoglycosides: activity and resistance. Antimicrob Agents Chemother 43, 727–737 (1999).

59. Azucena, E. & Mobashery, S. Aminoglycoside-modifying enzymes: mechanisms of catalytic processes and inhibition. Drug Resist. Updat. 4, 106–117 (2001).

60. Pedersen, L. C., Benning, M. M. & Holden, H. M. Structural investigation of the antibiotic and ATP-binding sites in kanamycin nucleotidyltransferase. Biochemistry 34, 13305–13311 (1995).

61. Xu, Y. et al. Structure of the N-terminal domain of Escherichia coli glutamine synthetase adenylyltransferase. Structure 12, 861–869 (2004).

62. Almassy, R. J., Janson, C. A., Hamlin, R., Xuong, N. H. & Eisenberg, D. Novel subunit-subunit interactions in the structure of glutamine synthetase. Nature 323, 304–309 (1986).

63. Lehninger, A. Lehninger Principles of Biochemistry. 5th edition.

64. Goody, R. S. et al. The versatile Legionella effector protein DrrA. Commun Integr Biol 4, 72–74 (2011).

65. Murata, T. et al. The Legionella pneumophila effector protein DrrA is a Rab1 guanine nucleotide-exchange factor. Nat. Cell Biol. 8, 971–977 (2006).

66. Yarbrough, M. L. et al. AMPylation of Rho GTPases by Vibrio VopS disrupts effector binding and downstream signaling. Science 323, 269–272 (2009).

67. Yarbrough, M. L. & Orth, K. AMPylation is a new post-translational modiFICation. Nat Chem Biol 5, 378–379 (2009).

68. Utsumi, R., Nakamoto, Y., Kawamukai, M., Himeno, M. & Komano, T. Involvement of cyclic AMP and its receptor protein in filamentation of an Escherichia coli fic mutant. J Bacteriol 151, 807–812 (1982).

69. Roy, C. R. & Mukherjee, S. Bacterial FIC Proteins AMP Up Infection. Science signaling 2, pe14 (2009).

70. Komano, T., Utsumi, R. & Kawamukai, M. Functional analysis of the fic gene involved in regulation of cell division. Res Microbiol 142, 269–277 (1991).

71. Utsumi, R. et al. Identification of a membrane protein induced concurrently with cell filamentation by cyclic AMP in an Escherichia coli K-12 fic mutant. J Bacteriol 155, 398–401 (1983).

72. Kawamukai, M. et al. Cloning of the fic-1 gene involved in cell filamentation induced by cyclic AMP and construction of a delta fic Escherichia coli strain. J Bacteriol 170, 3864–3869 (1988).

73. Kawamukai, M., Matsuda, H., Fujii, W., Utsumi, R. & Komano, T. Nucleotide sequences of fic and fic-1 genes involved in cell filamentation induced by cyclic AMP in Escherichia coli. J Bacteriol 171, 4525–4529 (1989).

74. Utsumi, R., Noda, M., Kawamukai, M. & Komano, T. Control mechanism of the Escherichia coli K-12 cell cycle is triggered by the cyclic AMP-cyclic AMP receptor

protein complex. J Bacteriol 171, 2909–2912 (1989).

75. Worby, C. A. et al. The fic domain: regulation of cell signaling by adenylylation. Molecular cell 34, 93–103 (2009).

76. Casselli, T., Lynch, T., Southward, C. M., Jones, B. W. & DeVinney, R. Vibrio parahaemolyticus inhibition of Rho family GTPase activation requires a functional chromosome I type III secretion system. Infect Immun 76, 2202–2211 (2008).

77. Das, D. et al. Crystal structure of the Fic (Filamentation induced by cAMP) family protein SO4266 (gi|24375750) from Shewanella oneidensis MR-1 at 1.6 A resolution. Proteins 75, 264–271 (2009).

78. Finn, R. D. et al. Pfam: the protein families database. Nucleic Acids Res 42, D222–30 (2014).

79. Kinch, L. N., Yarbrough, M. L., Orth, K. & Grishin, N. V. Fido, a novel AMPylation domain common to fic, doc, and AvrB. PLoS ONE 4, e5818 (2009).

80. Xiao, J., Worby, C. A., Mattoo, S., Sankaran, B. & Dixon, J. E. Structural basis of Fic-mediated adenylylation. Nat Struct Mol Biol 17, 1004–1010 (2010).

81. Gazit, E. & Sauer, R. T. The Doc toxin and Phd antidote proteins of the bacteriophage P1 plasmid addiction system form a heterotrimeric complex. J Biol Chem 274, 16813–16818 (1999).

82. Luong, P. et al. Kinetic and structural insights into the mechanism of AMPylation by VopS FIC domain. Journal of Biological Chemistry 285, 20155 (2010).

83. Palanivelu, D. V. et al. Fic domain-catalyzed adenylylation: insight provided by the structural analysis of the type IV secretion system effector BepA. Protein science : a publication of the Protein Society 20, 492–499 (2011).

84. Garcia-Pino, A. et al. crystallization communications. Acta Cryst (2008). F64, 1034-1038, 1–5 (2008).

85. Garcia-Pino, A. et al. Doc of prophage P1 is inhibited by its antitoxin partner Phd through fold complementation. J Biol Chem 283, 30821–30827 (2008).

86. Goepfert, A., Harms, A., Schirmer, T. & Dehio, C. in Prokaryotic Toxin-Antitoxins 177–187 (Springer Berlin Heidelberg, 2012).

87. Watson, J. D. & Milner-White, E. J. A novel main-chain anion-binding site in proteins: the nest. A particular combination of phi,psi values in successive residues gives rise to anion-binding sites that occur commonly and are found often at functionally important regions. J Mol Biol 315, 171–182 (2002).

88. Garcia-Pino, A., Zenkin, N. & Loris, R. The many faces of Fic: structural and functional aspects of Fic enzymes. Trends in Biochemical Sciences 39, 121–129 (2014).

89. Lee, C. C. et al. Crystal structure of the type III effector AvrB from Pseudomonas syringae. Structure 12, 487–494 (2004).

90. Desveaux, D. et al. Type III effector activation via nucleotide binding, phosphorylation, and host target interaction. PLoS Pathog 3, e48 (2007).

91. Mattoo, S., Xiao, J., Dixon, J. E. & Worby, C. A. Comparative analysis of Histophilus somni immunoglobulin-binding protein A (IbpA) with other fic domain-containing enzymes reveals differences in substrate and nucleotide specificities. J

Biol Chem 286, 32834–32842 (2011).

92. Rahman, M. et al. Visual neurotransmission in Drosophila requires expression of Fic in glial capitate projections. Nature Neuroscience (2012).

93. Salomon, D. & Orth, K. What Pathogens Have Taught Us About Posttranslational Modifications. Cell Host Microbe 14, 269–279 (2013).

94. Bennett, B. D. et al. Absolute metabolite concentrations and implied enzyme active site occupancy in Escherichia coli. Nat Methods 5, 593–599 (2009).

95. Pan, X., Lührmann, A., Satoh, A., Laskowski-Arce, M. A. & Roy, C. R. Ankyrin repeat proteins comprise a diverse family of bacterial type IV effectors. Science 320, 1651–1654 (2008).

96. Campanacci, V., Mukherjee, S., Roy, C. R. & Cherfils, J. Structure of the Legionella effector AnkX reveals the mechanism of phosphocholine transfer by the FIC domain. EMBO J 32, 1469–1477 (2013).

97. Castro-Roa, D. et al. The Fic protein Doc uses an inverted substrate to phosphorylate and inactivate EF-Tu. Nat Chem Biol 1–9 (2013).

98. Cruz, J. W. et al. Doc toxin is a kinase that inactivates elongation factor tu. J Biol Chem 289, 7788–7798 (2014).

99. Pieles, K., Glatter, T., Harms, A., Schmidt, A. & Dehio, C. An experimental strategy for the identification of AMPylation targets from complex protein samples. Proteomics 14, 1048–1052 (2014).

100. Goody, P. R. et al. Reversible phosphocholination of Rab proteins by Legionella pneumophila effector proteins. EMBO J 31, 1774–1784 (2012).

101. Lewallen, D. M. et al. Inhibiting AMPylation: a novel screen to identify the first small molecule inhibitors of protein AMPylation. ACS Chem. Biol. 9, 433–442 (2014).

102. Duarte, J. M., Srebniak, A., Schärer, M. A. & Capitani, G. Protein interface classification by evolutionary analysis. BMC Bioinformatics 13, 334 (2012).

103. Arbing, M. A. et al. Crystal structures of Phd-Doc, HigA, and YeeU establish multiple evolutionary links between microbial growth-regulating toxin-antitoxin systems. Structure 18, 996–1010 (2010).

104. Li, J., Mahajan, A. & Tsai, M.-D. Ankyrin repeat: a unique motif mediating protein-protein interactions. Biochemistry 45, 15168–15178 (2006).

105. Doublet, P., Vincent, C., Grangeasse, C., Cozzone, A. J. & Duclos, B. On the binding of ATP to the autophosphorylating protein, Ptk, of the bacterium Acinetobacter johnsonii. FEBS Lett 445, 137–143 (1999).

106. Grangeasse, C. et al. Autophosphorylation of the Escherichia coli protein kinase Wzc regulates tyrosine phosphorylation of Ugd, a UDP-glucose dehydrogenase. J Biol Chem 278, 39323–39329 (2003).

107. Soulat, D. et al. Tyrosine-kinase Wzc from Escherichia coli possesses an ATPase activity regulated by autophosphorylation. FEMS microbiology letters 274, 252–259 (2007).

108. Grangeasse, C., Nessler, S. & Mijakovic, I. Bacterial tyrosine kinases: evolution, biological function and structural insights. Philos. Trans. R. Soc. Lond., B, Biol. Sci. 367, 2640–2655 (2012).

109. Harms, A. FIC domains of Bartonella effector proteins - AMPylation and beyond. University of Basel, Basel (2011).

110. Engel, P. et al. Parallel Evolution of a Type IV Secretion System in Radiating Lineages of the Host-Restricted Bacterial Pathogen Bartonella. PLoS Genet 7, e1001296 (2011).

111. Cogli, L., Progida, C., Bramato, R. & Bucci, C. Vimentin phosphorylation and assembly are regulated by the small GTPase Rab7a. Biochimica et Biophysica Acta (BBA) - Molecular Cell Research 1833, 1283–1293 (2013).

112. Pieles, K. From FIC to BID: target identification and functional characterization of Bartonella effector proteins. University of Basel, Basel (2013).

113. Parker, A. L., Kavallaris, M. & McCarroll, J. A. Microtubules and Their Role in Cellular Stress in Cancer. Front. Oncol. 4, (2014).

114. Al-Bassam, J. & Chang, F. Regulation of microtubule dynamics by TOG-domain proteins XMAP215/Dis1 and CLASP. Trends in cell biology 21, 604–614 (2011).

115. Ayaz, P., Ye, X., Huddleston, P., Brautigam, C. A. & Rice, L. M. A TOG:αβ-tubulin complex structure reveals conformation-based mechanisms for a microtubule polymerase. Science 337, 857–860 (2012).

116. Wang, J. C. Interaction between DNA and an Escherichia coli protein omega. J Mol Biol 55, 523–533 (1971).

117. Liu, L. F. & Wang, J. C. Supercoiling of the DNA template during transcription. Proc Natl Acad Sci USA 84, 7024–7027 (1987).

118. Postow, L., Crisona, N. J., Peter, B. J., Hardy, C. D. & Cozzarelli, N. R. Topological challenges to DNA replication: conformations at the fork. Proc Natl Acad Sci USA 98, 8219–8226 (2001).

119. Schoeffler, A. J. & Berger, J. M. DNA topoisomerases: harnessing and constraining energy to govern chromosome topology. Q Rev Biophys 41, 41–101 (2008).

120. Tretter, E. M., Lerman, J. C. & Berger, J. M. A naturally chimeric type IIA topoisomerase in Aquifex aeolicus highlights an evolutionary path for the emergence of functional paralogs. Proceedings of the National Academy of Sciences 107, 22055–22059 (2010).

121. Berg, J. M., Stryer, L. & Tymoczko, J. L. in 1100 (Granite Hill Publishers, 2002).

122. Papillon, J. et al. Structural insight into negative DNA supercoiling by DNA gyrase, a bacterial type 2A DNA topoisomerase. Nucleic Acids Res (2013).

123. Wigley, D. B., Davies, G. J., Dodson, E. J., Maxwell, A. & Dodson, G. Crystal structure of an N-terminal fragment of the DNA gyrase B protein. Nature 351, 624–629 (1991).

124. Brino, L. et al. Dimerization of Escherichia coli DNA-gyrase B provides a structural mechanism for activating the ATPase catalytic center. J Biol Chem 275, 9468–9475 (2000).

125. Deibler, R. W., Rahmati, S. & Zechiedrich, E. L. Topoisomerase IV, alone, unknots DNA in E-coli. Genes Dev. 15, 748–761 (2001).

126. Lopez, V., Martinez-Robles, M. L., Hernandez, P., Krimer, D. B. & Schvartzman, J. B. Topo IV is the topoisomerase that knots and unknots sister duplexes during DNA

replication. Nucleic Acids Res 40, 3563–3573 (2012).

127. Schvartzman, J. B., Martínez-Robles, M.-L., Hernández, P. & Krimer, D. B. The benefit of DNA supercoiling during replication. Biochem Soc Trans 41, 646–651 (2013).

128. Schmidt, B. H., Osheroff, N. & Berger, J. M. Structure of a topoisomerase II-DNA-nucleotide complex reveals a new control mechanism for ATPase activity. Nat Struct Mol Biol 19, 1147–1154 (2012).

129. Roca, J. & Wang, J. C. The capture of a DNA double helix by an ATP-dependent protein clamp: a key step in DNA transport by type II DNA topoisomerases. Cell 71, 833–840 (1992).

130. Dong, K. C. & Berger, J. M. Structural basis for gate-DNA recognition and bending by type IIA topoisomerases. Nature 450, 1201–1205 (2007).

131. Liu, L. F. & Wang, J. C. DNA-DNA gyrase complex: the wrapping of the DNA duplex outside the enzyme. Cell 15, 979–984 (1978).

132. Roca, J., Berger, J. M. & Wang, J. C. On the simultaneous binding of eukaryotic DNA topoisomerase II to a pair of double-stranded DNA helices. J Biol Chem 268, 14250–14255 (1993).

133. Ali, J. A., Jackson, A. P., Howells, A. J. & Maxwell, A. The 43-kilodalton N-terminal fragment of the DNA gyrase B protein hydrolyzes ATP and binds coumarin drugs. Biochemistry 32, 2717–2724 (1993).

134. Berger, J. M. & Wang, J. C. Recent developments in DNA topoisomerase II structure and mechanism. Curr Opin Struct Biol 6, 84–90 (1996).

135. Fass, D., Bogden, C. E. & Berger, J. M. Quaternary changes in topoisomerase II may direct orthogonal movement of two DNA strands. Nat Struct Biol 6, 322–326 (1999).

136. Roca, J. & Wang, J. C. DNA transport by a type II DNA topoisomerase: evidence in favor of a two-gate mechanism. Cell 77, 609–616 (1994).

137. Williams, N. L. & Maxwell, A. Probing the two-gate mechanism of DNA gyrase using cysteine cross-linking. Biochemistry 38, 13502–13511 (1999).

138. Bates, A. D., Berger, J. M. & Maxwell, A. The ancestral role of ATP hydrolysis in type II topoisomerases: prevention of DNA double-strand breaks. Nucleic Acids Res 39, 6327–6339 (2011).

139. Sissi, C. & Palumbo, M. In front of and behind the replication fork: bacterial type IIA topoisomerases. Cell Mol Life Sci 67, 2001–2024 (2010).

140. Maxwell, A. & Gellert, M. The DNA dependence of the ATPase activity of DNA gyrase. Journal of Biological Chemistry 259, 14472–14480 (1984).

141. Gross, C. H. et al. Active-site residues of Escherichia coli DNA gyrase required in coupling ATP hydrolysis to DNA supercoiling and amino acid substitutions leading to novobiocin resistance. Antimicrob Agents Chemother 47, 1037–1046 (2003).

142. Bates, A. D. & Maxwell, A. Energy coupling in type II topoisomerases: why do they hydrolyze ATP? Biochemistry 46, 7929–7941 (2007).

143. Gubaev, A. & Klostermeier, D. DNA-induced narrowing of the gyrase N-gate coordinates T-segment capture and strand passage. Proc Natl Acad Sci USA 108, 14085–14090 (2011).

144. Baird, C. L., Harkins, T. T., Morris, S. K. & Lindsley, J. E. Topoisomerase II drives DNA transport by hydrolyzing one ATP. Proceedings of the National Academy of Sciences 96, 13685–13690 (1999).

145. Smith, C. V. & Maxwell, A. Identification of a residue involved in transition-state stabilization in the ATPase reaction of DNA gyrase. Biochemistry 37, 9658–9667 (1998).

146. Wei, H., Ruthenburg, A. J., Bechis, S. K. & Verdine, G. L. Nucleotide-dependent domain movement in the ATPase domain of a human type IIA DNA topoisomerase. J Biol Chem 280, 37041–37047 (2005).

147. Corbett, K. D. & Berger, J. M. Structure of the topoisomerase VI-B subunit: implications for type II topoisomerase mechanism and evolution. EMBO J 22, 151–163 (2003).

148. Corbett, K. D. & Berger, J. M. Structural dissection of ATP turnover in the prototypical GHL ATPase TopoVI. Structure 13, 873–882 (2005).

149. Van Melderen, L. Molecular interactions of the CcdB poison with its bacterial target, the DNA gyrase. International Journal of Medical Microbiology 291, 537–544 (2001).

150. Kampranis, S. C., Bates, A. D. & Maxwell, A. A model for the mechanism of strand passage by DNA gyrase. Proc Natl Acad Sci USA 96, 8414–8419 (1999).

151. Dao-Thi, M.-H. et al. Molecular basis of gyrase poisoning by the addiction toxin CcdB. J Mol Biol 348, 1091–1102 (2005).

152. Tryptic fragments of the Escherichia coli DNA gyrase A protein. J Biol Chem 264, 19648–19653 (1989).

153. Bernard, P. & Couturier, M. Cell killing by the F plasmid CcdB protein involves poisoning of DNA-topoisomerase II complexes. J Mol Biol 226, 735–745 (1992).

154. Critchlow, S. E. et al. The interaction of the F plasmid killer protein, CcdB, with DNA gyrase: induction of DNA cleavage and blocking of transcription. J Mol Biol 273, 826–839 (1997).

155. Smith, A. B. & Maxwell, A. A strand-passage conformation of DNA gyrase is required to allow the bacterial toxin, CcdB, to access its binding site. Nucleic Acids Res 34, 4667–4676 (2006).

156. Barbosa, L. C. B. et al. Design and synthesis of peptides from bacterial ParE toxin as inhibitors of topoisomerases. European journal of medicinal chemistry (2012).

157. Maxwell, A. DNA gyrase as a drug target. Trends in microbiology 5, 102–109 (1997).

158. Maxwell, A. DNA gyrase as a drug target. Biochem Soc Trans 27, 48–53 (1999).

159. Collin, F., Karkare, S. & Maxwell, A. Exploiting bacterial DNA gyrase as a drug target: current state and perspectives. Appl. Microbiol. Biotechnol. 92, 479–497 (2011).

160. Lamour, V., Hoermann, L., Jeltsch, J. M., Oudet, P. & Moras, D. Crystallization of the 43 kDa ATPase domain of Thermus thermophilus gyrase B in complex with novobiocin. Acta Crystallogr D Biol Crystallogr 58, 1376–1378 (2002).

161. Lamour, V., Hoermann, L., Jeltsch, J.-M., Oudet, P. & Moras, D. An open conformation of the Thermus thermophilus gyrase B ATP-binding domain. J Biol Chem 277, 18947–18953 (2002).

162. Forsythe, E., Achari, A. & Pusey, M. L. Trace fluorescent labeling for high-throughput crystallography. Acta Crystallogr D Biol Crystallogr 62, 339–346 (2006).

163. Pusey, M., Forsythe, E. & Achari, A. in Structural Proteomics 426, 377–385 (Humana Press, 2008).

164. Wriggers, W., Chakravarty, S. & Jennings, P. A. Control of protein functional dynamics by peptide linkers. Biopolymers 80, 736–746 (2005).

165. Chen, X., Zaro, J. L. & Shen, W.-C. Fusion protein linkers: Property, design and functionality. Advanced Drug Delivery Reviews (2012).

166. Vanwart, H. E., Lewis, A., Scheraga, H. A. & Saeva, F. D. Disulfide Bond Dihedral Angles From Raman Spectroscopy. Proc Natl Acad Sci USA 70, 2619–2623 (1973).

167. Boyd, D. B. Conformational dependence of the electronic energy levels in disulfides. J Am Chem Soc 94, 8799–8804 (1972).

168. Kabsch, W. XDS. Acta Crystallogr D Biol Crystallogr 66, 125–132 (2010).

169. Evans, P. R. & Murshudov, G. N. How good are my data and what is the resolution? Acta Crystallogr D Biol Crystallogr 69, 1204–1214 (2013).

170. Engel, P. et al. Adenylylation control by intra- or intermolecular active-site obstruction in Fic proteins. Nature 482, 107–110 (2012).

171. Emsley, P., Lohkamp, B., Scott, W. G. & Cowtan, K. Features and development of Coot. Acta Crystallogr D Biol Crystallogr 66, 486–501 (2010).

172. Murshudov, G. N. et al. REFMAC5 for the refinement of macromolecular crystal structures. Acta Crystallogr D Biol Crystallogr 67, 355–367 (2011).

173. Adams, P. D. et al. PHENIX: a comprehensive Python-based system for macromolecular structure solution. Acta Crystallogr D Biol Crystallogr 66, 213–221 (2010).

174. Chen, V. B. et al. MolProbity: all-atom structure validation for macromolecular crystallography. Acta Crystallogr D Biol Crystallogr 66, 12–21 (2010).

175. Goepfert, A., Stanger, F. V., Dehio, C. & Schirmer, T. Conserved inhibitory mechanism and competent ATP binding mode for adenylyltransferases with fic fold. PLoS ONE 8, e64901 (2013).

176. Smith, J. A., Francis, S. H. & Corbin, J. D. Autophosphorylation - a Salient Feature of Protein-Kinases. Mol. Cell. Biochem. 128, 51–70 (1993).

177. Yu, X. et al. Click chemistry-based detection of global pathogen-host AMPylation on self-assembled human protein microarrays. Mol. Cell Proteomics mcp.M114.041103 (2014).

178. Müller, M. P., Albers, M. F., Itzen, A. & Hedberg, C. Exploring adenylylation and phosphocholination as post-translational modifications. Chembiochem : a European journal of chemical biology 15, 19–26 (2014).

Acknowledgements

6. Acknowledgments

Foremost, I'd like to thank my supervisors, Prof. Tilman Schirmer and Prof. Christoph Dehio, for giving me the opportunity to work at the interface of structural biology and microbiology, in a very close collaboration between these two research groups. I especially enjoyed the context and atmosphere in which I conducted my research projects, developing my ideas and challenging the resulting hypotheses with a well-balanced freedom to guidance ratio.

Thank you also for supporting my choices in terms of education, giving me the chance to join two incredibly stimulating summer schools (FEBS Advanced Crystallization school 2012 and CCP4 summer school 2013) and several conferences.

I'd like to thank Prof. Timm Maier who accepted to be part of my PhD committee, thanks for the fruitful input and crystallographic discussions.

Thanks to the FIC team, in particular to Arnaud Goepfert and Alexander Harms. Our daily interactions highly enhanced the quality of our respective projects.

I'd also like to thank all the great researchers with whom I had the chance to directly collaborate. This includes Philipp Engel, Arnaud Goepfert, Björn Burmann, Alexander Harms, Tim Sharpe, Adam Mazur and Prof. Sebastian Hiller.

Thanks to all lab members from the Schirmer lab and Dehio lab, past and present, with whom I enjoyed working and interacting: Houchaima Ben Tekaya, Aline Borer, Alain Casanova, Raquel Conde, Tjaart De Beer, Mathias Dick, Badri Dubey, Simone Eicher, Mario Emmenlauer, Stefan Emming, Philipp Engel, Arnaud Goepfert, Alexander Harms, Tillmann Heinisch, Shyan Huey Low, Cedric Hutter, Valentin Köhler, Jonas Körner, Yun-Yueh Lu, Zora Markovic-Housley, Simon Marlaire, Claudia Massa, Claudia Mistl, Simone Muntwiler, Damian Murezzan, Rusudan Okujava, Camille Peitsch, Caroline Peneff-Verheyden, Maxime Québatte, Pauli Rämö, Sayantan Saha, Dietrich Samoray, Christoph Schmutz, Sabrina Siamer, Isabel Sorg, Sarah Stiegeler, Amit Sundriyal, Matthias Truttmann and Franziska Zähringer. Special thank to David Hinnen, Chee-Seng Hee and Stefanie Kauer for the great time.

Special thank to Arnaud Goepfert, Alexander Harms and Kathrin Pieles for critical reading of my thesis.

I would like to acknowledge the constant support by the many people of the technical and administrative staff of the 3rd and 4th floors.

I would like to thank the staff of beamlines PXI and PXIII at the SLS and a special thank to Roman Jakob for sharing long nights at the SLS, shooting a tremendous number of crystals and sharing your crystallographic experience.

I would also like to thank the French train company “SNCF” for providing rather comfortable and on-time transportation on the 150’000 km that I travelled between Colmar and Basel in the last 4 years.

Un très grand merci à ma famille et mes amis qui m’ont soutenu tout au long de mes études, m’apportant tout le soutien nécessaire pour toujours aller de l’avant dans mes projets. Merci spécialement à mes parents, d’avoir laisser libre-cours à mon imagination tout au long de mon cursus.

Enfin, le dernier de mes remerciements, mais pas des moindre, va à mon épouse Emma, pour ton soutien inconditionnel et notre amour, et bien sur la stabilité que m’apporte la joie de notre couple ! ps: I love you !

Curriculum Vitae

7. Curriculum Vitae

Frédéric V. Stanger **PhD student, Structural Biology**

Born on 7th of April, 1987 (27 years old) in Mulhouse, France

Married

French citizen

Office address:

Biozentrum, University of Basel

Structural Biology and Biophysics

Klingelbergstrasse 50/70

CH-4056 Basel, Switzerland

Phone: +41 61 267 20 92

frederic.stanger@unibas.ch

Private address:

87 Noehlenweg

68 000 Colmar, France

Phone: +33 6 19 96 66 39

frederic.stanger@gmail.com

EDUCATION AND RESEARCH EXPERIENCE

2010 - present	**PhD Thesis** Focal Area Structural Biology and Biophysics and Focal Area Infection Biology Biozentrum, *University of Basel, Basel, Switzerland* Supervisors: Prof. Tilman Schirmer and Prof. Christoph Dehio PhD committee member: Prof. Timm Maier Title: Tightly regulated FIC domain proteins modulate bacterial topoisomerases by adenylylation
June 2013	**CCP4/APS Summer School in Macromolecular Crystallography**: from data collection to structure refinement and beyond, *Argonne, Illinois, USA*
June 2012	**FEBS practical course**: Advanced methods in Macromolecular Crystallization, *Nové Hrady, Czech Republic*
2008 - 2010	**Master of Sciences in Chemistry and Biology** – Interfaces and Applications, Biomolecules: Structure and Function *University of Strasbourg, France*

January - July 2010	**Master thesis** at the Institute of Molecular and Cellular Biology (IBMC), *Strasbourg, France* Supervisor: Dr. Claude Sauter Title: Physico-chemical and structural characterization of the plant membrane protein VDAC
2005 - 2008	**Bachelor of Biochemistry and Molecular Biology** *University Louis Pasteur, Strasbourg, France*
2005	***Baccalauréat Scientifique*** (equivalent of the European Matura), Life Science *Lycée Jeanne d'Arc, Mulhouse, France*

TEACHING EXPERIENCE

2010 - 2014	Assistant and tutor for undergraduate students in practical courses of Structural Biology and Microbiology Focal Area Structural Biology and Biophysics and Focal Area Infection Biology, Biozentrum, *University of Basel, Switzerland*
2012 - 2013	Tutor for undergraduate students in exercises of Structural Biology

ORAL AND POSTER PRESENTATION

2012	**Poster Presentation** at the "FEBS practical course: Advanced methods in Macromolecular Crystallization", *Nové Hrady, Czech Republic* Title: Fic proteins AMPylate a bacterial target: crystallization trials of the FIC/Target/ATP complex
2013	**Poster Presentation** at the Biozentrum Symposium, *St Chrischona, Switzerland* Title: Fic-mediated adenylylation inhibits GyrB by interfering with ATP hydrolysis
2013	**Oral Presentation** at the 27th Rhine-Knee Regional Meeting on Biocrystallography, *Schluchsee, Germany* Title: Fic-mediated adenylylation inhibits GyrB by interfering with ATP hydrolysis
2014	**Poster Presentation** at the Gordon Research Conference "DNA Topoisomerase in Biology and Medicine", *Sunday River Resort, Newry, Maine, USA* Title: Structure of the N-terminal gyrase B fragment in complex with ADP·P_i reveals rigid-body motion induced by ATP hydrolysis

PUBLICATIONS

2014 Stanger F.V., Dehio C. & Schirmer T. Structure of the N-terminal gyrase B fragment in complex with ADP·P_i reveals rigid-body motion induced by ATP hydrolysis. *PLoS one, in press.*

2013 Goepfert A., Stanger F.V., Dehio C. & Schirmer T. Conserved inhibitory mechanism and competent ATP binding mode for adenylyltransferases with Fic fold. *PLoS one* **8(5)**: e64901.

2012 Engel P., Goepfert A., Stanger F.V., Harms A., Schmidt A., Schirmer T. & Dehio C. Adenylylation control by intra- or intermolecular active-site obstruction in Fic proteins. *Nature* **482**, 107-110 (2012).

LANGUAGE AND COMPUTING

Language	French: mother tongue English: fluent German: conversant
Computing	Mac OS X, Unix, Windows Unix commands and scripts Office, Adobe CS5, Geneious, Python (user)
Crystallography	CCP4 suite, Phenix suite, Coot, XDS, Pymol, Dino, Modtrafo

REFERENCES

Prof. Tilman Schirmer
Principal Investigator
Biozentrum
University of Basel
Klingelbergstrasse 50-70
CH-4056 Basel, Switzerland
+ 41 61 267 20 89
tilman.schirmer@unibas.ch

Prof. Christoph Dehio
Principal Investigator
Biozentrum
University of Basel
Klingelbergstrasse 50-70
CH-4056 Basel, Switzerland
+ 41 61 267 21 40
christoph.dehio@unibas.ch

Dr. Claude Sauter
Research scientist
Institute for Molecular and Celluar Biology (IBMC)
University of Strasbourg
15 Rue René Descartes
67 000 Strasbourg,
France
+ 33 3 88 41 71 02
c.sauter@unistra.fr

Appendix

8. Appendix

8.1. Plasmids constructed

A comprehensive list of the plasmids constructed in the frame of my PhD thesis work appears on the next pages using the following color code:

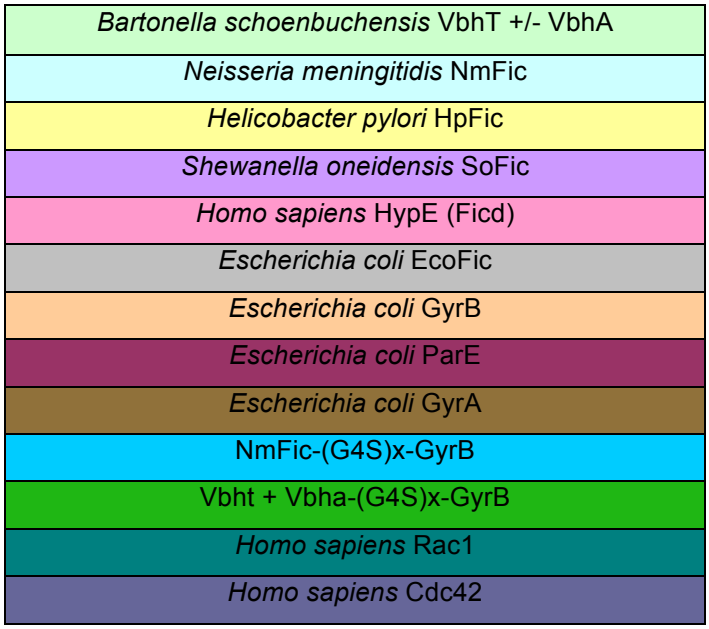

Plasmid	Description	FIC domain	Inhibition helix	Vector type
		Mutations		
pFVS0001	VbhT FL wt	wt	-	pRSFDuet1
pFVS0002	VbhT FL wt + VbhA wt	wt	wt	pRSFDuet1
pFVS0003	VbhT 1-248 His136Ala	His136Ala	-	pRSFDuet1
pFVS0004	VbhT 1-248 His136Ala + VbhA wt	His136Ala	wt	pRSFDuet1
pFVS0005	VbhT 1-308 His136Ala	His136Ala	-	pRSFDuet1
pFVS0006	VbhT 1-308 His136Ala + VbhA wt	His136Ala	wt	pRSFDuet1
pFVS0010	VbhT FL His136Ala	His136Ala	-	pRSFDuet1
pFVS0011	VbhT 1-198 wt + VbhA wt	wt	wt	pRSFDuet1
pFVS0012	VbhT 1-198 wt	wt	-	pRSFDuet1
pFVS0013	VbhT 8-198 wt + VbhA wt	wt	wt	pRSFDuet1
pFVS0014	VbhT 8-198 wt	wt	-	pRSFDuet1
pFVS0015	NmFic wt (10-191)	wt	wt	pRSFDuet1
pFVS0016	NmFic Δ8 (10-167)	wt	-	pRSFDuet1
pFVS0017	VbhT FL Glu35Asn	Glu35Asn	-	pRSFDuet1
pFVS0018	VbhT 1-198 Glu35Asn + VbhA wt	Glu35Asn	wt	pRSFDuet1
pFVS0019	HpFic wt	wt	wt	pRSFDuet1
pFVS0020	HpFic Δ8	wt	-	pRSFDuet1
pFVS0021	NmFic Asp15Ala	Asp15Ala	wt	pRSFDuet1
pFVS0022	NmFic Δ8 Asp15Ala (10-167)	Asp15Ala	-	pRSFDuet1
pFVS0023	NmFic Glu186Ala	wt	Glu186Ala	pRSFDuet1
pFVS0024	VbhT FL His136Ala + VbhA wt	His136Ala	wt	pRSFDuet1
pFVS0025	VbhT FL Glu35Asn + VbhA wt	Glu35Asn	wt	pRSFDuet1
pFVS0026	HpFic Δ8 Asp4Ala	Asp4Ala	-	pRSFDuet1
pFVS0027	HpFic Asp4Ala	Asp4Ala	wt	pRSFDuet1
pFVS0028	HpFic Ser171Ala Glu175Ala	wt	Ser171Ala Glu175Ala	pRSFDuet1
pFVS0029	VbhT FL wt + VbhA Ser20Ala	wt	Ser20Ala	pRSFDuet1
pFVS0030	VbhT 1-198 wt + VbhA Ser20Ala	wt	Ser20Ala	pRSFDuet1
pFVS0031	VbhT FL wt + VbhA Ser20Ala Glu24Ala	wt	Ser20Ala Glu24Ala	pRSFDuet1
pFVS0032	VbhT FL Glu35Asn + VbhA Ser20Ala Glu24Ala	Glu35Asn	Ser20Ala Glu24Ala	pRSFDuet1

Plasmid	Description	FIC domain	Inhibition helix	Vector type
		Mutations		
pFVS0033	VbhT 1-198 Glu35Asn + VbhA Ser20Ala Glu24Ala	Glu35Asn	Ser20Ala Glu24Ala	pRSFDuet1
pFVS0034	HpFic Asp4Ala Ser171Ala Glu175Ala	Asp4Ala	Ser171Ala Glu175Ala	pRSFDuet1
pFVS0035	NmFic Asp15Ala Glu186Ala	Asp15Ala	Glu186Ala	pRSFDuet1
pFVS0036	S. oneidensis Fic FL from DNASU in pSpeed	wt	wt	pSpeed
pFVS0037	NmFic Ser182Ala Glu186Ala	wt	Ser182Ala Glu186Ala	pRSFDuet1
pFVS0038	NmFic Asp15Ala Ser182Ala Glu186Ala	Asp15Ala	Ser182Ala Glu186Ala	pRSFDuet1
pFVS0039	VbhT 1-198 Glu35Asn	Glu35Asn	-	pRSFDuet1
pFVS0040	SoFic wt	wt	wt	pRSFDuet1
pFVS0041	VbhT 1-198 His136Ala + VbhA wt	His136Ala	wt	pRSFDuet1
pFVS0042	VbhT 1-198 His136Ala	His136Ala	-	pRSFDuet1
pFVS0043	HpFic helix8 (MCS1) + Fic Δ8 (MCS2)	wt	wt	pRSFDuet1
pFVS0044	NmFic Tyr183Ala	wt	Tyr183Ala	pRSFDuet1
pFVS0045	VbhT 1-198 Arg144Ala + VbhA wt	Arg144Ala	wt	pRSFDuet1
pFVS0046	VbhT 1-198 Arg147Ala + VbhA wt	Arg147Ala	wt	pRSFDuet1
pFVS0047	VbhT 1-198 wt + VbhA Gln22Ala	wt	Gln22Ala	pRSFDuet1
pFVS0048	VbhT 1-198 Arg144Ala	Arg144Ala	-	pRSFDuet1
pFVS0049	VbhT 1-198 Arg147Ala	Arg147Ala	-	pRSFDuet1
pFVS0050	NmFic Tyr183Ala Tyr188Ala	wt	Tyr183Ala Tyr188Ala	pRSFDuet1
pFVS0051	NmFic His107Ala	His107Ala	wt	pRSFDuet1
pFVS0052	VbhT 1-198 Arg144Ala Arg147Ala + VbhA wt	Arg144Ala Arg147Ala	wt	pRSFDuet1
pFVS0053	VbhT 1-198 Arg144Ala Arg147Ala	Arg144Ala Arg147Ala	-	pRSFDuet1
pFVS0054	VbhT 1-198 wt + VbhA Ser20Ala Glu24Ala	wt	Ser20Ala Glu24Ala	pRSFDuet1
pFVS0055	VbhT 1-198 wt + VbhA Gln22Ala Leu27Ala	wt	Gln22Ala Leu 27Ala	pRSFDuet1
pFVS0056	NmFic Glu111Gln Ser182Ala Glu186Ala	Glu111Gln	Ser182Ala Glu186Ala	pRSFDuet1
pFVS0057	SoFic Glu73Ala	wt	Glu73Ala	pRSFDuet1
pFVS0058	SoFic Glu73Gly	wt	Glu73Gly	pRSFDuet1
pFVS0059	NmFic Glu186Gly	wt	Glu186Gly	pRSFDuet1
pFVS0060	VbhT 1-198 Ala188Val + VbhA Glu24Gly	Ala188Val	Glu24Gly	pRSFDuet1

Plasmid	Description	FIC domain	Inhibition helix	Vector type
		Mutations		
pFVS0061	Human HYPE wt in pET-GSTx (from Seema Mattoo)	wt	wt	pET-GSTx
pFVS0062	Human HYPE H295A in pET-GSTx (from Seema Mattoo)	His295Ala	wt	pET-GSTx
pFVS0063	Human HYPE Glu234Ala in pET-GSTx	wt	Glu234Ala	pET-GSTx
pFVS0064	Human HYPE Glu234Gly in pET-GSTx	wt	Glu234Gly	pET-GSTx
pFVS0065	VbhT 1-198 wt + VbhA Glu24Gly	wt	Glu24Gly	pRSFDuet1
pFVS0066	NmFic Δ8 (10-167) His107Ala	His107Ala	-	pRSFDuet1
pFVS0067	NmFic His107Ala Ser182Ala Glu186Ala	His107Ala	Ser182Ala Glu186Ala	pRSFDuet1
pFVS0068	Human HYPE Thr230Ala Glu234Gly in pET-GSTx	wt	Thr230Ala Glu234Gly	pET-GSTx
pFVS0069	Human HYPE His225Tyr Thr230Ala Glu234Gly in pET-GSTx	wt	Thr230Ala Glu234Ala	pET-GSTx
pFVS0070	SoFic His198Ala	His198Ala	wt	pRSFDuet1
pFVS0071	SoFic Glu73Gly Ser69Ala Asp136Gly	wt	Glu73Gly Ser69Ala	pRSFDuet1
pFVS0072	Human HYPE Thr230Ala Glu234Ala in pET-GSTx	wt	Thr230Ala Glu234Ala	pET-GSTx
pFVS0073	Human HYPE His295Ala Glu234Ala in pET-GSTx	His295Ala	Glu234Ala	pET-GSTx
pFVS0074	Human HYPE His295Ala Glu234Gly in pET-GSTx	His295Ala	Glu234Gly	pET-GSTx
pFVS0075	Human HYPE wt in pcDNA3.1	wt	wt	pcDNA3.1
pFVS0076	Human HYPE His295Ala in pcDNA3.1	His295Ala	wt	pcDNA3.1
pFVS0077	Human HYPE Thr230Ala Glu234Ala in pcDNA3.1	wt	Thr230Ala Glu234Ala	pcDNA3.1
pFVS0078	Human HYPE Glu234Gly in pcDNA3.1	wt	Glu234Gly	pcDNA3.1
pFVS0079	VbhT FL wt + VbhA Glu24Gly	wt	Glu24Gly	pRSFDuet1
pFVS0080	VbhT 1-198 His136Ala + VbhA Glu24Gly	His136Ala	Glu24Gly	pRSFDuet1
pFVS0081	NmFic Tyr183Phe	wt	Tyr183Phe	pRSFDuet1
pFVS0082	NmFic Tyr188Phe	wt	Tyr188Phe	pRSFDuet1
pFVS0083	NmFic Tyr183Phe Glu186Gly	wt	Tyr183Phe Glu186Gly	pRSFDuet1
pFVS0084	NmFic Tyr183Phe Glu186Gly Tyr188Ser	wt	Tyr183Phe Glu186Gly Tyr188Ser	pRSFDuet1
pFVS0085	Human HYPE Fic wt (187-437)	wt	wt	pRSFDuet1
pFVS0086	Human HYPE Tpr Fic wt (104-437)	wt	wt	pRSFDuet1
pFVS0087	Human HYPE Fic His295Ala (187-437)	His295Ala	wt	pRSFDuet1
pFVS0088	Human HYPE Tpr Fic His295Ala (104-437)	His295Ala	wt	pRSFDuet1
pFVS0089	Human HYPE Fic Thr230Ala Glu234Ala (187-437)	wt	Thr230Ala Glu234Ala	pRSFDuet1

Plasmid	Description	FIC domain	Inhibition helix	Vector type
		Mutations		
pFVS0090	Human HYPE Tpr Fic Thr230Ala Glu234Ala (104-437)	wt	Thr230Ala Glu234Ala	pRSFDuet1
pFVS0091	Human HYPE Fic Glu234Gly (187-437)	wt	Glu234Gly	pRSFDuet1
pFVS0092	Human HYPE Tpr Fic Glu234Gly (104-437)	wt	Glu234Gly	pRSFDuet1
pFVS0093	NmFic Tyr183Phe Tyr188Phe	wt	Tyr183Phe Tyr188Phe	pRSFDuet1
pFVS0094	NmFic Tyr183Phe Glu186Gly Tyr188Phe	wt	Tyr183Phe Glu186Gly Tyr188Phe	pRSFDuet1
pFVS0095	NmFic Glu186Gly Tyr188Phe	wt	Glu186Gly Tyr188Phe	pRSFDuet1
pFVS0096	Human HYPE Fic wt (187-437) in pcDNA3.1	wt	wt	pcDNA3.1
pFVS0097	Human HYPE Fic His295Ala (187-437) in pcDNA3.1	His295Ala	wt	pcDNA3.1
pFVS0098	VbhT 1-198 wt in pACYC-Duet	wt	-	pACYC-Duet
pFVS0099	VbhT 1-198 His136Ala in pACYC-Duet	His136Ala	-	pACYC-Duet
pFVS0100	NmFic Δ8 (10-167) Nter Strep-II Tag	wt	-	pRSFDuet1
pFVS0101	VbhA wt in pBSK	-	wt	pBSK
pFVS0102	VbhA Glu24Gly in pBSK	-	Glu24Gly	pBSK
pFVS0103	E. coli GyrB 1-220 wt Nter HisTag	-	-	pRSFDuet1
pFVS0104	E. coli GyrB 1-220 wt NO-TAG	-	-	pRSFDuet1
pFVS0105	E. coli GyrB 1-220 wt Cter HisTag	-	-	pRSFDuet1
pFVS0106	E. coli GyrB 15-220 wt Nter HisTag	-	-	pRSFDuet1
pFVS0107	E. coli GyrB 15-220 wt NO-TAG	-	-	pRSFDuet1
pFVS0108	E. coli GyrB 15-220 wt Cter HisTag	-	-	pRSFDuet1
pFVS0109	E. coli GyrB 1-392 wt Nter HisTag	-	-	pRSFDuet1
pFVS0110	E. coli GyrB 1-392 wt NO-TAG	-	-	pRSFDuet1
pFVS0111	E. coli GyrB 1-392 wt Cter HisTag	-	-	pRSFDuet1
pFVS0112	E. coli GyrB 15-392 wt Nter HisTag	-	-	pRSFDuet1
pFVS0113	E. coli GyrB 15-392 wt NO-TAG	-	-	pRSFDuet1
pFVS0114	E. coli GyrB 15-392 wt Cter HisTag	-	-	pRSFDuet1
pFVS0115	NmFic wt Nter Strep-II-Tag	wt	wt	pRSFDuet1
pFVS0116	E. coli GyrB 15-390 wt Nter HisTag	-	-	pRSFDuet1
pFVS0117	NmFic His107Ala Glu186Gly	His107Ala	Glu186Gly	pRSFDuet1

Plasmid	Description	FIC domain	Inhibition helix	Vector type
		Mutations		
pFVS0118	E. coli GyrB 1-220 Y109F Nter HisTag	-	-	pRSFDuet1
pFVS0119	E. coli GyrB 15-220 Y109F Nter HisTag	-	-	pRSFDuet1
pFVS0120	E. coli GyrB 1-392 Y109F Nter HisTag	-	-	pRSFDuet1
pFVS0121	E. coli GyrB 15-392 Y109F Nter HisTag	-	-	pRSFDuet1
pFVS0122	E. coli GyrB 15-392 Y109F Cter HisTag	-	-	pRSFDuet1
pFVS0123	HpFic Glu175Gly	wt	Glu175Gly	pRSFDuet1
pFVS0124	NmFic Arg71Ala	Arg71Ala	wt	pRSFDuet1
pFVS0125	NmFic Glu102Arg	Glu102Arg	wt	pRSFDuet1
pFVS0126	NmFic Glu156Arg	Glu156Arg	wt	pRSFDuet1
pFVS0127	NmFic Glu102Ala	Glu102Ala	wt	pRSFDuet1
pFVS0128	NmFic Lys99Arg Glu102Ala	Lys99Arg Glu102Ala	wt	pRSFDuet1
pFVS0129	E. coli Fic Gly55Arg Nter HisTag + YhfG HA-Tag	Gly55Arg	wt	pRSFDuet1
pFVS0130	E. coli Fic wt Nter HisTag + YhfG Glu28Gly HA-Tag	wt	Glu28Gly	pRSFDuet1
pFVS0131	E. coli ParE 1-390 wt Nter Histag	-	-	pRSFDuet1
pFVS0132	E. coli ParE 1-217 wt Nter Histag	-	-	pRSFDuet1
pFVS0133	E. coli Fic Gly55Arg Nter HisTag + YhfG Glu28Gly HA-Tag	Gly55Arg	Glu28Gly	pRSFDuet1
pFVS0134	NmFic Glu102Arg Glu156Arg	Glu102Arg Glu156Arg	wt	pRSFDuet1
pFVS0135	NmFic Glu156Arg Tyr183Phe	Glu156Arg	Tyr183Phe	pRSFDuet1
pFVS0136	NmFic Glu156Arg Tyr188Phe	Glu156Arg	Tyr188Phe	pRSFDuet1
pFVS0137	NmFic Glu102Arg His107Ala	Glu102Arg His107Ala	wt	pRSFDuet1
pFVS0138	NmFic His107Ala Glu156Arg	His107Ala Glu156Arg	wt	pRSFDuet1
pFVS0139	E. coli GyrA FL wt Nter HisTag	-	-	pRSFDuet1
pFVS0140	E. coli GyrA FL wt Cter HisTag	-	-	pRSFDuet1
pFVS0141	E. coli GyrB FL wt Nter HisTag	-	-	pRSFDuet1
pFVS0142	E. coli GyrB FL wt Cter HisTag	-	-	pRSFDuet1
pFVS0143	NmFic Glu102Arg His107Ala Glu156Arg	Glu102Arg His107Ala Glu156Arg	-	pRSFDuet1
pFVS0144	NmFic Glu102Arg Glu156Arg Tyr183Phe	Glu102Arg Glu156Arg	Tyr183Phe	pRSFDuet1
pFVS0145	NmFic Glu102Arg Glu156Arg Tyr188Phe	Glu102Arg Glu156Arg	Tyr188Phe	pRSFDuet1
pFVS0146	NmFic Tyr183Phe	-	Tyr183Phe	pNDM220

Plasmid	Description	FIC domain	Inhibition helix	Vector type
		Mutations		
pFVS0147	NmFic Tyr183Phe Glu186Gly	-	Tyr183Phe Glu186Gly	pNDM220
pFVS0148	NmFic His107Ala Glu186Gly	His107Ala	Glu186Gly	pNDM220
pFVS0149	NmFic Glu102Arg	Glu102Arg	-	pNDM220
pFVS0150	NmFic Glu156Arg	Glu156Arg	-	pNDM220
pFVS0151	NmFic His107Ala	His107Ala	-	pNDM220
pFVS0152	NmFic Arg149Glu Glu156Arg	Arg149Glu Glu156Arg	-	pRSFDuet1
pFVS0153	NmFic Arg71Glu	Arg71Glu	-	pRSFDuet1
pFVS0154	NmFic Arg71Glu Glu102Arg	Arg71Glu Glu102Arg	-	pRSFDuet1
pFVS0155	NmFic Tyr183Trp	-	Tyr183Trp	pRSFDuet1
pFVS0156	E. coli GyrB 1-392 Cys58Ser Nter HisTag	-	-	pRSFDuet1
pFVS0157	E. coli GyrB 1-392 Cys268Ser Nter HisTag	-	-	pRSFDuet1
pFVS0158	E. coli GyrB 1-392 Ser244Cys Nter HisTag	-	-	pRSFDuet1
pFVS0159	E. coli GyrB 1-392 Glu300Cys Nter HisTag	-	-	pRSFDuet1
pFVS0160	E. coli GyrB 1-392 Glu363Cys Nter HisTag	-	-	pRSFDuet1
pFVS0161	E. coli GyrB 1-392 Thr366Cys Nter HisTag	-	-	pRSFDuet1
pFVS0162	E. coli GyrB 1-392 Glu359Cys Nter HisTag	-	-	pRSFDuet1
pFVS0163	NmFic Arg149Glu	Arg149Glu	-	pRSFDuet1
pFVS0164	NmFic Tyr183Ala Glu186Gly	-	Tyr183Ala Glu186Gly	pRSFDuet1
pFVS0165	NmFic Glu102Arg His107Ala Glu156Arg Tyr183Phe	Glu102Arg His107Ala Glu156Arg	Tyr183Phe	pRSFDuet1
pFVS0166	NmFic Tyr183Arg	-	Tyr183Arg	pRSFDuet1
pFVS0167	NmFic Glu102Arg Tyr183Phe	Glu102Arg	Tyr183Phe	pRSFDuet1
pFVS0168	NmFic Glu102Arg Tyr188Phe	Glu102Arg	Tyr188Phe	pRSFDuet1
pFVS0169	NmFic Δ8 (10-167) Glu102Arg Glu156Arg	Glu102Arg Glu156Arg	Δ8	pRSFDuet1
pFVS0170	NmFic Δ8 (10-167) Glu102Arg His107Ala Glu156Arg	Glu102Arg His107Ala Glu156Arg	Δ8	pRSFDuet1
pFVS0171	NmFic Δ8 (10-167) Glu102Arg	Glu102Arg	Δ8	pRSFDuet1
pFVS0172	NmFic Δ8 (10-167) Glu156Arg	Glu156Arg	Δ8	pRSFDuet1
pFVS0173	NmFic Glu102Arg Glu156Arg	Glu102Arg Glu156Arg	-	pNDM220
pFVS0174	NmFic Glu102Arg Tyr183Phe	Glu102Arg	Tyr183Phe	pNDM220

Plasmid	Description	FIC domain	Inhibition helix	Vector type
		Mutations		
pFVS0175	NmFic Glu156Arg Tyr183Phe	Glu156Arg	Tyr183Phe	pNDM220
pFVS0176	NmFic Δ8 (10-167) His107Ala	His107Ala	Δ8	pNDM220
pFVS0177	NmFic Glu102Arg His107Ala	Glu102Arg His107Ala	-	pNDM220
pFVS0178	NmFic Glu102Arg Glu156Arg Tyr183Phe	Glu102Arg Glu156Arg	Tyr183Phe	pNDM220
pFVS0179	NmFic His107Ala Glu156Arg	His107Ala Glu156Arg	-	pNDM220
pFVS0180	NmFic Δ8 (10-167)	-	Δ8	pNDM220
pFVS0181	VbhT 1-198 wt + VbhA-STOP-(G4s)**1**-GyrB	wt	wt	pRSFDuet1
pFVS0182	NmFic-STOP-(G4S)**1**-GyrB	wt	wt	pRSFDuet1
pFVS0183	NmFic-STOP-(G4S)**3**-GyrB	wt	wt	pRSFDuet1
pFVS0184	NmFic-STOP-(G4S)**2**-GyrB	wt	wt	pRSFDuet1
pFVS0185	VbhT 1-198 wt + VbhA-STOP-(G4s)**2**-GyrB	wt	wt	pRSFDuet1
pFVS0186	VbhT 1-198 wt + VbhA-STOP-(G4s)**3**-GyrB	wt	wt	pRSFDuet1
pFVS0187	NmFic-(G4S)**1**-GyrB (fusion protein)	wt	wt	pRSFDuet1
pFVS0188	NmFic-(G4S)**3**-GyrB (fusion protein)	wt	wt	pRSFDuet1
pFVS0189	VbhT 1-198 wt + VbhA-(G4s)**1**-GyrB **V118I** (fusion protein)	wt	wt	pRSFDuet1
pFVS0190	NmFic Tyr183Phe Tyr185Phe	-	Tyr183Phe Tyr185Phe	pRSFDuet1
pFVS0191	NmFic Tyr183Phe Tyr185Phe Glu186Gly	-	Tyr183Phe Tyr185Phe Glu186Gly	pRSFDuet1
pFVS0192	NmFic Glu102Arg Glu156Arg Tyr183Phe Tyr185Phe	Glu102Arg Glu156Arg	Tyr183Phe Tyr185Phe	pRSFDuet1
pFVS0193	NmFic Glu102Arg His107Ala Glu156Arg Tyr183Phe Tyr185Phe Glu186Gly	Glu102Arg His107Ala Glu156Arg	Tyr183Phe Tyr185Phe Glu186Gly	pRSFDuet1
pFVS0194	VbhT 1-198 wt + VbhA-(G4s)**3**-GyrB (fusion protein)	wt	wt	pRSFDuet1
pFVS0195	VbhT 1-198 wt + VbhA-(G4s)**1**-GyrB (fusion protein)	wt	wt	pRSFDuet1
pFVS0196	NmFic Glu102Arg His107Ala Glu156Arg Tyr183Phe Tyr185Phe	Glu102Arg His107Ala Glu156Arg	Tyr183Phe Tyr185Phe	pRSFDuet1
pFVS0197	NmFic Glu102Arg His107Ala Glu156Arg	Glu102Arg His107Ala Glu156Arg	-	pNDM220
pFVS0198	NmFic-GGGDSGGGGS-GyrB (fusion protein)	wt	wt	pRSFDuet1
pFVS0199	NmFic-(G4S)**2**-GyrB (fusion protein)	wt	wt	pRSFDuet1
pFVS0200	VbhT 1-198 wt + VbhA-(G4S)**2**-GyrB (fusion protein)	wt	wt	pRSFDuet1
pFVS0201	VbhT 1-198 wt + VbhA-STOP-(G4S)**4**-GyrB	wt	wt	pRSFDuet1
pFVS0202	NmFic_Glu186Gly-(G4S)**1**-GyrB (fusion protein)	wt	Glu186Gly	pRSFDuet1
pFVS0203	NmFic_Glu186Gly-(G4S)**2**-GyrB (fusion protein)	wt	Glu186Gly	pRSFDuet1

Plasmid	Description	FIC domain	Inhibition helix	Vector type
		Mutations		
pFVS0204	NmFic_Glu186Gly-(G4S)**3**-GyrB (fusion protein)	wt	Glu186Gly	pRSFDuet1
pFVS0205	NmFic_His107Ala-(G4S)**1**-GyrB (fusion protein)	His107Ala	wt	pRSFDuet1
pFVS0206	NmFic_His107Ala-(G4S)**2**-GyrB (fusion protein)	His107Ala	wt	pRSFDuet1
pFVS0207	NmFic_His107Ala-(G4S)**3**-GyrB (fusion protein)	His107Ala	wt	pRSFDuet1
pFVS0208	VbhT 1-198 wt + VbhA_Glu24Gly-(G4S)**1**-GyrB (fusion protein)	wt	Glu24Gly	pRSFDuet1
pFVS0209	VbhT 1-198 wt + VbhA_Glu24Gly-(G4S)**2**-GyrB (fusion protein)	wt	Glu24Gly	pRSFDuet1
pFVS0210	VbhT 1-198 wt + VbhA_Glu24Gly-(G4S)**3**-GyrB (fusion protein)	wt	Glu24Gly	pRSFDuet1
pFVS0211	VbhT 1-198 His136Ala + VbhA-(G4S)**1**-GyrB (fusion protein)	His136Ala	wt	pRSFDuet1
pFVS0212	VbhT 1-198 His136Ala + VbhA-(G4S)**2**-GyrB (fusion protein)	His136Ala	wt	pRSFDuet1
pFVS0213	VbhT 1-198 His136Ala + VbhA-(G4S)**3**-GyrB (fusion protein)	His136Ala	wt	pRSFDuet1
pFVS0214	NmFic_His107Ala_Glu186Gly-(G4S)**1**-GyrB (fusion protein)	His107Ala	Glu186Gly	pRSFDuet1
pFVS0215	NmFic_His107Ala_Glu186Gly-(G4S)**2**-GyrB (fusion protein)	His107Ala	Glu186Gly	pRSFDuet1
pFVS0216	NmFic_His107Ala_Glu186Gly-(G4S)**3**-GyrB (fusion protein)	His107Ala	Glu186Gly	pRSFDuet1
pFVS0217	VbhT 1-198 His136Ala + VbhA_Glu24Gly-(G4S)**1**-GyrB (fusion protein)	His136Ala	Glu24Gly	pRSFDuet1
pFVS0218	VbhT 1-198 His136Ala + VbhA_Glu24Gly-(G4S)**2**-GyrB (fusion protein)	His136Ala	Glu24Gly	pRSFDuet1
pFVS0219	VbhT 1-198 His136Ala + VbhA_Glu24Gly-(G4S)**3**-GyrB (fusion protein)	His136Ala	Glu24Gly	pRSFDuet1
pFVS0220	NmFic Δhelix1 (32-191) Nter HisTag	Δhelix1	wt	pRSFDuet1
pFVS0221	NmFic Δhelix1 (32-191) Cter HisTag	Δhelix1	wt	pRSFDuet1
pFVS0222	NmFic Δ½-helix1 (22-191) Nter HisTag	Δ½-helix1	wt	pRSFDuet1
pFVS0223	VbhT 1-198 Ser175Cys + VbhA wt	Ser175Cys	wt	pRSFDuet1
pFVS0224	VbhT 1-198 His136Ala Ser175Cys + VbhA wt	His136Ala Ser175Cys	wt	pRSFDuet1
pFVS0225	VbhT 1-198 His136Ala Ser175Cys + VbhA Glu24Gly	His136Ala Ser175Cys	Glu24Gly	pRSFDuet1
pFVS0226	NmFic Met147Cys	Met147Cys	wt	pRSFDuet1
pFVS0227	NmFic His107Ala Met147Cys	His107Ala Met147Cys	wt	pRSFDuet1
pFVS0228	NmFic His107Ala Met147Cys Glu186Gly	His107Ala Met147Cys	Glu186Gly	pRSFDuet1
pFVS0229	VbhT 1-198 Ser175Cys + VbhA Glu24Gly	Ser175Cys	Glu24Gly	pRSFDuet1
pFVS0230	NmFic Met147Cys Glu186Gly	Met147Cys	Glu186Gly	pRSFDuet1
pFVS0231	NmFic Δhelix1 Glu186Gly (32-191) Nter HisTag	Δhelix1	Glu186Gly	pRSFDuet1

Plasmid	Description	FIC domain	Inhibition helix	Vector type
		Mutations		
pFVS0232	NmFic Δhelix1 Glu186Gly (32-191) Cter HisTag	Δhelix1	Glu186Gly	pRSFDuet1
pFVS0233	NmFic Δ½-helix1 Glu186Gly (22-191) Nter HisTag	Δ½-helix1	Glu186Gly	pRSFDuet1
pFVS0234	NmFic Glu102Arg Glu186Gly	Glu102Arg	Glu186Gly	pNDM220
pFVS0235	NmFic Glu156Arg Glu186Gly	Glu156Arg	Glu186Gly	pNDM220
pFVS0236	NmFic Glu102Arg Glu156Arg Glu186Gly	Glu102Arg Glu156Arg	Glu186Gly	pNDM220
pFVS0237	NmFic Glu102Arg Glu186Gly Nter HisTag	Glu102Arg	Glu186Gly	pRSFDuet1
pFVS0238	NmFic Glu102Arg Glu156Arg Glu186Gly Nter HisTag	Glu102Arg Glu156Arg	Glu186Gly	pRSFDuet1
pFVS0239	Human GST-Cdc42 Lys27Ala	-	-	pGex6p1
pFVS0240	Human GST-Cdc42 Ser30Gly	-	-	pGex6p1
pFVS0241	Human GST-Cdc42 Lys27Ala Q61L (constitutively active)	-	-	pGex6p1
pFVS0242	Human GST-Cdc42 Ser30Gly Q61L (constitutively active)	-	-	pGex6p1
pFVS0243	Human GST-Rac1 Ala27Lys	-	-	pGex6p1
pFVS0244	Human GST-Rac1 Gly30Ser	-	-	pGex6p1
pFVS0245	Human GST-Rac1 Ala27Lys Q61L (constitutively active)	-	-	pGex6p1
pFVS0246	Human GST-Rac1 Gly30Ser Q61L (constitutively active)	-	-	pGex6p1

8.2. Strains constructed

A comprehensive list of the strains obtained in the frame of my PhD thesis work appears below.

Name (TS strain collection)	Name (CHD strain collection)	Description	Plasmid name	Vector type	Cell type	Resistance
FVS001	FVSE101	Hbep FL (wt) schoenbuchensis Cter HisTag	pFVS0001	pRSFDuet1	Novablue	Kan |
FVS002	FVSE102	Hbep FL (wt) + AT schoenbuchensis Cter HisTag	pFVS0002	pRSFDuet1	Novablue	Kan |
FVS003	FVSE103	Hbep cst1 (HxxxA) schoenbuchensis Cter HisTag	pFVS0003	pRSFDuet1	Novablue	Kan |
FVS004	FVSE104	Hbep cst1 (HxxxA) + AT schoenbuchensis Cter HisTag	pFVS0004	pRSFDuet1	Novablue	Kan |

Name (TS strain collection)	Name (CHD strain collection)	Description	Plasmid name	Vector type	Cell type	Resistance
FVS005	FVSE105	Hbep cst2 (HxxxA) schoenbuchensis Cter HisTag	pFVS0005	pRSFDuet1	Novablue	Kan |
FVS006	FVSE106	Hbep cst2 (HxxxA) + AT schoenbuchensis Cter HisTag	pFVS0006	pRSFDuet1	Novablue	Kan |
FVS007	FVSE107	Bep1ro FicΔ8 (HxxxA) rochalimae Cter HisTag	pFVS0007	pRSFDuet1	Novablue	Kan |
FVS008	FVSE108	Bep1ro FicOB (HxxxA) rochalimae Cter HisTag	pFVS0008	pRSFDuet1	Novablue	Kan |
FVS009	FVSE109	Bep1ro FicOBex (HxxxA) rochalimae Cter HisTag	pFVS0009	pRSFDuet1	Novablue	Kan |
FVS010	FVSE110	Hbep FL (wt) schoenbuchensis Cter HisTag	pFVS0001	pRSFDuet1	BL21	Kan |
FVS011	FVSE111	Hbep FL (wt) + AT schoenbuchensis Cter HisTag	pFVS0002	pRSFDuet1	BL21	Kan |
FVS012	FVSE112	Hbep cst1 (HxxxA) schoenbuchensis Cter HisTag	pFVS0003	pRSFDuet1	BL21	Kan |
FVS013	FVSE113	Hbep cst1 (HxxxA) + AT schoenbuchensis Cter HisTag	pFVS0004	pRSFDuet1	BL21	Kan |
FVS014	FVSE114	Hbep cst2 (HxxxA) schoenbuchensis Cter HisTag	pFVS0005	pRSFDuet1	BL21	Kan |
FVS015	FVSE115	Hbep cst2 (HxxxA) + AT schoenbuchensis Cter HisTag	pFVS0006	pRSFDuet1	BL21	Kan |
FVS016	FVSE116	Bep1ro FicΔ8 (HxxxA) rochalimae Cter HisTag	pFVS0007	pRSFDuet1	BL21	Kan |
FVS017	FVSE117	Bep1ro FicOB (HxxxA) rochalimae Cter HisTag	pFVS0008	pRSFDuet1	BL21	Kan |
FVS018	FVSE118	Bep1ro FicOBex (HxxxA) rochalimae Cter HisTag	pFVS0009	pRSFDuet1	BL21	Kan |
FVS019	FVSE119	Hbep FL (HxxxA) schoenbuchensis Cter HisTag	pFVS0010	pRSFDuet1	Novablue	Kan |
FVS020	FVSE120	Hbep FL (HxxxA) schoenbuchensis Cter HisTag	pFVS0010	pRSFDuet1	BL21	Kan |
FVS021	FVSE121	Hbep FL (wt) schoenbuchensis Cter HisTag	pFVS0001	pRSFDuet1	Rosetta	Kan | + Cam |
FVS022	FVSE122	Hbep FL (wt) + AT schoenbuchensis Cter HisTag	pFVS0002	pRSFDuet1	Rosetta	Kan | + Cam |
FVS023	FVSE123	Hbep cst1 (HxxxA) schoenbuchensis Cter HisTag	pFVS0003	pRSFDuet1	Rosetta	Kan | + Cam |
FVS024	FVSE124	Hbep cst1 (HxxxA) + AT schoenbuchensis Cter HisTag	pFVS0004	pRSFDuet1	Rosetta	Kan | + Cam |
FVS025	FVSE125	Hbep cst2 (HxxxA) schoenbuchensis Cter HisTag	pFVS0005	pRSFDuet1	Rosetta	Kan | + Cam |
FVS026	FVSE126	Hbep cst2 (HxxxA) + AT schoenbuchensis Cter HisTag	pFVS0006	pRSFDuet1	Rosetta	Kan | + Cam |
FVS027	FVSE127	Bep1ro FicΔ8 (HxxxA) rochalimae Cter HisTag	pFVS0007	pRSFDuet1	Rosetta	Kan | + Cam |
FVS028	FVSE128	Bep1ro FicOB (HxxxA) rochalimae Cter HisTag	pFVS0008	pRSFDuet1	Rosetta	Kan | + Cam |
FVS029	FVSE129	Bep1ro FicOBex (HxxxA) rochalimae Cter HisTag	pFVS0009	pRSFDuet1	Rosetta	Kan | + Cam |
FVS030	FVSE130	Hbep FL (HxxxA) schoenbuchensis Cter HisTag	pFVS0010	pRSFDuet1	Rosetta	Kan | + Cam |
FVS031	FVSE131	Hbep 1-198 (wt) + AT schoenbuchensis Cter HisTag	pFVS0011	pRSFDuet1	Novablue	Kan |
FVS032	FVSE132	Hbep 1-198 (wt) schoenbuchensis Cter HisTag	pFVS0012	pRSFDuet1	Novablue	Kan |
FVS033	FVSE133	Hbep 8-198 (wt) schoenbuchensis Cter HisTag	pFVS0014	pRSFDuet1	Novablue	Kan |
FVS034	FVSE134	Hbep 1-198 (wt) + AT schoenbuchensis Cter HisTag	pFVS0011	pRSFDuet1	BL21	Kan |
FVS035	FVSE135	Hbep 1-198 (wt) + AT schoenbuchensis Cter HisTag	pFVS0011	pRSFDuet1	Rosetta	Kan | + Cam |
FVS036	FVSE136	Hbep 1-198 (wt) schoenbuchensis Cter HisTag	pFVS0012	pRSFDuet1	BL21	Kan |
FVS037	FVSE137	Hbep 1-198 (wt) schoenbuchensis Cter HisTag	pFVS0012	pRSFDuet1	Rosetta	Kan | + Cam |
FVS038	FVSE138	Hbep 8-198 (wt) schoenbuchensis Cter HisTag	pFVS0014	pRSFDuet1	BL21	Kan |

Name (TS strain collection)	Name (CHD strain collection)	Description	Plasmid name	Vector type	Cell type	Resistance
FVS039	FVSE139	Hbep 8-198 (wt) schoenbuchensis Cter HisTag	pFVS0014	pRSFDuet1	Rosetta	Kan | + Cam |
FVS040	FVSE140	Hbep 8-198 (wt) + AT schoenbuchensis Cter HisTag	pFVS0013	pRSFDuet1	Novablue	Kan |
FVS041	FVSE141	Neisseria meningitidis Fic wt (10-191) Nter HisTag	pFVS0015	pRSFDuet1	Novablue	Kan |
FVS042	FVSE142	Neisseria meningitidis Fic Δ8 (10-167) Nter HisTag	pFVS0016	pRSFDuet1	Novablue	Kan |
FVS043	FVSE143	VbhT FL Glu35Asn Cter HisTag	pFVS0017	pRSFDuet1	Novablue	Kan |
FVS044	FVSE144	VbhA wt + VbhT 1-198 Glu35Asn Cter HisTag	pFVS0018	pRSFDuet1	Novablue	Kan |
FVS045	FVSE145	Hbep 8-198 (wt) + AT schoenbuchensis Cter HisTag	pFVS0013	pRSFDuet1	BL21	Kan |
FVS046	FVSE146	Hbep 8-198 (wt) + AT schoenbuchensis Cter HisTag	pFVS0013	pRSFDuet1	Rosetta	Kan | + Cam |
FVS047	FVSE147	Neisseria meningitidis Fic wt (10-191) Nter HisTag	pFVS0015	pRSFDuet1	BL21	Kan |
FVS048	FVSE148	Neisseria meningitidis Fic wt (10-191) Nter HisTag	pFVS0015	pRSFDuet1	Rosetta	Kan | + Cam |
FVS049	FVSE149	Neisseria meningitidis Fic Δ8 (10-167) Nter HisTag	pFVS0016	pRSFDuet1	BL21	Kan |
FVS050	FVSE150	Neisseria meningitidis Fic Δ8 (10-167) Nter HisTag	pFVS0016	pRSFDuet1	Rosetta	Kan | + Cam |
FVS051	FVSE151	Helicobacter pylori Fic (G27) FL wt (1-176) Nter HisTag	pFVS0019	pRSFDuet1	Novablue	Kan |
FVS052	FVSE152	Helicobacter pylori Fic (G27) Δ8 (1-155) Nter HisTag	pFVS0020	pRSFDuet1	Novablue	Kan |
FVS053	FVSE153	NO VbhA + VbhT FL Glu35Asn Cter HisTag	pFVS0017	pRSFDuet1	BL21	Kan |
FVS054	FVSE154	NO VbhA + VbhT FL Glu35Asn Cter HisTag	pFVS0017	pRSFDuet1	Rosetta	Kan | + Cam |
FVS055	FVSE155	VbhA wt + VbhT 1-198 Glu35Asn Cter HisTag	pFVS0018	pRSFDuet1	BL21	Kan |
FVS056	FVSE156	VbhA wt + VbhT 1-198 Glu35Asn Cter HisTag	pFVS0018	pRSFDuet1	Rosetta	Kan | + Cam |
FVS057	FVSE157	Helicobacter pylori Fic (G27) FL wt (1-176) Nter HisTag	pFVS0019	pRSFDuet1	BL21	Kan |
FVS058	FVSE158	Helicobacter pylori Fic (G27) FL wt (1-176) Nter HisTag	pFVS0019	pRSFDuet1	Rosetta	Kan | + Cam |
FVS059	FVSE159	Helicobacter pylori Fic (G27) Δ8 (1-155) Nter HisTag	pFVS0020	pRSFDuet1	BL21	Kan |
FVS060	FVSE160	Helicobacter pylori Fic (G27) Δ8 (1-155) Nter HisTag	pFVS0020	pRSFDuet1	Rosetta	Kan | + Cam |
FVS061	FVSE161	Neisseria meningitidis Fic (10-191) Asp15Ala Nter HisTag	pFVS0021	pRSFDuet1	Novablue	Kan |
FVS062	FVSE162	Neisseria meningitidis Fic Δ8 (10-167) Asp15Ala Nter HisTag	pFVS0022	pRSFDuet1	Novablue	Kan |
FVS063	FVSE163	Neisseria meningitidis Fic (10-191) Glu186Ala Nter HisTag	pFVS0023	pRSFDuet1	Novablue	Kan |
FVS064	FVSE164	Neisseria meningitidis Fic (10-191) Asp15Ala Nter HisTag	pFVS0021	pRSFDuet1	BL21	Kan |
FVS065	FVSE165	Neisseria meningitidis Fic (10-191) Asp15Ala Nter HisTag	pFVS0021	pRSFDuet1	Rosetta	Kan | + Cam |
FVS066	FVSE166	Neisseria meningitidis Fic Δ8 (10-167) Asp15Ala Nter HisTag	pFVS0022	pRSFDuet1	BL21	Kan |
FVS067	FVSE167	Neisseria meningitidis Fic Δ8 (10-167) Asp15Ala Nter HisTag	pFVS0022	pRSFDuet1	Rosetta	Kan | + Cam |
FVS068	FVSE168	Neisseria meningitidis Fic (10-191) Glu186Ala Nter HisTag	pFVS0023	pRSFDuet1	BL21	Kan |
FVS069	FVSE169	Neisseria meningitidis Fic (10-191) Glu186Ala Nter HisTag	pFVS0023	pRSFDuet1	Rosetta	Kan | + Cam |
FVS070	FVSE170	VbhT FL (HxxxA) + VbhA schoenbuchensis Cter HisTag	pFVS0024	pRSFDuet1	Novablue	Kan |
FVS071	FVSE171	VbhA wt + VbhT FL Glu35Asn Cter HisTag	pFVS0025	pRSFDuet1	Novablue	Kan |
FVS072	FVSE172	Helicobacter pylori Fic (G27) Δ8 (1-155) Asp4Ala	pFVS0026	pRSFDuet1	Novablue	Kan |
FVS073	FVSE173	Helicobacter pylori Fic (G27) FL (1-176) Asp4Ala	pFVS0027	pRSFDuet1	Novablue	Kan |

Name (TS strain collection)	Name (CHD strain collection)	Description	Plasmid name	Vector type	Cell type	Resistance
FVS074	FVSE174	Helicobacter pylori Fic (G27) FL (1-176) Ser171Ala Glu175Ala	pFVS0028	pRSFDuet1	Novablue	Kan |
FVS075	FVSE175	VbhT FL (HxxxA) + VbhA schoenbuchensis Cter HisTag	pFVS0024	pRSFDuet1	BL21	Kan |
FVS076	FVSE176	VbhT FL (HxxxA) + VbhA schoenbuchensis Cter HisTag	pFVS0024	pRSFDuet1	Rosetta	Kan | + Cam |
FVS077	FVSE177	VbhA wt + VbhT FL Glu35Asn Cter HisTag	pFVS0025	pRSFDuet1	BL21	Kan |
FVS078	FVSE178	VbhA wt + VbhT FL Glu35Asn Cter HisTag	pFVS0025	pRSFDuet1	Rosetta	Kan | + Cam |
FVS079	FVSE179	Helicobacter pylori Fic (G27) Δ8 (1-155) Asp4Ala	pFVS0026	pRSFDuet1	BL21	Kan |
FVS080	FVSE180	Helicobacter pylori Fic (G27) Δ8 (1-155) Asp4Ala	pFVS0026	pRSFDuet1	Rosetta	Kan | + Cam |
FVS081	FVSE181	Helicobacter pylori Fic (G27) FL (1-176) Asp4Ala	pFVS0027	pRSFDuet1	BL21	Kan |
FVS201	FVSE201	Helicobacter pylori Fic (G27) FL (1-176) Asp4Ala	pFVS0027	pRSFDuet1	Rosetta	Kan | + Cam |
FVS202	FVSE202	Helicobacter pylori Fic (G27) FL (1-176) Ser171Ala Glu175Ala	pFVS0028	pRSFDuet1	BL21	Kan |
FVS203	FVSE203	Helicobacter pylori Fic (G27) FL (1-176) Ser171Ala Glu175Ala	pFVS0028	pRSFDuet1	Rosetta	Kan | + Cam |
FVS204	FVSE204	VbhA Ser21Ala + VbhT FL wt Cter HisTag	pFVS0029	pRSFDuet1	Novablue	Kan |
FVS205	FVSE205	VbhA Ser21Ala + VbhT 1-198 wt Cter HisTag	pFVS0030	pRSFDuet1	Novablue	Kan |
FVS206	FVSE206	VbhA Ser21Ala Glu25Ala + VbhT FL wt Cter HisTag	pFVS0031	pRSFDuet1	Novablue	Kan |
FVS207	FVSE207	VbhA Ser21Ala Glu25Ala + VbhT FL Glu35Asn Cter HisTag	pFVS0032	pRSFDuet1	Novablue	Kan |
FVS208	FVSE208	VbhA Ser21Ala Glu25Ala + VbhT 1-198 Glu35Asn Cter HisTag	pFVS0033	pRSFDuet1	Novablue	Kan |
FVS209	FVSE209	Helicobacter pylori Fic (G27) FL (1-176) Asp4Ala Ser171Ala Glu175Ala	pFVS0034	pRSFDuet1	Novablue	Kan |
FVS210	FVSE210	Neisseria meningitidis Fic (10-191) Asp15Ala Glu186Ala Nter HisTag	pFVS0035	pRSFDuet1	Novablue	Kan |
FVS211	FVSE211	VbhA Ser21Ala + VbhT FL wt Cter HisTag	pFVS0029	pRSFDuet1	BL21	Kan |
FVS212	FVSE212	VbhA Ser21Ala + VbhT 1-198 wt Cter HisTag	pFVS0030	pRSFDuet1	BL21	Kan |
FVS213	FVSE213	VbhA Ser21Ala Glu25Ala + VbhT FL wt Cter HisTag	pFVS0031	pRSFDuet1	BL21	Kan |
FVS214	FVSE214	VbhA Ser21Ala Glu25Ala + VbhT FL Glu35Asn Cter HisTag	pFVS0032	pRSFDuet1	BL21	Kan |
FVS215	FVSE215	VbhA Ser21Ala Glu25Ala + VbhT 1-198 Glu35Asn Cter HisTag	pFVS0033	pRSFDuet1	BL21	Kan |
FVS216	FVSE216	Helicobacter pylori Fic (G27) FL (1-176) Asp4Ala Ser171Ala Glu175Ala	pFVS0034	pRSFDuet1	BL21	Kan |
FVS217	FVSE217	Neisseria meningitidis Fic (10-191) Asp15Ala Glu186Ala Nter HisTag	pFVS0035	pRSFDuet1	BL21	Kan |
FVS218	FVSE218	VbhA Ser21Ala + VbhT FL wt Cter HisTag	pFVS0029	pRSFDuet1	Rosetta	Kan | + Cam |
FVS219	FVSE219	VbhA Ser21Ala + VbhT 1-198 wt Cter HisTag	pFVS0030	pRSFDuet1	Rosetta	Kan | + Cam |
FVS220	FVSE220	VbhA Ser21Ala Glu25Ala + VbhT FL wt Cter HisTag	pFVS0031	pRSFDuet1	Rosetta	Kan | + Cam |
FVS221	FVSE221	VbhA Ser21Ala Glu25Ala + VbhT FL Glu35Asn Cter HisTag	pFVS0032	pRSFDuet1	Rosetta	Kan | + Cam |
FVS222	FVSE222	VbhA Ser21Ala Glu25Ala + VbhT 1-198 Glu35Asn Cter HisTag	pFVS0033	pRSFDuet1	Rosetta	Kan | + Cam |
FVS223	FVSE223	Helicobacter pylori Fic (G27) FL (1-176) Asp4Ala Ser171Ala Glu175Ala	pFVS0034	pRSFDuet1	Rosetta	Kan | + Cam |
FVS224	FVSE224	Neisseria meningitidis Fic (10-191) Asp15Ala Glu186Ala Nter HisTag	pFVS0035	pRSFDuet1	Rosetta	Kan | + Cam |
FVS225	FVSE225	Shewanella oneidensis Fic protein in pSpeed vector (from DNASU)	pFVS0036	pSpeed vector	DH5 α	Kan |

Name (TS strain collection)	Name (CHD strain collection)	Description	Plasmid name	Vector type	Cell type	Resistance
FVS226	FVSE226	Neisseria meningitidis Fic (10-191) Ser182Ala Glu186Ala Nter HisTag	pFVS0037	pRSFDuet1	Novablue	Kan |
FVS227	FVSE227	Neisseria meningitidis Fic (10-191) Asp15Ala Ser182Ala Glu186Ala Nter HisTag	pFVS0038	pRSFDuet1	Novablue	Kan |
FVS228	FVSE228	Shewanella oneidensis Fic protein in pSpeed vector (from DNASU)	pFVS0036	pSpeed vector	Novablue	Kan |
FVS229	FVSE229	Shewanella oneidensis Fic protein in pSpeed vector (from DNASU)	pFVS0036	pSpeed vector	BL21	Kan |
FVS230	FVSE230	Shewanella oneidensis Fic protein in pSpeed vector (from DNASU)	pFVS0036	pSpeed vector	Rosetta	Kan | + Cam |
FVS231	FVSE231	Neisseria meningitidis Fic (10-191) Ser182Ala Glu186Ala Nter HisTag	pFVS0037	pRSFDuet1	BL21	Kan |
FVS232	FVSE232	Neisseria meningitidis Fic (10-191) Ser182Ala Glu186Ala Nter HisTag	pFVS0037	pRSFDuet1	Rosetta	Kan | + Cam |
FVS233	FVSE233	Neisseria meningitidis Fic (10-191) Asp15Ala Ser182Ala Glu186Ala Nter HisTag	pFVS0038	pRSFDuet1	BL21	Kan |
FVS234	FVSE234	Neisseria meningitidis Fic (10-191) Asp15Ala Ser182Ala Glu186Ala Nter HisTag	pFVS0038	pRSFDuet1	Rosetta	Kan | + Cam |
FVS235	FVSE235	VbhT 1-198 Glu35Asn Cter HisTag	pFVS0039	pRSFDuet1	Novablue	Kan |
FVS236	FVSE236	VbhT 1-198 Glu35Asn Cter HisTag	pFVS0039	pRSFDuet1	BL21	Kan |
FVS237	FVSE237	VbhT 1-198 Glu35Asn Cter HisTag	pFVS0039	pRSFDuet1	Rosetta	Kan |
FVS238	FVSE238	Shewanella oneidensis Fic wt in Duet	pFVS0040	pRSFDuet1	Novablue	Kan |
FVS239	FVSE239	VbhA wt + VbhT 1-198 H136A Cter HisTag	pFVS0041	pRSFDuet1	Novablue	Kan |
FVS240	FVSE240	VbhT 1-198 H136A Cter HisTag	pFVS0042	pRSFDuet1	Novablue	Kan |
FVS241	FVSE241	Helicobacter pylori Fic (G27) helix α8 (MCS1) + Fic Δ8 (MCS2)	pFVS0043	pRSFDuet1	Novablue	Kan |
FVS242	FVSE242	Neisseria meningitidis Fic (10-191) Tyr183Ala Nter HisTag	pFVS0044	pRSFDuet1	Novablue	Kan |
FVS243	FVSE243	VbhA wt + VbhT 1-198 Arg144Ala Cter HisTag	pFVS0045	pRSFDuet1	Novablue	Kan |
FVS244	FVSE244	VbhA wt + VbhT 1-198 Arg147Ala Cter HisTag	pFVS0046	pRSFDuet1	Novablue	Kan |
FVS245	FVSE245	Shewanella oneidensis Fic wt in Duet	pFVS0040	pRSFDuet1	BL21	Kan |
FVS246	FVSE246	Shewanella oneidensis Fic wt in Duet	pFVS0040	pRSFDuet1	Rosetta	Kan | + Cam |
FVS247	FVSE247	VbhA wt + VbhT 1-198 H136A Cter HisTag	pFVS0041	pRSFDuet1	BL21	Kan |
FVS248	FVSE248	VbhA wt + VbhT 1-198 H136A Cter HisTag	pFVS0041	pRSFDuet1	Rosetta	Kan | + Cam |
FVS249	FVSE249	VbhT 1-198 H136A Cter HisTag	pFVS0042	pRSFDuet1	BL21	Kan |
FVS250	FVSE250	VbhT 1-198 H136A Cter HisTag	pFVS0042	pRSFDuet1	Rosetta	Kan | + Cam |
FVS251	FVSE251	Helicobacter pylori Fic (G27) helix α8 (MCS1) + Fic Δ8 (MCS2)	pFVS0043	pRSFDuet1	BL21	Kan |
FVS252	FVSE252	Helicobacter pylori Fic (G27) helix α8 (MCS1) + Fic Δ8 (MCS2)	pFVS0043	pRSFDuet1	Rosetta	Kan | + Cam |
FVS253	FVSE253	Neisseria meningitidis Fic (10-191) Tyr183Ala Nter HisTag	pFVS0044	pRSFDuet1	BL21	Kan |
FVS254	FVSE254	Neisseria meningitidis Fic (10-191) Tyr183Ala Nter HisTag	pFVS0044	pRSFDuet1	Rosetta	Kan | + Cam |
FVS255	FVSE255	VbhA wt + VbhT 1-198 Arg144Ala Cter HisTag	pFVS0045	pRSFDuet1	BL21	Kan |
FVS256	FVSE256	VbhA wt + VbhT 1-198 Arg144Ala Cter HisTag	pFVS0045	pRSFDuet1	Rosetta	Kan | + Cam |
FVS257	FVSE257	VbhA wt + VbhT 1-198 Arg147Ala Cter HisTag	pFVS0046	pRSFDuet1	BL21	Kan |
FVS258	FVSE258	VbhA wt + VbhT 1-198 Arg147Ala Cter HisTag	pFVS0046	pRSFDuet1	Rosetta	Kan | + Cam |
FVS259	FVSE259	VbhA Gln22Ala + VbhT 1-198 wt Cter HisTag	pFVS0047	pRSFDuet1	Novablue	Kan |
FVS260	FVSE260	VbhT 1-198 Arg144Ala Cter HisTag	pFVS0048	pRSFDuet1	Novablue	Kan |

Name (TS strain collection)	Name (CHD strain collection)	Description	Plasmid name	Vector type	Cell type	Resistance
FVS261	FVSE261	VbhT 1-198 Arg147Ala Cter HisTag	pFVS0049	pRSFDuet1	Novablue	Kan |
FVS262	FVSE262	Neisseria meningitidis Fic (10-191) Tyr183Ala Tyr188Ala Nter HisTag	pFVS0050	pRSFDuet1	Novablue	Kan |
FVS263	FVSE263	Neisseria meningitidis Fic (10-191) His107Ala Nter HisTag	pFVS0051	pRSFDuet1	Novablue	Kan |
FVS264	FVSE264	VbhA wt + VbhT Arg144Ala Arg147Ala Cter HisTag	pFVS0052	pRSFDuet1	Novablue	Kan |
FVS265	FVSE265	VbhT 1-198 Arg144Ala Arg147Ala Cter HisTag	pFVS0053	pRSFDuet1	Novablue	Kan |
FVS266	FVSE266	VbhA Ser21Ala Glu25Ala + VbhT 1-198 wt Cter HisTag	pFVS0054	pRSFDuet1	Novablue	Kan |
FVS267	FVSE267	VbhA Gln22Ala Leu27Ala + VbhT 1-198 wt Cter HisTag	pFVS0055	pRSFDuet1	Novablue	Kan |
FVS268	FVSE268	Neisseria meningitidis Fic (10-191) Glu111Gln Ser182Ala Glu186Ala Nter HisTag	pFVS0056	pRSFDuet1	Novablue	Kan |
FVS269	FVSE269	Shewanella oneidensis Fic Glu73Ala in Duet	pFVS0057	pRSFDuet1	Novablue	Kan |
FVS270	FVSE270	Shewanella oneidensis Fic Glu73Gly in Duet	pFVS0058	pRSFDuet1	Novablue	Kan |
~~FVS271~~	~~FVSE271~~	~~Neisseria meningitidis Fic (10-191) Glu186Gly Nter HisTag~~ *(contaminated with wt)*	~~pFVS0059~~	~~pRSFDuet1~~	~~Novablue~~	~~Kan |~~
FVS272	FVSE272	VbhA Glu25Gly + VbhT 1-198 Val188Ala Cter HisTag	pFVS0060	pRSFDuet1	Novablue	Kan |
FVS273	FVSE273	HYPE wt Nter GST-Tag Cter HisTag	pFVS0061	pET-GSTx	Novablue	Amp ||
FVS274	FVSE274	HYPE His295Ala Nter GST-Tag Cter HisTag	pFVS0062	pET-GSTx	Novablue	Amp ||
FVS275	FVSE275	HYPE Glu234Ala Nter GST-Tag Cter HisTag	pFVS0063	pET-GSTx	Novablue	Amp ||
FVS276	FVSE276	HYPE Glu234Gly Nter GST-Tag Cter HisTag	pFVS0064	pET-GSTx	Novablue	Amp ||
FVS277	FVSE277	HYPE wt Nter GST-Tag Cter HisTag	pFVS0061	pET-GSTx	Rosetta	Amp || + Cam |
FVS278	FVSE278	HYPE His295Ala Nter GST-Tag Cter HisTag	pFVS0062	pET-GSTx	Rosetta	Amp || + Cam |
FVS279	FVSE279	HYPE Glu234Ala Nter GST-Tag Cter HisTag	pFVS0063	pET-GSTx	Rosetta	Amp || + Cam |
FVS280	FVSE280	HYPE Glu234Gly Nter GST-Tag Cter HisTag	pFVS0064	pET-GSTx	Rosetta	Amp || + Cam |
FVS281	FVSE281	VbhA Glu25Gly + VbhT 1-198 wt Cter HisTag	pFVS0065	pRSFDuet1	Novablue	Kan |
FVS301	FVSE301	Neisseria meningitidis Fic Δ8 (10-167) His107Ala Nter HisTag	pFVS0066	pRSFDuet1	Novablue	Kan |
FVS302	FVSE302	Neisseria meningitidis Fic (10-191) His107Ala Ser182Ala Glu186Ala Nter HisTag	pFVS0067	pRSFDuet1	Novablue	Kan |
FVS303	FVSE303	HYPE Thr230Ala Glu234Gly Nter GST-Tag Cter HisTag	pFVS0068	pET-GSTx	Novablue	Amp ||
FVS304	FVSE304	HYPE Thr230Ala Glu234Ala His225Tyr Nter GST-Tag Cter HisTag	pFVS0069	pET-GSTx	Novablue	Amp ||
FVS305	FVSE305	Neisseria meningitidis Fic (10-191) Glu186Gly Nter HisTag	pFVS0059	pRSFDuet1	Novablue	Kan |
FVS306	FVSE306	Shewanella oneidensis Fic His198Ala in Duet	pFVS0070	pRSFDuet1	Novablue	Kan |
FVS307	FVSE307	Shewanella oneidensis Fic Ser69Ala Glu73Gly Asp136Gly in Duet	pFVS0071	pRSFDuet1	Novablue	Kan |
FVS308	FVSE308	HYPE Thr230Ala Glu234Ala Nter GST-Tag Cter HisTag	pFVS0072	pET-GSTx	Novablue	Amp ||
FVS309	FVSE309	HYPE His295Ala Glu234Ala Nter GST-Tag Cter HisTag	pFVS0073	pET-GSTx	Novablue	Amp ||
FVS310	FVSE310	HYPE His295Ala Glu234Gly Nter GST-Tag Cter HisTag	pFVS0074	pET-GSTx	Novablue	Amp ||
FVS311	FVSE311	HYPE Thr230Ala Glu234Gly Nter GST-Tag Cter HisTag	pFVS0068	pET-GSTx	Rosetta	Amp || + Cam |
FVS312	FVSE312	HYPE Thr230Ala Glu234Ala Nter GST-Tag Cter HisTag	pFVS0072	pET-GSTx	Rosetta	Amp || + Cam |

Name (TS strain collection)	Name (CHD strain collection)	Description	Plasmid name	Vector type	Cell type	Resistance
FVS313	FVSE313	Neisseria meningitidis Fic (10-191) Tyr183Ala Tyr188Ala Nter HisTag	pFVS0050	pRSFDuet1	BL21	Kan |
FVS314	FVSE314	Neisseria meningitidis Fic (10-191) His107Ala Nter HisTag	pFVS0051	pRSFDuet1	BL21	Kan |
FVS315	FVSE315	Neisseria meningitidis Fic (10-191) Glu186Gly Nter HisTag	pFVS0059	pRSFDuet1	BL21 AI	Kan |
FVS316	FVSE316	HYPE wt Nter HA-Tag	pFVS0075	pcDNA3.1	Novablue	Amp ||
FVS317	FVSE317	HYPE His295Ala Nter HA-Tag	pFVS0076	pcDNA3.1	Novablue	Amp ||
FVS318	FVSE318	HYPE Thr230Ala Glu234Ala Nter HA-Tag	pFVS0077	pcDNA3.1	Novablue	Amp ||
FVS319	FVSE319	HYPE Glu234Gly Nter HA-Tag	pFVS0078	pcDNA3.1	Novablue	Amp ||
FVS320	FVSE320	VbhA Glu25Gly + VbhT FL wt Cter HisTag	pFVS0079	pRSFDuet1	Novablue	Kan |
FVS321	FVSE321	VbhA Glu25Gly + VbhT 1-198 His136Ala Cter HisTag	pFVS0080	pRSFDuet1	Novablue	Kan |
FVS322	FVSE322	Neisseria meningitidis Fic (10-191) Tyr183Phe Nter HisTag	pFVS0081	pRSFDuet1	Novablue	Kan |
FVS323	FVSE323	Neisseria meningitidis Fic (10-191) Tyr188Phe Nter HisTag	pFVS0082	pRSFDuet1	Novablue	Kan |
FVS324	FVSE324	Neisseria meningitidis Fic (10-191) Tyr183Phe Glu186Gly Nter HisTag	pFVS0083	pRSFDuet1	Novablue	Kan |
FVS325	FVSE325	Neisseria meningitidis Fic (10-191) Tyr183Phe Glu186Gly Tyr188Ser Nter HisTag	pFVS0084	pRSFDuet1	Novablue	Kan |
FVS326	FVSE326	Homo sapiens HYPE FIC (187-437) wt Nter HisTag	pFVS0085	pRSFDuet1	Novablue	Kan |
FVS327	FVSE327	Homo sapiens HYPE TPR FIC (104-437) wt Nter HisTag	pFVS0086	pRSFDuet1	Novablue	Kan |
FVS328	FVSE328	Homo sapiens HYPE FIC (187-437) His295Ala Nter HisTag	pFVS0087	pRSFDuet1	Novablue	Kan |
FVS329	FVSE329	Homo sapiens HYPE TPR FIC (104-437) His295Ala Nter HisTag	pFVS0088	pRSFDuet1	Novablue	Kan |
FVS330	FVSE330	Homo sapiens HYPE FIC (187-437) Thr230Ala Glu234Ala Nter HisTag	pFVS0089	pRSFDuet1	Novablue	Kan |
FVS331	FVSE331	Homo sapiens HYPE TPR FIC (104-437) Thr230Ala Glu234Ala Nter HisTag	pFVS0090	pRSFDuet1	Novablue	Kan |
FVS332	FVSE332	Homo sapiens HYPE FIC (187-437) Glu234Gly Nter HisTag	pFVS0091	pRSFDuet1	Novablue	Kan |
FVS333	FVSE333	Homo sapiens HYPE TPR FIC (104-437) Glu234Gly Nter HisTag	pFVS0092	pRSFDuet1	Novablue	Kan |
FVS334	FVSE334	Neisseria meningitidis Fic (10-191) Tyr183Phe Tyr188Phe Nter HisTag	pFVS0093	pRSFDuet1	Novablue	Kan |
FVS335	FVSE335	Neisseria meningitidis Fic (10-191) Tyr183Phe Glu186Gly Tyr188Phe Nter HisTag	pFVS0094	pRSFDuet1	Novablue	Kan |
FVS336	FVSE336	Neisseria meningitidis Fic (10-191) Glu186Gly Tyr188Phe Nter HisTag	pFVS0095	pRSFDuet1	Novablue	Kan |
FVS337	FVSE337	Homo sapiens HYPE FIC (187-437) wt Nter HisTag	pFVS0096	pcDNA3.1	Novablue	Amp ||
FVS338	FVSE338	Homo sapiens HYPE FIC (187-437) His295Ala Nter HisTag	pFVS0097	pcDNA3.1	Novablue	Amp ||
FVS339	FVSE339	VbhT 1-198 wt Cter HisTag in pACYCDuet vector	pFVS0098	pACYC-Duet	DH5 α	Cam |
FVS340	FVSE340	VbhT 1-198 His136Ala Cter HisTag in pACYCDuet vector	pFVS0099	pACYC-Duet	DH5 α	Cam |
FVS341	FVSE341	Neisseria meningitidis Fic Δ8 (10-167) Nter Strep-II Tag	pFVS0100	pRSFDuet1	DH5 α	Kan |
FVS342	FVSE342	VbhA wt in pBSK vector	pFVS0101	pBSK	DH5 α	Amp ||
FVS343	FVSE343	VbhA E24G in pBSK vector	pFVS0102	pBSK	DH5 α	Amp ||
FVS344	FVSE344	Neisseria meningitidis Fic Δ8 (10-167) Nter Strep-II Tag	pFVS0100	pRSFDuet1	BL21 AI	Kan |
FVS345	FVSE345		pFVS0101			
FVS346	FVSE346		pFVS0102			
FVS347	FVSE347	Escherichia coli GyrB wt 1-220 Nter HisTag	pFVS0103	pRSFDuet1	DH5 α	Kan |

Name (TS strain collection)	Name (CHD strain collection)	Description	Plasmid name	Vector type	Cell type	Resistance
FVS348	FVSE348	Escherichia coli GyrB wt 1-220 NO-TAG	pFVS0104	pRSFDuet1	DH5 α	Kan |
FVS349	FVSE349	Escherichia coli GyrB wt 1-220 Cter HisTag	pFVS0105	pRSFDuet1	DH5 α	Kan |
FVS350	FVSE350	Escherichia coli GyrB wt 15-220 Nter HisTag	pFVS0106	pRSFDuet1	DH5 α	Kan |
FVS351	FVSE351	Escherichia coli GyrB wt 15-220 NO-TAG	pFVS0107	pRSFDuet1	DH5 α	Kan |
FVS352	FVSE352	Escherichia coli GyrB wt 15-220 Cter HisTag	pFVS0108	pRSFDuet1	DH5 α	Kan |
FVS353	FVSE353	Escherichia coli GyrB wt 1-392 Nter HisTag	pFVS0109	pRSFDuet1	DH5 α	Kan |
FVS354	FVSE354	Escherichia coli GyrB wt 1-392 NO-TAG	pFVS0110	pRSFDuet1	DH5 α	Kan |
FVS355	FVSE355	Escherichia coli GyrB wt 1-392 Cter HisTag	pFVS0111	pRSFDuet1	DH5 α	Kan |
FVS356	FVSE356	Escherichia coli GyrB wt 15-392 Nter HisTag	pFVS0112	pRSFDuet1	DH5 α	Kan |
FVS357	FVSE357	Escherichia coli GyrB wt 15-392 NO-TAG	pFVS0113	pRSFDuet1	Novablue	Kan |
FVS358	FVSE358	Escherichia coli GyrB wt 15-392 Cter HisTag	pFVS0114	pRSFDuet1	DH5 α	Kan |
FVS359	FVSE359	Neisseria meningitidis Fic (10-191) wt Nter Strep-II-Tag	pFVS0115	pRSFDuet1	DH5 α	Kan |
FVS360	FVSE360	Escherichia coli GyrB wt 15-390 Nter HisTag	pFVS0116	pRSFDuet1	DH5 α	Kan |
FVS361	FVSE361	Escherichia coli GyrB wt 1-220 Nter HisTag	pFVS0103	pRSFDuet1	BL21	Kan |
FVS362	FVSE362	Escherichia coli GyrB wt 15-220 Nter HisTag	pFVS0106	pRSFDuet1	BL21	Kan |
FVS363	FVSE363	Neisseria meningitidis Fic (10-191) His107Ala Glu186Gly Nter HisTag	pFVS0117	pRSFDuet1	DH5 α	Kan |
FVS364	FVSE364	Escherichia coli GyrB Y109F 1-220 Nter HisTag	pFVS0118	pRSFDuet1	DH5 α	Kan |
FVS365	FVSE365	Escherichia coli GyrB Y109F 15-220 Nter HisTag	pFVS0119	pRSFDuet1	DH5 α	Kan |
FVS366	FVSE366	Escherichia coli GyrB Y109F 1-392 Nter HisTag	pFVS0120	pRSFDuet1	DH5 α	Kan |
FVS367	FVSE367	Escherichia coli GyrB Y109F 15-392 Nter HisTag	pFVS0121	pRSFDuet1	DH5 α	Kan |
FVS368	FVSE368	Escherichia coli GyrB Y109F 15-392 Cter HisTag	pFVS0122	pRSFDuet1	DH5 α	Kan |
FVS369	FVSE369	Neisseria meningitidis Fic (10-191) wt Nter HisTag	pFVS0015	pRSFDuet1	BL21	Kan |
FVS370	FVSE370	Neisseria meningitidis Fic (10-191) His107Ala Nter HisTag	pFVS0051	pRSFDuet1	BL21	Kan |
FVS371	FVSE371	Neisseria meningitidis Fic (10-191) His107Ala Glu186Gly Nter HisTag	pFVS0117	pRSFDuet1	BL21	Kan |
FVS372	FVSE372	VbhA wt / VbhT 1-198 wt Cter HisTag	pFVS0011	pRSFDuet1	BL21	Kan |
FVS373	FVSE373	VbhA wt / VbhT 1-198 H136A Cter HisTag	pFVS0041	pRSFDuet1	BL21	Kan |
FVS374	FVSE374	VbhA E24G / VbhT 1-198 H136A Cter HisTag	pFVS0080	pRSFDuet1	BL21	Kan |
FVS375	FVSE375	H pylori (G27) Fic Glu175Gly Nter HisTag	pFVS0123	pRSFDuet1	DH5 α	Kan |
FVS376	FVSE376	Neisseria meningitidis Fic (10-191) Arg71Ala Nter HisTag	pFVS0124	pRSFDuet1	DH5 α	Kan |
FVS377	FVSE377	Neisseria meningitidis Fic (10-191) Glu102Arg Nter HisTag	pFVS0125	pRSFDuet1	DH5 α	Kan |
FVS378	FVSE378	Neisseria meningitidis Fic (10-191) Glu156Arg Nter HisTag	pFVS0126	pRSFDuet1	DH5 α	Kan |
FVS379	FVSE379	Neisseria meningitidis Fic (10-191) Glu102Ala Nter HisTag	pFVS0127	pRSFDuet1	DH5 α	Kan |
FVS380	FVSE380	Neisseria meningitidis Fic (10-191) Lys99Arg Glu102Ala Nter HisTag	pFVS0128	pRSFDuet1	DH5 α	Kan |
FVS381	FVSE381	Escherichia coli Fic Gly55Arg (MCS1) + YhfG (MCS2)	pFVS0129	pRSFDuet1	DH5 α	Kan |

Name (TS strain collection)	Name (CHD strain collection)	Description	Plasmid name	Vector type	Cell type	Resistance
FVS401	FVSE401	Escherichia coli Fic wt (MCS1) + YhfG Glu28Gly (MCS2)	pFVS0130	pRSFDuet1	DH5 α	Kan |
FVS402	FVSE402	Escherichia coli ParE wt 1-390 Nter HisTag	pFVS0131	pRSFDuet1	DH5 α	Kan |
FVS403	FVSE403	Escherichia coli ParE wt 1-217 Nter HisTag	pFVS0132	pRSFDuet1	DH5 α	Kan |
FVS404	FVSE404	Escherichia coli ParE wt 1-390 Nter HisTag	pFVS0131	pRSFDuet1	BL21	Kan |
FVS405	FVSE405	Escherichia coli ParE wt 1-217 Nter HisTag	pFVS0132	pRSFDuet1	BL21	Kan |
FVS406	FVSE406	Escherichia coli Fic Gly55Arg (MCS1) + YhfG Glu28Gly (MCS2)	pFVS0133	pRSFDuet1	DH5 α	Kan |
FVS407	FVSE407	Neisseria meningitidis Fic (10-191) Glu102Arg Glu156Arg Nter HisTag	pFVS0134	pRSFDuet1	DH5 α	Kan |
FVS408	FVSE408	Neisseria meningitidis Fic (10-191) Glu156Arg Tyr183Phe Nter HisTag	pFVS0135	pRSFDuet1	DH5 α	Kan |
FVS409	FVSE409	Escherichia coli GyrB wt 1-392 Nter HisTag	pFVS0109	pRSFDuet1	BL21	Kan |
FVS410	FVSE410	Escherichia coli Fic Gly55Arg (MCS1) + YhfG (MCS2)	pFVS0129	pRSFDuet1	BL21	Kan |
FVS411	FVSE411	Escherichia coli Fic wt (MCS1) + YhfG Glu28Gly (MCS2)	pFVS0130	pRSFDuet1	BL21	Kan |
FVS412	FVSE412	Escherichia coli Fic wt (MCS1) + YhfG wt (MCS2)	pPE0038	pRSFDuet1	BL21	Kan |
FVS413	FVSE413	Neisseria meningitidis Fic (10-191) Glu156Arg Tyr188Phe Nter HisTag	pFVS0136	pRSFDuet1	DH5 α	Kan |
FVS414	FVSE414	Neisseria meningitidis Fic (10-191) Glu102Arg His107Ala Nter HisTag	pFVS0137	pRSFDuet1	DH5 α	Kan |
FVS415	FVSE415	Neisseria meningitidis Fic (10-191) His107Ala Glu156Arg Nter HisTag	pFVS0138	pRSFDuet1	DH5 α	Kan |
FVS416	FVSE416	Escherichia coli GyrA full lenght wt Nter HisTag	pFVS0139	pRSFDuet1	DH5 α	Kan |
FVS417	FVSE417	Escherichia coli GyrA full lenght wt Cter HisTag	pFVS0140	pRSFDuet1	DH5 α	Kan |
FVS418	FVSE418	Escherichia coli GyrB full lenght wt Nter HisTag	pFVS0141	pRSFDuet1	DH5 α	Kan |
FVS419	FVSE419	Escherichia coli GyrB full lenght wt Cter HisTag	pFVS0142	pRSFDuet1	DH5 α	Kan |
FVS420	FVSE420	Neisseria meningitidis Fic (10-191) Glu102Arg His107Ala Glu156Arg Nter HisTag	pFVS0143	pRSFDuet1	DH5 α	Kan |
FVS421	FVSE421	Neisseria meningitidis Fic (10-191) Glu102Arg Glu156Arg Tyr183Phe Nter HisTag	pFVS0144	pRSFDuet1	DH5 α	Kan |
FVS422	FVSE422	Neisseria meningitidis Fic (10-191) Glu102Arg Glu156Arg Tyr188Phe Nter HisTag	pFVS0145	pRSFDuet1	DH5 α	Kan |
FVS423	FVSE423	empty	pFVS0000	pRSFDuet1	Novablue	Kan |
FVS424	FVSE424	empty	pET-28a	pET-28a	Novablue	Kan |
FVS425	FVSE425	Neisseria meningitidis Fic (10-191) Y183F in pNMD220 (no Tag)	pFVS0146	pNMD220	DH5 α	Amp30 ||
FVS426	FVSE426	Neisseria meningitidis Fic (10-191) E186G Y183F in pNMD220 (no Tag)	pFVS0147	pNDM220	DH5 α	Amp30 ||
FVS427	FVSE427	Neisseria meningitidis Fic (10-191) H107A E186G in pNMD220 (no Tag)	pFVS0148	pNMD220	DH5 α	Amp30 ||
FVS428	FVSE428	Neisseria meningitidis Fic (10-191) E102R in pNMD220 (no Tag)	pFVS0149	pNDM220	DH5 α	Amp30 ||
FVS429	FVSE429	Neisseria meningitidis Fic (10-191) E156R in pNMD220 (no Tag)	pFVS0150	pNMD220	DH5 α	Amp30 ||
FVS430	FVSE430	Neisseria meningitidis Fic (10-191) H107A in pNMD220 (no Tag)	pFVS0151	pNMD220	DH5 α	Amp30 ||
FVS431	FVSE431	Neisseria meningitidis Fic (10-191) Arg149Glu Glu156Arg Nter HisTag	pFVS0152	pRSFDuet1	DH5 α	Kan |
FVS432	FVSE432	Neisseria meningitidis Fic (10-191) Arg71Glu Nter HisTag	pFVS0153	pRSFDuet1	DH5 α	Kan |
FVS433	FVSE433	Neisseria meningitidis Fic (10-191) Arg71Glu Glu102Arg Nter HisTag	pFVS0154	pRSFDuet1	DH5 α	Kan |
FVS434	FVSE434	Neisseria meningitidis Fic (10-191) Tyr183Trp Nter HisTag	pFVS0155	pRSFDuet1	DH5 α	Kan |

Name (TS strain collection)	Name (CHD strain collection)	Description	Plasmid name	Vector type	Cell type	Resistance
FVS435	FVSE435	Escherichia coli GyrB Cys58Ser 1-392 Nter HisTag	pFVS0156	pRSFDuet1	DH5 α	Kan |
FVS436	FVSE436	Escherichia coli GyrB Cys268Ser 1-392 Nter HisTag	pFVS0157	pRSFDuet1	DH5 α	Kan |
FVS437	FVSE437	Escherichia coli GyrB Ser244Cys 1-392 Nter HisTag	pFVS0158	pRSFDuet1	DH5 α	Kan |
FVS438	FVSE438	Escherichia coli GyrB Glu300Cys 1-392 Nter HisTag	pFVS0159	pRSFDuet1	DH5 α	Kan |
FVS439	FVSE439	Escherichia coli GyrB Glu363Cys 1-392 Nter HisTag	pFVS0160	pRSFDuet1	DH5 α	Kan |
FVS440	FVSE440	Escherichia coli GyrB Thr366Cys 1-392 Nter HisTag	pFVS0161	pRSFDuet1	DH5 α	Kan |
FVS441	FVSE441	Escherichia coli GyrB Glu359Cys 1-392 Nter HisTag	pFVS0162	pRSFDuet1	DH5 α	Kan |
FVS442	FVSE442	Neisseria meningitidis Fic (10-191) Arg149Glu Nter HisTag	pFVS0163	pRSFDuet1	DH5 α	Kan |
FVS443	FVSE443	Neisseria meningitidis Fic (10-191) Glu102Arg His107Ala Glu156Arg Nter HisTag	pFVS0143	pRSFDuet1	BL21	Kan |
FVS444	FVSE444	Neisseria meningitidis Fic (10-191) Tyr183Ala Glu186Gly Nter HisTag	pFVS0164	pRSFDuet1	DH5 α	Kan |
FVS445	FVSE445	Neisseria meningitidis Fic (10-191) Glu102Arg His107Ala Glu156Arg Y183F Nter HisTag	pFVS0165	pRSFDuet1	DH5 α	Kan |
FVS446	FVSE446	Neisseria meningitidis Fic (10-191) Tyr183Arg Nter HisTag	pFVS0166	pRSFDuet1	DH5 α	Kan |
FVS447	FVSE447	Neisseria meningitidis Fic (10-191) Glu102Arg Tyr183Phe Nter HisTag	pFVS0167	pRSFDuet1	DH5 α	Kan |
FVS448	FVSE448	Neisseria meningitidis Fic (10-191) Glu102Arg Tyr188Phe Nter HisTag	pFVS0168	pRSFDuet1	DH5 α	Kan |
FVS449	FVSE449	Neisseria meningitidis Fic (10-191) Glu102Arg E156R Delta8 (Δ8) Nter HisTag	pFVS0169	pRSFDuet1	DH5 α	Kan |
FVS450	FVSE450	Neisseria meningitidis Fic (10-191) Glu102Arg His107Ala E156R Delta8 (Δ8) Nter HisTag	pFVS0170	pRSFDuet1	DH5 α	Kan |
FVS451	FVSE451	Escherichia coli GyrB Ser244Cys 1-392 Nter HisTag	pFVS0158	pRSFDuet1	BL21	Kan |
FVS452	FVSE452	Escherichia coli GyrB Glu300Cys 1-392 Nter HisTag	pFVS0159	pRSFDuet1	BL21	Kan |
FVS453	FVSE453	Escherichia coli GyrB Glu363Cys 1-392 Nter HisTag	pFVS0160	pRSFDuet1	BL21	Kan |
FVS454	FVSE454	Escherichia coli GyrB Thr366Cys 1-392 Nter HisTag	pFVS0161	pRSFDuet1	BL21	Kan |
FVS455	FVSE455	Escherichia coli GyrB Glu359Cys 1-392 Nter HisTag	pFVS0162	pRSFDuet1	BL21	Kan |
FVS456	FVSE456	Neisseria meningitidis Fic (10-191) Glu102Arg His107Ala Glu156Arg Y183F Nter HisTag	pFVS0165	pRSFDuet1	BL21	Kan |
FVS457	FVSE457	Neisseria meningitidis Fic (10-191) Glu102Arg Delta8 (Δ8) Nter HisTag	pFVS0171	pRSFDuet1	DH5 α	Kan |
FVS458	FVSE458	Neisseria meningitidis Fic (10-191) Glu156Arg Delta8 (Δ8) Nter HisTag	pFVS0172	pRSFDuet1	DH5 α	Kan |
FVS459	FVSE459	Neisseria meningitidis Fic (10-191) E102R E156R in pNMD220 (no Tag)	pFVS0173	pNDM220	DH5 α	Amp30 ||
FVS460	FVSE460	Neisseria meningitidis Fic (10-191) E102R Y183F in pNMD220 (no Tag)	pFVS0174	pNDM220	DH5 α	Amp30 ||
FVS461	FVSE461	Neisseria meningitidis Fic (10-191) E156R Y183F in pNMD220 (no Tag)	pFVS0175	pNMD220	DH5 α	Amp30 ||
FVS462	FVSE462	Neisseria meningitidis Fic (10-191) H107A Δ8 (stop codon) in pNMD220 (no Tag)	pFVS0176	pNDM220	DH5 α	Amp30 ||
FVS463	FVSE463	Neisseria meningitidis Fic (10-191) E102R H107A in pNMD220 (no Tag)	pFVS0177	pNDM220	DH5 α	Amp30 ||
FVS464	FVSE464	Neisseria meningitidis Fic (10-191) E102R E156R Y183F in pNMD220 (no Tag)	pFVS0178	pNMD220	DH5 α	Amp30 ||
FVS465	FVSE465	Neisseria meningitidis Fic (10-191) H107A E156R in pNMD220 (no Tag)	pFVS0179	pNDM220	DH5 α	Amp30 ||
FVS466	FVSE466	Neisseria meningitidis Fic (10-191) Δ8 (stop codon) in pNMD220 (no Tag)	pFVS0180	pNDM220	DH5 α	Amp30 ||
FVS467	FVSE467	B. schoenbuchensis VbhT 1-198 wt + VbhA-(G4s)1-STOP-GyrB E. coli in Duet	pFVS0181	pRSFDuet1	DH5 α	Kan |
FVS468	FVSE468	N. meningitidis NmFic-(G4S)1-STOP-GyrB E. coli in Duet	pFVS0182	pRSFDuet1	DH5 α	Kan |

Name (TS strain collection)	Name (CHD strain collection)	Description	Plasmid name	Vector type	Cell type	Resistance
FVS469	FVSE469	N. meningitidis NmFic-(G4S)3-STOP-GyrB E. coli in Duet	pFVS0183	pRSFDuet1	DH5 α	Kan |
FVS470	FVSE470	N. meningitidis NmFic-(G4S)2-STOP-GyrB E. coli in Duet	pFVS0184	pRSFDuet1	DH5 α	Kan |
FVS471	FVSE471	B. schoenbuchensis VbhT 1-198 wt + VbhA-(G4s)2-STOP-GyrB E. coli in Duet	pFVS0185	pRSFDuet1	DH5 α	Kan |
FVS472	FVSE472	B. schoenbuchensis VbhT 1-198 wt + VbhA-(G4s)2-STOP-GyrB E. coli in Duet	pFVS0186	pRSFDuet1	DH5 α	Kan |
FVS473	FVSE473	N. meningitidis NmFic-(G4S)1-GyrB E. coli fusion protein in Duet	pFVS0187	pRSFDuet1	DH5 α	Kan |
FVS474	FVSE474	N. meningitidis NmFic-(G4S)3-GyrB E. coli fusion protein in Duet	pFVS0188	pRSFDuet1	DH5 α	Kan |
FVS475	FVSE475	B. schoenbuchensis VbhT 1-198 wt + VbhA-(G4s)1-GyrB V118I E. coli fusion protein in Duet	pFVS0189	pRSFDuet1	DH5 α	Kan |
FVS476	FVSE476	Neisseria meningitidis Fic Y183F Y185F in Duet	pFVS0190	pRSFDuet1	DH5 α	Kan |
FVS477	FVSE477	Neisseria meningitidis Fic Y183F Y185F E186G in Duet	pFVS0191	pRSFDuet1	DH5 α	Kan |
FVS478	FVSE478	Neisseria meningitidis Fic E102R E156R Y183F Y185F in Duet	pFVS0192	pRSFDuet1	DH5 α	Kan |
FVS479	FVSE479	Neisseria meningitidis Fic E102R H107A E156R Y183F Y185F E186G in Duet	pFVS0193	pRSFDuet1	DH5 α	Kan |
FVS480	FVSE480	B. schoenbuchensis VbhT 1-198 wt + VbhA-(G4s)3-GyrB E. coli fusion protein in Duet	pFVS0194	pRSFDuet1	DH5 α	Kan |
FVS481	FVSE481	B. schoenbuchensis VbhT 1-198 wt + VbhA-(G4s)1-GyrB E. coli fusion protein in Duet	pFVS0195	pRSFDuet1	DH5 α	Kan |
FVS501	FVSE501	N. meningitidis NmFic-(G4S)1-GyrB E. coli fusion protein in Duet	pFVS0187	pRSFDuet1	BL21	Kan |
FVS502	FVSE502	N. meningitidis NmFic-(G4S)3-GyrB E. coli fusion protein in Duet	pFVS0188	pRSFDuet1	BL21	Kan |
FVS503	FVSE503	B. schoenbuchensis VbhT 1-198 wt + VbhA-(G4s)3-GyrB E. coli fusion protein in Duet	pFVS0194	pRSFDuet1	BL21	Kan |
FVS504	FVSE504	B. schoenbuchensis VbhT 1-198 wt + VbhA-(G4s)1-GyrB E. coli fusion protein in Duet	pFVS0195	pRSFDuet1	BL21	Kan |
FVS505	FVSE505	Neisseria meningitidis Fic E102R H107A E156R Y183F Y185F in Duet	pFVS0196	pRSFDuet1	DH5 α	Kan |
FVS506	FVSE506	Neisseria meningitidis Fic (10-191) E102R H107A E156R in pNMD220 (no Tag)	pFVS0197	pNDM220	DH5 α	Amp30 ||
FVS507	FVSE507	N. meningitidis NmFic-GGGDSGGGGS-GyrB E. coli fusion protein in Duet	pFVS0198	pRSFDuet1	DH5 α	Kan |
FVS508	FVSE508	N. meningitidis NmFic-(G4S)2-GyrB E. coli fusion protein in Duet	pFVS0199	pRSFDuet1	DH5 α	Kan |
FVS509	FVSE509	B. schoenbuchensis VbhT 1-198 wt + VbhA-(G4s)2-GyrB E. coli fusion protein in Duet	pFVS0200	pRSFDuet1	DH5 α	Kan |
FVS510	FVSE510	B. schoenbuchensis VbhT 1-198 wt + VbhA-(G4s)4-STOP-GyrB E. coli in Duet	pFVS0201	pRSFDuet1	DH5 α	Kan |
FVS511	FVSE511	B. henselae BepA (Fic-OB) / BipA (antitoxin Bhe) in Duet	pAG0052	pRSFDuet1	DH5 α	Kan |
FVS512	FVSE512	B. henselae BepA (Fic-OB) / BipA (antitoxin Bhe) in Duet	pAG0052	pRSFDuet1	BL21	Kan |
FVS513	FVSE513	N. meningitidis NmFic_E186G-(G4S)1-GyrB E. coli fusion protein in Duet	pFVS0202	pRSFDuet1	DH5 α	Kan |
FVS514	FVSE514	N. meningitidis NmFic_E186G-(G4S)2-GyrB E. coli fusion protein in Duet	pFVS0203	pRSFDuet1	DH5 α	Kan |
FVS515	FVSE515	N. meningitidis NmFic_E186G-(G4S)3-GyrB E. coli fusion protein in Duet	pFVS0204	pRSFDuet1	DH5 α	Kan |
FVS516	FVSE516	N. meningitidis NmFic_H107A-(G4S)1-GyrB E. coli fusion protein in Duet	pFVS0205	pRSFDuet1	DH5 α	Kan |
FVS517	FVSE517	N. meningitidis NmFic_H107A-(G4S)2-GyrB E. coli fusion protein in Duet	pFVS0206	pRSFDuet1	DH5 α	Kan |
FVS518	FVSE518	N. meningitidis NmFic_H107A-(G4S)3-GyrB E. coli fusion protein in Duet	pFVS0207	pRSFDuet1	DH5 α	Kan |
FVS519	FVSE519	B. sch VbhT 1-198 wt + VbhA_E24G-(G4s)1-GyrB E. coli fusion protein in Duet	pFVS0208	pRSFDuet1	DH5 α	Kan |
FVS520	FVSE520	B. sch VbhT 1-198 wt + VbhA_E24G-(G4s)2-GyrB E. coli fusion protein in Duet	pFVS0209	pRSFDuet1	DH5 α	Kan |
FVS521	FVSE521	B. sch VbhT 1-198 wt + VbhA_E24G-(G4s)3-GyrB E. coli fusion protein in Duet	pFVS0210	pRSFDuet1	DH5 α	Kan |

Name (TS strain collection)	Name (CHD strain collection)	Description	Plasmid name	Vector type	Cell type	Resistance
FVS522	FVSE522	B. sch VbhT 1-198 H136A + VbhA-(G4s)1-GyrB E. coli fusion protein in Duet	pFVS0211	pRSFDuet1	DH5 α	Kan |
FVS523	FVSE523	B. sch VbhT 1-198 H136A + VbhA-(G4s)2-GyrB E. coli fusion protein in Duet	pFVS0212	pRSFDuet1	DH5 α	Kan |
FVS524	FVSE524	B. sch VbhT 1-198 H136A + VbhA-(G4s)3-GyrB E. coli fusion protein in Duet	pFVS0213	pRSFDuet1	DH5 α	Kan |
FVS525	FVSE525	N. meningitidis NmFic_H107A_E186G-(G4S)1-GyrB E. coli fusion protein in Duet	pFVS0214	pRSFDuet1	DH5 α	Kan |
FVS526	FVSE526	N. meningitidis NmFic_H107A_E186G-(G4S)2-GyrB E. coli fusion protein in Duet	pFVS0215	pRSFDuet1	DH5 α	Kan |
FVS527	FVSE527	N. meningitidis NmFic_H107A_E186G-(G4S)3-GyrB E. coli fusion protein in Duet	pFVS0216	pRSFDuet1	DH5 α	Kan |
FVS528	FVSE528	B. sch VbhT 1-198 H136A + VbhA_E24G-(G4s)1-GyrB E. coli fusion protein in Duet	pFVS0217	pRSFDuet1	DH5 α	Kan |
FVS529	FVSE529	B. sch VbhT 1-198 H136A + VbhA_E24G-(G4s)2-GyrB E. coli fusion protein in Duet	pFVS0218	pRSFDuet1	DH5 α	Kan |
FVS530	FVSE530	B. sch VbhT 1-198 H136A + VbhA_E24G-(G4s)3-GyrB E. coli fusion protein in Duet	pFVS0219	pRSFDuet1	DH5 α	Kan |
FVS531	FVSE531	N. meningitidis Fic Δhelix1 (32-191) Nter HisTag in Duet	pFVS0220	pRSFDuet1	DH5 α	Kan |
FVS532	FVSE532	N. meningitidis Fic Δhelix1 (32-191) Cter HisTag in Duet	pFVS0221	pRSFDuet1	DH5 α	Kan |
FVS533	FVSE533	N. meningitidis Fic Δ½-helix1 (22-191) Nter HisTag in Duet	pFVS0222	pRSFDuet1	DH5 α	Kan |
FVS534	FVSE534	B. schoenbuchensis VbhA + VbhT 1-198 S175C Cter HisTag	pFVS0223	pRSFDuet1	DH5 α	Kan |
FVS535	FVSE535	B. schoenbuchensis VbhA + VbhT 1-198 H136A S175C Cter HisTag	pFVS0224	pRSFDuet1	DH5 α	Kan |
FVS536	FVSE536	B. schoenbuchensis VbhA E24G + VbhT 1-198 H136A S175C Cter HisTag	pFVS0225	pRSFDuet1	DH5 α	Kan |
FVS537	FVSE537	N. meningitidis Fic M147C Nter HisTag	pFVS0226	pRSFDuet1	DH5 α	Kan |
FVS538	FVSE538	N. meningitidis Fic H107A M147C Nter HisTag	pFVS0227	pRSFDuet1	DH5 α	Kan |
FVS539	FVSE539	N. meningitidis Fic H107A M147C E186G Nter HisTag	pFVS0228	pRSFDuet1	DH5 α	Kan |
FVS540	FVSE540	B. schoenbuchensis VbhA E24G + VbhT 1-198 S175C Cter HisTag	pFVS0229	pRSFDuet1	DH5 α	Kan |
FVS541	FVSE541	N. meningitidis Fic M147C E186G Nter HisTag	pFVS0230	pRSFDuet1	DH5 α	Kan |
FVS542	FVSE542	N. meningitidis Fic Δhelix1 (32-191) E186G Nter HisTag in Duet	pFVS0231	pRSFDuet1	DH5 α	Kan |
FVS543	FVSE543	N. meningitidis Fic Δhelix1 (32-191) E186G Cter HisTag in Duet	pFVS0232	pRSFDuet1	DH5 α	Kan |
FVS544	FVSE544	N. meningitidis Fic Δ½-helix1 (22-191) E186G Nter HisTag in Duet	pFVS0233	pRSFDuet1	DH5 α	Kan |
FVS545	FVSE545	N. meningitidis Fic E102R E186G in pNDM220	pFVS0234	pNMD220	DH5 α	Amp30 ||
FVS546	FVSE546	N. meningitidis Fic E156R E186G in pNDM220	pFVS0235	pNDM220	DH5 α	Amp30 ||
FVS547	FVSE547	N. meningitidis Fic E102R E156R E186G in pNDM220	pFVS0236	pNDM220	DH5 α	Amp30 ||
FVS548	FVSE548	N. meningitidis Fic E102R E186G Nter HisTag in Duet	pFVS0237	pRSFDuet1	DH5 α	Kan |
FVS549	FVSE549	N. meningitidis Fic E102R E156R E186G Nter HisTag in Duet	pFVS0238	pRSFDuet1	DH5 α	Kan |
FVS550	FVSE550	Human GST-Cdc42 K27A in pGex6p1	pFVS0239	pGex6p1	DH5 α	Amp100 ||
FVS551	FVSE551	Human GST-Cdc42 S30G in pGex6p1	pFVS0240	pGex6p1	DH5 α	Amp100 ||
FVS552	FVSE552	Human GST-Cdc42 K27A Q61L (constitutively active) in pGex6p1	pFVS0241	pGex6p1	DH5 α	Amp100 ||
FVS553	FVSE553	Human GST-Cdc42 S30G Q61L (constitutively active) in pGex6p1	pFVS0242	pGex6p1	DH5 α	Amp100 ||
FVS554	FVSE554	Human GST-Rac1 A27K in pGex6p1	pFVS0243	pGex6p1	DH5 α	Amp100 ||
FVS555	FVSE555	Human GST-Rac1 G30S in pGex6p1	pFVS0244	pGex6p1	DH5 α	Amp100 ||

Name (TS strain collection)	Name (CHD strain collection)	Description	Plasmid name	Vector type	Cell type	Resistance
FVS556	FVSE556	Human GST-Rac1 A27K Q61L (constitutively active) in pGex6p1	pFVS0245	pGex6p1	DH5 α	Amp100 II
FVS557	FVSE557	Human GST-Rac1 G30S Q61L (constitutively active) in pGex6p1	pFVS0246	pGex6p1	DH5 α	Amp100 II

8.3. Diphosphate-containing molecules from *E. coli*

This section contains a list of putative substrates for Fic proteins. Note that this list is non-comprehensive and still needs to be cured for phosphodiester containing molecules.

Compound name	**Formula**	**MW (Da)**
isopentenyl diphosphate	$C_5H_9O_7P_2$	243.069
dimethylallyl diphosphate	$C_5H_9O_7P_2$	243.069
2-amino-4-[(phosphonomethyl)hydroxy-phosphinyl]butanoate	$C_4H_9N_1O_7P_2$	245.065
diimidotriphosphate	$H_7N_2O_8P_3$	255.985
1-hydroxy-2-methyl-2-(E)-butenyl 4-diphosphate	$C_5H_9O_8P_2$	259.069
2,3-diphospho-D-glycerate	$C_3H_3O_{10}P_2$	260.998
1,3-bisphospho-D-glycerate	$C_3H_4O_{10}P_2$	262.006
hexanediol 1,6-bisphosphate	$C_6H_{12}O_8P_2$	274.104
2-C-methyl-D-erythritol-2,4-cyclodiphosphate	$C_5H_{10}O_9P_2$	276.076
5-phospho-α-D-ribose 1,2-cyclic phosphate	$C_5H_7O_{10}P_2$	289.052
4-amino-2-methyl-5-diphosphomethylpyrimidine	$C_6H_8N_3O_7P_2$	296.093
alpha-D-ribose-1-methylphosphonate-5-phosphate	$C_6H_{11}O_{10}P_2$	305.094
alpha-D-ribose 1,5-bisphosphate	$C_5H_8O_{11}P_2$	306.059
geranyl diphosphate	$C_{10}H_{17}O_7P_2$	311.188
4-amino-2-methoxy-5-hydroxymethylpyrimidine pyrophosphate	$C_6H_8N_3O_8P_2$	312.092
tetraphosphate	$O_{13}P_4$	331.887
alpha-glucose 1,6-bisphosphate	$C_6H_{10}O_{12}P_2$	336.085
beta-glucose-1,6-diphosphate	$C_6H_{10}O_{12}P_2$	336.085
beta-D-fructose 2,6-bisphosphate	$C_6H_{10}O_{12}P_2$	336.085
tagatose-1,6-bisphosphate	$C_6H_{10}O_{12}P_2$	336.085
fructose-1,6-bisphosphate	$C_6H_{10}O_{12}P_2$	336.085
bromohydrin of isopentenyl pyrophosphate	$C_5H_{10}O_8P_2Br_1$	339.981
4-amino-2-trifluoromethyl 5-hydroxymethylpyrimidine pyrophosphate	$C_6H_5N_3O_7F_3P_2$	350.064
(2-amino-4-hydroxy-7,8-dihydropteridin-6-yl)methyl diphosphate	$C_7H_8N_5O_8P_2$	352.116
D-glycero-β-D-manno-heptose 1,7-bisphosphate	$C_7H_{12}O_{13}P_2$	366.112
D-sedoheptulose-1,7-bisphosphate	$C_7H_{12}O_{13}P_2$	366.112
(2E,6E)-farnesyl diphosphate	$C_{15}H_{25}O_7P_2$	379.306
5-phospho-α-D-ribose 1-diphosphate	$C_5H_8O_{14}P_3$	385.031
ribose triphosphate	$C_5H_9O_{14}P_3$	386.039

(S)-farnesyl thiopyrophosphate	$C_{15}H_{25}O_6P_2S_1$	395.366
bis(glycerophosphoglycerol)	$C_9H_{20}O_{13}P_2$	398.197
6-phosphonouridine 5'-monophosphate	$C_9H_{11}N_2O_{12}P_2$	401.14
6-azauridine diphosphate	$C_8H_{10}N_3O_{12}P_2$	402.127
deoxyinosine diphosphate	$C_{10}H_{11}N_4O_{10}P_2$	409.165
P1-uridyl-P2-methyl diphosphate	$C_{10}H_{14}N_2O_{12}P_2$	416.174
2'-chloro-2'-deoxyuridine-5'-diphosphate	$C_9H_{10}N_2O_{11}P_2Cl_1$	419.585
thiamin diphosphate	$C_{12}H_{16}N_4O_7P_2S_1$	422.288
adenosine 3',5'-bisphosphate	$C_{10}H_{11}N_5O_{10}P_2$	423.172
adenosine-2',5'-bisphosphate	$C_{10}H_{11}N_5O_{10}P_2$	423.172
inosine diphosphate	$C_{10}H_{11}N_4O_{11}P_2$	425.165
2'-azido-2'-deoxyuridine-5'-diphosphate	$C_9H_{10}N_5O_{11}P_2$	426.152
2'-methoxythiamin pyrophosphate	$C_{12}H_{16}N_4O_8P_2S_1$	438.288
geranylgeranyl diphosphate	$C_{20}H_{33}O_7P_2$	447.424
all-trans-geranylgeranyl diphosphate	$C_{20}H_{33}O_7P_2$	447.424
thiamine thiothiazolone pyrophosphate	$C_{12}H_{15}N_4O_7P_2S_2$	453.341
α-D-ribose-1-methylphosphonate-5-triphosphate	$C_6H_{12}O_{16}P_4$	464.046
2-(α-hydroxyethyl)thiamine diphosphate	$C_{14}H_{20}N_4O_8P_2S_1$	466.341
P1-uridyl-P2-phenyl diphosphate	$C_{15}H_{16}N_2O_{12}P_2$	478.245
7,8-dihydromonapterin triphosphate	$C_9H_{12}N_5O_{13}P_3$	491.141
7,8-dihydroneopterin triphosphate	$C_9H_{12}N_5O_{13}P_3$	491.141
uridine-5'-diphosphate chloroacetol	$C_{12}H_{15}N_2O_{13}P_2Cl_1$	492.657
2-thiouridine 5'-triphosphate	$C_9H_{11}N_2O_{14}P_3S_1$	496.172
thiamin triphosphate	$C_{12}H_{16}N_4O_{10}P_3S_1$	501.26
2-hydroxydeoxyadenosine 5'-triphosphate	$C_{10}H_{12}N_5O_{13}P_3$	503.152
phosphoadenosine-5'-phosphosulfate	$C_{10}H_{11}N_5O_{13}P_2S_1$	503.23
di-trans,di-cis-pentaprenyl diphosphate	$C_{25}H_{41}O_7P_2$	515.542
geranylfarnesyl diphosphate	$C_{25}H_{41}O_7P_2$	515.542
8-hydroxydeoxyguanosine 5'-triphosphate	$C_{10}H_{12}N_5O_{14}P_3$	519.151
4-(cytidine 5'-diphospho)-2-C-methyl-D-erythritol	$C_{14}H_{23}N_3O_{14}P_2$	519.295
succinate semialdehyde-thiamine diphosphate	$C_{16}H_{22}N_4O_{10}P_2S_1$	524.378
uridine-5'-diphosphate bromoacetol	$C_{12}H_{15}N_2O_{13}P_2Br_1$	537.108
1-(5-phospho-β-D-ribosyl)-AMP	$C_{15}H_{19}N_5O_{14}P_2$	555.288
D-myo-inositol (1,3,4,5,6)-pentakisphosphate	$C_6H_7O_{21}P_5$	569.977
D-myo-inositol (1,2,4,5,6)-pentakisphosphate	$C_6H_7O_{21}P_5$	569.977
1D-myo-inositol (1,2,3,4,6)-pentakisphosphate	$C_6H_7O_{21}P_5$	569.977
D-myo-inositol (1,2,3,4,5)-pentakisphosphate	$C_6H_7O_{21}P_5$	569.977

phosphoribulosylformimino-AICAR-P	$C_{15}H_{21}N_5O_{15}P_2$	573.303
1-(5-phospho-β-D-ribosyl)-5-[(5-phosphoribosylamino)methylideneamino]imidazole-4-carboxamide	$C_{15}H_{21}N_5O_{15}P_2$	573.303
adenosine tetraphosphate	$C_{10}H_{13}N_5O_{16}P_4$	583.132
di-trans,poly-cis-hexaprenyl diphosphate	$C_{30}H_{49}O_7P_2$	583.66
all-trans-hexaprenyl diphosphate	$C_{30}H_{49}O_7P_2$	583.66
2-phospho-4-(cytidine 5'-diphospho)-2-C-methyl-D-erythritol	$C_{14}H_{22}N_3O_{17}P_3$	597.259
guanosine tetraphosphate	$C_{10}H_{13}N_5O_{17}P_4$	599.131
p-(bromoacetamido)phenyl uridyl pyrophosphate	$C_{17}H_{18}N_3O_{13}P_2Br_1$	614.193
1D-myo-inositol 1,2,3,4,5,6-hexakisphosphate	$C_6H_6O_{24}P_6$	647.942
di-trans,poly-cis-heptaprenyl diphosphate	$C_{35}H_{57}O_7P_2$	651.779
all-trans-heptaprenyl diphosphate	$C_{35}H_{57}O_7P_2$	651.779
3'-dephospho-CoA	$C_{21}H_{33}N_7O_{13}P_2S_1$	685.538
1-(5-phospho-β-D-ribosyl)-ATP	$C_{15}H_{20}N_5O_{20}P_4$	714.24
di-trans,poly-cis-octaprenyl diphosphate	$C_{40}H_{65}O_7P_2$	719.897
all-trans-octaprenyl diphosphate	$C_{40}H_{65}O_7P_2$	719.897
adenosine thiamine triphosphate	$C_{22}H_{28}N_9O_{13}P_3S_1$	751.497
5',5'''-diadenosine triphosphate	$C_{20}H_{24}N_{10}O_{16}P_3$	753.388
di-trans,poly-cis-nonaprenyl diphosphate	$C_{45}H_{73}O_7P_2$	788.015
all-trans-nonaprenyl diphosphate	$C_{45}H_{73}O_7P_2$	788.015
Phosphatidylglycerophosphate (dihexadec-9-enoyl, n-C16:1)	$C_{38}H_{69}O_{13}P_2$	795.903
1,2-dipalmitoyl-phosphatidylglycerol-phosphate	$C_{38}H_{73}O_{13}P_2$	799.934
5',5'''-diadenosine tetraphosphate	$C_{20}H_{24}N_{10}O_{19}P_4$	832.36
phosphatidylglycerophosphate (dioctadecanoyl, n-C18:0)	$C_{42}H_{81}O_{13}P_2$	856.042
ω, mono-trans,octa-cis-decaprenyl diphosphate	$C_{50}H_{81}O_7P_2$	856.133
di-trans,poly-cis-decaprenyl diphosphate	$C_{50}H_{81}O_7P_2$	861.173
P1,P4-bis(5'-guanosyl) tetraphosphate	$C_{20}H_{24}N_{10}O_{21}P_4$	864.359
2'-(5''-phosphoribosyl)-3'-dephospho-CoA	$C_{26}H_{42}N_7O_{19}P_3S1$	881.635
5',5'''-diadenosine pentaphosphate	$C_{20}H_{24}N_{10}O_{22}P_5$	911.332
di-trans,octa-cis-undecaprenyl diphosphate	$C_{55}H_{89}O_7P_2$	924.251
2'-(5''-triphospho-α-D-ribosyl)-3'-dephospho-CoA	$C_{26}H_{41}N_7O_{26}P_5S_1$	1054.57
N-acetyl-α-D-glucosaminyl-diphospho-trans,octacis-decaprenol	$C_{58}H_{95}N_1O_{12}P_2$	1060.335
N-acetyl-α-D-glucosaminyl-diphospho-ditrans,octacis-undecaprenol	$C_{63}H_{103}N_1O_{12}P_2$	1128.454

8.4. Structure gallery of FIC domain proteins

This appendix contains a comprehensive list of FIC domain structures that have been determined to date and are either deposited in the protein data bank (www.pdb.org) or have been determined in the frame of the collaboration between the Schirmer group and the Dehio group at the Biozentrum, University of Basel.

Table A1. FIC domain structures determined to date.

Organism	Description	Note	PDB code	Figure
L. pneumophilae	AnkX	Apo	4BEP	A1
L. pneumophilae	AnkX in complex with CDP-choline	Substrate	4BET	A1
L. pneumophilae	AnkX in complex with CMP and phosphocholine	Products	4BES	A1
L. pneumophilae	AnkX in complex with CMP	Side-product	4BER	A1
P. syringae	AvrB	Apo	1NH1	A2
P. syringae	AvrB in complex with ADP	Putative side-product?	2NUN	A2
P. syringae	AvrB in complex with RIN4	Target peptide	2NUD	A2
B. henselae	BepA FIC-OB	Apo	2VY3	A3
B. henselae	BepA FIC-OB in complex with PP_i	Side-product	2JK8	A3
B. quintana	BepC	Apo	4LU4	A3
B. quintana	BepC in complex with ADP	Putative side-product?	4N67	A3
B. rochalimae	Bep1 in complex with its antitoxin	Apo	A. Goepfert, *unpublished*	A4
B. Clarridgeiae	Bep1 FIC-OB	Apo		A4
B. sp. ar 15-3	Bep8	Apo	4M16	A4
B. sp. ar 15-3	Bep8	Apo	4PY3	A4
B. schoenbuchensis	VbhT in complex with VbhA	Apo	3SHG	A5
B. schoenbuchensis	VbhT in complex with VbhA and ATP	ATP, incompetent form	3ZC7	A5
B. schoenbuchensis	VbhT in complex with $VbhA_{E24G}$ and ATP (adenylylase form)	ATP, adenylylase competent form	3ZCB	A5
B. schoenbuchensis	VbhT in complex with $VbhA_{E24G}$ and ATP (kinase form)	ATP, kinase competent form	A. Goepfert, *unpublished*	A5
B. schoenbuchensis	$VbhT_{S175C}$ in complex with $VbhA_{E24G}$ and 2'-S-ATP	Covalently bound ATP, competent form	F.V. Stanger, *unpublished*	A5

E. coli	$EcFicT_{G55R}$ in complex with EcFicA	Apo	F.V. Stanger, *unpublished*	A6
E. coli	EcFicT in complex with $EcFicA_{E28G}$	Apo	F.V. Stanger, *unpublished*	A6
S. oneidensis	SoFic	Apo	3EQX	A7
S. oneidensis	SoFic in complex with ATP	ATP, incompetent form	3ZCN	A7
S. oneidensis	SoFic in complex with AMPPNP	AMPPNP, competent form	3ZEC	A7
B. thetaiotaomicron	BtFic	Apo	3CUC	A7
V. parahaemolyticus	VopS	Apo	3LET	A8
H. somni	IbpA	Apo		A8
H. somni	IbpA in complex with Cdc42	Complex with adenylylated-target	3N3V, 4ITR	A8
Bacteriophage P1	Doc in complex with PhD	Complex with antitoxin PhD	3KH2, 3K33	A9
Bacteriophage P1	Doc_{H66Y} in complex with PhD	Disturbed fold	3DD9	A9
N. meningitidis	NmFic wt	Apo	2G03	A10
N. meningitidis	NmFic wt in complex with AMPPNP	ATP, incompetent form	3S6A	A10
N. meningitidis	NmFic wt tetramer	Tetramer	F.V. Stanger, *unpublished*	A10
N. meningitidis	NmFic S182A,E186A	ATP, competent form	3SN9	A10
N. meningitidis	NmFic E186G in complex with AMPPNP	ATP, competent form	3ZLM	A10
N. meningitidis	NmFic Y183F,E186G	ATP	F.V. Stanger, *unpublished*	A10
N. meningitidis	NmFic Δ8	Tetramer, ATP, competent form	3SE5	A10
N. meningitidis	NmFic E102R	Dimer, apo	F.V. Stanger, *unpublished*	A11
N. meningitidis	NmFic E156R	Dimer, apo	F.V. Stanger, *unpublished*	A11
N. meningitidis	NmFIc E102R,E156R	Monomer, apo	F.V. Stanger, *unpublished*	A11
N. meningitidis	NmFic E156R in complex with ATP	Dimer, ATP, competent kinase form	F.V. Stanger, *unpublished*	A11
N. meningitidis	NmFic E156R,Y183F in complex with ATP	Dimer, ATP, competent kinase form	F.V. Stanger, *unpublished*	A11
H. pylori	HpFic	Apo	2F6S	A11

In the following figures, note that the view slightly differs from one figure to the other, depending on the presence of additional domains (as a compromise to find a view in which most of the features of each structure are visible).

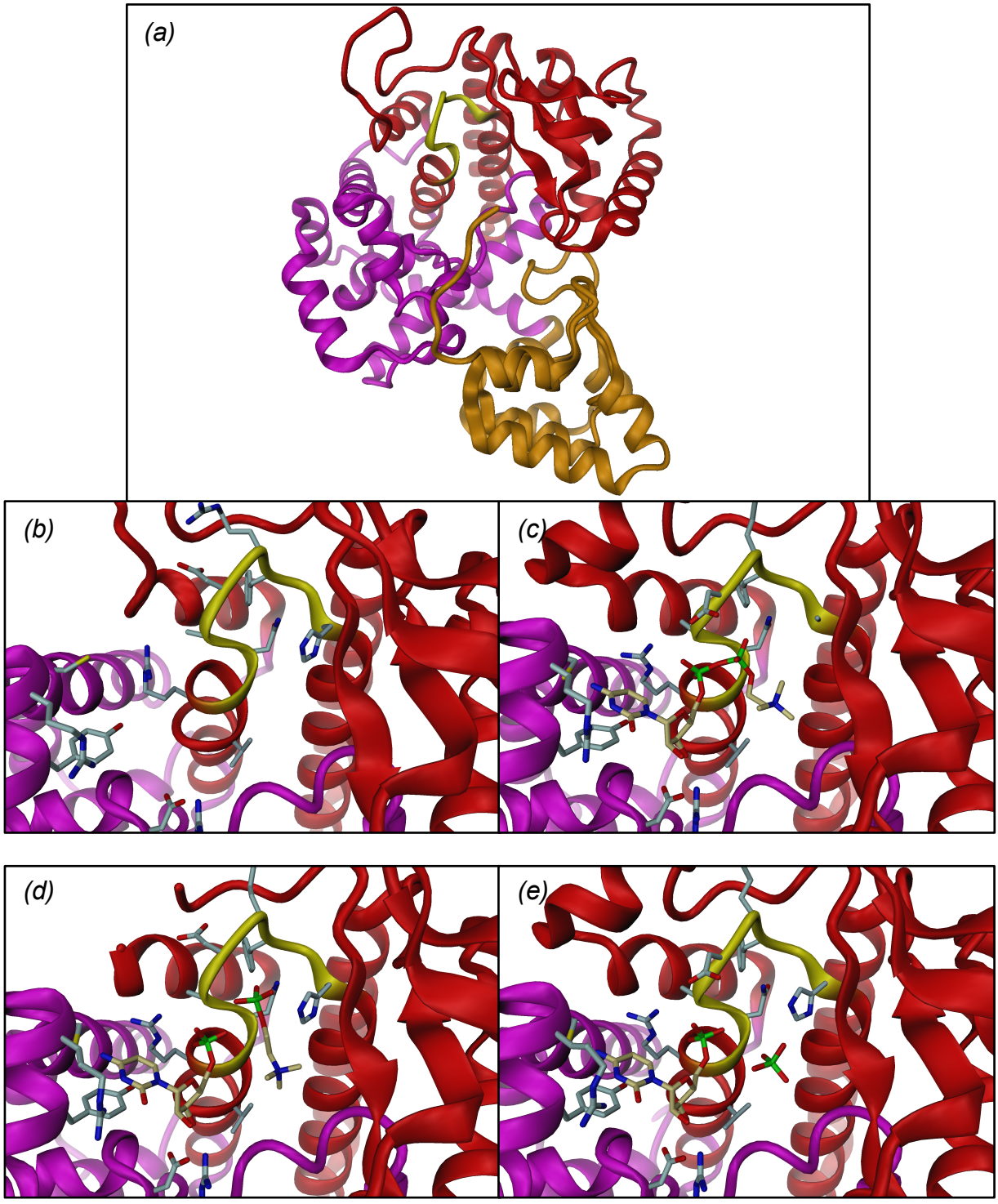

Figure A1. Structure of *Legionella pneumophilae* AnkX. *(a)* Overall structure. The FIC domain and insert domain are colored in red, the CMP domain is colored in magenta, the Fic active site motif is colored in yellow and ankyrin repeats are colored in orange. Details of the active site of *(b)* the apo structure of AnkX (PDB: 4BEP), *(c)* $AnkX_{H229A}$ in complex with the substrate CDP-choline (PDB: 4BET), *(d)* AnkX in complex with the products CMP and phosphocholine (PDB: 4BES) and *(e)* AnkX in complex with CMP and phosphate (PDB: 4BER). The substrate is shown with beige carbon atoms and residues part of the Fic active site motif or interacting with the substrate are displayed as sticks.

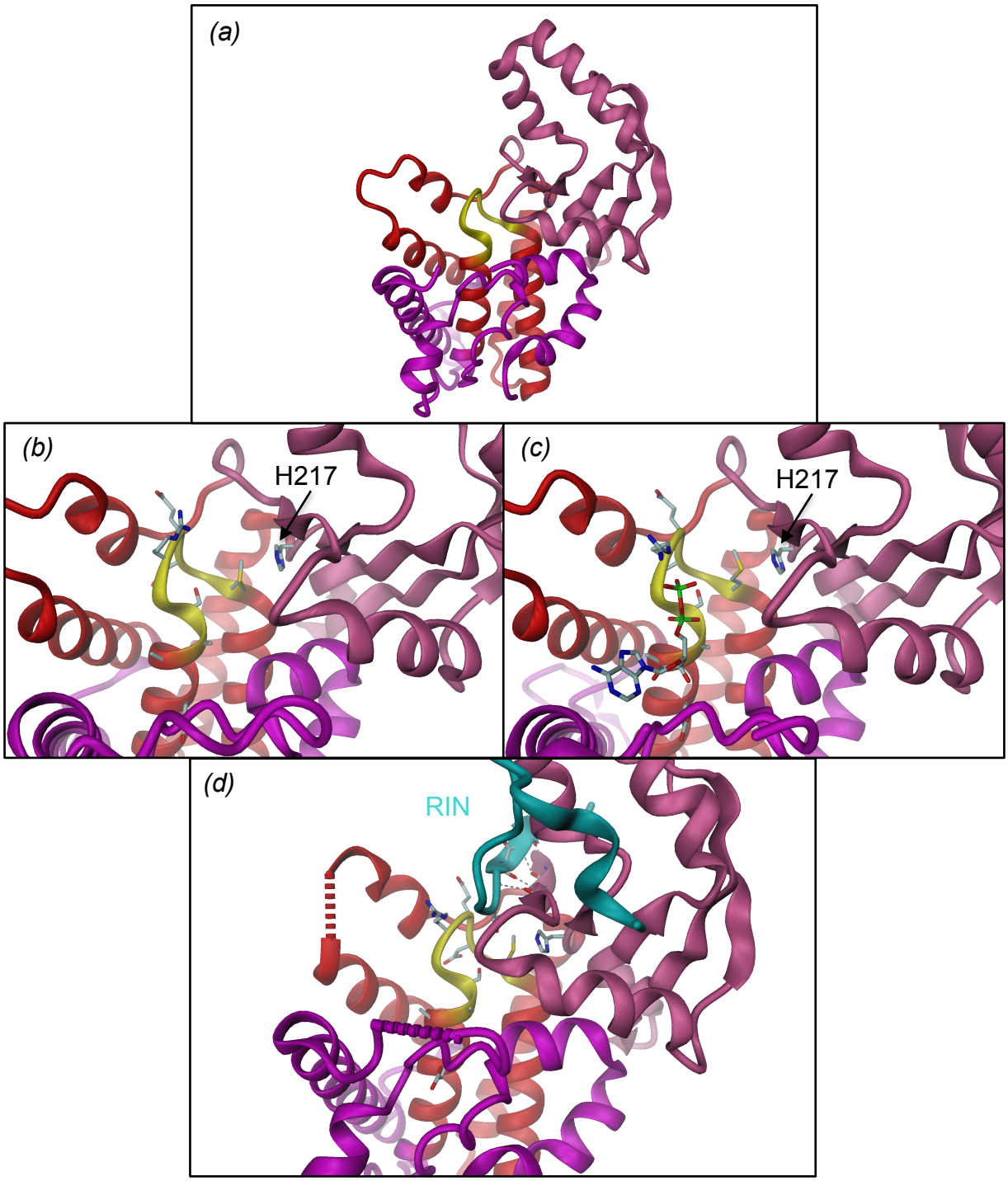

Figure A2. Structure of AvrB from *Pseudomonas syringae*. *(a)* Overall structure of AvrB. The Fic core is colored in red, the Fic active site is colored in yellow and the additional domains are colored in magenta and light pink. *(b)* Active site details of the apo structure of AvrB (PDB: 1NH1). Note the absence of the histidine at the first position of the active site motif (replaced by a methionine). H217, part of the neighboring domain (light pink) may act as a general base in this case. *(c)* AvrB in complex with, presumably, the product of the reaction, ADP (PDB: 2NUN). AvrB is thought to act as a kinase. *(d)* AvrB in complex with the RIN4 peptide (PDB: 2NUD).

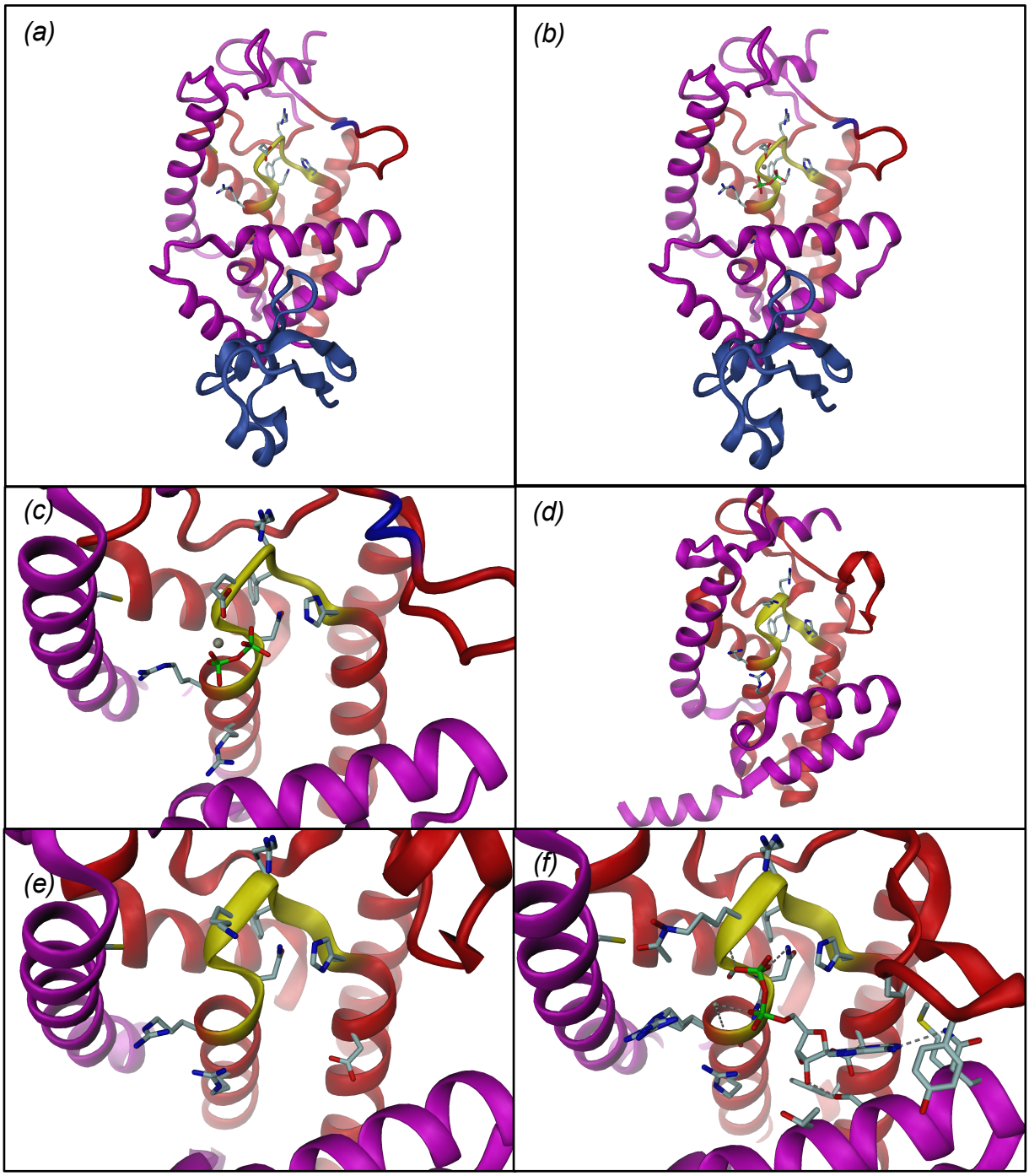

Figure A3. Structures of *Bartonella* effector proteins from lineage 4. *(a)* Overall structure of BepA from *Bartonella henselae* (PDB code: 2VY3). The Fic core is colored in red, the Fic active site is colored in yellow, the additional helices are colored in magenta and the OB (oligonucleotide-binding) fold in blue. *(b)* Overall structure of BepA from *Bartonella henselae* in complex with PP_i (PDB code: 2JK8). *(c)* Details of the active site of BepA in complex with PP_i and Mg^{2+} (as in *(b)*). *(d)* Overall structure of BepC from *Bartonella quintana* (PDB code: 4LU4) using the same color code as in *(a)*. *(e)* Details of the active site of (d). *(f)* Details of the active site of BepC from *Bartonella quintana* in complex with ADP and Mg^{2+} (PDB code: 4N67). Note the modification of the lysine side chain in the active site.

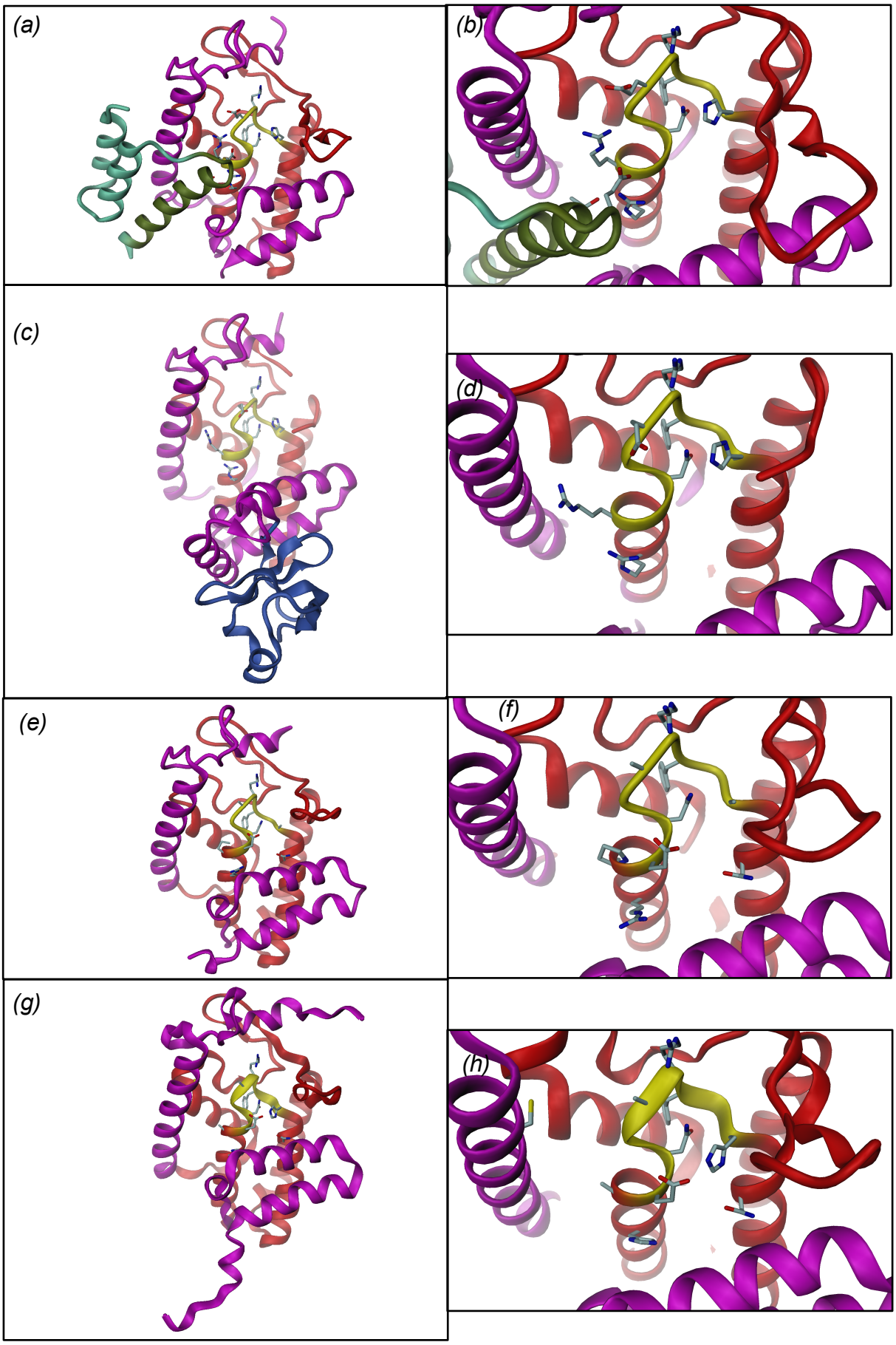
(a)
(b)
(c)
(d)
(e)
(f)
(g)
(h)

Figure A4. Structures of *Bartonella* effector proteins from lineage 3. *(a)* Overall structure of Bep1 from *Bartonella rochalimae* (Arnaud Goepfert, *unpublished*) in complex with its cognate antitoxin. The Fic core is colored in red, the Fic active site is colored in yellow, the additional helices are colored in magenta and the antitoxin is colored in aquamarine except the α_{inh}-helix in dark green. *(b)* Details of the active site of *(a)*. *(c)* Overall structure of Bep1 from *Bartonella clarridgeiae* (PDB code: 4NPS) using the same color code as in (a). Additionally, the OB-fold is colored in blue. *(d)* Details of the active site of *(c)*. Note that the fold is highly similar between these two proteins with or without the antitoxin. *(e)* Overall structure of Bep8 from *Bartonella sp. ar 15-3* (PDB code: 4M16). *(f)* Details of the active site of *(e)*. *(g)* Overall structure of Bep8 from *Bartonella sp. 1-1C*. (PDB code: 4PY3). *(h)* Details of the active site of *(g)*.

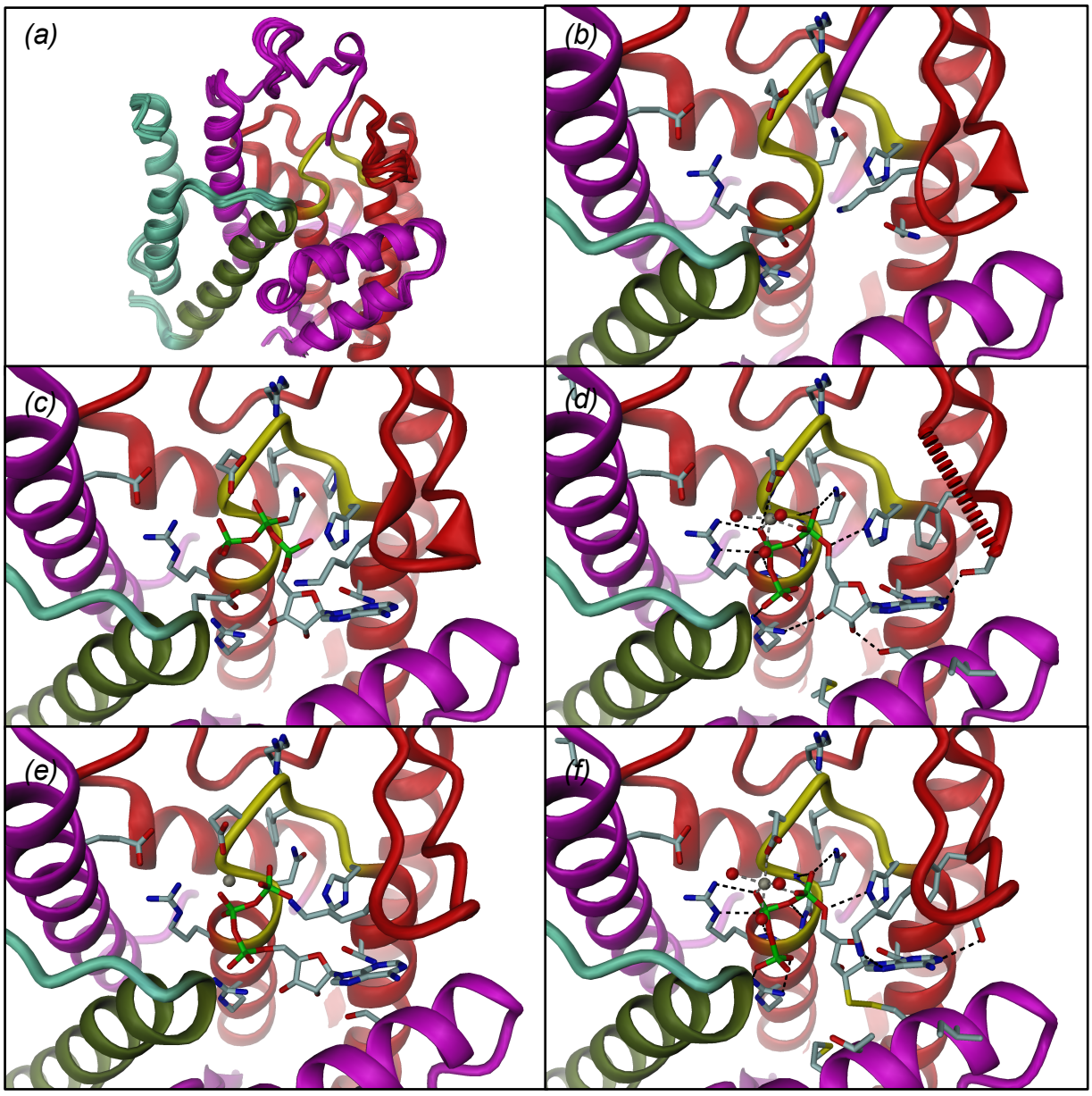

Figure A5. Structures of *Bartonella* effector proteins from lineage 2: VbhT from *B. schoenbuchensis* in complex with its cognate antitoxin VbhA. *(a)* Superimposition of the five structures of VbhT/VbhA described in detail in *(b-f)*. *(b)* Details of the active site of the apo structure of VbhT/VbhA (PDB code: 3SHG). Details of the active site of *(c)* VbhT/VbhA in complex with ATP (PDB code: 3ZC7), *(d)* VbhT/VbhA$_{E24G}$ (inhibition-relieved mutant) in complex with ATP (PDB code: 3ZCB), *(e)* VbhT/VbhA$_{E24G}$ in complex with ATP in which the ATP adopts a kinase-competent conformation (Arnaud Goepfert, *unpublished*) and *(f)* VbhT$_{S175C}$A$_{E24G}$ cross-linked to 2'-S-ATP via a disulfide bond with cysteine 175 (*unpublished*).

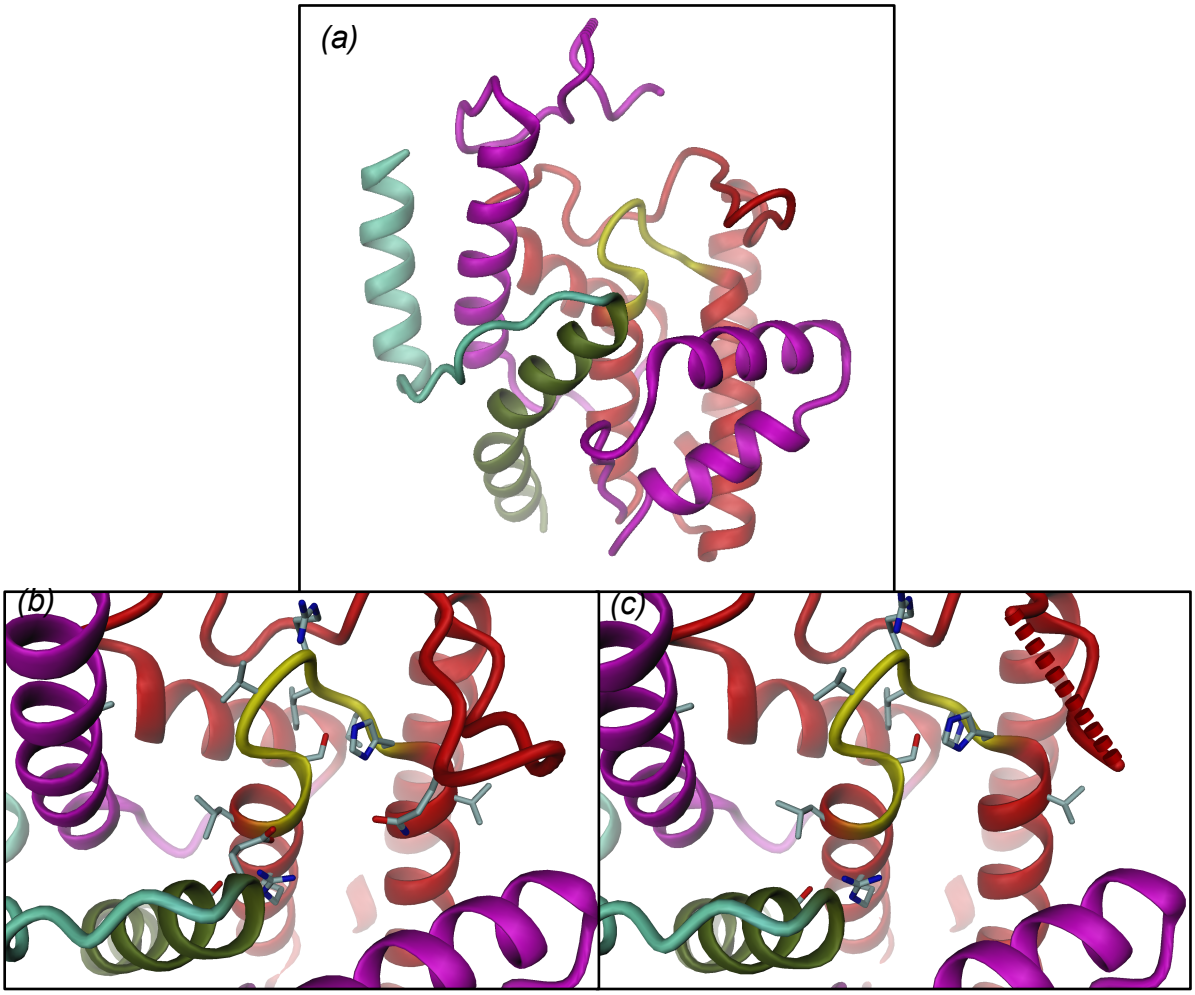

Figure A6. Structures of the class I Fic protein EcFicT in complex with its cognate antitoxin EcFicA. *(a)* Overall structure of $EcFicT_{G55R}$/EcFicA (*unpublished*) using the same color code as in Figure A4. Details of the active site of *(b)* $EcFicT_{G55R}$/EcFicA (*unpublished*) and *(c)* EcFicT/$EcFicA_{E28G}$ (*unpublished*).

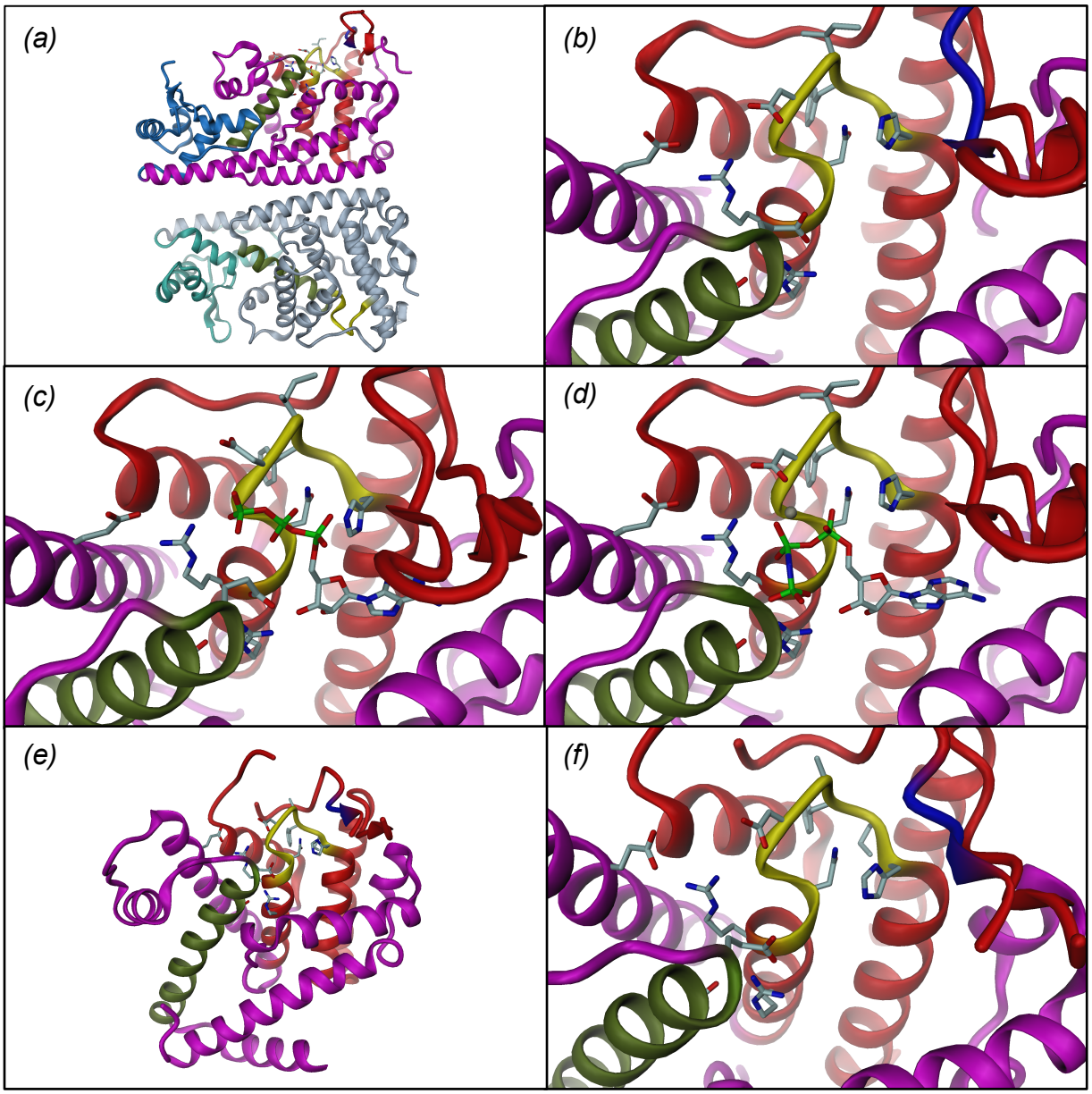

Figure A7. Structures of the class II Fic protein SoFic from *Shewanella oneidensis* and BtFic from *Bacteroides thetaiotaomicron*. *(a)* Overall structure of the SoFic dimer (PDB code: 3EQX) using the same color code as the previous figures with the OB-fold in blue. *(b)* Details of the active site of *(a)*. Details of the active site of *(c)* SoFic in complex with ATP (PDB code: 3ZCN) and *(d)* $SoFic_{E73G}$ (inhibition-relieved mutant) in complex with AMPPNP (PDB code: 3ZEC). *(e)* Overall structure of the BtFic dimer (PDB code: 3CUC) and *(f)* respective active site details.

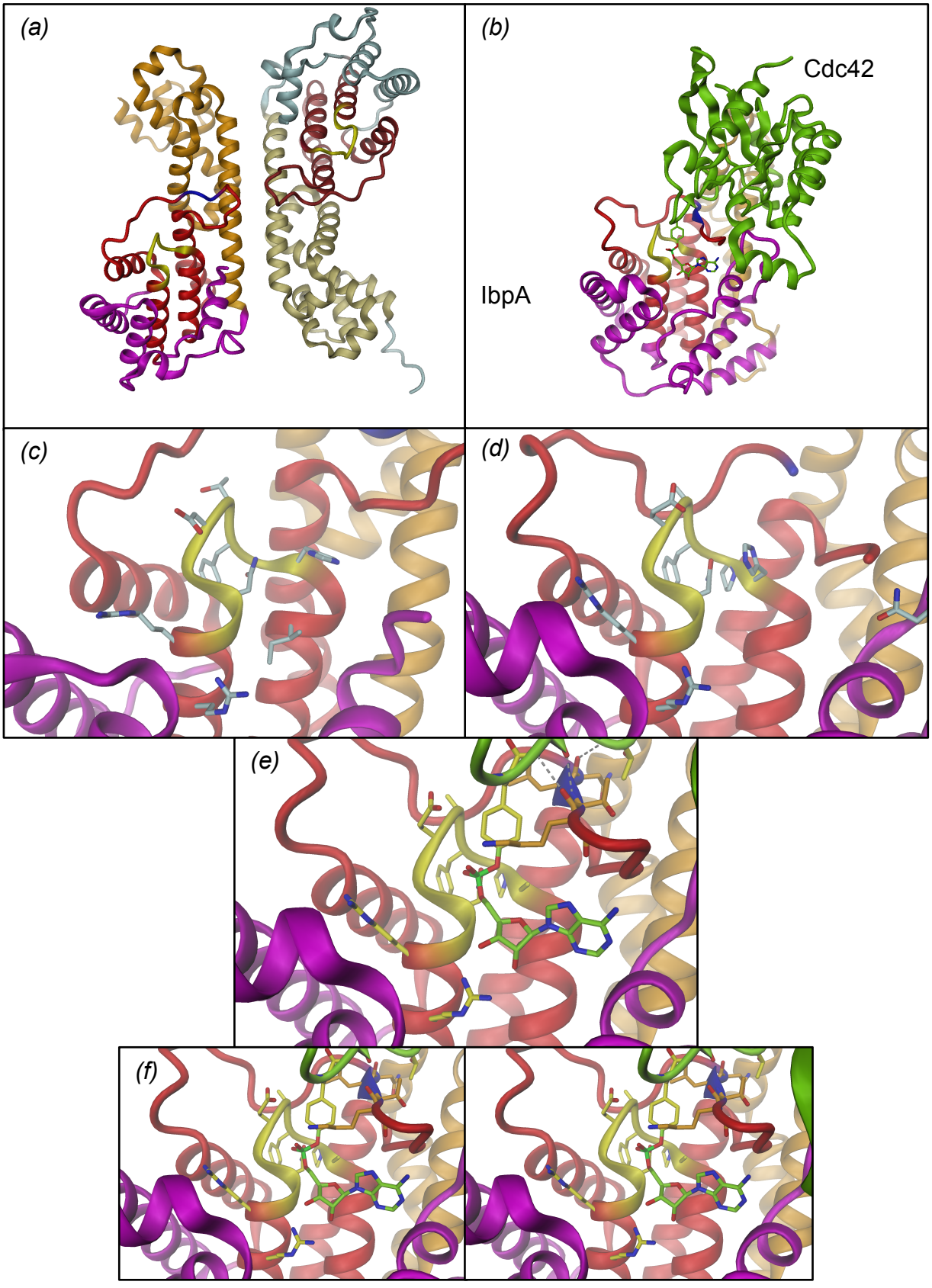
(a)
(b)
Cdc42
IbpA
(c)
(d)
(e)
(f)

Figure A8. Structures of VopS from *Vibrio parahaemolyticus*, IbpA from *Histophilus somni* and IbpA in complex with its target Cdc42. *(a)* Overall structure of the VopS dimer (PDB code: 3LET) using the same color code as the previous figures, the B-subunit of the dimer is colored in slightly different color hue. *(b)* Overall structure of IbpA in complex with Cdc42 (PDB code: 3N3V or 4ITR). *(c)* Details of the active site of *(a)*. *(d)* Details of the active site of IbpA (PDB code: 3N3U). *(e)* Details of the active site of *(b)*. Note that AMP is covalently attached to Y32 of Cdc42. *(f)* Stereoview of *(e)*.

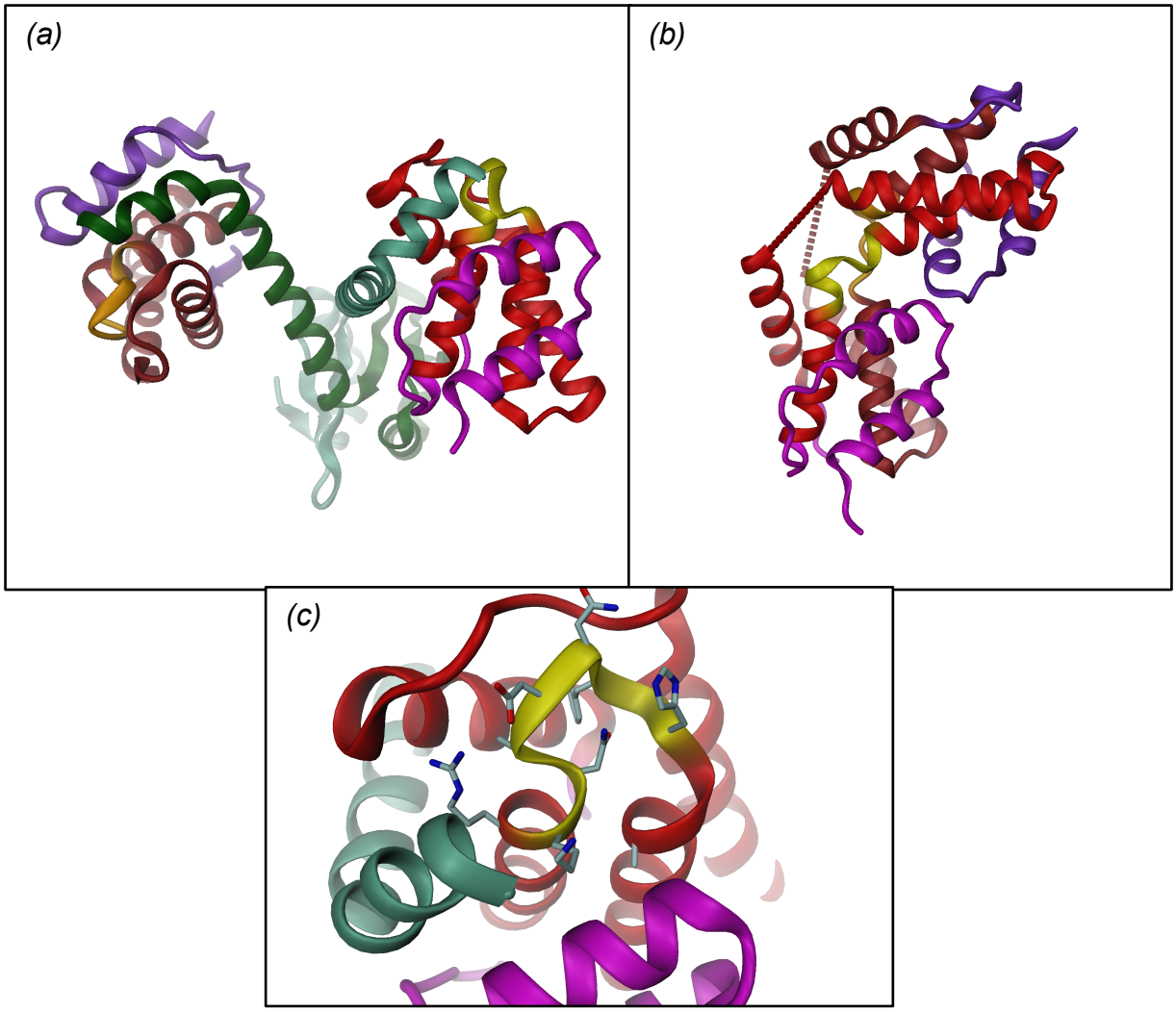

Figure A9. Structures of Doc from Bacteriophage P1. *(a)* Overall structure of the Doc-PhD complex that forms an heterotetramer (2 Doc and 2 PhD) *via* dimerization of the antitoxin PhD (PDB code: 3KH2) using the same color code as the previous figures. *(b)* Overall structure of the Doc_{H66Y} dimer. Note that the Fic fold has been disrupted by this mutation and is now splitted within this dimeric structure. *(c)* Details of the active site of *(a)*.

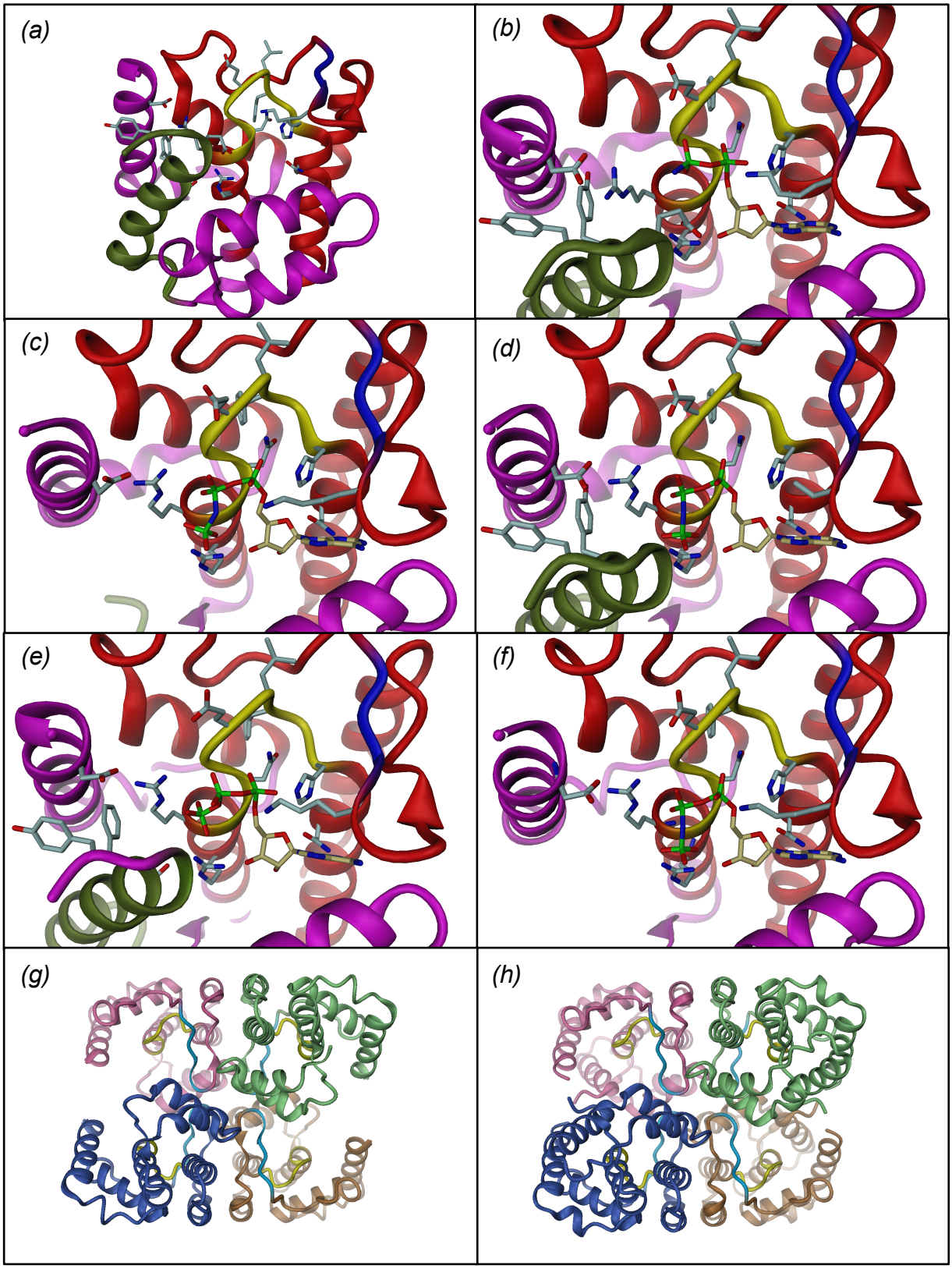

Figure A10. Structures of NmFic from *Neisseria meningitidis*. *(a)* Overall structure of NmFic (PDB code: 2G03) using the same color code as the previous figures. Active site details of *(b)* NmFic in complex with AMPPNP (PDB code: 3S6A), *(c)* $NmFic_{S182A,E186G}$ in complex with AMPPNP (PDB code: 3SN9), *(d)* $NmFic_{E186G}$ in complex with AMPPNP (PDB code: 3ZLM), *(e)* $NmFic_{Y183F,E186G}$ in complex with ATP

(*unpublished*) and *(f)* $NmFic_{\Delta 8}$ in complex with AMPPNP (PDB code: 3SE5). Tetramer observed in the structure of *(g)* $NmFic_{\Delta 8}$ (PDB code: 3SE5) and *(h)* $NmFic_{wt}$ crystallized at high protein concentration (*unpublished*).

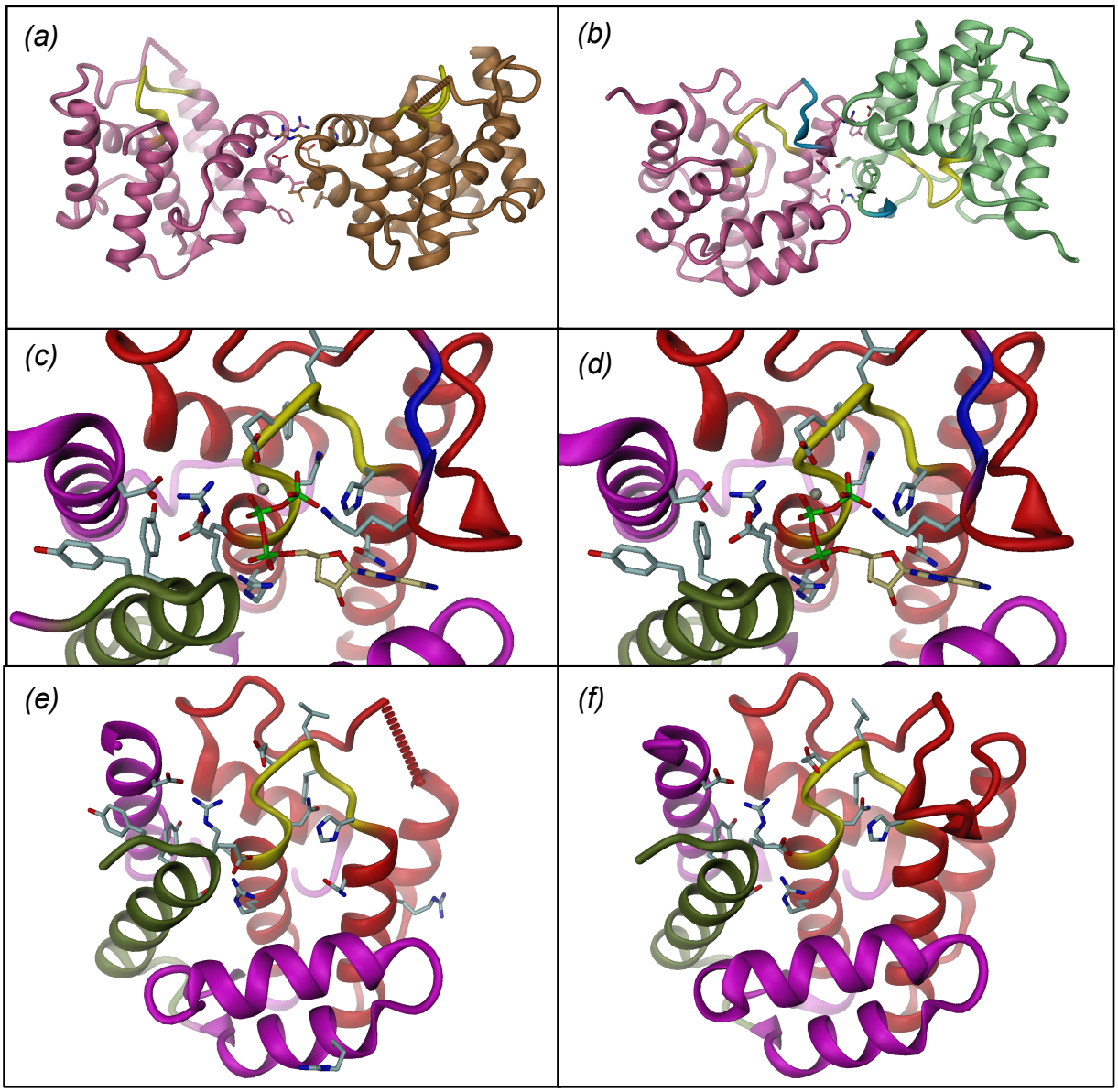

Figure A11. Structures of NmFic from *Neisseria meningitidis* and HpFic from *Helicobacter pylori*. *(a)* Overall dimeric structure of $NmFic_{E102R}$ (*unpublished*) with the monomer A in pink and B in brown. The active site loop is colored is yellow and the residues involved in contacts are shown as sticks. Note that the FLAP region is not ordered in the crystal. *(b)* Overall dimeric structure of $NmFic_{E156R}$ (*unpublished*) with the monomer A in pink and B in green. The active site loop is colored is yellow, the FLAP in blue and the residues involved in contacts are shown as sticks. Details of the active site of *(c)* $NmFic_{E156R}$ in complex with ATP and *(d)* $NmFic_{E156R,Y183F}$ in complex with ATP. Note that ATP adopts a kinase conformation in these two structures. *(e)* Structure of monomeric $NmFic_{E102R,E156R}$ and *(f)* structure of HpFic.